THE EFFECT OF SEA INDUCED MOTION ON OFFSHORE PROCESS EQUIPMENT.

Graeme White

Submitted for the Degree of Doctor of Philosophy

Heriot-Watt University

Department of Chemical and Process Engineering

May 1990

TABLE OF CONTENTS.

Additional Material External to this Report :

1) Computer Listing of Numerical Simulation Program.
2) Computer Listing of Motion Simulatior Data Logging and Control Programs.
3) Computer Listing of Data Processing Program.

LIST OF FIGURES

LIST OF GRAPHS

LIST OF PHOTOGRAPHS

LIST OF TABLES

ACKNOWLEDGEMENTS.

Firstly, I wish to thank Professor Brian Waldie not only for his time and patient supervision throughout this project but for his foresight into the importance of marine motion on offshore process equipment. Under his influence, the departments offshore processing laboratory is not only well equipped but attractive to the offshore industry.

Secondly, I would like to thank Mr Alastair Thomas whose technical advice was much appreciated. It was Mr Thomas, along with Professor Waldie, who designed and built the motion simulator. I would also mention Mr Jack Paterson whose interest and support in electrical matters was also appreciated.

Finally, for financial support both direct and into the simulator project in general, I would like to thank SERC, The Marine Technology Directorate and the company Britoil. Without Britoil's scholarship at the beginning, I may never have started the research project.

ABSTRACT.

The performance of offshore process equipment on floating production platforms may be reduced through imposed sea motion. Fluid sloshing inside primary separators and non-segregated storage tanks may lead to oil/water mixing.

The aim of previous work into sloshing has been to prevent damage to LNG tankers and increase the stability of space rockets. Work into oil/water sloshing appears limited.

A computer controlled motion simulator was developed to conduct experiments with two rectangular vessels filled with air, refined oil and water. Two single sinusoidal forcing motions were applied, pitch and surge at various amplitudes and periods. Additional experiments were conducted with combined forcing motions pitch/roll and pitch/surge. Air/water interface profiles were measured and analysed using a computer based data logging and processing system. Air/oil and oil/water profiles were recorded using high speed video equipment. Also studied were the effect of baffles in reducing interface amplitude and the effect of forcing on oil/water transfer.

A linear theory was derived to predict natural frequencies of three fluid systems and a numerical model was developed to predict near resonant behaviour. Air/water experiments and numerical model showed a coupling of natural and forcing frequencies in the free surface frequency spectrum. Favourable comparisons were also seen between the numerical model and oil/water experiments. Additional experiments indicated that oil/water mixing is promoted by resonant forcing in an unbaffled vessel. The presence of baffles reduces interfacial breakup and hence reduces oil content of water.

LIST OF MAJOR ABBREVIATIONS.

The following list all major abbreviations used throughout this report, all other symbols are defined where required. Note some symbols have multiple meanings.

Ai = Amplitude of motion i (i=p for pitch, =h for heave, =l for sway) .

A - General constant.

a = Distance from a point. Vector quantity with elements a_i, i=x,y,z.

= Pitch angle at any time t.

= Vessel length or half length.

B = General constant.

b = Distance from a point. Vector quantity with elements b_i, i=x,y,z.

C = General constant.

D = Position term of rotating vessel origin from fixed origin.

= General constant.

F = Force.

f = General term.

g = Acceleration due to gravity.

H = Vessel height.

h = Heave position at any time t.

h_i = Liquid fill depth of fluid i.

k = Wave number.

l = Sway position at any time t.

= Vessel length.

m = Mass.

n = General index n=1,2,3...

O_i = Offset in motion i (see definition from symbol A).

P = Pressure.

p = Pressure.

q = Velocity vector term.

R = Distance from a point. Vector quantity with elements R_i, i=x,y,z.

r = Distance from a point.

r_{ij} = density ratio of fluid i and j (= ρ_i/ρ_j)

T = General term for time.

$T_i(t)$ = Function of time, element i=0,1,2,3...

t = Time.

u = Velocity in x direction.

u_i = Velocity of tensor component i.

v = Velocity in y direction.

= General symbol for velocity.

X_i = General Body force of tensor component i. Split into components X & Y.

x = Distance from origin.

x_i = Distance tensor component i.

x_o = Amplitude of sway motion for simple linear theory.

ε = Phase angle.

ε_{ijk} = Krondecadelta.

ε_i = Phase angle of motion i (See A above).

μ = Coefficient of viscosity.

μ_v = Coefficient of Bulk viscosity.

η_i = Equation of the free surface of fluid i.

Ω = Rotation of a frame of reference. Vector quantity with elements Ω_i, i=x,y,z.

= General term for forcing frequency.

ω_i = Frequency of motion i (See A above).

ω = General term for natural frequency. Expression for natural frequency modes ω_{2n-1}, n=1,2,3...

ρ = Density.

σ_{ik} = Stress tensor component ik.

θ = Angle of rotating vessel to fixed frame of reference.

ϕ_i = Velocity potential of fluid i.

∇ = Operator $\frac{\partial}{\partial x} + \frac{\partial}{\partial y}$

ACF = Amplitude Conversion Factor used in FFT frequency spectra calculations.

AMFC = Amplitude of the Major Frequency Component used in FFT frequency spectra calculations.

CHAPTER 1.

INTRODUCTION TO THE EFFECT OF SEA INDUCED MOTION ON OFFSHORE PROCESS EQUIPMENT.

1.1 BACKGROUND TO MOTION EFFECTS ON OFFSHORE EQUIPMENT.

To develop oil fields in deep water or fields which are small in size, design engineers have turned to the use of *Floating Production Systems* rather than conventional fixed structures. In comparison with fixed platforms, the advantages of floating systems are their relatively low capital cost, shorter installation time and reusability once the field has been depleted.

Conventional fixed platforms use gravity based separation equipment to separate gas, oil, water and sand. The performance of offshore separation equipment used on floating platforms will be affected by platform motion (1). As a means to reduce platform capital cost, the possibility exists to store produced oil and ballast water in the same container. Therefore, imposed sea motion will also influence the design and operation of these non-segregated oil/water storage vessels.

Partially filled liquid containers (e.g. a vessel filled with gas, oil and water) all have the basic property that, under the influence of some physical force the unrestricted liquid free surface (i.e. the gas/oil and oil/water interface) will deform. Depending on the applied force, waves on the free surface can give rise to large impact pressures on the vessel walls, leading to breaking of the interface (2). This phenomenon, called *fluid sloshing*, has obvious relevance to the design of non-segregated oil/water storage systems and to offshore process equipment.

Due to interest in LNG carriers, definite procedures exist to design vessels to withstand the high impact pressures that can arise in sloshing (3,4). However, little work appears to have been done to find the

extent of fluid mixing caused by breaking waves which arise due to sloshing.

1.2 OBJECTIVE OF RESEARCH PROJECT.

The objective of this research project was to investigate some of the features of fluid sloshing in relation to non-segregated oil/water storage systems and to the performance of offshore separators. In particular, this project studied the effects of imposed motion on the behaviour of air/water, oil/water and air/oil interfaces in closed rectangular vessels. A two dimensional numerical model was developed and compared to physical experiments.

1.3 PREVIOUS WORK RELATED TO FLOATING PRODUCTION SYSTEMS.

The theory behind fluid sloshing can be considered to have its origins in the development of basic wave theory in the 1800's (5). It was not until the late 1950's and early 1960's with the advent of spaceflight and large Liquid Natural Gas tankers, that a more detailed understanding of fluid sloshing became important (6-10).

By experiment and simple theoretical analysis, it was found that oscillations of a partially filled liquid container at a certain frequency and amplitude could result in large *impact pressures* and *large turning forces*. These forces were found to be important for the control and stability of space rockets and a vast number of papers were published on this topic (6).

More recently, with large LNG cargo ships, attention has been paid to the design of storage tanks to withstand the high impact pressures that might occur under various sea conditions (2,8). Work in this area has dealt mainly with the effects of fluid properties, cargo tank design and scale up parameters for the prediction of impact pressures.

Besides spacecraft and LNG carriers, sloshing is also a concern with rail/road transport and the effect of earthquakes on large shore based liquid storage tanks (11).

For floating production systems, designers of offshore process equipment realised that sea motion could affect gas/oil/water separation (12). To minimize liquid motion, even under severe sea conditions *internals (baffles)* were devised. Rice (1) described test facilities used by the company *C-E Natco* in the USA, to test process equipment using a *motion simulator.* However his paper presented a summary of work, no details of specific process equipment were given. Very few papers appear to have been written on the subject of oil/water sloshing.

Chapter 2 presents a review of floating production systems and introduces the problems associated with platform motion.

1.4 THE THEORY OF SLOSHING AND SOLUTION TECHNIQUES.

As with wave theory in general, sloshing is a highly non-linear problem, producing complex equations which are specific to one geometry. The major stumbling block with such theories, is accounting for fluid acceleration terms.

Simplifications can be made to the fluid equations, to yield the prediction of the *natural period* of the fluid/container system i.e. the frequency at which waves will oscillate once external forcing has stopped. This parameter is of paramount importance to gauge the conditions which may cause structural damage to LNG tanks and cause mixing of oil and water in offshore separators. Chapter 3 presents a review of previous work with linear and non-linear theories, including results of some experiments. As various authors adopt different mathematical notation, chapter 4 presents the derivation of a basic sloshing equation and solutions of a simple linearized form by Laplace Transform.

With the advent of large computing systems, it has now become feasible to employ numerical techniques to solve fluid equations (3,13-15). Of the numerical techniques currently available, the *Marker And Cell (MAC)* method as described by Harlow & Welch in 1965 (16) appeared to be applicable to numerical simulation of fluid sloshing.

Chapter 4 also describes modifications to the MAC code due to Nichols et al (17) to model fluid behaviour in two dimensional rectangular vessels. Comparisons between numerical model and physical experiments are presented in chapter 12.

1.5 USE OF A MOTION SIMULATOR.

Although the effect of sea waves on floating structures involves six degrees of freedom, previous experimental studies have concentrated on single forcing motions. Scale models of prototype vessels would be placed on a *motion simulator* and a single forcing motion applied. This makes the analysis of results simpler to interpret by either analytical or numerical means.

Prior to the start of this project, the Chemical and Process Engineering Department, undertook the design and construction of a motion simulator, capable of generating three simultaneous forcing motions. During the course of this project, a full computer control and data logging facility was developed for the simulator. Details of the motion simulator and control system are described in chapter 5. Chapter 6 then presents experimental procedures to study the effect of forcing motion on rectangular vessels filled with air/water, oil/water and air/oil/water.

1.6 RANGE OF EXPERIMENTS PERFORMED IN THIS PROJECT.

Unlike previous studies, which have tended to study pressure and force distributions, this project required information on the mixing of oil and water i.e. the interface and fluid flow profiles. The experiments conducted during this project were divided into three sections. Firstly, experiments were conducted with air and water, recording the interface profile as a function of time. Secondly, interface profiles in an air/oil/water system were recorded using high speed video equipment. The third set of experiments attempted to measure the actual amount of oil transferred to the water. Data from these *physical experiments* were used to check and assist the development of the numerical model.

Chapters 7 and 8 discuss the results of experiments with two rectangular vessels of different sizes, using air and water as test fluids. For the large rectangular vessel, chapter 8 includes a section on the effects of *simultaneous* forcing motions and the effects of baffles on air/water behaviour. Chapters 9 and 10 discuss experiments in the same vessels, using oil and water. The effect of baffles on oil/water behaviour is included in chapter 10. Then, chapter 11 describes a series of experiments to determine the amount of oil transferred to water as a result of forcing in the large vessel.

Using the numerical model, *simulation experiments* were conducted and results compared to *physical experiments*. These comparisons are discussed in chapter 12.

The overall significance of the results are discussed in chapter 13 and the main conclusions of this work presented in chapter 14.

CHAPTER 2.

REVIEW OF SEA MOTION EFFECTS ON FLOATING PRODUCTION SYSTEMS.

2.1 INTRODUCTION.

Development of smaller, remote and deep water oil fields, has lead to the use of floating rather than fixed production platforms. A major difference between fixed and floating platform concerns the effect of sea motion on platform stability and performance of separation equipment.

Although floating production systems are not new (18,19), published information relates mainly to overall operation of the facility rather than specific parameters concerning the design of processing equipment. A literature survey was conducted to provide details on the effects of sea induced motion on the performance of both gas/oil/water separators and gas/liquid contacting columns. Such information was useful in deciding the motion conditions for experimental work carried out during this project. This chapter presents a review of floating production systems currently in operation and some of the problems caused by sea motion.

2.2 REVIEW OF CURRENT FLOATING PRODUCTION SYSTEMS.

2.2.1 Function of a Offshore Production Platform.

The basic function of a offshore production system is to separate *well head fluids* (gas, oil, water and sand) and transport the oil to shore based refineries. For the other fluids, gas may be transported, reinjected or flared, water and sand must be disposed of. First stage, *primary*, separation involves gravity settling of well head fluids in pressure vessels. The size of these vessels is determined by flowrate and product (oil or water) quality. Subsequent separation stages may involve further gravity settling or use of coalescence/filtration units until the oil, water and gas streams reach specification (e.g. depending on the platform

position, discharge water has been stated as not to exceed an oil content of 40ppm (20)). As an example, figure 2.1 presents an flowscheme for separating oil from well head fluids.

The normal conception of a north sea platform consists of both processing and living facilities placed on top of a steel/concrete structure which extends and is secured to, the sea bed. The cost of production facilities for any field must be matched to the revenue that might be gained from that field. In the case of a small sized field or one in deep water, or both, the cost of a fixed structure might prohibit field development. Oil companies trying to develop these *marginal* fields are considering and installing floating rather than fixed production facilities (21).

2.2.2 Semi-Submersible & Ship Based Floating Production Systems.

Floating production systems currently in use fall mainly into two catagories, semi-submersibles and ship based units. Semi-submersibles are based upon conventional steel platforms with buoyant pontoons supporting the working area. These systems are positioned over the well head by mooring lines (figure 2.2a). Recently, the company Conoco, has successfully developed the Tension Leg Platform (TLP) (22). Unlike conventional semi-submersible units, tensioned wires attached the TLP to the sea bed. The oil produced from semi-submersibles must be shipped to shore based refineries by either pipeline or shuttle tanker. In the case of shuttle tanker export, no effective means for berthing a tanker to a semi-submersible have yet been found (19). In this case produced oil must be stored in another floating structure (e.g. the reservoir tanker as depicted in figure 2.2a). Other than their own buoyancy compartments, semi-submersibles may have no inherent storage capacity for produced oil.

In the case of ship based units, separation and treatment equipment can be placed on either converted oil tankers or purpose built ships. Produced oil is then stored in the ships own cargo tanks prior to export by shuttle tanker. Figure 2.2b serves to illustrate such a ship based floating production system, attached to a well by means of a moveable arm (swivel). A recent development in ship based systems is BP's Single Well Offshore Production System (SWOPS) (figure 2.3) (23). This vessel is designed to unhook from the sea bed and transport oil to shore before returning to the well for further production. Dynamic positioning is used to keep the vessel over the well head. It is worth noting that the Norwegian Companies, like BP, are currently involved with ship based floating production units (24).

2.2.3 Proposals for Produced Oil Storage on Semi-Submersible Systems.

One major difference between ship and semi-submersible based floating production systems is that semi-submersibles may require an additional floating storage unit for produced oil. It would then appear, that ship based floating production systems offer a better alternative to semi-submersibles as regards storage of oil. However, as swivel moorings pose technical difficulties (19), suggestions have been made to add produced oil storage compartments to semi-submersibles.

1) A conceptual study was made by Hisamatsu (25) to add a storage unit to a TLP system. Computer predictions were made in regards to the loading forces involved in placing such a unit and during platform operation. To maintain a constant weight, Hisamatsu envisaged a completely filled container i.e. a *non-segregated* oil/water storage area for oil. Water would replace oil taken off by shuttle tanker.

2) The company Britoil, suggested a course of research into the possibility of storing produced oil and water in the pontoons of a semi-submersible. In a similar manner to Hisamatsu, non-segregated oil/water storage tanks were proposed.

As with separation equipment, the effects of sea motion on these non-segregated oil/water storage systems is relatively unknown.

2.3 SEA INDUCED MOTION EFFECTS ON PROCESS EQUIPMENT.

2.3.1 Effects of Motion on Partially Filled Liquid Containers.

Separation equipment and non-segregated oil/water storage systems involve vessels which contain a *free surface*, i.e an unrestricted gas/liquid or liquid/liquid interface. The effects of forcing motion on partially filled liquid containers (i.e. those with a free surface), can lead to (6) :

1) Waves forming on the gas/liquid and liquid/liquid interface.

2) At certain forcing conditions, interface breakup occurs causing mixing across the free surface.

3) In large containers high impact pressures caused by waves slamming on container walls, may result in structural damage.

As will be shown in the next chapter, wave motion in gas/liquid containers may be reduced through the use of baffles (6).

2.3.2 Effects of Forcing Motion on Processing Equipment.

In the case of separation equipment, either primary gas/oil/water or *secondary* oil/water separators, the effects of imposed forcing motion were studied by Karve et al (12) and Rice (1). These effects may be summarized as :

1) Primary turbulence: Interface breakup may lead to mixing of oil and water thereby reducing separator performance. A system of mechanical *baffles* may reduce primary turbulence.

2) Secondary Turbulence: Flow round internal obstacles, such as baffles, may cause eddy currents which degrade separation. As baffles may reduce primary but increase secondary turbulence, the design of baffles must be optimized (figure 2.4).

3) Level Control: Waves on the free surface may results in problems with liquid level control systems, giving false high and low level alarms.

In relation to the proposed non-segregated oil/water storage system, imposed forcing motion may be considered to cause similar effects to those above. Prolonged mixing of oil and water in storage tanks may in addition, generate emulsions (26).

Forcing motion also affects the performance of gas/liquid contacting columns. Work by Hoerner et al (27) may be summarized as :

1) Random imposed motion has a relatively small effect of column efficiency.

2) Column characteristics (e.g. flooding, weeping) are affected by permanent inclination.

2.4 RANGE OF PLATFORM MOTIONS IN RESPONSE TO SEA MOTION.

2.4.1 Introduction.

A floating structure is potentially subject to six degrees of movement, as indicated in figure 2.5. The amplitude of each motion will depend on the design of the platform and on sea state. To design both platform and process equipment, information is needed on platform response to *worst sea state* conditions expected during the working life of the

platform. The *sea keeping* characteristics between ship and semi-submersible based units is then one factor in deciding which system to use (28).

During initial design stages of proposed floating systems, computer models have been used (29) to simulate the effect of various seas. In the absence of specific design details and access to the predicting models, motion conditions must be obtained from published experimental data.

2.4.2 Selection of Semi-submersible and Ship Based Floating Production Systems.

It has been claimed that ship based systems have better sea keeping characteristics than a semi-submersible (28,30). Table 2.1 lists some of the floating production systems that have or are, currently in operation throughout the world and shows that the majority of systems are based on semi-submersibles. This may indicate that semi-submersible are better suited for floating production systems. However, table 2.1 and 2.2 show that floating production systems have been situated in relatively calm seas as compared to the North Sea.

Available published literature (21,30,31) dealing with both semi-submersible and ship based floating production systems, have noted no abnormal operational difficulties. However, these floating production systems were placed in relatively calm seas, compared to the North Sea. It may be expected that sea motion will have a greater influence on the choice of vessel and separation equipment for North Sea floating production systems.

2.4.3 Typical Design Motion Conditions.

In the absence of specific environmental conditions, several standards have been laid down for design purposes. Baitis et al (32), quoted United States Federal Regulations (1974) that LNG tankers be designed to withstand :

Rolling	±30°	amplitude,	10	second	period
Pitching	±6°	" ,	7	"	"
Heaving	L/80 feet	,	8	"	" .

(L = Vessel length in direction of movement)

Without quoting specific figures, the authors state that these regulations should be amended to *stricter* limits as in European designs. Tables 2.3 and 2.4 present motion response data for BP's SWOPS vessel (23), and those used by Hisamatsu (25) in the design of a TLP oil/water storage unit. In addition, Remery (26) quoted ship based floating production systems operating satisfactorily at up to ±10° roll. He further commented that ±4° would be expected from a similar system in the North Sea.

Comparisons of motion data, suggest that motion amplitudes of ship and semi-submersibles are less than those for LNG tanker design. Figure 2.6 shows the response of both semi-submersibles and ship based units in terms of significant wave height.

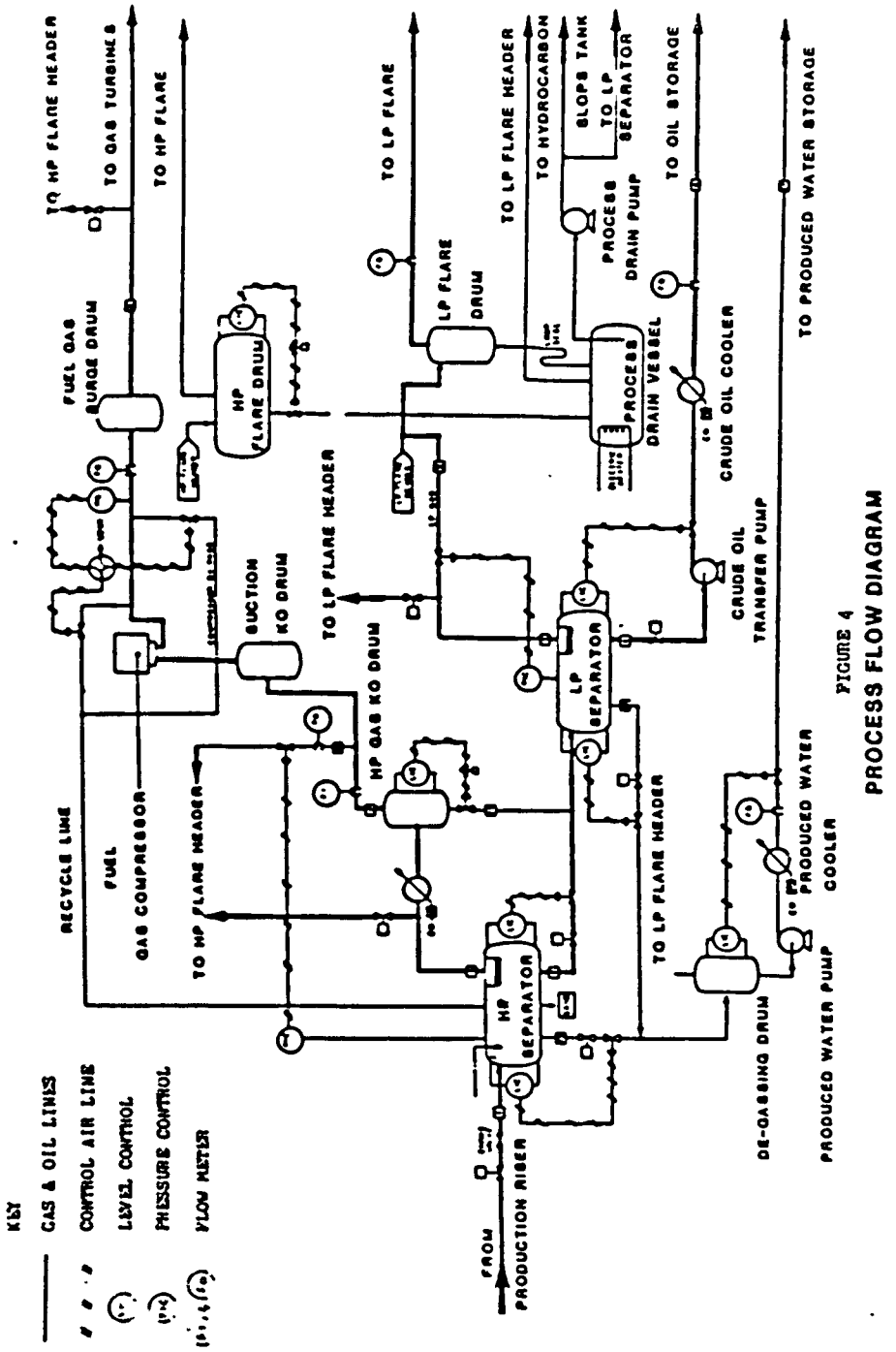

Figure 2.1: Flowscheme for gas/oil/water separation on BP's SWOPS floating production system (23).

Santa Fe Drilling Co. Deepwater Floating Production System

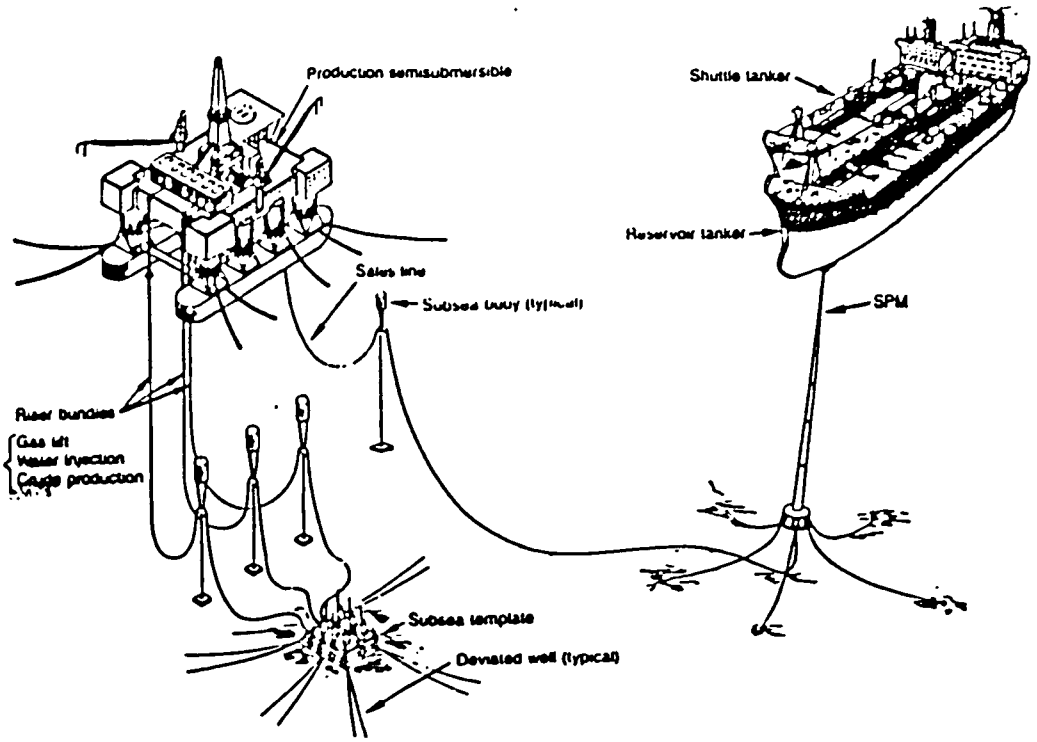

Figure 2.2a: Example of a semi-submersible based floating production system for deep water (33).

Exxon's Offshore Storage & Treating Facility
Santa Barbara Channel, California

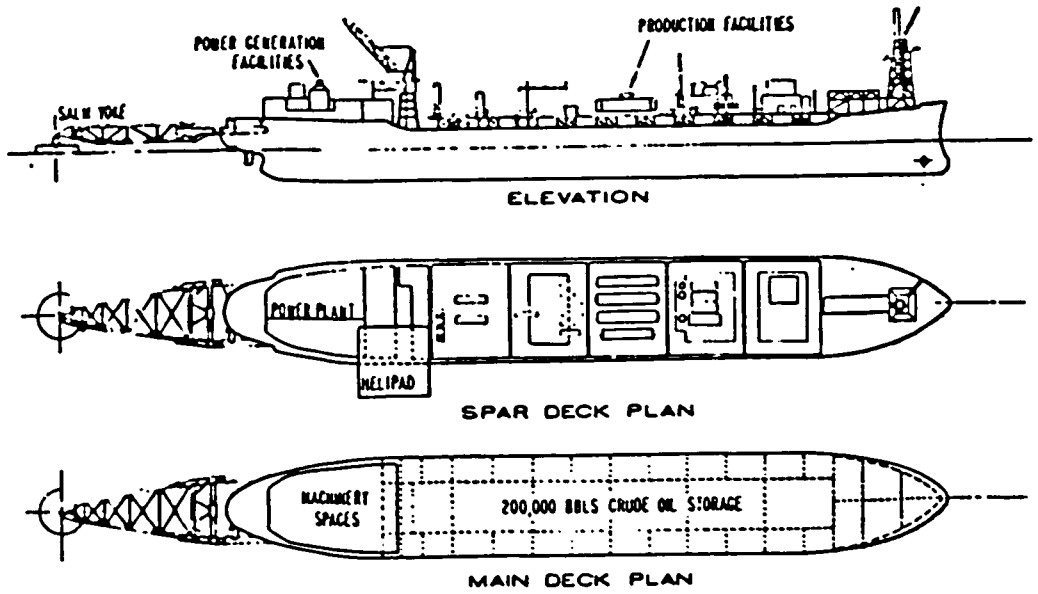

Figure 2.2b: Example of a ship based floating production system (34).

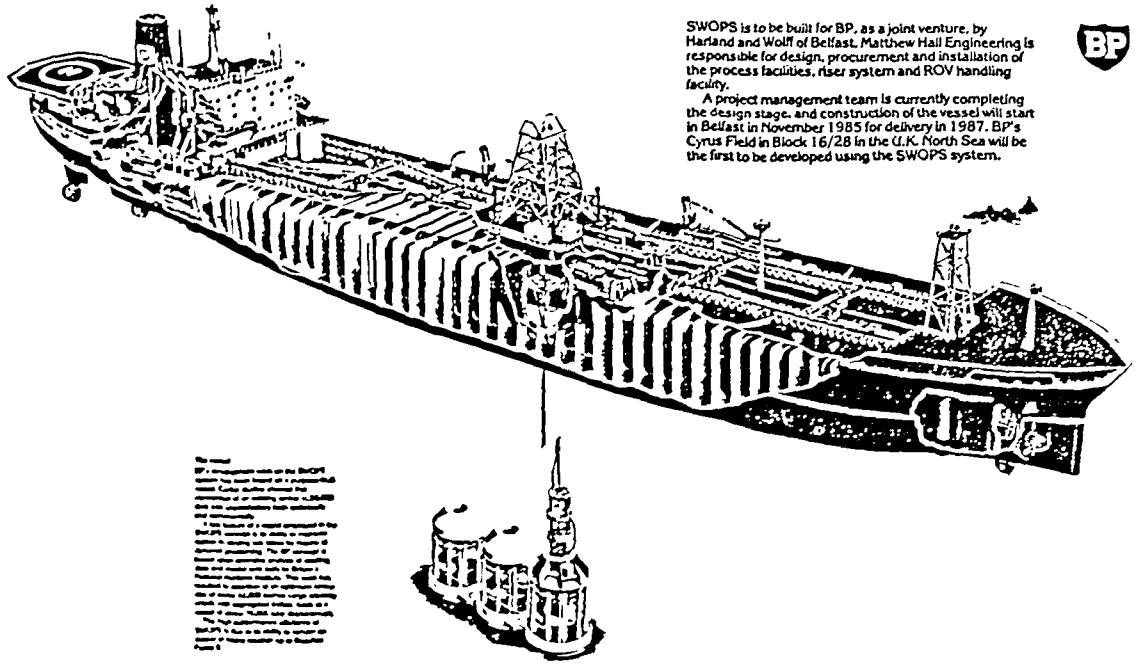

Figure 2.3: BP's Single Well Oil Production System (SWOPS) for development of marginal fields (35).

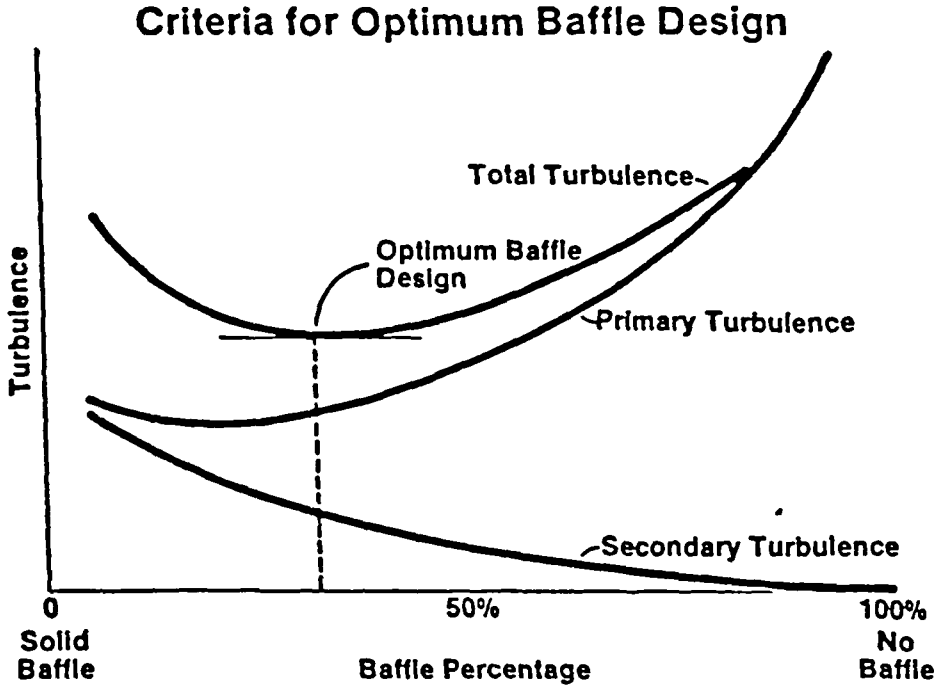

Figure 2.4: Example of optimum baffle design to reduce primary and secondary turbulence in an primary separator, due to Karve and Fenner (12).

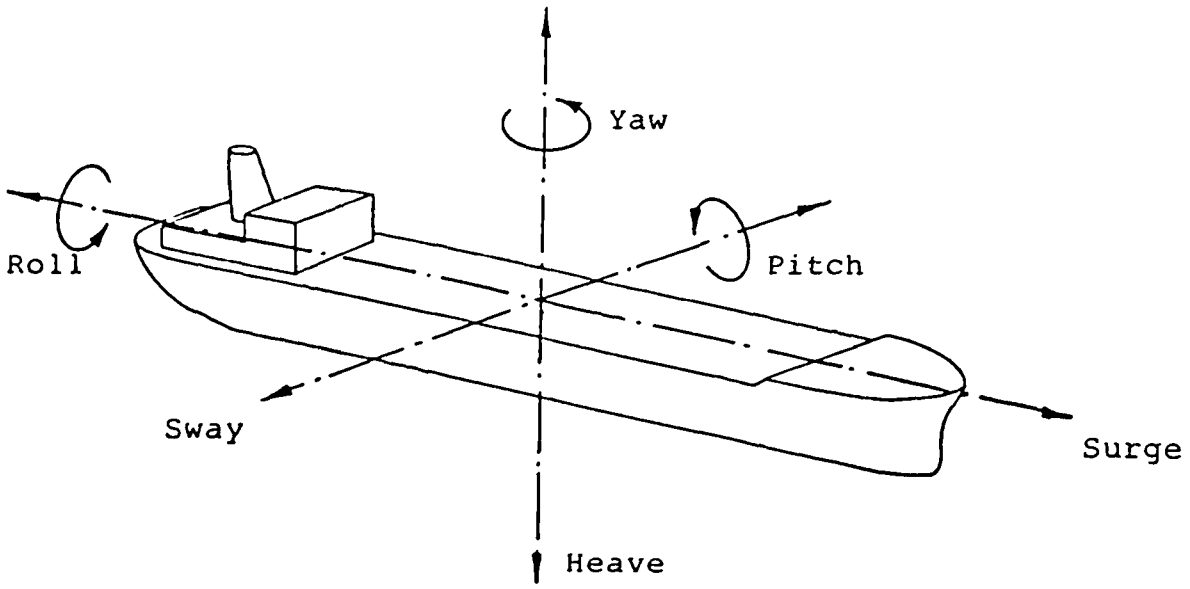

Figure 2.5: Designation used to describe the six degrees of motion of a floating structure.

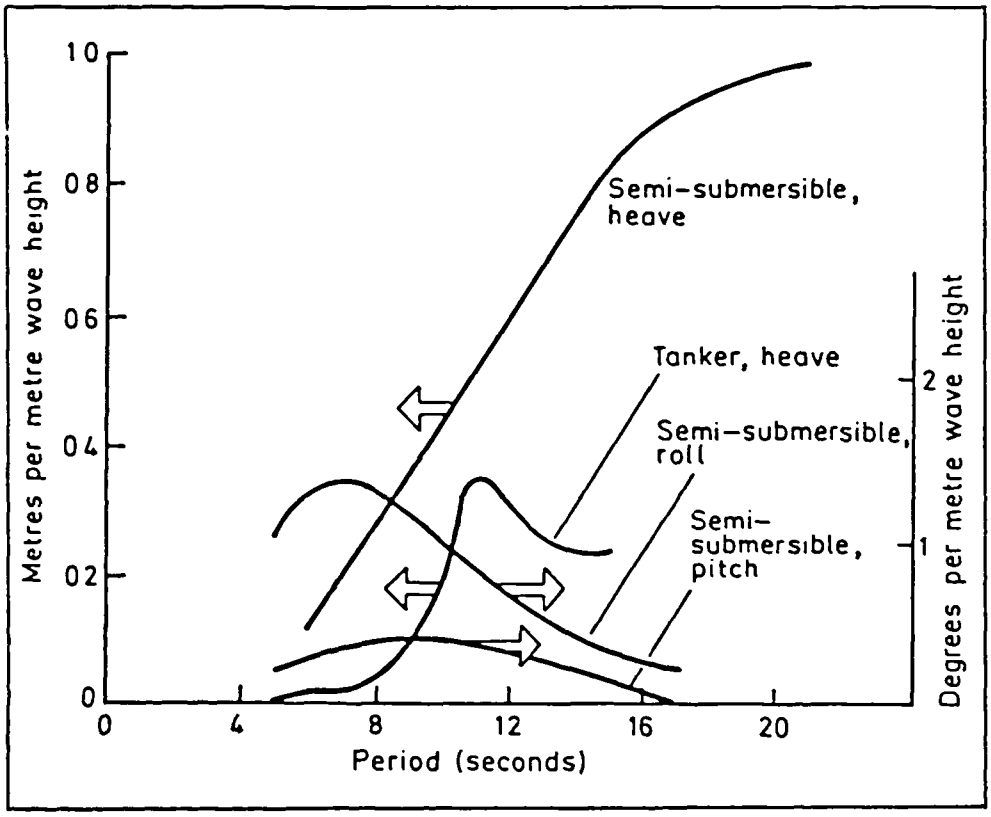

Figure 2.6: Response of semi-submersible and ship based floating productions systems to given sea states (36).

Field Name	Operator	Water Depth (m)	Design Capacity (barrels per day)	Date	Location	Ref
Casellon	Shell	118		1977	Spain	37
Garoupa	Petrobras	124		1979	Brazil	37
Nilde	AGIP	82		1980	Sicily	37
Cadlao	Amoco	92	30,000	1981	Philippines	21
Tazerka	Shell	151		1982	Tunis	37
Cyrus*	BP	110	15,000	----	North Sea	35
Hondo	Exxon	260		1981	California	33

Table 2.1a: List of ship based floating production systems.

Notes: * Cyrus field is destined for BP's SWOPS floating production system and is as yet not in production.

Field Name	Operator	Water Depth (m)	Design Capacity (barrels per day)	Date	Location	Ref
Argyll/ Duncan	Hamilton	79	70,000	1975	North Sea	37
Enchova I	Petrobras	172		1977	Brazil	37
Dorada	Eniespa	93		1979	Spain	37
Casablanca	Eniespa	133		1980	Spain	37
Buchan	BP	118	72,000	1981	North Sea	37
Linguado	Petrobras	96		1982	Brazil	37
Bicudo	Petrobras	126		1982	Brazil	37
Bonito	Petrobras	186		1982	Brazil	37
Garouphina	Petrobras	106		1982	Brazil	37
Corvina	Petrobras	220		1983	Brazil	37
Pirauna	Petrobras	230		1983	Brazil	37
Parati	Petrobras	96		1984	Brazil	37
RJS-236	Petrobras	99		1984	Brazil	37
Viola	Petrobras	125		1984	Brazil	37
Innes	Hamilton	80	25,000	1984	North Sea	37
Hutton*	Conoco	148	85,000	1984	North Sea	22
AngulaC	Eniespa	117		1985	Spain	37
Balmoral	Sun Oil	143	65,000	1987	North Sea	37

Table 2.1b: List of semi-submersible based floating production systems.

Notes: * Conoco's Tension Leg Platform is producing from the Hutton field.

Field Location	Environmental Conditions Wave Condition (yrs)	Wave Height (m)	Mean Period (sec)
Gabon	1	3.1	6.0
	10	3.4	6.2
	100	4.6	7.3
Spain	1	5.5	8.3
	10	6.4	9.1
	100	8.5	10.6
North Sea	1	10.2	10.8
	10	12.3	11.9
	100	14.4	12.8

Table 2.2 : Wave height and periods due to different storm conditions in various sea areas. Due to Carlisle et al (21).

Applied Wave Condition	Height (m) Period (sec) Angle (deg)	4.5 7.2 30 s	4.5 7.2 15 s	15 11 15 b
Ship Motion		Response to the above		
Roll	(deg)	0.6	1.5	1.3
Pitch	(deg)	0.6	0.8	4.1
Yaw	(deg)	0.5	0.4	1.0
Surge	(m)	1.2	0.5	5.3
Sway	(m)	1.6	0.6	1.3
Heave	(m)	0.5	0.8	3.5
Vertical Acceleration	(m/s^2)	0.2	0.3	0.8

Table 2.3: Response of the BP SWOPS floating production system to various sea states (23).

Notes: The sea wave applied to the vessel is in relation to its Stern (s) or Bow (b).

Sea State (storm)	Wave Ht (m)	Surge (m)	Heave (m)	Roll (deg)
1yr	12	4.0	0.1	0.05
100yr	30	25.6	4.9	0.6

Table 2.4: TLP response used in a conceptual design study by Hisamatsu (25).

CHAPTER 3

REVIEW OF FLUID BEHAVIOR IN A MOVING VESSEL.

3.1 INTRODUCTION.

In the previous chapter, mention was made of the effect of forcing motion on a closed vessel partially filled with liquid and gas. The resulting wave action, *sloshing*, was seen to have a detrimental effect on offshore separator performance.

To date, fluid sloshing poses many practical problems to the safety of transporting liquid cargos in a variety of containers e.g. Liquified Natural Gas (LNG) tankers, rail and road carriers, liquid storage tanks and spacecraft. The motion of contained fluid under certain conditions can give rise to large impact pressures and significant turning forces which affect the stability of the vessel.

Investigations into the dynamics of partially filled liquid vessels concentrated at first on upright cylinders for application to spacecraft (6), then turned to prismatic containers, relevant to LNG tankers (8). Development of theoretical models followed closely with experimental investigations through application of basic wave theory, mechanical analogies and, more recently, the use of computer based numerical simulations.

This chapter introduces basic principles of fluid sloshing together with definitions used throughout this report. From a literature survey, theoretical aspects of air/water and gas/oil/water sloshing are presented. Also discussed are the effects of baffles to reduce wave motion and scaling laws applied to model experimental studies.

3.2 BASIC PRINCIPLES OF FLUID BEHAVIOUR.

3.2.1 Introduction.

Consider a closed container filled with gas and liquid so that a free surface exits between the two fluids. Suppose the container is moved from one position to another by some external force. Fluid particles will then be displaced from their current equilibrium position. Restoring forces within the fluid (e.g. gravity, surface tension), will then cause these particles to oscillate around a new equilibrium position. The amplitude of these oscillations will eventually die out due to viscous forces. On the free surface these oscillations appear as waves whose amplitude and period, termed the *natural period*, will be shown to depend on the external force and fluid properties. It is these fluid oscillations, in response to an external force that have been termed *fluid sloshing*.

Fluid sloshing can be said to fall into two catagories depending on the forcing motion. Natural oscillations result from a single displacement of the fluid container, with wave motion eventually dying out. Forced oscillations arise if the external force is time varying, either through a random nature as in sea/road transport, or by some periodic nature. The response of the fluid to forced oscillations, will be shown to depend on various factors including the relationship between the period of the forcing motion and the natural period of the fluid system. One important condition is that of *resonance*, when the forcing period equals the natural period of the system. This has some important consequences for the design of partially filled liquid containers (6).

3.2.2 The Effects of Fluid Sloshing.

Although treated in classical theoretical works (5), the practical significance of fluid sloshing has stemmed from the development of space

craft and more recently with the development of large LNG tankers. Some major effects of fluid sloshing can be summarized as :

1) In space craft, sloshing of liquid fuel can generate turning forces which affect the stability and control of the space vehicle (6).

2) In large liquid carriers, such as LNG tankers, impacting waves on the containers walls have lead to structural failure of some containers (8).

3) In relation to oil/water separation equipment on offshore floating production systems, the waves generated in fluid sloshing may lead to mixing of separated oil and water. Waves inside separation vessels can also cause problems with level control equipment (1).

3.2.3 Shape of the Free Surface.

The waves which occur during sloshing have been classified (8) in four ways (figure 3.1):

1) Standing Waves: Liquid particles on free surface appear to move vertically, with no horizontal motion.

2) Traveling Waves: Wave crests move back and forth between container walls. The basic form of this is a solitary wave with a smooth crest and no apparent trough.

3) Standing/Travelling Waves: A combination of the above waves.

4) Hydraulic Jump: A special case of a traveling wave whose front is turbulent. This wave form is similar in shape to waves breaking on a beach.

3.3 DESCRIPTION OF THE FLUID SYSTEM.

Before discussing previous theoretical and experimental work with fluid sloshing, a useful description of a fluid system will now be defined (see figure 3.2) :

1) Single Fluid Sloshing: Previous works (5) have referred to fluid sloshing in terms of a single fluid with a free surface and no account of the upper fluid e.g. air above water.

2) Twin Fluid Sloshing: In this case, the presence of an upper fluid cannot be ignored, as in the case of oil/water systems. From the literature survey, few works were found to deal with such a system.

3) Three Fluid Sloshing: This applies to the case of a gas/oil/water separator where all fluids in the container are accounted for. Here, two fluid interfaces (gas/oil and oil/water) have to be described by theory.

The effect of forcing motion on fluid systems may be gauged by the changes in interface profile i.e. the wave amplitude. It is then useful to define the term *interface amplitude* to be the wave amplitude (i.e. maximum-minimum wave height/2) along a particular interface.

3.4 LIQUID RESPONSE TO AN EXTERNAL FORCING MOTION.

3.4.1 Introduction.

The effects of forcing motion on a vessel can be divided into two cases, air/water and oil/water. Many papers deal with single fluid (air/water) sloshing but only a few with oil/water.

3.4.2 Experimental Results with Air/Water Sloshing.

Experiments into the effects of forcing frequency on free surface response (8,38,39) all indicate a basic characteristic that as the forcing frequency approaches the *resonant (natural)* frequency, interface amplitude rapidly increases to a high, finite value. This is the *fundamental (first) sloshing mode.* Additional *resonant sloshing modes* occur at shorter frequencies, where interface amplitude will again rise, but to a value lower than that at resonance. Such experiments have also indicated a hysteresis effect where interface amplitude response depends on how resonance is approached i.e. from shorter or longer forcing periods. Figure 3.3 provides a basic view of these features.

The shape of waves which develop on the air/water interface were found to depend on forcing conditions and additional factors including, water fill depth and location of pitch/roll axis (40).

3.4.3 Experimental Results from Oil/Water Sloshing.

Experimental investigations by Thorpe (41) and Handa & Tayima (42), revealed that the basic characteristics of two fluid sloshing are the same as those of a single fluid i.e. maximum interface disturbance occurs at resonance. One major difference between in the two fluid case is that, interfacial vortices may be formed, leading to fluid mixing (43)

Photographs by Handa & Tayima (reproduced in figure 3.4) indicate that a stream function can be defined that continues across the oil/water interface. The authors also presented photographs which showed that whilst the upper (air/oil) interface may be flat and free from waves, large amplitude waves may form on the lower (oil/water) interface.

3.5 THEORETICAL ASPECTS OF SINGLE FLUID SLOSHING.

3.5.1 Foundation of Theory.

The basic equations describing fluid sloshing derive from the both the continuity and Navier-Stokes equations, solved with appropriate boundary conditions. As full solution methods for the Navier-Stokes equations are not as yet possible, simplifications have been made. Several methods have then been proposed, the velocity potential method, a mechanical analogy and a numerical solution.

3.5.2 Principle of the Velocity Potential Theory.

Assuming the fluid motion is irrotational and incompressible, a velocity potential function can be defined which satisfies Laplaces equation :

$$\frac{\partial^2\phi}{\partial x^2} + \frac{\partial^2\phi}{\partial y^2} = 0 \qquad \forall\ x,y,t \quad \ldots\ 3.1$$

Further, assuming that viscosity and surface tension can be neglected, the Navier-Stokes equation can be reduced to a form of Eulers equation (44) :

$$\frac{\partial\phi}{\partial t} + \frac{(u^2+v^2)}{2} + \frac{P}{\rho} - \Omega = f(t) \qquad \forall\ x,y,t \quad \ldots\ 3.2$$

Where the term Ω represents external *body forces* acting on the fluid (e.g. gravity).

This reduces the sloshing problem to that based on shallow wave theory where fluid acceleration terms are accounted for (45).

Equation 3.1 can be solved applying three principle boundary conditions (46) :

1) The Dynamic Boundary Condition : The reduced Navier-Stokes equation can be considered a form of boundary condition at the free surface i.e. at $y=h+\eta$:

$$g\eta + \frac{\partial\phi}{\partial t} + \frac{1}{2}\left[\left[\frac{\partial\phi}{\partial x}\right]^2 + \left[\frac{\partial\phi}{\partial y}\right]^2\right] = 0 \qquad \forall\, x,t \qquad \ldots\ 3.3$$

The differences between equation 3.2 and 3.3 are :

a) Inclusion of a gravity force term ($g\eta$): This could incorporate a time varying force.

b) The absence of a pressure term: Since the presence of any upper fluid is neglected in this theory, the pressure anywhere along the free surface can be arbitrarily set to zero.

c) The absence of the general time function f(t): It usual when dealing with a velocity potential (ϕ) function to incorporate such terms within ϕ itself (44).

A description of the transformation process from the full Navier-Stokes equation to equation 3.3 is presented in Chapter 4.

2) The Kinematic Boundary Condition : The continuity of the free surface is governed by this boundary condition, given as:

$$\frac{\partial\eta}{\partial t} + \frac{\partial\phi}{\partial y} + \frac{\partial\phi\partial\eta}{\partial x\partial x} = 0 \qquad \ldots\ 3.3$$

3) Wall Boundary Conditions : The wall conditions refer to fluid-vessel interaction, and are time dependant e.g. the no slip boundary condition on a moving vessel wall. It is through this boundary condition that the effect of an external force may be introduced.

As the boundary conditions are time varying (i.e. the container is moving in relation to a fixed frame of reference), solution of the velocity potential equation is difficult. Simplifications have been made

to allow solutions of varying complexity ranging from simple linear to non-linear theories.

3.5.3 Simple Linear Solution to Velocity Potential Theory.

Assuming that fluid accelerations can be neglected, equation 3.2 can be reduced to a simple form which allows solution of Laplaces equation, by a separation of variables technique.

Bauer (47) presented worked examples for free and forced horizontal oscillations of a single fluid in a rectangular vessel. The equation for the velocity potential and free surface amplitude under forced oscillations were given as :

$$\phi(x,y,t) = x_o \Omega \mathrm{Sin}(\Omega t)\left[\frac{a}{2} + \frac{4a}{\pi^2}\sum_{n=1}^{\infty}\frac{\gamma_{2n-1}^2}{(1-\gamma_{2n-1}^2)}\frac{\mathrm{Cosh}\left[\frac{(2n-1)\pi}{a}(z+h)\right]\mathrm{Cos}\left[\frac{(2n-1)\pi x}{a}\right]}{(2n-1)^2\mathrm{Cosh}\left[\frac{(2n-1)\pi h}{a}\right]}\right] \quad \ldots 3.4a$$

for the velocity potential, and for the free surface profile :

$$z(x,t) = \frac{\Omega^2}{g} x_o \mathrm{Cos}(\Omega t)\left[(x - \frac{a}{2}) - \frac{4a}{\pi^2}\sum_{n=1}^{\infty}\frac{\mathrm{Cos}\left[\frac{(2n-1)\pi x}{a}\right]}{(1-\gamma_{2n-1}^2)}\frac{\gamma_{2n-1}^2}{(2n-1)^2}\right] \quad \ldots 3.4b$$

where :

$$\gamma_{2n-1} = \frac{\Omega}{\omega_{2n-1}} = \text{ratio of forcing to natural frequency.}$$

$$\omega_{2n-1}^2 = \omega_{2n-1}^2 = \frac{g(2n-1)\pi}{a}\mathrm{Tanh}\left[\frac{(2n-1)\pi h}{a}\right] \quad \ldots 3.4c$$

Ω = frequency of forcing motion

$2\pi/\omega_{2n-1}$ = natural period of mode n, n=1,2,3...

other terms are defined in figure 3.5.

Binnie (48) presented an analysis of a rectangular vessel undergoing pitch motion, a displacement given by :

$$\theta = \theta_o \mathrm{Sin}(\Omega t)$$

The elevation of the free surface at motion extremes, was derived as :

$$\eta = \frac{-\Omega^2 \theta_o a}{g}\left[-H + \frac{8}{\pi^2}\sum_{n=0}^{\infty}\frac{g-\Omega H^2-2g\,\mathrm{Sech}\left[\frac{(2n+1)\pi h}{2a}\right]}{(\omega_{2n+1}^2 - \Omega^2)(2n+1)^2}\right] \quad \ldots 3.5$$

Graham & Rodriguez (10,49) presented three sets of equations relating to pitch, horizontal sway and yaw motion for a rectangular vessel :

1) Horizontal Sway Motion Parallel to the x-Axis.

Applied motion : $X(t) = A\mathrm{Sin}(\Omega t)$

Free surface profile :

$$\eta(x,t) = \frac{A\Omega^2}{g}\mathrm{Sin}(\Omega t)\left[x + \sum_{n=0}^{\infty}\frac{4a(-1)^n}{\pi^2(2n+1)^2}\left[\frac{\Omega^2}{\omega_n^2 - \Omega^2}\right]\mathrm{Sin}\left[\frac{(2n+1)\pi x}{a}\right]\right] \quad \ldots 3.6a$$

2) Sinusoidal Pitching about the y-Axis.

Applied Motion : $\theta(t) = B\mathrm{Sin}(\Omega t)$

Free Surface Profile :

$$\eta(x,t) = \frac{B\Omega^2}{g}\mathrm{Sin}(\Omega t)\left[\sum_{n=0}^{\infty}\frac{4a(-1)^n}{\pi^2(2n+1)^2}\left[\frac{h}{2} - \frac{2a\,\mathrm{Tanh}\left[\frac{(2n-1)\pi h}{2a}\right]}{(2n-1)\pi} + \frac{g}{\omega_n^2}\right]\frac{\omega_n^2}{(\omega_n^2 - \Omega^2)}\mathrm{Sin}\left[\frac{(2n-1)\pi x}{a}\right]\right] \quad \ldots 3.6b$$

In both equations, ω_n is the *nth odd harmonic of the fundamental mode of oscillation in the stationary vessel*, given by :

$$\omega_n^2 = g(2n+1)\frac{\pi}{a}\text{Tanh}[(2n+1)\pi\frac{h}{a}] \quad n=0,1,2,3... \qquad ... 3.6c$$

where a = length of the vessel

h = liquid fill depth

x = distance from the centre of the vessel i.e. walls are at $\pm a/2$

Ω = the forcing frequency

Note that equations 3.4c and 3.6c are essentially the same apart from the expression in "n". Differences are due to authors preference in starting the series expansions from n=0 or n=1.

Equations 3.4b and 3.6a appear to be similar apart from differences in the applied forcing functions.

Note that all solutions produce a series summation equation involving several frequency modes. The condition of resonance is given when $\Omega = \omega_{(i=1)}$, that is when the forcing period equals the natural period of the lowest mode. At this point, the amplitude of the free surface approaches an infinite value. Therefore, linear theory breaks down near resonance as experimentally, interface amplitude reaches a finite value.

To demonstrate the differences between rectangular and cylindrical geometry, the prediction of natural frequency in a upright cylindrical vessel is given as (7) :

$$\omega_{mn}^2 = \left[\left[\frac{2\epsilon_{mn}^2}{d}\right]\frac{\gamma}{\rho} + \frac{2\epsilon_{mn}g}{d}\right]\text{Tanh}\left[\frac{2\epsilon_{mn}h}{l}\right] \qquad ... 3.7$$

where ω_{mn} = natural frequency of mode mn

d = tank diameter

h = liquid depth

γ = liquid surface tension

ρ = liquid density

ε_{mn} = roots of $J_m'(\varepsilon_{mn}) = 0$

J_m = Bessel function of the first kind, m^{th} order.

In the absence of surface tension ($\gamma=0$), equations 3.7 and 3.4c are similar except for the term ε_{mn} which is due to cylindrical co-ordinates.

3.5.4 Non-linear Analytical Velocity Potential Theory.

The non-linear velocity potential solution method attempts to retain the fluid acceleration terms neglected in equation 3.2. To do this, previous workers have used series expansion methods applied to both the free surface and the velocity potential.

Skalak & Yarymovych (50) dealt with vertical oscillations of a rectangular vessel, presenting series forms of both the velocity potential and free surface amplitude :

$$\phi = \sum_{n=0}^{\infty} \alpha_n e^n \mathrm{Cos}(nx) \quad \text{and} \quad \eta = \frac{1}{2} a_o + \sum_{n=0}^{\infty} a_n \mathrm{Cos}(nx) \qquad \ldots 3.8a/b$$

Where α_n and a_n are both unknown functions of time.

Results of this work indicated the presence of half sub-harmonic waves i.e. the surface wave frequency is half that of the excitation frequency.

In a similar manner, Chu (51) applied a perturbation method (series expansion) to an arbitrary shaped vessel using :

$$\phi = \varepsilon \sum_{n=0}^{\infty} \phi_n \varepsilon^n \quad \text{and} \quad \eta = \varepsilon \sum_{n=0}^{\infty} \alpha_n \varepsilon^n \qquad \ldots 3.9a/b$$

Where ε was defined in terms of the amplitude of the tank base.

As the author states, this type of analysis although in agreement with previous theory and experiments, is limited in application due to the complex method of solution.

Faltinsen (46) developed a non-linear theory applied to a rectangular vessel undergoing small amplitude harmonic sway oscillations. In this case :

$$\phi = \sum_{n=1}^{\infty} \phi_n \varepsilon^{n/3} \quad \text{and} \quad \eta = \sum_{n=1}^{\infty} \eta_n \varepsilon^{n/3} \qquad \ldots 3.10$$

Where ε is the ratio of excitation amplitude to tank dimension.

To introduce forcing, the velocity potential was modified such that :

$$\phi_T = \phi + \phi_c, \ \phi_c = 2a\omega\varepsilon x \cos(\omega t) \qquad \ldots 3.11$$

Solutions were presented for forced sway and roll to third order i.e. expanding the summation series to three terms. The theory was compared to unpublished data on a rectangular container of dimensions 1m by 1m by 0.1m.

Apart from amplitude expansion terms, time series expansions have been carried out by Chwang & Wang (52), applied to impulsive forcing of a rectangular and upright cylindrical vessel :

$$\phi(x,z,t) = \sum_{n=1}^{\infty} t^n \phi_n(x,z) \text{ and } \eta(x,t) = \sum_{n=1}^{\infty} t^n \eta_n(x) \qquad \ldots 3.12$$

By this analysis, the authors found that a circular vessel has more influence on internal fluid motion than a rectangular one.

Sakata et al (53), studied the response of liquid in a cylindrical vessel when subject to external forcing by earthquakes. Again, this force was impulsive and consequently the resulting equations were derived with a varying time function :

$$\phi = \sum_{m=0}^{\infty} \sum_{n=1}^{\infty} \left[A_{mn}(t)\mathrm{Cos}(n\theta) + B_{mn}(t)\mathrm{Sin}(m\theta) \right]$$

$$\times J_m(\lambda_{mn} r) \frac{\mathrm{Cosh}[\lambda_{mn}(z+h)]}{\mathrm{Cosh}(\lambda_{mn} h)} \qquad \ldots 3.13$$

J_m is the Bessel function of the first kind, mth order.

3.5.5 Non-linear Alternative Analytic Theory.

Describing resonant or near resonant sloshing effects by velocity potential method has proved difficult and complex. To study near resonant sloshing, several workers have adopted different approaches. Verhagen & Wijngaarden (54) and Chester (55) applied theory based upon shock waves in gas dynamics to describe fluid sloshing in rectangular containers. Here, equations were derived giving actual velocity components as functions of forcing conditions.

Following previous analytical work (46), Faltinsen (56) presented a numerical method based on the distribution of *sources and sinks* along the boundary walls of a rectangular vessel. This analysis allowed the introduction of artificial damping terms, akin to a viscosity, to account for non-linear effects. Results from numerical analysis were compared to those by linear theory, comparisons with experimental data were not presented.

3.5.6 Mechanical Analogies.

In section 3.2, the generation of free surface waves were described as originating from fluid oscillations around an equilibrium state. This is then similar to those oscillations produced when a single mass attached to the end of a spring is displaced then released. Mechanical analogies have therefore been proposed where the fluid system is replaced by a

number of masses fixed to springs (figure 3.6) (10). The configuration of masses are determined by the number of frequency modes.

Vandiver & Mitome (57), applied this technique to demonstrated the action of a storage tank on damping the motion of offshore platforms. Karve & Fenner (12) found that a single fixed mass and one spring-mass component, could be used to describe the response of a gas/oil interface in offshore separators. The data was then used to determine the response of tne oil/water interface.

3.5.7 Numerical Techniques.

Solving the full Navier-Stokes equations for fluid sloshing by analytical means has at this time proved very difficult. Consequently, no exact solutions exist. Numerical methods solving either velocity potential equations or the full Navier Stokes equations have proved useful in situations without a free surface (58).

The particular problem with fluid sloshing is to deal with the free surface. The Marker & Cell (MAC) technique developed by Harlow & Welch (16) is a *finite difference* numerical technique that can deal with a free surface. The original free surface boundary conditions were later improved (59). Feng (13) applied the MAC method to study the dynamic loads caused by sloshing of liquid in propellant tanks, associated with the space shuttle. Here, two and three dimensional codes were developed for rigid rectangular boundaries, curved surfaces were approximated.

Although the usual MAC method employs a finite difference mesh calculation, Liu & Ma (60) used a *finite element* technique to look at earthquake effects on nuclear reactors. The equations to solve, were derived with a view to study the effects of a flexible container wall on fluid response. Results indicated that due to the flexible wall, the free

surface profile is not a simple function of time oscillating at only one frequency, but a number of different frequencies.

To determine the location of the free surface, the original MAC method used marker particles. Free surface boundary conditions could then be applied once the free surface location was known. Nichols et al (17) proposed a new method based on a volume of fluid technique (SOLA-VOF) to track the free surface. Bridges (14) applied SOLA-VOF to solve large amplitude gas/liquid sloshing in rectangular containers.

Although individual companies will inevitably adopt their own design methods to evaluating slosh loads, Mikelis et al (3) described the development of a numerical model for use by Lloyds Register of Shipping to evaluate slosh imposed loads on cargo tanks. Previously, Lloyds applied the non-linear theory due to Verhagen & Wijngaarden (54) for shallow liquid fill depths (fill depth to length ratio, $h/l<0.21$) and a linear theory for high fill depths ($h/l>0.21$). According to the authors, SOLA-VOF was stable for approximately two forcing oscillations, therefore the method due to Navickas (61) (SOLA-SURF) was adopted as the solution program. Comparison tests were carried out on experimental data and showed good agreement.

3.6 THEORETICAL ASPECTS OF MULTIFLUID SLOSHING.

3.6.1 Introduction.

Published work regarding theoretical and practical aspects of multifluid (e.g. air/oil/water) sloshing, appears to be limited. Using the velocity potential method has resulted in simple linear solutions for natural period and interface amplitude applied to both air/oil and oil/water interfaces (42). Other authors have concentrated on both mechanical analogies and non-linear theory (62,63).

3.6.2 Linear Velocity Potential Theory for Multifluid Sloshing.

Unlike single fluid theory, the assumption that above the fluid/fluid interface the pressure can be set to zero, becomes no longer valid (section 3.5). To derive the dynamic *free surface* boundary condition the pressure on that interface must be determined. It is then assumed that the pressure just above and below the interface is equal. The linear form of equation 3.2 (i.e. neglecting fluid acceleration terms) can then be applied to each fluid so that on the interface (11) :

$$\rho_1\left[\frac{\partial^2\phi_1}{\partial t^2} + g\frac{\partial\phi_1}{\partial z}\right] = \rho_2\left[\frac{\partial^2\phi_2}{\partial t^2} + g\frac{\partial\phi_2}{\partial z}\right] \qquad \ldots 3.14$$

Where subscripts 1 & 2 refer to lower and upper fluids respectively.

The case of a rectangular container filled with two liquids, with the upper liquid having a free surface (i.e. a gas/liquid interface), was treated by Handa & Tayima (42). Solutions from simple linear theory were presented for the amplitude of the oil/water and air/oil interfaces under the influence of a sway oscillation :

$$\eta_1 = -\frac{1}{g(1-\mu)}\left[\frac{\partial\phi_1}{\partial t} - \mu\frac{\partial\phi_2}{\partial t}\right]$$

$$= -\frac{1}{g(1-\mu)}X_o\omega^2 j e^{j\omega t}\left[(1-\mu)x + \sum_{n=1}^{\infty} S_{1n}\sin(\beta_n x)\right] \qquad \ldots 3.15a$$

$$\eta_2 = -\frac{1}{g}\frac{\partial\phi_2}{\partial t} = -\frac{1}{g}X_o\omega^2 j e^{j\omega t}\left[x + \sum_{n=1}^{\infty} S_{2n}\sin(\beta_n x)\right] \qquad \ldots 3.15b$$

Where :

$$S_{1n} = L_n\cosh(\beta_n 1) - \mu N_n$$

$$S_{2n} = N_n\cosh(\beta_n h) + L_n\sinh(\beta_n 1)\sinh(\beta_n h)$$

$$\beta_n = \frac{(2n-1)\pi}{2a}$$

μ = ratio of fluid densities

h and l relate to the depth of each fluid in the container.

L_n and N_n are complex relations involving ω, μ and are not included here for clarity.

The period of interfacial waves was determined from the roots of the expression :

$$\omega^4[\text{Cosh}(\beta_n l)\text{Cosh}(\beta_n h)+\mu\text{Sinh}(\beta_n l)\text{Sinh}(\beta_n h)] - \omega^2 g\beta_n \text{Sinh}(\beta_n(l+h))$$

$$+ (1-\mu)(g\beta_n)^2\text{Sinh}(\beta_n l)\text{Sinh}(\beta_n h) = 0 \qquad \ldots 3.16$$

As this paper was obtained in Japanese and no translation was available, the exact interpretation of equations 3.15 and 3.16 was therefore difficult. However, equation 3.16 results in two roots, one for the upper (gas/oil) interface and one for the lower (oil/water) interface.

Bauer (62) presented a similar expression for the natural period of waves in a two and three fluid system, but included the effect of surface tension. The natural period expression for the two fluid system was given as :

$$\omega_n^2 = \left[\frac{(1 - \rho_1/\rho_2)(n\pi g/a) + (\sigma_{12}/\rho_{12}a^3)n^3\pi^3}{1 + \dfrac{(\rho_1/\rho_2)\text{Tanh}(n\pi h_2/a)}{\text{Tanh}(n\pi h_1/a)}}\right] x\ \text{Tanh}(n\pi h_2/a)$$

$\ldots 3.17a$

When the upper fluid has a free surface (i.e. a gas cap), Bauer derived an expression of the form :

$$\omega_n^2 = [\alpha \pm \sqrt{(\alpha_n^2 - \beta_n)}]/\gamma_n \qquad \ldots 3.17b$$

Where α, β, γ are terms involving density (ρ_1, ρ_2), interfacial tension (σ_{12}) and fill depth (h_i), and are not presented here.

In the case of an upright cylinder, Haroun & Chang (11) derived a similar expression to equation 3.17a as :

$$\omega_n^2 = \frac{g\varepsilon_n(\rho_1 - \rho_2)}{R\left[\rho_1 \text{Coth}(\frac{\varepsilon_1 h_1}{R}) + \rho_2 \text{Coth}(\frac{\varepsilon_1 h_2}{R})\right]} \quad \ldots 3.18$$

In this case the term ε_n arises due to the use of cylindrical co-ordinates.

Development of equations to predict natural periods for two and three fluid systems are presented in Appendix I.

3.6.3 Non-linear Velocity Potential Theory for Multifluid Sloshing.

Apart from the mechanical analogy models due to Haroun & Chang (42) and Bauer (62), Manna (63) proposed a full analytical theory for forced waves at a fluid interface based upon a generalized Fourier transform method. In this case, initial wave motion was introduced by a time varying pressure distribution applied to the interface. As with the majority of non-linear single fluid theories, the effort involved in producing a result was substantial. Manna states that his work indicates that surface waves (i.e. interfacial waves) consist of two distinct parts, one due to the single fluid/homogenous case with modified amplitude and a part which deals with stratification.

3.7 THE USE OF BAFFLES TO REDUCE THE EFFECTS OF SLOSHING.

3.7.1 Introduction.

The forcing period which result in the *worst case* fluid sloshing, that is resonance, can be predicted from simple linear theory. Consider the example of a LNG tanker. If the expected sea conditions result in the period of ships motion to be close to the natural period of one cargo tank, then damage to that cargo tank may occur. If the cargo tank were partitioned, then the natural period as predicted by equation 3.4c, of the

liquid, would be shifted towards lower values (64). Hopefully, these would be beyond the range of ship motion periods.

While solid partitions, *baffles*, may be acceptable in some cases, perforated baffles have been used (12) where weight has been important. Not only do baffles alter natural periods, they also aid the decay of waves once forcing motion has ceased (65) i.e. baffles are said to increase *damping* in the fluid system.

3.7.2 Description of Damping.

The degree of damping in a baffled or unbaffled vessel, is usually expressed in terms of a logarithmic decrement, defined as (65) :

$$\delta = \text{Ln}\left[\frac{\text{Peak Wave Amplitude at one cycle}}{\text{Peak Wave Amplitude one cycle later}}\right] \qquad \ldots 3.20$$

(see figure 3.7)

A damping factor can then be defined as $\gamma = \delta/2\pi$.

To measure damping, the wave profile must be recorded once forcing motion has ceased.

3.7.3 Damping in a Unbaffled Vessel.

Keulegan (66) presented a theoretical and experimental study of damping in rectangular vessels. The results suggest that damping may be divided into effects due to viscosity and surface tension. The results may be summarized as :

1) Damping increases with increasing fluid viscosity and decreasing vessel size.

2) Contributions to damping by surface tension, became negligeable for vessel widths larger than 200mm.

Keulegan defined a modulus of decay as:

$$\alpha = \frac{T}{t_r} \text{Ln}\left[\frac{a_o}{a_r}\right] = \delta \frac{T}{t_r} \qquad \ldots 3.21$$

Damping due to viscous and surface tension were given by $\alpha = \alpha_1 + \alpha_2$, where :

$$\alpha_1 = f(\upsilon^{1/2} T^{1/2}/B) \text{ and } \alpha_2 = g(\sigma T^2/\rho B^3)$$

The viscous term (α_1) was derived from second order wave theory in terms of contributions to damping from boundary walls and internal bulk fluid, as :

$$\alpha_1 = \frac{\pi^{-1/2} x \nu^{1/2} T^{1/2}}{B} + 2k^2 \nu T \qquad \ldots 3.22$$

Where :

$$x = (\pi + Bk) + \frac{Bk(\pi + 2kH)}{\text{Sinh}(2kH)} \quad \text{and } k = \pi/L$$

T = The natural period i.e. the period of the decaying wave.

H = The liquid fill depth

B,L = Vessel width/breadth and length

ν = Kinematic viscosity

The first term in equation 3.22 represents viscous damping on the vessel walls, the second term represents viscous damping in the bulk fluid.

For α_2, Keulegan's experiments provided an empirical relation as :

$$\alpha_2 = 0.1 \frac{\sigma T^2}{\rho B^3}$$

Where σ = surface tension coefficient of liquid in contact with air

ρ = liquid density

In a study of damping in upright cylinders, Case & Parkinson (67) found that wall surface roughness may introduce an additional factor of 2 to 4 in logarithmic decrement.

In the case of upright cylinders, a correlation was found to predict logarithmic decrement (68) :

$$\delta = 4.98\nu^{1/2}R^{-3/4}g^{-1/4}\left[1+\frac{0.318}{\mathrm{Sinh}[\frac{1.84h}{R}]}\left[\frac{1-h/R}{\mathrm{Cosh}[\frac{1.84h}{R}]}+1\right]\right] \quad \ldots 3.23$$

Where ν = kinematic viscosity

R = radius of container

h = liquid fill depth from base

3.7.4 Damping due to Baffles.

The use of baffles to reduce wave motion has resulted in many different designs, from annular rings in space rockets (64,68,69) to perforated plates in offshore separators (12). As yet, no adequate theory is available to describe the effects of baffles on either damping of wave motion or on natural period. Attempts to predict natural periods in the presence of baffles, have resulted in complex relations (70,71).

The general effects of baffles can be summarized as (68) :

1) A significant weight saving can be achieved without the loss in damping or shift in natural period through the use of perforated baffles. However, increasing hole size may reduce baffle performance in reducing sloshing effects.

2) Damping, from any source including baffles, may be represented by an equivalent viscous damping.

3) The effectiveness of baffles depends both on design and location within the fluid.

4) For oil/water separation equipment, baffles may increase oil/water turbulence (12).

3.8 SCALING CONSIDERATIONS.

3.8.1 Introduction.

In the absence of precise theory, either analytic or via numerical model, laboratory experiments must be carried out to test a new vessel, e.g. a oil/water separator or LNG cargo tank. The use of laboratory models requires scaling of both fluid properties and forcing motions from the full scale vessel. Dimensional analysis has been used (72,73) to scale impact pressures in LNG tankers.

3.8.2 Dimensional Analysis.

Abramson (72) presented a dimensional analysis method to evaluate liquid impact pressures in space rockets as :

$$\frac{P}{ad\rho_l} = \phi\left[\frac{\sigma_l \rho_l d}{\mu_m^2}, \frac{\rho_l}{\mu_l}\left[ad^3\right]^{\frac{1}{2}}, t\left[\frac{a}{d}\right]^{\frac{1}{2}}, \frac{\mu_g \rho_g}{\mu_l \rho_l}\right] \qquad \ldots 3.24$$

where a = acceleration

d = diameter or length of vessel

t = time

ρ = density

μ = coefficient of viscosity

σ = surface tension

P = Pressure

For pressure loads in LNG tankers Abramson et al (2), presented a dimensional analysis as :

$$\frac{P}{\rho(L/T)^2} = F\left[Fr, Re, Wb, Ca, Cv, geometry\right] \qquad \ldots 3.25$$

Where : Re = Reynolds Number : $\rho L(L/T)/\mu$

Fr = Froude " : $g/(\rho(L/T)^2)$

Wb = Weber " : $\rho L(L/T)^2/\sigma$

Ca = Cauchy " : $\rho(L/T)^2/E_L$

Cv = Cavitation " : $\Delta P/(\rho(L/T)^2)$

Geometry numbers include X_o/L and h/L

L = Vessel length or principle dimension

h = liquid fill depth

T = Forcing period

X_o = Forcing amplitude

ρ = liquid density

μ = liquid viscosity

σ = surface tension

E_L = Bulk modulus

In application of equation 3.25, the authors consider that surface tension, wall elasticity can be neglected.

3.8.3 Froude Scaling.

In a survey of LNG slosh related experiments, Bass et al (73) state that Froude and Euler scaling may be appropriate. If λ is the ratio of model (L_m) to full prototype (L_p) size, then Froude scaling laws become :

Velocity $V_m = V_p\lambda^{1/2}$

Time $T_m = T_p\lambda^{1/2}$

Acceleration $A_m = A_p$

The work concluded :

1) Froude scaling is required to scale gross wave action.

2) Viscosity and surface tension are of secondary importance.

3) Model experiments involving compressible effects can be simplified through the use of Froude scaling. Although such experiments may result in conservative estimates of slosh induced loads.

Froude scaling suggests that acceleration between model and prototype must be the same. Motion conditions can then be scaled using this law.

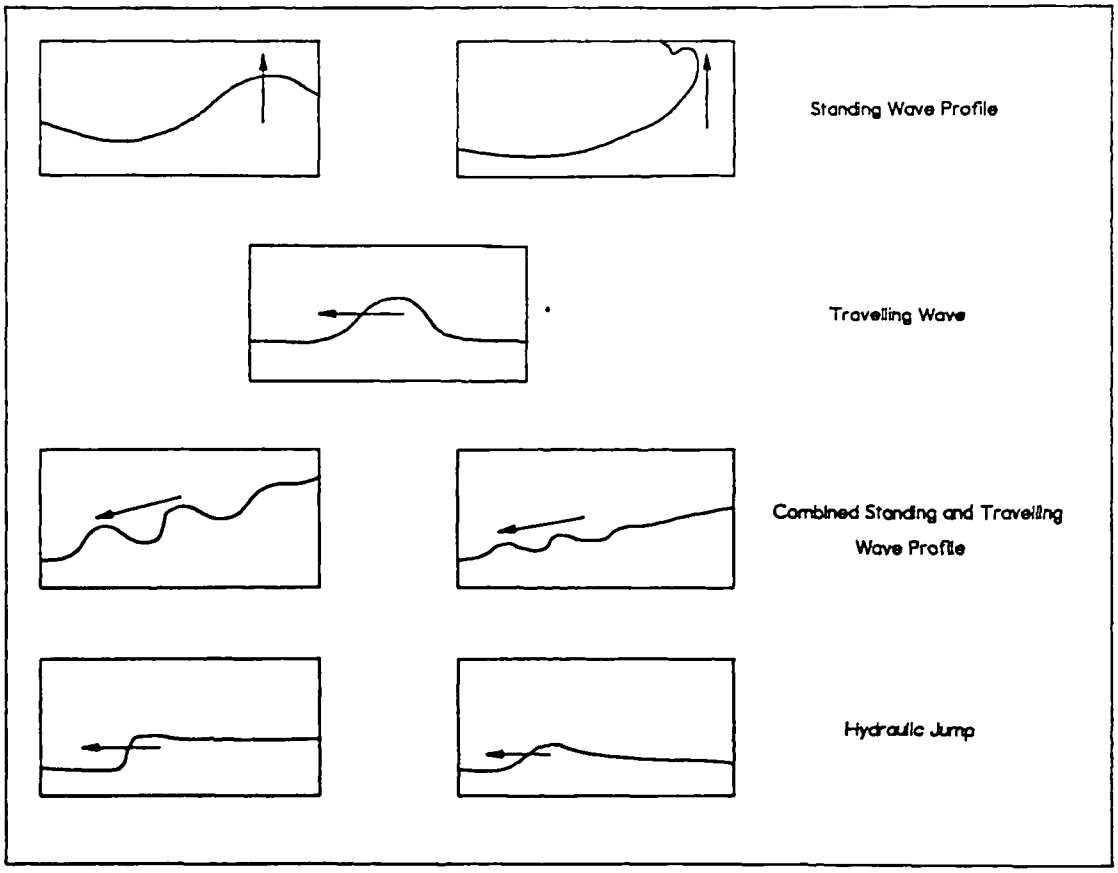

Figure 3.1: Description of free surface wave forms that occur in sloshing, due to Olsen (8).

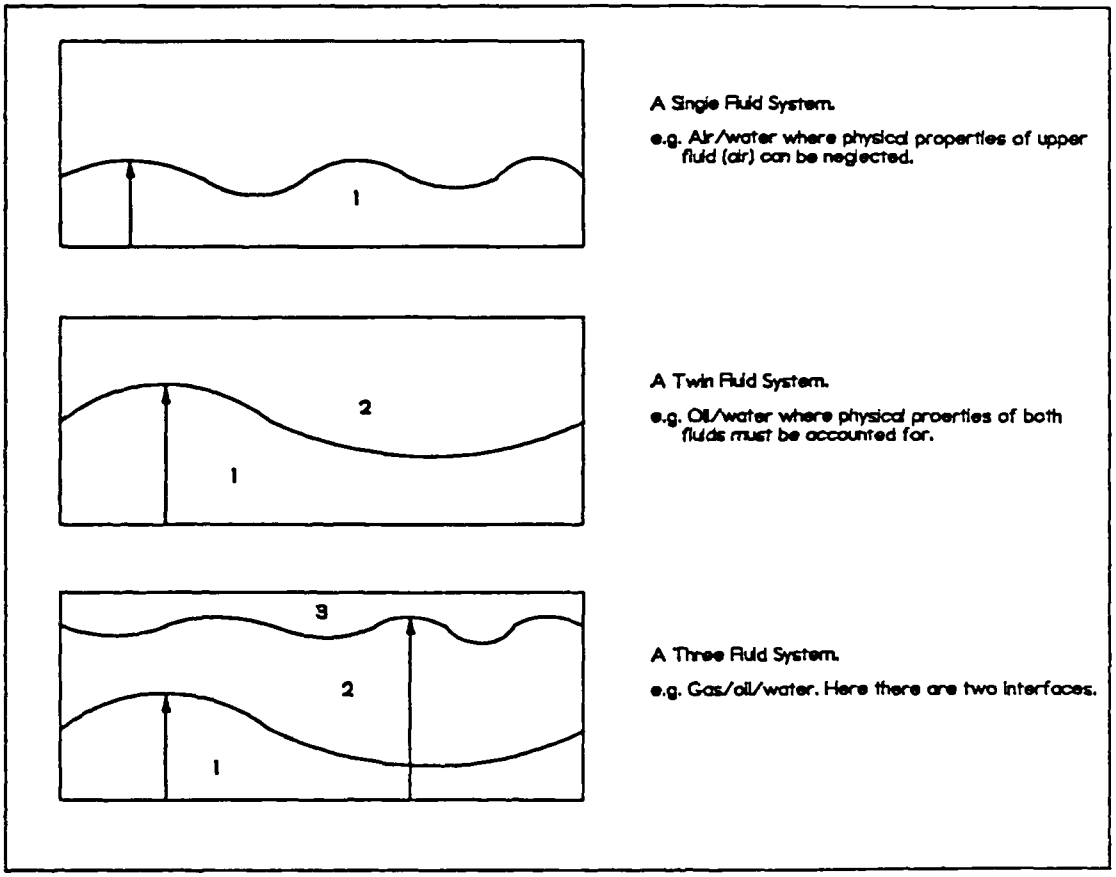

Figure 3.2: Description of a single, twin and three fluid system.

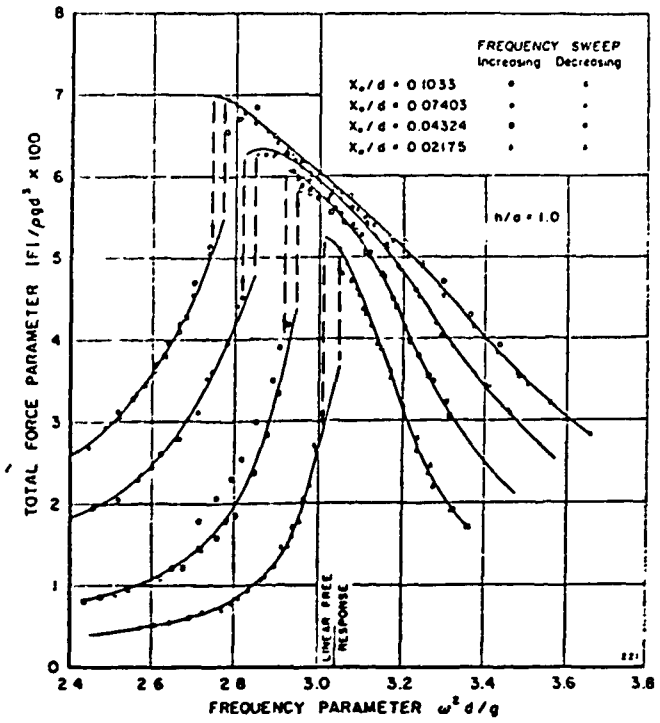

Figure 3.3: Effect of forcing frequency on free surface response. Results from experiments by Abramson (38).

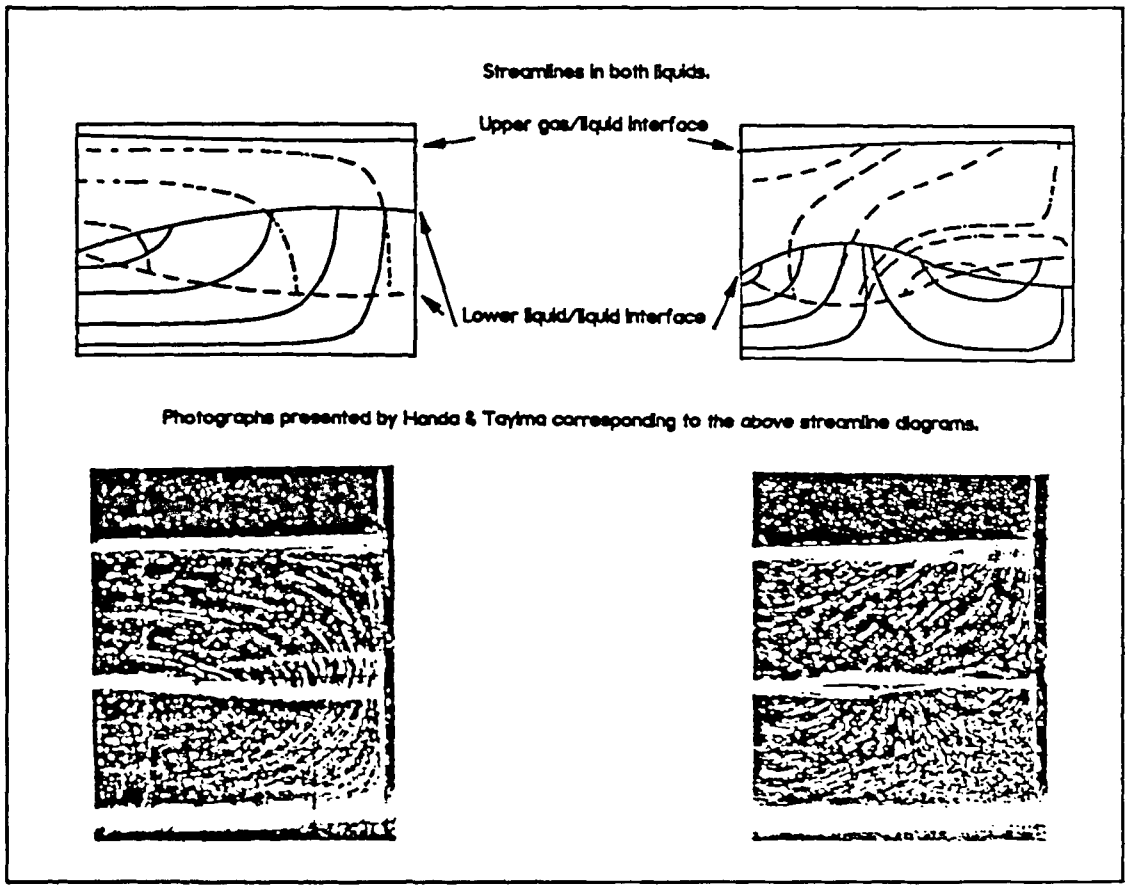

Figure 3.4: Streamlines as observed by Handa & Tayima in oil/water sloshing experiments (42).

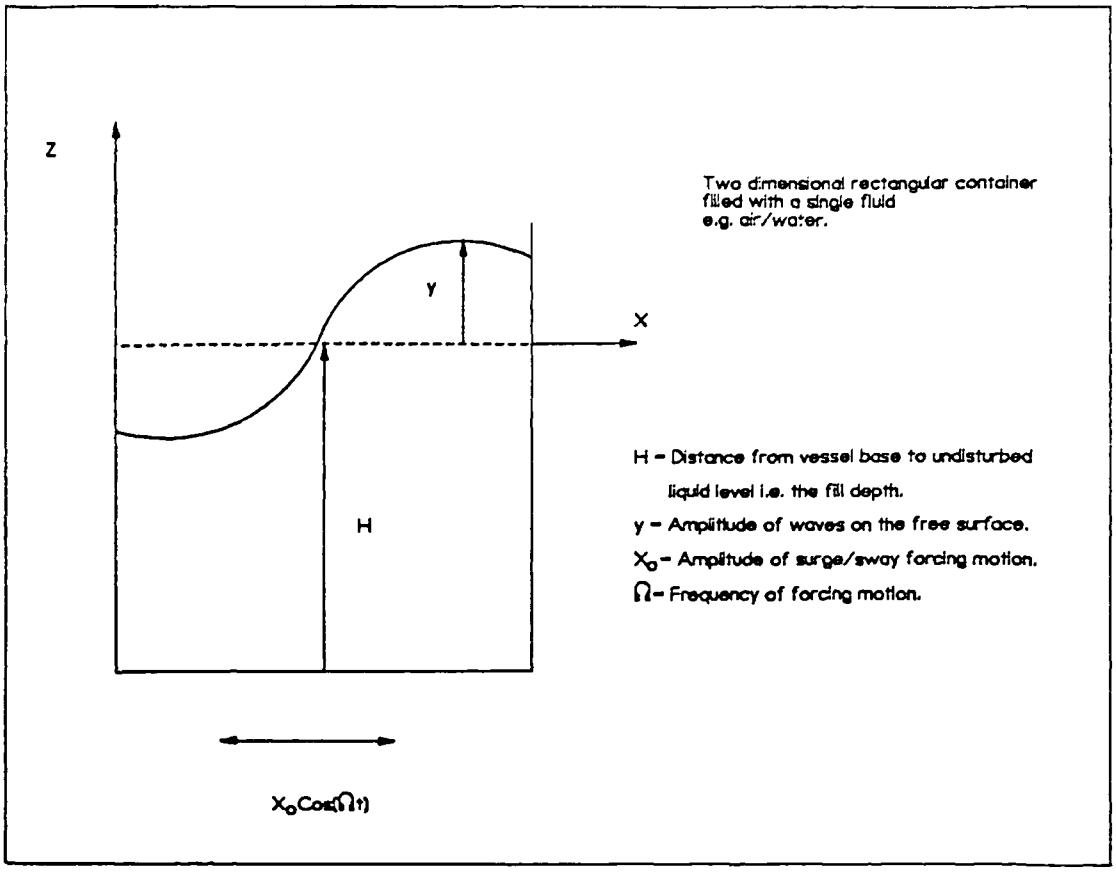

Figure 3.5: Description of a rectangular vessel used by Bauer (47) in a linear solution of sloshing.

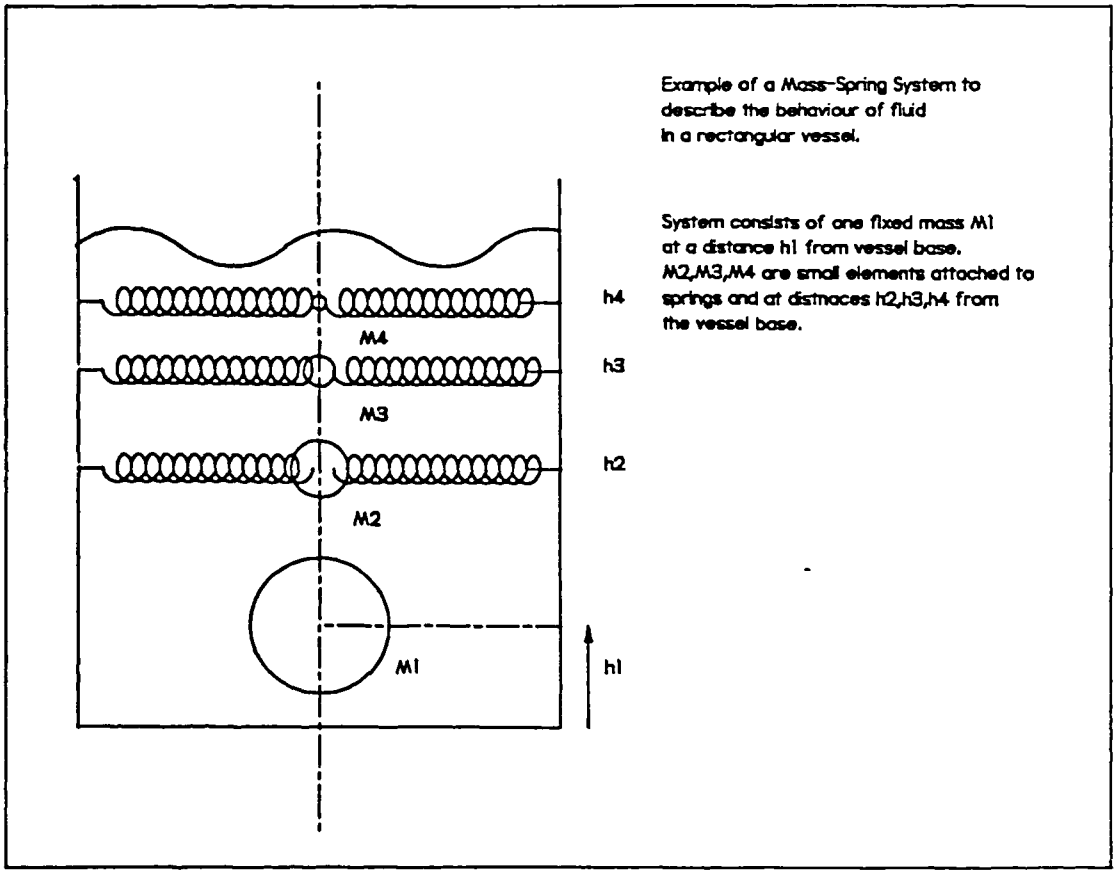

Figure 3.6: Description of a mechanical mass-spring system to model fluid sloshing (10).

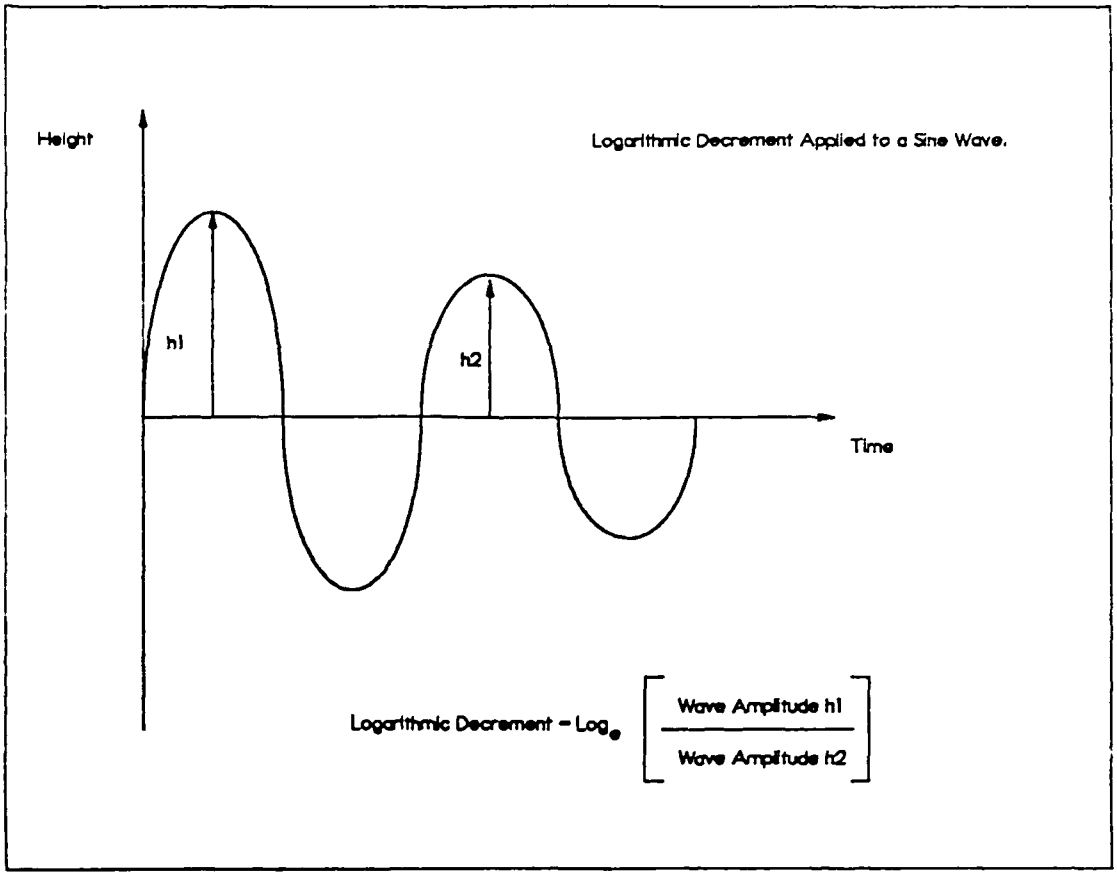

Figure 3.7: Description of logarithmic decrement as determined from wave height data (65).

CHAPTER 4

DEVELOPED LINEAR THEORY AND SOLUTION OF THE NON-LINEAR SLOSHING PROBLEM BY NUMERICAL SIMULATION.

4.1 INTRODUCTION.

The mathematical theory behind fluid sloshing derives from solutions of the Navier-Stokes equations together with the appropriate boundary conditions. The non-linear nature of the basic sloshing equations gives rise to solution instability and problem complexity. As shown in chapter 3, previous workers have concentrated on obtaining either full analytical solutions through the use of various mathematical devices, or simulating the problem by mechanical analogy or by direct numerical solution of the equations. Sloshing theory has tended to apply to single fluid systems i.e. a gas and one liquid. For the offshore industry however, there has to be a concern with multiple fluid sloshing e.g. gas, oil and water.

The equations presented in chapter 3, taken from previous works, fail to provide a full understanding of problems in deriving linear and non-linear sloshing theories. In this chapter a *basic sloshing equation* is derived from the Navier-Stokes equation, through the use of a rotational co-ordinate system. Simplifications are then applied to derive a *linear sloshing equation* which is subsequently solved for a closed rectangular vessel under simple surge/sway motion. The derived linear theory is capable of predicting natural periods for gas/liquid, liquid/liquid and gas/liquid/liquid systems. Unlike previous works (chapter 3), the equations derived here predict a frequency response containing terms due to both natural and forcing periods.

The full solution of the sloshing Navier-Stokes equation can be completed through the use of a numerical model. One of the simplest to

use, is an adaption of the classic Marker And Cell (MAC) technique to account for interfacial breaking.

This chapter presents the derivation of a two dimensional sloshing equation from the Navier-Stokes equation modified with a rotational reference frame. Applying Laplace transforms, three worked solutions are then given of a simple linear theory. This chapter also introduces the numerical model, comparisons between model and physical experiments will be presented in chapter 12.

4.2 THE BASIC FLUID EQUATIONS.

4.2.1 Introduction.

A derivation of the Navier-Stokes equation from Newtons Second law, is presented for clarity. The velocity components are then modified for a rotational co-ordinate system. Simplifications of the resulting equations produce the basic sloshing equation for pitch, heave and surge/sway forcing motions.

4.2.2 Derivation of the Navier-Stokes Equation.

As a fluid element obeys Newton Second law, then :

$$\bar{F} = \frac{d(m\bar{v})}{dt} \qquad \ldots 4.1$$

Equating the force $\bar{F}$ with the stress acting on the fluid element, the above can be written using tensor notation as (74,75) :

$$\frac{D(\rho u_i)}{Dt} = \rho X_i + \frac{\partial \sigma_{ik}}{\partial x_k} \qquad \ldots 4.2$$

But for a Newtonian fluid, the stress tensor can be written as :

$$\sigma_{ik} = (Ke_v + \mu\varepsilon_v)\delta_{ik} + 2\mu e_{ik(d)} \qquad \ldots 4.3$$

Following from the assumptions associated with a Newtonian fluid :

$$\sigma_{ik} = (-p + (\mu_v - \frac{2}{3}\mu)\nabla.\bar{q})\delta_{ik} + 2\mu\varepsilon_{ik(d)} \qquad \ldots 4.4$$

Combining equations 4.2 & 4.4 :

$$\frac{D(\rho u_i)}{Dt} = \rho X_i - \frac{\partial P}{\partial x_i} + \frac{\partial}{\partial x_i}\left[(\mu_v - \frac{2}{3}\mu)\nabla.\bar{q}\right] + \frac{\partial}{\partial x_k}\left[\mu(\frac{\partial u_i}{\partial x_k} + \frac{\partial u_k}{\partial x_i})\right]$$

$$\ldots 4.5$$

To arrive at the usual Navier-Stokes equation, the assumptions that $\mu_v = 0$ and that the fluid is incompressible are made and noting that :

$$1) \quad \frac{\partial(\nabla.\bar{q})}{\partial x_i} = \frac{\partial}{\partial x_i}\left[\frac{\partial u_i}{\partial x_j}\right]$$

$$2) \quad \frac{\partial \rho}{\partial t} + \frac{\partial (\rho u_i)}{\partial x_i} = 0 \qquad \ldots 4.6$$

Then, equation 4.5 reduces to :

$$\rho\frac{D(u_i)}{Dt} = \rho X_i - \frac{\partial P}{\partial x_i} + \mu\frac{\partial}{\partial x_k}\left[\frac{\partial u_i}{\partial x_k} + \frac{\partial u_k}{\partial x_i}\right] \qquad \ldots 4.7$$

4.2.3 Moving Co-ordinate System.

Equation 4.7 relates to a fixed co-ordinate system with a general body force X_i acting on every fluid element. Consider a moving vessel and the time dependant boundary conditions required to solve 4.7. Simplifications can give rise to a case where the body force can be expressed in terms of a simple sinusoid. However, for a general equation perhaps the easiest way to introduce a sloshing force is to employ a moving co-ordinate system (14,44,75). The derivation following Raudkivi and Callander (75), centres around the addition of extra acceleration terms using a fixed and moving reference frame.

The velocity and acceleration of a particle at "A" (figure 4.1), can be expressed in terms of three position vectors, each of which describe motion relative to a particular frame of reference. Then, the velocity and acceleration of point "A" relative to the fixed frame can be written as :

$$\frac{d\bar{R}_\theta}{dt} = \frac{d\bar{a}}{dt} + \bar{\Omega}x\bar{R} + \frac{d\bar{R}}{dt}$$

$$\frac{d^2\bar{R}_\theta}{dt^2} = \frac{d^2\bar{a}}{dt^2} + 2\bar{\Omega}x\frac{d\bar{R}}{dt} + \bar{\Omega}x(\bar{\Omega}x\bar{R}) + \frac{d\bar{\Omega}}{dt}x\bar{R} + \frac{d^2\bar{R}}{dt^2}$$

where $\bar{R} = \bar{r} + \bar{b}$

In tensor notation, the velocity can be written as :

$$u_i^\theta = u_i^1 + \frac{da_i}{dt} + \varepsilon_{ijk}\Omega_j R_k + \frac{db_i}{dt} \qquad \ldots 4.8$$

where ε_{ijk} is the *krondecadelta.*

Replacing for the velocity term on the left hand side of 4.7, gives :

$$\frac{\rho D}{Dt}(u_i + \frac{da_i}{dt} + \frac{db_i}{dt} + \varepsilon_{ijk}\Omega_j R_k) = \rho X_i - \frac{\partial P}{\partial x_i} + \mu\frac{\partial}{\partial x_k}\left[\frac{\partial u_i}{\partial x_k} + \frac{\partial u_k}{\partial x_i}\right]$$

Collecting the pure velocity terms gives the *Sloshing Navier-Stokes* equation as :

$$\frac{\rho Du_i}{Dt} = \rho X_i - \frac{\partial P}{\partial x_i} + \mu\frac{\partial}{\partial x_k}\left[\frac{\partial u_i}{\partial x_k} + \frac{\partial u_k}{\partial x_i}\right]$$

$$-\rho\left[\frac{d\,a_i^2}{dt^2} + \frac{d\,b_i^2}{dt^2} + 2\varepsilon_{ijk}\Omega_j(u_k + \frac{db_k}{dt})\right.$$

$$\left. + \varepsilon_{ijk}\Omega_j(\varepsilon_{klm}\Omega_l R_m) + \varepsilon_{ijk}\frac{d\chi_j}{dt}R_k\right] \qquad \ldots 4.9$$

Comparing 4.9 with 4.7, the only difference is the introduction of another body force term involving a moving boundary. Note that it is not

necessary to replace the viscous velocity terms as the motion involves only time, not distance.

4.2.4 Derivation of the Basic Sloshing Equation.

Equation 4.9 applies to a general three dimensional situation. For further treatment, the simplification to two dimensional sloshing, aids solution of equation 4.9. For a rectangular vessel, the forcing motions of pitch, heave and sway can be represented into terms of a rotational term and a positional vector (figure 4.2).

Applying simple sinusoidal relations :

$$\text{Pitch} \quad a = A_p \text{Sin}(\omega_p t + \varepsilon_p) + O_p$$

$$\text{Heave} \quad h = A_h \text{Sin}(\omega_h t + \varepsilon_h) + O_h \qquad \ldots 4.10$$

$$\text{Sway} \quad l = A_l \text{Sin}(\omega_l t + \varepsilon_l) + O_l$$

Then for a two dimensional vessel :

$$\bar{a} = (a_x, a_y, 0) \quad \bar{b} = (b_x, b_y, 0) \quad \bar{\chi} = (0, 0, \Omega_z)$$

Replacing the forcing relations into the above gives :

$$a_x = l \qquad a_y = 0$$

$$b_x = D \text{ Cos}(\theta) \qquad b_y = D \text{ Sin}(\theta)$$

$$\Omega = \Omega_z = \frac{da}{dt}$$

Where :

$$D = \sqrt{(h^2 + O_l^2)} \ , \quad \theta = \tan^{-1}\left(\frac{O_l}{h}\right) \qquad \ldots 4.11$$

Expanding equation 4.9 into the x and y velocity terms, gives :

$$\rho\frac{Du}{Dt} = \rho X - \frac{\partial P}{\partial x} + \mu\left[\frac{\partial^2 u}{\partial x^2} + \frac{\partial^2 u}{\partial y^2}\right] - \rho\left[\frac{d^2 a_x}{dt^2} + \frac{d^2 b_x}{dt^2} - 2\Omega(v + \frac{db_y}{dt}) - \Omega^2(x + b_x) - \frac{d\chi}{dt}(y + b_y)\right] \quad \ldots 4.12a$$

$$\rho\frac{Dv}{Dt} = \rho Y - \frac{\partial P}{\partial y} + \mu\left[\frac{\partial^2 v}{\partial x^2} + \frac{\partial^2 v}{\partial y^2}\right] - \rho\left[\frac{d^2 a_y}{dt^2} + \frac{d^2 b_y}{dt^2} + 2\Omega(u + \frac{db_x}{dt}) - \Omega^2(y + b_y) - \frac{d\chi}{dt}(x + b_x)\right] \quad \ldots 4.12b$$

Where the derivatives of a_n and b_n (n= x,y) are obtained from equations 4.10.

The solution of 4.12, as with the Navier-Stokes equations in general, cannot be solved using simple techniques, some approximations are required.

4.3 LINEAR SOLUTION OF THE SLOSHING EQUATION.

4.3.1 Conversion to Velocity Potential Form.

The non-linear rotational terms in 4.12 poses problems in finding a *simple linear solution*. The first stage is then to exclude motions in pitch and heave but concentrate on a simple *traversal* (surge/sway) forcing function (i.e. $\Omega = b_i = 0$). Intuitively, under such a forcing function, 4.12 could have been derived through the addition of an extra force in the expression for velocity in the x-axis (u).

Neglecting viscosity and assuming the motion is irrotational, 4.12 can be expressed as (see Appendix I) :

$$-\frac{\partial\phi}{\partial t} + \left[\frac{u^2 + v^2}{2}\right] + \frac{P}{\rho} - \Omega = f(t) \quad \ldots 4.13$$

Appendix I presents three worked solutions of 4.13 as applied to single, twin and three fluid systems in a rectangular vessel. The

treatment provides expressions predicting the natural period as well as interface amplitude. However when predicting interface amplitudes, the linear theory breaks down near resonant forcing periods.

4.3.2 A Single Fluid System.

Using Laplace transforms, the equation of the free surface of a single fluid under a traverse forcing motion is given by (Appendix I):

$$\eta(x,t) = \sum_{n=1}^{\infty} \frac{4lx_o\Omega^2\omega(\Omega\sin(\omega t)-\omega\sin(\Omega t))}{((2n-1)\pi)^2(\omega^2-\Omega^2)g}\cos\left(\frac{(2n-1)\pi x}{l}\right) \qquad \ldots 4.14$$

Where $\omega = \omega_{2n-1}$, is the natural frequency given by :

$$\omega_{2n-1}^2 = \frac{g(2n-1)\pi}{l}\tanh\left[\frac{(2n-1)\pi h}{l}\right] \qquad \ldots 4.15$$

Where Ω is the forcing frequency of the motion with amplitude x_o, as defined in figure 4.3.

Unlike previous workers (47-49), equation 4.14 predicts that the free surface profile is not just a function of the forcing frequency, rather a combination with the natural frequency. In practical terms, experiments should show the free surface oscillating at its natural frequency whilst the vessel is forced at another frequency.

Graphs 4.1 & 4.2 illustrate the result of the above equation, plotting interface amplitude against forcing period. Where :

$$\text{Interface Amplitude} = \frac{\text{Max}(\eta(x,t))-\text{Min}(\eta(x,t))}{2} \qquad \ldots 4.16$$

As expected, the theory breaks down ($\eta=\infty$) around the resonant period. Graphs 4.1 & 4.2 refer to a calculation with a closed rectangular container of length 1.78m and height 0.612 m, filled with water to a depth measured from the base. Interface amplitude measurements taken from a point 300mm from the left hand wall i.e. x=300mm in equation 4.14.

4.3.3 A Twin Fluid System.

In this case, the upper fluid cannot be neglected e.g oil on top of water. With reference to figure 4.4, the equation of the interface profile can be derived as (Appendix I) :

$$\eta(x,t) = -\sum_{n=1}^{\infty}\left[\frac{4lx_o\Omega^2[(\omega^2+\Omega^2(1-f))\mathrm{Sin}(\Omega t)-\Omega\omega f\,\mathrm{Sin}(\omega t)]}{[(2n-1)\pi^2]^2 g(\omega^2-\Omega^2)} * \mathrm{Cos}\left(\frac{(2n-1)\pi x}{l}\right)\right] \quad \ldots 4.17$$

Where :

$$f = \frac{\mathrm{Sinh}(k(h_2-h_1))\mathrm{Cosh}(kh_1) - r\mathrm{Sinh}(kh_1)\mathrm{Cosh}(k(h_2-h_1))}{\mathrm{Sinh}(k(h_2-h_1))\mathrm{Cosh}(kh_1) + r\mathrm{Sinh}(kh_1)\mathrm{Cosh}(k(h_2-h_1))}$$

$$r = r_{21} = \frac{\rho_2}{\rho_1} \quad , \quad k = k_n = \frac{(2n-1)\pi}{l}$$

$$\omega^2 = \omega_{2n-1}^2 \qquad \text{Natural period} = \frac{2\pi}{\omega}$$

The natural frequency is given by :

$$\omega_{2n-1}^2 = g(1-r)\frac{(2n-1)\pi}{l}[\mathrm{Coth}(kh_1) + r\mathrm{Coth}(k(h_2-h_1)]^{-1} \quad \ldots 4.18$$

Note that if r=0 (i.e. $\rho_2 << \rho_1$), then both equations 4.17 and 4.18 reduce to the single fluid expressions, equations 4.14 and 4.15 respectively.

Looking at the natural frequency expression, not only is there an effect of density, but also of fill depth. Graph 4.3 shows the variation in natural frequency with fill depth ratio for a vessel of same dimensions as referred to in graphs 4.1 & 4.2. Each curve on 4.3, refers to a different density.

As the density of the upper fluid is increased, so is the natural period. An important point to note, is that at low and high fill depths of

the lower fluid, the natural period becomes very high and will reach infinite values. In mathematical terms, this is due to the equations breaking down (i.e. $h_1=h_2$, $\omega=0$ hence infinite period) and in practical terms, this implies the slightest movement may be sufficient to cause interface breakup.

4.3.4 A Three Fluid System.

With oil/water separation equipment, there will be a significant gas cap over the oil, which will effect the theory. In this case, it can be shown (Appendix I) that the equations for natural frequency of both fluid interfaces involve the solution of a quadratic, of the form :

$$(s^4+(\omega_1^2+\omega_3^2)s^2+\omega_1^2\omega_3^2-c_1c_3)(s^2+\Omega^2)$$

$$= (s^2+\omega_1'^2)(s^2+\omega_3'^2)(s^2+\Omega^2) \qquad \ldots 4.19$$

Subscript 1 and 3 refer to the lower and upper fluids. The ω' terms are given as :

$$\omega_1'^2 = \frac{g(1-r_{21})k\mathrm{Sinh}(kh_1)}{[\mathrm{Cosh}(kh_1)-r_{21}(a_1\mathrm{Sinh}(kh_1)+b_1\mathrm{Cosh}(kh_1))]}$$

$$\omega_3'^2 = \frac{g(1-r_{23})k\mathrm{Sinh}(kh_2-H)}{[\mathrm{Cosh}(k(h_2-H)-r_{23}(a_3\mathrm{Sinh}(kh_2)+b_3\mathrm{Cosh}(kh_2))]} \qquad \ldots 4.20a/b$$

$$r_{ij} = \frac{\rho_i}{\rho_j} \qquad k = k_n = \frac{(2n-1)\pi}{l}$$

$$\omega^2 = \omega_{2n-1}^2 \qquad \text{Natural period} = \frac{2\pi}{\omega}$$

Fill depth and density terms are as defined in figure 4.5.

Graph 4.4 plots natural period against fill depth to length ratio for a three fluid system (water, oil of density 800 Kg/m^3 and air), again in a container of length 1.78m and height 0.612m. The difference between this graph and 4.3, is the effect of changing the gas cap size as indicated by the curves.

4.3.5 Properties of the Linear Solution.

As with all previous linear theories, graphs 4.1 & 4.2 show that interface amplitude approaches infinite values as the forcing frequency approaches the natural frequency. This has been attributed to the theory breaking down due to exclusion of the velocity product term in equation 4.13 (46). However, a simple explanation can be found by looking at the kinematic boundary condition. In the derivation (74), mean flow is neglected for small waves and thus :

$$\frac{\partial \phi}{\partial y} = \frac{\partial \eta}{\partial t} + u\frac{\partial \eta}{\partial x} = \frac{\partial \eta}{\partial t} \qquad \ldots 4.21$$

In physical terms, this means that particles at the free surface remain at the free surface, hence the break down of treatments which use the above assumption at resonance. Any linear analysis, such as the one presented in this chapter, derives equations for the free surface profile which can only be applied far from resonance where the assumption in equation 4.21 is valid.

Linear theory can however, provide some information on the period of oscillation of the free surface. Previous work (10,47-48) solving a velocity potential by separation of variables technique, have assumed a time function (i.e. $\phi(x,y,t) = \bar{\Phi}(x,y)\mathrm{Cos}(\Omega t)$) and then used boundary conditions to solve the various constants. In this present analysis, the time function and constants, were obtained through the use of Laplace

transform methods. This results in equations which contain terms linking the natural frequency to the forcing frequency.

Taking equation 4.14 as an example, if the forcing frequency is lower than the natural frequency, the free surface will consist of waves which oscillate at the forcing frequency. If the forcing frequency is greater than the natural frequency, the free surface waves will oscillate at the natural frequency. Therefore, there will be a transition region between the two.

The theory presented in this chapter does not account for the effects of surface tension and viscosity on the prediction of free surface profile and natural period. Following discussions on scaling of slosh experiments (chapter 3), it is suggested that surface tension effects are negligible. It will be shown later, that viscosity too might be considered negligible (chapter 12).

4.4 NUMERICAL SIMULATION OF FLUID SLOSHING.

4.4.1 Background to the Numerical Solution Technique.

The sloshing Navier-Stokes equation 4.12, can be solved by analytical techniques, making simplifications and assumptions. Yet, these solutions are only obtained after quite some effort and are case specific in that they only apply to one particular vessel configuration. The simple linear theory neglects viscous effects, surface tension and the presence of internal obstructions and its use is therefore restricted to the prediction of natural frequency. However, by numerical techniques, the basic sloshing equation may be solved accounting for both viscous and surface tension effects as well as internals.

Theoretically there are two ways in which to describe fluid motion. The Eulerian system is one with a fixed frame of reference, the Lagrange system provides a moving frame of reference. In fluid sloshing, the

Lagrange system appears to offer advantages over the Eulerian one with the possibility of tracking the free surface. However, Hirt et al (76) quotes a disadvantage of the Lagrange method in that the system will break down as a result of large fluid distortions. In an attempt to overcome difficulties with each method, previous workers have developed coupled Eulerian-Lagrangian systems (77) which are difficult to program. However other techniques are available for tackling problems with a free surface.

The Marker And Cell numerical technique, developed at Los-Alamos Laboratory USA (16) for solving fluid flow problems with a free surface, have proved successful in both two and three dimensions (13). However, simulation of large amplitude sloshing, requires new surface tracking procedures. To study large amplitude single fluid sloshing, Bridges (14) used a method due to Nichols et al (17), the SOLution Algorithm by Volume Of Fluid (SOLA-VOF) technique. The program was modified to study sloshing, through the use of a rotational coordinate system. Instead of marker particles, free surfaces are tracked by a volume of fluid function. Comments have been made both to the instability (3) of the code and to errors in the applied free surface boundary conditions (78).

A full copy of the original SOLA-VOF code was obtained (17) without the modifications by Bridges. This general fluid dynamic program was converted to run on the Universities *Burroughs B6390* mainframe, providing *GINO* graphical output of the fluid velocity and surface profiles. Later, the program was transported to a *Acorn Cambridge Work Station* (ACW) to allow further development and the inclusion of code to simulate fluid sloshing. Subsequent replacement of the B6930, by a *VAX CLUSTER*, required minor modifications of the ACW program for mainframe application.

A full listing of the program with modifications carried out for this project, is presented with material external to this report. The

program provided represents the most recent version and will therefore contain some additional modifications not reported here.

4.4.2 The SOLA-VOF Solution Method.

As with other MAC codes, the SOLA-VOF program operates on a finite difference mesh system, where the fluid region is mapped onto a grid. The partial differentials in the Navier-Stokes equations are converted into *their difference format, according to standard techniques* (53).

At any given time cycle, for each mesh cell, the velocity components are estimated explicitly i.e. from previous known values. The pressure terms are calculated iteratively ensuring the continuity equation is adhered to at each step. If the number of iterations exceeds a specific value, then the mesh configuration can be considered unstable. Calculation of the new pressure terms is carried out not from the Navier-Stokes equations, but from a modified form of the continuity equation. This tries to account for *limited compressibility.* Once satisfactory convergence has been determined, the mesh values are updated and the simulation time incremented. To maintain control of the fluid motion, ideally the maximum fluid velocity throughout the whole mesh should be such that fluid cannot travel more than one cell distance in any time step. This introduces the prospect of reducing time steps to such small values that again, the mesh can be considered to be unstable.

In the original MAC method, marker particles were used to track the free surface, positions of which, were updated once a time interval was complete. For the SOLA-VOF method, the free surface is followed using a special function F, the volume of fluid function, which takes a value of 1 for a full cell and 0 for a void cell. This offers the possibility of bubble formation and certainly interface breaking, as would occur in large amplitude near resonant sloshing.

Other variations of the basic MAC method have been employed in the design of ships and space craft. Lloyds Register of Shipping (3) have tested SOLA-SURF which, according to Nichols (17), uses a height function to position the free surface. As such, SOLA-SURF cannot deal with breaking waves. Although the current SOLA-VOF program is two dimensional, three dimensional versions of the MAC technique have been applied by Feng (13) for work with the space shuttle. Such a program even with current computing power, would be slow and require significant computer time to complete.

4.4.3 Introduction of Sloshing into SOLA-VOF.

Bridges introduced forcing terms by means of a rotational reference frame to simulate pitch/roll motion on a large vessel. As the SOLA-VOF code arrived with no forcing terms (only gravity) an attempt was made to introduce three forcing motions, pitch, heave and sway. In a two dimensional model the terms pitch and surge are then synonymous with the terms roll and sway respectively (chapter 2, figure 2.5).

Modification to the code, dealt with altering the calculation of the new velocity components and to the volume of fluid function. The program derived fluid velocities from the equation :

$$\frac{Du_i}{Dt} = \rho X_i - \frac{\partial P}{\partial x_i} + \mu \frac{\partial^2 u_i}{\partial x_k^2} + \Omega_i \qquad \ldots 4.21$$

The appropriate terms for Ω_i were encoded according to the formulation presented earlier (equation 4.12). This required modification to the calculation of velocity (subroutine TILDE) and to the calculation of the fluid configuration routine (subroutine VFCONV). These alterations were made through the use of general subroutines to aid further enhancements and problem solving.

Caution had to be exercised in calculating the derivatives of the motion terms. To prevent instability, it was found that these terms had to be expressed in their finite differences form and not the exact derivatives. Also, following Bridges recommendations, all apparent acceleration terms due to the co-ordinate system were evaluated using time centered values (i.e. times at $T-\Delta T/2$). The other acceleration terms based on the previous velocity values, were evaluated at previous time levels (i.e. $T-\Delta T$).

4.4.4 Modifications to the Input/Output of Data.

The original program had three modes of output, direct numerical values of the velocity and pressure, graphical drawings of particle positions and lastly, a graphical output of the velocity and free surface profile. All of these modes were time stepped so that anyone output mode could be given independent of the others. Enhancements and additions were made to these :

1) Modified Graphical Presentation: The graphical output from the original program was re-written for use with GINO then ACW graphics, with options to save all data to disk file for later viewing or obtaining hard copies by pen plotter.

2) Improved presentation of vectors: Special code was added to draw both the direction and magnitude of velocity components.

3) Output of Velocity profile to Video Recorder: To provide an animated sequence of fluid profiles, code was included to drive a VHS video recorder. Video output from the ACW was send to a domestic video recorder whose recording features were controlled directly from software. The application of this method relied on running the program on the ACW not on the mainframe. Transfer of

the large screen data files from the mainframe would have proved time consuming and *costly*.

4) Printed Summary Data: Instead of printing vast amounts of velocity and pressure data for each mesh cell, additional code was written to determine maximum values within the mesh.

5) Internals: To aid placement of baffles and other internals, a custom internal object generator was included. Two types of internals are currently defined, covering solid or perforated, horizontal or vertical plates. With the perforated plates, although input data specifies position, length and hole size, the program fits this data to the current mesh size. Therefore, the minimum hole size and plate thickness, will ultimately be defined by the overall mesh used in the simulation.

6) Addition of a Dump Routine: Working the VAX computer, a maximum of 5 hours CPU time was allocated per user. As some simulation runs aborted after this time, a special routine was added to save all system variables at specific times to disk. Corresponding re-start code was then written to restore the simulation where it had left off. Although useful for singular runs, the matching of two sets of data files has proved difficult.

7) Detection of the Fluid Interface: As will be described in later chapters, data from physical experiments obtained during this project, were recorded using a computer based data logging/processing system. To allow direct comparison between numerical and physical experiments, code was included into the simulation program to generate compatible data files to those produced by the data logging system. In this case, *wave probes* determined the interface position with respect to vessel base, by calculating the total volume of fluid at specific points inside the

rectangular grid. Data from these probes together with motion positions was then stored on disk. As all data processing was carried out locally on the ACW, simulations running on the VAX mainframe required transfer of data files to the ACW.

4.4.5 Stability of Solution.

Stability is one of the major considerations in numerical solution procedures, SOLA-VOF is no exception. To check for stability, the program uses two methods :

1) Conservation of Mass: Loss of fluid can result from numerical rounding errors during the calculation. The program therefore calculates the cumulative total mass lost or gained throughout the simulation. In practical terms this means that liquid level inside simulated (two dimensional) vessels can rise or fall. As will be seen in later *simulation experiments*, such fluid losses remained below 0.5%.

2) High Velocity values: One principle of the volume of fluid finite difference mesh is in the transportation of fluid from one cell to the next. Ideally between each time step, a fluid element must travel only to adjacent cells. Then if the fluid velocity becomes too high, time steps have to be reduced accordingly. For an unstable mesh, it was found in practice that time steps approached 10^{-6} seconds. Therefore checks were added to detect such low time steps and abort the calculation.

Bridges reported that increased mesh stability may be achieved by applying a higher fluid viscosity than the physical case. It was assumed here, that this would introduce fluid damping and hence reduce overall

velocity values. However, it will be shown (chapter 12) that simulation viscosity has little effect on free surface profile.

4.4.6 Description of Graphical Output Produced by Simulation.

Examples of velocity profile data are presented in figures 4.6a-f dealing with a rectangular vessel (1780mm by 612mm) filled with water and oil. To the right of the vessel is a weir plate, as found in offshore separators.

Figure 4.6a presents initial run information. As the simulation deals with two fluids (e.g. gas/liquid or liquid/liquid) the term *fill depth* refers to the position of the oil/water interface with respect to the vessel base. Information is also given as to the actual fluid density, forcing conditions (i.e. pitch motion at $\pm 4°$) and duration of forcing and decay. In this project, it was envisaged that experiments would yield the oil/water interface profile during applied forcing and once forcing had ceased. This explains the *Time to Finish* and *Time to Stop* motion values in the profile plot information page.

The second page (figure 4.6b) shows the *initial finite difference mesh* used in this problem. Here, the mesh is seen to be uneven, converging at a point near the right hand wall. The original SOLA-VOF code allowed the generation of a variable mesh to aid resolution along fluid/wall boundaries. It has been reported (79) that a variable mesh can increase the stability of the solution.

The next successive plots (figures 4.6c-f) show the actual velocity profile at specific time intervals (in this case 0.5 seconds) :

1) The top line provides information on the current simulation time, the current cycle number and the volume of fluid change.
2) On the bottom of each plot, is the current position of the simulated vessel, with pitch in degrees, sway and heave in mm. Note

that in this case, the term sway should strictly be surge. In terms of sign, these terms are in accordance with usual cartesian conventions i.e. +ve angles are anti-clockwise, +ve distances are to the right.

3) The middle of each plot shows the rectangular boundary (in correct proportions), the free surface profile and the velocity vectors emanating from the center of a mesh cell. As time increases, the dots seen in the initial plots change into full vector arrows, the size of which determines the strength of the velocity field at that point. To save plotting time and storage space, in some cases the arrow tips are not shown when the velocity is small as compared with the rest of the mesh.

This type of output, provides a vast amount of information regarding the flow of fluid, more that would be gained by numerical figures from a printout. However, although a large number of simulation experiments were eventually carried out (chapter 12), the time and effort involved in producing such velocity plots was too restrictive. Only a few plots were made for general visual examples of the simulated fluid response to sloshing.

4.4.7 Comparisons with Physical Experiments.

Chapter 12 presents comparisons between *simulation* and *physical* experiments on two rectangular vessels filled with air/water and oil/water. General discussions on the operation, advantages and limitations of the model are also presented.

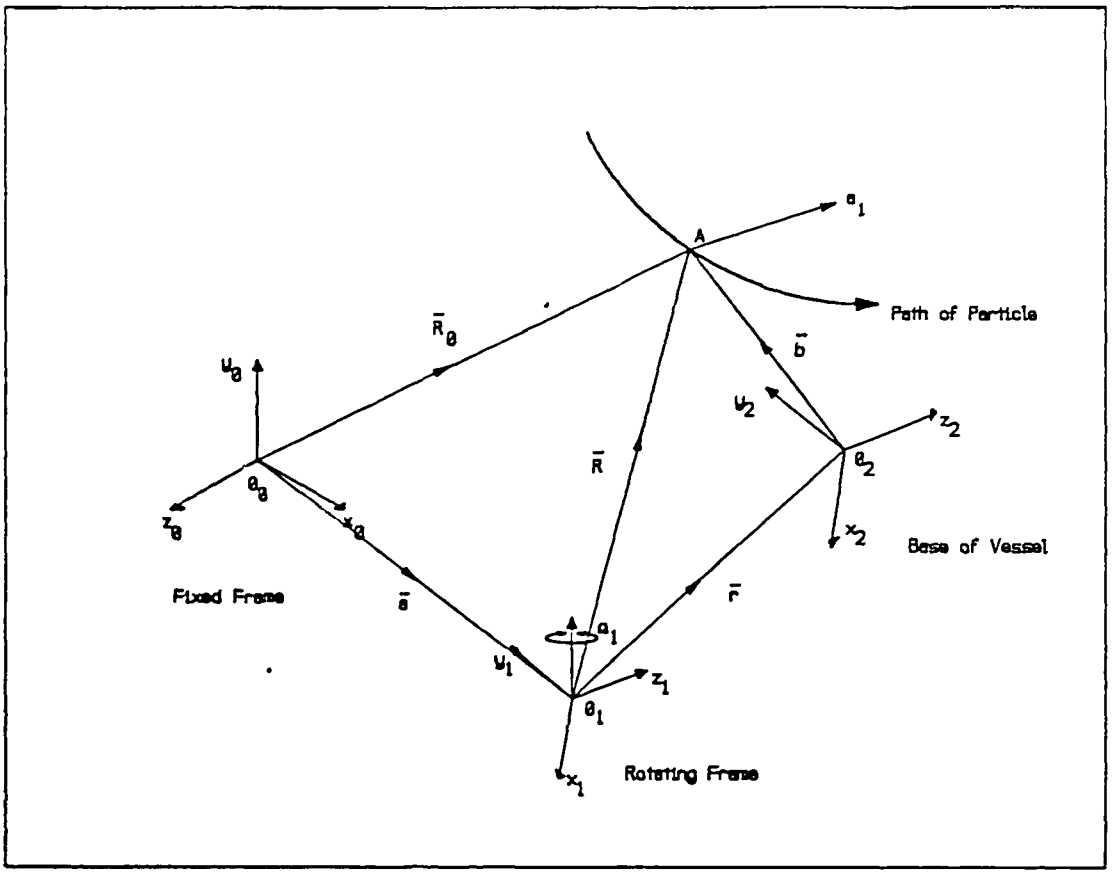

Figure 4.1: Description of the rotating co-ordinate system following Raudkivi & Callander (75).

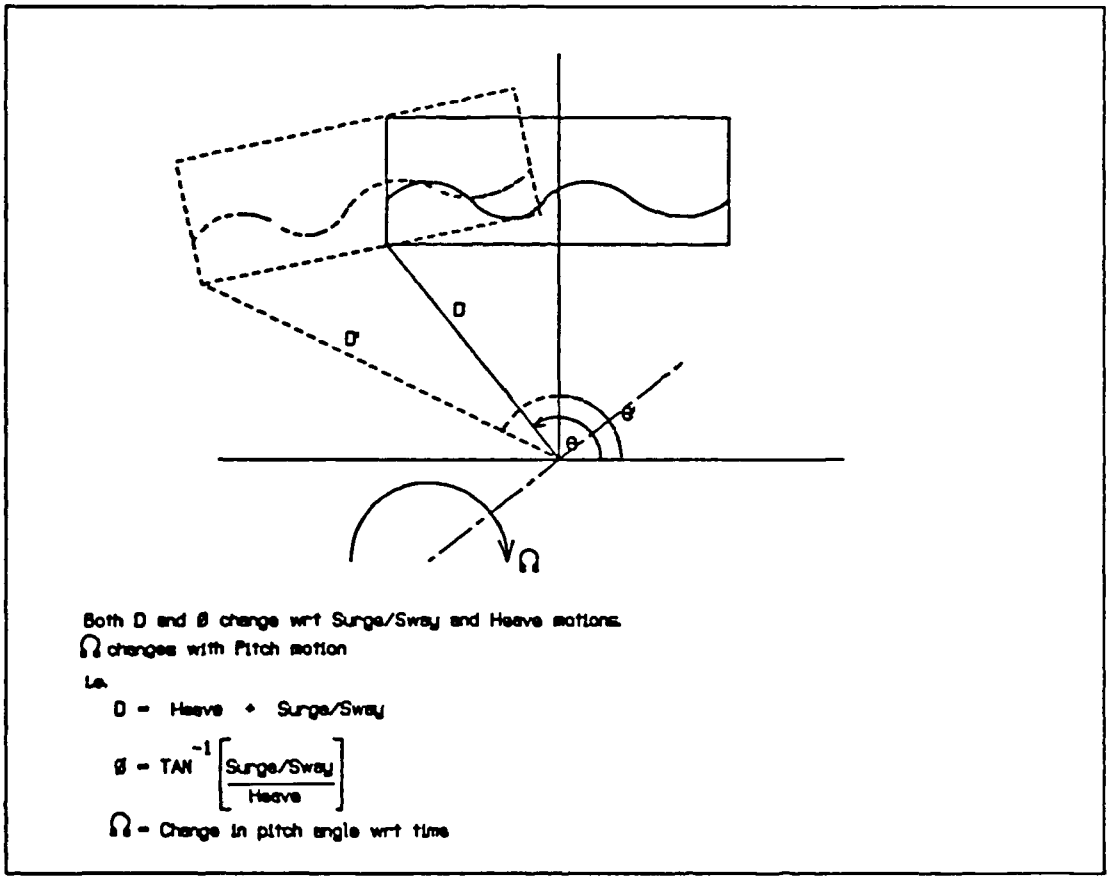

Figure 4.2: Representation of two dimensional forcing motions acting on a rectangular container.

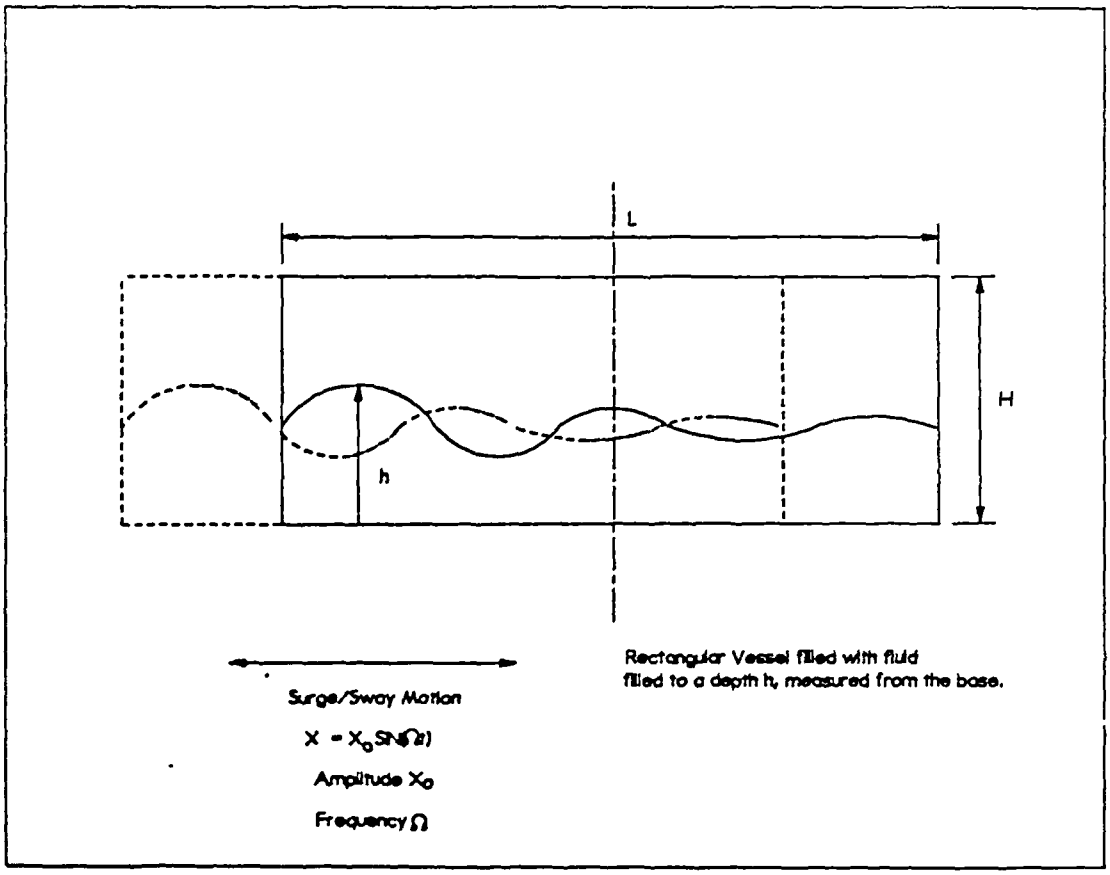

Figure 4.3: Definition used for surge motion applied to a rectangular container for a twin fluid system.

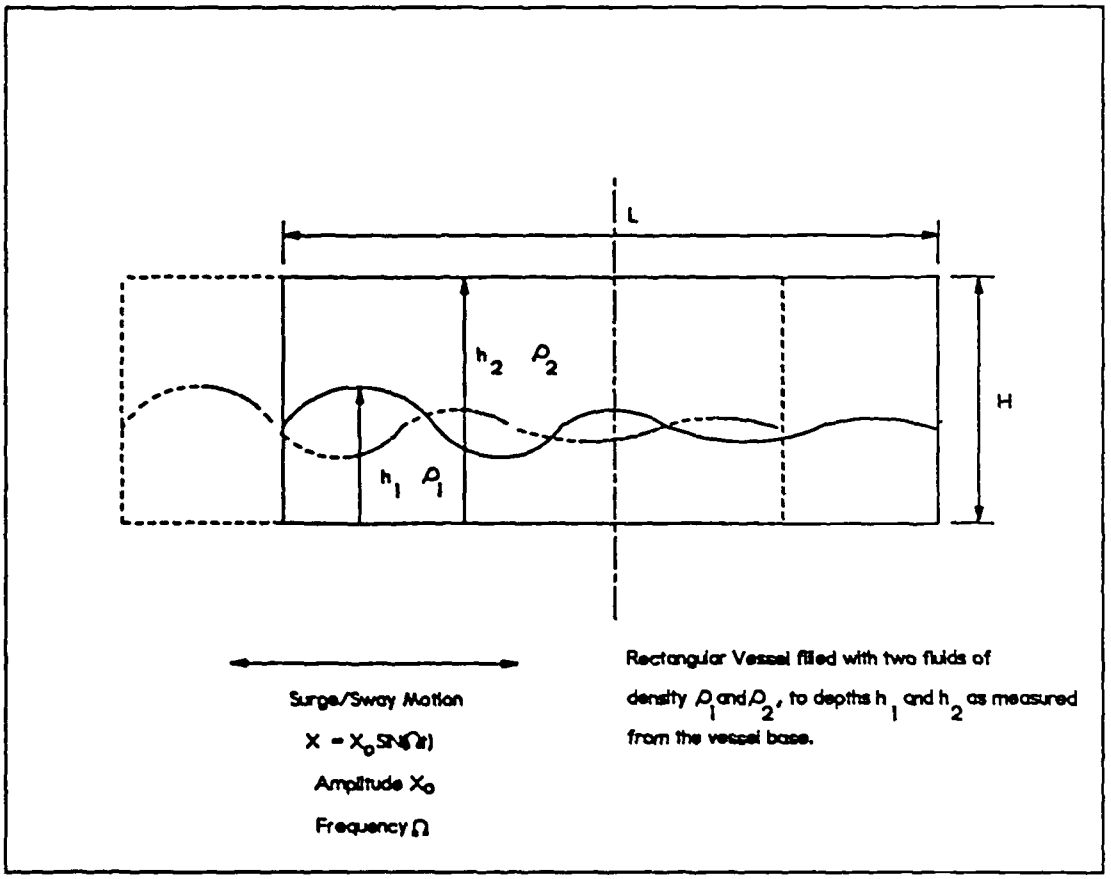

Figure 4.4: Definition used for surge motion applied to a rectangular container for a twin fluid system.

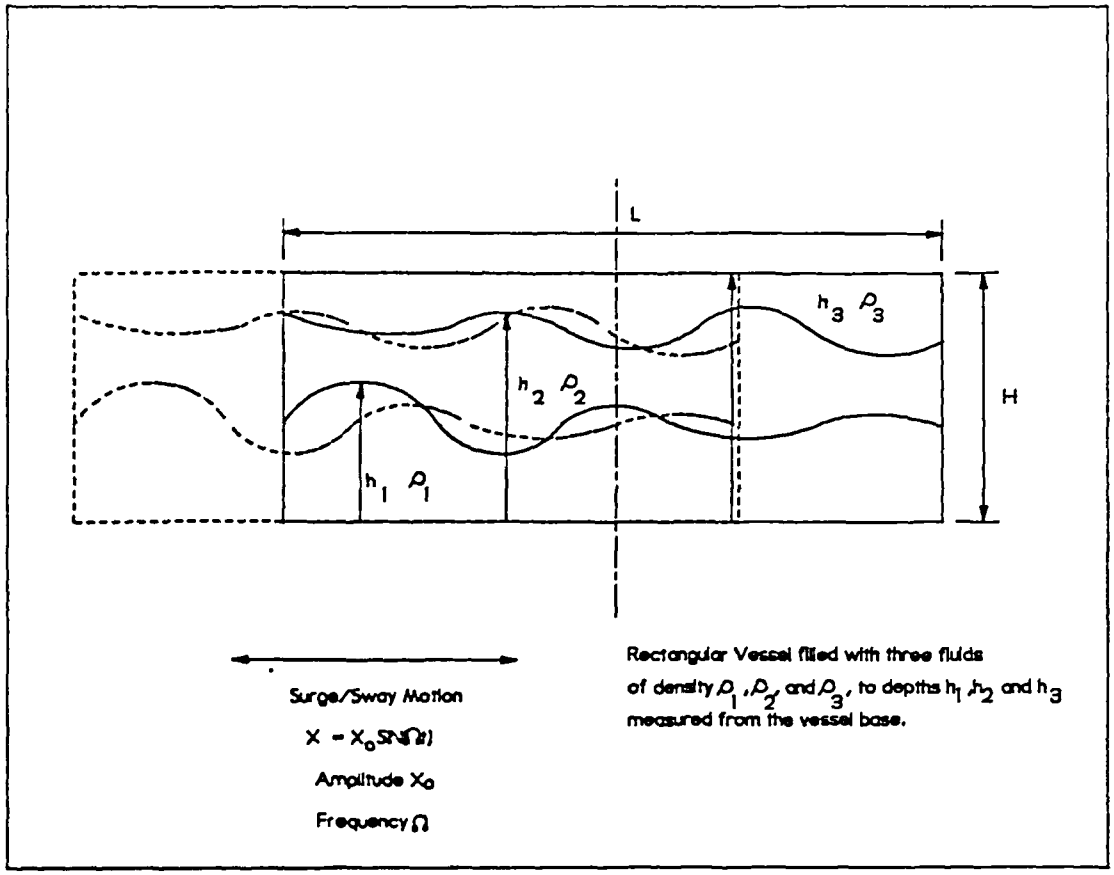

Figure 4.5: Definition used for surge motion applied to a rectangular container for a three fluid system.

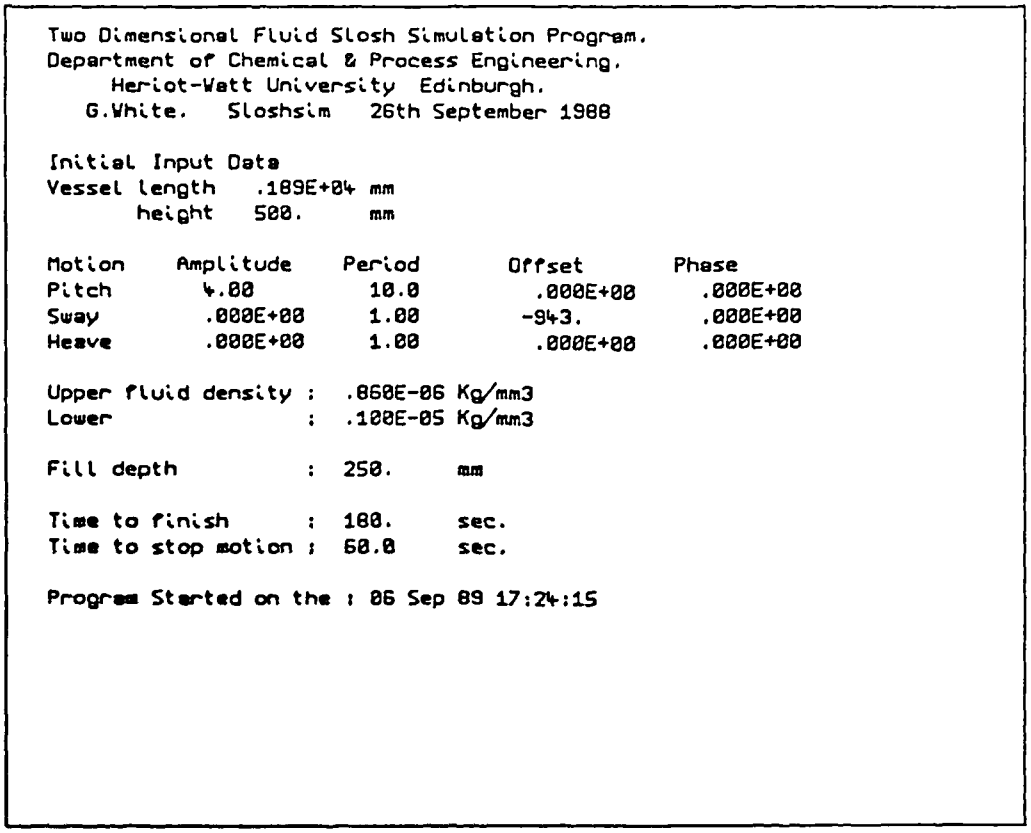

Figure 4.6a: Example of velocity vector plot for a rectangular vessel filled with oil and water. The initial information page.

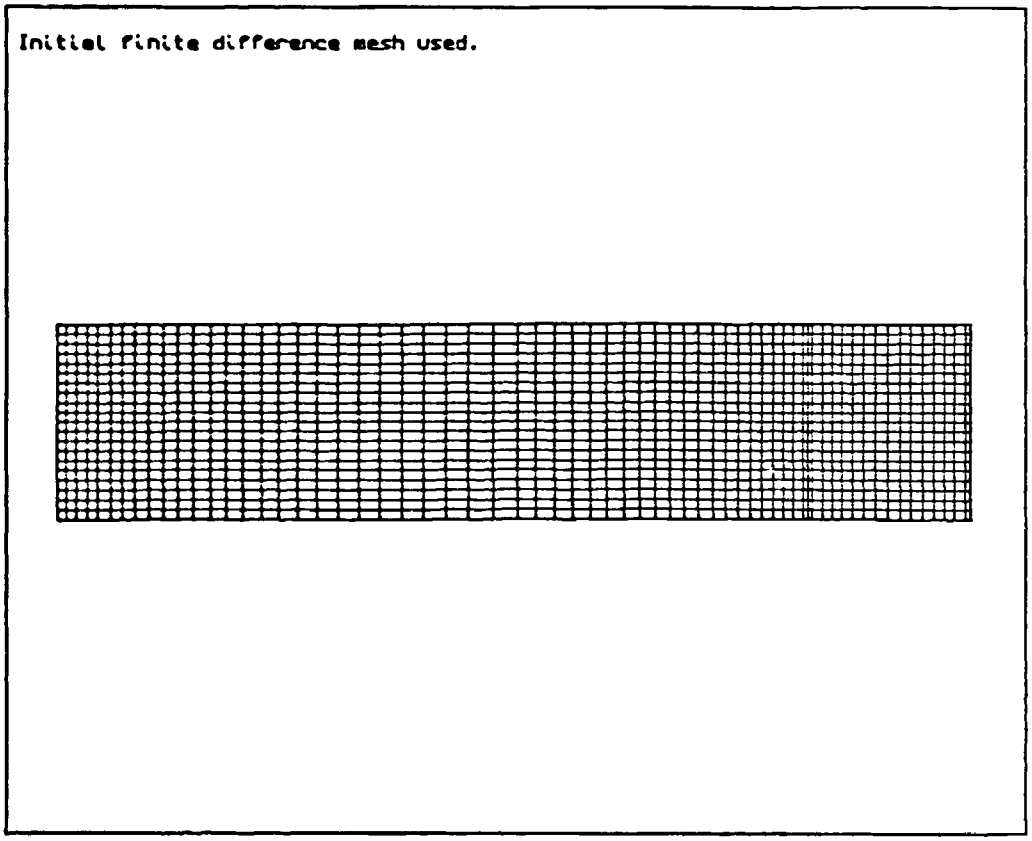

Figure 4.6b: Example of velocity vector plot for a rectangular vessel filled with oil and water. The initial mesh configuration.

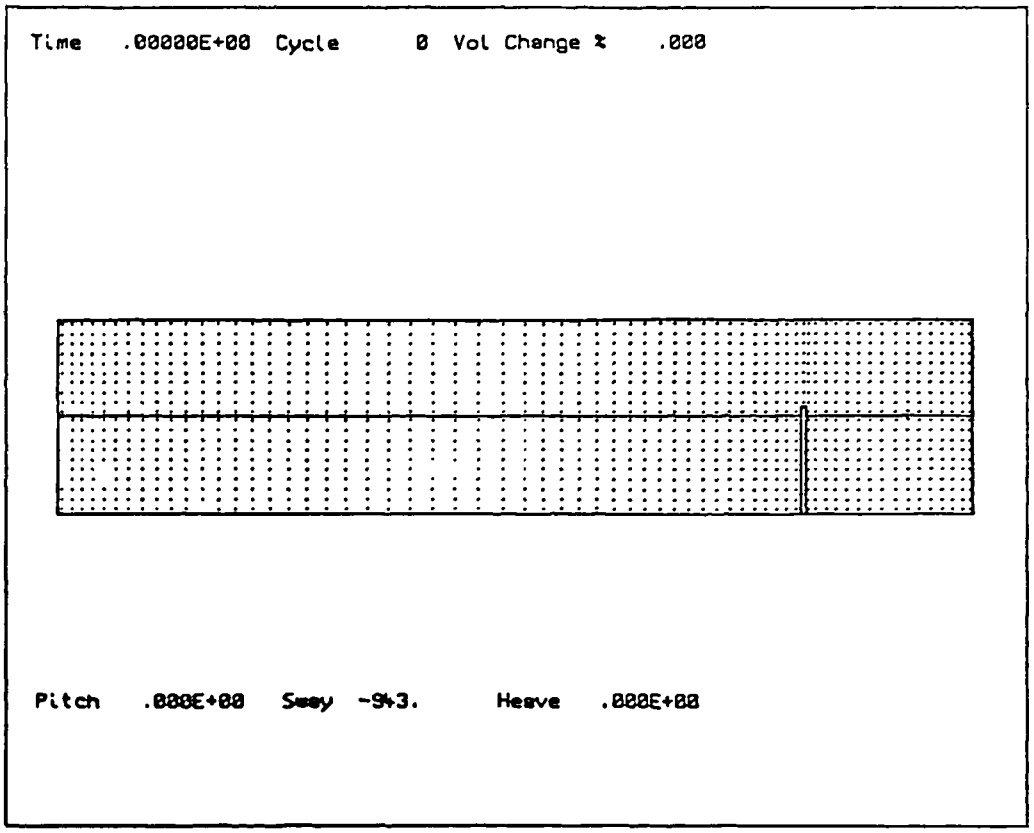

Figure 4.6c: Example of velocity vector plot for a rectangular vessel filled with oil and water. Profile plot at time 0 seconds.

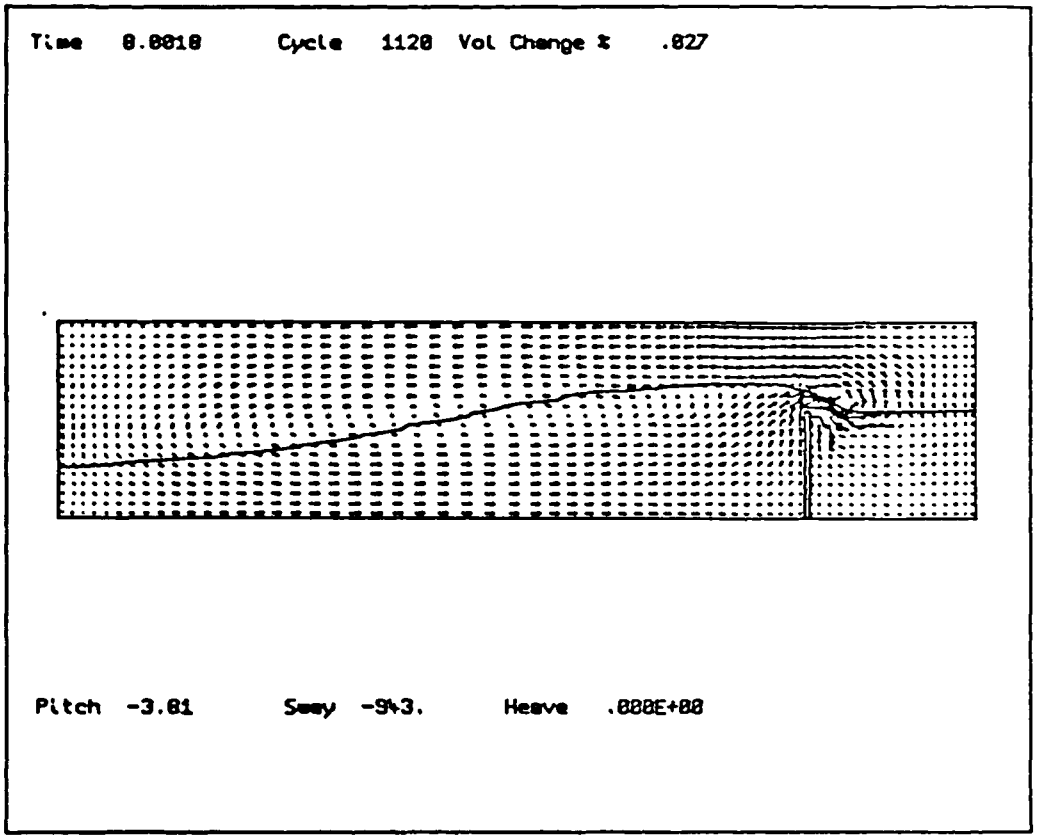

Figure 4.6d: Example of velocity vector plot for a rectangular vessel filled with oil and water. Profile plot at time 8 seconds.

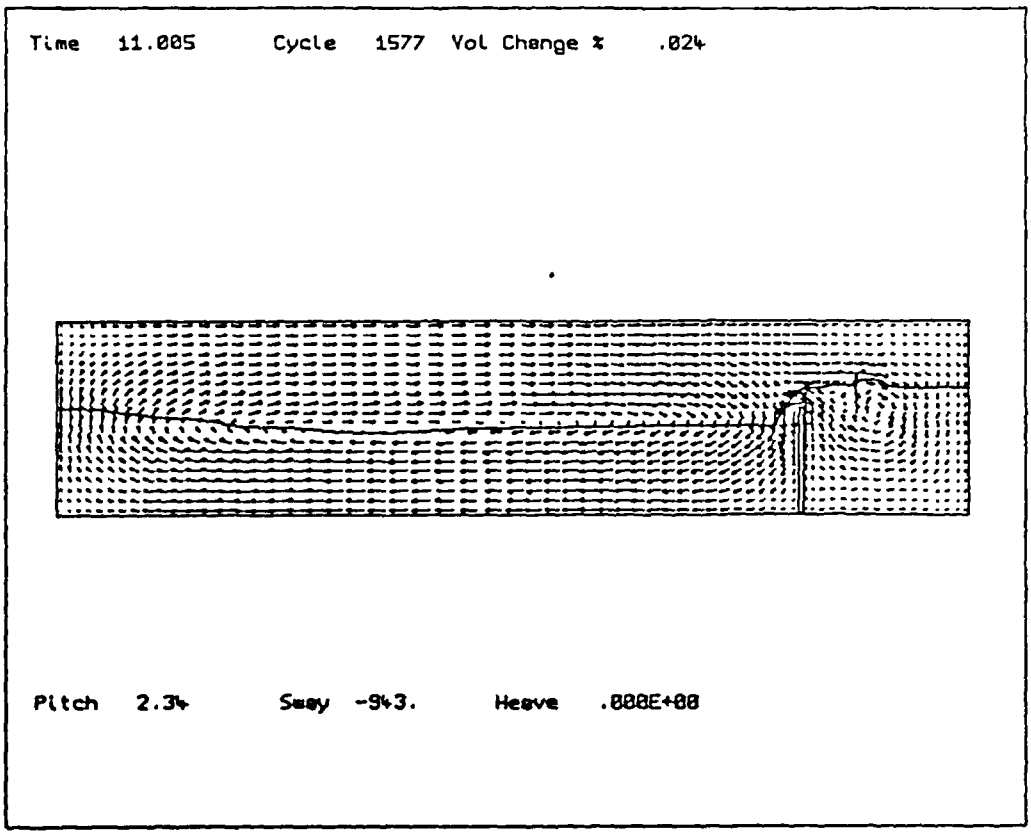

Figure 4.6e: Example of velocity vector plot for a rectangular vessel filled with oil and water. Profile plot at time 11 seconds.

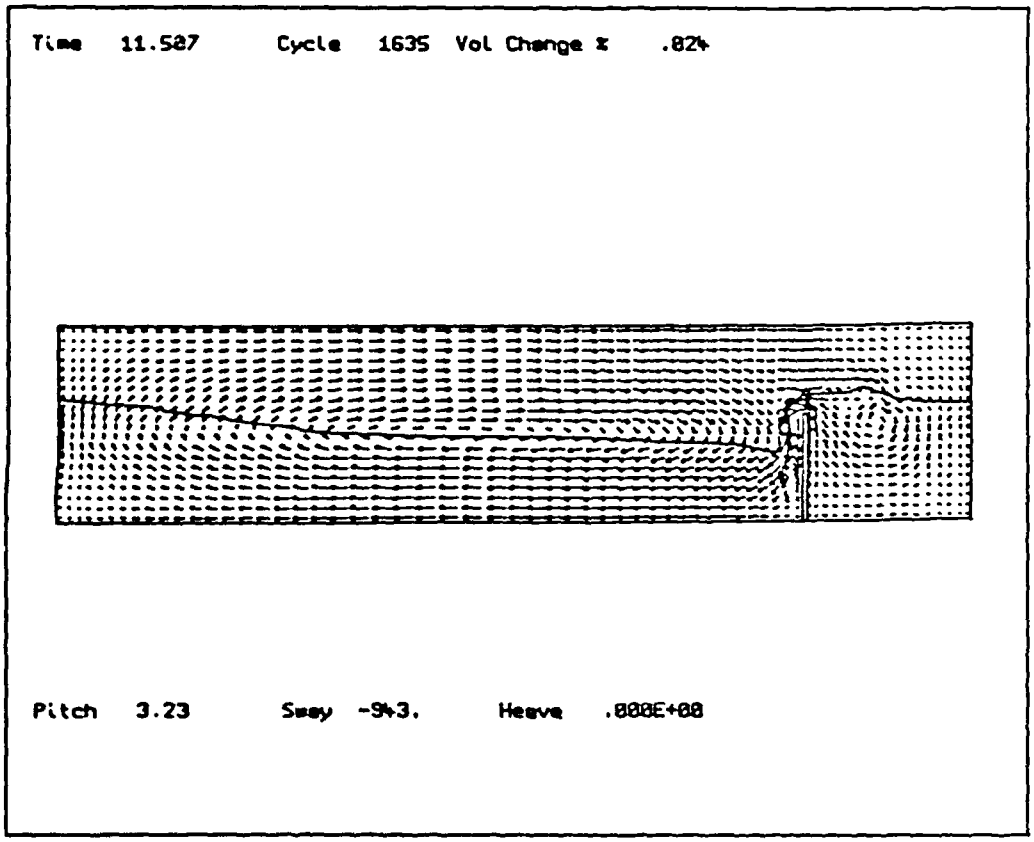

Figure 4.6f: Example of velocity vector plot for a rectangular vessel filled with oil and water. Profile plot at time 11.5 seconds.

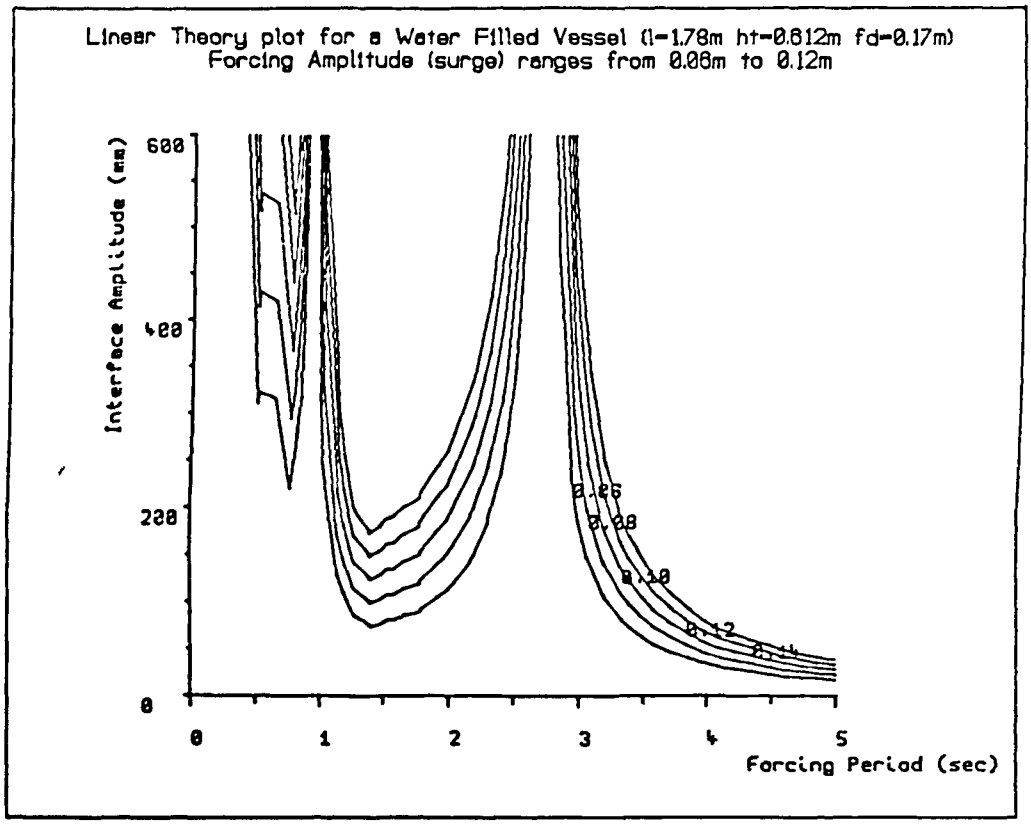

Graph 4.1: Linear theory prediction of interface amplitude for a rectangular vessel with fluid to a depth of 0.17m subject to surge forcing motion at different periods and amplitudes.

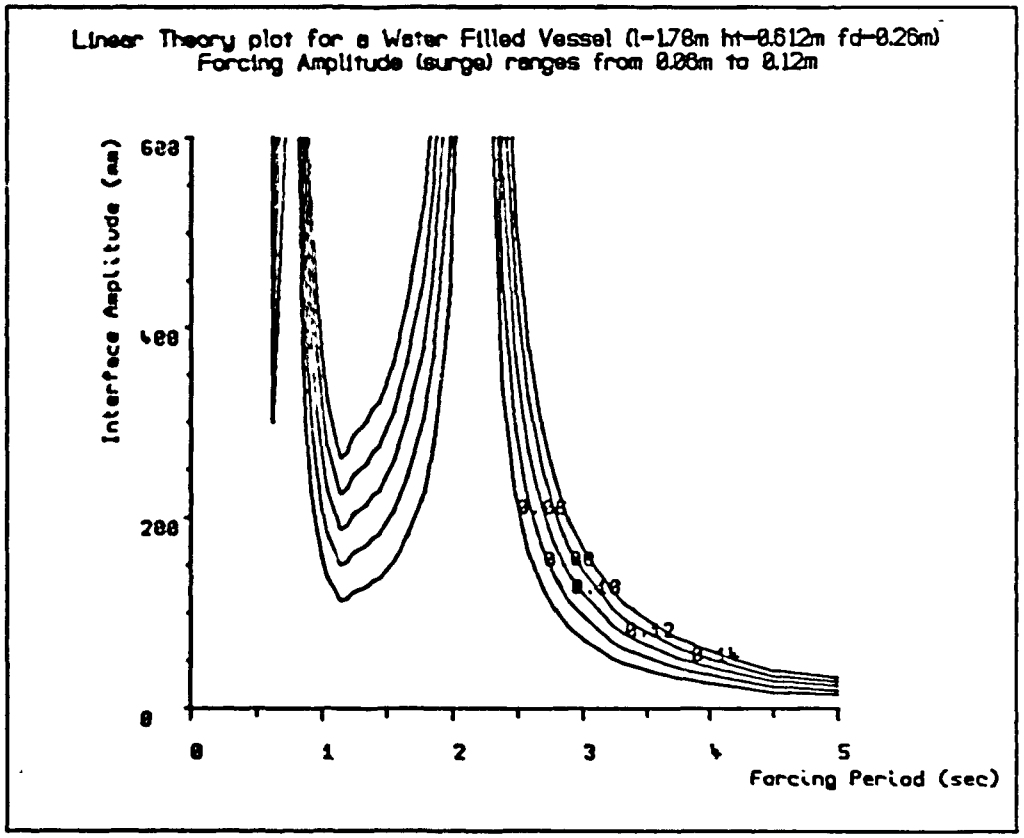

Graph 4.2: Linear theory prediction of interface amplitude for a rectangular vessel with fluid to a depth of 0.26m subject to surge forcing motion at different periods and amplitudes.

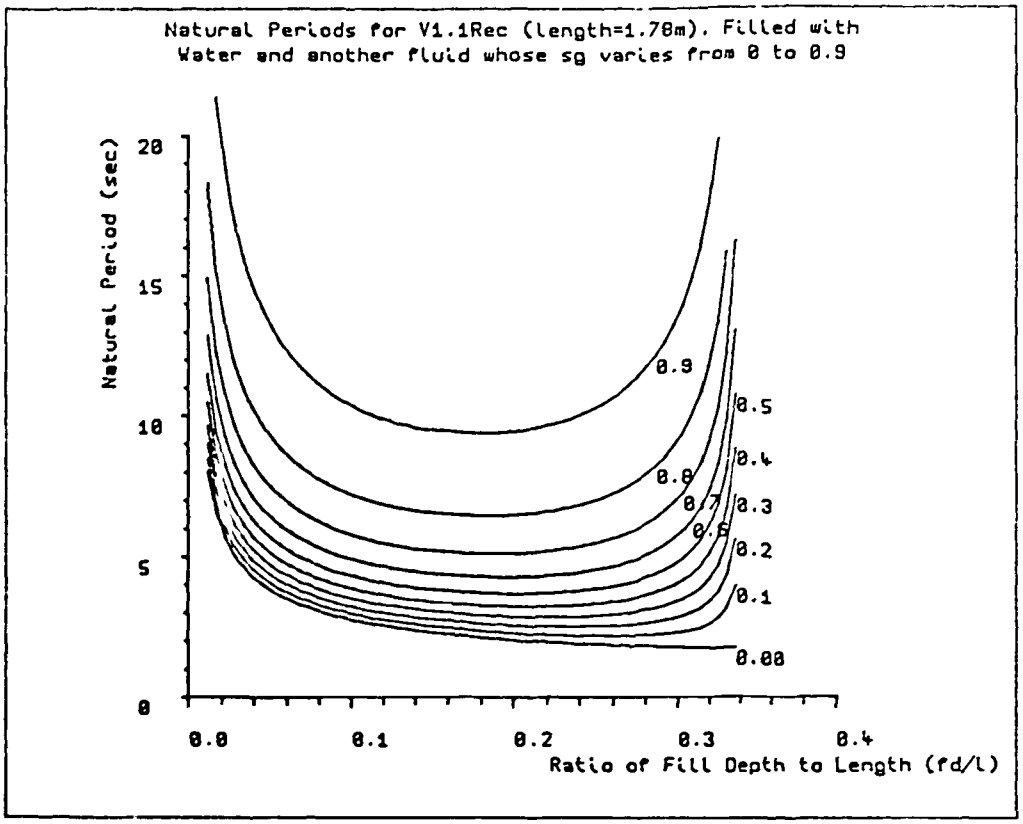

Graph 4.3: Predicted natural periods of a twin fluid system in a rectangular vessel of length 1.78m as a function of upper fluid density.

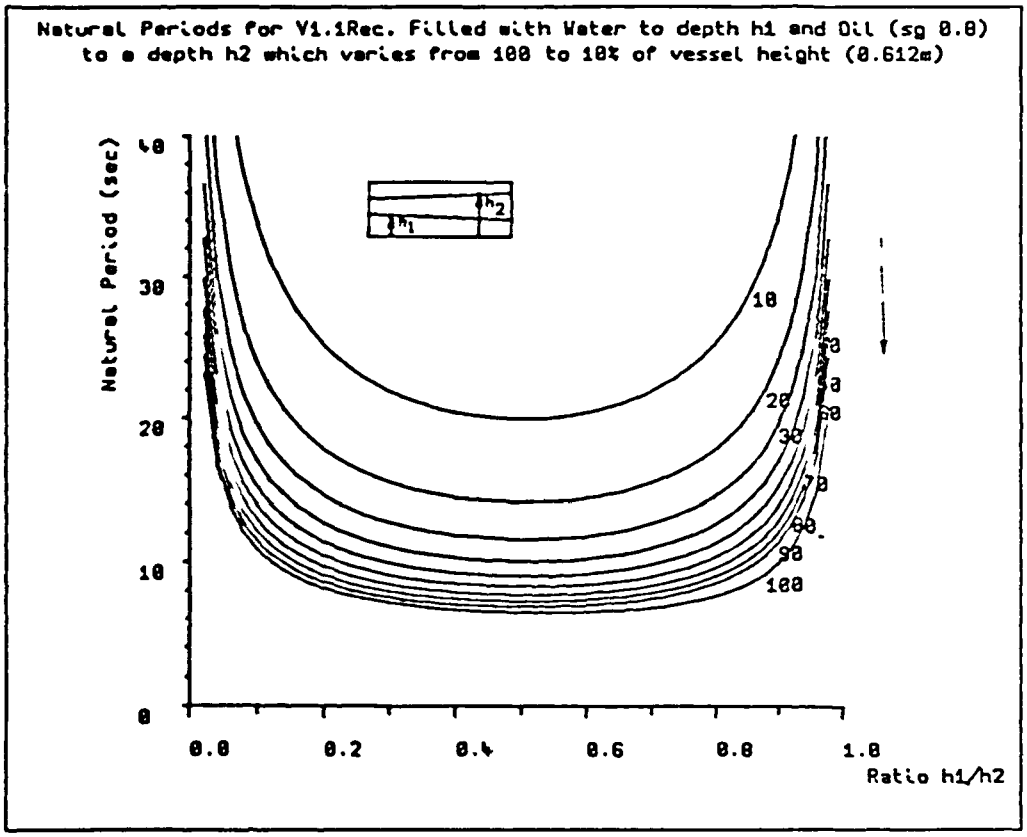

Graph 4.4: Predicted natural periods as a function of fill depth ratio, in a three fluid system for a rectangular vessel where middle fluid is of sg 0.8.

CHAPTER 5.

THE MOTION SIMULATOR & CONTROL SYSTEM.

5.1 INTRODUCTION.

Prior to the start of this project, the motion simulator had been constructed and was undergoing testing. This simulator was designed to subject test vessels to three forcing motions. Initially, the control system used three signal generators to specify the forcing motion. The initial objective of this project was to design and commission a computer based control and data logging system for the motion simulator.

Powered by hydraulics, the motion simulator is controlled from two microcomputers, one acting as the *motion controller*, the other the *data logger*. A protocol was devised for the data logger to communicate with the motion controller and to store experimental data in a reliable form. This same protocol was then used for a data processing system. The computer software, for both motion controller and data logger, has been continually modified to improve both reliability and safety of the simulator system.

This chapter provides details on the design of the motion simulator, computer based control system and the data logging system. During the following discussions, reference will be made to previous motion control and data logging systems.

5.2 DESIGN OF THE MOTION SIMULATOR.

5.2.1 Mechanical Design.

The motion simulator, referred to as the *Wave Motion Simulator* (WMS), consists of a table mounted on a trolley via a universal joint which, in turn, sits on a pair of rails (photograph 5.1). Powered by three hydraulic cylinders (photograph 5.2), three forcing motions can be generated :

1) Angular motion of the table, parallel to the rails, i.e. pitch, with limits ±10°.

2) Angular motion of the table, at 90° to the rails, i.e. roll, with limits ±10°.

3) Lateral motion of the trolley along the rails i.e. surge/sway (depending on vessel orientation), with limits ±1m.

The diagram in figure 5.1 presents simplified schematic details of the table/trolley arrangement.

Limits in forcing period were a function of the control system and the capacity of the hydraulic power unit. Mechanical vibration of the simulator and resolution accuracy in generating the forcing motion, required the forcing periods to be longer than 1 second. This minimum limit was thought to pose no difficulty in scaling motion conditions that might occur on floating production platforms.

5.2.2 The Hydraulic Power System.

With reference to the flow system diagram in figure 5.2, hydraulic oil from the power unit is split into three separate lines, each of which form the input to a servo value. Under an external control signal, these servo valves allow oil to flow from the power unit to one end of a cylinder. At the same time, oil from the cylinders other end is forced back to the power unit via a return line. Three linear potentiometers, one for each motion placed close to each cylinder, were used to feedback information on the position of each cylinder, hence the simulators position, to a central control unit.

5.2.3 Principal of Generating Motion.

The control unit referred to above, was specifically purchased to control hydraulic servo valves. Inside the unit were three control cards, one for each servo valve with associated adjustments including offsets and controller gain. Each card compares the signal from its associated potentiometer with another signal from some external source. If the two are not balanced the card sends a further signal to its servo valve allowing hydraulic oil to flow thereby causing the cylinder to move. The flow of oil is halted as soon as the potentiometer signal balances the incoming external signal.

As an example of this process, consider movement of the trolley from one end of its stroke to the other. Consider an initial external voltage of -10 Volts is applied to the surge/sway control card and the trolley remains at a position -1m from centre (figure 5.3). That is, -10 Volts corresponds to physical position of -1m. If the external signal is then changed to +10 Volts, the control card will allow the trolley to move. Since the system has been pre-scaled the trolley will stop once +1m has been reached. The time taken for this operation is a function of the control card's internal settings. Now instead of a step change, suppose the external signal is sinusoidal with amplitude 10 volts (i.e. varying between -10 and +10) with period 10 seconds. The control card will then respond by moving the simulator in the same sinusoidal manner from -1m to +1m with a period 10 seconds.

5.3 THE PREVIOUS CONTROL AND DATA LOGGING SYSTEM.

5.3.1 Generation of Motion.

Generation of sinusoidal motion relies on the application of a sinusoidal signal, to the hydraulic control box. The obvious source of such signals was therefore a signal generator providing a variety of

amplitudes and periods of various wave forms (e.g. sine, cosine, sawtooth). With three independent signal generators it was possible to generate a wide range of combined pitch, roll and surge motions.

Several disadvantages of the signal generator system became apparent :

1) Motions were not linked together so that the phase difference between each would pose problems in performing experiments with two or three degrees of freedom e.g. combined pitch and roll motion.

2) Exact positioning of the simulator could not be achieved with signal generators. This was important from a safety point of view.

It was for these reasons that a computer based system was designed.

5.3.2 Previous Non-Computer Based Data Logging System.

Studies with a small simulator in previous work (80), measured the depth of water at various positions in a cylindrical vessel using conductive type level probes. Several probes were multiplexed into one meter using a rotary switch system and results recorded on a UV chart recorder. This method had several drawbacks :

1) Chart recorder paper deteriorated in the presence of sunlight.

2) Identification of probes used was difficult in some cases where the switch system combined probe signals. This resulted in distorted UV traces which were difficult to analyze.

3) Analysis of the data from such recordings was time consuming.

For this project, using the same conductive probes, a computer based data logging system was devised.

5.3.3 Development of Previous Computer Based Control and Data Logging Systems.

The problem of motion generator/controller was solved using a microcomputer linked to a digital to analogue convertor. Although the operating program has undergone five revisions, the current one retains most of the basic features of previous versions. On the data logging side, during testing of the motion control system the rotary switch remained in service. Following purchase of a digital multiplexer, work began on the data logging system.

To aid the operator in using both motion controller and data logging system, both systems were combined into essentially one unit using the two computers. As a further aid, all operating programs were programed into the firmware of the microcomputer. That is, the code currently resides in ROM (Read Only Memory) and is active as soon as the control system is powered on.

5.4 THE MOTION CONTROL SYSTEM.

5.4.1 Overview of System.

The motion controller consists of an ACORN ATOM microcomputer fitted with a four channel, 8 bit digital to analogue (D/A) convertor. Each D/A channel scales a number between 0 and 255 to a specific voltage. This voltage is sent to the hydraulic control box and hence converts the number to a physical simulator position (figure 5.4). For example, a number of 0 on the pitch channel places the table at an angle of -10° while 255 places it at +10°. The fourth channel was provided for expansion and is currently used in turning the hydraulic pump unit on and off line.

To generate a sinusoidal voltage on any channel, the following equation can be applied :

Channel Value = Amplitude*SIN(Frequency*Time+Phase)

+ Offset ... 5.1

Where the channel value varies between 0 to 255.

This "value" is then sent to one of the D/A channels causing the simulator to move to the corresponding physical position. The offset was required as a horizontal positioning device, to take account of any physical inaccuracies in positioning of a test vessel on the simulator table. This introduces the concept of a *default center*. A calibration procedure had to be carried out to convert the computers digital numbers to an actual physical simulator positions.

5.4.2 Computer Generation of Sinusoidal Motion.

With Acorn ATOM BASIC, the interpretation of equation 5.1 was found to be too slow, putting a severe restriction on the lowest forcing period possible. To overcome this, assembly code (6502) was written to generate a machine code program to be used in conjunction with a BASIC program. While the machine code provided control of simulator motion, the BASIC section allowed for easier input of periods and amplitudes. A listing of all simulator programs is presented in material external to this report.

Evaluating the sine function within assembly language could be performed in two ways. The first method was to use the computers own floating point calculation routines. However, it was again thought that this would be too slow to facilitate short forcing periods. The second method was to use a *look-up-table* whose values for one complete cycle, evaluated prior to the start of motion.

Using the BASIC program, an individual 800 point look-up-table was generated for each forcing motion. Amplitude limits were dictated by the required motion amplitude. Stepping through the table within a delay counter loop and outputting the value to the simulator, the forcing motion

was generated according to equation 5.1. At the end of the table, a jump was made back to the start and the whole cycle repeats itself (figure 5.5)

For each forcing motion, the user then supplied the amplitude, offsets and period. These where then used to calculate three sine tables, and the values of each delay counter. As with amplitude conversion values, the value of the delay counter had to be calibrated for motion periods. The phase value entered by the user was simply converted to a starting position in the look-up-table.

A convention was set up to distinguish between the computer values (0 to 255) and vessel physical positions (±10°, ±1m) (see figure 5.3).

5.4.3 Resolution and Accuracy of Motion.

The reproduction of sinusoidal motion in relation to period and amplitude was governed by the use of 8 bit D/A conversion and the response time of the hydraulic control unit. In relation to amplitude, the computer system was capable of resolving to 0.08° and 0.008m (that is 20°/255 and 2m/255). Therefore, by virtue of the physical distance travelled, pitch/roll resolution is higher than that of surge/sway.

The resolution of period was governed by the delay counter loop used to output signals to the simulator. This has been estimated to be approximately 0.2 seconds. However when entering period values to the computer system, the correct motion period would be displayed on computer monitor. A finer resolution than the 0.2 seconds would require either program re-coding or a computer upgrade.

Although amplitude resolutions are quoted above, during initial testing at short forcing periods (less than 2 seconds), a degradation was observed in the amplitude of the motions. In effect, the response time of the hydraulic control unit began to infringe on the requested motion amplitude. In experiments which will be referred to in later chapters,

this effect of short forcing periods on large motion amplitude did not cause difficulties. The motion conditions selected for the various experiments performed during this project, accounted for this degradation effect.

5.4.4 Basic Operating Procedure for the Motion Control Program.

All initial versions of the motion control program were similar in layout :

1) Set the default centre: Before power was applied to the hydraulic unit, a default centre had to be specified. This value was used to relate the horizontal position of a test vessel to the simulator. It was envisaged that construction methods could introduce positioning errors in placing a test vessel onto the simulator table. The default centre was then used to locate the exact centre of such vessels.

2) Enter Run Information: All conditions were entered for each motion required (e.g. period, amplitude and phase angle). If any motion was not required then its amplitude would be set to zero.

3) Calculation of Run Table: From the motion conditions, the computer would calculate the three look-up-tables, based currently on a sine function.

4) Performing a Forcing Experiment: The program waits till the operator is ready before starting a run. The length of each run would be dictated by the user. After a run had finished, it was decided to leave the simulator in one position until the user was ready.

5) Move to Default Centre: When finished, the computer would move the simulator to its default centre.

With the advent of a second microcomputer for the data logging side, it was considered prudent to have all user input through one computer. This would avoid confusion between programs and ensure that the data logging system would be closely linked to the motion controller. Therefore, although the above instruction list was adhered to, all requests for a user response came via the data logging computer.

5.5 THE DATA LOGGING SYSTEM.

5.5.1 Quantity to Measure.

One of the major concerns in previous sloshing studies, has been the production of large impact pressures on container walls, as a result impacting slosh induced waves. Pressure transducers were then employed to record such impacts. As the ultimate aim of this project was to study the effect of induced motion on oil/water systems, a means of recording the oil/water interface had to be found. As will be explained later, this has posed some problems. For air/water studies, used to gain an appreciation of sloshing effects (chapter 6), a simple conductivity method was already in use by the department to record the air/water interface profile inside a test vessel.

5.5.2 Application of a Multiplexer.

As stated in previous sections, prior to the start of this project a system of conductivity probes were used to record the water depth during sloshing experiments. Although details of this technique will be described later (chapter 6), it is sufficient to state that several of these *Wave Probes* were linked to one conductivity meter. Only one meter was used for several reasons :

1) It was thought that two meters connected to two separate wave

probes would cause interference between probes. This was observed in practice.

2) The cost of a system using multiple meters would have been prohibitive.

This required a data logging system to :

1) Switch one probe into the meter.

2) Record the conductivity reading by chart recorder.

3) Switch to the next probe in the sequence and repeat step 2.

The disadvantages of the rotary switch system developed for this application have already been outlined. As a result, a digital multiplexer was purchased which allowed any one of 16 wave probes to be switched to one meter under the control of a microcomputer.

During the design of the data logging system, consideration was given to the response time of both the meter and multiplexer switching.

5.5.3 Description of the Data Logging Program.

The standard memory inside an Acorn ATOM did not allow for the data logger to be combined with the motion control program. In fact such a program would have been too slow in operation. A second ACORN ATOM was therefore used as the data logger, designed to take data from the waves probes and to store that data along with simulator position on tape.

As well as the direct connection to the multiplexer, this computer was fitted with a 16 channel 8 bit analogue to digital (A/D) convertor. The A/D convertor was used to take external voltage readings from the three linear potentiometers, used in the control of the simulator, and a fourth input from the conductivity meter used for the wave probes. The

conductivity meter had in turn, its input supplied by the multiplexer. Figure 5.6 provides details of this system.

5.5.4 Resolution of the Recorded Data.

Resolution of wave data was then a function of the multiplexer switching rate, A/D settling time and tape storage rate. Of these, the *tape baud rate* (operating at a standard speed of 300 bits per second) was found to be the major factor. By careful design, the delay in storing a single byte of tape information was used to provide the A/D conversion time thus achieving maximum efficiency from the system. However, at some short forcing periods, such as 2 seconds, it was found that even this baud rate required continual output from one probe for sufficient resolution. Via additional code, the computers standard baud rate of 300 bits per second was increased to 1200 bits per second. Thus, a four fold increase in data collection rate was achieved, together with a four fold increase in the size of stored data file.

In relation to the conductivity meter, experiments were carried out with delay loops of differing sizes to determine if the meter could cope with switching multiple probes. That is, several probes were linked to the computer under static (no motion) conditions. The value of the delay loop was then adjusted until the A/D convertor gave a stable reading for every probe. It was found that use of a small timing delay loop and the tape storage loop provided sufficient time for both conductivity response and A/D conversion.

With the increase of tape baud rate to 1200, it was found preferable to transfer wave data directly to the hard disk on a Acorn Cambridge Work Station (ACW) as it was collected. This not only saved time, but reduced the error in tape to disk transfer. This microcomputer

was then used to process data from experiments. The data processing system will be described in the next chapter.

5.5.5 Communication Between Computers.

The communication system between motion controller and data logger, centres on the use of one 8 bit parallel communication port built into each computer. In the current program versions, a form of serial communication has been achieved, allowing data to be sent from either computer to the other. All appropriate handshaking routines were placed in subroutines to allow future expansion.

To allow identification of all runs and check the data sent between computers, it was decided to employ a *header data block* system. With these header blocks, the data logging system would send run information obtained from the user, to the motion control system. The motion controller would then check certain information contained in the data block for errors. If an error occurred, then the system would inform the user to take appropriate action. The format of header blocks and structure of the raw data files are presented in Appendix II.

5.6 SAFETY CONSIDERATIONS.

5.6.1 General Considerations.

Using a hydraulic operated machine required some thought to the interaction of the operator with the computer and simulator. Physical barriers between the simulator area and the rest of the laboratory catered for the safety of other personnel not involved with the project.

5.6.2 Experimental Procedure.

With regards to the experimental procedure, the motion controller was allowed to store 18 separate run conditions with each run lasting a

specified time. Some sort of convention had also to be adhered to, as to what position a test vessel would be in at the end of each run. It was decided to leave the test vessel in its *stopped position* until the user requested another run. Then and only then, would the motion controller return the vessel to its default center. Although the control system could be made fully automatic, performing up to 18 consecutive experiments with data logging, it was considered prudent to involve the operator at the end of each run. This forced operator presence and involvement with the simulator at all stages, and hence increase overall safety of the system.

5.6.3 Personnel Safety Considerations.

Since visual as well as quantitative experimental results were required, there was a necessity for close machine and operator contact (e.g. removal of physical barriers for video camera viewing). Some method was therefore required to halt the forcing motion sequence and shut down the hydraulic unit, in the advent of any operator or equipment failure which would endanger the operator.

Although the hydraulic pump was fitted with an emergency stop, it was discovered that during a forcing test, as soon as the stop button was activated, sufficient hydraulic pressure remained in the system, to allow the simulator to move for a short time. Following this, it was observed that although the surge/sway motion ceased, the simulator table was susceptible to tilting over (to $\pm$ 10°). A person could then be trapped under the simulator table and remain trapped until the computer could be programed to move the table away. Determining the exact position the simulator stopped at would posed a further complication.

To avoid this potentially dangerous scenario, it was decided to stop the actual forcing motion itself before activating the simulator emergency stop. To this end, a remote emergency stop system was designed

around the computers *Non Maskable Interrupt* lines (NMI). When an NMI interrupt is received by the computer, it immediately starts another program. This program was designed to abort any motion run with the result of leaving the simulator in a known fixed position. The user was then given several options :

1) Completely reset the system by putting the hydraulics on *stand-bye*. This means that hydraulic power to the simulator is removed and the table allowed to fall to some unspecified position.

2) Move the simulator to its default centre thereby placing the system in a known controlled state.

3) Restating a motion run if the system was interrupted during one. This prevents breaking an experimental sequence.

4) Moving the simulator to any position in a controlled safe manner. This, for example, would allow the simulator to be moved away from a trapped person.

Another source of equipment failure was determined to be the signal lines from the computers or the signals from the simulator trolley/table, to the central control box. If one of these lines broke, then it is possible for the control box to move the test trolley/table to an end limit, almost instantaneously and without warning. At this time, no solution has been derived for such a failure. Possible solutions have been suggested from discussions with departmental advisors :

1) Placing current limits on the hydraulic pump. It was noted that moving the simulator from one extremity to another tended to increase the amount of current drawn by the power unit. Therefore, it has been suggested that some sort of measuring system could be introduced to detect a sudden surge in current and shut down the unit.

2) Upgrading of signal cables. Cable flexing may result in failure of feedback signals from potentiometer to control unit. In addition to simple upgrading, some sort of automatic checking facility may be necessary to test the integrity of all important signal lines.

3) Complete removal of all personnel from the simulator area. This policy has been adopted by enclosing the simulator with physical barriers. However due to the nature of some research work, access to this area has to be allowed in some cases.

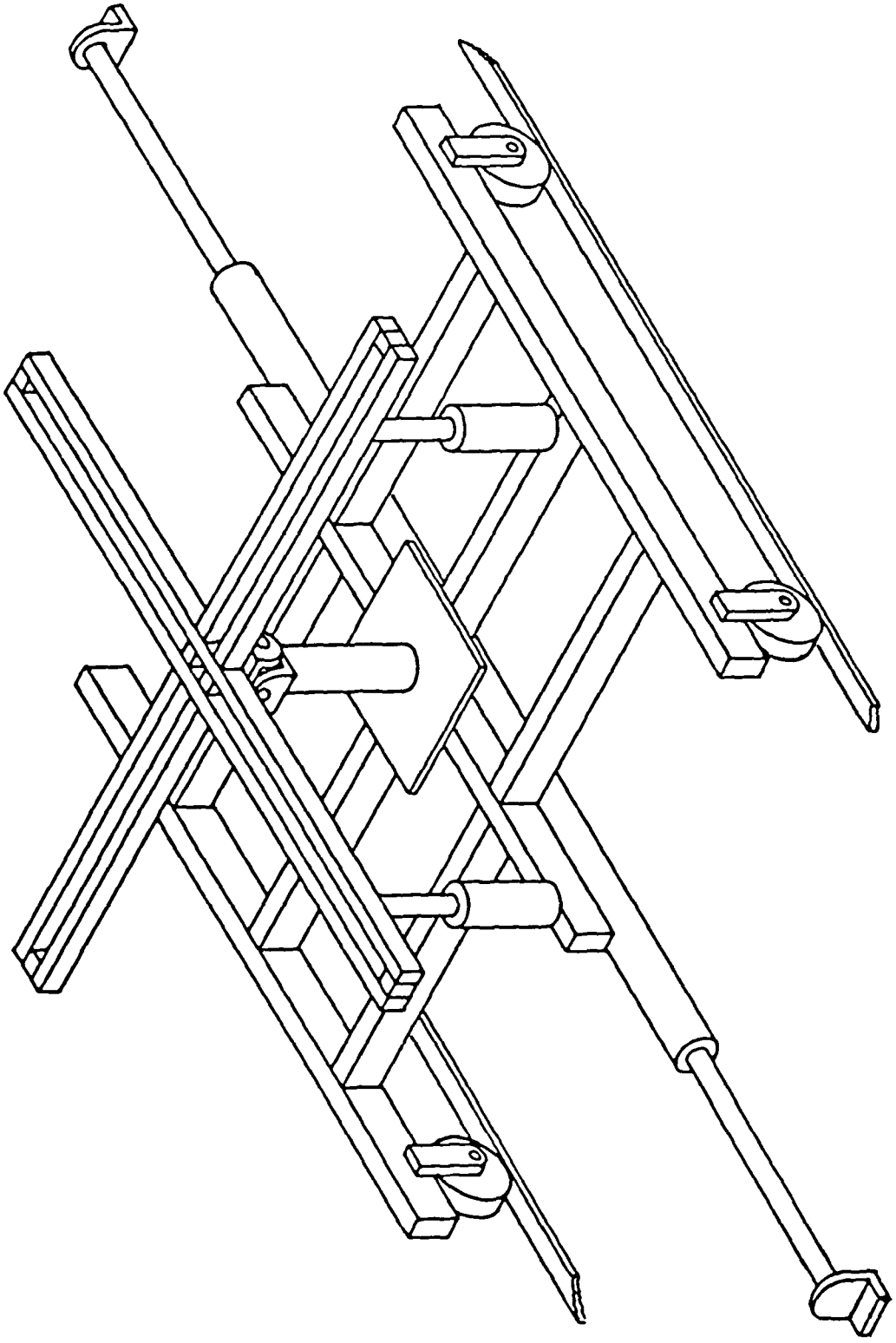

Figure 5.1: Details of the motion simulator table and trolley.

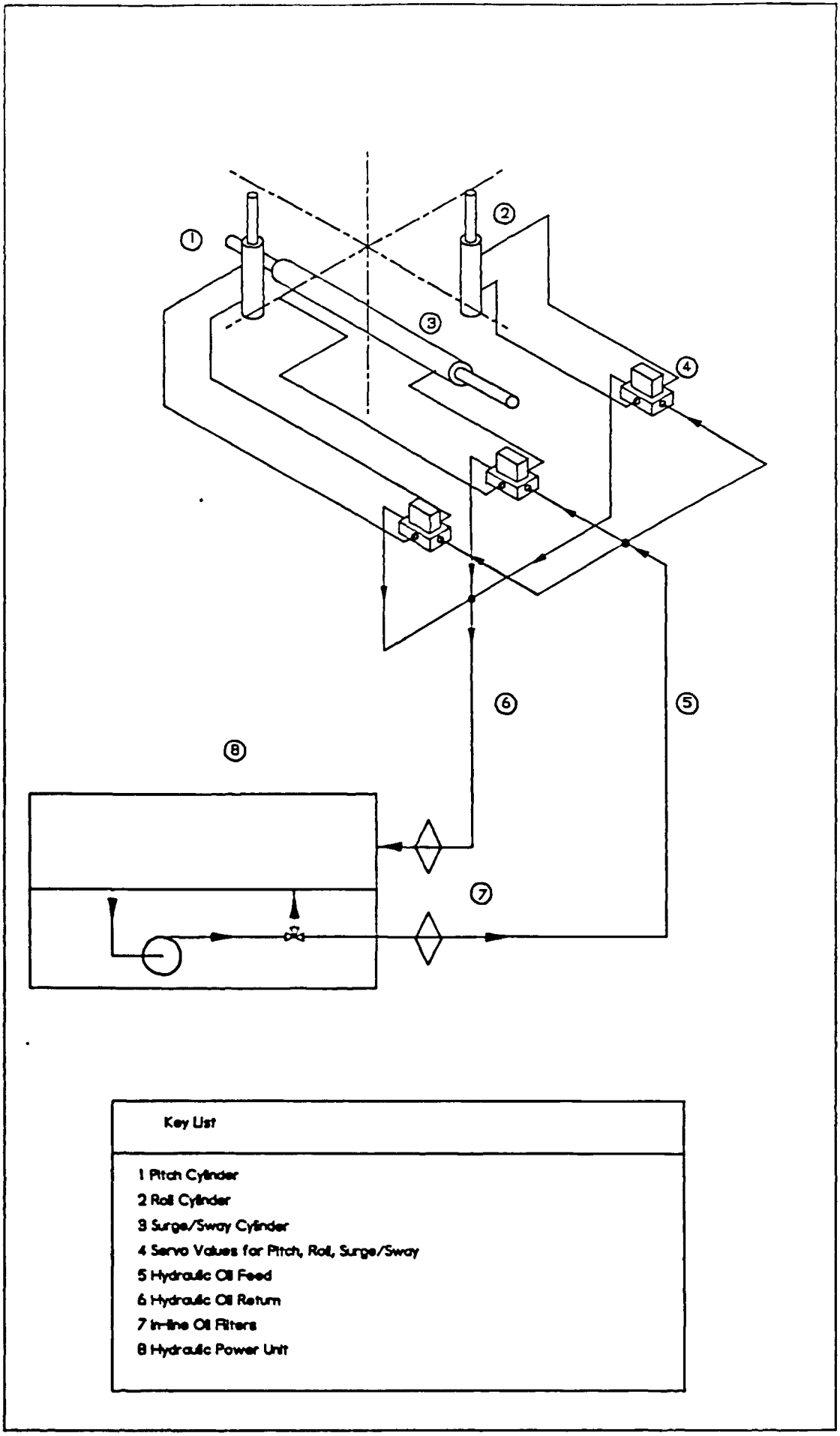

Figure 5.2: The hydraulic circuit from pump to cylinders.

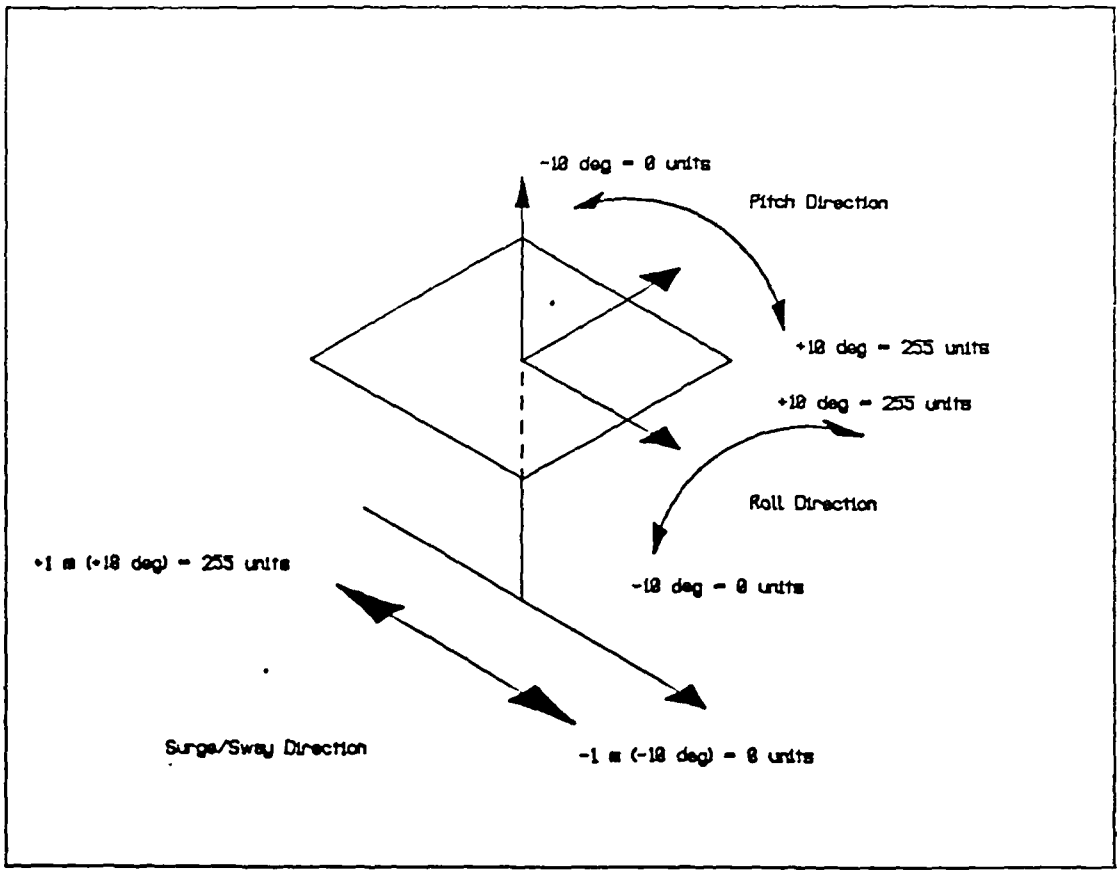

Figure 5.3: Angle conventions relating computer values (0-255) to physical angles and positions.

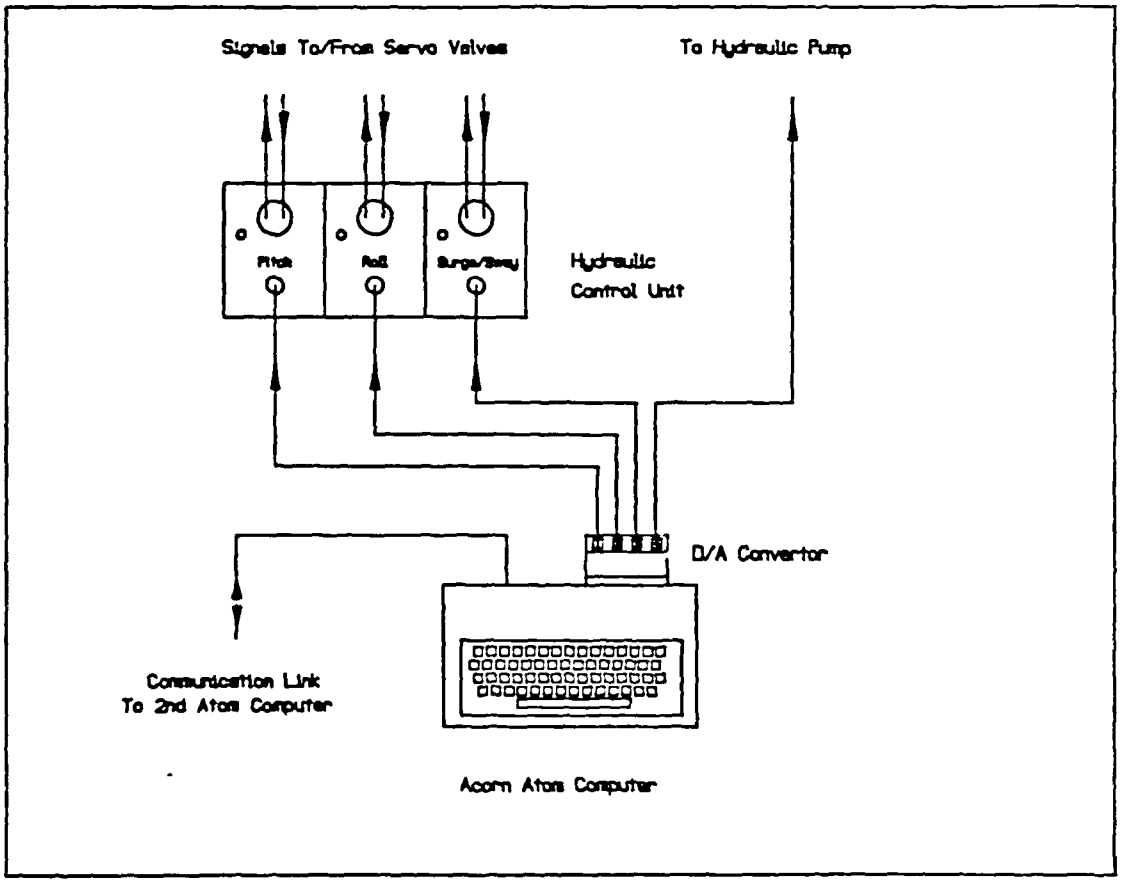

Figure 5.4: Simplified block diagram of the motion controller for the simulator.

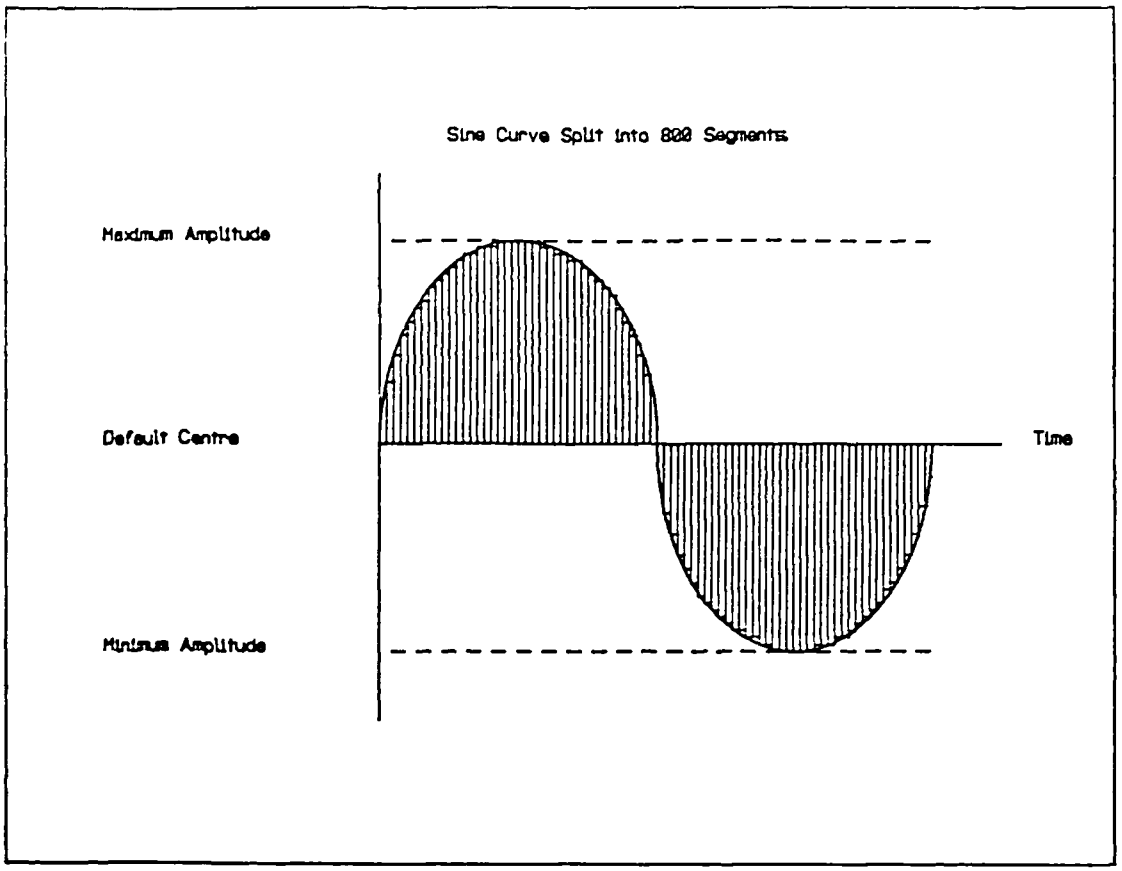

Figure 5.5: Representation of a sine wave used to generate sinusoidal motion from within a machine code program.

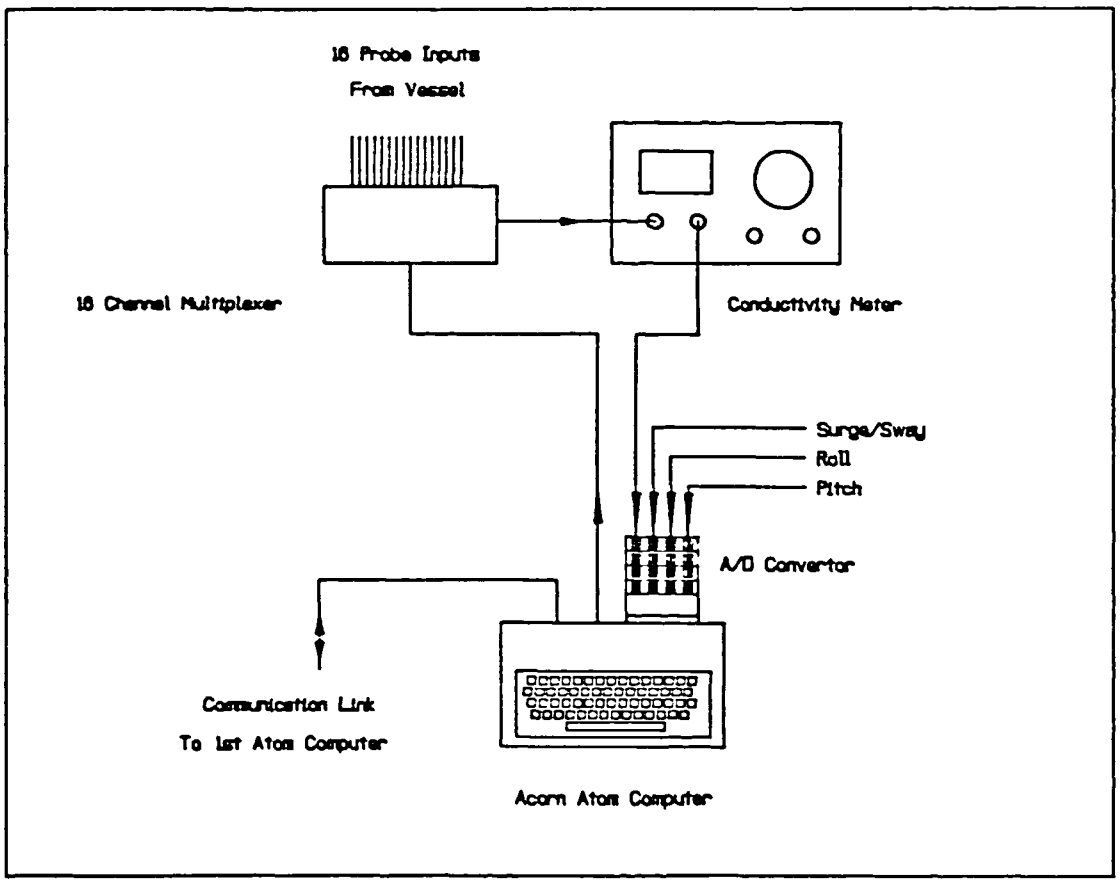

Figure 5.6: Block diagram of the data logging system designed to record interface profiles during sloshing experiments.

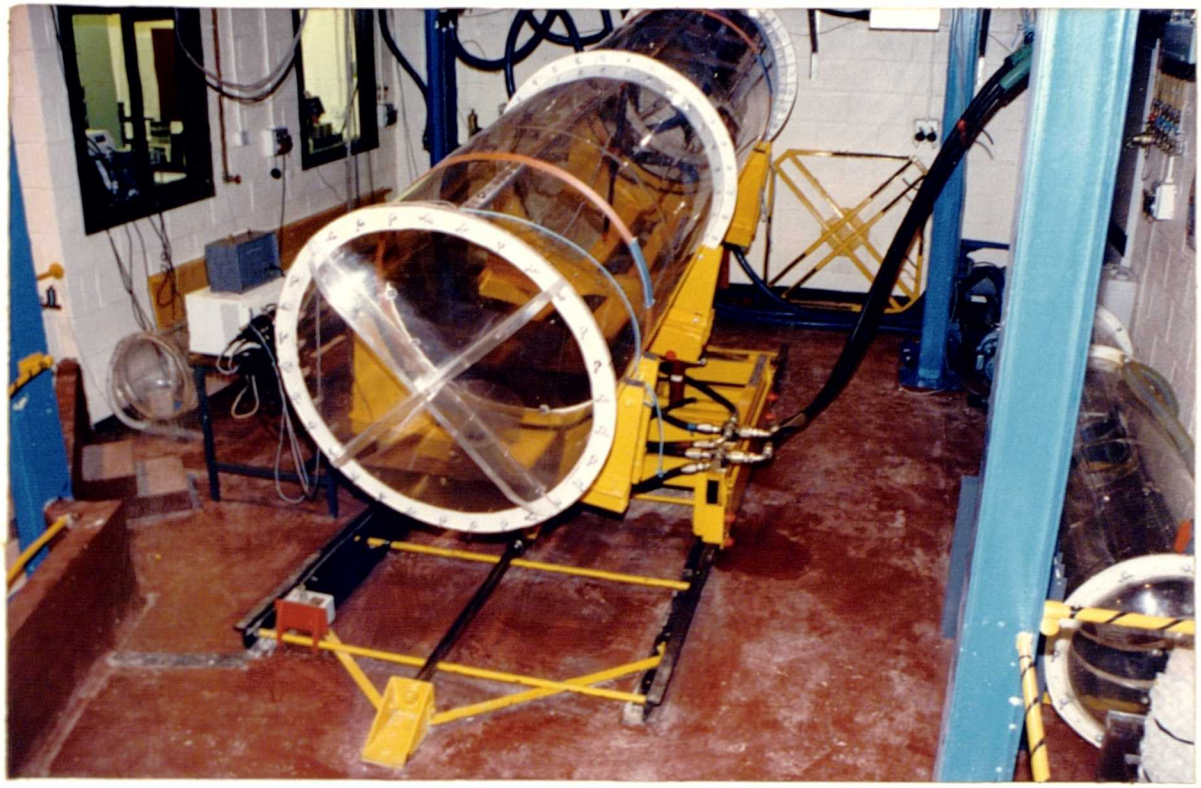

Photograph 5.1: The Motion Simulator showing trolley and table arrangement.

Photograph 5.2: The three hydraulic cylinders proving movement of trolley and table.

CHAPTER 6

TEST VESSELS, INTERFACE MEASUREMENT AND DATA LOGGING/PROCESSING SYSTEMS.

6.1 INTRODUCTION.

During this project, the effects of forcing motion on air/water and air/oil/water interfaces were measured in two rectangular tanks of size ratio 2:1. It was intended to relate the results from these experiments to non-segregated oil/water storage tanks and offshore separators. In addition, to study the effects of vessel internals on interface behaviour, a series of baffles were designed for use in the large rectangular vessel. Preliminary experiments were conducted with air and water to gain an appreciation of the effects of forcing motion.

This chapter provides details of the computer based data logging and processing system designed for air/water experiments. Experimental procedures are presented for *wave probe* calibration and data logging. In addition, procedures are presented for detection and analysis of oil/water interface profiles.

6.2 DETAILS OF TEST VESSELS USED AND INTERNALS.

6.2.1 Rectangular Vessels.

Two rectangular vessels of size ratio 2:1 were made available for this project. For viewing the various wave forms which occur in sloshing, both vessels were constructed from transparent *Acrylic*. Referred to in this report as the *small and large rectangular vessels*, their physical dimensions are shown in figures 6.1 & 6.2. Both vessels were positioned such that their mid-points coincided with the simulators pivot point and supported to provide a uninterrupted length wise view. In addition, the small rectangular vessel was mounted on an adjustable frame allowing the

vessel to be positioned at two different heights from the simulators pivot point (figure 6.3).

6.2.2 Application of Rectangular Vessels in Relation to Offshore Equipment.

While easier to model from a theoretical aspect, the use of rectangular vessels may appear to limit the practical application of experimental results to offshore process equipment. In addition consideration must be given to the scale factors involved between the model and physical vessels.

In relation to offshore primary separators which are essentially horizontal cylinders, the use of rectangular vessels might seem limiting. However, it was hoped that the range of experiments planned would provide basic information of the effect of induced motion on oil/water and gas/oil interfaces. From departmental activities, it was known that offshore separators could be of length 9m, diameter 2m and larger. Therefore a scale factor of approximately 5:1 and upwards, would exist between the large rectangular vessel and primary separators.

In relation to non-segregated oil/water storage systems, exact construction details of such vessels would vary with the floating production system but are likely to contain near rectangular section elements.

6.2.3 Design of Internals used in Experiments.

As mentioned in previous chapters (chapter 2), reduction of sloshing effects can be achieved through the use of baffles. Such baffles usually consist of vertical perforated plates positioned at various points inside a vessel. Although such baffles are likely to reduce gas/liquid sloshing, in oil/water separation equipment reference has been made to

possible detrimental effects of such devices (12). To investigate the effect of baffles on the oil/water interface, several baffle designs were considered for use in the large rectangular vessel. Physical details of all baffles are presented in figure 6.4.

Each baffle was inserted into the large rectangular vessel through a slit in the vessel's roof (figure 6.1) and secured. This allowed the baffle to be positioned so that its base would rest at specific distances from the vessels base. The range of baffles included :

1) Solid Plate Baffle: This consisted of a solid plate made from acrylic.

2) Two perforated Baffles: The first one with 22% free area with a square pitch, constructed from acrylic and the second with 53% free area with a triangular pitch, constructed from *PVC.*

3) Interfacial Strips: Following experiments with the solid plate baffle, two interfacial baffles were constructed. Each consisted of a strip of PVC of different heights and again positioned on the air/water or oil/water interface.

6.2.4 Determination of Default Centres for Each Vessel.

As mentioned in the previous chapter, allowance was made for a default centre in the simulator operating programs. When any vessel had to be removed and then replaced on the simulator table, a new default centre was calculated. The procedure adopted followed :

1) Filling the vessel to a certain depth with water.

2) Recording the depth of water at each corner.

3) Moving the simulator table by fractions of a degree in both pitch and roll until the depth at all corners became equal.

6.3 OVERVIEW OF EXPERIMENTS AND OF TEST FLUIDS USED.

6.3.1 Range of Experiments.

The experimental programme was divided into three section. Firstly, experiments were required to evaluate the performance of the data logging/simulator system. Secondly, to gain an appreciation of the fundamentals of fluid sloshing, extensive experiments with air/water were carried out using both rectangular vessels at various forcing conditions. The third section related to the effect of forcing motion on an air/oil/water interface.

All experiments were carried out at room conditions with air, mains water and various oils.

6.3.2 Physical Properties of Oils used.

Preliminary trials with *Forties* crude oil posed several problems :

1) Crude oil had a tendency to adhere to the sides of the vessels resulting in a loss of vision of the oil/water interface.

2) Physical properties and composition of crude oils vary from field to field.

For these reasons, it was decided to use two refined oils of known physical properties :

1) Kerosene, supplied as a colourless liquid in 45 gallon drums.

2) Gas oil, supplied as a red liquid in 45 gallon drums and by bulk tanker.

To provide a range of oils with differing densities but with the same viscosity and composition, the fluorocarbon 112 Trichlorotrifluoroethane was used to increase the density of the pure kerosene. This gave two *pseudo* oils labeled FK851 and FK890, where the

numbers identify the density of each oil. To distinguish between the "kerosene" oils and to assist viewing the oil/water interface, waxoline dye (supplied by ICI Grangemouth) was added.

The physical properties of all oils used are shown in table 6.1.

6.4 EXPERIMENTAL TECHNIQUE FOR ALL AIR/WATER EXPERIMENTS.

6.4.1 Type of Experiments Performed with Air/Water.

The experiments performed using air/water were designed to gain an understanding of the sloshing problem, the relation between physical and theoretical effects and to gauge the effectiveness of baffles. Using the data logging system, interface profiles were recorded for different water fill depths with various forcing conditions. Results of these experiments will be described in chapters 7 and 8.

6.4.2 Measurement of the Air/Water Interface.

As mentioned in chapter 5, conductive wave probes had been used in a previous research project to detect air/water interface positions at various point inside a vessel. The following types of level detection (81) equipment were rejected :

1) Float type devices would in principle interfere with the air/water or oil/water interface.

2) Capacitative devices rely on the water acting as the other conductor from an insulated metal probe. Both the possible interference between adjacent probes and the construction of capacitative measuring equipment for multiple probes, ruled out such devices for this present project.

3) Ultrasonic devices were ruled out on similar grounds to capacitative devices.

Conductive type probes proved to be viable. These *wave probes* were constructed from basic materials without involving great expense and were adaptive to different situations. Such devices have already been applied to the measurement of ocean waves with some success (82).

6.4.3 Construction of the Conductivity based "Wave Probes".

The wave probes used here, consisted of two parallel, solid wires at a uniform spacing, insulated from each other to form part of the input circuit to a standard conductivity meter (Model P310, supplied by Portland Electronics Ltd). When such a probe is immersed in a polar liquid, the measured conductivity is a function of the immersion depth. Placing several of these probes in a test vessel, it is fairly easy to build up an image of the air/water interface profile by multiplexing all probes through a single conductivity meter.

One important consideration was the physical construction of these probes with regards to disruption of the fluid profile and meniscus effects giving positive errors on interface position.

For both rectangular vessels, 0.1mm diameter stainless wire (supplied by United Wire Ltd, Edinburgh) probes of separation 3mm, were stretched from the vessel roof to its base (figure 6.5) and held under tension by small fasteners. By keeping the wire diameter small, the wave probes could be made non-disruptive and reduce errors due to meniscus effects. The main problem with this construction was to keep the wires under tension throughout experiments and not to alter in length so as to change the physical properties of the wire.

Prior to any set of experiments, each probe would be calibrated in situ. It was hoped that such a procedure would remove any inherent errors within the measuring system (i.e. probe, connecting wires and conductivity meter).

Details of the position of probes inside both rectangular vessels are given in figures 6.6 and 6.7.

6.4.4 Wave Probe Calibration Procedure.

Before a calibration sequence could begin, the simulator operating program was used to check the connections between probes and computer :

1) The vessel was placed in its horizontal position and filled with water so that all probe wires were covered.

2) The conductivity meter *range* was then adjusted to obtain a maximum digital reading for each probe (i.e. a number of 255). This ensured maximum accuracy from all probes with a resolution of 2.4mm (=612mm/255) for the large vessel and 1.06mm (=271/255) for the small vessel.

3) Conductivity meter settings and water temperature were then noted. The vessel was then drained.

To calibrate each wave probe, the following procedure was adopted :

1) Up to 5 different water depths were selected for calibration. The last fill depth was chosen to be that used for subsequent forcing experiments. This ensured that no fresh water would enter the system, avoiding water quality problems with the calibration.

2) The vessel was then filled to the first fill depth.

3) Data logging was started, for 10 cycles with a number of pitch and roll angles, once residual waves from filling/draining had decayed.

4) Steps 2-4 were repeated for all fill depths.

The raw data stored on the ACW was then processed to calculate the best straight line fit of probe reading to water fill depth. A poor

residual of the fit would indicate either a bad connection in the probe/computer circuit, or failure of the data logging system.

6.4.5 Operating Procedure during an Experiment.

As stated in the previous chapter, up to 18 different run conditions could be selected at any one time. Prior to staring a run sequence, decisions would be taken regarding the exact run conditions, the liquid fill depth, the number and the specific sequence of probes to be used. It was envisaged that different vessels would be fitted with more than 16 probes and therefore the probe numbering system was left to the user to define.

After probe calibration, the sequence to start a run was as follows

1) The water fill depth would be checked and recorded, forcing conditions and probes to used, decided.

2) The run *header* was entered, giving run set identification (date, vessel, probes), length of run and how long to record the decaying wave profile once forcing motion had ceased. This was used as a starting base for all runs with an incrementing sequence number distinguishing between individual runs in a set.

3) Next, for each run in the set, the motion conditions for pitch, roll and surge/sway were entered together with the number of probes required for each run. The variable number of probes allowed control over wave profile resolution at different short periods.

4) The data logging system would then send appropriate information to the motion controller for the first run. The run would only start after the user was ready.

5) Data would be recorded for the duration of the run and for the decay profile. The system then waits for the user to respond before

starting the next run in the set (step 4) or terminate the data logging section.

As regards the data storage, before starting any experiments, the ACW was set running with a program which automatically stored received data in separate files. The storage of raw data was then transparent to the user. Processing of the collected data would be carried out later. No data loss occurred in communications between the data logger and the ACW once logging had begun. This testifies to the robustness of the system.

6.5 DATA PROCESSING FOR AIR/WATER EXPERIMENTAL DATA.

6.5.1 Overview of the Data Processing System.

The accumulation of large amounts of experimental data required an effective management and processing system which lent itself to changes in procedure that occurred with new tests and analysis methods. For this reason, the data file header could be manipulated in a variety of ways, not only to convey information to the user, but also specific information about the type and size of the data file. Following a set of experiments, the processing system had two tasks :

1) Calibrating the wave probes based on user supplied water depth information and by accessing the calibration data files.

2) Finding the number of data points within a forcing data file and allowing the user processing options on that data.

The data processors task when accessing a data file for the first time, was to ask the user for the actual probe connections and then to store this information, along with the number of data points, at the end of the file.

There are currently four data processing methods. Firstly a direct plot of wave height in time, secondly a numerical analysis locating peak wave amplitudes and thirdly a frequency analysis of the wave probe spectrum. The fourth method, relied on the frequency analysis results to produce condensed wave profile plots. The term *wave height* or *wave profile* represents the result from a single wave probe rather than the *free surface wave profile* along the vessel length.

6.5.2 Direct Profile Plots from a Single Probe.

For the direct plot of wave height with time, figure 6.8 presents a plotted copy of the computer screen showing a time fragment from one probe in a large data file. Split into three sections, the top shows the simulator position made up of three lines, one for each forcing motion. This provides information about the amplitude, period and phase of each forcing motion in relation to the other and to the wave profile itself. The next section gives numerical data on the run condition. Finally, the last section shows a plot of wave height from a single probe.

All the profile plots are scaled according to a maximum i.e. -10° to +10° for the forcing motions and 0 to 600 mm for the wave height. The program allowed changes to be made regarding window size (time scale), probe number, start of the window with respect to time, and the scaling parameters. Hard copies of screen display by printer or pen plotter, and the positioning of markers which helped in two other numerical processing techniques, were provided.

6.5.3 Peak Amplitude Detection by Numerical Analysis.

The second type of data analysis provided, was to scan through all points in the file, locating the maximum/minimum amplitudes and periods for the probe readings and simulator response. In this case, the data files was split into three parts, *startup*, *main* and *decay* sections. Normally, the startup region was specified as lasting 60 seconds and only the main region was analyzed. The type of algorithm used, was found to be susceptible to data file errors, mainly *spikes* which gave rise to abnormal wave heights and periods. Attempts were made, however to eliminate these by :

1) Using the first analysis technique (section 6.5.2) with markers to start and stop the calculations.

2) Check on the rate of change between one value and the next. This then had the potential danger of missing important peaks.

In practice, for normal cases, these precautions were not required.

6.5.4 The Fast Fourier Frequency Analysis.

The third technique was perhaps the most useful as it not only produced a frequency spectrum (using a Fast Fourier Transform (FFT) (83,84) calculation) of the wave profile at specific times, but also averaged out wave amplitudes.

Any periodic wave can be represented by a Fourier series of sine and cosine terms of specific frequency, phase and amplitude. The numerical calculation by FFT, transforms the normal time domain into a frequency domain consisting of both real and imaginary components. This can then give the amplitudes of the various frequency components. An inverse transform process can then be used to generate (predict) the original wave profile.

The basic FFT method involved taking 256 data points of the wave profile and transforming this into 128 frequency components of individual magnitude and phase. Plotting out these components for both the forcing and decay regions, provided instant comparison between forcing conditions.

Figure 6.9 shows a example of a frequency spectrum (bottom box), of one wave profile (top box). Other information in the diagram relates to the frequency interval of the spectrum, the time taken for the calculation, general run identification and the amplitude conversion factor (ACF). As realized, each frequency component in the spectrum has its amplitude in terms of a percentage of the amplitude of the major/primary frequency component (AMFC/APFC). The ACF was used to relate the amplitude a particular component to the real physical amplitude of the wave form, by the following expression :

$$\text{Wave Factor (WF)} = \frac{\text{Percentage value of a component}}{128 * \text{ACF}} \quad \ldots 6.1$$

Where WF has units of 'mm'

The WF (ACF) value does not give a direct reading of interface amplitude but rather a guide. Using the ACF, it should have then been possible to calculate the average amplitude of the wave during the particular time interval, over which the FFT was taken. However, such a calculation would have required phase differences between frequency components to be accurately determined. Phase components were found to depended on which point the FFT was started together with the period of the wave. Thus, no wave amplitude calculation was deemed obtainable by this method.

Using the FFT technique, it is then possible to match experimental results more closely to derived theory than just considering overall maximum and minimum wave heights and periods.

From written work on the FFT (83,84), the errors associated with such an analysis, were found to concern the sampling rate. If an odd number of wave cycles were contained in the 256 block, *aliasing* between frequency components was to be expected (i.e. small frequency component round the major one). Such errors were of little consequence as visual examinations of the frequency spectrum would located all major frequency components. To determine the position of these peaks numerically, required software to detect changes in magnitude between adjacent components. Further filtering was done by considering the resolution of the probe data.

6.5.5 Production of Condensed Profile Plots.

The fourth type of analysis originated in the need to analyse the full probe profiles with respect to fluid response due to forcing and the following decay profile. Since the FFT analysis provided a figure for the average wave amplitude in a particular analysis block, it was deemed probable, that by performing the FFT at small time intervals on a probe profile, that the average amplitude for that probe could be plotted with respect to time. In this way, a *condensed probe profile* plot could be obtained.

The procedure to collect information for the condensed profile plots, involved:

1) At small time intervals, the FFT was started and 11 major components located and stored. This was performed from time 0 to the end of the raw data file.

2) Using the condensed frequency spectrum, for the time associated with forcing and decay, the saved frequency data was then averaged. This would determine the *average FFT spectrum* for forcing and decay.

6.6 PROCEDURE FOR AIR/OIL/WATER INTERFACE RESPONSE EXPERIMENTS.

6.6.1 Scope of Experiments Performed.

In the case of air/oil/water, similar experiments were carried out as those for air/water i.e. to record the effect of different forcing motion conditions on the oil/water and air/oil interfaces. Again, a method had to be found to record the position of each interface with respect to time.

In addition to the above, two other sets of experiments were conducted. Firstly, to gauge the transfer of material (i.e. a tracer) from oil to water and secondly to attempt to measure the amount of dissolved oil in water, resulting from forcing. The experimental procedure and results for both sets of experiments will be presented in later chapters.

6.6.2 Supply of Oil in Interface Response Experiments.

With the small rectangular vessel, the effect of oil density was studied using kerosene and the two pseudo oils FK851 and FK890. For each experiment, the oil was supplied from 25l drums and carefully pumped onto a water layer in such a manner as not to cause mixing of oil with water.

In the case of the large rectangular container, due to the quantity of oil required, experiments were conducted with gas oil. In this case, oil was supplied from the departmental oil storage system.

6.6.3 Oil/Water Interface Measurement Technique.

It was hoped that the conductive air/water interface detection system could be applied to the oil/water interface. However, it found that oil would adhere to the probe wires even when the wires were degreased. The method eventually adopted was to record the interface profile on video tape and then digitize several frames by computer.

All video recordings were made using a NAC HSV-400 High Speed Video System comprising of camera, recording unit and strobe light. The stored frames would then be passed through a Genlock unit (supplied by Video Electronics Ltd, Beeb-Lock system), attached to a Acorn BBC Model B microcomputer. This was used in conjunction with a Bit-Pad graphics tablet to digitize each frame throughout one complete forcing cycle. The stored results on disk, were later converted to produce similar results as those from air/water experiments i.e. interfacial heights from specific points inside each vessel corresponding to the wave probe positions used in the air/water experiments (see figures 6.6 and 6.7).

The features of the HSV-400 which made for easy analysis included :

1) Excellent single frame advance facility allowing stepping backwards and forwards in time.

2) A built in timer which displayed the exact time (in minutes, seconds and 500^{th} of a second) on the video screen.

To analyze each frame, the following procedure was adopted :

1) Enter the time at which the frame corresponds to.

2) Mark the vessel outline with 4 straight lines. This provided a reference point for the interface profile data.

3) For each interface (air/oil and oil/water), mark out the outline from one end of the vessel to the other.

4) Steps 2-3 were repeat for further frames taken at small time intervals, until one complete forcing cycle had been processed.

The stored information would then be converted to give the position of the appropriate interface with respect to a level vessel base. The software written for this application is not included in this report.

An example of the output from this procedure, is shown in Appendix III.

6.6.4 Experimental Procedure.

For all experiments involving the effect of induced motion on the oil/water interface, the following procedure was adopted :

1) Using the simulator control system, a vessel would be placed in its horizontal position.

2) Mains water would then be pumped into the vessel to a specific depth

3) Stored oil would then be pumped slowly on top of the water layer to minimize mixing. This would prevent the formation of emulsions.

4) The HSV-400 camera would then be positioned so that it had a full length wise view of the vessel.

5) The simulator control system was set up so that one forcing run could be performed. To by-pass the data logging section, the system was allowed to run as normal without any calibration procedure or data storage.

6) Once the run was complete, the camera and control system was reset for another run.

7) Once all runs were completed, in the case of the large rectangular vessel, the oil and water were transferred back into settling tanks to enable the oil to be recovered. For the small rectangular vessel, the oil was stored in its original containers and the water disposed of.

As a check on oil quality, after each run samples of oil were taken and left to settle. No water was seen in these samples.

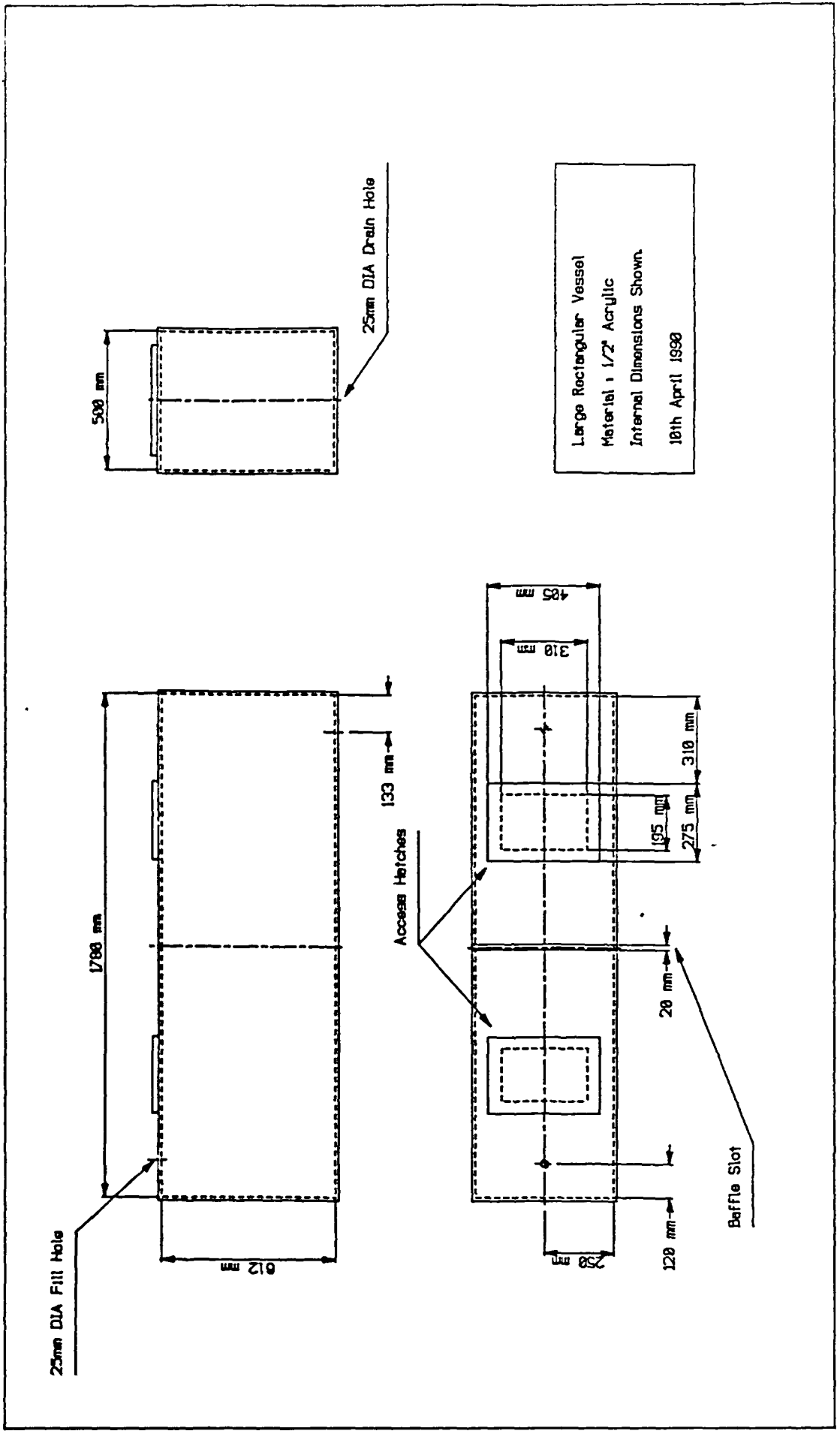

Figure 6.1: Physical details of the large rectangular vessel of length 1.78m, used in experiments.

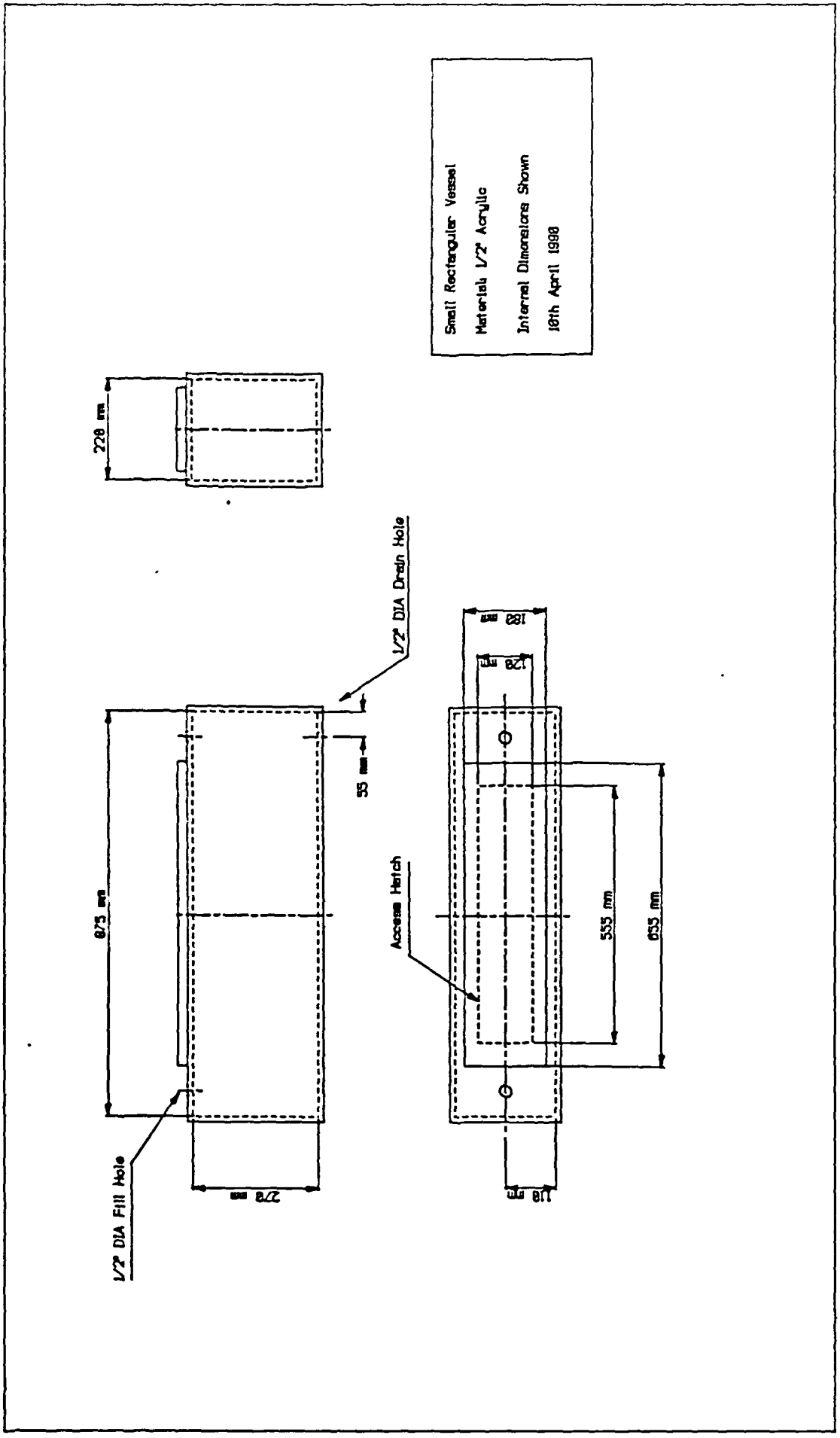

Figure 6.2: Physical details of the small rectangular vessel of length 0.87m, used in experiments.

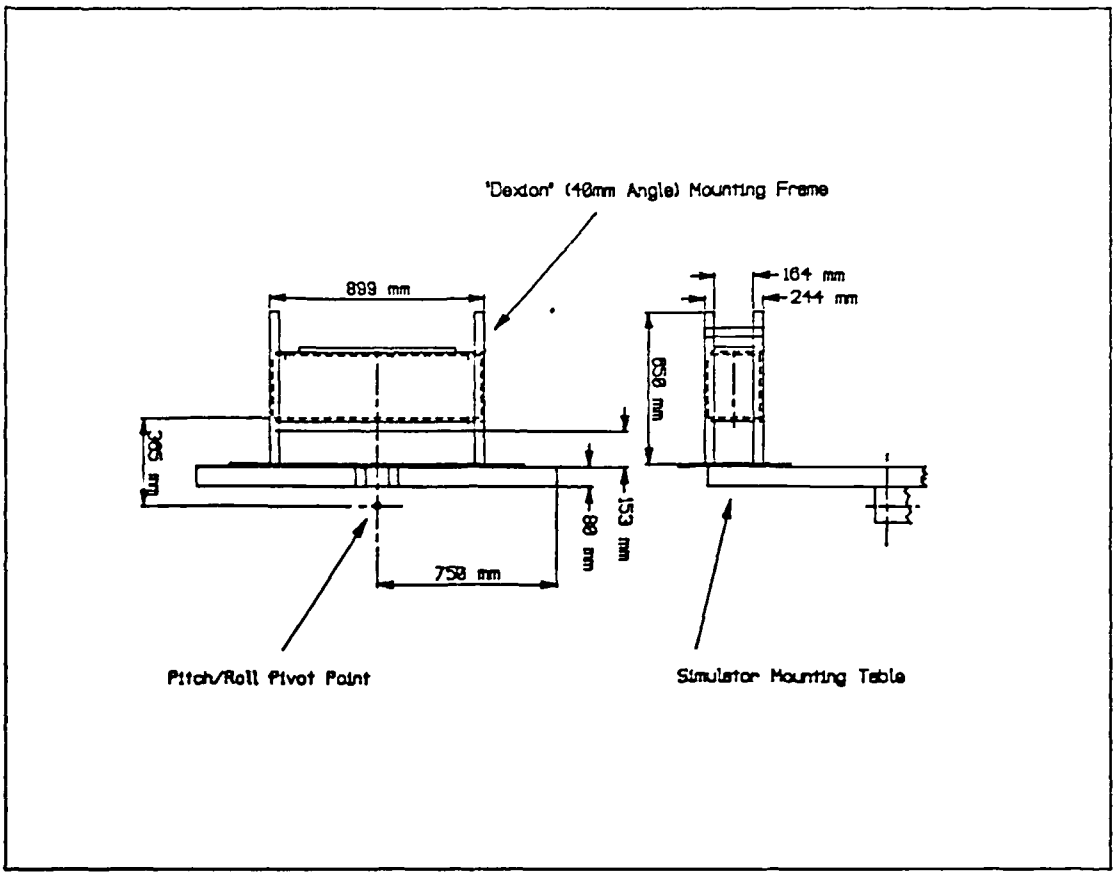

Figure 6.3: Details of mounting frame used for the small rectangular vessel.

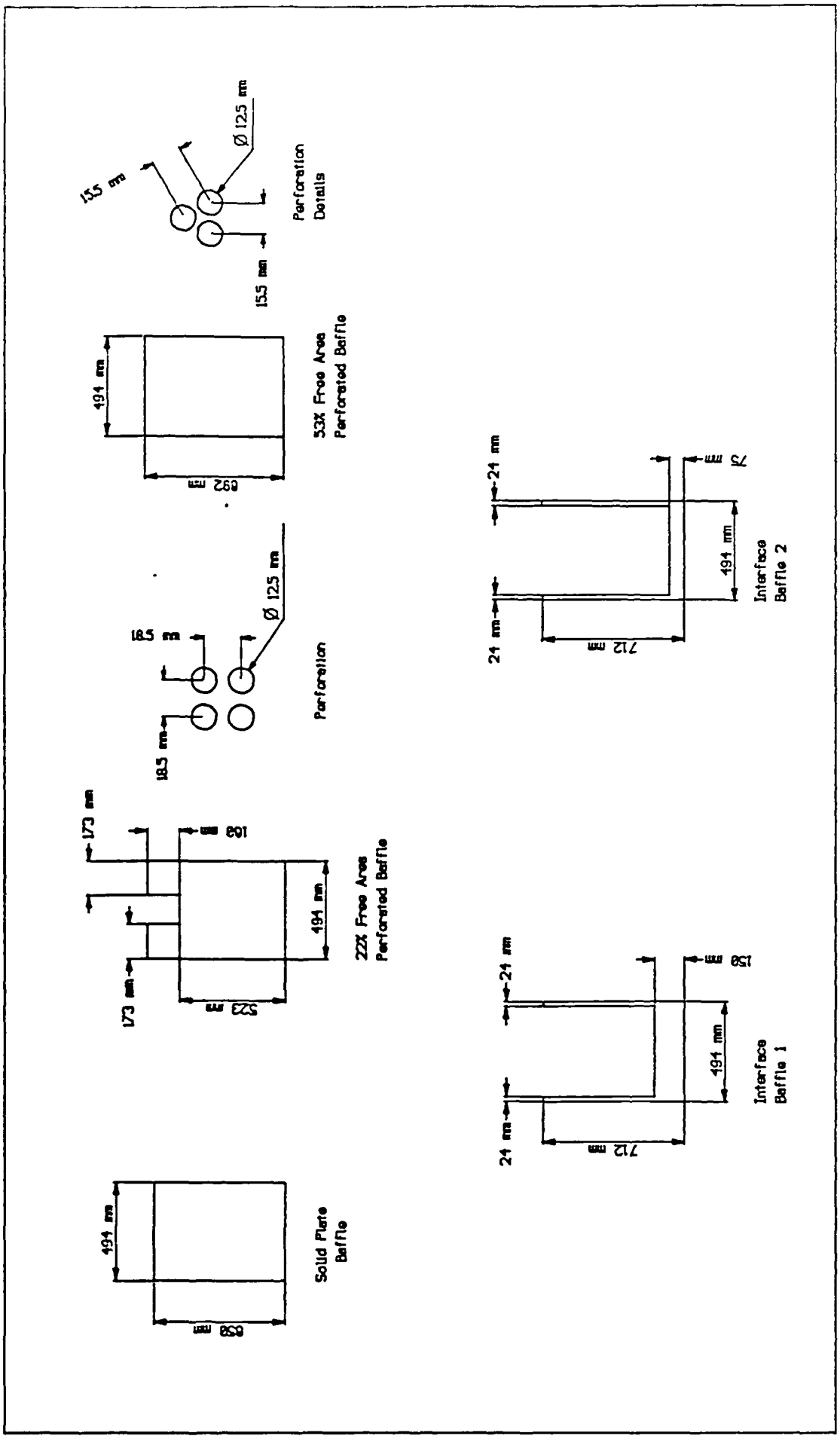

Figure 6.4: Details of baffles used in experiments with the large rectangular vessel.

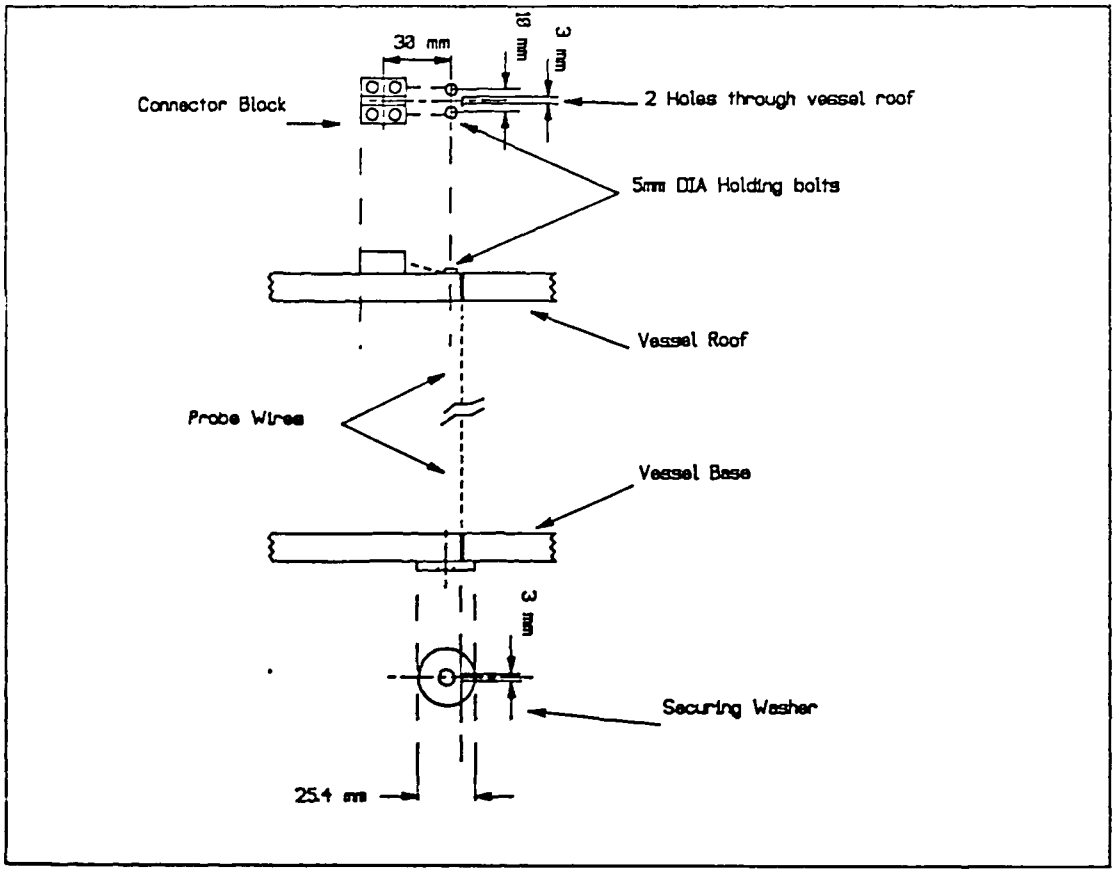

Figure 6.5: Details of the wave probes used to detect the air/water interface in the rectangular vessels.

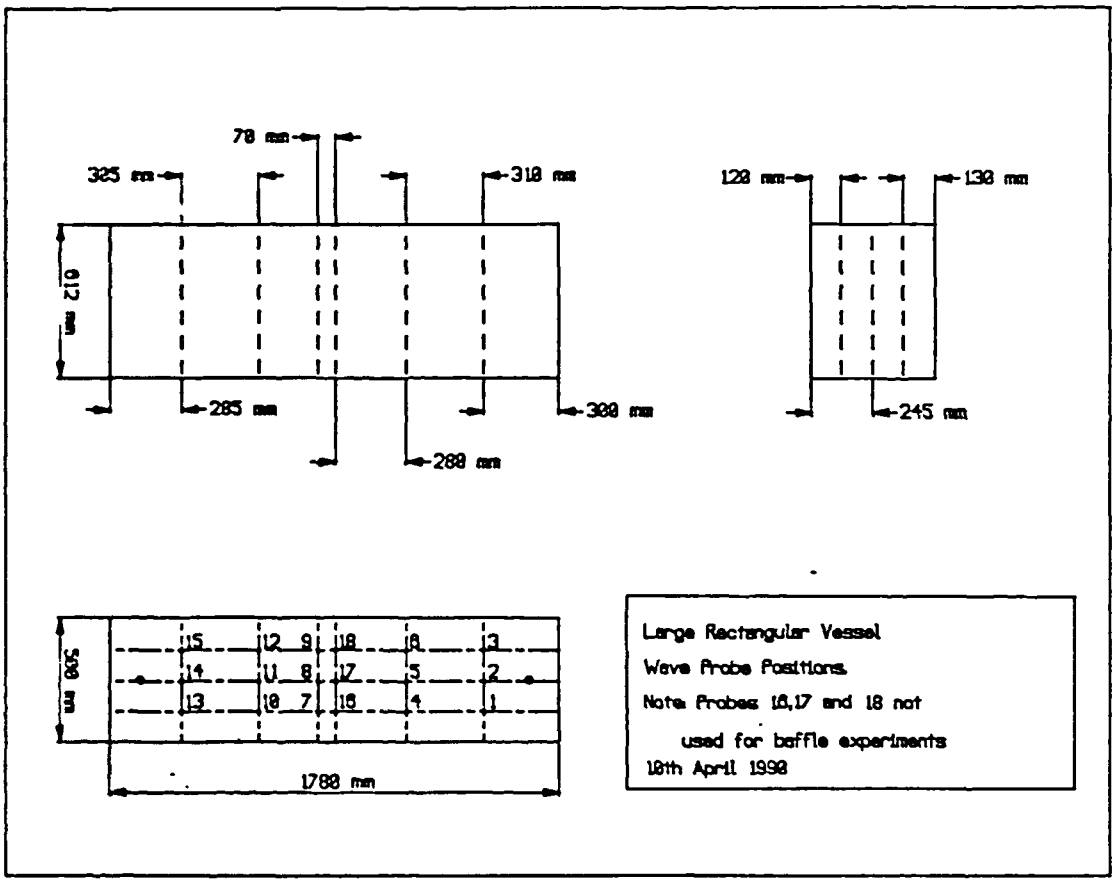

Figure 6.6: Positions of waves probes inside the large rectangular vessel.

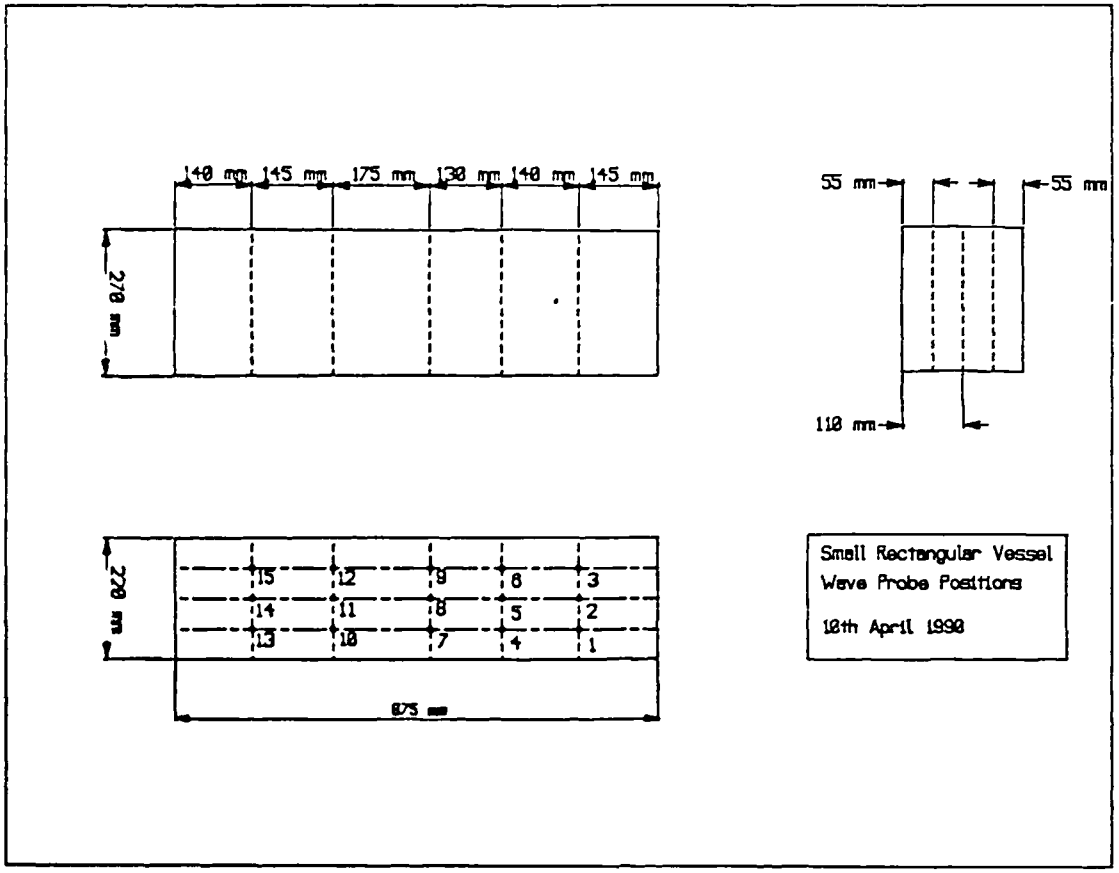

Figure 6.7: Positions of waves probes inside the small rectangular vessel.

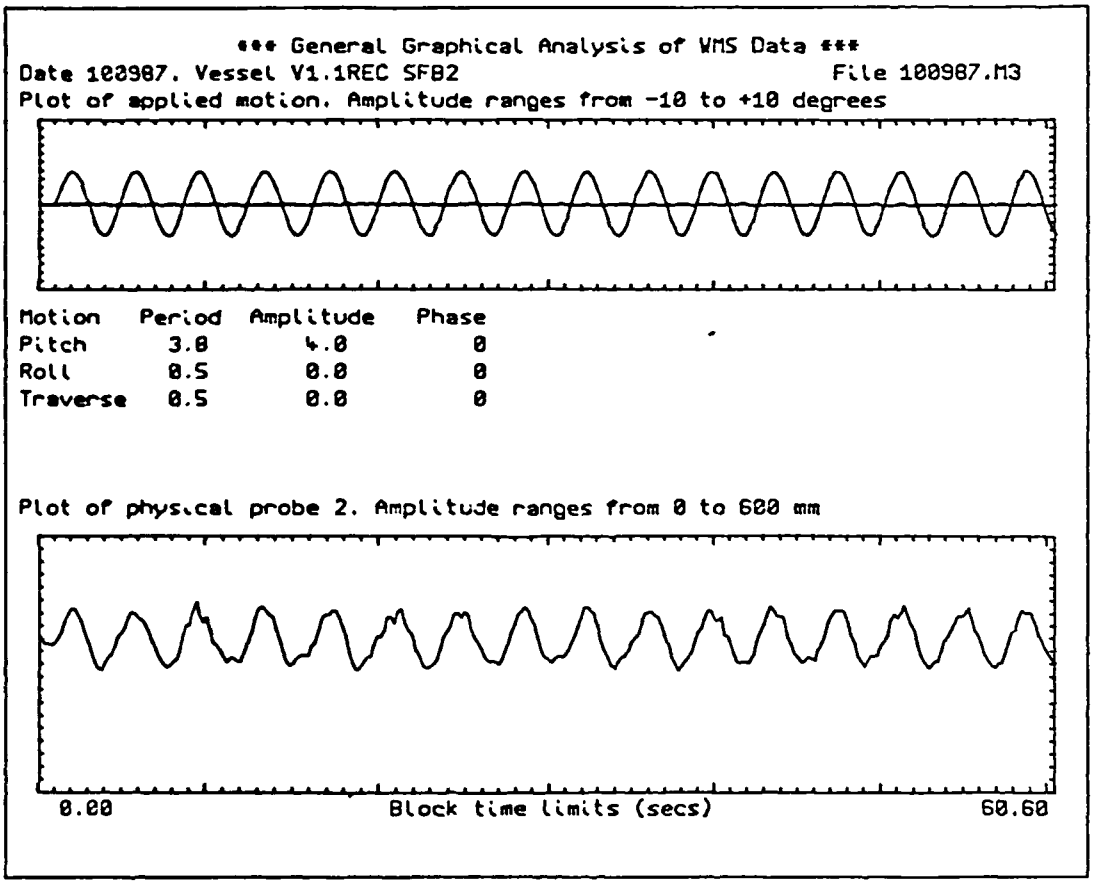

Figure 6.8: Example of wave profile data for probe 2 in the large rectangular vessel.

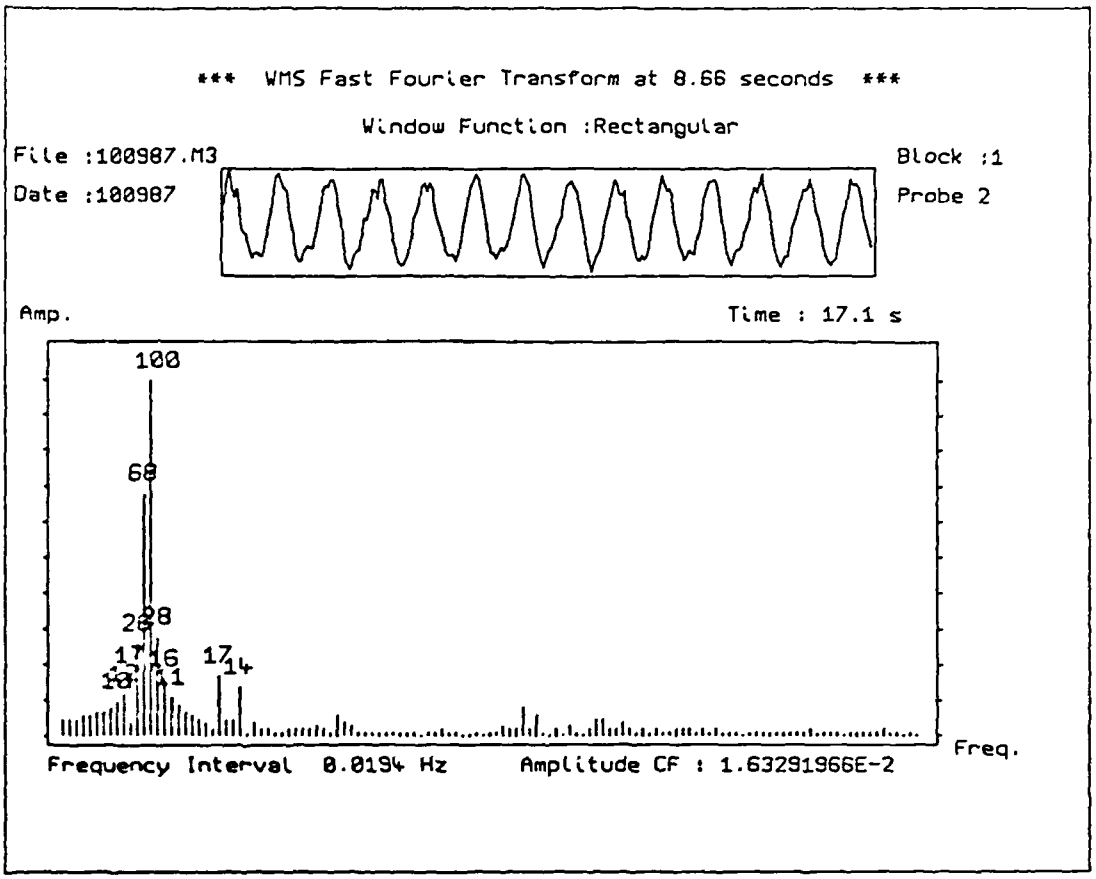

Figure 6.9: Example of a FFT frequency spectrum for probe 2 in the large rectangular vessel.

Oil	Density* (Kg/m^3)	Viscosity* (Ns/m^2)	Oil/Water* Interfacial Tension (N/m)	Flash Point+ (°C)
Kerosene	796	0.001	0.0337	39
FK851	858	0.001		
FK890	885	0.001		
Gas Oil	860	0.005	0.0246	76

Table 6.1: Physical properties of all oils used in related oil/water experiments.

Notes: *Measurements made at 19 °C, by :

Density : Parr Scientific DMA 35 Density Meter.

Viscosity : Contraves Rheomat 15T Viscometer.

Interfacial Tension : *Ring-pull* Torsion Balance

+Flash point taken from literature (85).

CHAPTER 7.

RESULTS FROM AIR/WATER EXPERIMENTS IN THE SMALL RECTANGULAR VESSEL.

7.1 INTRODUCTION.

Air/Water experiments with the small rectangular vessel were conducted during the initial stages of simulator control and data logging system development. As a consequence, wave profile results were found to be unsuited to detailed frequency analysis. However, the experiments show some effects of fill depth and forcing period on air/water interface amplitude.

In previous work (40), some reference has been made regarding the effect of pivot point location in reducing interface amplitude. The relative small size of this vessel allowed comparative results at two pitch pivot point locations.

7.2 RANGE OF APPLIED FORCING CONDITIONS.

Several different liquid fill depths were used with a *standard set* of pitch forcing conditions as :

1) Fill Depths : 43mm, 83mm, 139mm, 174mm
2) Periods : 3, 6, 12 seconds
3) Amplitudes : $\pm 2°$, $\pm 4°$, $\pm 6°$

In addition, at two fill depths (43mm & 174mm), the pitch pivot point location was changed from its normal 356mm to 262mm away from vessel base (chapter 6, figure 6.3).

All experiments with air/water in the small rectangular vessel were conducted following procedures given in chapter 6.

7.3 EFFECT OF DATA LOGGING SYSTEM PARAMETERS ON RESULTS.

The data logging system was initially designed around a data recording rate of 300 baud, as dictated by the computer's tape cassette storage mechanism (chapter 6). Due to the multiplexing nature of data collection, this baud rate was found to limit the number of probes which could be accessed to obtain reasonable resolution of air/water interface profiles.

Graphs 7.1a-d demonstrate the effects of sampling a differing number of probes. Table 7.1 provides reference to the number of probes used and corresponding graphs.

The graphs demonstrate that profile resolution decreases as the number of probes accessed increases. Although maximum/minimum wave amplitudes could be obtained at 300 baud, the frequency information obtained from multiple probes was found to be of little value.

It was from these tests, that the data logging system was improved to allow a four fold increase in data collection rate. Experiments using the improved data logging system were carried out exclusively on the large rectangular vessel, results of which, will be presented in a later chapter.

7.4 THE EFFECT OF WATER DEPTH ON INTERFACE AMPLITUDE.

7.4.1 Summary of Results.

Graphs 7.2a-c show the influence of water fill depth on interface amplitude at different forcing amplitudes and periods. Results are for probe number 2 placed 145mm from the vessel's right wall, along the centre line (see figure 6.7). Comparisons between each graph indicate :

1) A 3 second forcing period results in higher interface amplitude values than 6 or 12 second periods. At 3 seconds, interface amplitude appears to depend on water fill depth.

2) At forcing periods of 6 and 12 seconds, interface amplitude is independent on water fill depth, for any forcing amplitude.

Using equation 4.15, natural periods were calculated for each fill depth used, and are given in table 7.2.

7.4.2 Discussion.

Natural periods for this vessel fall below 3 seconds for all fill depths. Simple linear theory would suggest, that forcing periods 6 and 12 seconds should have little influence on interface amplitude. The experiments follow this predicted trend. Differences between each forcing amplitude arise due to *spirit level effects* i.e. values of interfacial amplitude that would exist if the vessel were tilted from +ve to -ve angles. Hence, interface amplitude value for $\pm 2°$ amplitude is lower than $\pm 4°$.

Equation 4.15 predicts that a forcing period of 3 seconds produces a resonant (i.e. formation of hydraulic jump) at only 43mm fill depth. At this forcing period, interface amplitude would be independent of all other fill depths. The results for a 3 second forcing period contradicts this in that interface amplitude for 83mm fill depth is higher that for 43mm. For this forcing period (Ω=3 secs), visual observations at each fill depth characterise the free surface profile as :

1) For 43mm fill depth: At all forcing amplitudes, a hydraulic jump develops.

2) At 83mm fill depth: For $\pm 2°$ and $\pm 4°$ a hydraulic jump formed after the 1^{st} forcing cycle which degrades into a *three dimensional profile*. However, a jump remained throughout the experiment for amplitude $\pm 6°$.

3) At 139mm: A calm unbroken surface resulted from ±2° and ±4° forcing amplitude. At ±6° amplitude, a three dimensional profile developed.

4) At 174mm: A calm unbroken profile developed from ±2° and ±4° forcing amplitude. At ±6° amplitude, a standing/travelling wave developed (chapter 3, figure 3.1).

Note: A three dimensional profile was one which can be described as generating waves along the vessel length and width. Such profiles usually consisted of standing/travelling waves.

From the above observations typical resonant behaviour occurred at a fill depth of 43mm indicating theory was correct. However, the jump formation at 83mm fill depth indicates, to some extent, the validation of linear theory i.e. becomes invalid for large forcing amplitudes. Previous workers (7) have applied a non-linear analysis to arrive at a stability diagram in terms of forcing amplitude against forcing period (figure 7.1).

7.5 EFFECT OF ADJUSTING PITCH PIVOT POINT LOCATION.

Previous workers (40) suggested that adjusting the pivot position of a vessel may assist in reducing sloshing effects. Experiments were carried out covering the standard forcing periods and amplitudes for this vessel at two different pitch pivot point locations for two liquid fill depths (see chapter 6, figure 6.3):

1) Base of vessel at 262mm and 365mm above pivot point.

2) Fluid fill depths 43mm and 174mm.

Due to the physical construction of the motion simulator and vessel supports, it was not possible to locate the pivot point lower than 262mm.

Table 7.3 lists the conditions and interface amplitudes obtained from wave probe number 2.

According to the results, altering the pivot point location of this vessel has no effect on interface amplitude over the conditions tested. Lou et al (40) have suggested that optimum pivot position to reduce interface amplitude, is located above the undisturbed free surface. With these experiments, such a pivot point location was not possible.

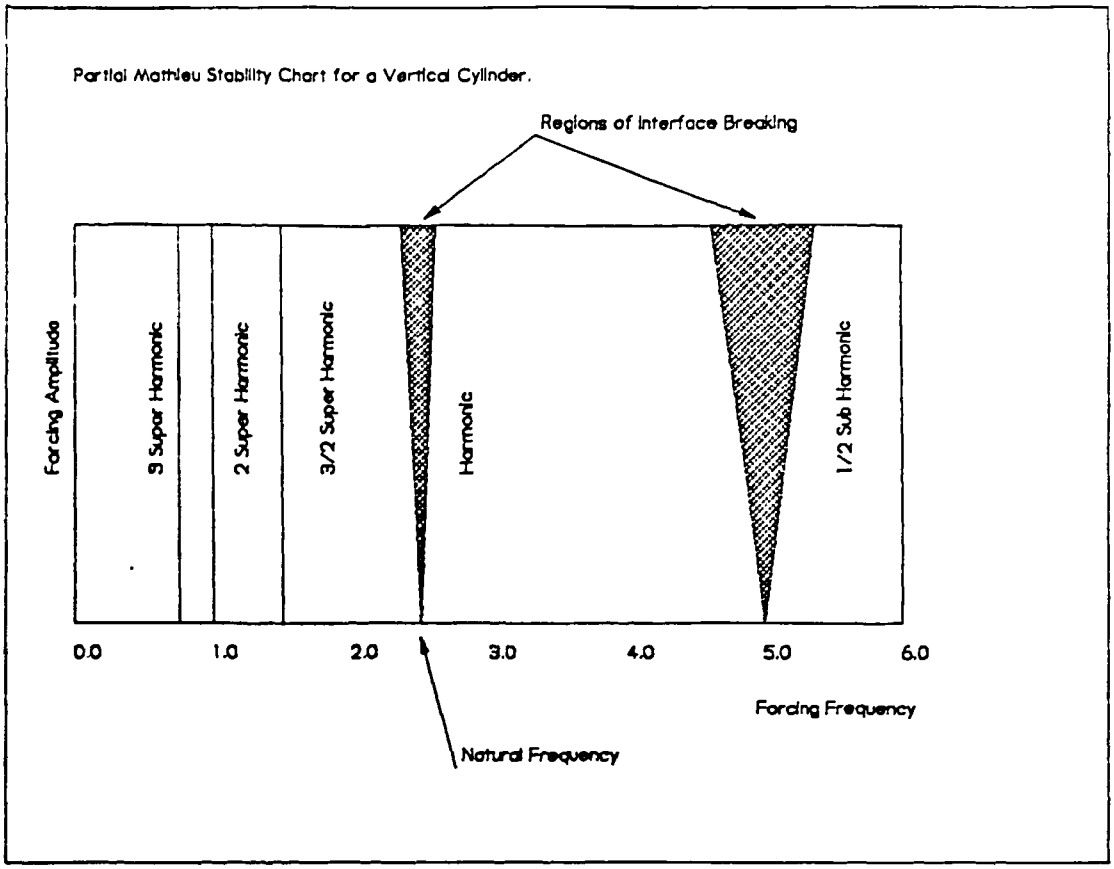

Figure 7.1: Stability of the air/water interface in relation to applied forcing period and amplitude (7).

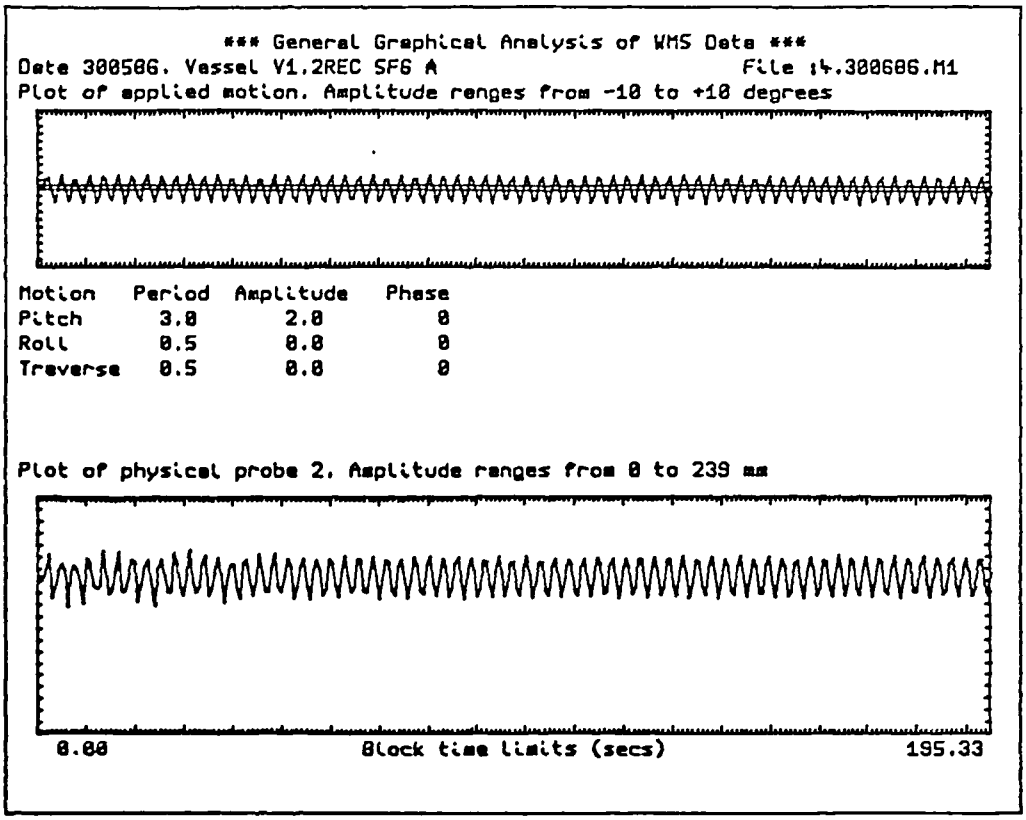

Graph 7.1a: Wave profile results from probe 2 in the small rectangular vessel, when accessing 15 probes.

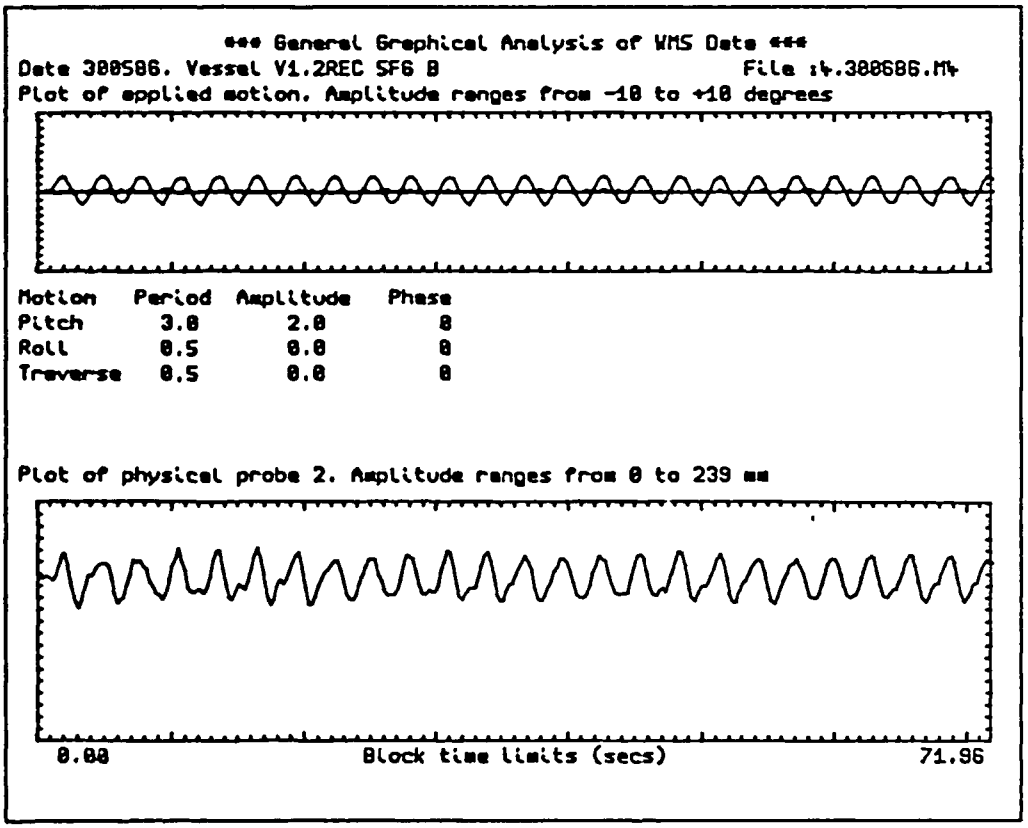

Graph 7.1b: Wave profile results from probe 2 in the small rectangular vessel, when accessing 3 probes.

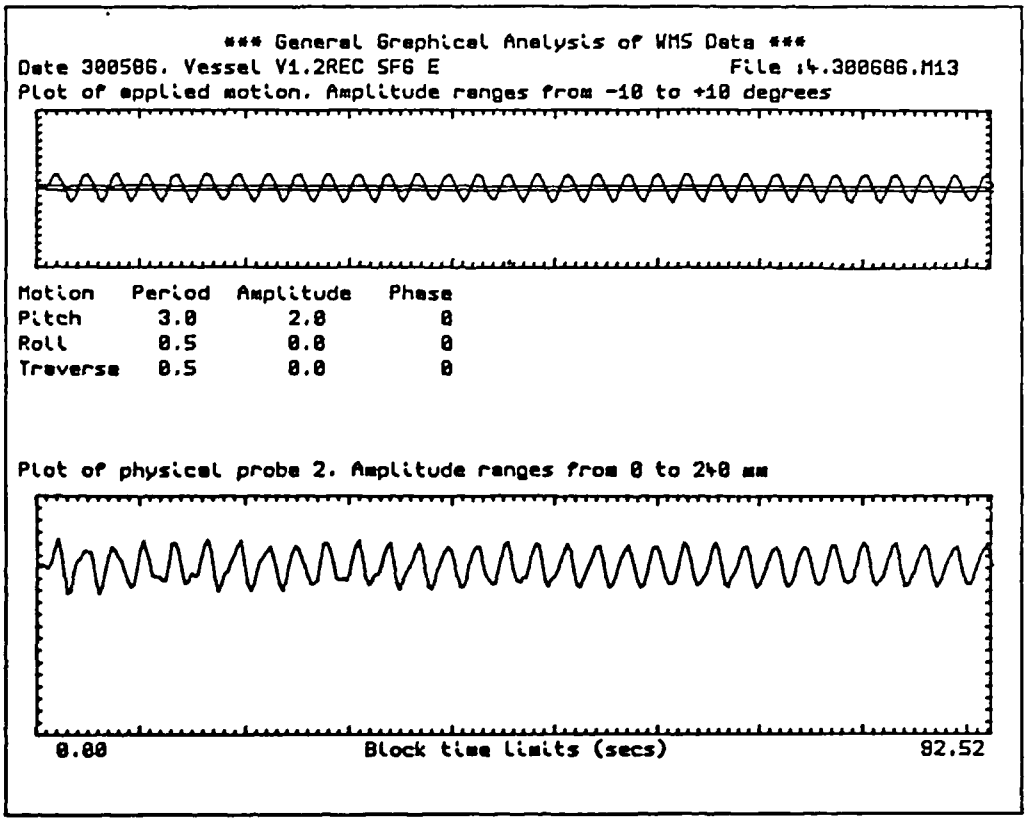

Graph 7.1c: Wave profile results from probe 2 in the small rectangular vessel, when accessing 5 probes.

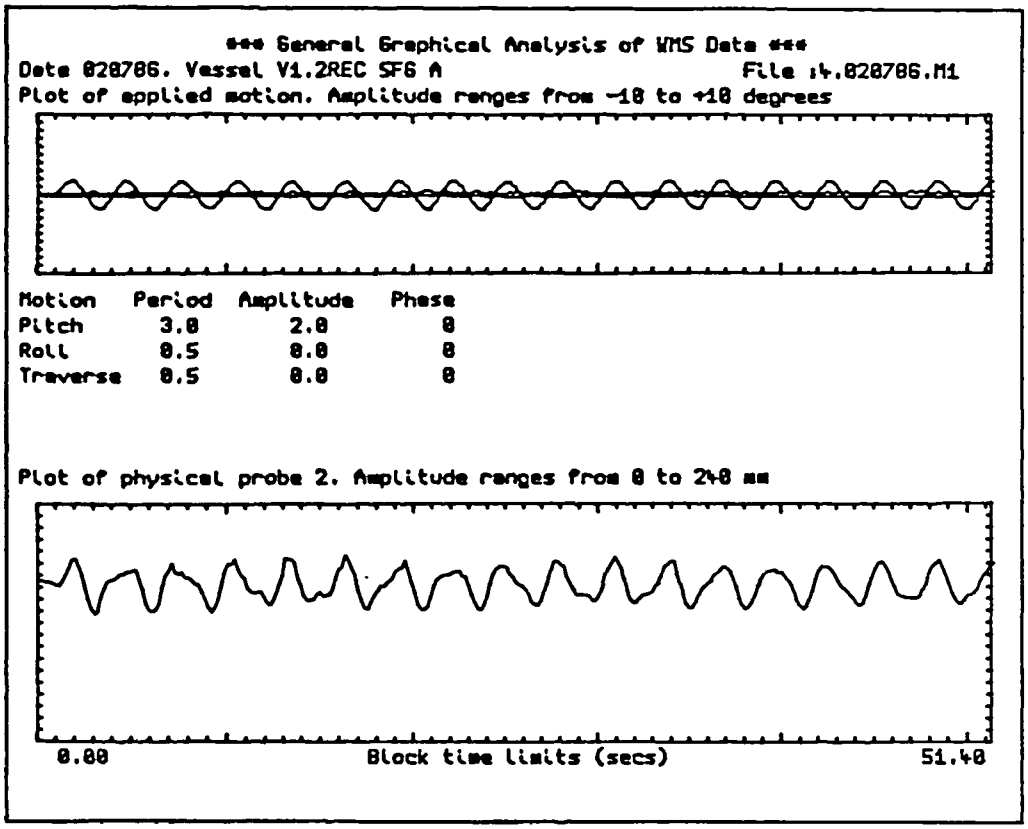

Graph 7.1d: Wave profile results from a single probe (probe 2) in the small rectangular vessel.

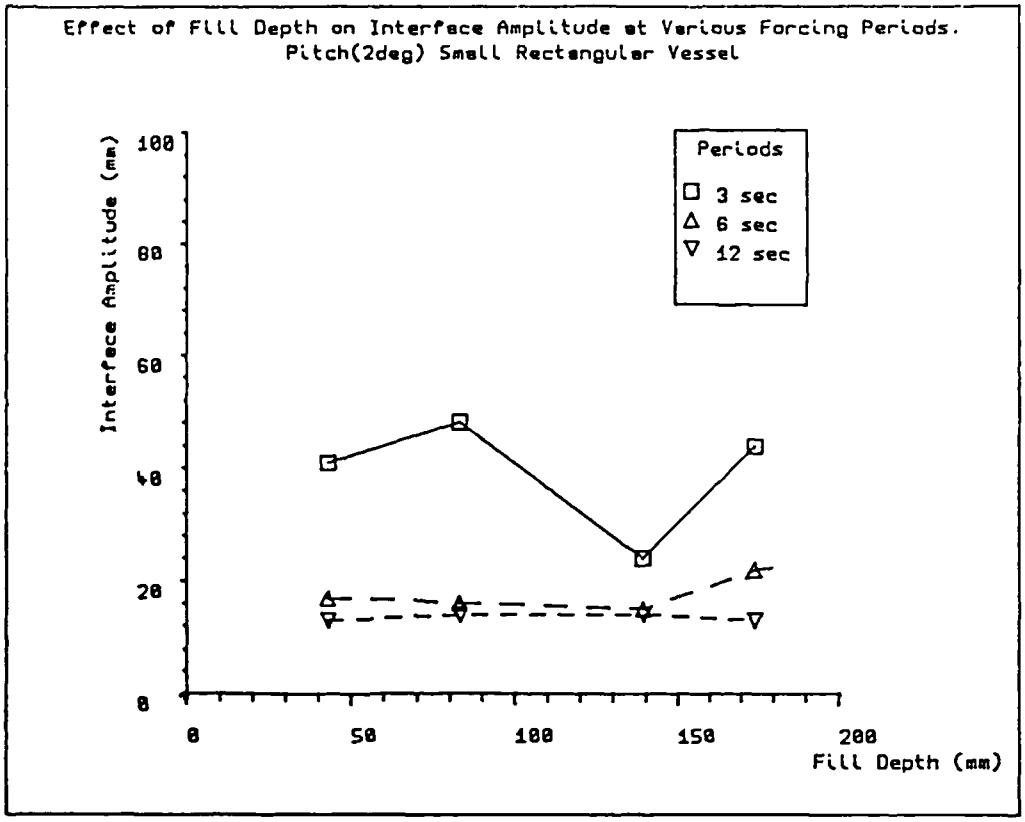

Graph 7.2a: Effect of water fill depth on Interface Amplitude (measured by probe 2) with pitch forcing motion at ±2° amplitude.

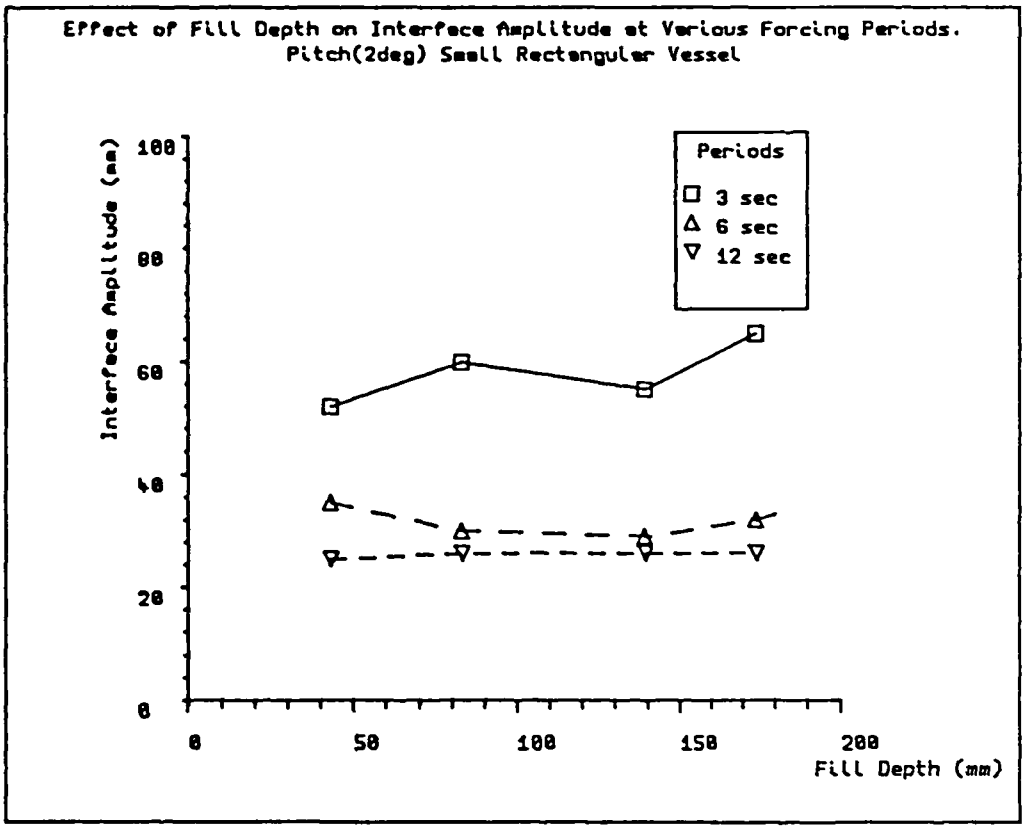

Graph 7.2b: Effect of water fill depth on Interface Amplitude (measured by probe 2) with pitch forcing motion at ±4° amplitude.

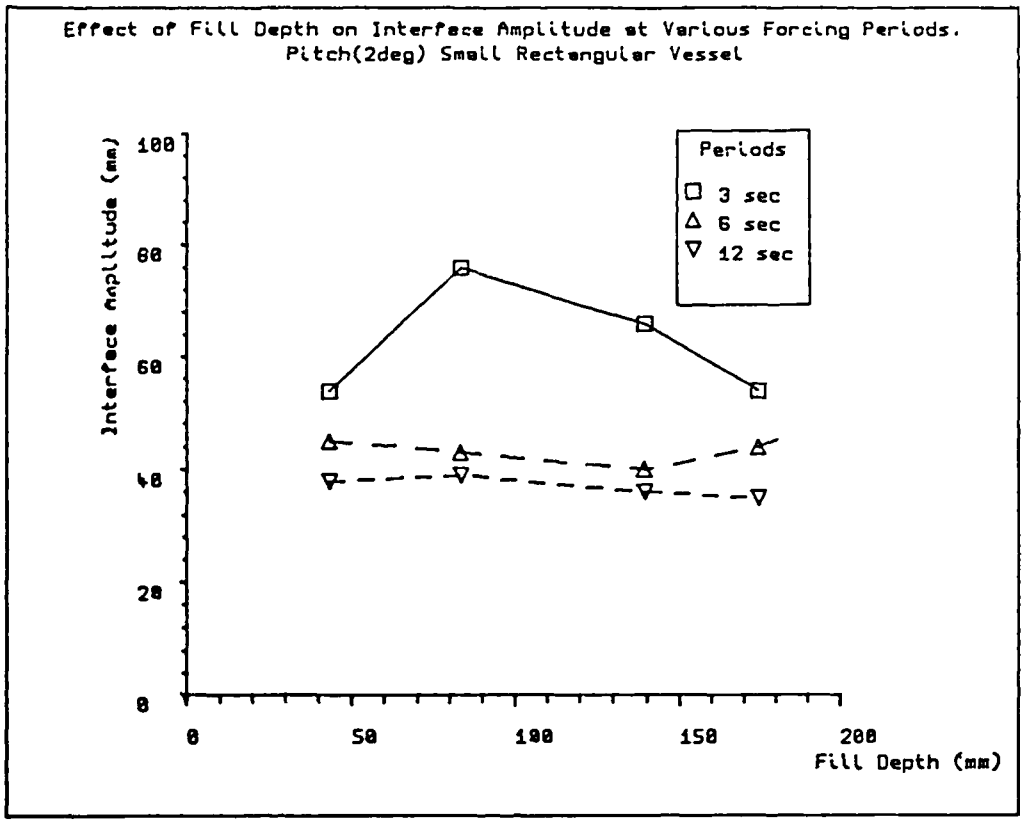

Graph 7.2c: Effect of water fill depth on Interface Amplitude (measured by probe 2) with pitch forcing motion at $\pm 6°$ amplitude.

Graph	Number of Probes
7.1a	15
b	3
c	5
d	1

Table 7.1: Number of Wave Probes Accessed.

Fill Depth (mm)	Natural Periods (eq 4.15) Mode 1 (sec)	Mode 2 (sec)
43	2.69	0.92
83	1.96	0.72
139	1.55	0.64
174	1.43	0.62

Table 7.2: Predicted natural periods for 5 water fill depths in the small rectangular vessel.

Fill Depth (mm)	Pitch Conditions Period (sec)	Amplitude (deg)	Probe 2 Interface Amplitude for Pivot Point 262 mm	365 mm
43	3	2	40	41
		4	50	52
		6	55	54
	6	2	16	17
		4	32	35
		6	44	45
	12	2	13	13
		4	24	25
		6	36	38
174	3	2	39	44
		4	63	65
		6	51	54
	6	2	15	22
		4	27	32
		6	50	44
	12	2	15	13
		4	24	26
		6	35	35

Table 7.3: Effect of pivot point location on interface amplitude at various forcing conditions.

CHAPTER 8.

RESULTS FROM AIR/WATER EXPERIMENTS IN THE LARGE RECTANGULAR VESSEL.

8.1 INTRODUCTION.

The results from the small rectangular vessel while useful in gaining experience, were found lacking for detailed analysis. Improvements in both wave probe and data logging system design allowed collection of accurate large amplitude wave data.

For preliminary experiments, the *standard forcing conditions* as applied to the small rectangular vessel were also applied for this vessel. Later, attention was paid to two forcing motions, pitch at ±4° amplitude and surge at ±120mm amplitude, at various periods. Experiments demonstrate the effects of forcing amplitude, liquid fill depth, combination of forcing motions and the effect of baffles on interfacial amplitude.

For analysis purposes, peak interfacial amplitudes were combined with Fast Fourier Transform analysis to measure the average frequency spectra for both the duration of forcing and decay.

8.2 EXPERIMENTAL OVERVIEW.

All experiments followed the method laid out in chapters 5 & 6 :

1) Checking the probe system.

2) Probe calibration with known water fill depths.

3) Record data and decay collection for a known time.

An important addition in this sequence, was the constant checking of probe wire tension to ensure a linear response between conductivity and fill depth. Positions of all waves probes used in the vessel are presented in figure 8.1.

8.3 EFFECT OF FORCING PERIOD ON INTERFACE AMPLITUDE.

8.3.1 Introduction.

Results from the small rectangular vessel showed that interface amplitude increased when the forcing period was close to the natural period. Graphs 8.1 & 8.2 show the effect of forcing period on interface amplitude for pitch motion at ±4° and surge motion at ±120mm amplitude. Water fill depth in each case was 173mm, natural period as predicted by equation 4.15 was therefore 2.7 seconds. Each graph shows interface amplitude as measured from several wave probes situated along the vessel's centre line. Figure 8.1 shows probe positions.

Several comments can be made :

1) Independent of applied motion, each graph has a peak interface amplitude value which occurs at forcing period about 2.5 seconds. This compares to the predicted resonant period of 2.7 seconds.

2) For surge motion, there appears a second peak at forcing period of around 6 seconds. A small peak occurs around 6.5 seconds in pitch motion.

3) The profile response is symmetrical for probes equidistant from the vessel's midpoint (i.e. probes 2/14, 5/11, 8/17).

8.3.2 Wave Probe Responses in Relation to Wall Effects.

To investigate the effect of vessel corners on interface amplitude, results from three probes placed in line, at one end of the vessel (figure 8.1) are presented in table 8.1. The results show that at all forcing periods, each probe records the same interface amplitudes. During these experiments, visual observations indicated :

1) At 3 seconds forcing period, low amplitude forcing of ±2° initially produced a standing/travelling wave profile (chapter 3, figure 3.1). At ±4° and ±6° a hydraulic jump developed.

2) At 6 seconds forcing period, all forcing amplitudes produced calm two dimensional profiles. In addition, at ±6° amplitude, a breaking waves was recorded but of insufficient amplitude to cause a three dimensional profile.

3) At 12 seconds forcing period, all forcing amplitudes gave smooth, calm two dimensional profiles.

8.3.3 Discussion.

According to simple linear theory (equation 4.14), the free surface should form a cosine wave profile and as a consequence of this, probes placed at opposing ends of a vessel should give similar trends. The experimental results (graphs 8.1 & 8.2) support this. It was therefore encouraging to note the symmetrical output produced by the probes and thus gave confidence of the operation of data logging and processing systems.

The presence of modes occurring at periods greater than the predicted natural period, *super-harmonic modes* (7), does however, pose some questions. Referring to graph 8.2 at around 6 seconds forcing period, all probes show similar trends of increasing interface amplitude. Therefore, the data logging system must have been functioning correctly. Visual observations during this experiment (surge at 6 second period, ±120mm amplitude) note the formation of a three dimensional profile. Such a profile can be attributed to the build up of waves in the *roll direction* i.e. waves traveling across the vessel's width. The effects noted in graph 8.2 could be due to :

1) When the vessel started moving, some abnormal motion of the simulator (i.e. non-sinusoidal) may have resulted in a breaking wave. Visual observations indicated that once breaking waves develop, a two dimensional free surface profile would degrade to a three dimensional one (figure 8.2).

2) Non-linear theory presented by Dodge et al (7) states that super-harmonic frequency responses occur over very narrow forcing conditions i.e. significant free surface response occurs over a smaller range of forcing amplitudes than harmonic responses around the resonant period.

It is suggested that no vessel vibration took place, and therefore the results of these experiments indicate the presence of super-harmonic modes during surge forcing motion. Such modes have been reported during previous work (7,42). Due to the absence of super-harmonic modes in pitch forcing experiments, is suggested that surge forcing motion is more susceptible to non-linear effects than pitch.

8.3.4 Recommendation to Use One wave Probe.

Performing many experiments at different fill depths, forcing conditions and internal configurations, resulted in a vast collection of wave data from multiple probes. As a consequence of the observed symmetry in multiple probe response (graphs 8.1 and 8.2), it was decided to concentrate detailed analysis on wave probe 2.

8.4 THE EFFECT OF FORCING AMPLITUDE ON INTERFACE AMPLITUDE.

8.4.1 Introduction.

Linear theory (equations 4.14 & 3.14) implies that interfacial amplitude is linearly dependant upon forcing amplitude, for both angular and linear forcing motions. To test if such a relationship exists, several experiments were conducted with pitch and surge forcing motion. Conditions are given in table 8.2.

Results from pitch forcing experiments are presented in graphs 8.3a-c in terms of interface amplitude against forcing amplitude, together

with condensed profiles (graphs 8.4a-c), produced from the Fast Fourier Transform analysis described in chapter 6. Unfortunately, only three surge amplitude configurations were applied and therefore, results relating to surge motion effects are presented in the form of condensed profiles (graphs 8.5a-c).

8.4.2 Pitch Motion Results from Three Wave Probes (Graphs 8.3a-c).

Close to resonance (Ω=3 secs, graph 8.3a) and below forcing amplitude of $\pm 3°$, all probes follow a similar trend of increasing interface amplitude with forcing amplitude. In this region, the relationship between forcing and interface amplitude is seen to be approximately linear. At a forcing amplitude of $\pm 3°$ and above, a distinct change occurs. Probes 2 & 14 continue to show increasing interface amplitude with increasing forcing amplitude, although the rate of change is reduced. Probe 17 at the vessel centre (figure 8.1) shows decreasing interface amplitude with increasing forcing amplitude. The relationship between interface amplitude and forcing amplitude appears now to be non-linear.

Away from resonance (Ω>3 seconds, graphs 8.3b-c), there appears to be a linear relationship between interface amplitude and forcing amplitude. However, an important note is that while theory (equation 4.14) would predict that there would be no interface amplitude at the vessel centre, this is contradicted by probe 17.

Visual observations from these experiments indicated :

1) For forcing periods of 3 seconds and forcing amplitudes less than $\pm 3°$, three dimensional wave profiles were produced (figure 8.2). Hydraulic jumps developed for all forcing amplitudes above $\pm 3°$.

2) For all other forcing periods (4 & 5 seconds), as the forcing amplitude increased above ±5°, two dimensional wave profiles gave way to a three dimensional profile.

8.4.3 FFT Condensed Single Probe Profiles for Pitch Motion.

The condensed probe profiles as produced by the fast fourier transform analysis for probe 2 (graphs 8.4a-c), draw attention to wave behavior after forcing has ceased i.e. the decay profile. During forcing, the *Amplitude of the Major Frequency Component* (AMFC) is seen to remain constant, falling quickly once forcing has ceased. The effect of increasing forcing amplitude can be clearly seen by the increase in AMFC values.

In some condensed FFT profiles the AMFC value is seen to decrease before motion has stopped. The reason for this lies in averaging AMFC values per FFT analysis window (see chapter 6). Consider a wave profile of large amplitude during forcing and as soon as motion stops, wave amplitude gradually decreases. The AMFC value will therefore decrease the moment the decay profile enters the 256 point analysis window. Once the point of motion stop leaves the analysis window, the AMFC will continue to decrease if the wave amplitude continues to decrease, or it will increase if the wave amplitude increases.

For the decay profiles, the following points can be made :

1) At forcing periods close to resonance (Ω=3 secs) and forcing amplitudes of ±1° & ±2°, the AMFC profile can be seen to sharply increase before gradually decreasing with time. As the forcing period is increased away from resonance (Ω>3 secs), the effect of rising AMFC prior to decay is noted at increasing forcing amplitudes i.e. up to ±4° for 4 second period, up to ±6° for the 5 second period.

2) Significant values of AMFC (>20mm) occur some time after motion has ceased for all experiments except the condition of period 4 seconds, amplitude ±1° (graph 8.4b).

8.4.4 FFT Condensed Single Probe Profiles for Surge Motion.

In a similar analysis as for pitch forcing, graphs 8.5a-c plot condensed FFT profiles for probe 2 as a results of surge forcing motion. The results indicate :

1) Close to resonance (Ω=2.3 secs) for ±150mm forcing amplitude (graph 8.5a), the maximum value of AMFC appears to be the same as that for pitch forcing at ±6° (graph 8.4a). However, unlike pitch forcing the decay profiles resulting from all forcing amplitudes are similar, with no increase in AMFC once motion has ceased. Visual observations indicated the free surface was dominated by large amplitude two dimensional standing waves. Such waves gradually built up in amplitude until they touched the vessel roof. This gave surface breaking and generation of a three dimensional profile.

2) At a forcing period of 3 seconds (graph 8.5b), there appears to be a significant difference between a forcing amplitude of ±150mm and ±100mm. This difference appears similar to the ±3° amplitude limit for pitch motion also at 3 seconds period. Visual observations indicate this particular profile was dominated by a three dimensional, breaking wave profile. At lower amplitudes (±50mm & ±100mm) the free surface consisted of a smooth three dimensional profile.

3) At a forcing period of 3.3 seconds (graph 8.5c), all forcing amplitudes produce similar profiles. Both the values of the AMFC and the trend in decay profiles are similar.

By comparing surge profile results with pitch at 3 second forcing period (graphs 8.4a and 8.5b), it would appear that surge amplitudes of ±150mm produce similar profile results as pitch amplitudes of ±3°, ±100mm with ±2° and ±50mm with ±1°.

8.4.5 Discussion.

The results from the pitch forcing indicate, that away from resonance (Ω>3 seconds in this case) a linear relationship exists between forcing and interface amplitude as predicted by simple linear theory (equation 4.14). However the presence of interface amplitude readings at the vessel's centre would tend to contradict the theory. As shown in section 8.3, various free surface profiles develop as a consequence of the proximity of forcing to natural period at one forcing amplitude. The results presented in this section indicate that forcing amplitude can also affect the shape of the free surface. The concept of *slosh severity* can be introduced to relate the effects of forcing conditions on free surface profile, which may be generalized as (figure 8.3) :

1) Low slosh severity results from forcing periods far from resonance over a wide range of forcing amplitudes. Free surface profiles may consist of smooth two dimensional profiles or be flat as predicted by simple linear theory.

2) If forcing period is close to resonance, low slosh severity will result from low forcing amplitudes. At higher forcing amplitudes, the free surface may become rough and susceptible to breaking waves. Once breaking waves occur, then a three dimensional profile may result. The exact forcing amplitude required to produce free surface breaking will then depend on the proximity of forcing to natural period.

3) A high slosh severity would result from near resonant large amplitude forcing and characterized by a hydraulic jump. As the hydraulic jump is essentially a two dimensional wave form, any three dimensional effects would therefore be an indication of low forcing amplitude.

In relation to the form of the decay profiles observed with different pitch and surge forcing conditions, use can be made of the severity concept. A *high* slosh severity gives an even decay, a *low* severity produces an increase in interface amplitude prior to decay.

8.5 THE EFFECT OF LIQUID FILL DEPTH ON INTERFACIAL AMPLITUDE.

The severity of sloshing depends both on the forcing amplitude, length of vessel and proximity of forcing to natural period. The principal effect of fill depth is its effect on natural period. Graph 8.6 shows results from two experiments of pitch forcing at ±4° for liquid fill depths of 173mm and 352mm. Predicted natural periods were 2.77 and 2.03 seconds respectively. The graph indicates that the higher fill depth produced the higher interface amplitude at the predicted resonant period. The difference in maximum interface amplitude, could be due to resolution of graphical data i.e more forcing period combinations were applied for 173mm than 352mm fill depth.

Both these fill depth conditions correspond to the case of a shallow liquid depth which is known to be characterised at resonance by hydraulic jumps (8). At higher liquid fill depths, previous workers (2) have concluded that standing waves impacting on vessel tops can produce large liquid impact pressures. While this is important for structural design, in terms of free surface disturbance, the hydraulic jump appears to be of more importance.

8.6 FREQUENCY ANALYSIS FROM SINGLE PROBE DATA.

8.6.1 Introduction.

Classical linear theories (Chapter 3), which suggest that the free surface oscillates at the same period as the applied forcing motion, solve the interfacial amplitude in terms of fill depth, forcing amplitude and natural period modes. Preliminary air/water experiments visually suggested the possibility of competition between forcing and natural period modes i.e. in some experiments, free surface waves were seen to oscillate at periods equal to the natural period and the forcing period. The developed linear theory presented in chapter 4, tended to support these observations although the theory itself was based on restricting assumptions (e.g. no viscosity).

The Fast Fourier Transform (FFT) analysis technique was applied principally to wave probes number 2 for various experiments. Resulting wave spectra were then split into two sections, one dealing with the duration of forcing motion, the other to the decaying wave profile. These two were then compared in an attempt to relate the forcing period to natural period modes. Chapter 6 presented details on this data processing technique.

. Experiments were conducted at a liquid fill depth of 173mm at various forcing periods for pitch at ±4° amplitude and surge at ±120mm amplitude. The first three natural period modes were calculated from equation 4.11 and are shown in table 8.9.

8.6.2 Frequency Analysis of Pitch Motion.

Appendix IV presents both waves profile data and frequency spectra for probe number 2 at various forcing periods. Data was analysed as outlined in chapter 6.

By tabulating the first three major frequency components of both forcing and decay regions (table 8.3), comparisons in each region can be made. The results indicate :

1) The first two natural periods modes, as determined by the FFT analysis (table 8.3) are 2.97 and 1.5 seconds respectively. The first mode compares favorably with predicted values from equation 4.15 (table 8.9), the second mode compares with predicted values based on half the vessel length. Natural periods were determined by referring to the second line of data presented for each forcing period.

2) Appendix IV shows that at a condition below predicted resonance (Ω=1.7 secs) the wave profile appears markedly irregular although the FFT was capable of locating the dominant frequency components. Observations indicated a three dimensional profile developed at this forcing period. However, there appears to be a contradiction between tabulated spectrum and the one as given in appendix IV. According to appendix IV, the second major component occurs at a longer period than the first component, the opposite trend occurs in table 8.3. This is an example of *initial start up effects* which will be discussed later in this section.

3) During forcing, table 8.3 shows the first major frequency component in the wave profile seem to be equal to that of the applied forcing motion. The second component appears to depend on the proximity of forcing to natural period. Close to resonance ($2.5<\Omega<5.0$ secs), all second frequency components correspond to that of the measured second natural period i.e. 1.5 seconds. Away from resonance ($\Omega>5.0$ secs) the second frequency component corresponds to the measured first natural period (i.e. 2.97 seconds).

8.6.3 Frequency Analysis of Surge Motion.

Table 8.4 shows the first three frequency components of both forcing and decay regions for the experiments with surge. Appendix IV presents corresponding profiles and spectra. The results indicate :

1) At forcing periods close to resonance ($3.0 < \Omega < 5.8$ secs), the first major frequency component in the forcing region corresponds to that of the forcing period. This is similar to the trend seen in pitch forcing.

2) At forcing periods away from resonance ($\Omega > 5.8$ secs) the first major frequency component corresponds to the natural period, the second component, to the forcing motion.

3) The amplitude of the major frequency components for forcing and decay are of similar magnitude except for resonance, This is unlike pitch forcing (table 8.3).

4) Visual observations during the surge experiments indicated that at no time did a hydraulic jump develop. At forcing periods away from resonance ($\Omega > 5.8$ secs), the free surface was dominated by a standing/travelling wave profile (chapter 3, figure 3.1). This would then be consistent with low sloshing severity, as defined in section 8.5.

8.6.4 Discussion.

In regards to the form of the wave profile and frequency spectra, both pitch and surge experiments indicate that the frequency spectrum away from resonance, consists of forcing and natural period modes. The natural period components appear more at low slosh severity conditions e.g. away from resonance. In the case of surge forcing, the natural components are seen to dominate the frequency spectrum. By comparison with pitch, it may

be suggested that the applied surge amplitude condition (±120mm) produced significantly lower slosh severity.

Although the measured and predicted natural period values are similar, several points can be made regarding the difference between the two. Firstly, it would require a water fill depth of 150mm to produce a predicted first natural period mode of 2.97 seconds not 175mm. Since a large error in fill depth measurement would have been noted, this suggests that prediction is in error. Secondly, a difference of 10% exists between measured (by FFT) and predicted first natural modes. If such an error was applied to the predicted second natural period mode, it would be insufficient to equal the measured second period mode i.e. 1.02+10%=1.22 secs. This suggests that measured second natural period mode is due to the predicted first mode based on vessel half length (1.44 secs as given in table 8.9).

This discrepancy continues over all applied forcing periods, near and far from resonance. If the natural period difference was due to non-linear effects, it is suggested that low slosh severity forcing combinations (e.g. Ω>5.0 secs) would show the predicted second natural period based on full vessel length. Therefore, the discrepancy between measured and predicted natural peirod is due to either problems with the data processor or errors in the prediction.

Considering the pitch forcing results, reference was made to *initial startup effects*. Observations made during initial trials with the small rectangular vessel had indicated that the free surface profile took some time to develop, depending on the forcing conditions. Therefore, in determining interface amplitudes the data processor allowed a period of 1 minute before data analysis began i.e. the results presented for comparison purposes were assume to be at steady state. Visual observations of changing wave profiles once forcing motion had started and evidence

presented from the frequency spectrum (Appendix IV) implies that natural period oscillations are involved in the wave frequency spectrum. For low slosh severity forcing combinations (e.g. surge at Ω>5 seconds, ±120mm amplitude) natural oscillations play a significant role in the frequency spectrum.

It is suggested that the equation describing the free surface should contain viscous terms which attenuate the natural period oscillation terms i.e. in a simplified form, the equation of the free surface may have a form :

$$\eta(x,t) = \left[F(\Omega,t) + G(\mu,t)H(\omega,t)\right]X(x,t) \qquad \ldots 8.1$$

Where Ω is the forcing period

ω corresponds to natural period oscillations

μ is a viscosity term, attenuating natural components

x is a distance term inside the vessel

η is the equation of the free surface.

F,G,H & X are complex functions incorporating time.

As yet, no linear or non-linear theory is able to incorporate viscosity into an analytical solution. However, as mentioned in chapter 3, Faltinsen (56) formed a numerical solution incorporating an artificial viscosity term. The resulting procedure was able to compare favorably with the start of wave motion, although no data was given for decay.

In the literature survey conducted during this project, the frequency analysis of fluid sloshing has not yet been considered. Previous linear theories (10,47) are incapable of deriving a free surface equation involving a frequency spectrum containing natural and forcing period terms. Non-linear theories involving series expansions, of some parameter in relation to time (chapter 3), contain terms which would result in a free surface profile having a suitable frequency spectrum (7,39).

8.7 THE EFFECT OF COMBINED FORCING MOTIONS ON INTERFACE RESPONSE.

8.7.1 Introduction.

A single forcing motion has been shown to generate waves which contain frequency terms due to the forcing period and to the natural period. It is suggested that combined forcing in two or more degrees of freedom (pitch & surge, surge & roll etc) could either increase or decrease slosh severity.

From literature sources, sloshing studies have previously involved only one forcing motion. Experiments were conducted with forcing combinations of pitch & roll and of pitch & surge. Motion amplitude, period and phase angle were altered. The relationships between forcing motions under various phase differences are presented in figure 8.4

8.7.2 Simultaneous Pitch & Roll.

Pitch & roll experiments were carried out with a liquid fill depth of 280mm. Table 8.5 lists forcing conditions and reference to associated condensed FFT profile plots. Full profile and FFT spectra are presented in Appendix V.

As wave motion will now be in two directions along the vessel length and breath, natural periods will now be defined as :

Define ω_l as the natural period based on the vessel length.

" ω_b " " " " " " " " breadth.

For the fill depth of 280mm, the predicted natural periods were ω_l=2.33 seconds, ω_b = 0.82 seconds.

According to the classic description of wave behavior (chapter 3) wave motion at this fill depth along the vessel length can be characterized as a *shallow fill depth* case i.e. fill depth/length ‹0.2. Across the vessel breadth, wave motion can be characterised as a *high fill depth* case (fill depth/breadth › 0.2).

The effect of phase difference at forcing periods away from resonance is shown in graphs A5.1-A5.2. As indicated by the magnitude of the second frequency component in the FFT spectrum, when pitch and roll forcing motions are out of phase by 90° the free surface seems less influenced by pitch than when both motions are in phase i.e. imposed roll motion acts as a damping influence on the wave motion when 90° out of phase with pitch. The effect of pitch forcing period closer to resonance (Ω=4.0 secs) while maintaining a long roll period (Ω=11.9 secs) is indicated in Graphs A5.3-A5.4. The FFT spectra shows that irrespective of phase angle, a frequency component due to roll appears along side one due to pitch. Once again, a phase difference of 0° seems to reduce the damping influence of roll motion.

The effect of increasing both forcing amplitudes while both periods were the same, is shown in graphs A5.5-A5.7. As both motions have the same period, one peak occurs in the spectrum relating to the motion. In addition, as the pitch period is closer to ω_l than roll is to ω_b, pitch is seen to have more influence on the resulting wave profile. Also apparent from these spectra, is the amplitude decrease of the natural period component w.r.t time (A5.5a-b). Doubling the forcing amplitude to ±4°, the natural oscillation components are quickly damped out (graph A5.6). Changing the phase angle to 90° has a calming influence on the wave profile compared to the 0° phase difference case.

These results then imply :

1) As expected, pitch motion has a greater influence than roll in determining wave profiles, due to the relationship between forcing periods and natural periods i.e. acceleration along the vessel length not width.

2) Roll motion, out of phase by 90° with pitch motion, has a calming influence on the wave profile.

8.7.3 Simultaneous Pitch & Surge.

Experiments were carried out with simultaneous pitch and surge where external forces act in either the same or opposing directions. Table 8.6 lists forcing conditions applied to the vessel, filled to a depth of 352mm. Unfortunately, due to computer error, comparative pitch & roll data at the same fill depth was lost.

In addition to full profile and FFT spectrum data presented in Appendix V, use is made of condensed profiles, presented in graphs 8.7 and 8.8

The effect of phase angle at forcing periods close to resonance (Ω=2.1 secs) is indicated in graphs A5.8-A5.9. These plots immediately indicate that slosh severity increases as a result of a phase difference of 180°. Also, the magnitude of the natural period component is reduced when pitch & surge are out of phase. In terminology used here, 180° phase results in imposed accelerations in the same directions (figure 8.4). Comparisons between condensed FFT profiles for single and combined forcing (graph 8.7) show that when pitch and surge are in phase, interface amplitude is reduced i.e. a lower slosh severity.

The effects of phase angle at forcing periods away from resonance (Ω=3.8 secs) are shown in graphs A5.10-A5.11. When both forcing motions are in phase (graph A5.10a) two frequency components are present, one relating to forcing period the other to natural period. Towards the end of forcing the natural component is still present (graph A5.10b). Therefore, the forcing motions must be sustaining natural oscillations. Visual observations during this experiments indicate the free surface adopts a standing/travelling wave profile. In the case where motions are out of phase (graph A5.11), the frequency spectrum is dominated by frequency components relating to the forcing motion. As a result, the wave profile becomes more regular since natural oscillations are no longer significant.

Turning to the condensed FFT profiles in graph 8.8 (Ω=4.0 secs), the effects of phase difference become clear :

1) When in phase, simultaneous pitch & surge motions produce lower interface amplitude values than pitch and surge forcing alone.

2) When out of phase, simultaneous pitch & surge forcing significantly increase interface amplitude.

8.7.4 Discussion.

The results from pitch & surge experiments demonstrate that when forcing motions combine to increase external forces (i.e. 180° out of phase), slosh severity can be increased to levels above those produced by a single forcing motion. The opposite effect occurs when combined motions are in phase. The presence of natural period oscillations when pitch & surge motions were in phase again suggest that the equation of the free surface should include both natural and forcing period terms. Observations from such experiments also show that a *beating* probe profile, as in graphs A5.10, are indications of a standing/travelling wave profile.

In the case of the angular motions pitch & roll, slosh severity was seen to be reduced when pitch & roll were 90° out of phase. The suggested reason for this behaviour occurs as a result of the proximity of forcing period to natural periods. Pitch motion was seen to dominate roll due to the vessel length/breadth ratio.

8.8 THE EFFECT OF BAFFLES ON INTERFACE RESPONSE.

8.8.1 Introduction.

From previous work on offshore separators and space rockets (4,12,68), it was known that perforated baffles could be a useful tool in reducing the effects of sloshing. In principal, baffles attempt to shift natural period modes away from expected forcing periods thus avoiding

resonant conditions. Extra baffling may not be required in large liquid storage tanks as structural members may be effective in shifting natural period modes (23).

To investigate the effect of perforated baffles and other internals on sloshing, experiments were conducted with several baffle designs. Construction details were presented in chapter 5.

Baffle configurations can be summarized as :

1) Perforated baffles of 22% and 53% free area: Either fully immersed or at some distance into the water.

2) Solid plate baffle: A solid plate extending from the vessel's roof placed at distances into the water. It should be noted that the vessel roof was not sealed and therefore the influence of air pressure on resulting wave profiles would be eliminated.

3) Interface baffles: Solid strips penetrating the air/water interface but not extending to the vessel's roof.

Figure 8.5 provided details of baffle configurations. Experiments were carried out with pitch forcing motion at $\pm 4^{\circ}$ amplitude with water fill depths of 175mm and 360mm.

In the following discussions, reference to the natural period will be in relation to an empty (unbaffled) vessel. The effect of baffles on natural period will be discussed later in this section.

8.8.2 The Effect Baffles on Interface Amplitude.

Graphs 8.9 & 8.10 compare the effect of forcing period on interface amplitude between baffled and unbaffled vessel. At 175mm water fill depth, the 22% baffle is seen to reduce interface amplitude over all forcing periods considered. In comparison, the fully immersed 53% baffle, causes little reduction in interface amplitude and even causes increases when its

tip touches the interface. At 360mm water depth (graph 8.10), the 22% baffle was again better than the 53% baffle at reducing interface amplitude. Photographs 8.1 and 8.2 show examples of free surface shape at a pitch forcing period of 3 seconds for both baffles immersed in water.

Turning to the effect of a solid plate baffle placed halfway into the water, at a water depth of 175mm, graph 8.9 shows that this baffle has similar characteristics to the 22% baffle except at resonance (Ω=3 secs). At the higher water depth of 360mm, graph 8.10 shows both solid plate baffle positions (169mm & 255mm) lead to a much greater reduction in interface amplitude than either perforated baffle. Photographs 8.3 and 8.4 show examples of free surface shape close to resonance (Ω=3 secs) and away from resonance (Ω=5 secs) with the solid plate baffle. These photographs show the hold up of water on one side of the baffle suggesting restricted flow beneath.

Placing the tip of the solid plate baffle on the air/water interface, appears to produce a *clipping effect* at the low water fill depth (175mm). Graph 8.9 shows that away from resonance (Ω>4 secs), the normal unbaffled response in followed. However, around resonance (2<Ω<4 secs) interface amplitude appears substantially reduced compared to both unbaffled and 53% baffle responses. In comparison, the 53% baffled placed on the air/water interface was seen to increase the interface amplitude at all forcing period conditions. For the high water depth of 360mm (graph 8.10), the solid plate baffle placed on the air/water interface seems to shift resonance towards longer forcing periods. This is indicated by a shift in the interface amplitude response, compared to the unbaffled vessel. Unfortunately, no comparisons with the 53% baffle in the same position are available. Photographs 8.5 and 8.6 show the generation of hydraulic jumps at 3 & 4 seconds forcing period for the 53% baffle touching the air/water interface. Photographs 8.7 and 8.8 show the

clipping effect of the solid plate baffle at similar conditions. For the solid plate baffle, the crest of the wave is seen to impact on the plate producing turbulence. Visual observations during further forcing cycles, indicated that the hydraulic jump appears to pass through the 53% baffle but is intercepted by the solid plate baffle. The disruption of the wave resulting from the impact on the solid plate baffle, seems sufficient to prevent hydraulic jump formation.

8.8.3 FFT Condensed Single Probe Profiles.

For several experiments, presented in the previous section, FFT condensed profile plots were compared for the baffled and unbaffled vessel. Table 8.7 lists pitch forcing period (amplitude at ±4°) together with water fill depth and baffle configuration. The FFT condensed profiles were constructed following procedures mentioned in chapter 6.

For a water fill depth of 175mm, graph 8.11 shows the effect of the solid plate baffle, both penetrating the fluid and touching the air/water interface, away from resonance (Ω=2 secs). Both baffled and unbaffled FFT profiles appear to coincide for the duration of forcing. However, once forcing ceases, then the profiles differ. In the unbaffled vessel, interface amplitude at first increases before reaching a steady decay value. This is in accordance with a low slosh severity as discussed in earlier in this chapter. For both baffle positions, wave amplitude is seen to decrease, such that the water surface is calm after about 2 minutes i.e. the AMFC reduces. As data logging was of the order of 5 minutes, the length of time taken for the wave amplitude in the unbaffled vessel to become calm cannot be estimated.

The performance of solid plate and perforated baffles at water fill depth of 175mm with forcing period closer to resonance (Ω=3 secs), are compared in graph 8.12. As can be seen, the solid plate baffle penetrating

the water has greater influence in reducing interface amplitude during forcing. Once forcing motion has ceased, decay profiles appear very similar for all baffle configurations although the solid plate baffle provides better damping than perforated baffles.

The performance of solid plate and interface baffles with the same fill depth/motion conditions as above, are shown in graph 8.13. During forcing, both interface baffle produce an increase in wave amplitude, compared to both the solid plate baffle and the unbaffled case. From the graph, interface baffle 2 increases the interface amplitude more than interface baffle 1. The decay profiles for all baffles are, however, very similar.

For a water depth of 360mm, graph 8.14 shows the effect of the solid plate baffle, again penetrating and touching the air/water interface. In this case during forcing, baffle performance is better than for the low water depth case (graph 8.11). Once the forcing motion has ceased, although both baffle positions rapidly reduce interface amplitude, the baffle touching the air/water interface gives similar responses to a low slosh severity forcing seen in earlier discussions.

Graph 8.15 compares the performance of solid plate and perforated baffles at a water fill depth of 360mm with applied forcing period of 3 seconds. Once again, the penetrating solid plate baffle appears better in reducing interface amplitude that any other baffle configuration. The decay profiles for all baffles differ, although each rapidly reduces interface amplitude, compared to the unbaffled vessel.

The performance of interface baffles at water depth 360mm, forcing period of 2 seconds is shown in graph 8.16. Interface baffle 1 is seen to both reduce interface amplitude and provide more damping than interface baffle 2. Increasing the forcing period to 3 seconds produces a different response (graph 8.17). In this case both baffles increase interface

amplitude to the same degree, although damping response is better than the unbaffled vessel.

8.8.4 Frequency Analysis of Single Probe Data in a Baffled Vessel.

Wave probe 2 profile results obtained from experiments with baffles at a water fill depth of 175mm, were analysed using techniques described in chapter 6, to produce numerical frequency spectrum data. Table 8.8a-f lists the first three major frequency components during applied forcing motion (upper line) and decay (lower line). For corresponding frequency data for an unbaffled vessel, reference is made to table 8.3.

Applying equation 4.15, the first three natural period modes were calculated for a vessel of length 1.78m and 0.87m, the results given in table 8.9. This data allows comparison with measured natural periods for the baffled and unbaffled vessel.

As regards the information provided by the decay data (lower line), it seems that the natural period in all experiments using baffles, equals the second natural period mode measured in the unbaffled vessel, that is 1.5 seconds. It should be noted that this period does not always correspond to the first major frequency component, but the second. In such cases, the first component corresponds to the forcing period.

Data relating to the duration of forcing (upper line) shows that for forcing periods away from resonance (Ω>3 secs) for all baffles that the second major frequency component corresponds to the measured natural period i.e. approximately 1.5 secs.

8.8.5 Discussion.

In relation to the quality of data, for the high water depth, insufficient forcing periods were applied around the predicted unbaffled vessel resonance condition. Although general trends regarding baffle

performance can be made, specific comparisons between high and low water depth resonant cases cannot. It was also unfortunate that insufficient forcing conditions were applied with the interface baffles to allow detailed comparisons with other baffles to be drawn.

Comparing the effect of baffles on reducing interface amplitude, it would appear that a solid plate penetrating the water has improved performance over perforated baffles. Calculating the effective *free area* for the solid baffle to be 50% when placed half way into the water, it would appear that the term *free area* as applied to baffles in general does not indicate performance. It would be expected that maximum fluid velocity would occur close to the free surface, at the centre of the vessel. Therefore, the solid obstruction at the vessel centre reduces fluid velocity more effectively than perforated baffles. Without velocity data from either non-linear theory prediction or measurement, further comments cannot be made.

Comparing the effectiveness of baffles to damp out wave motion once forcing has ceased, all baffles produce similar characteristics. The condensed profile plots show that a baffle with the same response as an unbaffled vessel during forcing, may result in a rapid decay of wave motion following forcing (e.g. graph 8.15 for the 53% baffle). The results from the interface baffles indicate that while interface amplitude may be significantly increased (graph 8.13), damping of wave motion following forcing may be rapid. As a consequence, measuring a baffles damping characteristics may have little consequence on the baffle performance during forcing.

In earlier sections, the discrepancy between measured and predicted natural period was discussed in relation to a unbaffled vessel. It was suggested that the second natural period mode of 1.5 seconds, corresponded to the predicted natural second mode, not that based on half the vessel

length. It would appear that with the presence of baffles, the first mode natural period is removed from the frequency spectrum. It may however be argued that the location of the baffles at the centre of the vessel supports, the theory of half length natural period modes. That is, the baffle effectively cuts the vessel in two halves. While this may be appreciated for the immersed perforated baffles and solid plate baffle, placed halfway into the water, difficulty arises when discussing either the interface baffles or the solid plate baffle touching the air/water interface. Therefore it is suggested that second natural period modes occur and not half length first period modes.

Although the solid plate baffle reduced air/water interface amplitude, observations show increased mixing round the baffle. The benefit of such baffles to offshore separators still needs to be addressed.

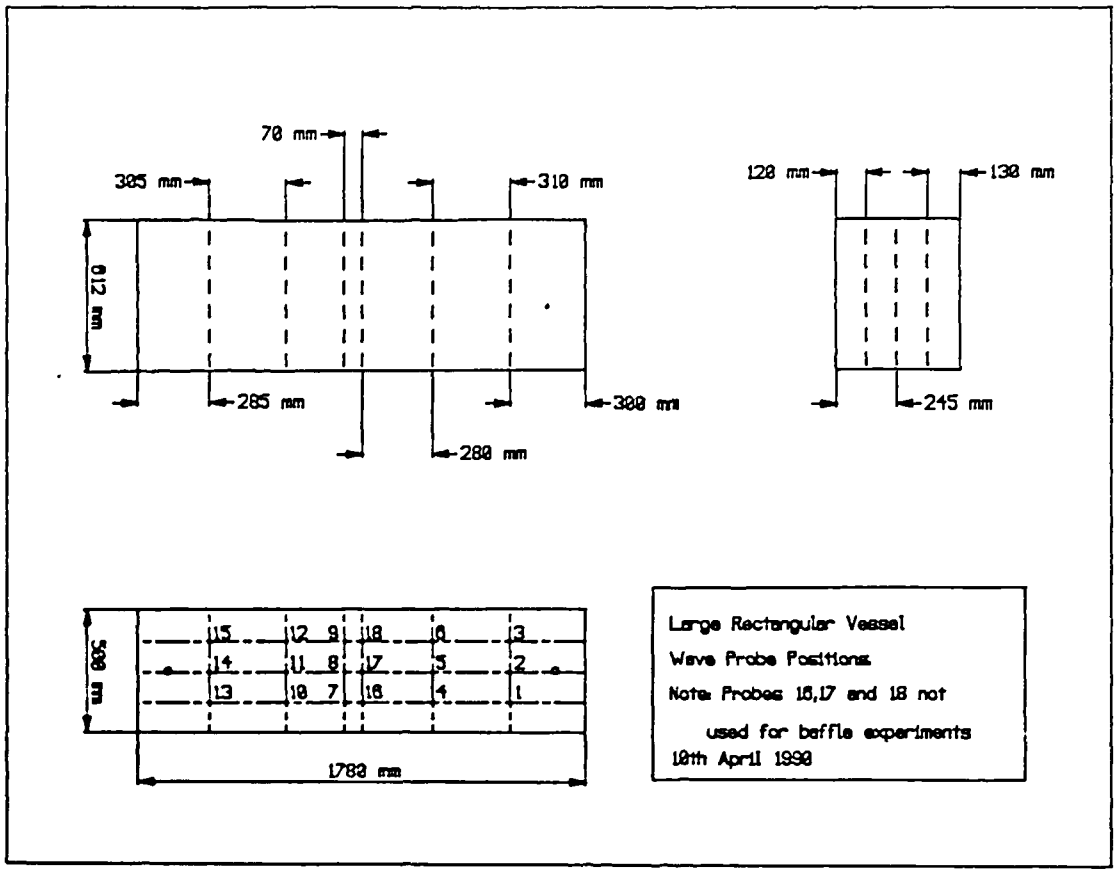

Figure 8.1: Wave probe positions in the large rectangular vessel.

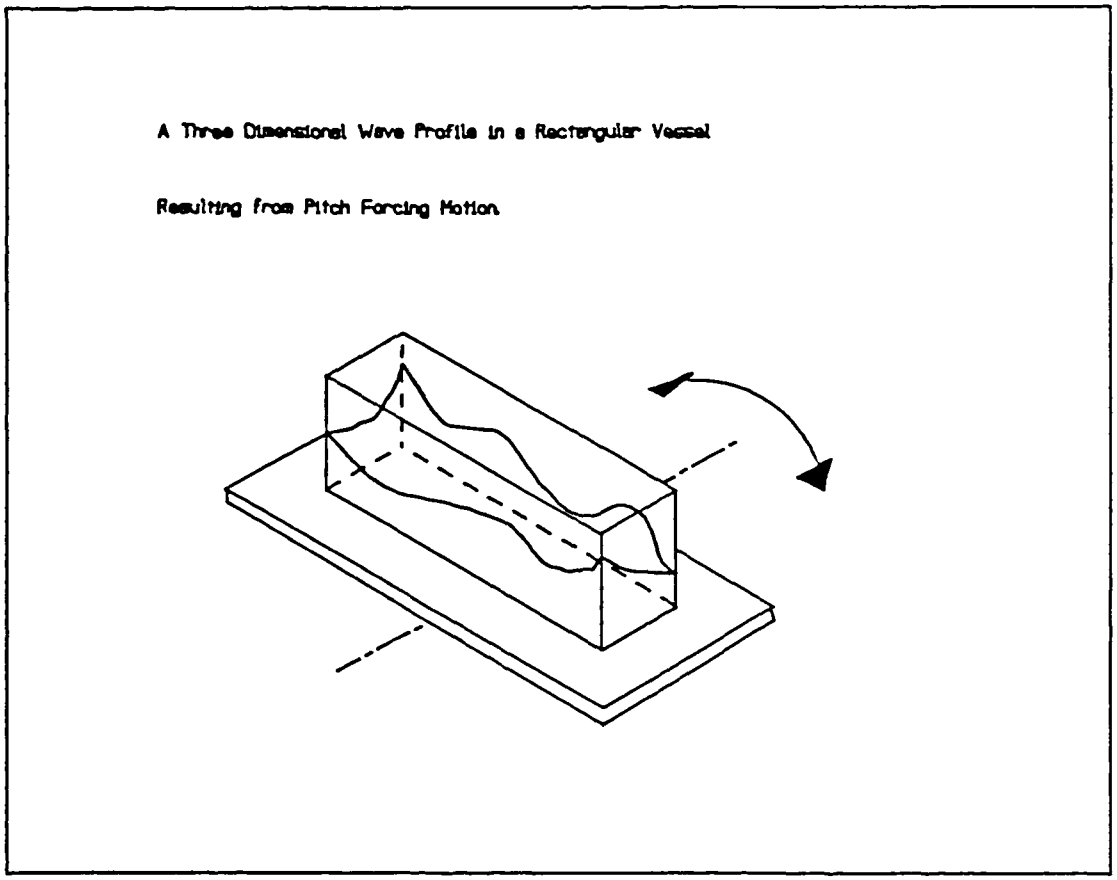

Figure 8.2: Sketch of three dimensional wave profiles observed in the large rectangular vessel.

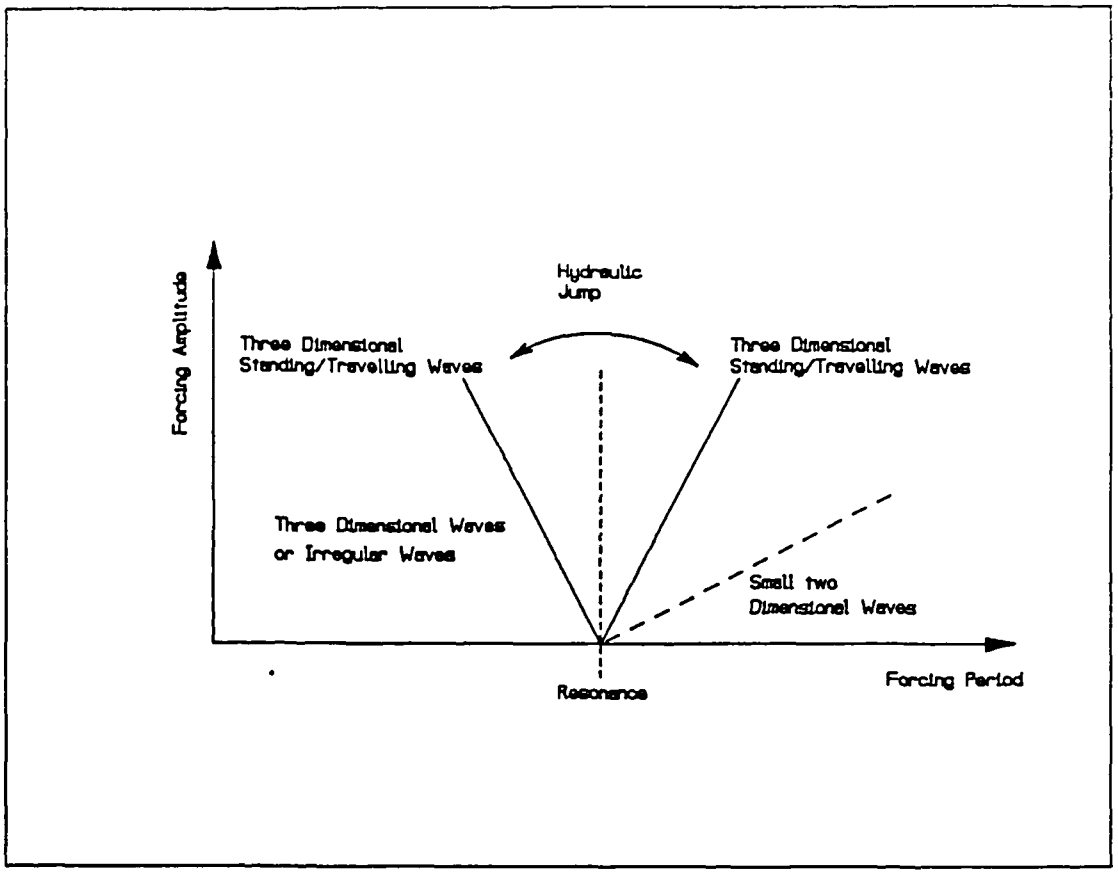

Figure 8.3: Sketch of the relationship between forcing period and amplitude to the shape of the free surface.

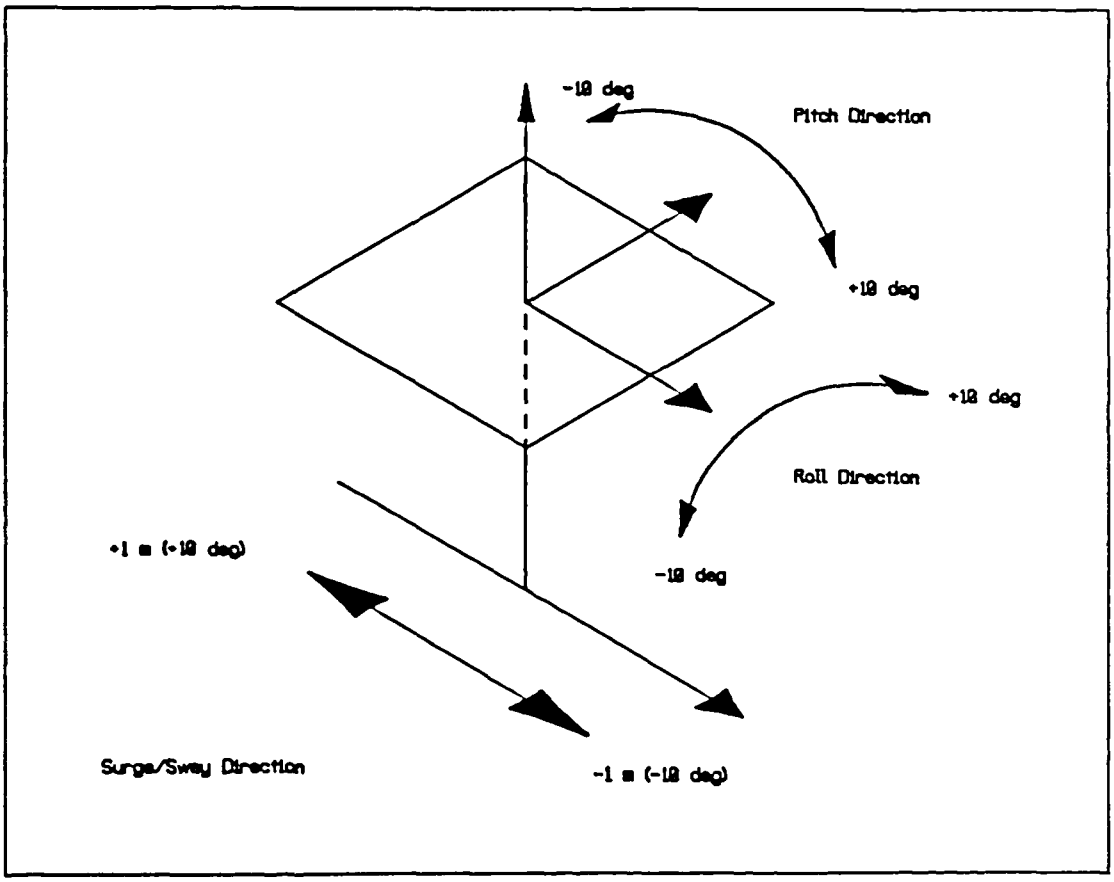

Figure 8.4: Relationship between simulator position and the phase angle of applied forcing motions.

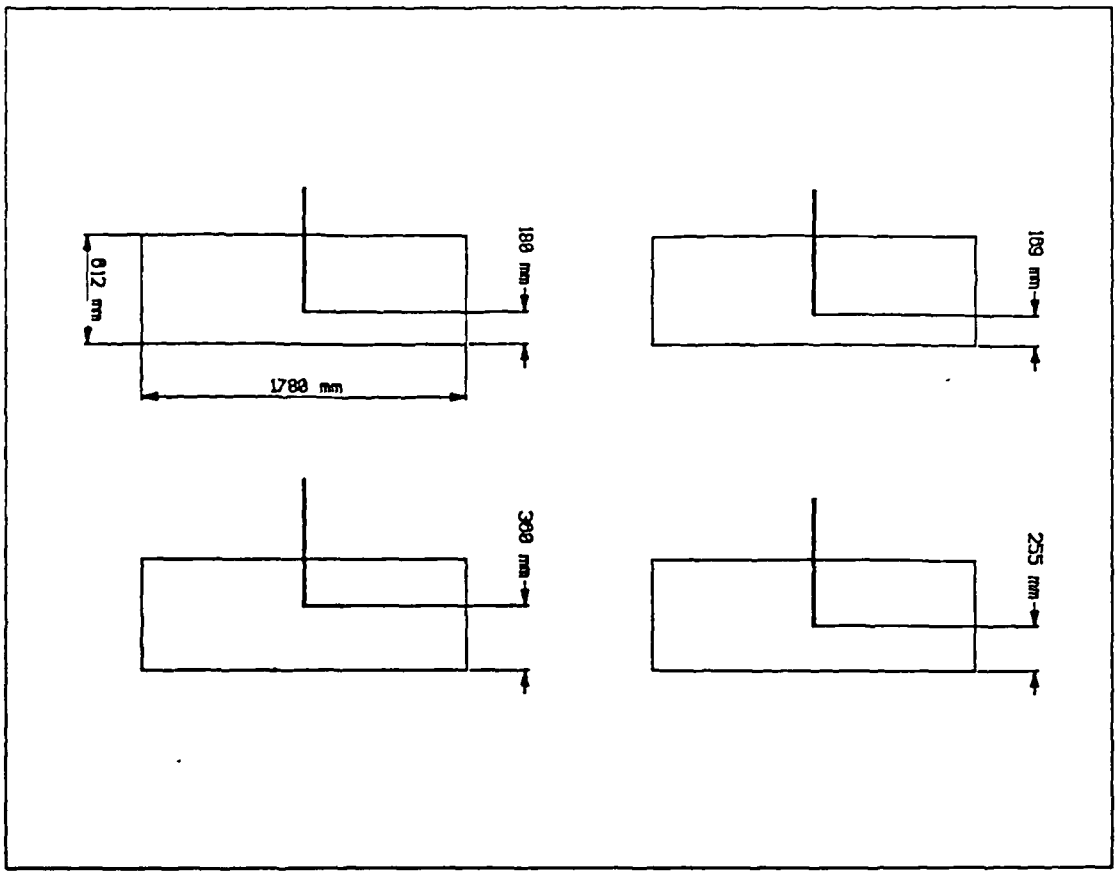

Figure 8.5: Details baffle placement in the large rectangular vessel.

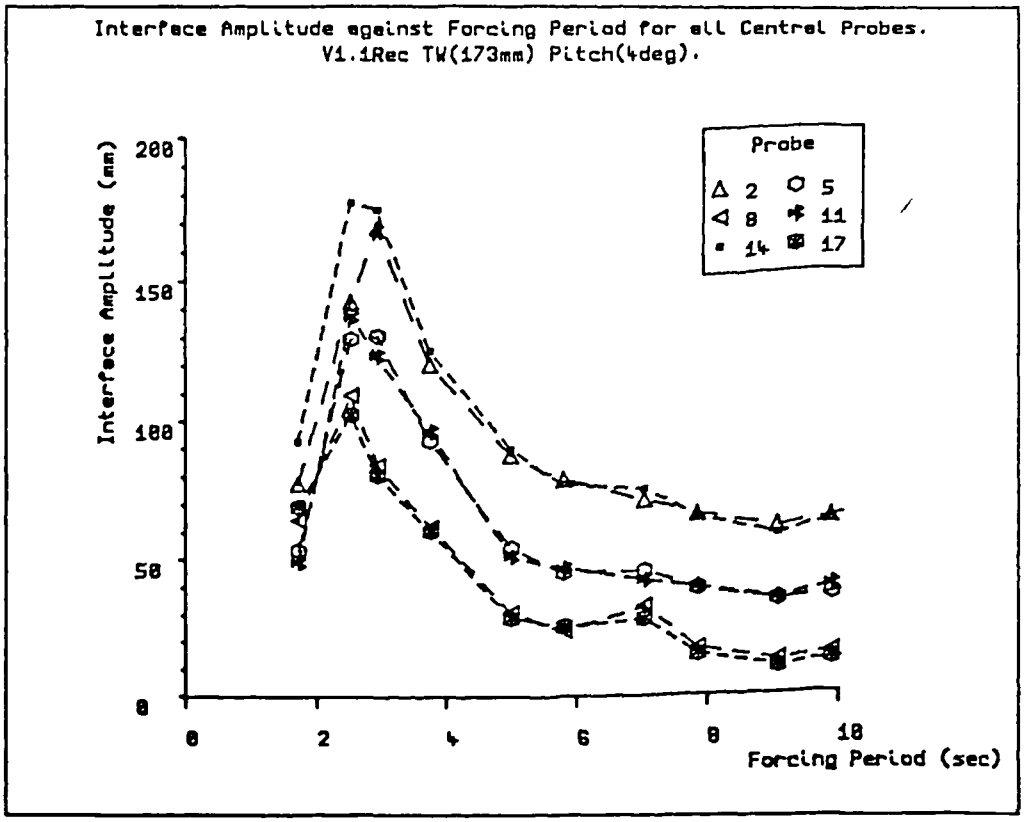

Graph 8.1: Effect of forcing period on interface amplitude at different positions inside the large rectangular vessel when subject to pitch forcing at ±4° amplitude.

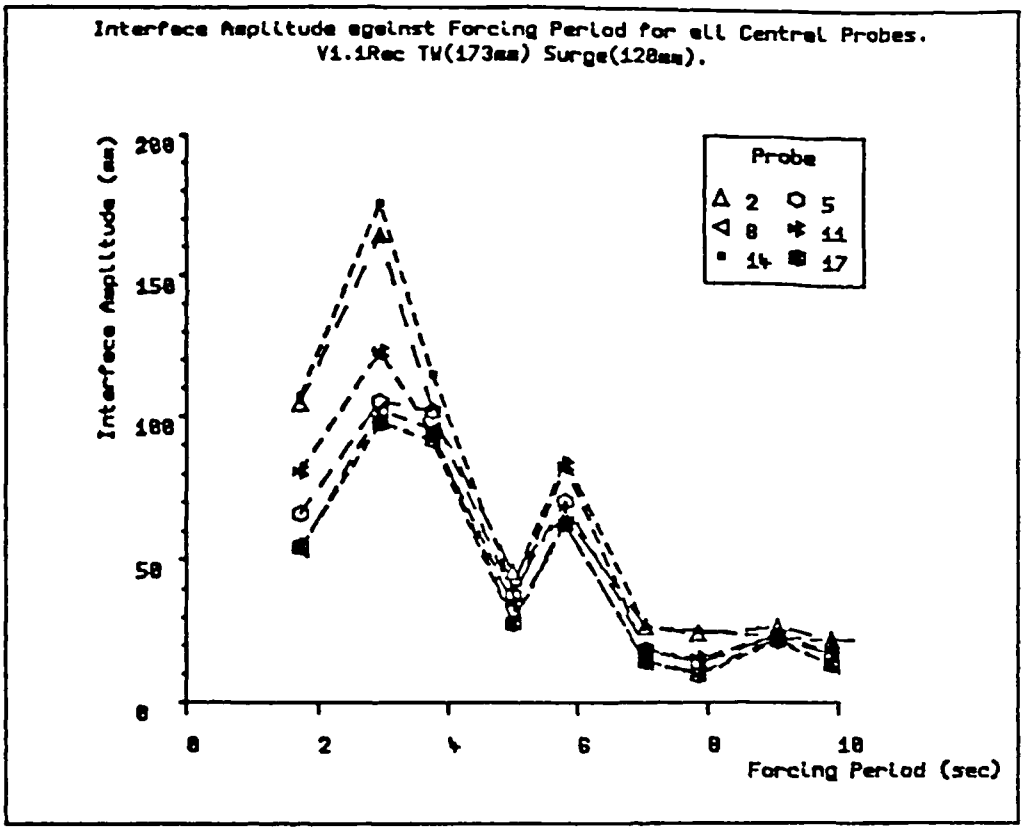

Graph 8.2: Effect of forcing period on interface amplitude at different positions inside the large rectangular vessel when subject to surge motion at ±120mm amplitude.

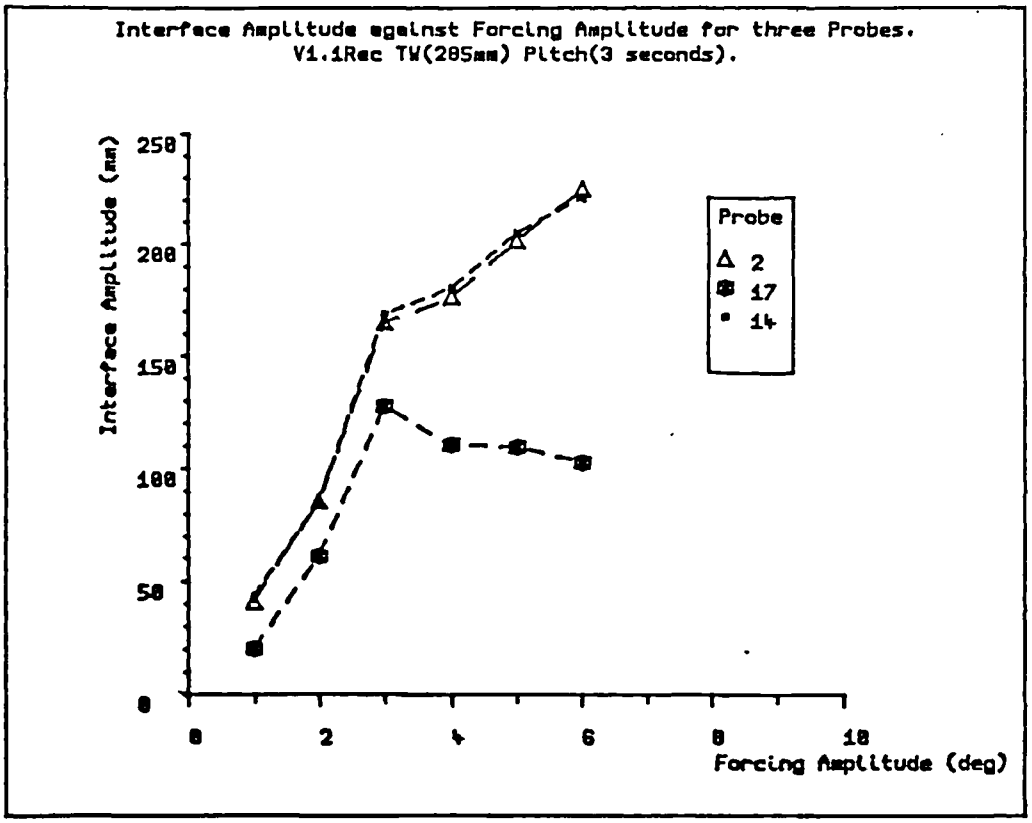

Graph 8.3a: Effect of forcing amplitude on interface amplitude for the large rectangular vessel under pitch motion at 3 seconds period.

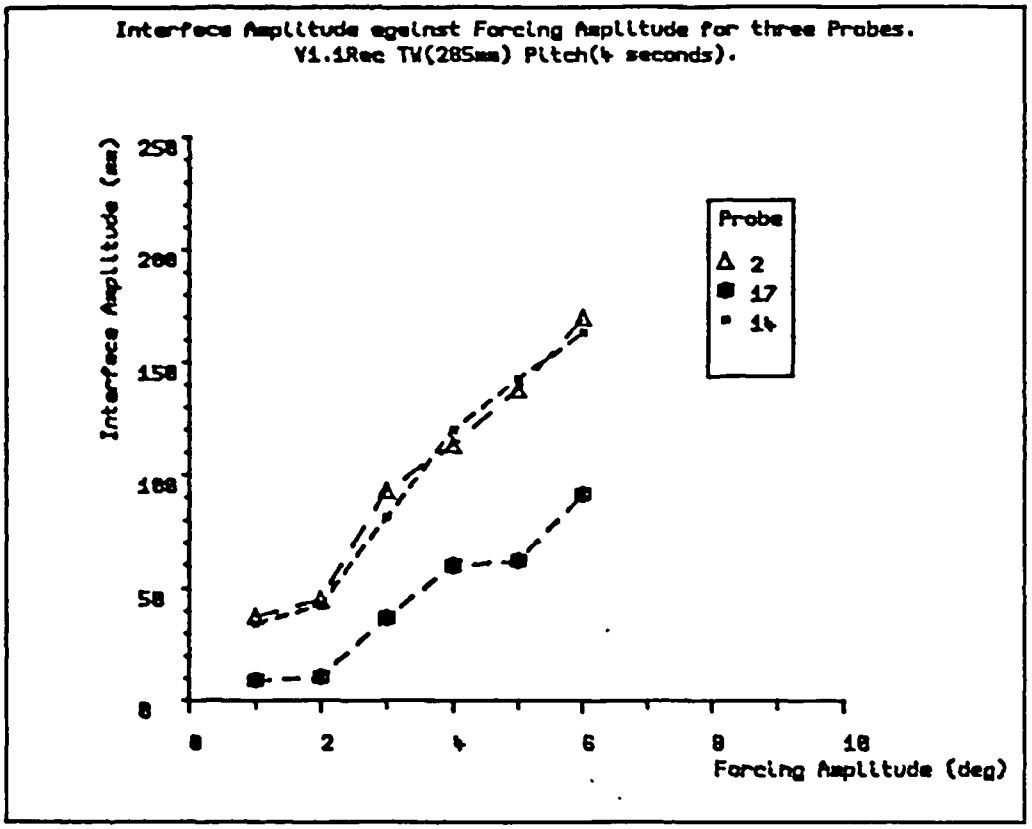

Graph 8.3b: Effect of forcing amplitude on interface amplitude for the large rectangular vessel under pitch motion at 4 seconds period.

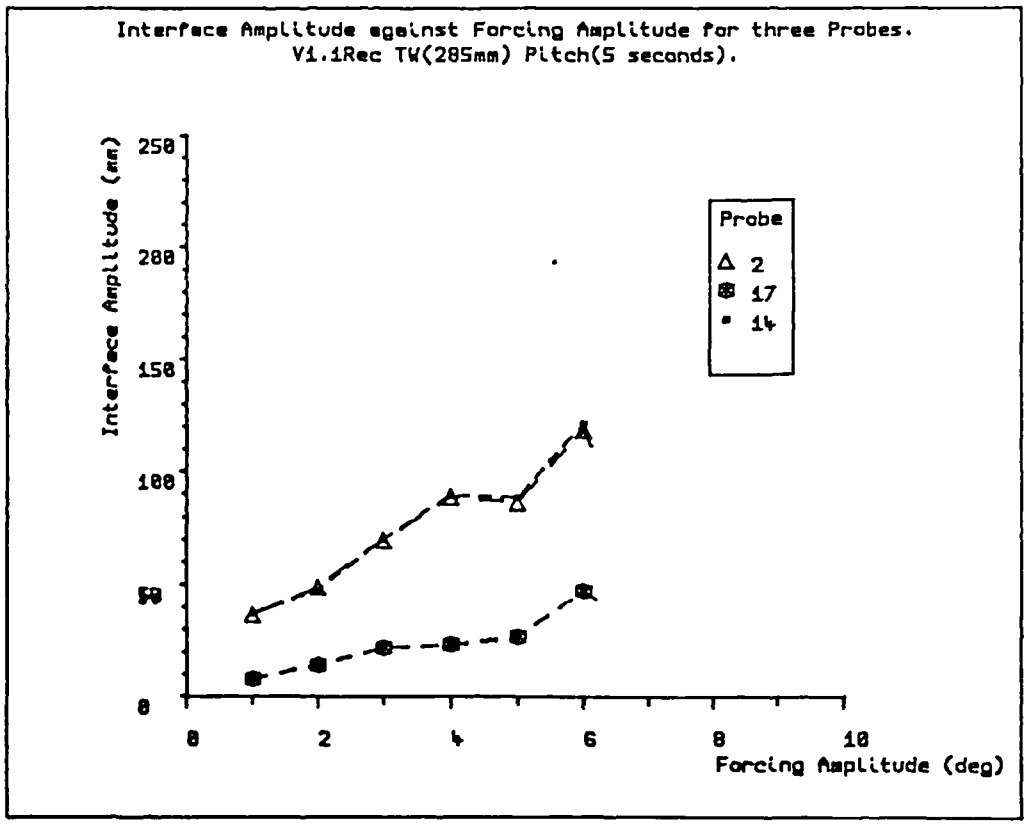

Graph 8.3c: Effect of forcing amplitude on interface amplitude for the large rectangular vessel under pitch motion at 5 seconds period.

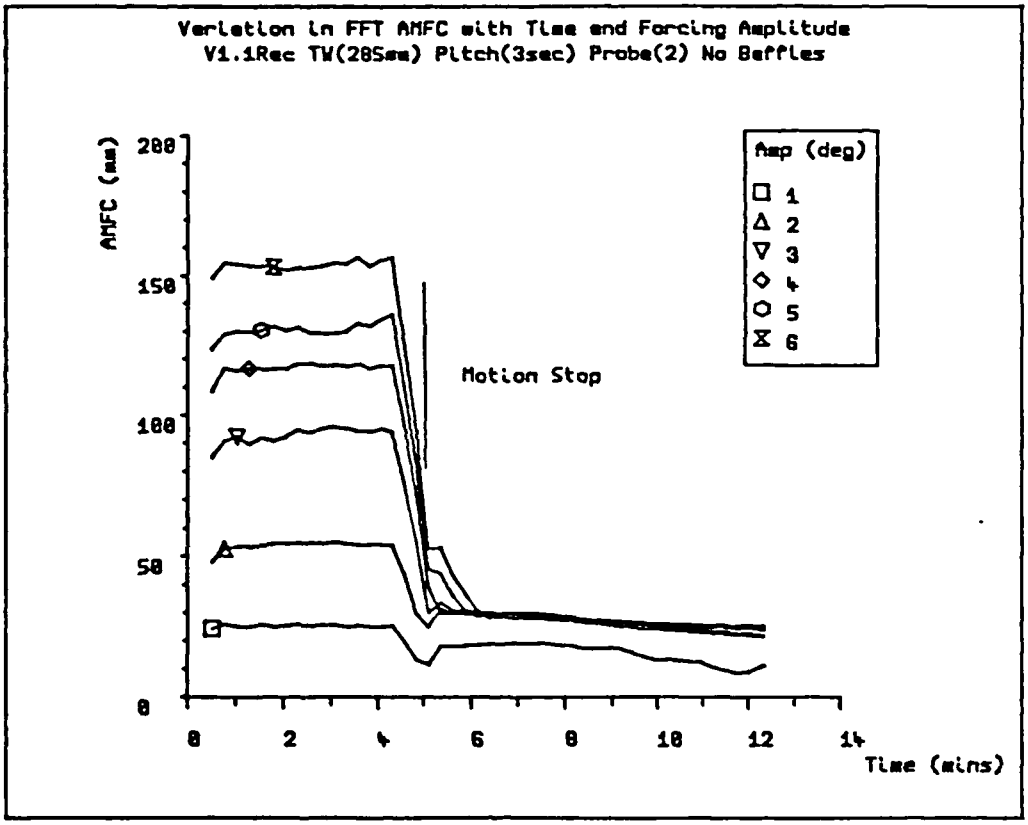

Graph 8.4a: Condensed FFT profile plots resulting from pitch forcing at 3 second period for the large rectangular vessel.

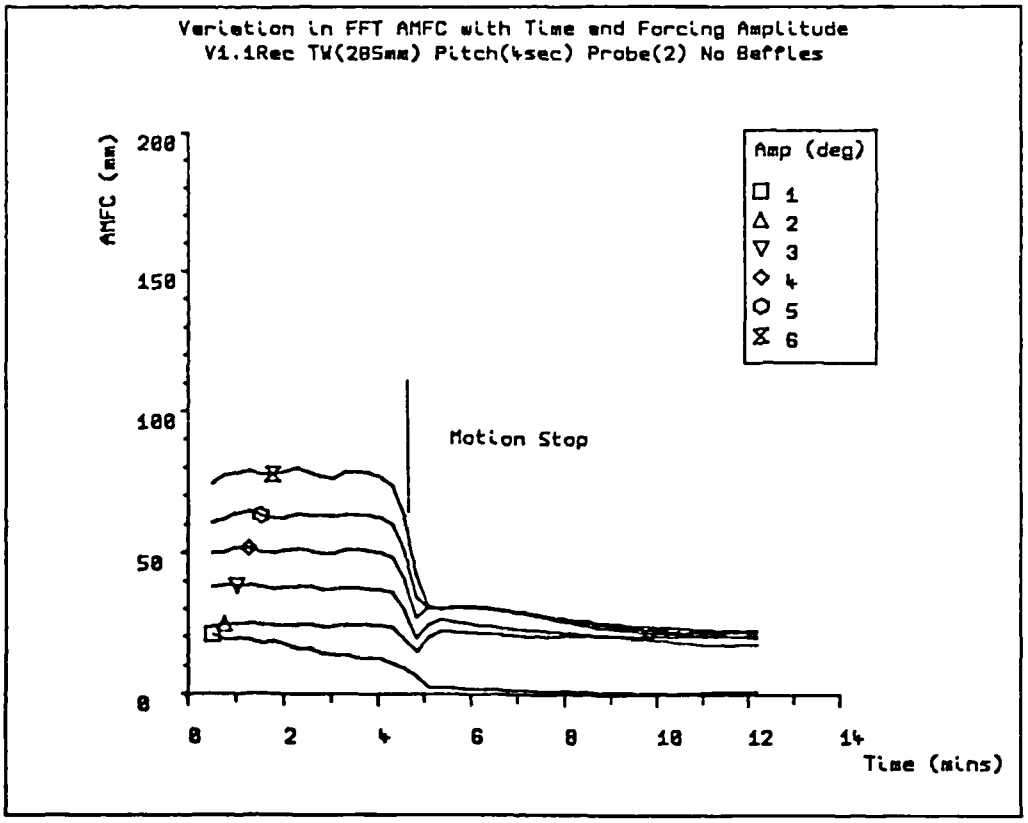

Graph 8.4b: Condensed FFT profile plots resulting from pitch forcing at 4 second period for the large rectangular vessel.

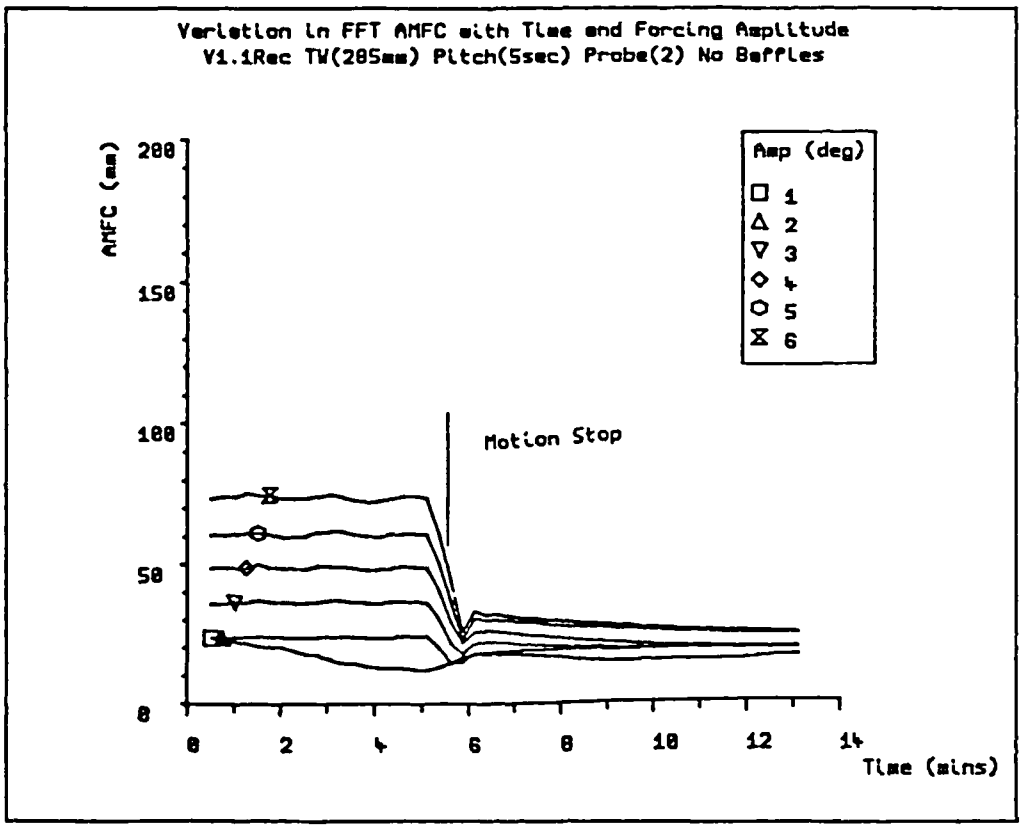

Graph 8.4c: Condensed FFT profile plots resulting from pitch forcing at 5 second period for the large rectangular vessel.

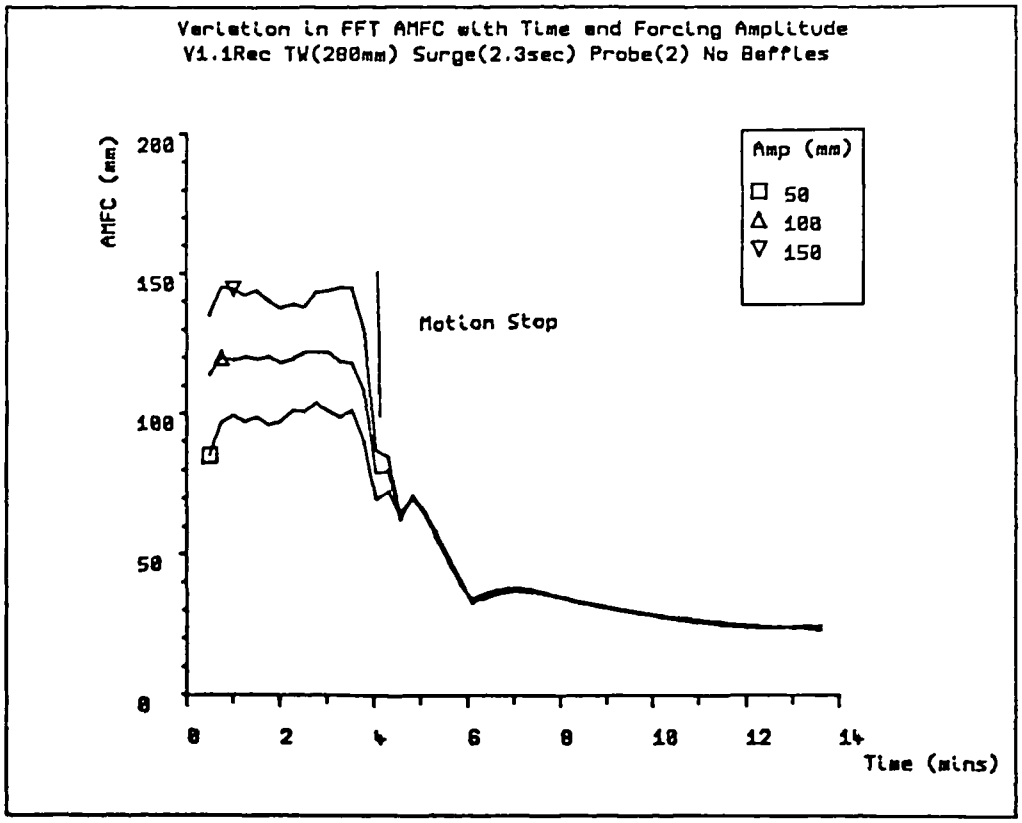

Graph 8.5a: Condensed FFT profile plots resulting from surge forcing at 2.3 second period for the large rectangular vessel.

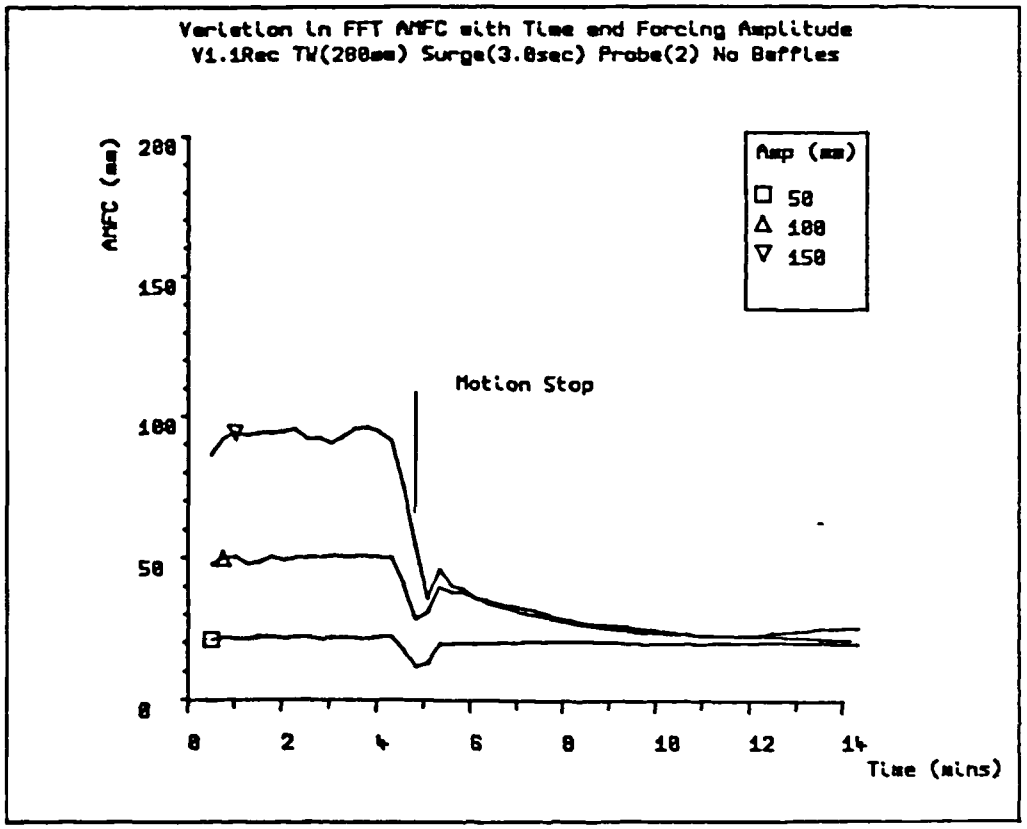

Graph 8.5b: Condensed FFT profile plots resulting from pitch forcing at 3.0 second period for the large rectangular vessel.

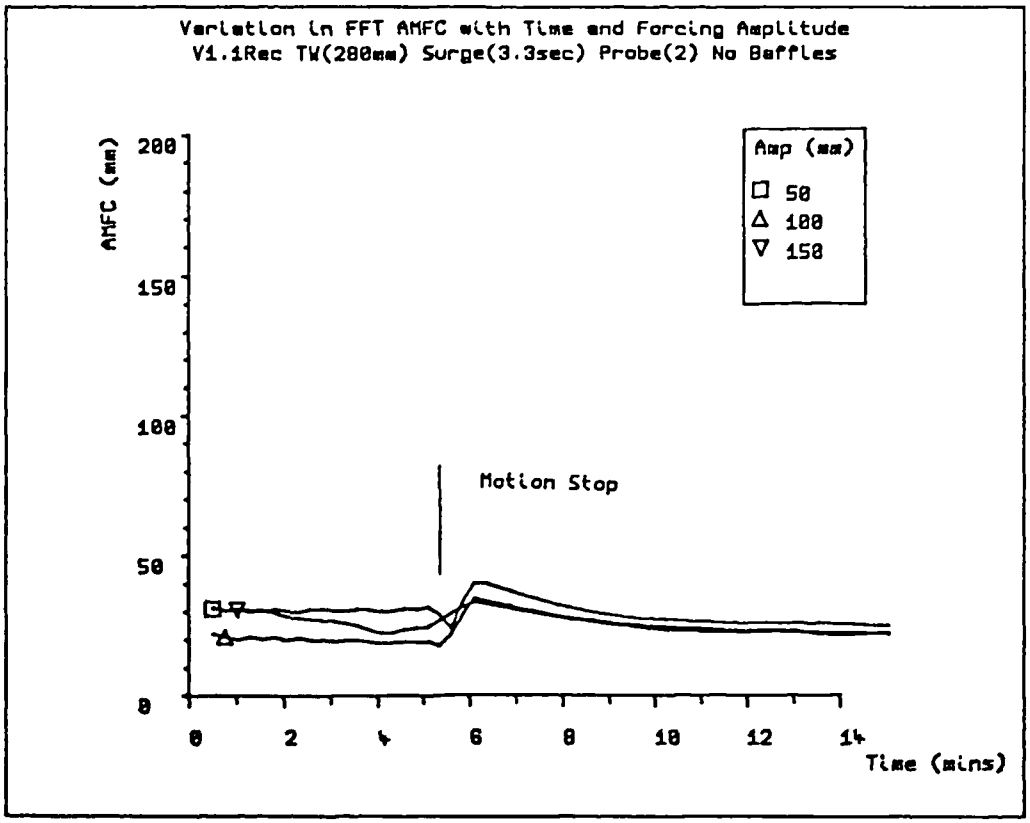

Graph 8.5c: Condensed FFT profile plots resulting from pitch forcing at 3.3 second period for the large rectangular vessel.

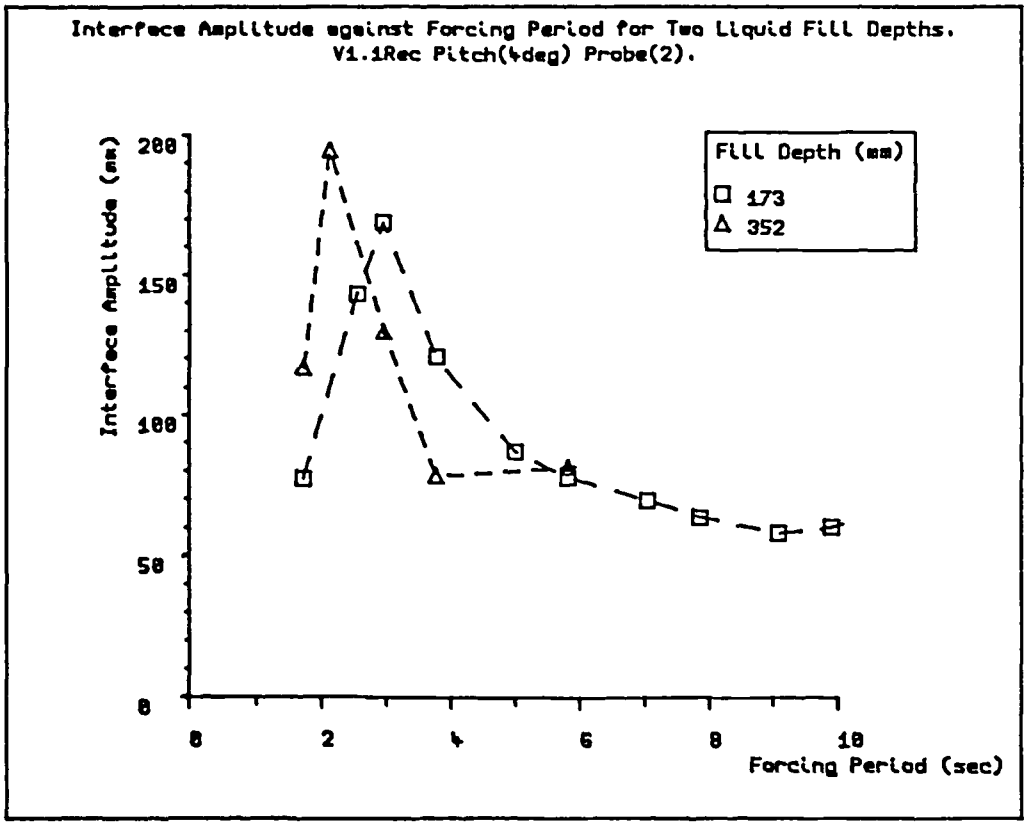

Graph 8.6: Effect of liquid fill depth and forcing period on interface amplitude for the large rectangular vessel under pitch forcing at ±4° amplitude.

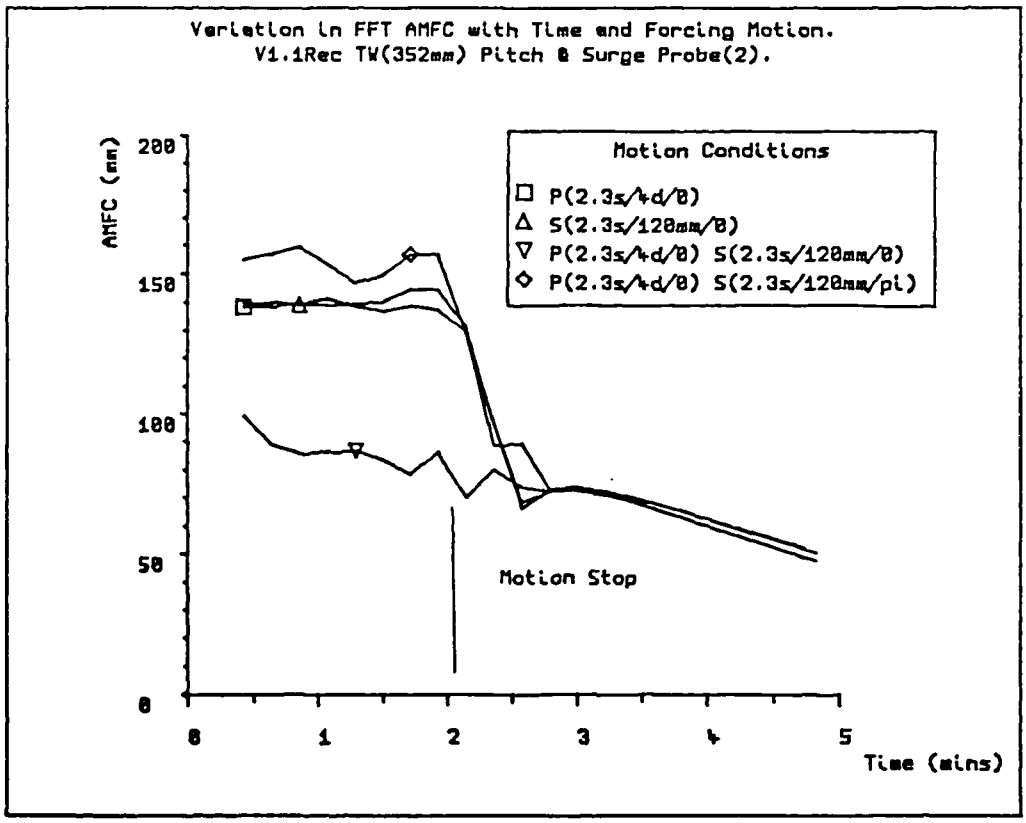

Graph 8.7: Condensed FFT profile plots resulting from combined pitch & surge forcing at 2.3 second period for the large rectangular vessel.

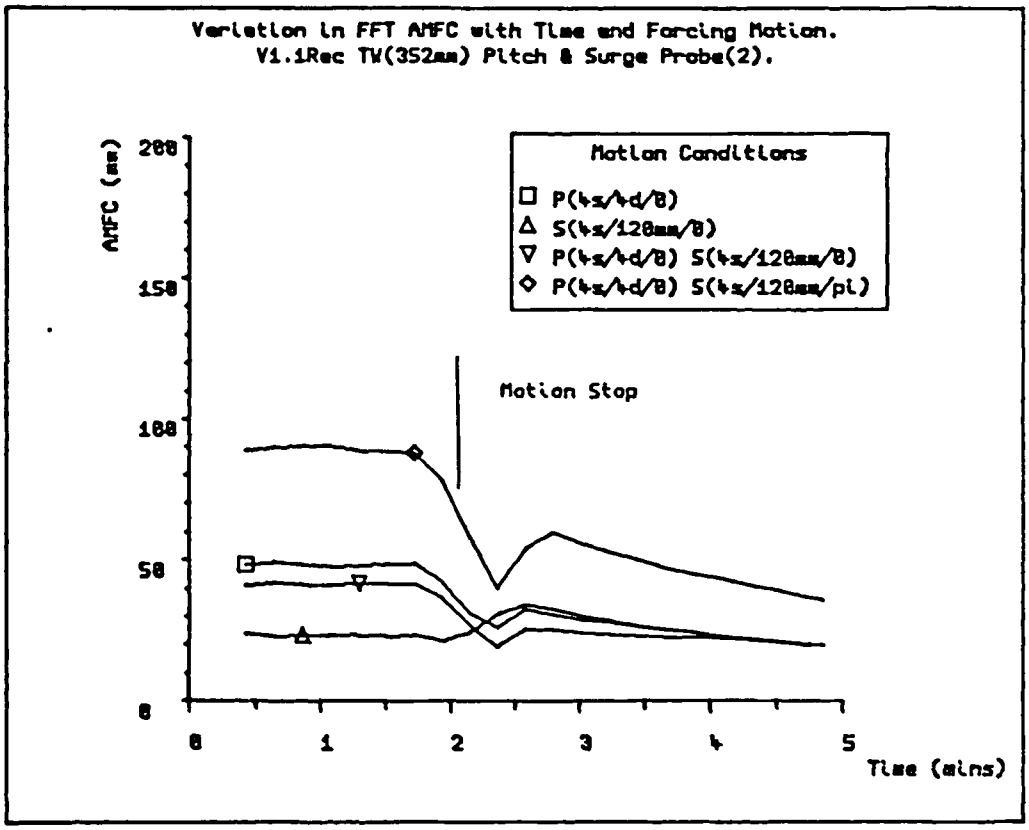

Graph 8.8: Condensed FFT profile plots resulting from combined pitch & surge forcing at 4 second period for the large rectangular vessel.

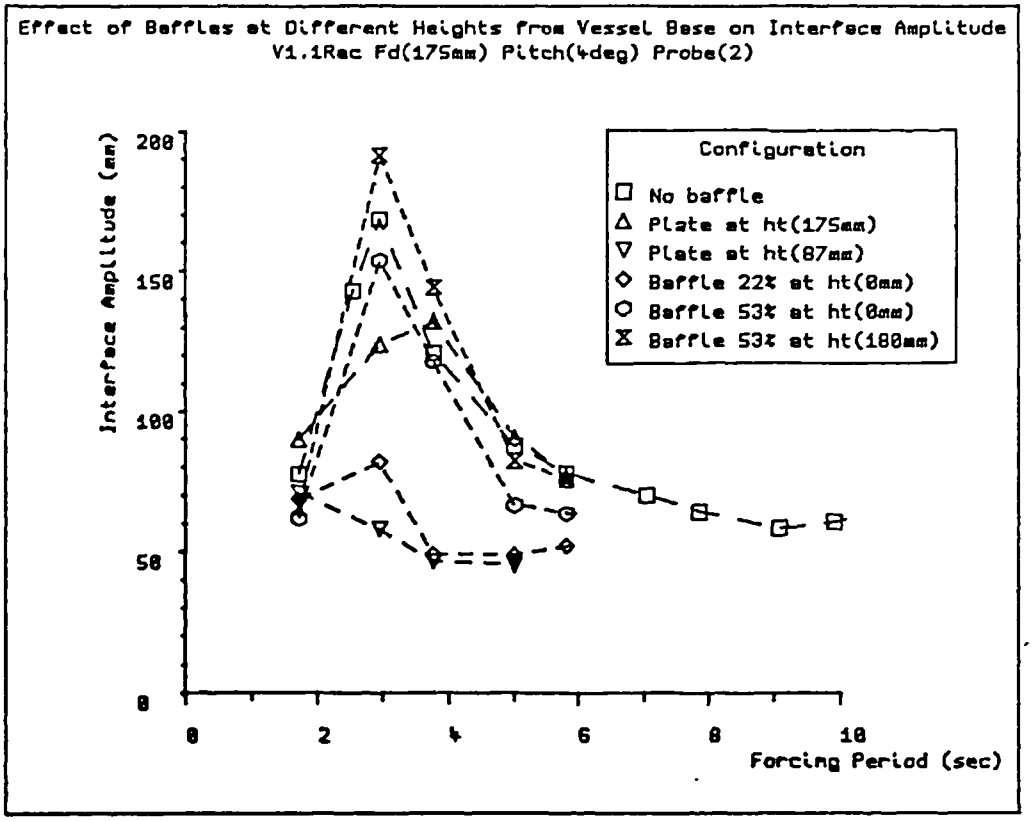

Graph 8.9: Effect of baffles on interface amplitude in relation to forcing period for pitch motion amplitude of ±4°, water depth of 175mm.

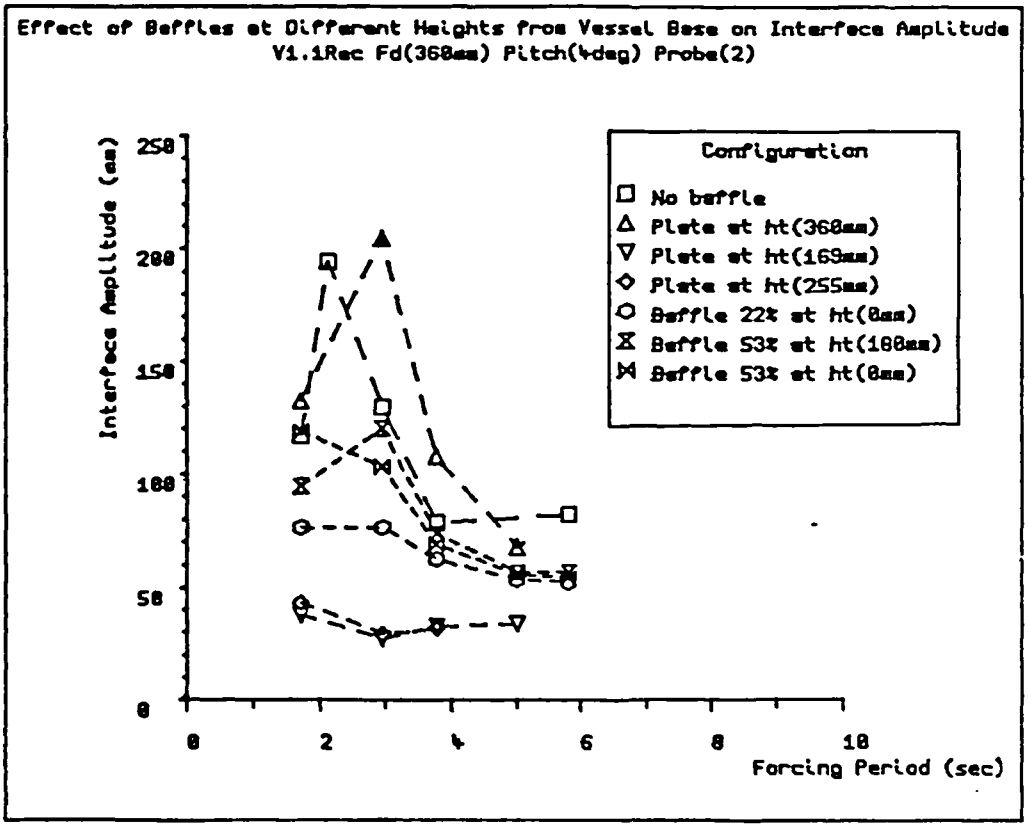

Graph 8.10: Effect of baffles on interface amplitude in relation to forcing period for pitch motion amplitude of ±4°, water depth of 360mm.

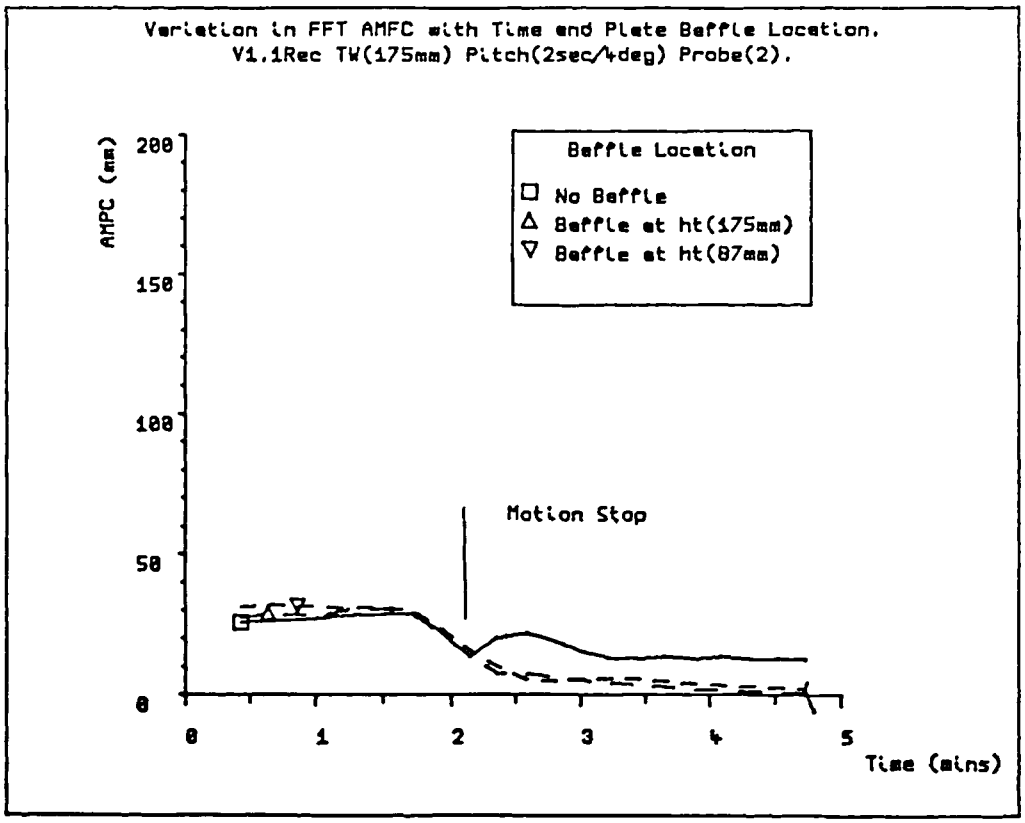

Graph 8.11: Effect of solid plate baffle on air/water interface profile under pitch forcing (2 secs, ±4°). Water depth 175mm.

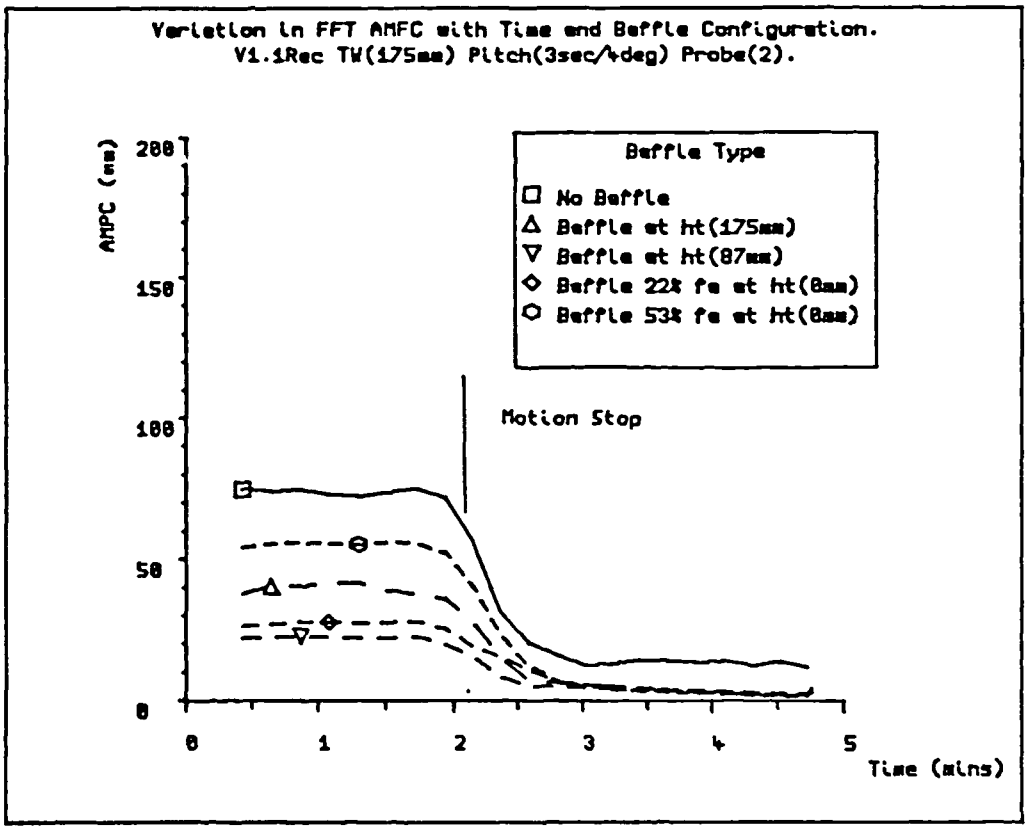

Graph 8.12: Effect of solid plate baffle and perforated baffles on air/water interface profile under pitch forcing (3 secs, ±4°). Water depth 175mm.

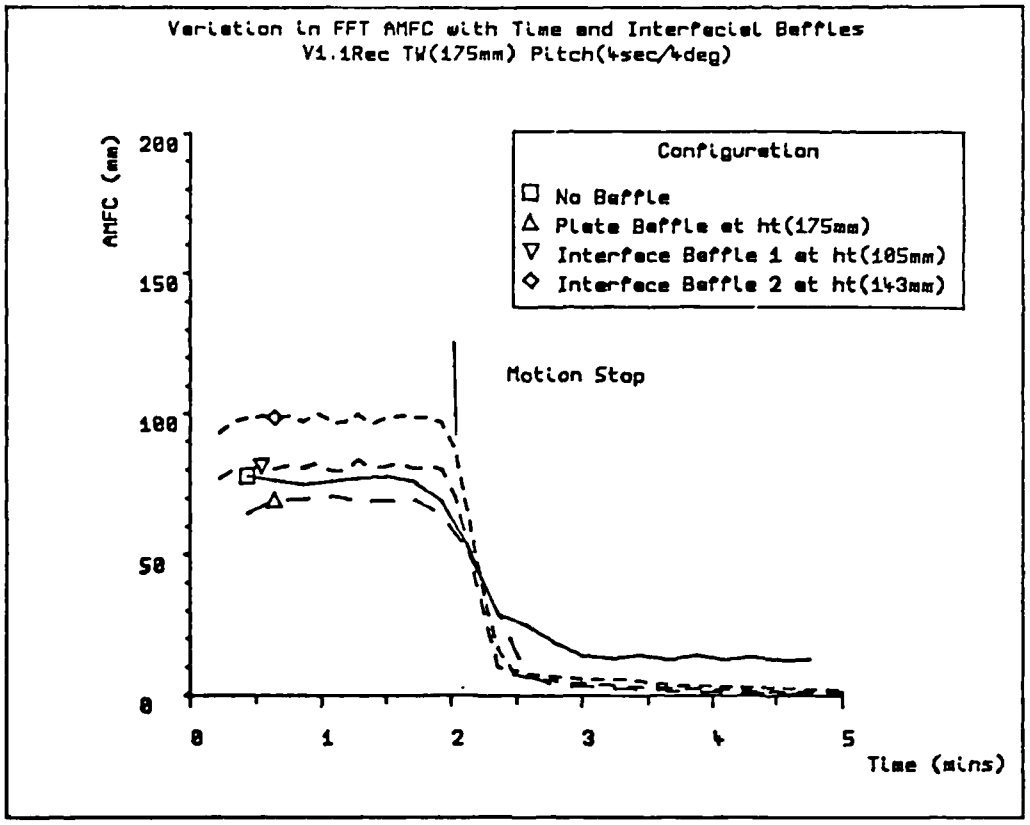

Graph 8.13: Effect of solid plate and interface location on air/water interface profile under pitch forcing (4 secs, ±4°). Water depth 175mm.

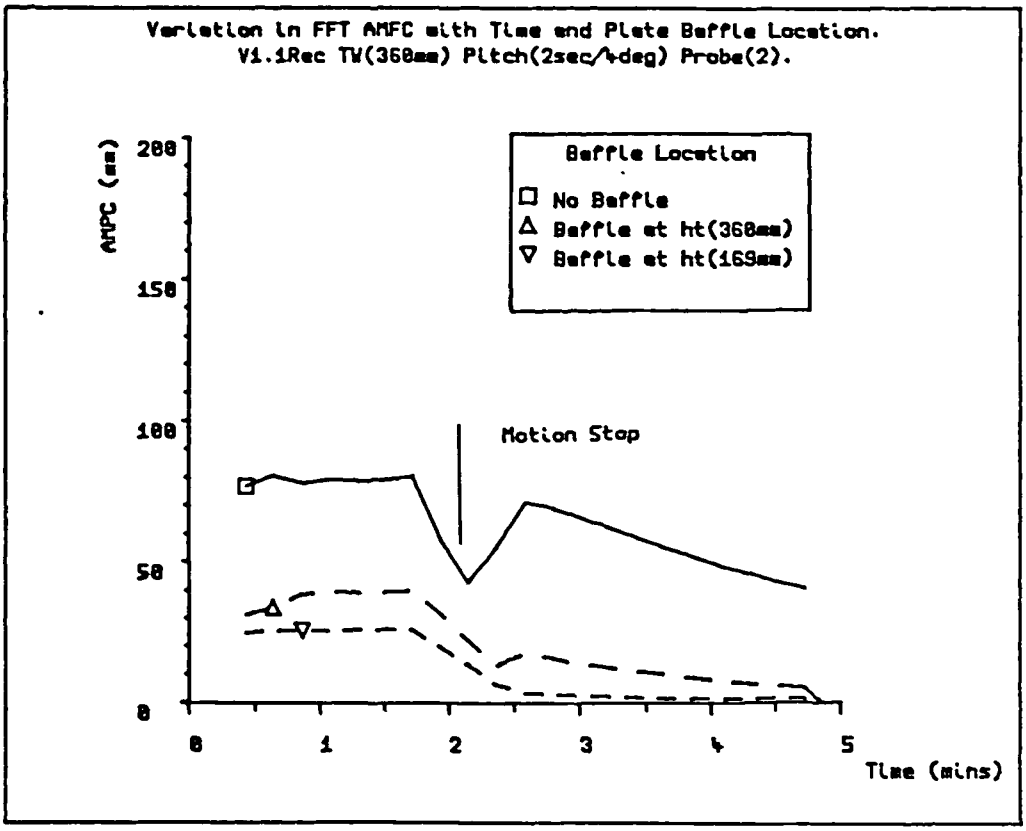

Graph 8.14: Effect of solid plate baffle on air/water interface profile under pitch forcing (2 secs, ±4°). Water depth 360mm.

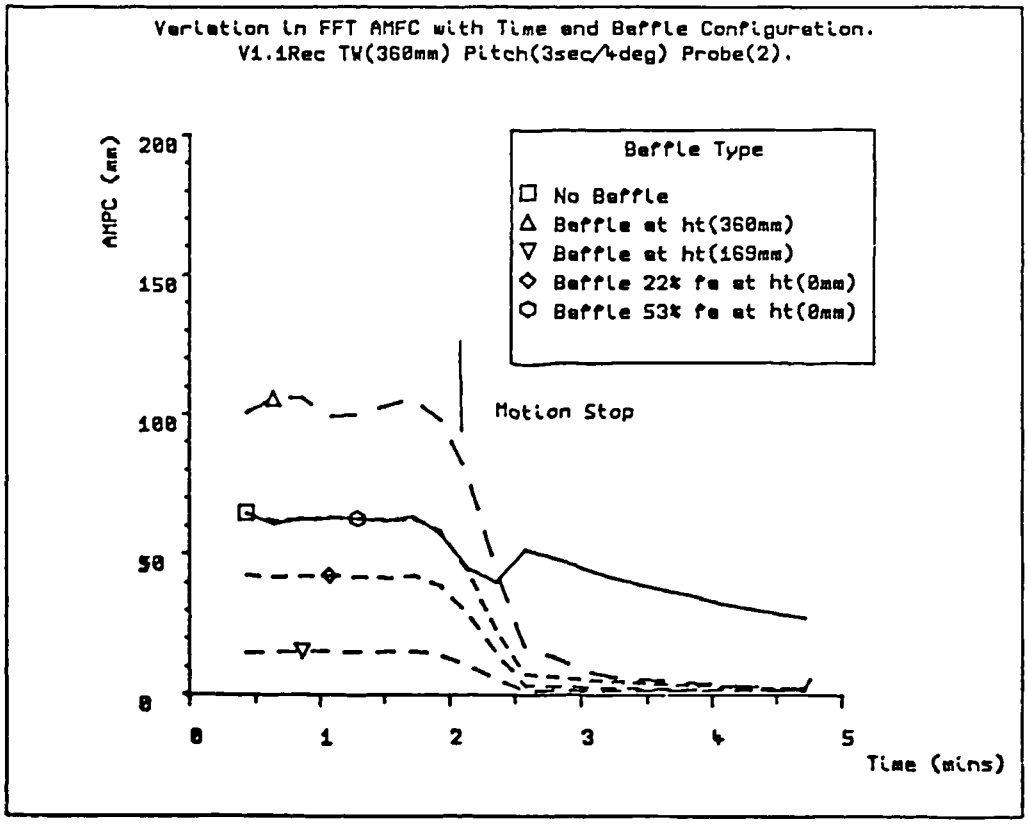

Graph 8.15: Effect of solid plate baffle and perforated baffles on air/water interface profile under pitch forcing (3 secs, ±4°). Water depth 360mm.

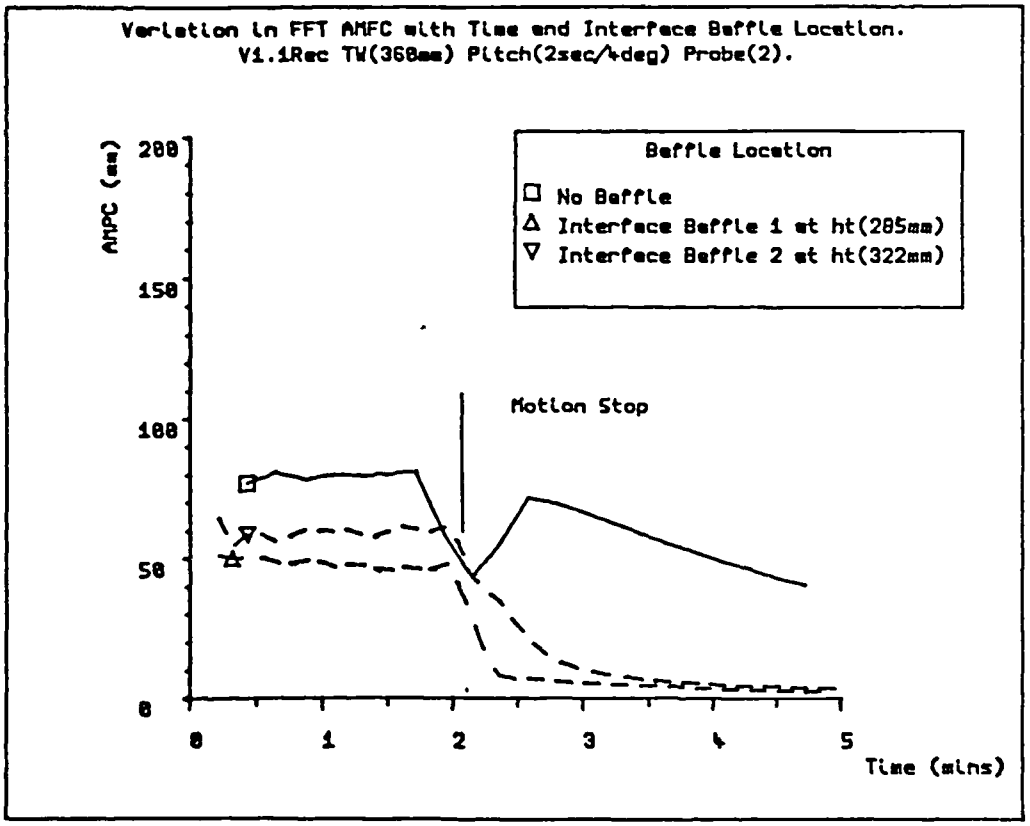

Graph 8.16: Effect of interface baffles on air/water interface profile under pitch forcing (2 secs, ±4°). Water depth 360mm.

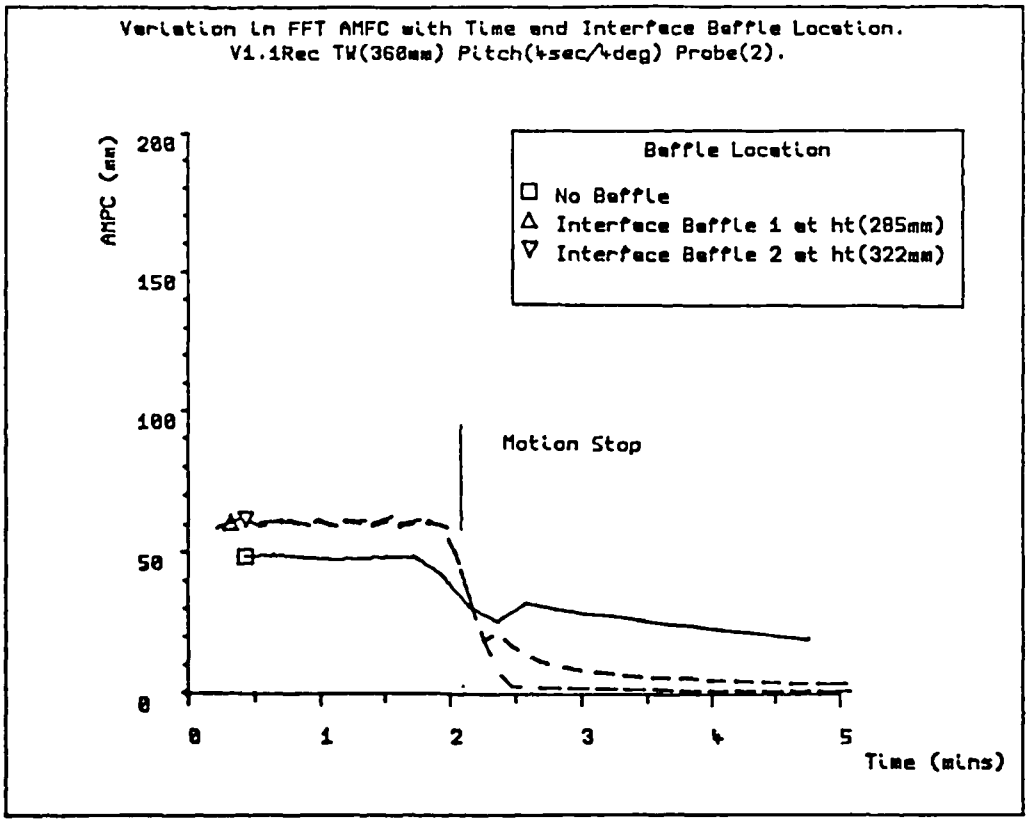

Graph 8.17: Effect of interface baffles on air/water interface profile under pitch forcing (4 secs, ±4°). Water depth 360mm.

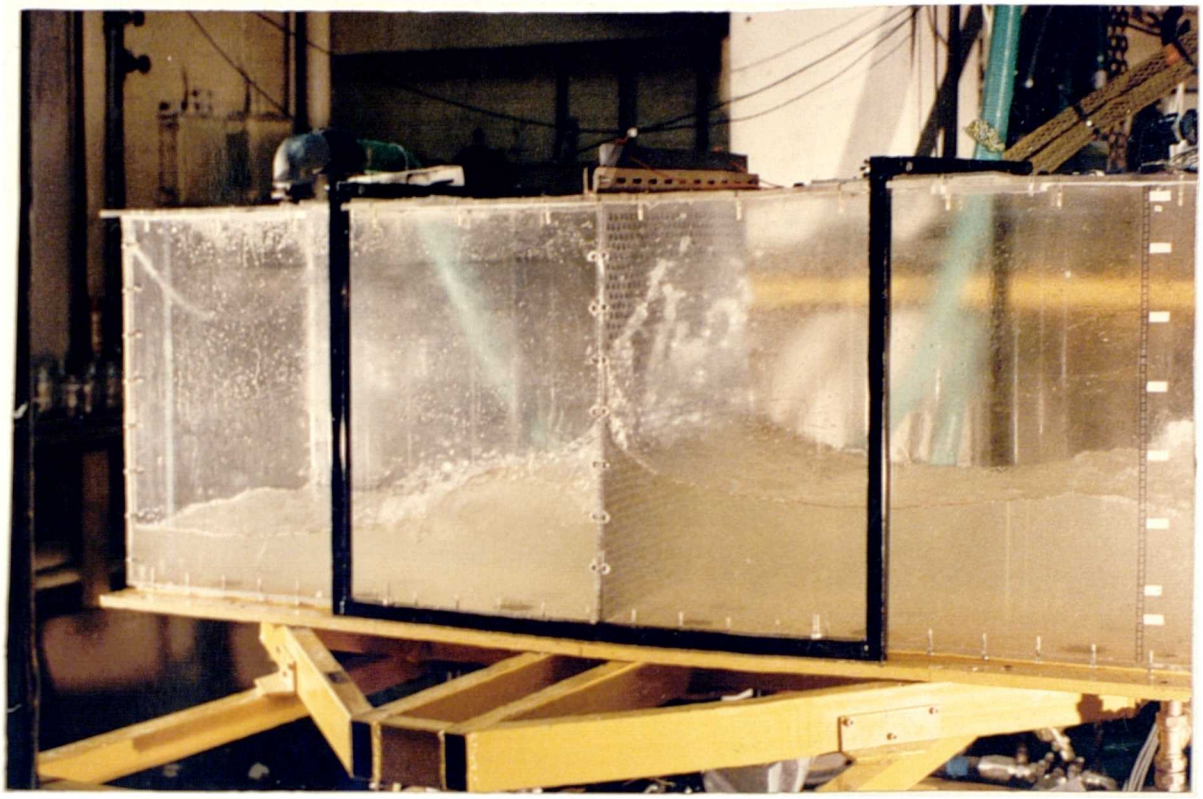

Photograph 8.1: Perforated baffle (53% free area) under pitch forcing motion (3 secs, ±4°). Water fill depth of 175mm.

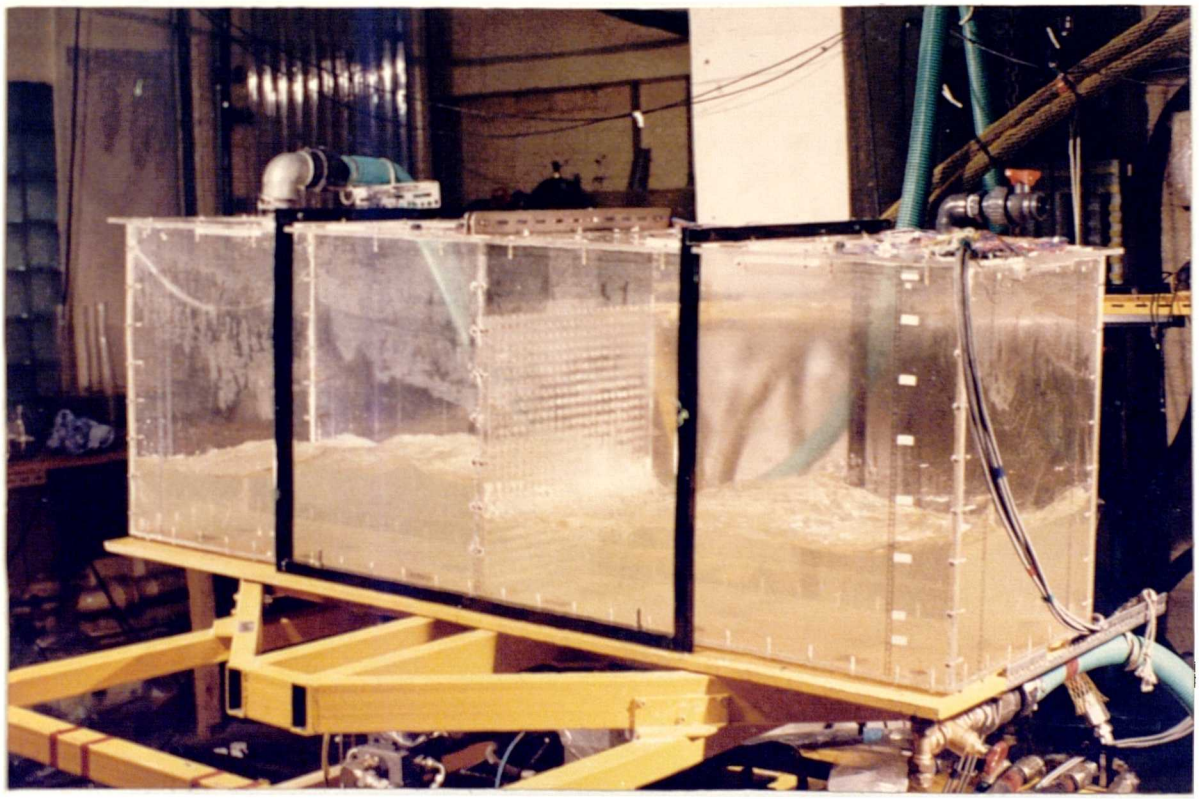

Photograph 8.2: Perforated baffle (22% free area) under pitch forcing motion (3 secs, ±4°). Water fill depth of 175mm.

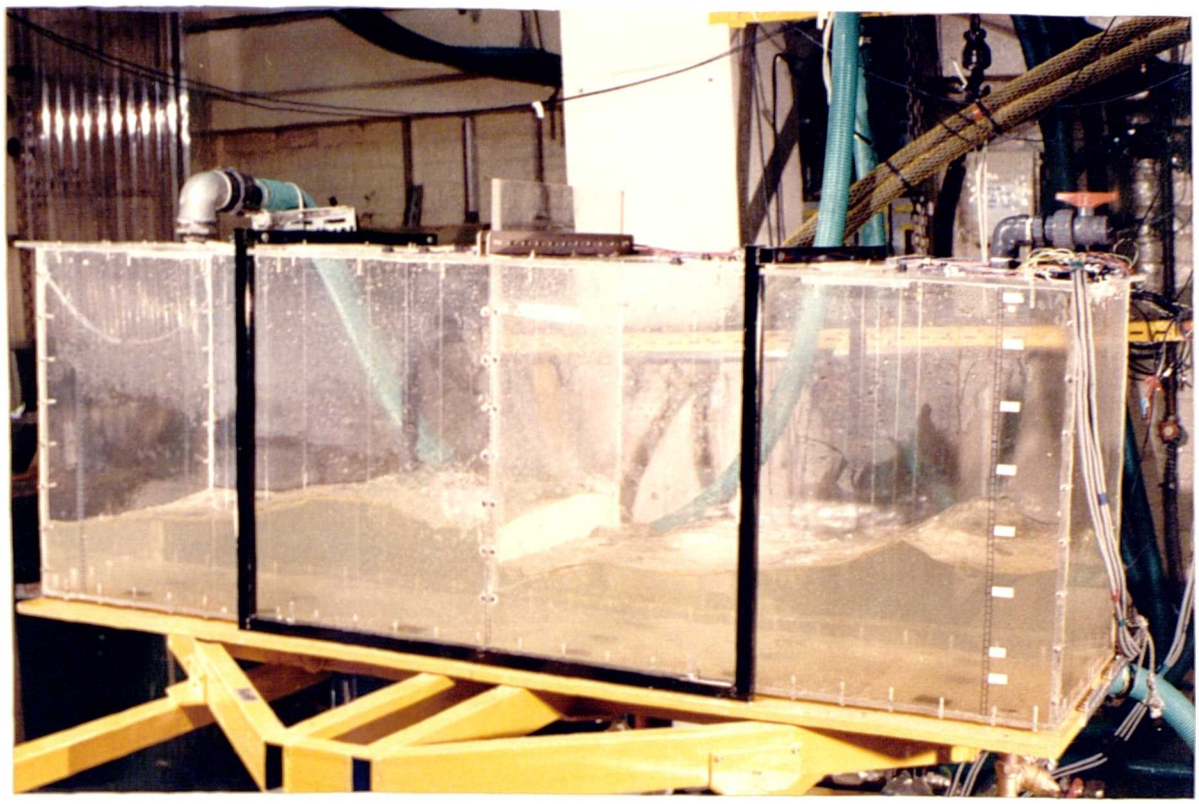

Photograph 8.3: Solid plate baffle penetrating the air/water interface to 87mm under pitch forcing motion (3 secs, ±4°). Water fill depth of 175mm.

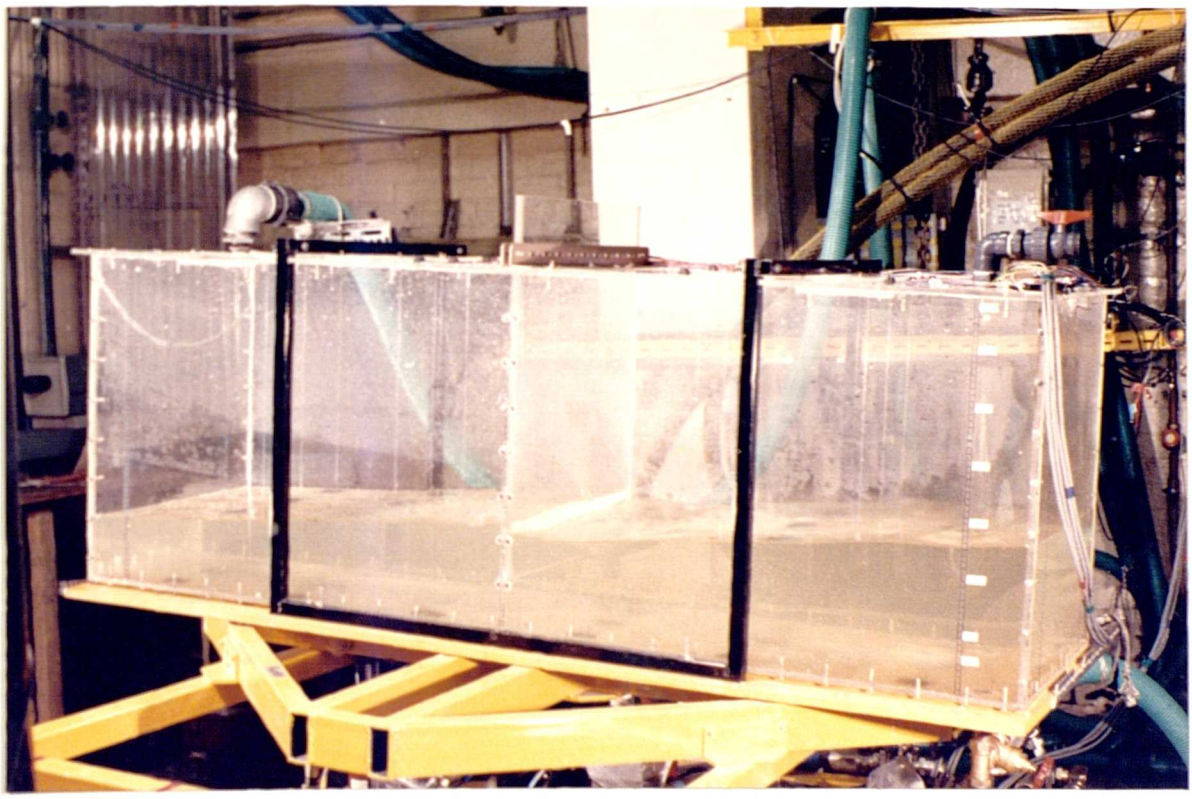

Photograph 8.4: Solid plate baffle penetrating the air/water interface to 87mm under pitch forcing motion (5 secs, ±4°). Water fill depth of 175mm.

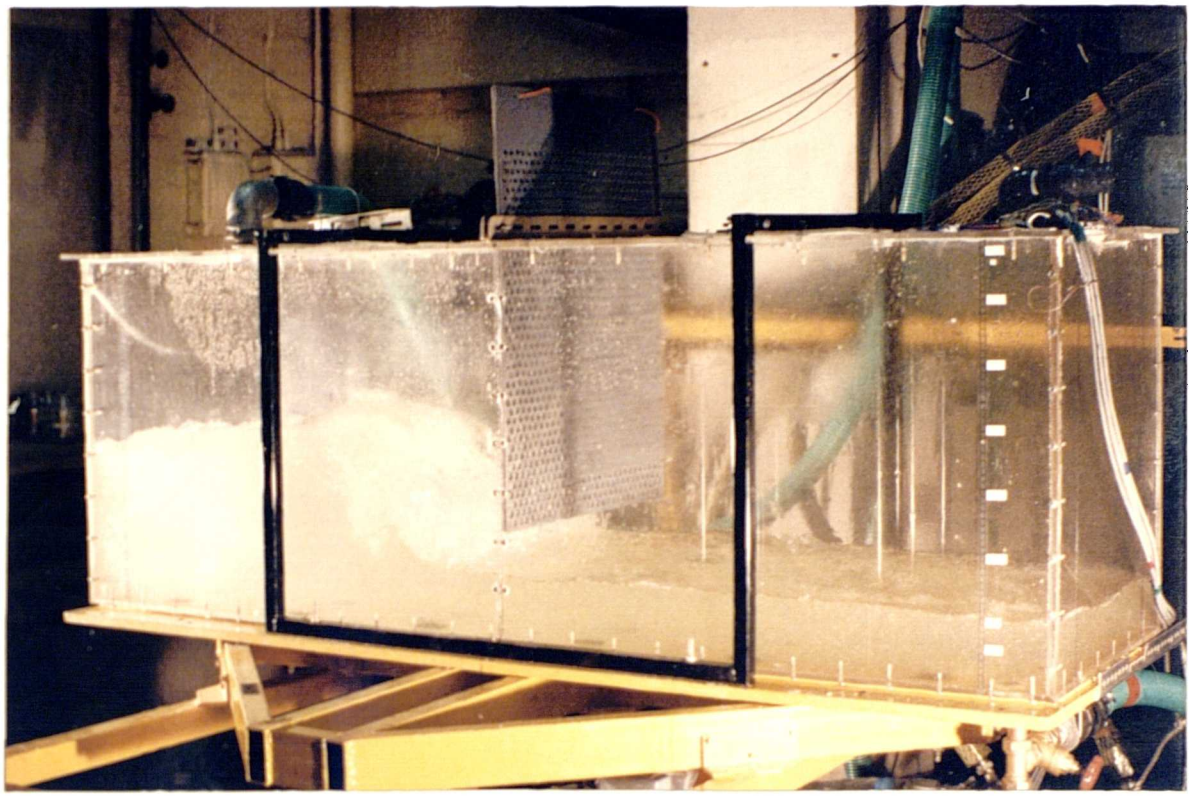

Photograph 8.5: Perforated baffle (53% free area) touching the air/water interface under pitch forcing motion (3 secs, ±4°). Water fill depth of 175mm.

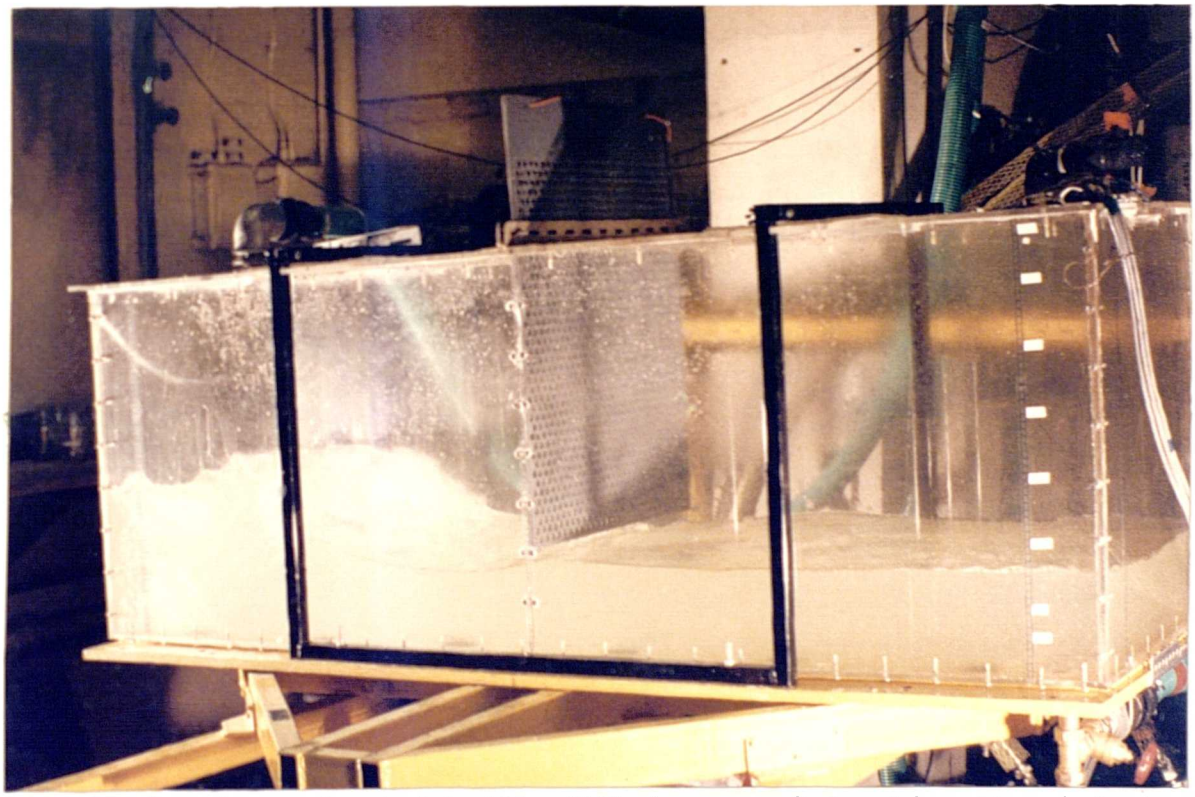

Photograph 8.6: Perforated baffle (53% free area) touching the air/water interface under pitch forcing motion (4 secs, ±4°). Water fill depth of 175mm.

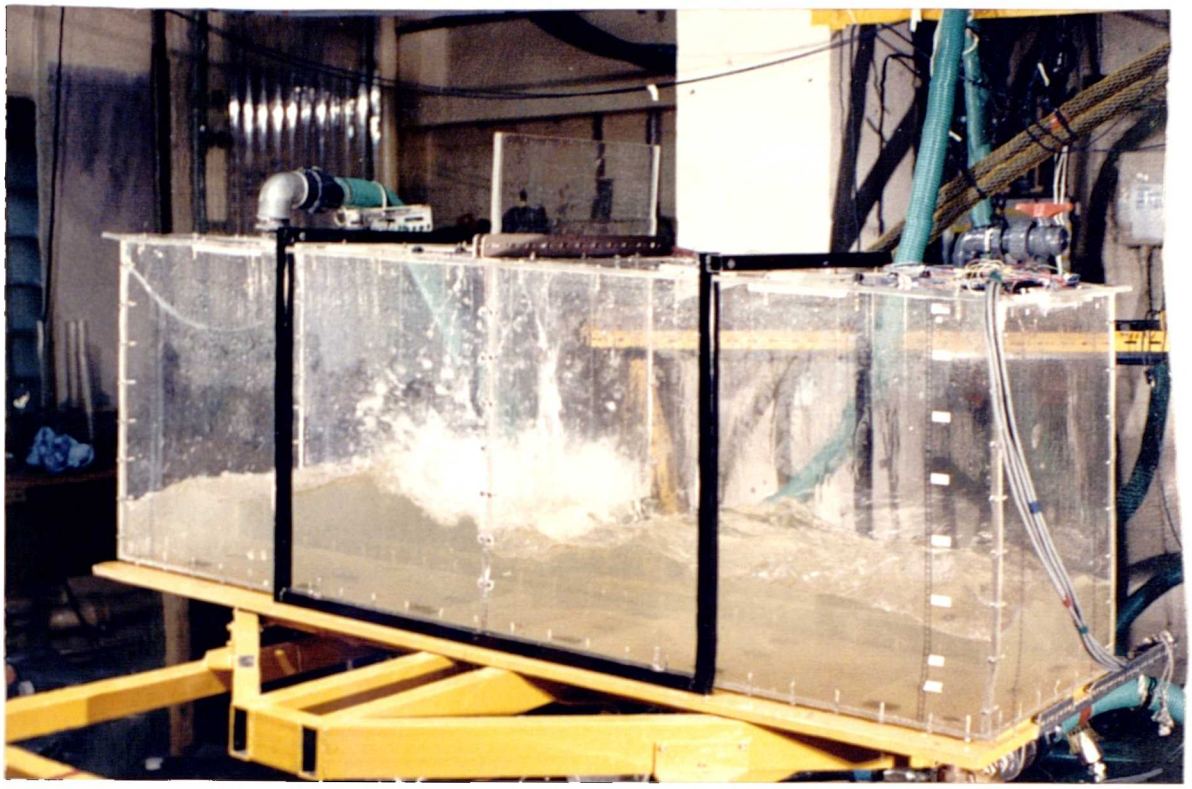

Photograph 8.7: Solid plate baffle touching the air/water interface under pitch forcing motion (3 secs, ±4°). Water fill depth of 175mm.

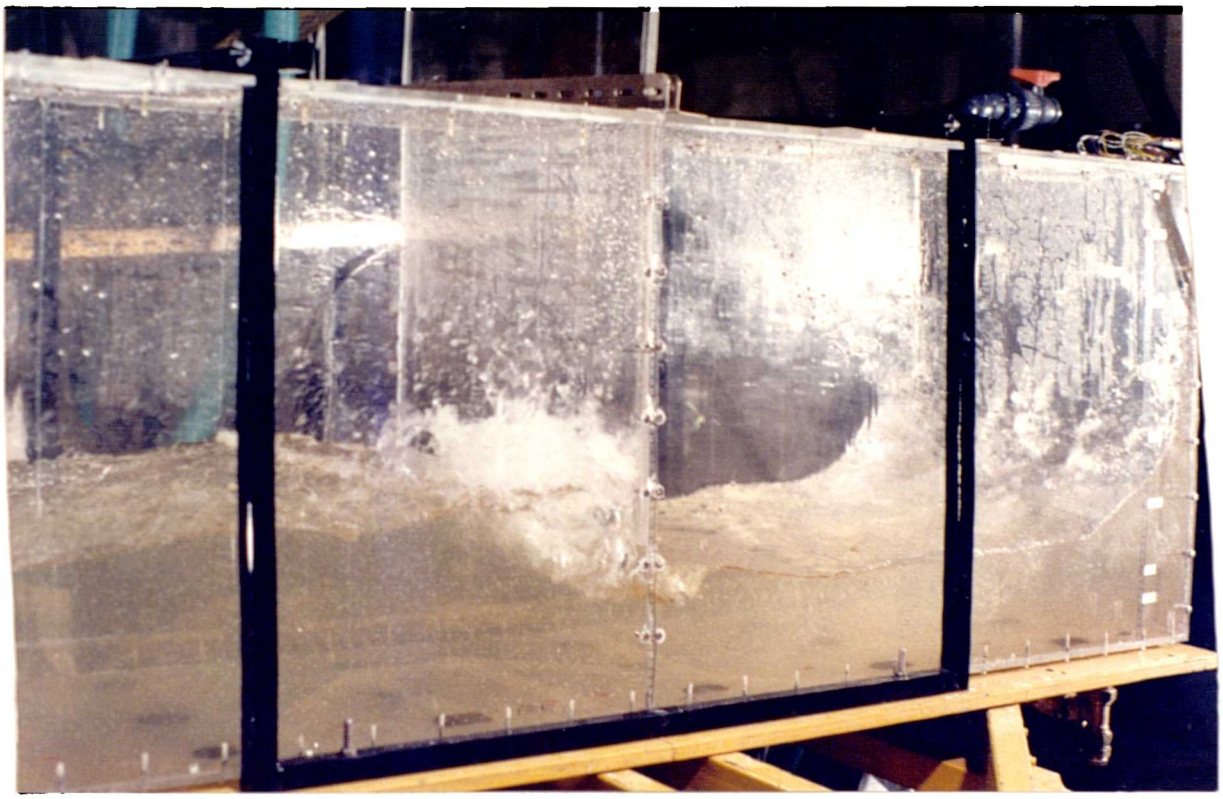

Photograph 8.8: Solid plate baffle touching the air/water interface under pitch forcing motion (4 secs, ±4°). Water fill depth of 175mm.

Fill Depth (mm)	Pitch Forcing Period (sec)	Amplitude (± deg)	Interfacial Amplitude for probe number*: 1 (mm)	2	3	Predicted Natural Period+ (sec)
285	3	2	139	140	162	2.21
		4	190	180	187	
		6	217	217	208	
285	6	2	29	30	30	2.21
		4	72	74	76	
		6	100	97	100	
276	12	2	25	25	26	2.24
		4	48	48	49	
		6	75	75	76	

Table 8.1: Interface Amplitude Values for three probes at stated forcing conditions.

Notes: *Probe positions are given in figure 8.1.

+Natural periods predicted from equation 4.15.

Motion	Liquid Fill Depth (mm)	Forcing Conditions Period (sec)	Amplitude	Graph
Pitch	285	3 4 5	±1° to ±6°	8.3a,8.4a 8.3b,8.4b 8.3c,8.4c
Surge	280	2.3 3.0 3.3	±50mm to ±150mm	8.5a 8.5b 8.5c

Table 8.2: Run conditions for the effect of forcing amplitude on interfacial amplitude.

Pitch Forcing Period (sec)	FFT Frequency Component Data					
	Mode 1		Mode 2		Mode 3	
	Period (sec)	Amp (mm)	Period (sec)	Amp (mm)	Period (sec)	Amp (mm)
1.7	1.7	27	0.65	13	0.84	10
	2.97	9	2.8	6	3.4	3
2.5	2.7	62	1.3	23	0.63	20
	2.8	10	2.97	6	3.35	6
3.0	2.97	74	1.5	25	0.74	18
	2.97	9	2.8	7	1.5	5
3.8	3.85	76	1.95	16	0.76	10
	2.97	8	2.8	8	1.5	5
5.0	5.5	64	0.46	6	2.66	4
	2.97	10	2.8	4	1.5	4
5.8	6.15	53	3.15	5	2.03	2
	2.97	10	1.5	5	2.8	5
7.0	8.08	52	2.79	7	1.59	1
	2.97	12	1.5	3	3.35	1
7.9	9.59	38	2.97	8	1.54	2
	2.97	11	1.46	2		
9.1	9.59	34	2.97	3	1.54	2
	2.97	11	1.46	2		
9.9	11.78	49	2.97	7	1.54	2
	2.97	13	1.5	2	3.35	1

Table 8.3: FFT analysis of wave profile data during pitch forcing at ±4° amplitude and various periods (probe 2 in the large rectangular vessel with water to depth 173mm). First line corresponds to duration of applied motion, second to decay.

Surge Forcing Period (sec)	FFT Frequency Component Data					
	Mode 1		Mode 2		Mode 3	
	Period (sec)	Amp (mm)	Period (sec)	Amp (mm)	Period (sec)	Amp (mm)
1.7	1.7	37	0.84	17	0.56	7
	2.97	11	2.8	2	3.35	2
3.0	2.97	65	1.5	26	0.74	23
	2.8	9	2.97	8	3.15	6
3.8	3.85	45	1.95	12	0.59	9
	2.97	13	0.59	4	1.5	4
5.0	5.5	20	2.97	7	2.66	7
	2.97	10	1.46	2	0.65	2
5.8	6.15	14	2.80	10	2.97	9
	2.97	10	1.5	9	3.15	3
7.0	2.97	9	8.08	9	3.85	4
	2.97	13	1.5	2	3.35	2
7.9	2.97	10	9.59	5	4.16	4
	2.97	12	1.46	2	3.35	1
9.1	2.97	6	9.59	4	1.50	4
	2.97	9				
9.9	2.97	10	11.78	4	3.59	2
	2.97	10	0.73	1	1.55	1

Table 8.4: FFT analysis of wave profile data during surge forcing at ±120mm amplitude and various periods (probe 2 in the large rectangular vessel with water to depth 173mm). First line corresponds to duration of applied motion, second to decay.

Pitch Conditions			Roll Conditions			Graph
Period (sec)	Amp (±deg)	Phase (deg)	Period (sec)	Amp (±deg)	Phase (deg)	
4.6	2.0	0	4.6	2.0	0	A5.1
4.6	2.0	0	4.6	2.0	90	A5.2
4.6	4.0	0	11.9	4.0	0	A5.3
4.6	4.0	0	11.9	4.0	90	A5.4
5.8	2.0	0	5.8	2.0	0	A5.5
5.8	4.0	0	5.8	4.0	0	A5.6
5.8	4.0	90	5.8	4.0	0	A5.7

Table 8.5: Run conditions for combined Pitch & Roll experiments at a fill depth 280mm. Reference to Appendix V given.

Pitch Conditions			Surge Conditions			Graph
Period (sec)	Amp (±deg)	Phase (deg)	Period (sec)	Amp (±mm)	Phase (deg)	
2.1	4.0	0	2.1	120	0	A5.8
2.1	4.0	0	2.1	120	180	A5.9
3.8	4.0	0	3.8	120	0	A5.10
3.8	4.0	0	3.8	120	180	A5.11

Table 8.6: Run conditions for combined Pitch & Surge experiments at a fill depth 352mm. Reference to Appendix V given.

Pitch Period (sec)	Fill Depth (mm)	Baffle Type	Distance From Base (mm)	Graph
2	175	Solid Plate	87,175	8.11
3	175	Solid Plate	87,175	8.12
3	175	Perforated	0	8.12
4	175	Solid Plate	175	8.13
4	175	Interface	-	8.13
2	360	Solid Plate	169,360	8.14
3	360	Solid Plate	169,360	8.15
3	360	Perforated	0	8.15
2	360	Interface	-	8.16
4	360	Interface	-	8.17

Table 8.7: Pitch Period (at ±4° amplitude), Baffle Type and Location for Condensed FFT Profile Plots.

Pitch Forcing Period (sec)	FFT Frequency Component Data Mode 1 Period (sec)	Amp (mm)	Mode 2 Period (sec)	Amp (mm)	Mode 3 Period (sec)	Amp (mm)
1.7	1.7	29	0.84	7	0.56	6
	0.84	3	1.5	1	0.55	1
3.0	2.97	40	1.5	25	0.98	10
	1.5	4	0.58	4	0.84	2
3.8	3.85	69	1.95	26	0.76	14
	3.85	3	0.84	2	11.78	1
5.0	5.15	62	3.32	8	0.67	5
	5.15	2	0.83	2	0.69	2
5.8	6.31	45	2.97	3	10.07	3
	6.31	2	1.47	1		

Table 8.8a: FFT analysis of wave profile data during pitch forcing at ±4° amplitude and various periods. Data for probe 2 in the large rectangular vessel with water to depth 175mm with solid plate baffle touching the air/water interface. First line corresponds to duration of applied motion, second to decay.

Pitch Forcing Period (sec)	FFT Frequency Component Data Mode 1 Period (sec)	Amp (mm)	Mode 2 Period (sec)	Amp (mm)	Mode 3 Period (sec)	Amp (mm)
1.7	1.7	31	0.84	22	0.56	6
	0.84	5	0.64	1	0.54	2
3.0	2.97	22	1.5	10	0.59	7
	1.5	4	0.84	2		
3.8	3.85	32	1.95	2	1.28	2
	3.85	1				
5.0	5.15	41	2.53	2		
	5.15	2				

Table 8.8b: FFT analysis of wave profile data during pitch forcing at ±4° amplitude and various periods. Data for probe 2 in the large rectangular vessel with water to depth 175mm with solid plate baffle at 87mm from vessel base. First line corresponds to duration of applied motion, second to decay.

Pitch Forcing Period (sec)	FFT Frequency Component Data Mode 1 Period (sec)	Amp (mm)	Mode 2 Period (sec)	Amp (mm)	Mode 3 Period (sec)	Amp (mm)
1.7	1.7	32	0.84	27	0.56	5
	0.84	8				
3.0	2.97	23	1.5	10	0.59	10
	1.5	4	0.58	3	0.65	2
3.8	3.85	34	1.95	4	1.28	2
	1.50	2	2.97	1	3.85	1
5.0	5.15	42	2.53	2	1.71	2
	5.15	2	1.50	1		
5.8	6.31	37	2.97	2	1.99	2
	6.31	2	1.50	2		

Table 8.8c: FFT analysis of wave profile data during pitch forcing at ±4° amplitude and various periods. Data for probe 2 in the large rectangular vessel with water to depth 175mm with the 22% free area perforated baffle. First line corresponds to duration of applied motion, second to decay.

Pitch Forcing Period (sec)	FFT Frequency Component Data Mode 1 Period (sec)	Amp (mm)	Mode 2 Period (sec)	Amp (mm)	Mode 3 Period (sec)	Amp (mm)
1.7	1.7	32	0.84	21	0.56	3
	0.84	4	1.5	3	2.97	1
3.0	2.97	55	1.5	28	0.59	26
	2.97	3	1.58	3	0.59	3
3.8	3.85	60	1.95	12	0.76	11
	1.50	4	3.85	2	0.58	2
5.0	5.15	58	4.14	4	24.99	3
	1.47	3	5.15	2	2.87	2
5.8	6.31	45	1.99	2	2.97	2
	1.47	3	5.87	3	2.87	1

Table 8.8d: FFT analysis of wave profile data during pitch forcing at ±4° amplitude and various periods. Data for probe 2 in the large rectangular vessel with water to depth 175mm with the 53% free area perforated baffle. First line corresponds to duration of applied motion, second to decay.

Pitch Forcing Period (sec)	FFT Frequency Component Data					
	Mode 1		Mode 2		Mode 3	
	Period (sec)	Amp (mm)	Period (sec)	Amp (mm)	Period (sec)	Amp (mm)
1.7	1.7	22	0.85	19	0.57	13
	0.85	4	1.4	3	3.08	2
3.0	3.08	71	0.75	18	0.59	9
	1.48	3	0.59	3	3.08	3
3.8	4.04	81	1.93	12	0.77	9
	1.48	3	0.59	2	3.08	2

Table 8.8e: FFT analysis of wave profile data during pitch forcing at ±4° amplitude and various periods. Data for probe 2 in the large rectangular vessel with water to depth 175mm with interface baffle 1 at 105mm from vessel base. First line corresponds to duration of applied motion, second to decay.

Pitch Forcing Period (sec)	FFT Frequency Component Data					
	Mode 1		Mode 2		Mode 3	
	Period (sec)	Amp (mm)	Period (sec)	Amp (mm)	Period (sec)	Amp (mm)
1.7	1.79	23	0.85	14	0.57	5
	3.08	4	1.48	3	0.85	3
3.8	4.04	97	1.93	14	0.77	12
	1.48	4	3.08	4	0.85	3

Table 8.8f: FFT analysis of wave profile data during pitch forcing at ±4° amplitude and various periods. Data for probe 2 in the large rectangular vessel with water to depth 175mm with interface baffle 2 at 143mm from vessel base. First line corresponds to duration of applied motion, second to decay.

Length Parameter (mm)	Natural Period Modes 1 (sec)	2 (sec)	3 (sec)
1780	2.77	1.02	0.71
890	1.44	0.63	0.48

Table 8.9: Predicted natural period modes for air/water fill vessel of specified length. Water fill depth of 175mm.

CHAPTER 9.

RESULTS FROM AIR/OIL/WATER EXPERIMENTS IN THE SMALL RECTANGULAR VESSEL.

9.1 INTRODUCTION.

As seen from air/water studies, the prediction of natural period gives a point at which the free surface will break, the severity of the break depending on the forcing amplitude. If the air is replaced by oil, theory (chapter 4) again predicts a point at which the interface will break but not the exact form of the break. For three fluids (air/oil/water), derived theory (equation 4.19) predicts two natural periods, one for the oil/water and the other for the air/oil interface. Both fluid fill depth and density were shown to be of prime importance in determining natural periods.

Previous experiments (chapters 7 and 8) have shown that air/water resonance at low fill depths is characterised by a hydraulic jump whose exact form/shape has yet to be predicted. In the same context, little information exists describing the form of an oil/water interface at or near resonance.

This chapter describes experiments with the small rectangular vessel conducted primarily, to gain information on the effect of density on the shape and amplitude of the oil/water interface. Three fluid sloshing experiments (air/oil/water) were conducted with a view to see the effect of a gas cap. For the oil, kerosene was selected both for handling properties and the possibility of adjusting its density by dilution with a fluorocarbon.

9.2 EXPERIMENTAL OVERVIEW.

As discussed in chapter 7, results from air/water forcing experiments demonstrated the formation of breaking waves at resonance i.e.

the hydraulic jump. It was assumed that such a condition in an oil/water filled vessel would result in water and oil mixing. Applications of experiments to offshore processing equipment would then include :

1) The shape of the oil/water and air/oil interfaces.

2) The amount of oil transferred into water or water into oil, as a result of interface breaking.

3) The formation of oil/water or water/oil emulsions on the oil/water interface, again as a result of interface breaking.

It was anticipated that *on-line-sampling* at intervals during an experiment would have to be performed to measure the amount of *oil-in-water* and *water-in-oil*. The earlier air/water experiments had shown that a change in liquid fill depth affects the natural period and hence the shape and form on the air/water interface. Consequently, it was decided that on-line-sampling could not be carried out on the small vessel, as the loss in fluid volume would significantly affect interface response. Therefore, only interface profiles resulting from forcing, were recorded.

Three oils, kerosene, FK851 and FK890 (different density and similar viscosities) were used in this vessel. Physical properties of each oil were given in section 6.2.

Experiments were conducted at various air/oil/water fill depths to compare two and three fluid sloshing. Table 9.1 presents predicted natural periods (by equation 4.19) for all fill depth combinations. In some experiments the natural period of the oil/water interface was measured by direct timing of decaying waves from the video recordings (using slow play-back mode). These results will be presented where appropriate. To reduce the amount of data, experiments concentrated on pitch forcing motion at $\pm 4^{\circ}$ amplitude.

As regards the photographs presented in this chapter, white backing paper was placed behind the vessel. Therefore the water phase will appear white. The oil was dyed using waxoline dye (see chapter 6).

The results from these experiments can be divided to two sections, those dealing with a twin fluid (oil/water) system and those to a three fluid system (air/oil/water) system.

9.3 RESULTS FROM A TWO FLUID (OIL/WATER) SYSTEM.

9.3.1 The Effect of Forcing Period on Oil/Water Interface Amplitude.

Graph 9.1 shows the effect of forcing period on interface amplitude for oil FK851 (density 858 Kg/m^3) at various positions inside the vessel (figure 6.7). From table 9.1, predicted natural period for this water depth (87mm) was calculated as 6.1 seconds.

The results from graph 9.1 demonstrate several important effects :

1) Allowing for the potential inaccuracies in measuring technique, the graph shows surprisingly well a symmetrical response e.g. probe 2 response is similar to probe 14. Therefore, as in previous air/water experiments, probe 2 will be used for comparative purposes.

2) The maximum interface amplitude occurs at forcing periods close to 6 seconds, which compares favourably to the predicted measured natural period.

3) The maximum interface amplitude reaches approximately 85mm which is then similar to the water fill depth. From the definition of interface amplitude (equation 4.16), this implies that the oil layer can extend to the vessel base.

Regarding the shape of the oil/water interface, away from resonance (Ω=3 secs), photograph 9.1 shows the interface as a smooth two dimensional

profile consisting of standing waves (photograph 9.4). Close to resonance (Ω=6 secs), photograph 9.2 shows a *travelling wave* with a distorted front. This distortion was seen to produce mixing of oil and water, resulting in the formation of *bubbles*. Photograph 9.3 shows these bubbles and the turbulence resulting from the traveling wave hitting the vessel end. The term *bubble* in this sense is taken to mean a volume of fluid A (water say), surrounded by a film of fluid B (oil) and suspended in the bulk fluid A. Evidence for this is supported by the colour of the oil-in-water bubbles, their destruction once motion had stopped and their size. The observed bubbles were light in colour, of large size (up to 20mm in some cases) and showed signs of flexible movement. True droplets of oil-in-water would have been darker in colour and of smaller size. Once forcing motion had ceased, these bubbles disintegrated on reaching the oil/water interface.

9.3.2 The Effect of Oil Density on Natural Period.

Graphs 9.2 and 9.3 show the effect of forcing period and oil density on oil/water interface amplitude for water depths 87mm and 174mm respectively. Oil was filled to the vessel top. Predicted natural periods for each oil at each water depth are presented in table 9.1. Measured natural periods of the oil water interface are presented in table 9.2.

The results show that :

1) For both water fill depths, as oil density increases so does natural period. This is indicated by the shift of interface amplitude response towards longer forcing periods.

2) For the high water depth (174mm) maximum interface amplitude appears higher than that for the low water depth (87mm).

3) Measured natural periods agree well with the ones predicted from

equation 4.19. However, the point at which maximum interface response occurs is at slightly longer forcing periods.

Examples of oil/water interface profiles at forcing periods lower than resonance (Ω=3 secs) for the low water fill depth (87mm), are shown for oils FK851 and FK890 in photographs 9.1 and 9.4. Photographs 9.5 and 9.6 show the oil/water interface profile at similar forcing conditions for the high water fill depth (174mm). For the more dense oil (FK890), the standing wave profile appears more pronounced. This is due to either differences in natural period (6.8 secs for FK890 low water fill depth and 6.1 secs for FK851), or time difference between each photograph.

In contrast to some air/water experiments that produced three dimensional wave profiles (see figure 8.2 for a description of a 3D wave profile), all oil/water experiments resulted in two dimensional profiles. Presumable this was due to the applied forcing periods being too far from the natural periods based on vessel breadth i.e. for 87mm, ρ=858 Kg/m^3 natural period = 2 secs.

9.3.3 Effect of Water Fill Depth on Oil/Water Interface Amplitude.

Graphs 9.4 and 9.5 show the effect of forcing period and water fill depth on interface amplitude for oils FK851 and FK890. These results show negligible difference in maximum interface amplitude between either fill depth.

Visual observations indicated significant differences in the shape of the oil/water interface, between fill depths at resonance. The effect of resonance for a low water depth (87mm) has already been seen (photograph 9.2) in the formation of a single travelling wave profile. For the high water depth (174mm), photograph 9.7 shows a turbulent interface profile, which could be classed as an *inverted travelling* wave. The fill

depth corresponding to the point of change between normal and inverted travelling wave, was not determined.

9.3.4 Discussion.

These two fluid (oil/water) experiments show that :

1) Natural periods as predicted by equation 4.19 agree well with measured natural periods for all oil densities. However, the point of maximum oil/water interface amplitude appears to occur at higher forcing periods than either predicted or measured.

2) Increasing oil density increases natural period, as predicted from equation 4.19.

3) At resonance, the oil/water interface breaks up to produce bubbles of oil-in-water and water-in-oil. These bubbles disperse once forcing motions had ceased.

4) At resonance, the oil/water interface was seen to reach close to the vessel's top and bottom. It was observed that contact between oil/vessel base and water/vessel roof did not occur.

With air/water sloshing experiments, it was shown that the point of maximum interface amplitude occurs at forcing periods close to predicted natural period. However, maximum oil/water interface amplitude occurs at longer forcing periods than either natural period predicted from equation 4.19 or measured e.g. +1 sec for FK851 and FK890 in graph 9.3. While predictions may be incorrect due to some underlying assumptions (e.g. irrotational motion) it would not be expected that measured natural periods would be in error.

Equation 4.19 was derived on the basis of homogeneous immiscible fluids with a continuous interface between each fluid. During oil water resonance the production of bubbles must surely alter the physical

properties (i.e. density) along the oil/water interface. Therefore, the effective density difference between oil and water layers would be reduced. Equation 4.19 shows that for any two fluids (oil/water), decreasing the density difference results in longer natural periods. This may explain deviations in predicted behaviour of the interface from pure oil and water.

In regards the formation of oil-in-water and water-in-oil bubbles, visual observations indicated that such bubbles formed as a result of vortex formation on the oil/water interface. These vortices must then be generated by competing flow profiles in both oil and water phases. Possible flow patterns derived from observations, are given in figure 9.1.

It was observed throughout these experiments, emulsions were not formed, even as a result of resonant forcing. Shaking kerosene and water together in a sample jar and left to settle, showed the oil/water interface *clean*, i.e. free from bubbles and emulsion. Therefore, it was doubtful that resonant forcing would also produce stable kerosene emulsions. It was expected that FK851 and FK890 would behave similar due to their kerosene base.

9.4 RESULTS FROM A THREE FLUID (AIR/OIL/WATER) SYSTEM.

9.4.1 Introduction.

In the majority of offshore operations, it may be assumed that gas would sit on top of oil/water layers i.e. gas from a production well for offshore separators or inert gas blanketing for storage tanks. A series of experiments were carried out concentrating on one water fill depth and different oil (kerosene/FK851) depths. Table 9.1 presents predicted natural periods for both air/oil and oil/water interfaces at all fill depth conditions studied.

9.4.2 Effect of Forcing Period On Air/Oil and Oil/Water Interface Amplitude.

Graphs 9.6a-b show the effect of forcing period on both oil/water and air/oil interfaces for oil FK851 under pitch forcing motion at ±4° amplitude. Predicted natural periods, from table 9.1, for the oil/water and air/oil interfaces were 6.5 and 1.3 seconds respectively.

From graph 9.6b, the upper air/oil interface is seen to remain calm throughout the applied forcing periods. Based on the predicted natural period, it would seem the applied forcing periods were not short enough to cause a resonant response (Ω<2 secs). As regards the lower oil/water interface, forcing motion resulted in a similar response to that in graph 9.1 and appears to occur at forcing period higher than predicted resonance.

Over the range of forcing periods applied, graph 9.6a indicates that the breadth of the response appears shorter than the equivalent oil/water case (graph 9.1) i.e that at the same water depth. Simple linear theory predicts that for a constant water depth, as gas cap size increases, the range of periods producing a resonant response decreases (see chapter 4, graph 4.4). Therefore, the experiments agree with linear theory.

As regards the shape of the free surface, photograph 9.8 applies to near resonant forcing period (Ω≈7.5 secs) for oil FK851 at the same fill depths referred to in graphs 9.6a-b. The oil/water interface profile is seen to be similar to that observed for the completely filled oil/water vessel (photograph 9.1). Photograph 9.9 refers to a similar case for kerosene but at a lower forcing period (Ω≈5.2 secs). In both cases, the upper air/oil interface remains smooth and free from any waves while the lower oil/water interface is turbulent.

9.4.3 Effect of Oil Layer/Gas Cap Size on Oil/Water Interface.

Graphs 9.7 and 9.8 show the effect of forcing period on oil/water interface amplitude for different oil fill depths. Measured oil/water natural periods taken from video recording are presented in table 9.3.

The results show that :

1) Predicted natural periods are in good agreement with measured natural periods.

2) Decreasing the oil layer size has the effect of reducing the oil/water interface amplitudes. For each oil, it appears that maximum oil/water interface amplitude is similar to half the oil fill depth. It was observed during the experiments that, the oil/water interface approached the both the air/oil interface and the base of the vessel. This effect is seen more clearly on graph 9.8.

3) The oil/water interface amplitude for the 131mm oil layer, increases for shorter forcing periods. Visual observation indicated that at such forcing periods, the upper air/oil interface approached its resonant condition.

In relation to the thick oil layer (small gas cap), the shape of the oil/water interface has been discussed in the previous section (photographs 9.8 and 9.9) i.e. a solitary travelling wave. In relation to the thin oil layer (large gas cap), photographs 9.10 and 9.11 show interface profiles near resonant forcing periods for oils FK851 (Ω=8.3 secs) and FK890 (Ω=9.5 secs). In both cases, observations at first indicate that a hydraulic type jump profile develops. However, subsequent observations suggest an inverted travelling wave formed, with a distinctive stepped tail (photograph 9.11).

For the thin oil layer (oil depth 131mm), it was noted in graphs 9.7 and 9.8, that the oil/water interface amplitude increased at short forcing periods. Photographs 9.12 and 9.13 show the shape of both air/oil and oil/water interfaces as a result of near resonant (air/oil) forcing periods for kerosene (Ω=2.5 secs) and FK851 (Ω=2 secs). In photograph 9.12, the air/oil interface is seen to produce a three dimensional profile similar to air/water profiles at similar total fill depth conditions (i.e. 131mm). Photograph 9.13 shows mixing of air and oil, as indicated by the *frothing* on the air/oil interface. From this and other observations, it appears that waves on the upper air/oil interface can influence waves on the lower oil/water interface.

9.4.4 Discussion.

The three fluid experiments indicate :

1) Equation 4.19 can predict natural periods of both upper air/oil and lower oil/water interfaces. Again, predicted oil/water natural periods agree well with measured oil/water natural periods, although the point of maximum interface response occurs at longer forcing periods.

2) At no time during the experiments, did the oil/water interface come in contact with either the air/oil interfaces or the base of the vessel.

3) At forcing period corresponding to oil/water resonance for a thick oil layer (oil depth 217mm), a traveling wave formed. An inverted travelling wave is observed for a thin oil layer (oil depth 131mm). This is then analogous to the two fluid (oil/water) low and high fill depth experiments.

Several points can be made regarding these results. Firstly, comparisons between two fluid (oil/water) and three fluid (air/oil/water) filled vessels can be summarized as :

1) Similar oil/water interfacial profiles are seen in both cases. That is, normal and inverted travelling waves at resonant forcing conditions.

2) Increasing gas cap size while maintaining constant water depth, has similar effects to increasing water depth in a two fluid system. Figure 9.2 depicts the various wave forms noted at resonant conditions for both two fluid (oil/water) and three fluid (air/oil/water) filled vessels. This shows that interface profiles are depend on oil/water ratio, not the type of fluid system.

The second point, regards the upper air/oil interface. Comparisons with air/water experiments would suggest that this interface behaves as if the vessel were filled with one liquid and a gas. The predicted natural periods for an air/water interface (equation 4.15) for fill depths 131mm (1.6 secs) and 217mm (1.3 secs) are found to equal those of the air/oil interface at the same fill depths (table 9.1), predicted by equation 4.19. This is to be expected as equation 4.19 reduces to equation 4.15 if density is ignored.

Throughout these experiments, the bubbles that formed as a result of resonant forcing periods, did not cause emulsions to form along the oil/water interface. It is suggested that emulsion formation is dependant on oil and water properties as well as conditions of oil/water mixing.

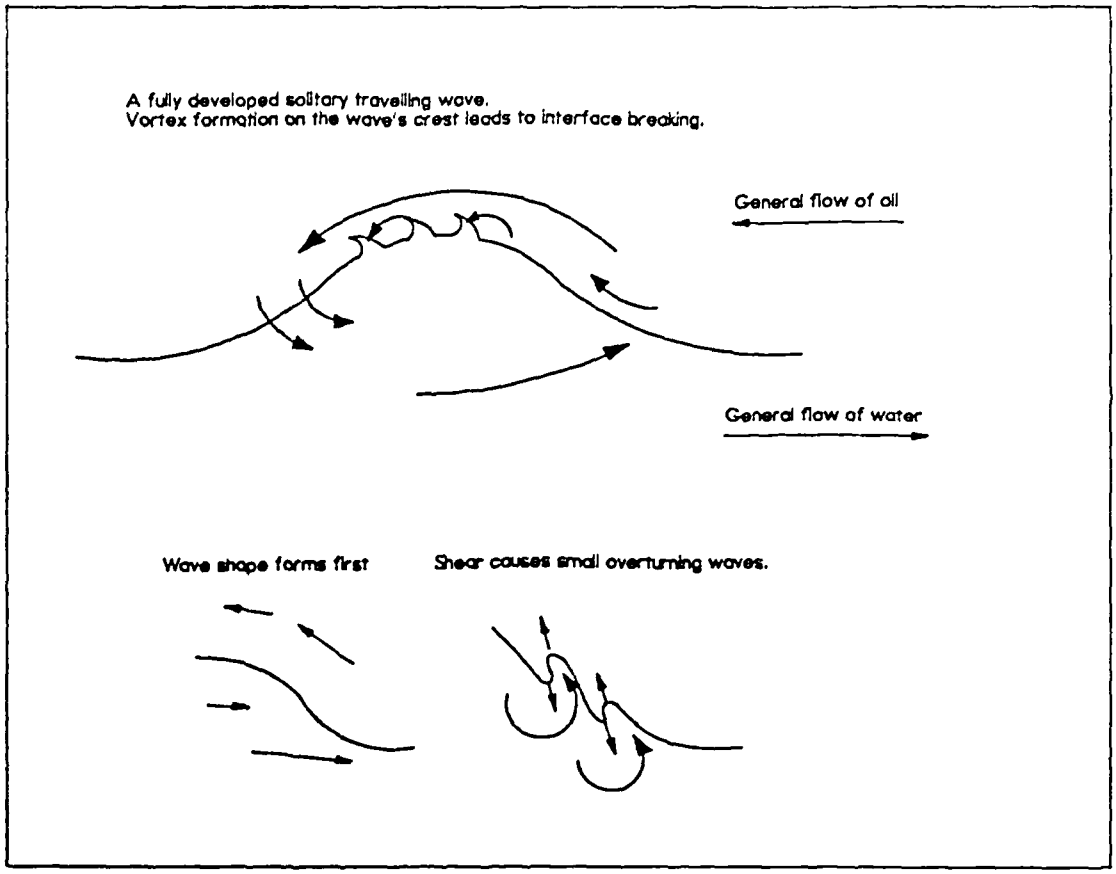

Figure 9.1: Possible flow profiles along the oil/water interface at resonant forcing conditions.

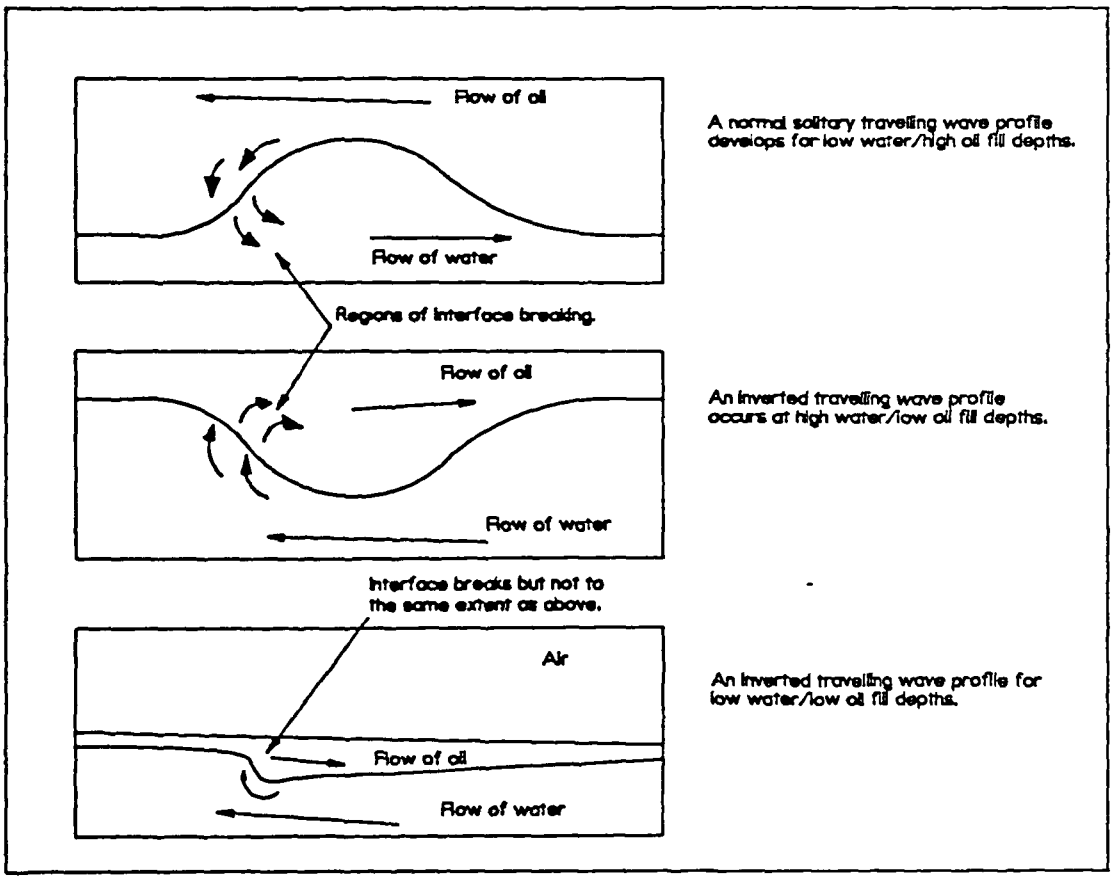

Figure 9.2: Oil/Water interface profiles observed during resonant forcing experiments in the small rectangular container.

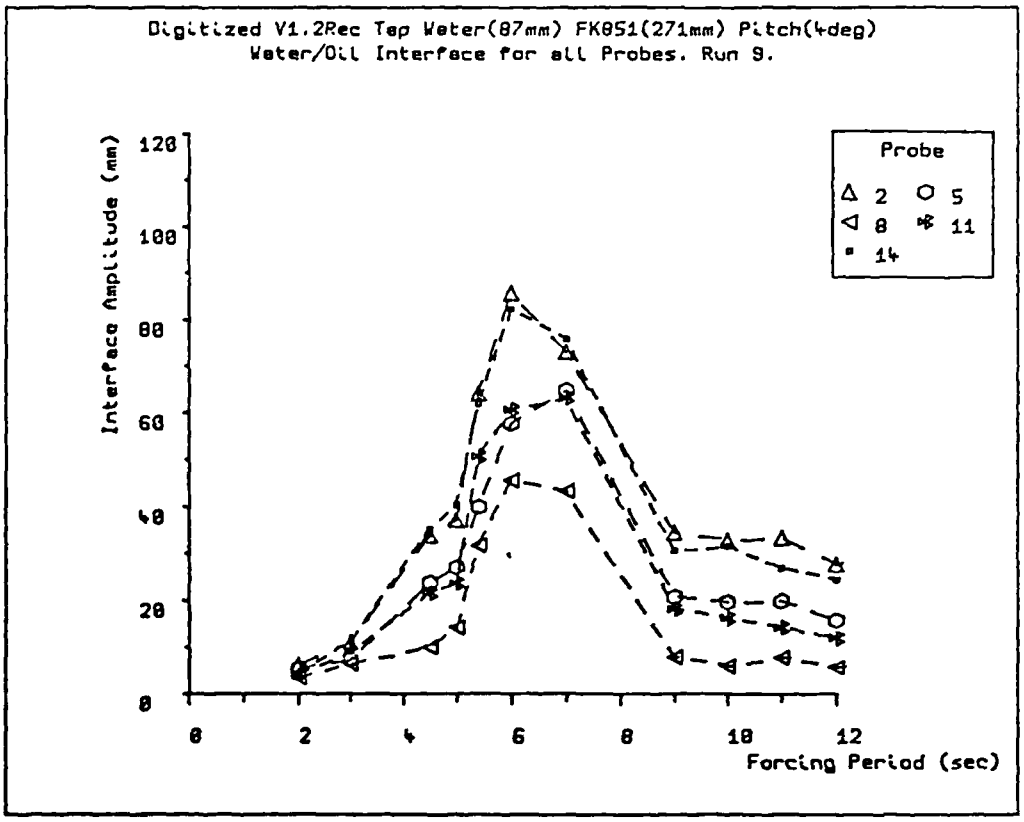

Graph 9.1: Effect of forcing period on oil/water interface amplitude for various probe positions in the small rectangular vessel under pitch forcing motion at ±4° amplitude. Oil: FK851, water fill depth 87mm.

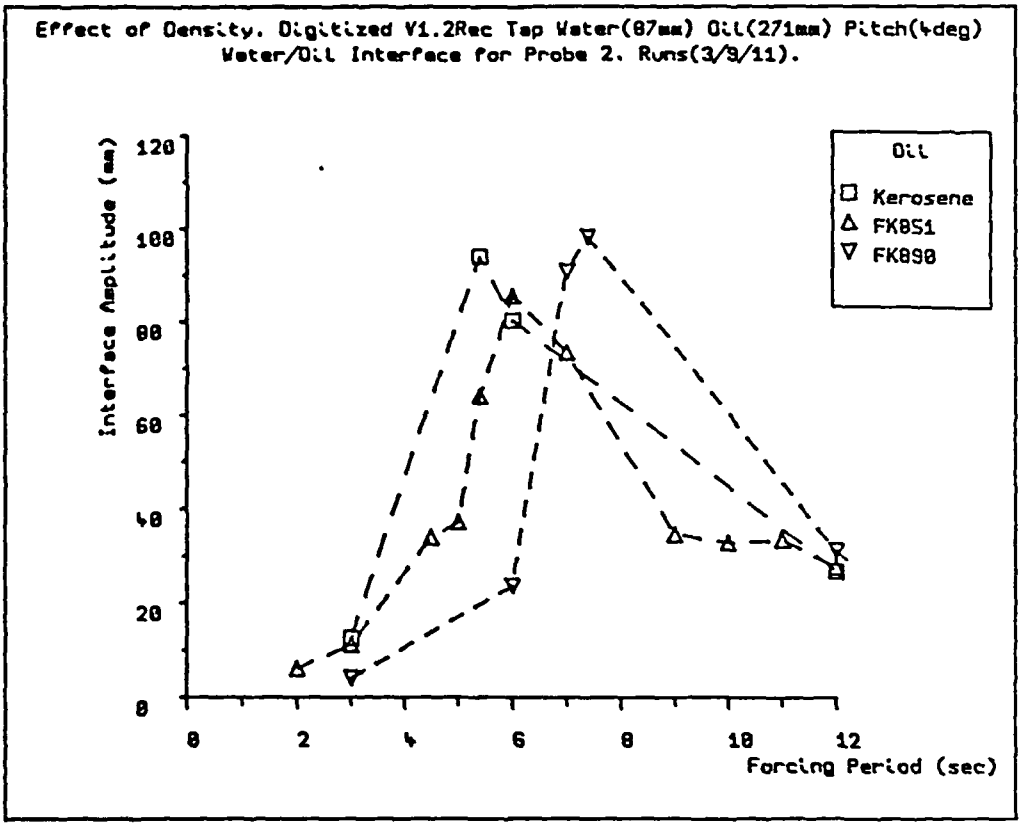

Graph 9.2: Effect of forcing period and oil density on oil/water interface amplitude in the small rectangular vessel under pitch forcing motion at ±4° amplitude. Water fill depth of 87mm.

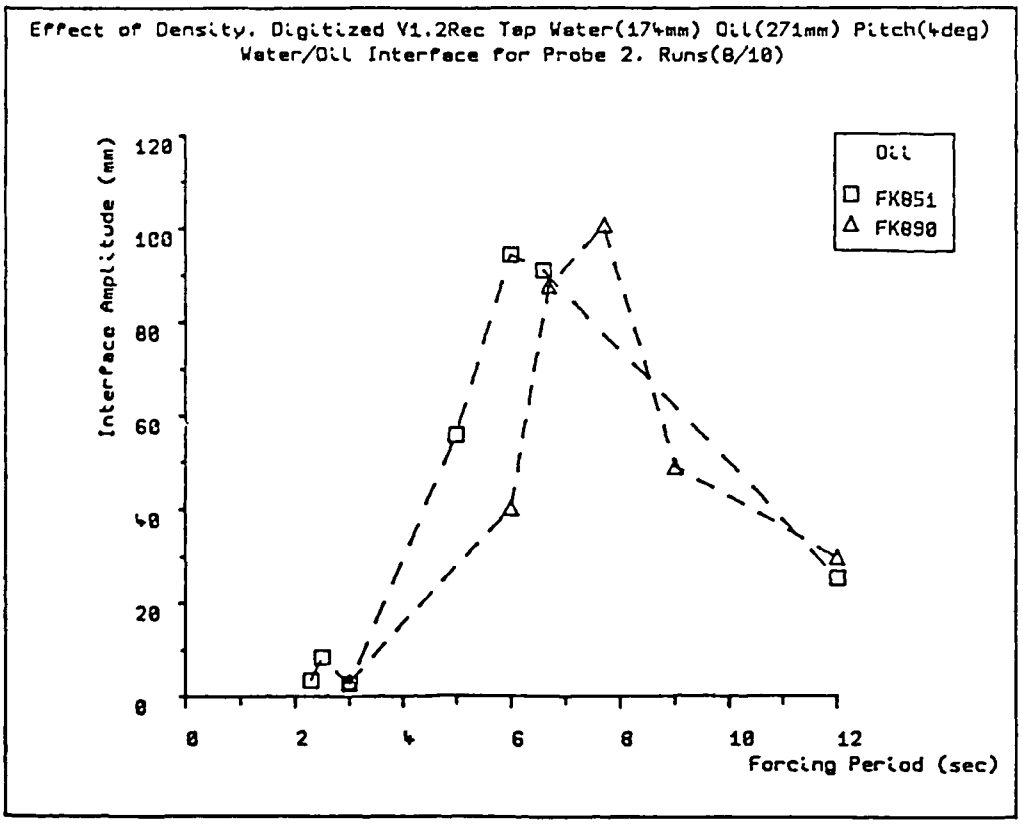

Graph 9.3: Effect of forcing period and oil density on oil/water interface amplitude in the small rectangular vessel under pitch forcing motion at ±4° amplitude. Water fill depth of 174mm.

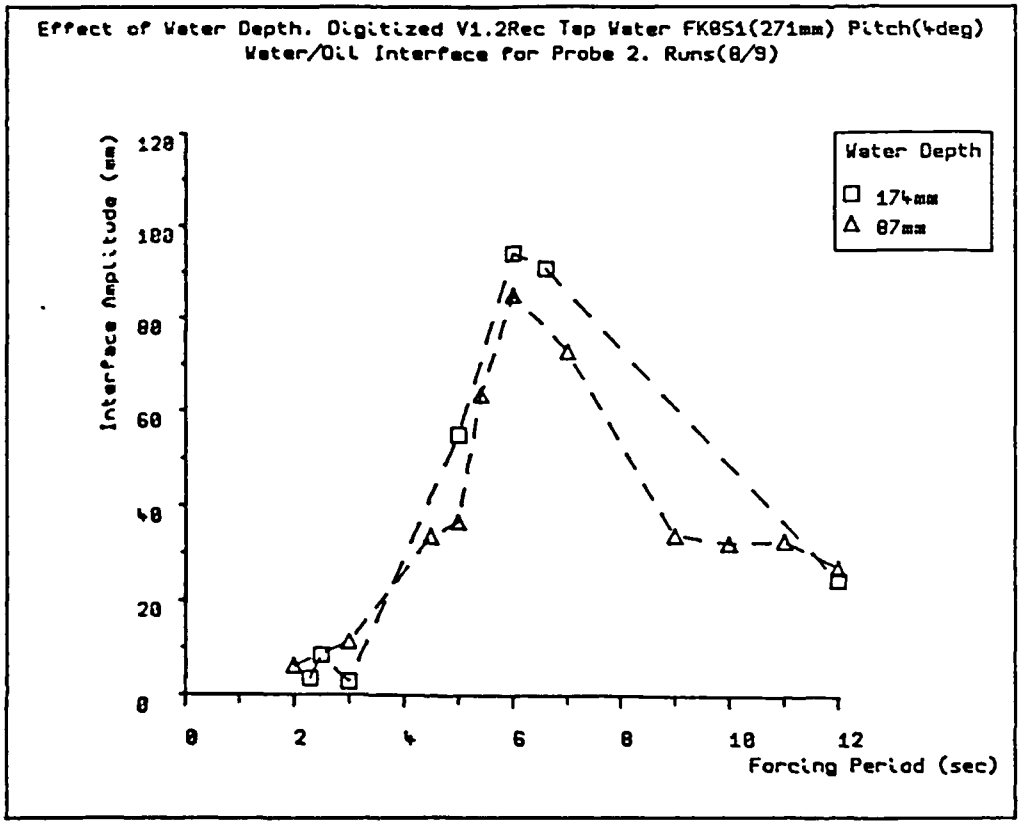

Graph 9.4: Effect of forcing period and water fill depth on oil/water interface amplitude in the small rectangular vessel under pitch forcing motion at ±4° amplitude. Oil: FK851.

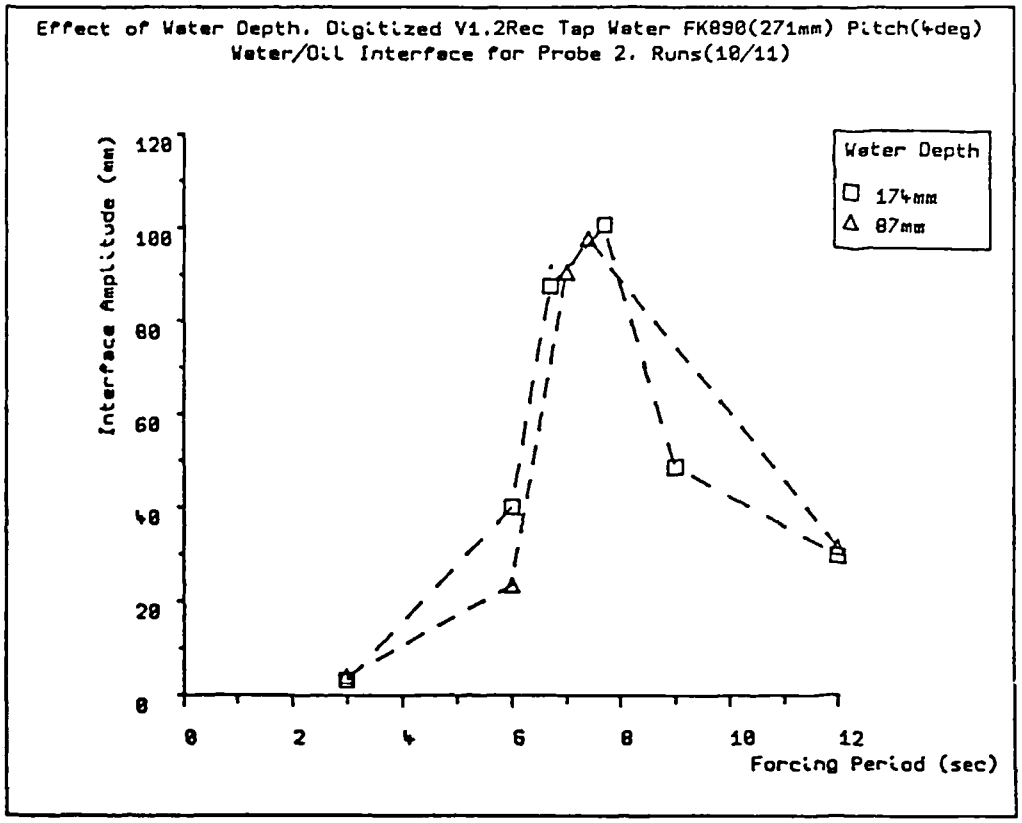

Graph 9.5: Effect of forcing period and water fill depth on oil/water interface amplitude in the small rectangular vessel under pitch forcing motion at ±4° amplitude. Oil: FK890.

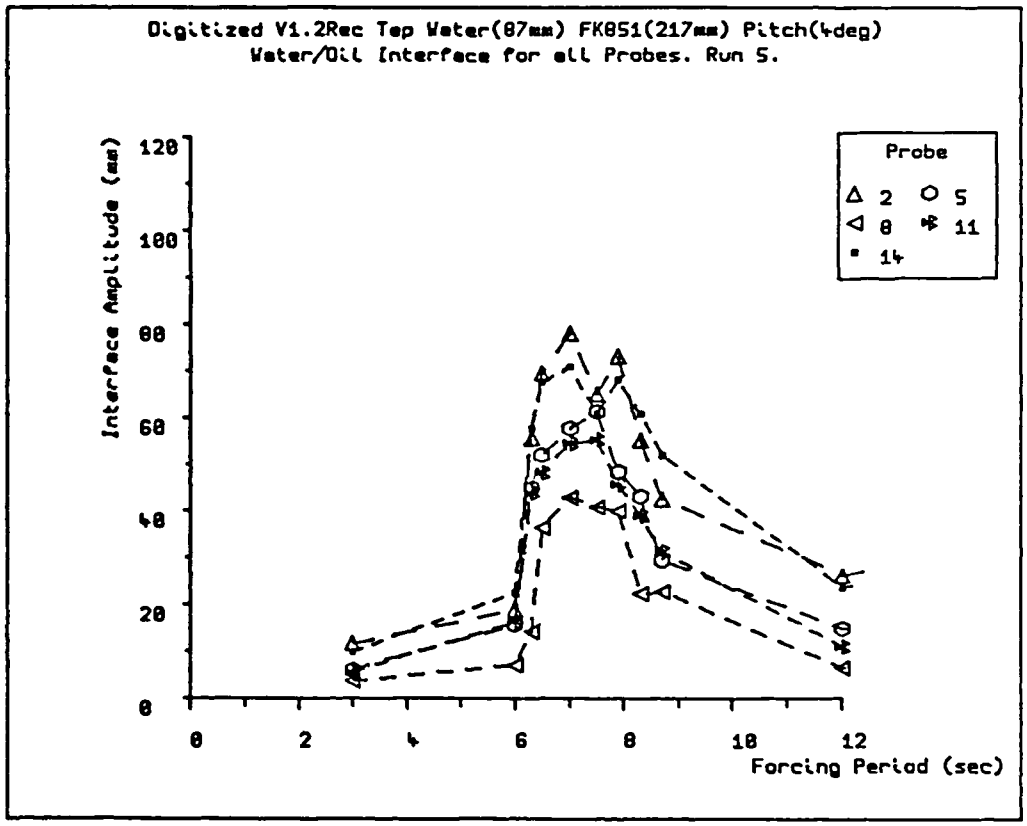

Graph 9.6a: Effect of forcing period on oil/water interface amplitude for various probe positions in the small rectangular vessel under pitch forcing motion at ±4° amplitude. Oil: FK851 at 217mm, water fill depth 87mm.

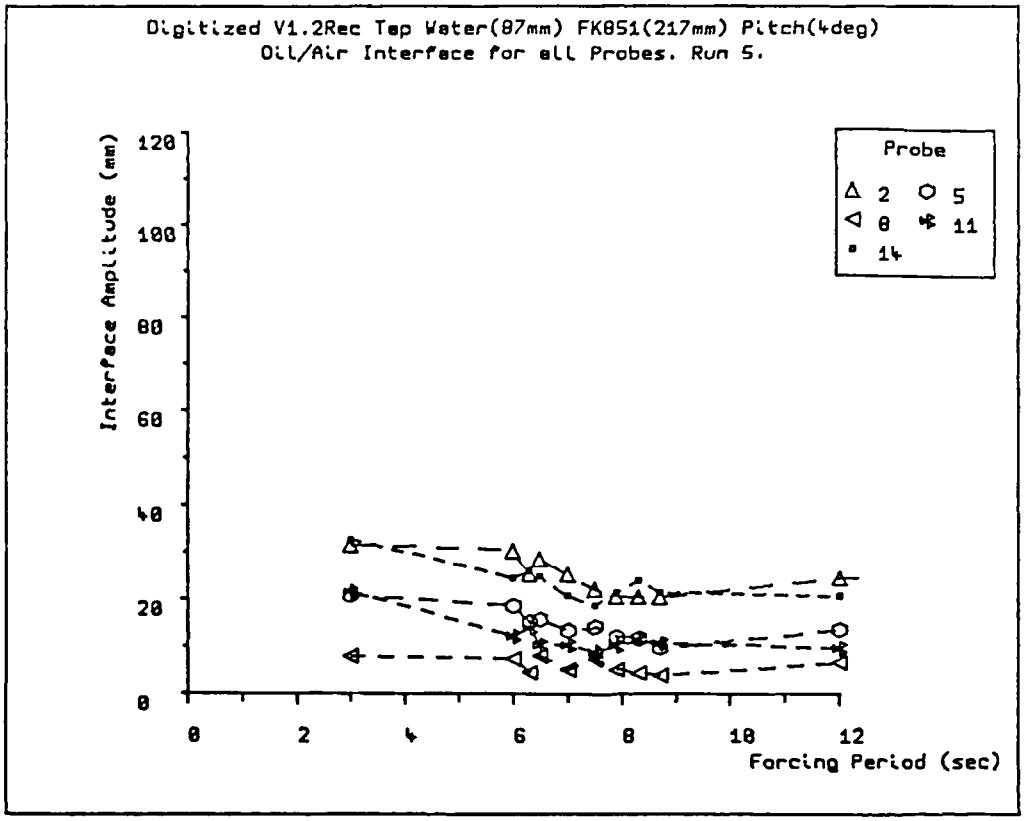

Graph 9.6b: Effect of forcing period on air/water interface amplitude for various probe positions in the small rectangular vessel under pitch forcing motion at ±4° amplitude. Oil: FK851 at 217mm, water fill depth 87mm.

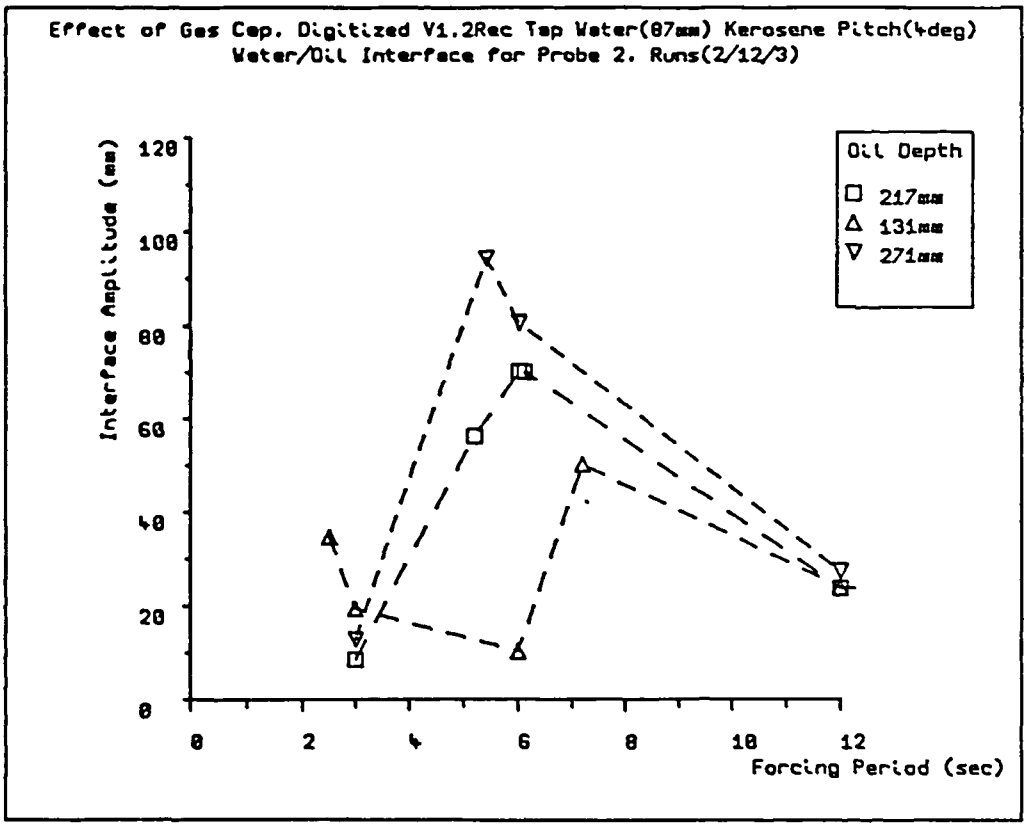

Graph 9.7: Effect of forcing period and oil layer size on oil/water interface amplitude in the small rectangular vessel under pitch forcing motion at ±4° amplitude. Oil: kerosene, water fill depth 87mm.

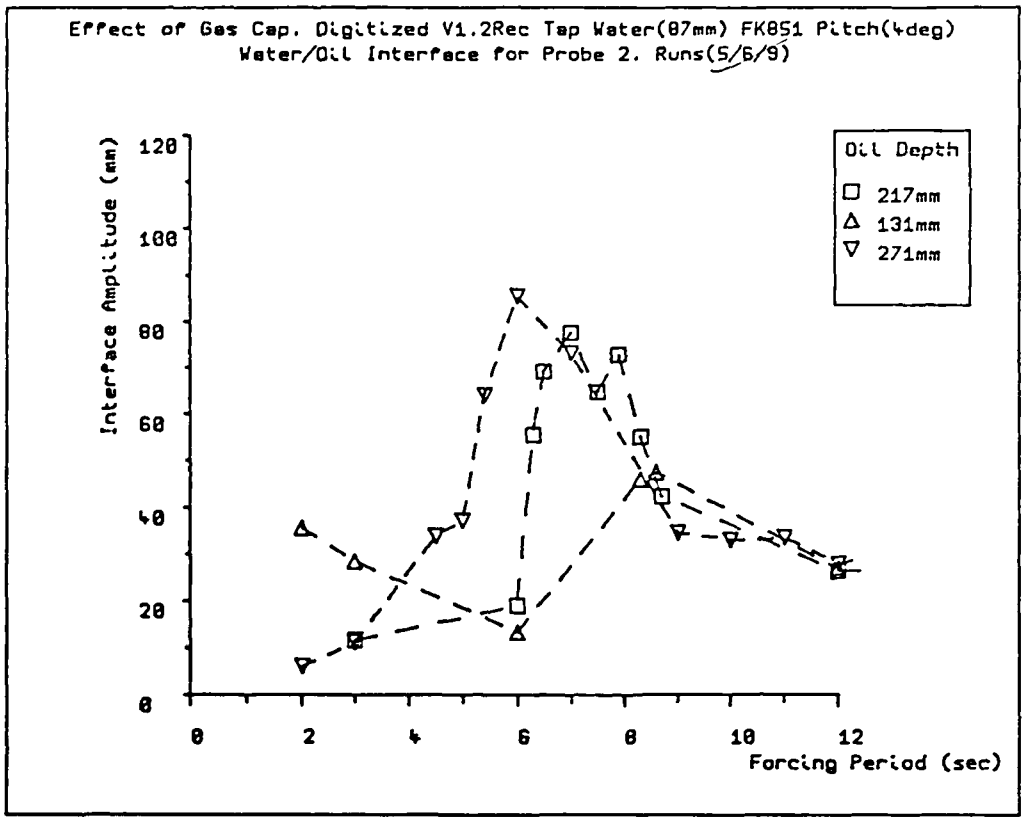

Graph 9.8: Effect of forcing period and oil layer size on oil/water interface amplitude in the small rectangular vessel under pitch forcing motion at ±4° amplitude. Oil: FK851, water fill depth 87mm.

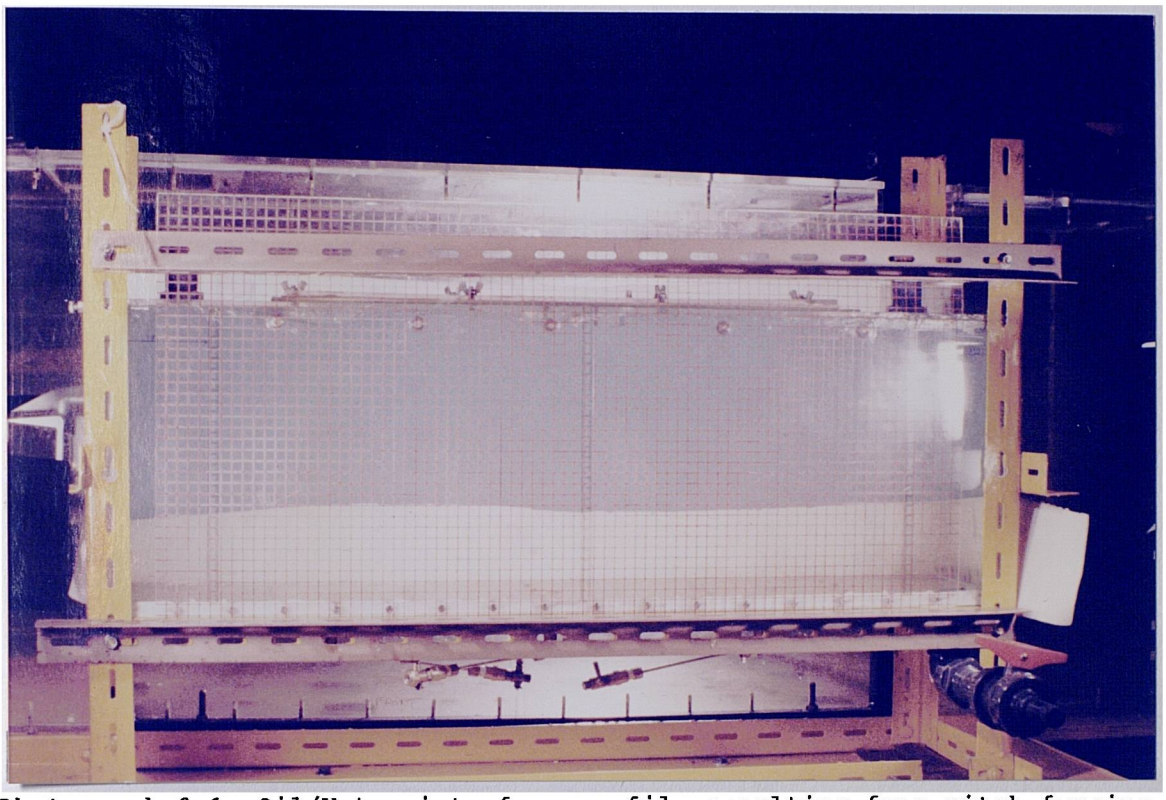

Photograph 9.1: Oil/Water interface profile resulting from pitch forcing motion at 3 seconds period, ±4° amplitude. Oil: FK851, water fill depth 87mm.

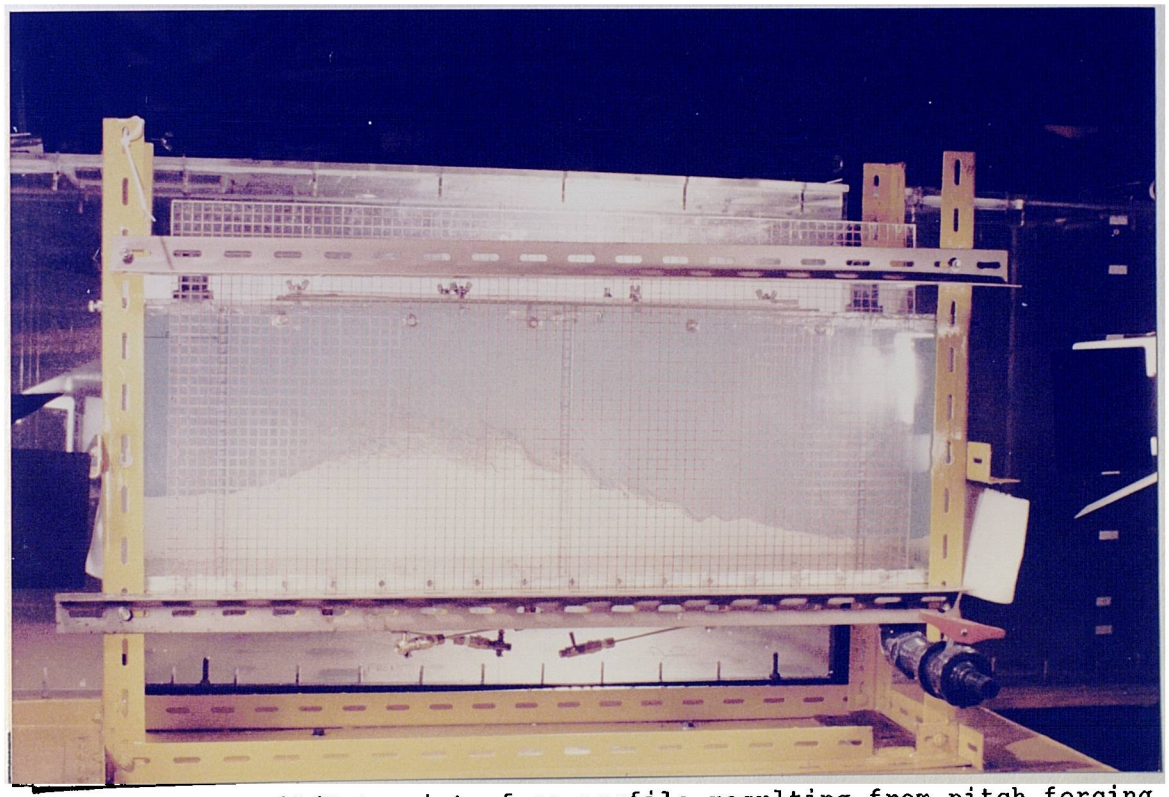

Photograph 9.2: Oil/Water interface profile resulting from pitch forcing motion at 6 seconds period, ±4° amplitude. Oil: FK851, water fill depth 87mm.

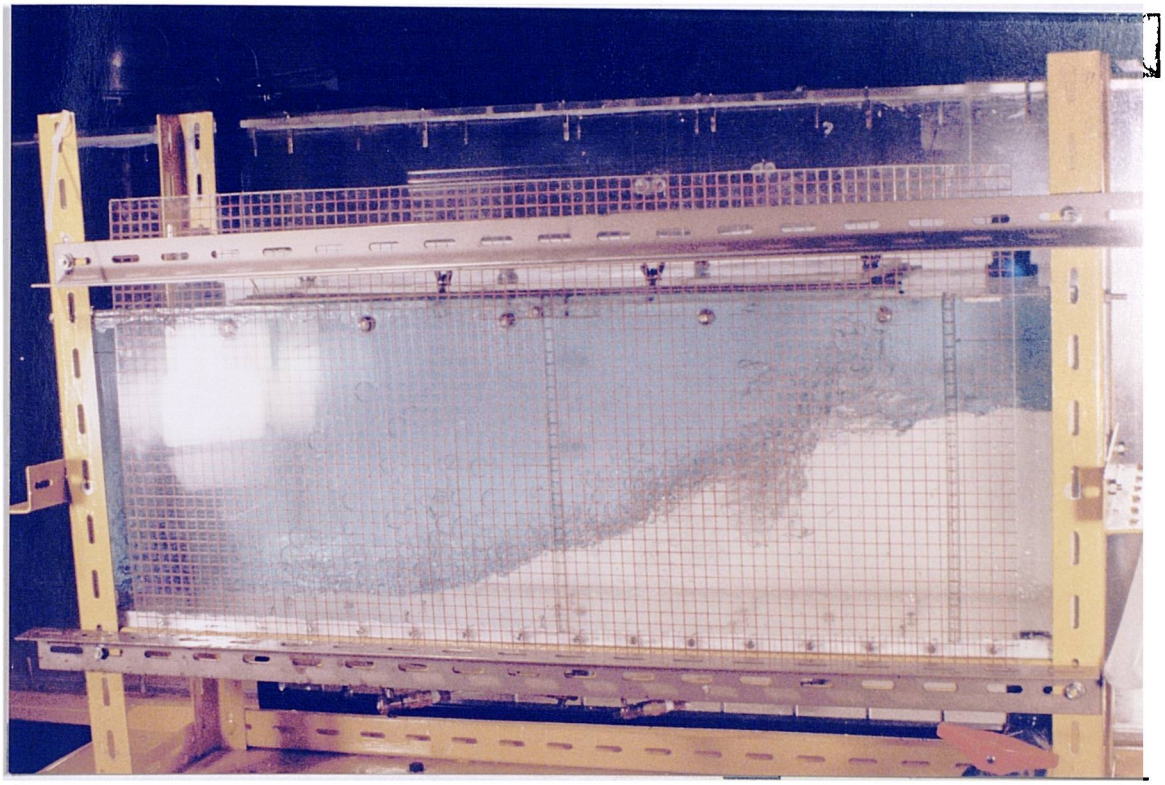

Photograph 9.3: Oil/Water interface profile resulting from pitch forcing motion at 5.4 seconds period, ±4° amplitude. Oil: FK851, water fill depth 87mm.

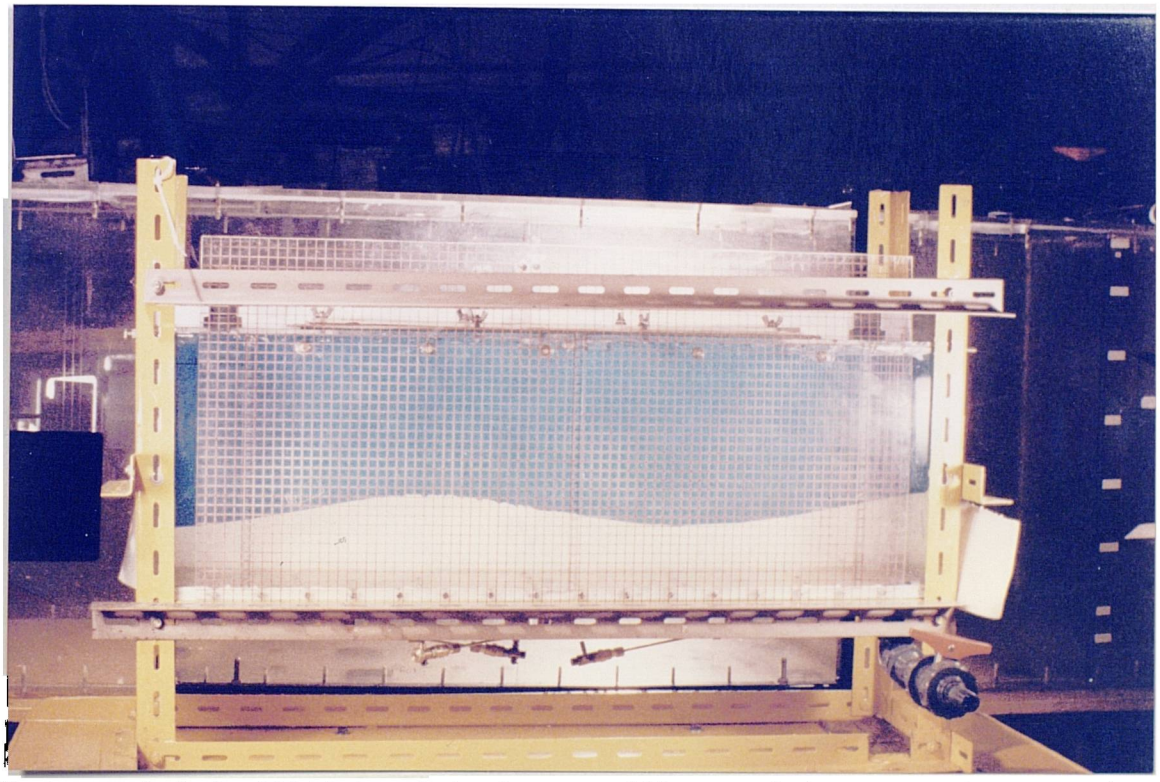

Photograph 9.4: Oil/Water interface profile resulting from pitch forcing motion at 3 seconds period, ±4° amplitude. Oil: FK890, water fill depth 87mm.

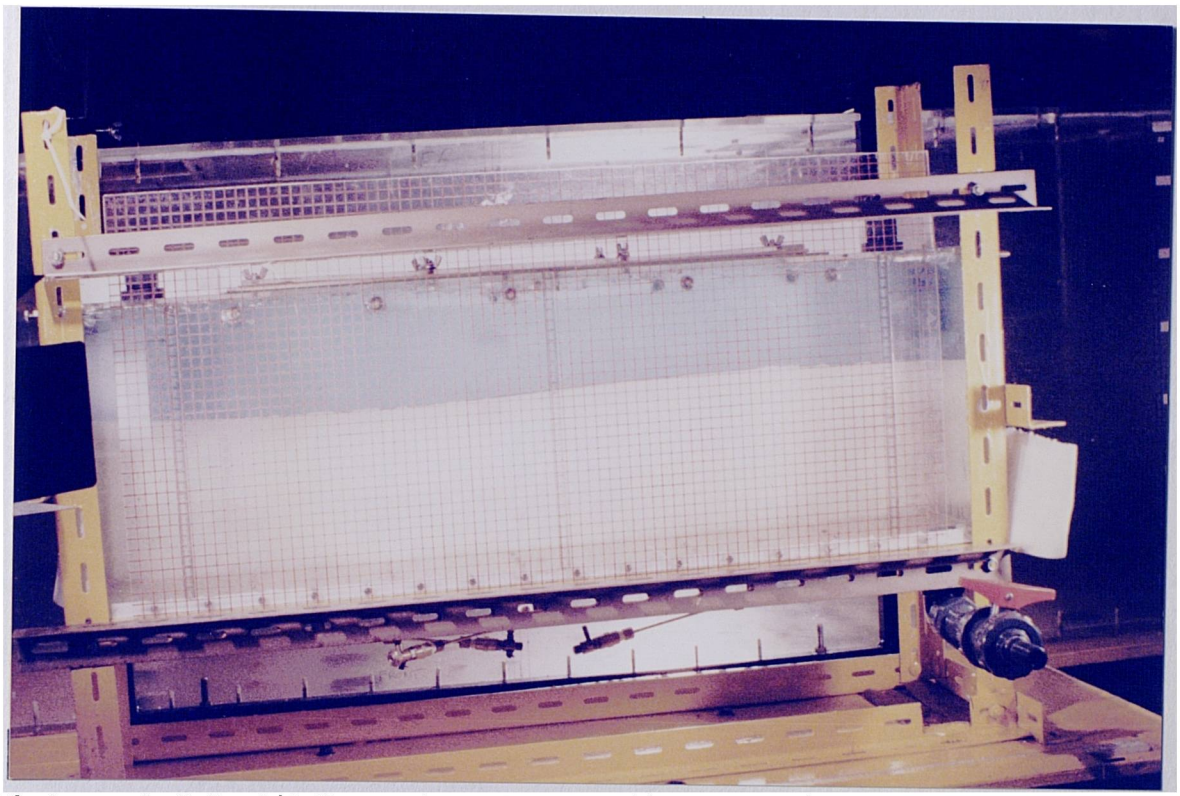

Photograph 9.5: Oil/Water interface profile resulting from pitch forcing motion at 3 seconds period, ±4° amplitude. Oil: FK851, water fill depth 174mm.

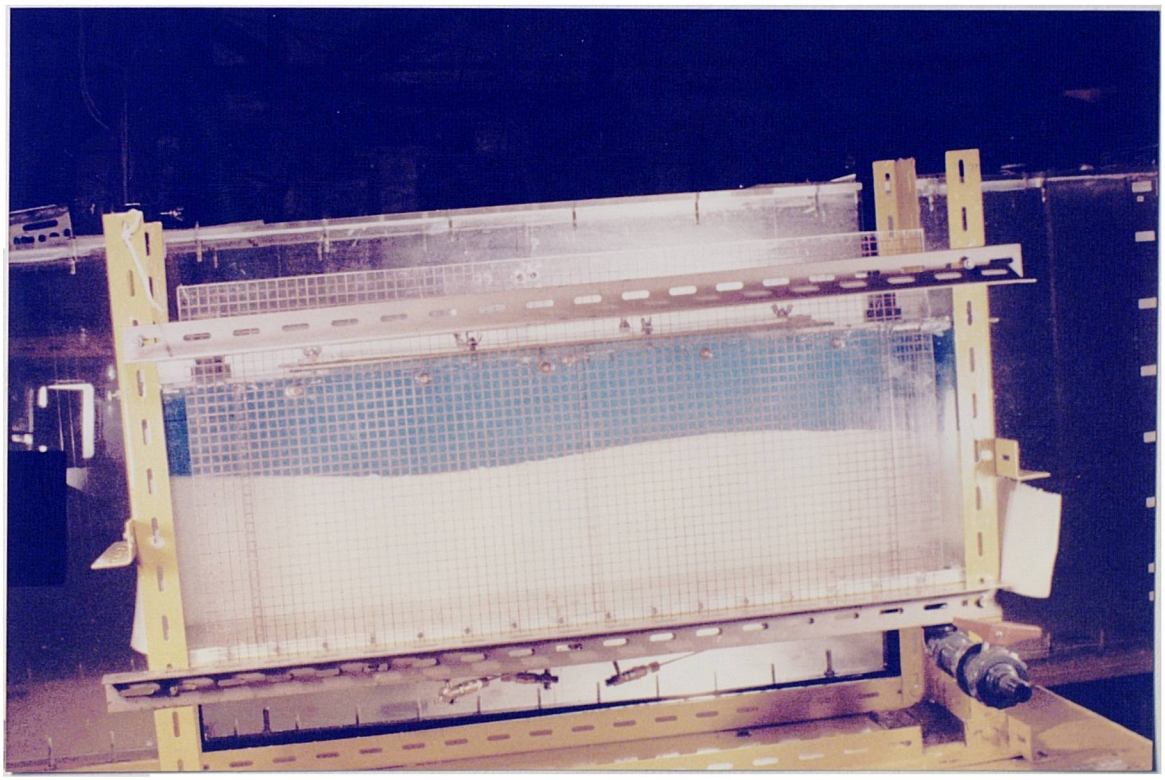

Photograph 9.6: Oil/Water interface profile resulting from pitch forcing motion at 3 seconds period, ±4° amplitude. Oil: FK890, water fill depth 174mm.

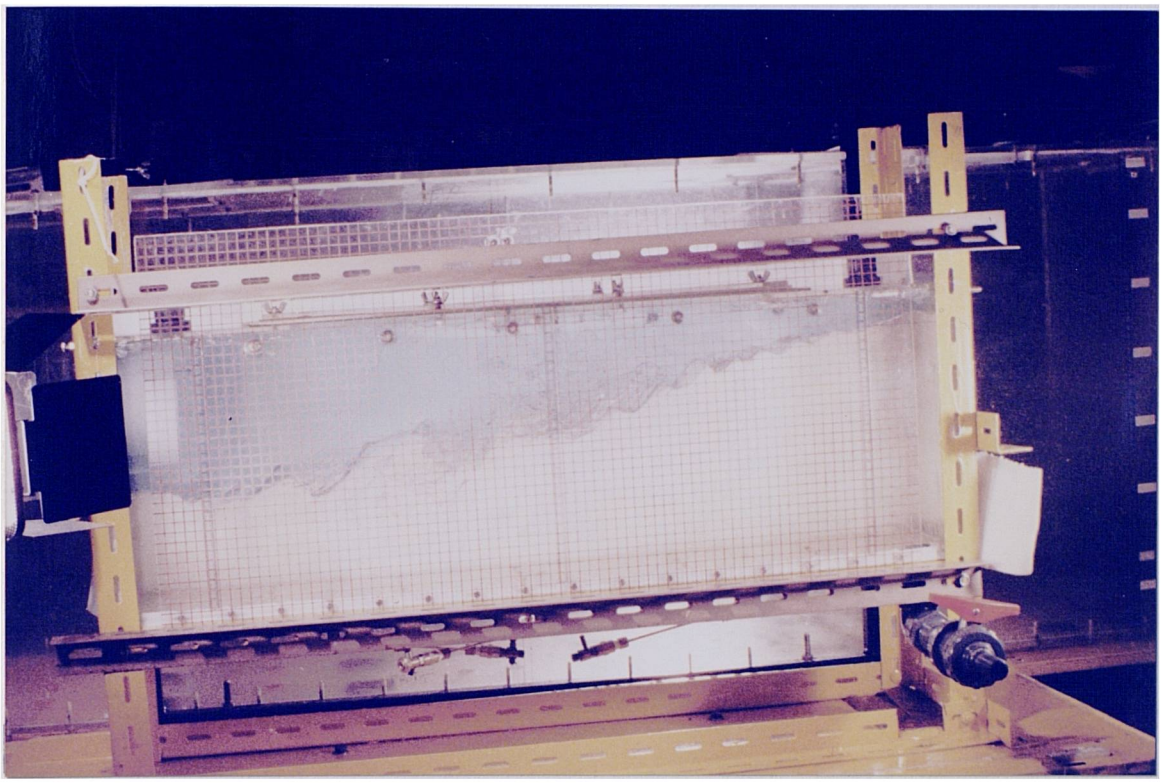

Photograph 9.7: Oil/Water interface profile resulting from pitch forcing motion at 6 seconds period, ±4° amplitude. Oil: FK851 water fill depth 174mm.

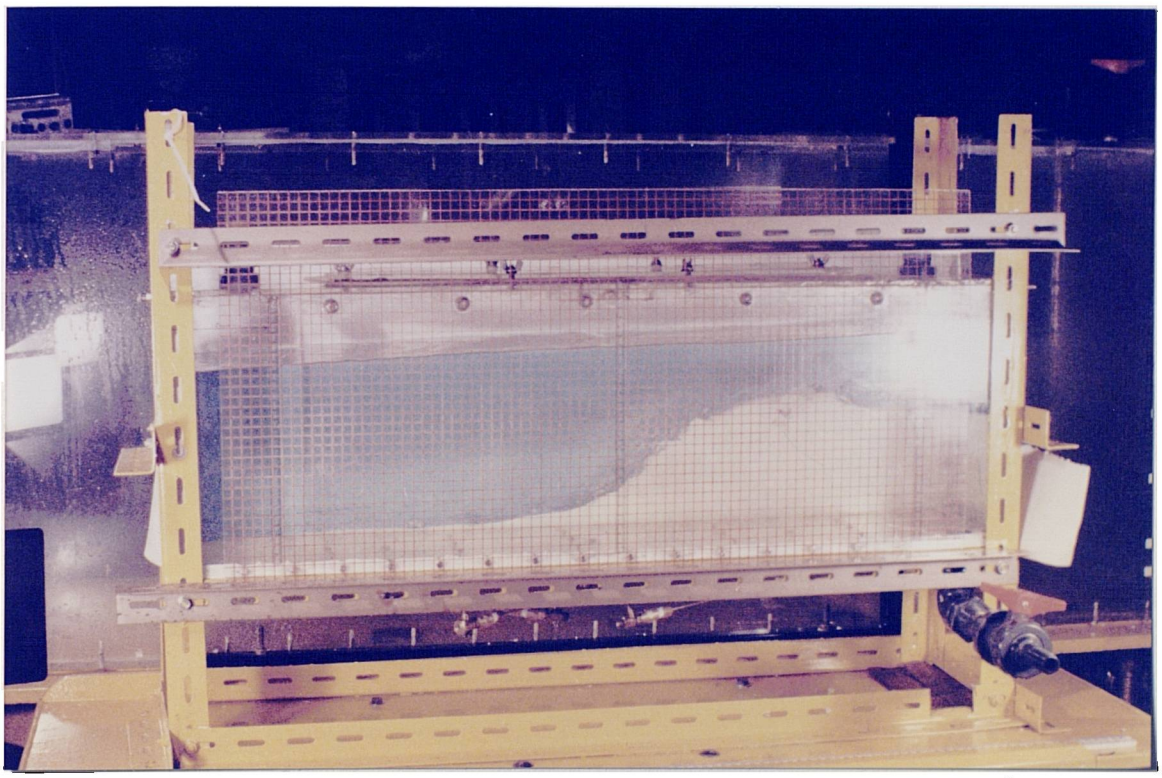

Photograph 9.8: Oil/Water and air/oil interface profiles resulting from pitch forcing motion at 7.5 seconds period, ±4° amplitude. Oil: FK851 at 217mm, water fill depth 87mm.

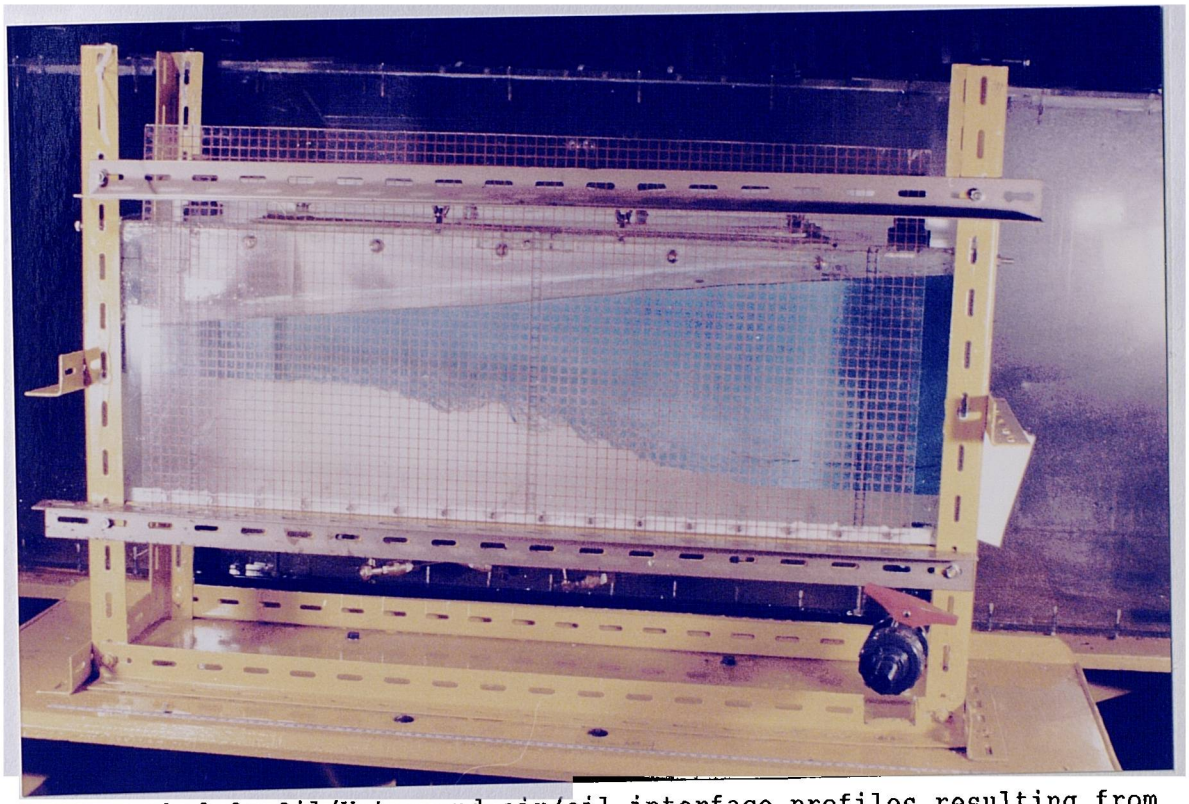

Photograph 9.9: Oil/Water and air/oil interface profiles resulting from pitch forcing motion at 5.2 seconds period, ±4° amplitude. Oil: kerosene at 217mm, water fill depth 87mm.

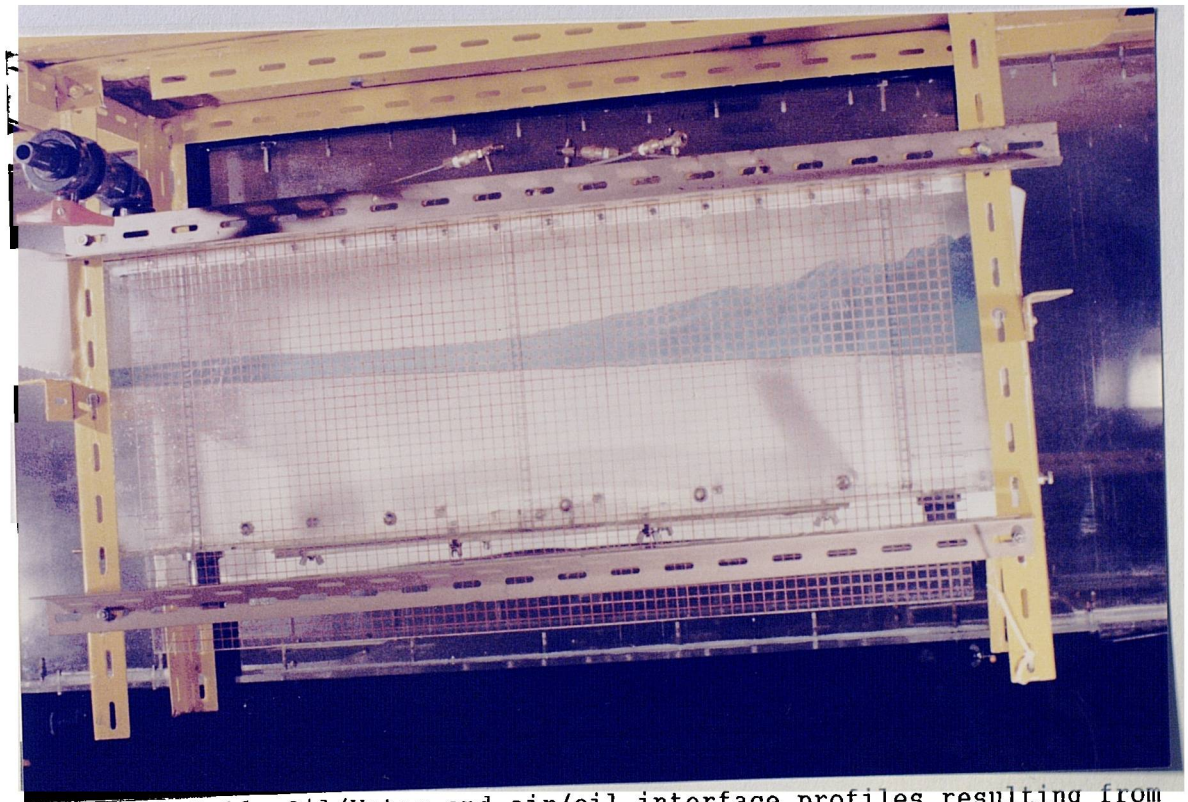

Photograph 9.10: Oil/Water and air/oil interface profiles resulting from pitch forcing motion at 8.3 seconds period, ±4° amplitude. Oil: FK851 at 131mm, water fill depth 87mm.

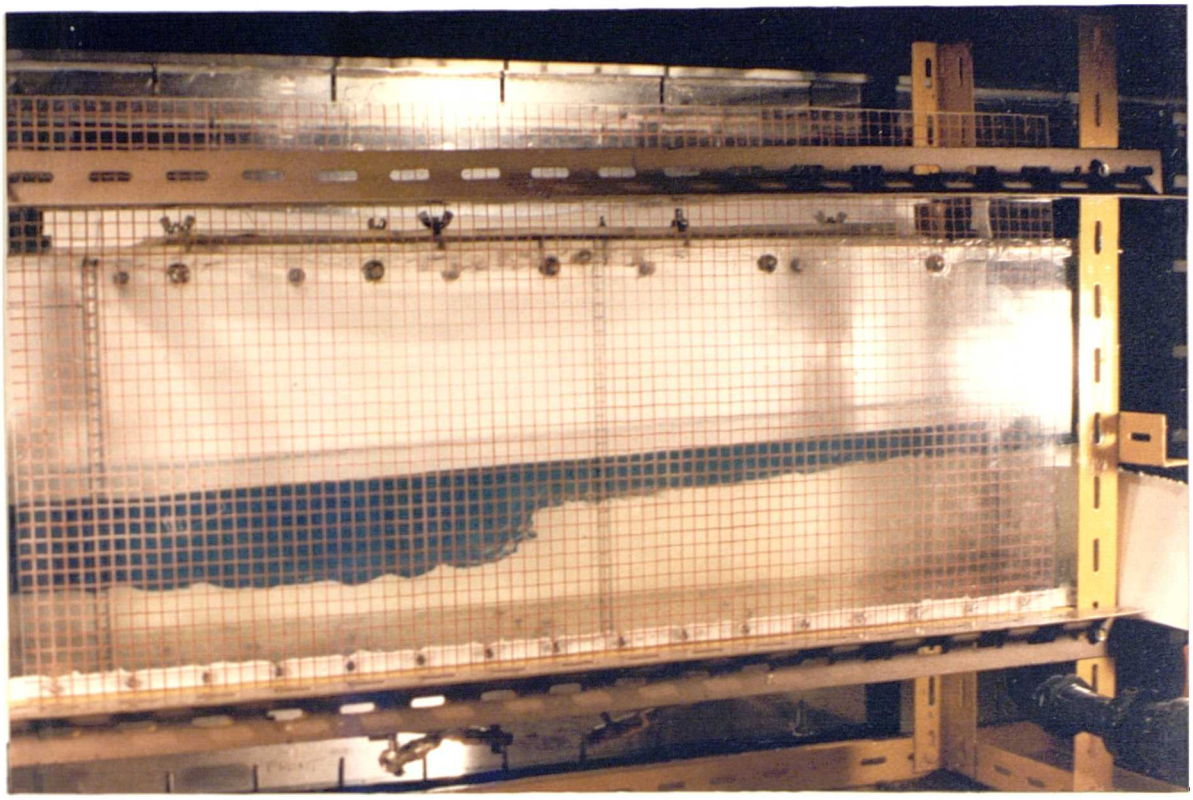

Photograph 9.11: Oil/Water and air/oil interface profiles resulting from pitch forcing motion at 9.5 seconds period, ±4° amplitude. Oil: FK890 at 131mm, water fill depth 87mm.

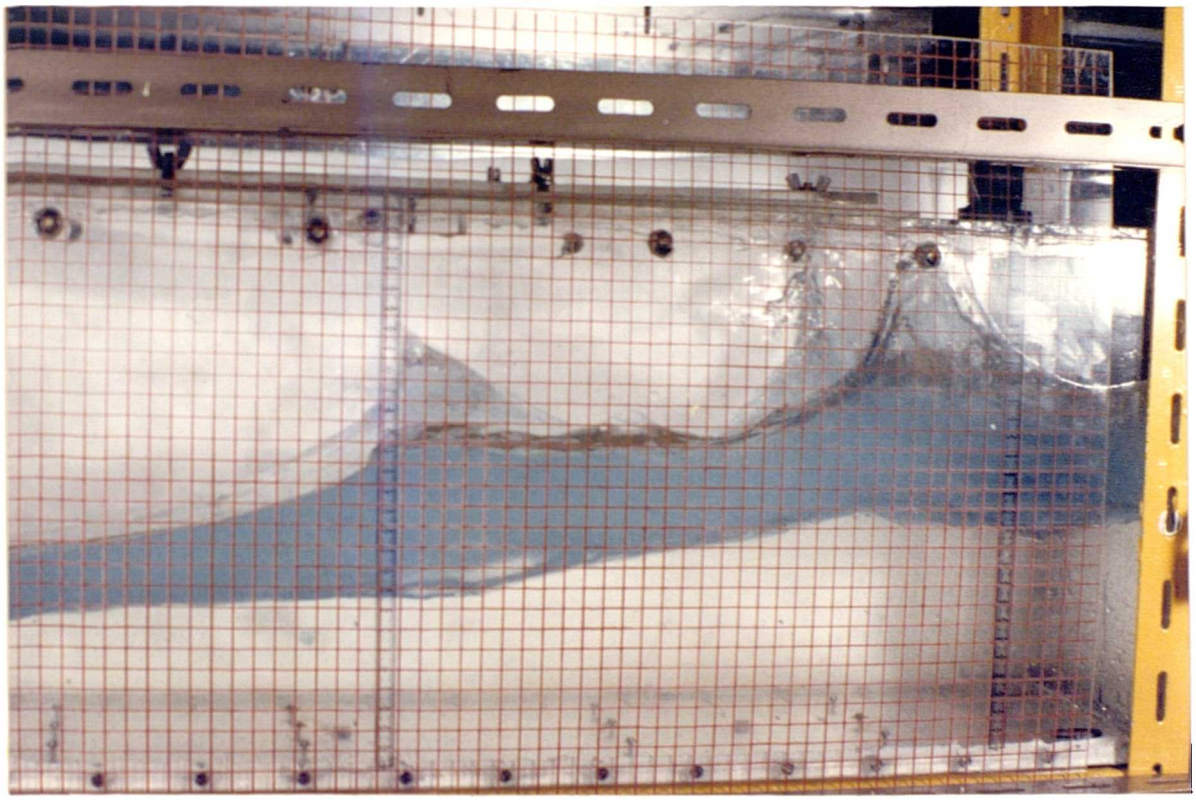

Photograph 9.12: Oil/Water and air/oil interface profiles resulting from pitch forcing motion at 2.5 seconds period, ±4° amplitude. Oil: kerosene at 131mm, water fill depth 87mm.

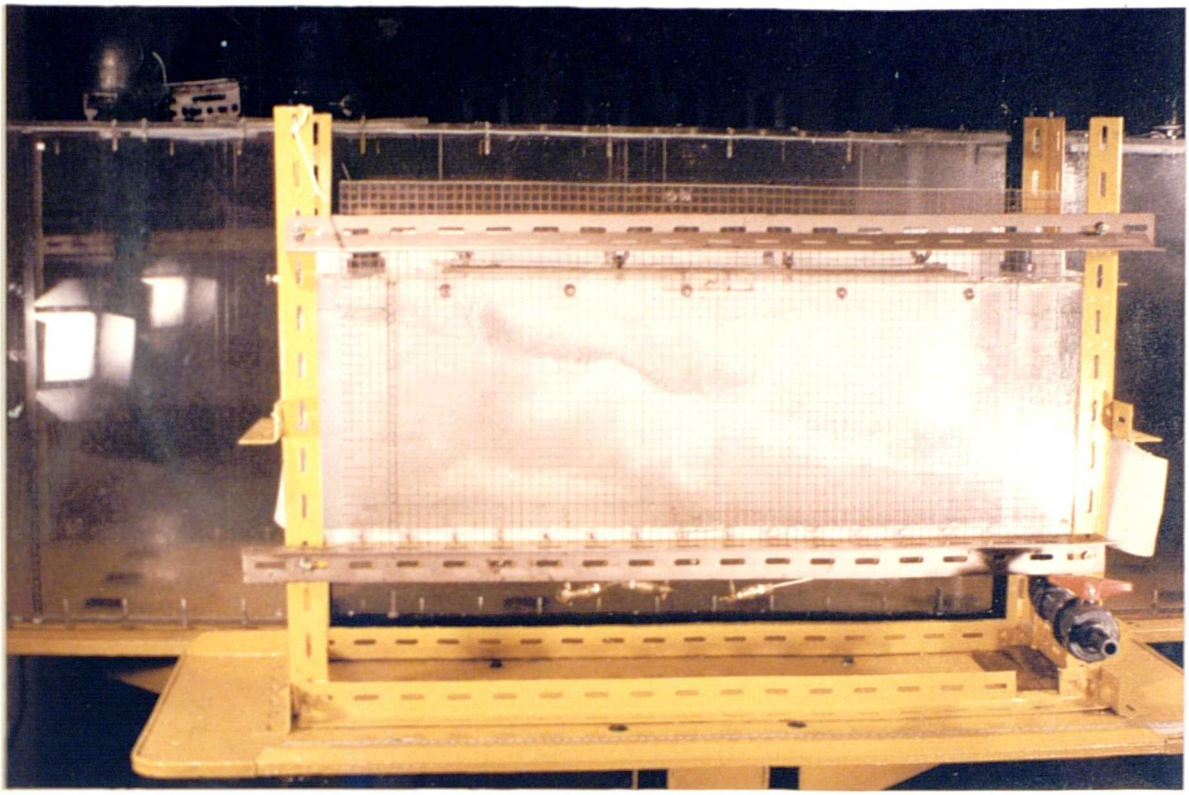

Photograph 9.13: Oil/Water and air/oil interface profiles resulting from pitch forcing motion at 2 seconds period, ±4° amplitude. Oil: FK851 at 131mm, water fill depth 87mm.

Oil Depth (mm)	Water Depth (mm)	Natural Periods* (secs) with Oils. (Density in Kg/m^3)					
		Kerosene ρ=796		FK851 ρ=858		FK890 ρ=885	
		A/O	O/W	A/O	O/W	A/O	O/W
271+	87		5.1		6.1		6.8
271+	174		4.8		5.8		6.5
217	87	1.3	5.4	1.3	6.5	1.3	7.2
131	87	1.6	7.1	1.6	8.5	1.6	9.5

Table 9.1: Predicted natural periods for oil/water (O/W) and air/oil (A/O) interfaces in the small rectangular container in relation to depth of oil and water and oil density.

Notes: *Predicted natural periods calculated from equation 4.19

+Vessel height is 271mm, therefore only oil/water period calculated.

Water Fill Depth (mm)	Oil Type	Oil Density (Kg/m^3)	Natural Period Predicted (sec)	Natural Period Measured (sec)	Graph
87	Kerosene	796	5.1	—	9.2
	FK851	858	6.1	6.1	
	FK890	885	6.8	6.9	
174	FK851	858	5.9	5.8	9.3
	FK890	885	6.5	6.7	

Table 9.2: Predicted and measured natural periods for oil/water experiments at different water fill depths.

Oil Type	Oil Density (Kg/m^3)	Oil Fill Depth (mm)	Natural Periods Predicted (sec)	Natural Periods Measured (sec)	Graph
FK851	858	271 217 131	6.1 6.5 8.6	6.0 6.5 ——	9.7
Kerosene	796	271 217 131	5.1 5.4 7.1	5.1 5.6 7.1	9.8

Table 9.3: Predicted and measured natural periods in for air/oil/water experiments at different oil fill depths. Water depth at 87mm.

CHAPTER 10.

RESULTS FROM AIR/OIL/WATER EXPERIMENTS IN THE LARGE RECTANGULAR VESSEL.

10.1 INTRODUCTION.

In chapter 2, the importance of baffles to reduce sloshing was stated, both in large scale LNG carriers and offshore separators. Outline reports of commercial model separator tests (12) suggested that perforated baffles whilst suppressing primary motion can cause secondary turbulence which may reduce separation performance. To provide specific details and to judge suitability of such baffles, oil/water sloshing experiments were conducted in the large rectangular vessel using the solid plate and perforated baffles described in chapter 8.

Due to the large volume of oil required for these experiments, Gas Oil was used instead of kerosene. This restricted experiments to a single density ratio as insufficient Freon 113 was available to modify gas oil density. Due to vessel sealing problems, all experiments were conducted with a gas cap, i.e. a three fluid (air/oil/water) system.

This chapter presents the results from two sets of experiments, to study the effects of forcing period on the unbaffled and baffled vessel.

10.2 EXPERIMENTAL OVERVIEW.

Oil/Water experiments with this vessel, were conducted with a view to study the effects of baffles on the oil/water interface. For this, interfacial profiles were recorded for different oil/water fill depths at pitch forcing motion of $\pm 4°$ amplitude. Forcing period was varied to cover predicted resonant periods of both upper air/oil and lower oil/water interfaces. Further experiments with this vessel were conducted to measure the amount of oil transferred into the water as a result of resonant forcing and will be described in chapter 11.

Oil/Water experiments with the large rectangular vessel posed several difficulties. Initially, oil was supplied by pumping from a single 45 gallon oil drum. Since total vessel volume was 120 gallons, the single oil drum severely restricted the range of oil fill depths. It was not until the department constructed a large oil/water storage facility, that oil/water experiments in this vessel became practical. A further difficulty was that results from preliminary experiments were recorded using conventional domestic video equipment (JVC VHS Camera and JVC VHS video recorder). This was found unsuited for detailed analysis. The purchase of the NAC HSV-400 video unit coincided with use of the oil/water storage facility. Therefore, the graphical results presented in this chapter concern those derived from the NAC HSV-400 recordings. However, some photographic evidence will refer to the preliminary experiments. It should be recognised that photographs presented in this chapter represent only samples of interface profiles both in time and of forcing conditions.

10.3 EFFECT OF FORCING PERIOD AND WATER/OIL DEPTH ON INTERFACE AMPLITUDE.

10.3.1 Introduction.

Oil/Water interface profiles were recorded following methods outlined in chapter 6, with different water and oil fill depths. Applied forcing motion was restricted to pitch at ±4° amplitude over a range of periods. Table 10.1 shows predicted first and second mode natural periods for both air/oil and oil/water interfaces (equation 4.19). Graph 10.1 shows the effect of forcing period on oil/water interface amplitude for different oil/water fill depths.

10.3.2 Interface Amplitude Response.

Graph 10.1 indicates :

1) The point of maximum interface amplitude occurs at forcing periods slightly higher than predicted resonance (table 10.1) for all oil/water fill depths. This may be due to the number of forcing periods used around predicted resonance and therefore actual resonance was not covered during this experiment.

2) The value of maximum interface amplitude appears to be approximately half that of oil layer size.

3) Oil/water interface amplitude is seen to increase at short forcing periods (Ω<4 secs) for low water/low oil (190/400mm) fill depths.

These observations are then similar to those noted in the small rectangular vessel (chapter 9).

The increase of oil/water interface amplitude at short forcing periods may be attributed to either the effects of upper air/oil interface or to a second natural period mode response. However, for the low water/low oil fill depth, table 10.1 indicates the observed increase in interface amplitude coincides at forcing periods equal to predicted air/oil first mode natural periods. In addition to discussions in chapter 9, and that low water/low oil interface amplitude is higher than for other fill depths, it is suggested that interaction between the air/oil and oil/water interfaces occurs at low oil depths.

10.3.3 Shape of the Oil/Water Interface.

Photographs 10.1 to 10.6 show oil/water interface profiles similar to those observed with the small rectangular vessel (chapter 9) :

1) At resonance for low water/high oil (180/535mm) fill depth (i.e. Ω=9 secs), a solitary travelling wave was observed, together with distinct regions where oil/water mixing occurred (photograph 10.1).

2) Close to resonance for the low water/low oil (190/400mm) fill depth (i.e. Ω=12 secs), an inverted solitary travelling wave was observed, with hydraulic jump similarities (photograph 10.2). Oil/Water mixing seemed to be confined to a region behind the jump, indicated by the step like presence in the photograph.

3) For low water/high oil (180/535mm) fill depth away from resonance (Ω=12 secs), a distinct sinusoidal profile formed (photograph 10.3), consisting of standing and travelling waves. The oil/water interface appears smooth and two dimensional in form.

4) For low water/low oil (180/285mm) depths, at forcing periods close to air/oil resonance (Ω=3 secs), interaction between oil/water and air/oil was clearly seen (photograph 10.4). At this forcing period the air/oil interface developed a three dimensional profile.

These observations then indicate similarities with the kerosene experiments in the small rectangular vessel (chapter 9). However, differences were noted in the oil-in-water and water-in-oil bubbles produced as a result of resonant forcing conditions. Photographs 10.5 & 10.6 show closeups of the point of oil/water interface breaking, with bubbles flowing away from the break. By their red colouration, individual drops of oil can be seen underneath the interface whereas the lighter coloured bubbles can be seen some distance away. Approximate size of oil-in-water bubbles were estimated (from one photograph) to be of the order of 10mm.

A further comment as regards the state of the oil, in some cases what appears to be feathery strands were seen stuck to the vessel wall. Observations show that these were produced in filling operations and not due to subsequent motion effects.

10.3.4 Discussion.

These results show that oil/water resonance occurs at much longer forcing periods than those for air/water or air/oil. Oil/water interfacial waves at such conditions are characterised by a single travelling wave for high oil depth (535mm) and an inverted travelling wave for low oil depths. The forcing period corresponding to maximum oil/water interface amplitude, may be slightly higher than predicted oil/water natural period. These effects are similar to those observed in the small rectangular container with kerosene (chapter 9), although they may be due to applied forcing periods not covering regions round resonance.

10.4 THE EFFECT OF BAFFLES ON OIL/WATER AND AIR/OIL INTERFACE AMPLITUDE.

10.4.1 Introduction.

The effect of solid plate and perforated baffles in reducing air/water interface amplitude has been discussed in chapter 8. Previous workers (12) have indicated that perforated baffles may increase oil/water mixing in offshore separation equipment. Several experiments were carried out to study the effect of solid plate baffles and the perforated baffles (22% and 53% free area) on oil/water interface profiles.

10.4.2 At Low Water/High Oil (180/535mm) Fill Depths.

Graphs 10.2a-b show the effect of forcing period on oil/water and air/oil interface amplitude, for baffled and unbaffled vessel at low water/high oil (180/535mm) fill depth. These results show :

1) For the oil/water interface (graph 10.2a), a similar response occurs in air/water sloshing at 180mm fill depth (chapter 8, graph 8.9). That is, baffles seem to chop the maximum interface amplitude at resonance as opposed to shifting the natural period. This is especially the case for the 53% free area baffle at both heights. The most effective baffle at reducing oil/water interface amplitude is firstly the 22% free area baffle followed by the solid plate baffle at a height of 180mm.

2) For the air/oil interface, all perforated baffles and unbaffled results (graph 10.2b), show increasing interface amplitude at short forcing periods. However, the solid plate baffle shows the opposite trend.

It would then appear from these results that the solid plate baffle touching the oil/water interface, is more effective at reducing oil/water and air/oil interface amplitude.

At forcing periods close to resonance for low water/high oil fill depths, similar wave forms were observed in baffled experiments as in the unbaffled vessel. However, the regions of interface breaking seemed to occur mainly at the baffle itself (photograph 10.7). Instead of bubbles, droplets of oil formed which were quickly absorbed back into the oil layer on contact with the interface. Photograph 10.8 shows a region of lighter coloured oil directly below oil/water interface next to the 53% perforated baffle. This photograph also shows indications of oil droplets in the water, not oil-in-water bubbles.

10.4.3 At High Water/High Oil (360/535mm) Fill Depths.

Graphs 10.3a-b show the effect of forcing period on oil/water and air/oil interface amplitude, for the baffled and unbaffled vessel at high water/high oil (180/535mm) fill depth. These results show :

1) For the oil/water interface (graph 10.3a), baffles seem to chop the maximum interface amplitude at resonance. The solid plate baffle appears to be more effective than the 53% perforated baffle.

2) Air/oil interface amplitude (graph 10.3b) follows similar trends as for low water/high oil fill depth (graph 10.2b) i.e. oil/water interface amplitude increases as short forcing periods except for the solid plate baffle.

Photographs 10.9 and 10.10 show for a short forcing period (Ω=3 secs), that the solid plate and 53% perforated baffles, touching the interface cause a series of small amplitude standing waves form on the oil/water interface. Breakup of the oil/water interface is seen away from the 53% perforated baffle and not for the solid plate baffle. At the same forcing period, two dimensional oil/water interface profiles were seen for the fully immersed 53% perforated baffle (photograph 10.11) and the unbaffled vessel (photograph 10.12). At forcing periods closer to resonance (Ω=12 secs), photographs 10.13 and 10.14 compare fully immersed 53% perforated and solid plate baffles. While the perforated baffle forms standing waves, interface break up is seen round the tip of the solid plate baffle.

10.4.4 At Low Water/Low Oil (180/360mm) Fill Depths.

At this oil/water fill depth, interface amplitudes were recorded using the conventional video system. The results were therefore, not digitized and the effect of forcing period on interface amplitude was not

measured. However, photographs of oil/water interface profiles were taken at forcing periods near oil/water resonance.

With the 53% perforated baffle fully immersed, although oil/water interface motion appears reduced (photograph 10.15), regions directly near the baffle perforations show severe oil/water mixing (photograph 10.16) with bubble formation replaced by droplet formation. Placing baffles on the oil/water interface, produces a very different profile, similar to standing waves. Photographs 10.17 and 10.18, show the marked difference between perforated and solid plate baffle. The light coloured patches appearing for the perforated baffle were identified as droplets of oil. These droplets were quickly reabsorbed with the bulk oil once forcing had ceased.

At longer forcing periods near to oil/water resonance (Ω=12 secs) the 53% perforated baffle is seen to allow unbaffled resonant waves pass unhindered (photograph 10.19). However, this was not found with the solid plate baffle (photograph 10.20). As a result, oil/water interface breakup occurs only round the tip of the solid plate baffle not along the length of the vessel.

10.4.5 Discussion.

These results indicate that at resonant forcing periods baffles can reduce oil/water interfacial amplitude. However, this effect does not necessarily prove that baffles have a beneficial affect on the oil/water interface. It was shown in some cases that perforated baffles may give rise to increased interfacial mixing of oil and water (photograph 10.7 and 10.8). Interfacial breakup which results from baffles consists of droplet rather than bubble formation.

At short forcing periods close to air/oil resonant conditions, only the solid plate baffle touching the oil/water interface, appears to reduce

air/oil interface amplitude. This is analogous with previous air/water experiments discussed in chapter 8. With the 53% perforated baffle in the same position, photograph 10.17 shows an oil/water profile which can only be due to flow through the baffle holes. Photograph 10.18 for the solid plate baffle, shows the air/oil interface smooth. The baffle appears to separate the vessel into two halves even though flow can occur under the baffle tip.

Evidence for emulsion formation was not found in these experiments. However, it must also be stated that for all experiments, forcing motion was applied for only 5 minutes. It is conceivable that sustained oil/water interfacial mixing would produce emulsions. Although the 5 minute forcing time was thought sufficient to study the general effects of forcing, it seems unsuited to study the long term effects experienced by a non-segregated oil-water storage vessel.

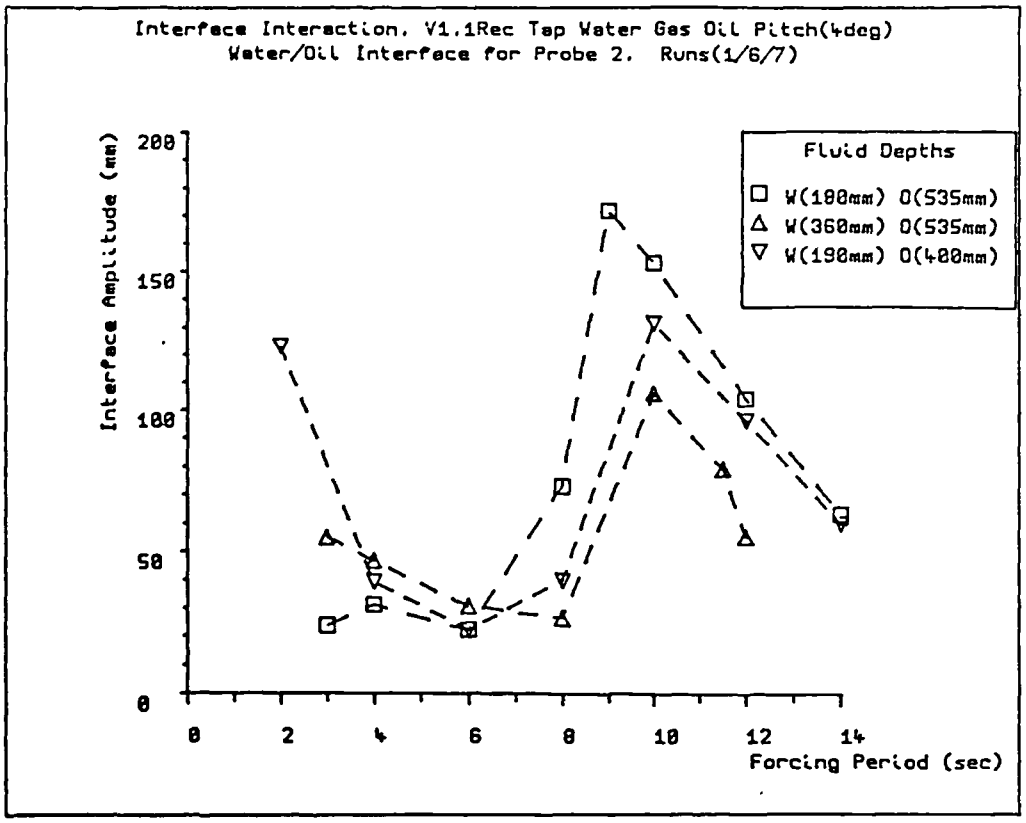

Graph 10.1: Effect of forcing period on oil/water interface amplitude for different oil/water fill depths under pitch forcing motion at ±4° amplitude.

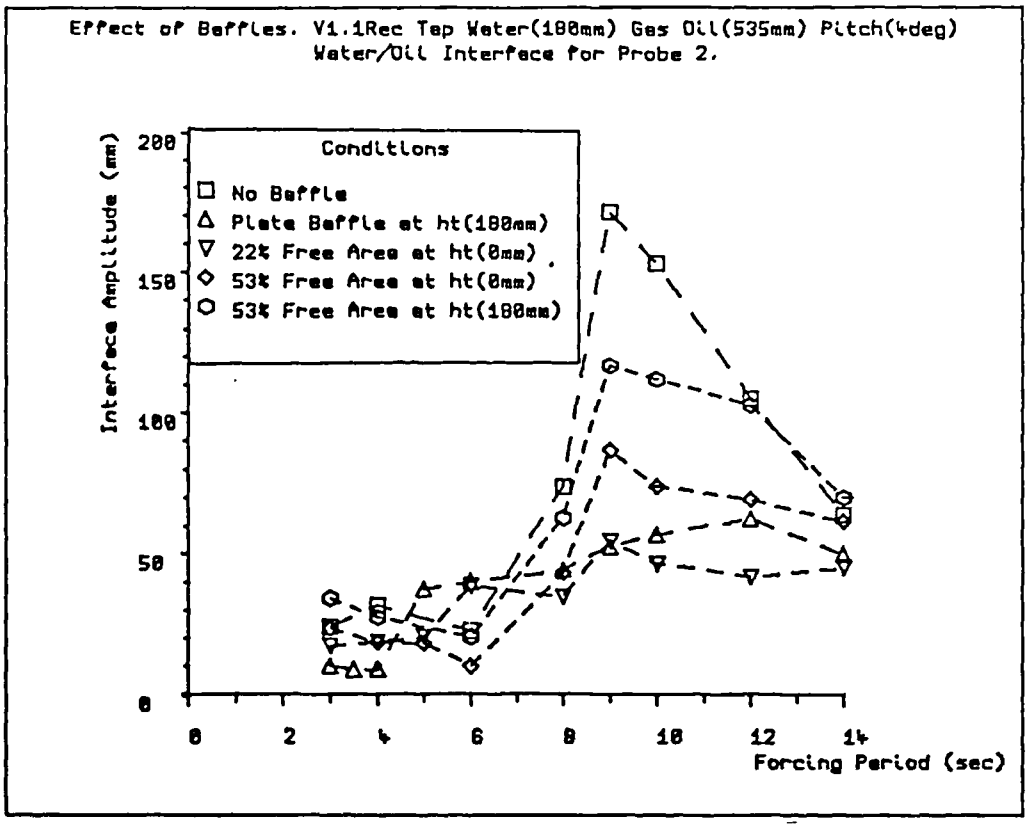

Graph 10.2a: Effect of forcing period on oil/water interface amplitude for different baffles under pitch forcing motion at ±4° amplitude. Oil depth 535mm, water depth 180mm.

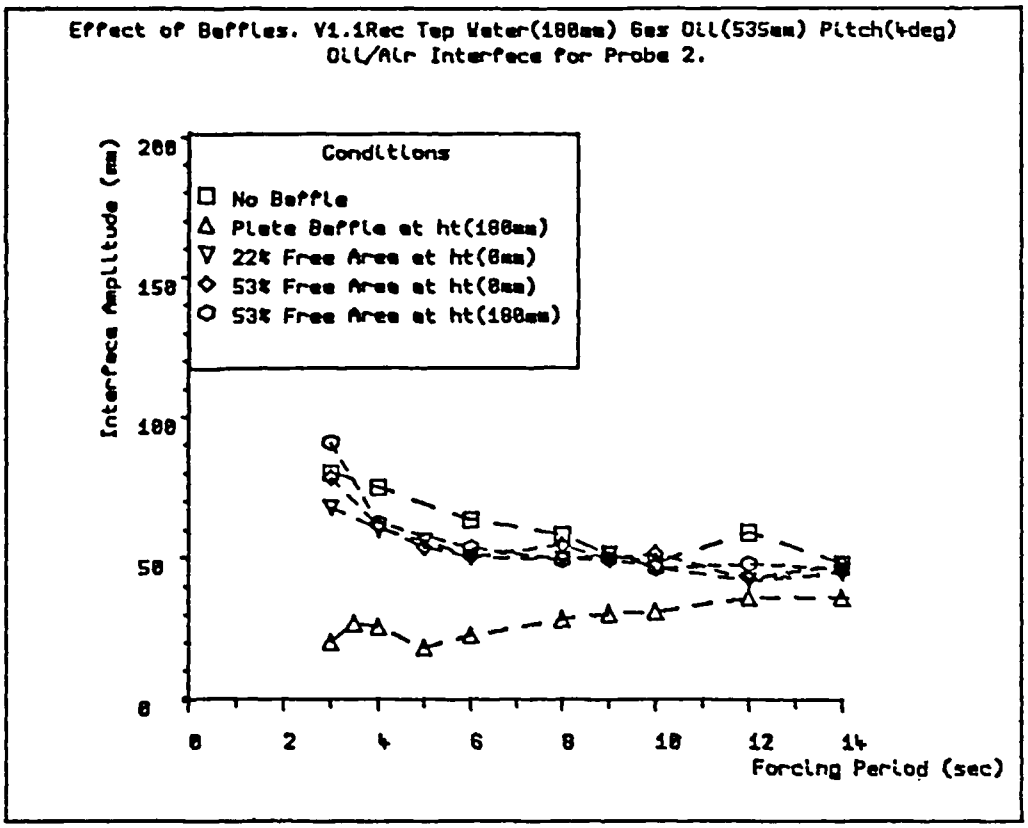

Graph 10.2b: Effect of forcing period on air/oil interface amplitude for different baffles under pitch forcing motion at ±4° amplitude. Oil depth 535mm, water depth 180mm.

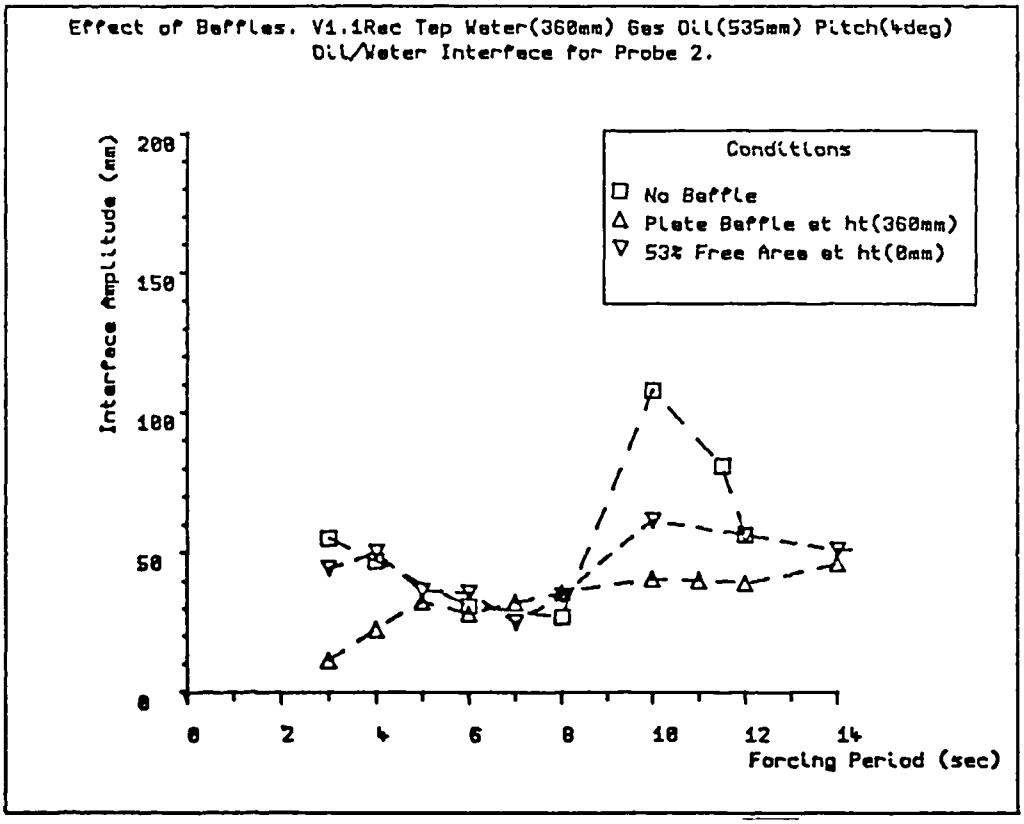

Graph 10.3a: Effect of forcing period on oil/water interface amplitude for different baffles under pitch forcing motion at ±4° amplitude. Oil depth 535mm, water depth 360mm.

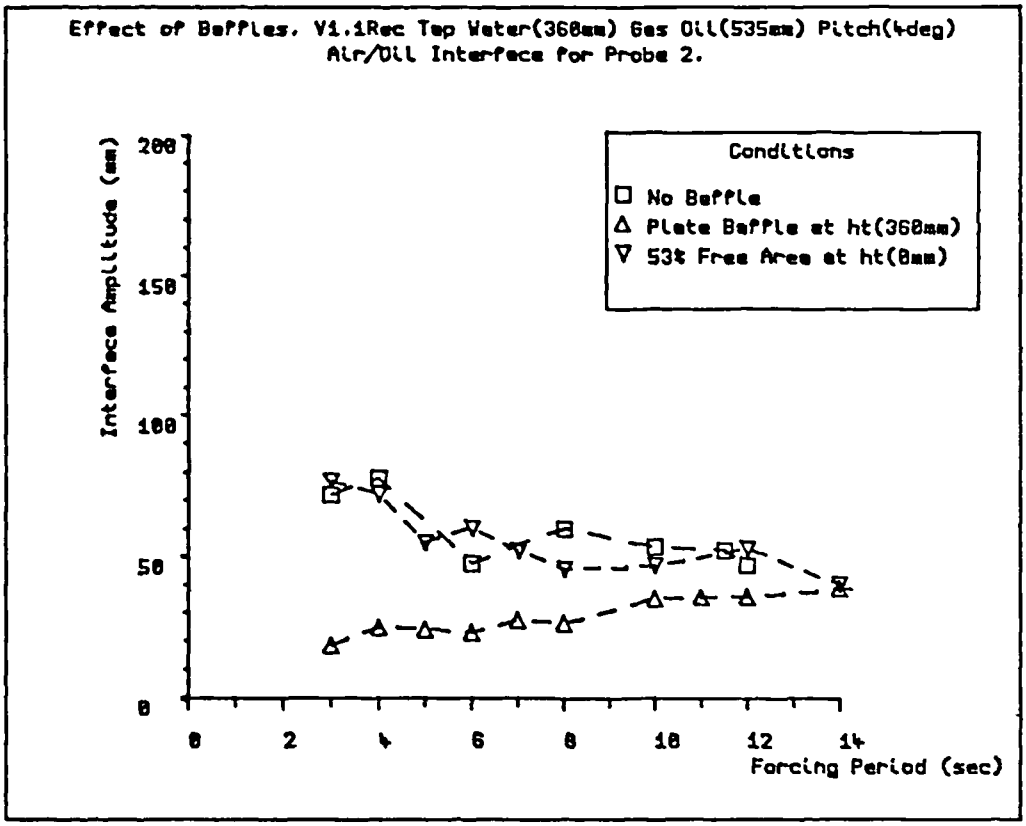

Graph 10.3b: Effect of forcing period on air/oil interface amplitude for different baffles under pitch forcing motion at ±4° amplitude. Oil depth 535mm, water depth 360mm.

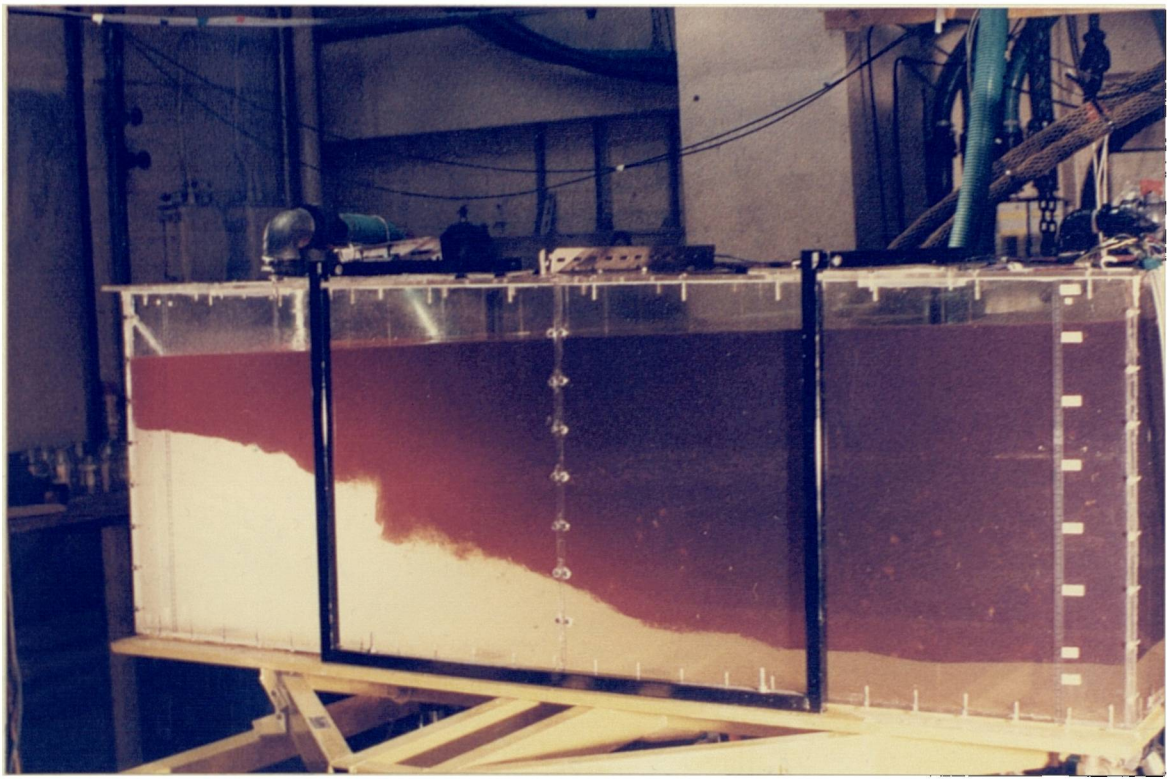

Photograph 10.1: Interface profiles under pitch forcing motion at 9 seconds, ±4° amplitude. Oil depth 536mm, water depth 180mm.

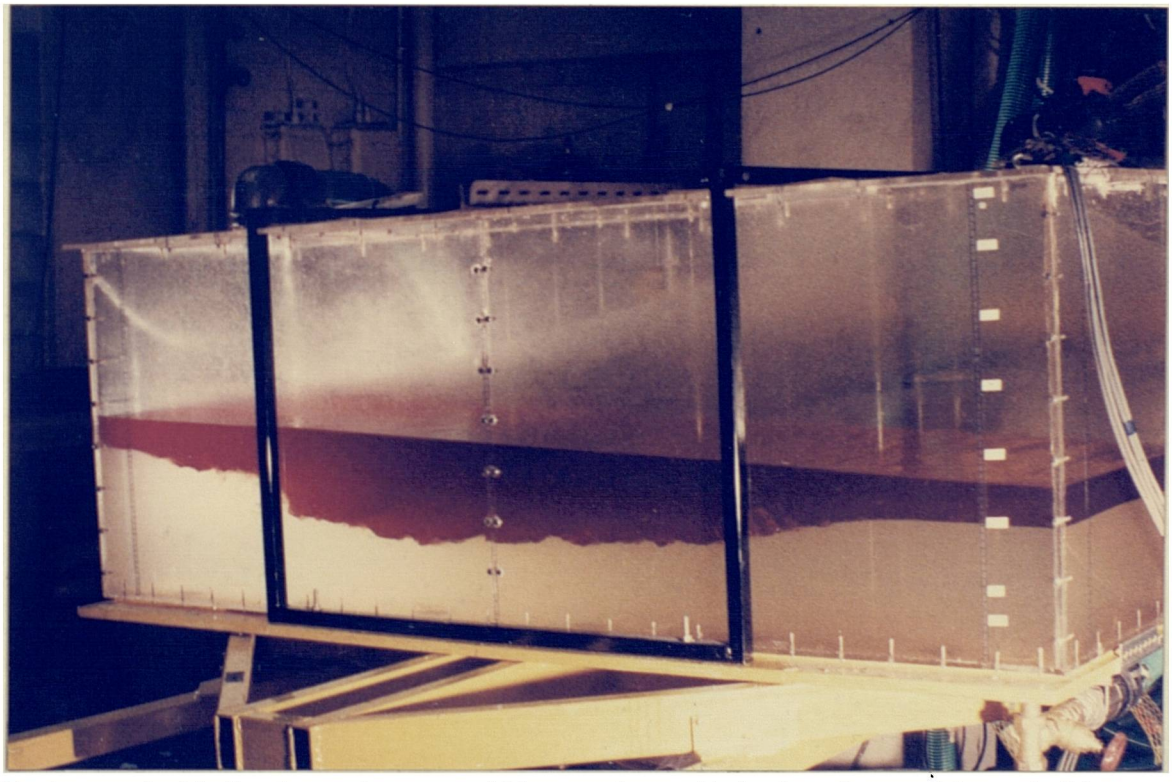

Photograph 10.2: Interface profiles under pitch forcing motion at 12 seconds, ±4° amplitude. Oil depth 285mm, water depth 180mm.

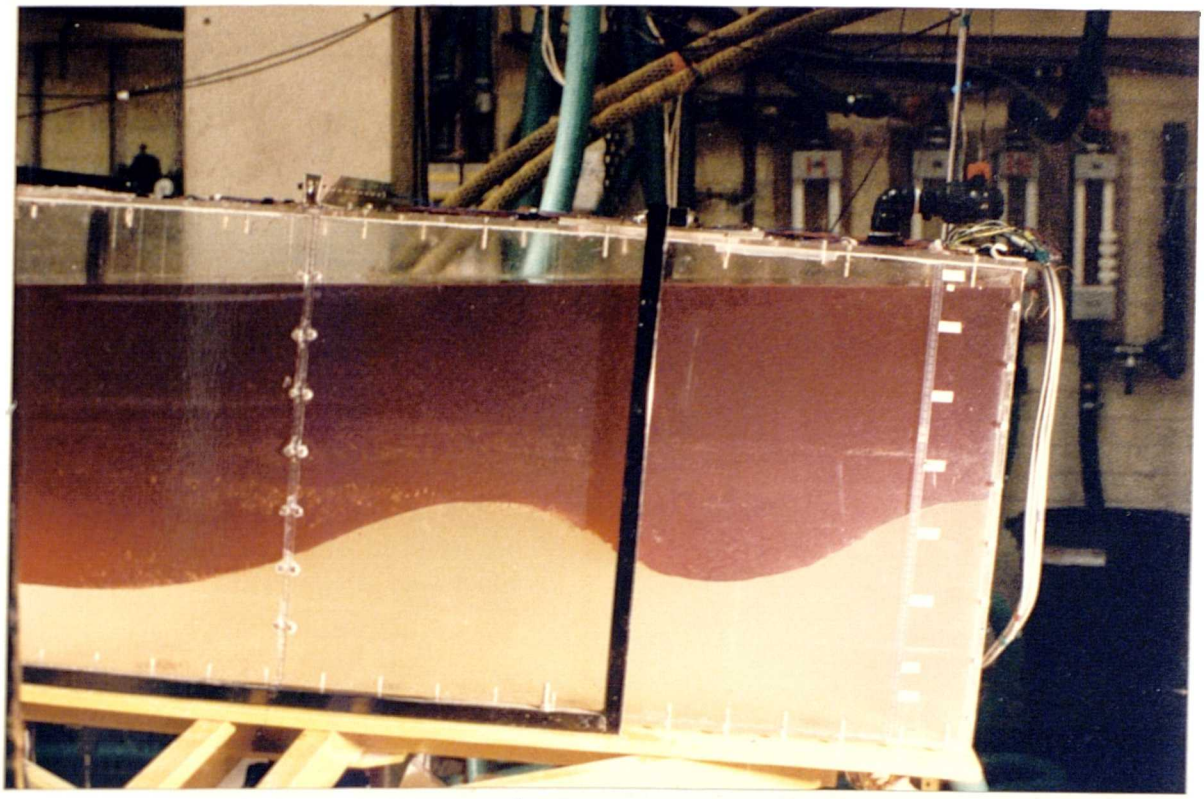

Photograph 10.3: Interface profiles under pitch forcing motion at 12 seconds, ±4° amplitude. Oil depth 536mm, water depth 180mm.

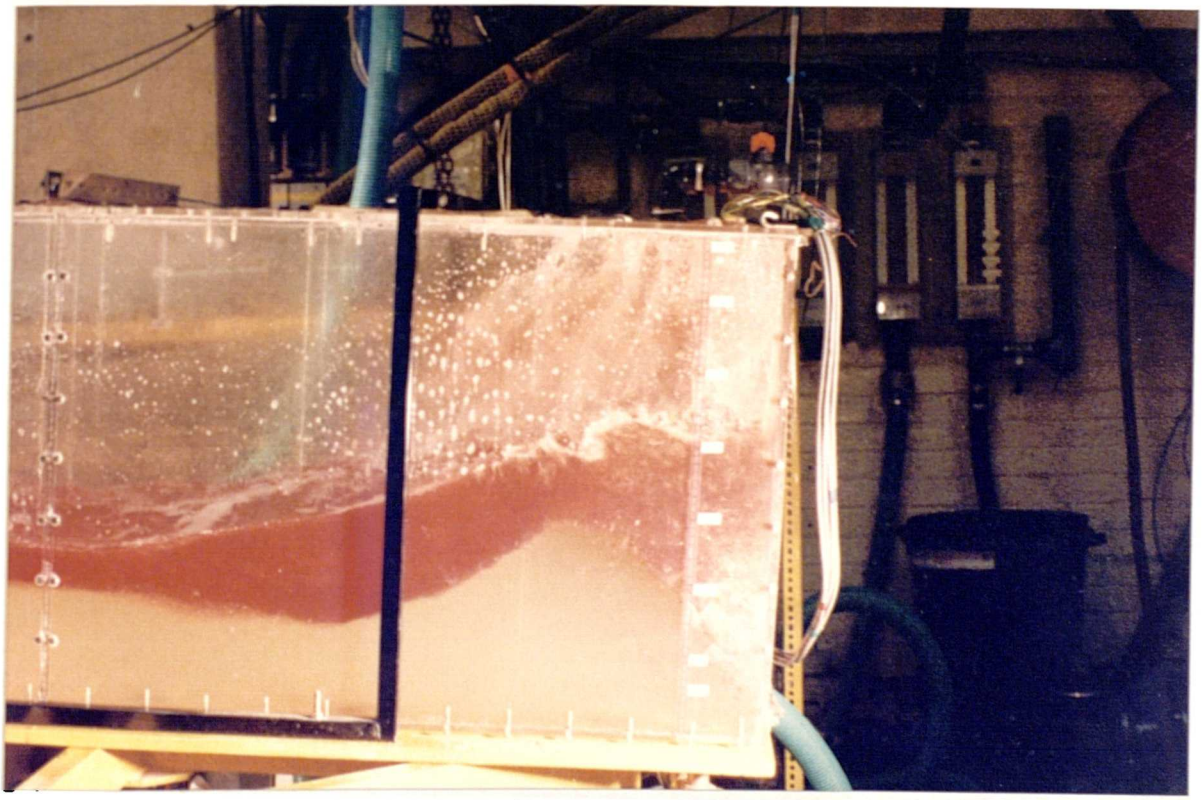

Photograph 10.4: Interface profiles under pitch forcing motion at 3 seconds, ±4° amplitude. Oil depth 285mm, water depth 180mm.

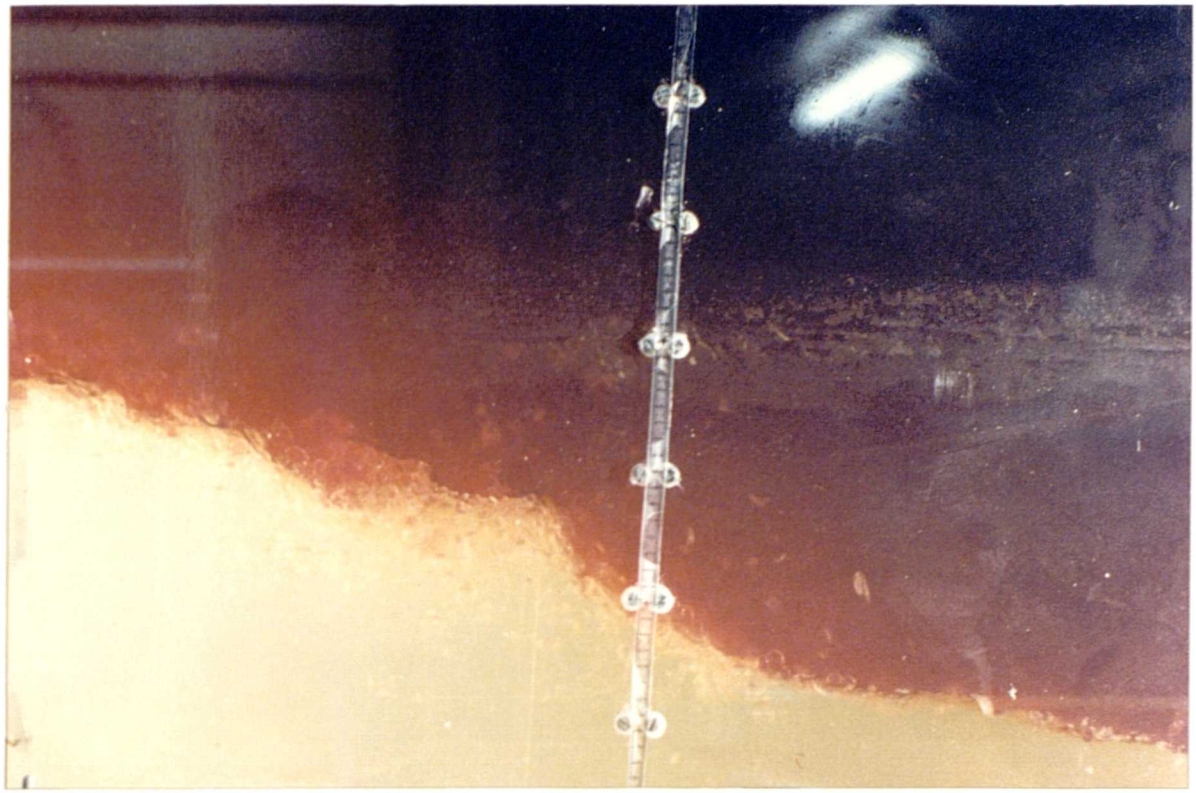

Photograph 10.5: Oil/water interface profiles under pitch forcing motion at 8.6 seconds, ±4° amplitude. Oil depth 536mm, water depth 180mm.

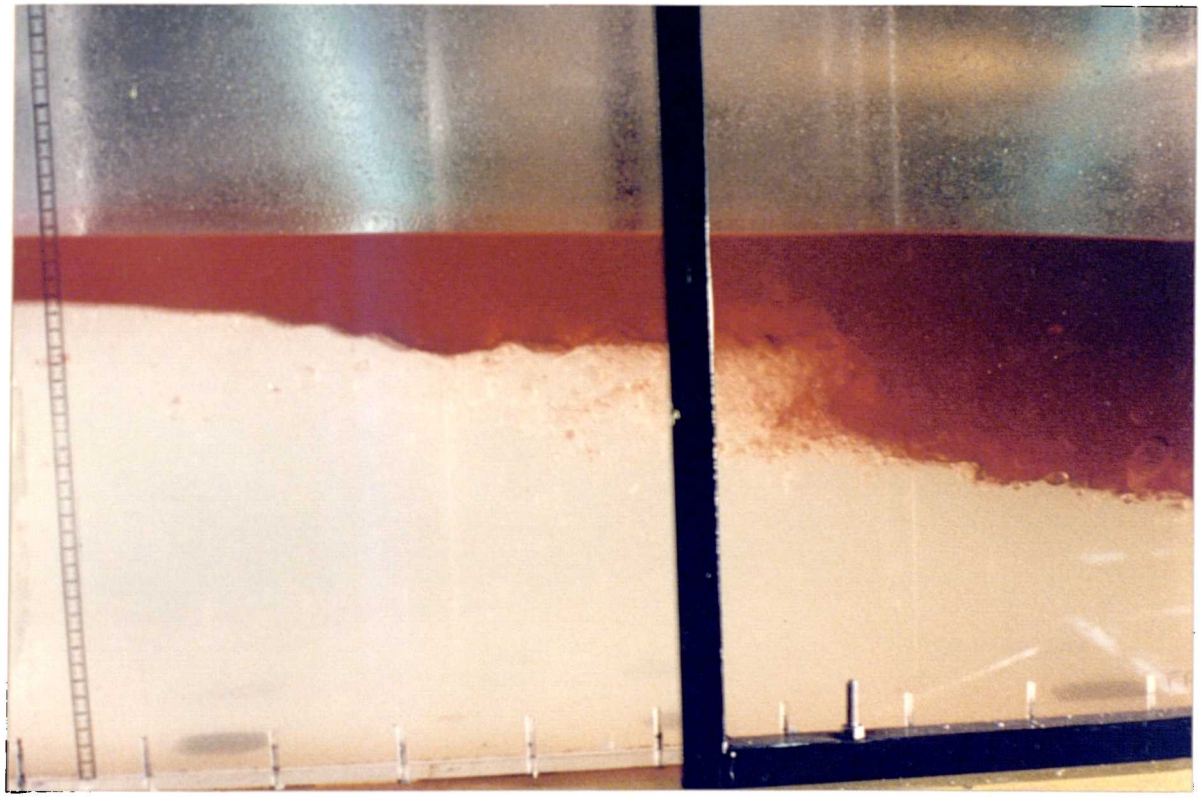

Photograph 10.6: Oil/water interface profiles under pitch forcing motion at 12 seconds, ±4° amplitude. Oil depth 285mm, water depth 180mm.

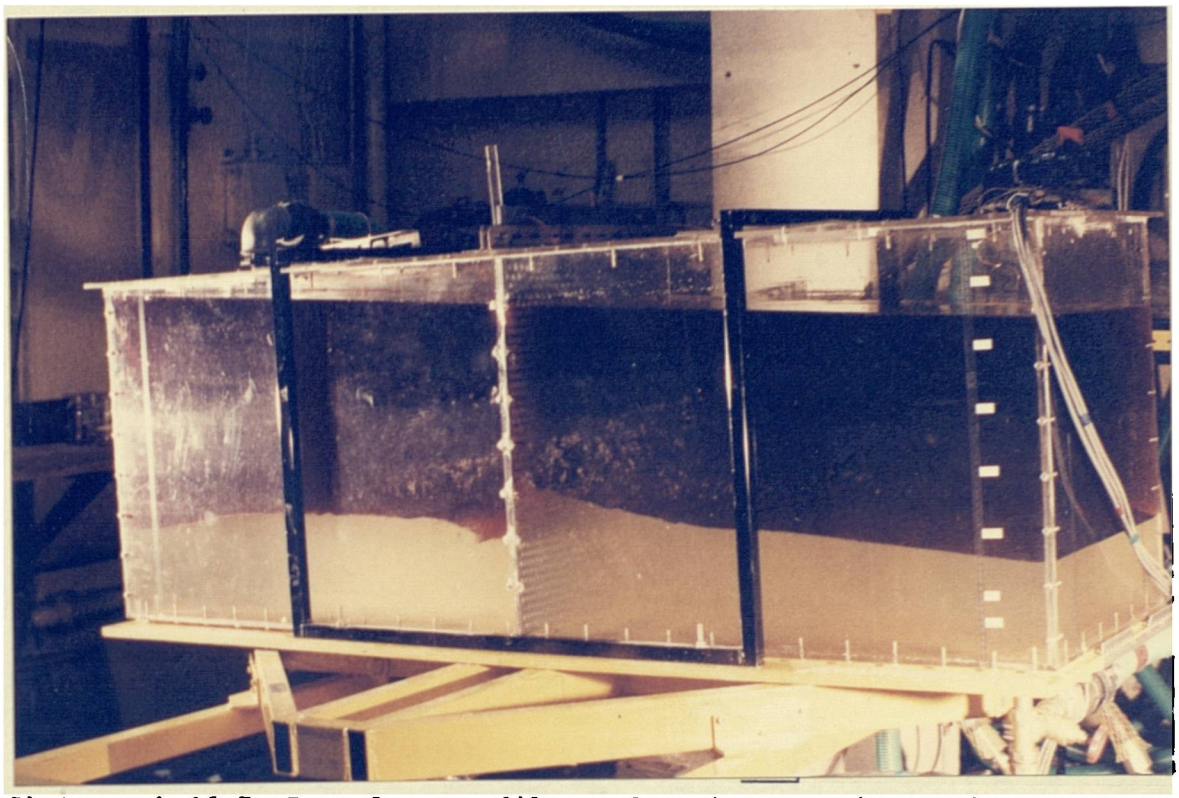

Photograph 10.7: Interface profiles under pitch forcing motion at 8.6 seconds, ±4° amplitude with the 53% perforated baffle. Oil depth 535mm, water depth 180mm.

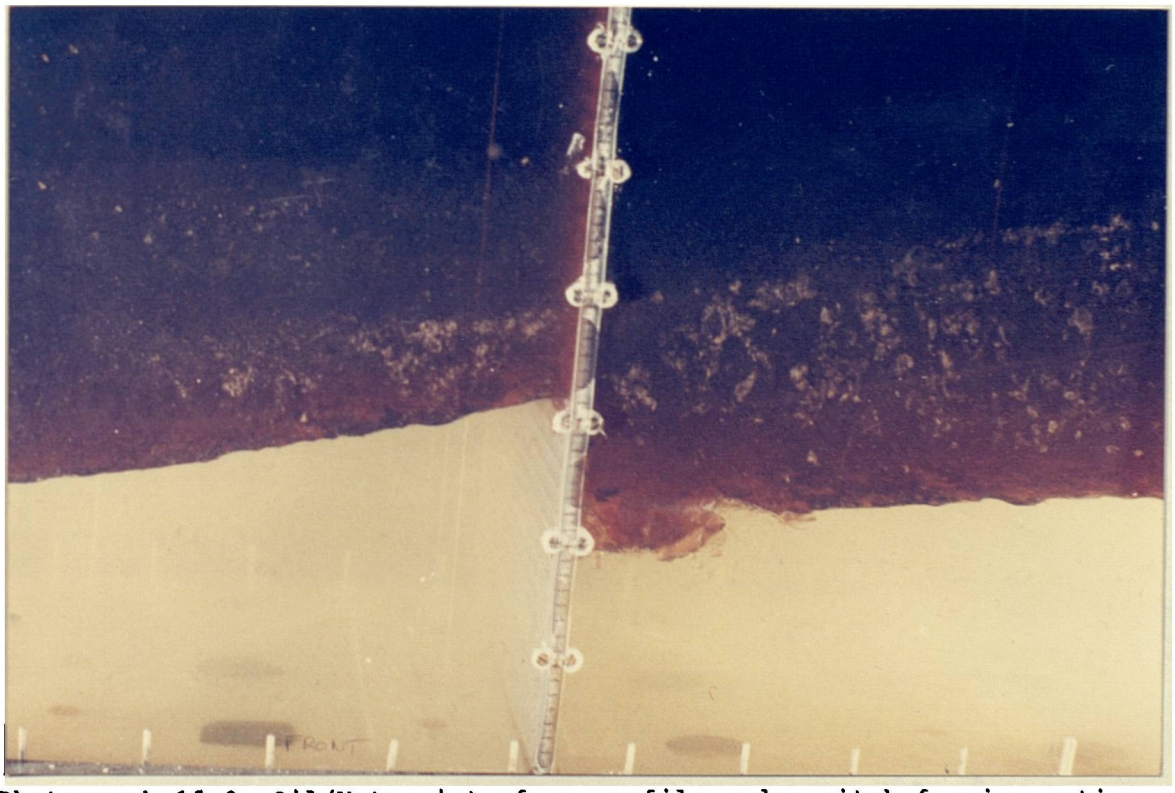

Photograph 10.8: Oil/Water interface profile under pitch forcing motion at 8.6 seconds, ±4° amplitude with the 53% perforated baffle. Oil depth 535mm, water depth 180mm.

Photograph 10.9: Interface profiles under pitch forcing motion at 3 seconds, ±4° amplitude with the 53% perforated baffle. Oil depth 460mm, water depth 355mm.

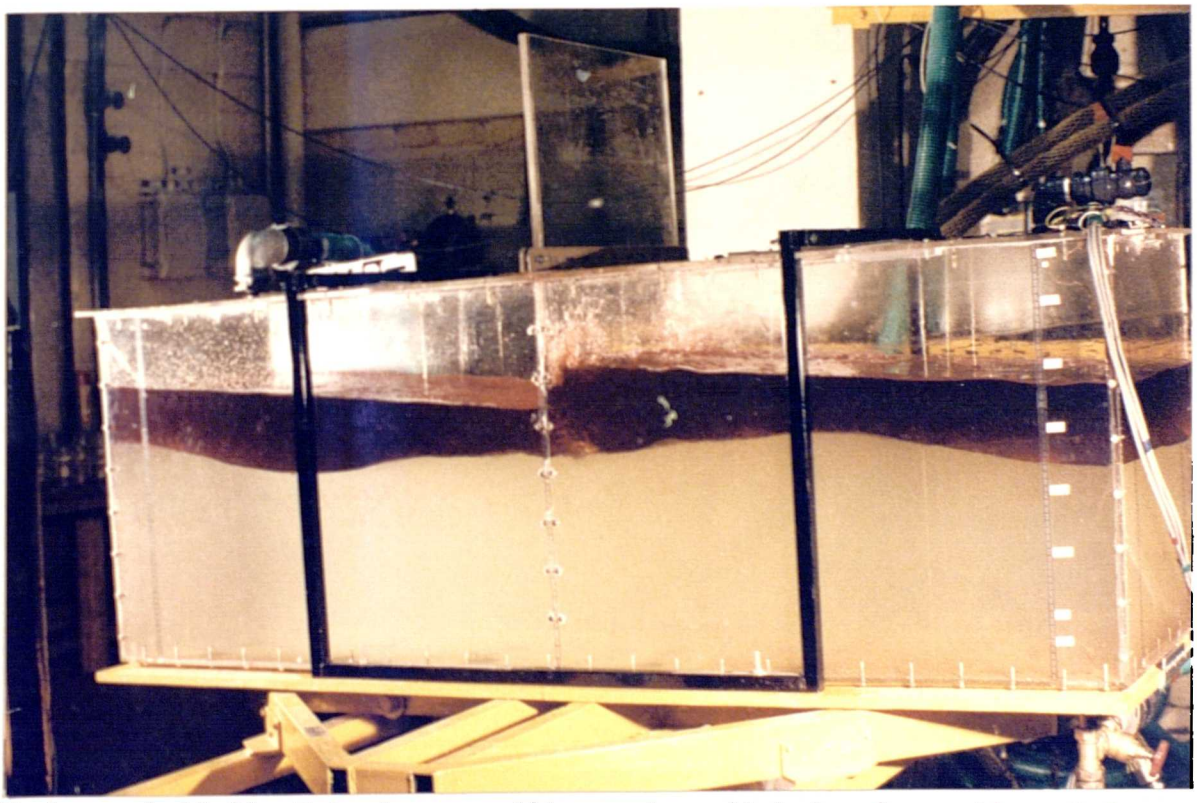

Photograph 10.10: Interface profiles under pitch forcing motion at 3 seconds, ±4° amplitude with solid plate baffle. Oil depth 460mm, water depth 355mm.

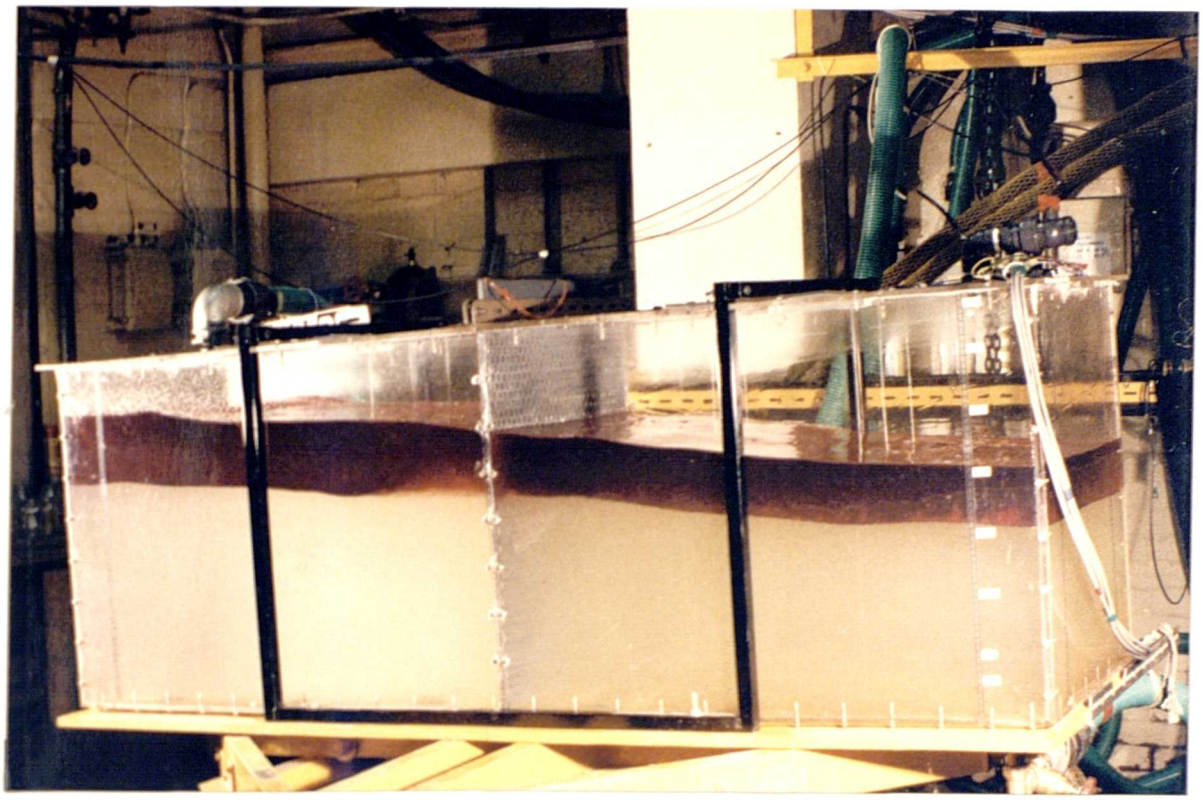

Photograph 10.11: Interface profiles under pitch forcing motion at 3 seconds, ±4° amplitude with the 53% perforated baffle. Oil depth 460mm, water depth 355mm.

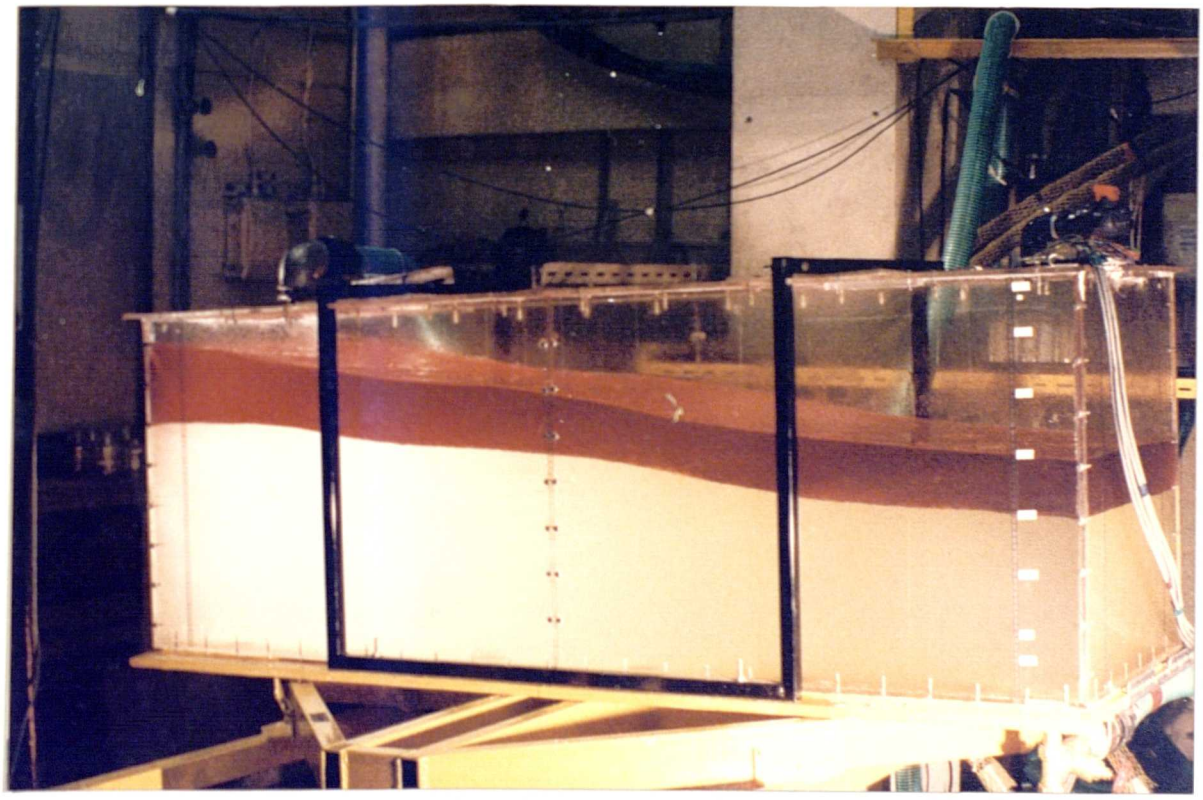

Photograph 10.12: Interface profiles under pitch forcing motion at 3 seconds, ±4° amplitude without baffles. Oil depth 460mm, water depth 356mm.

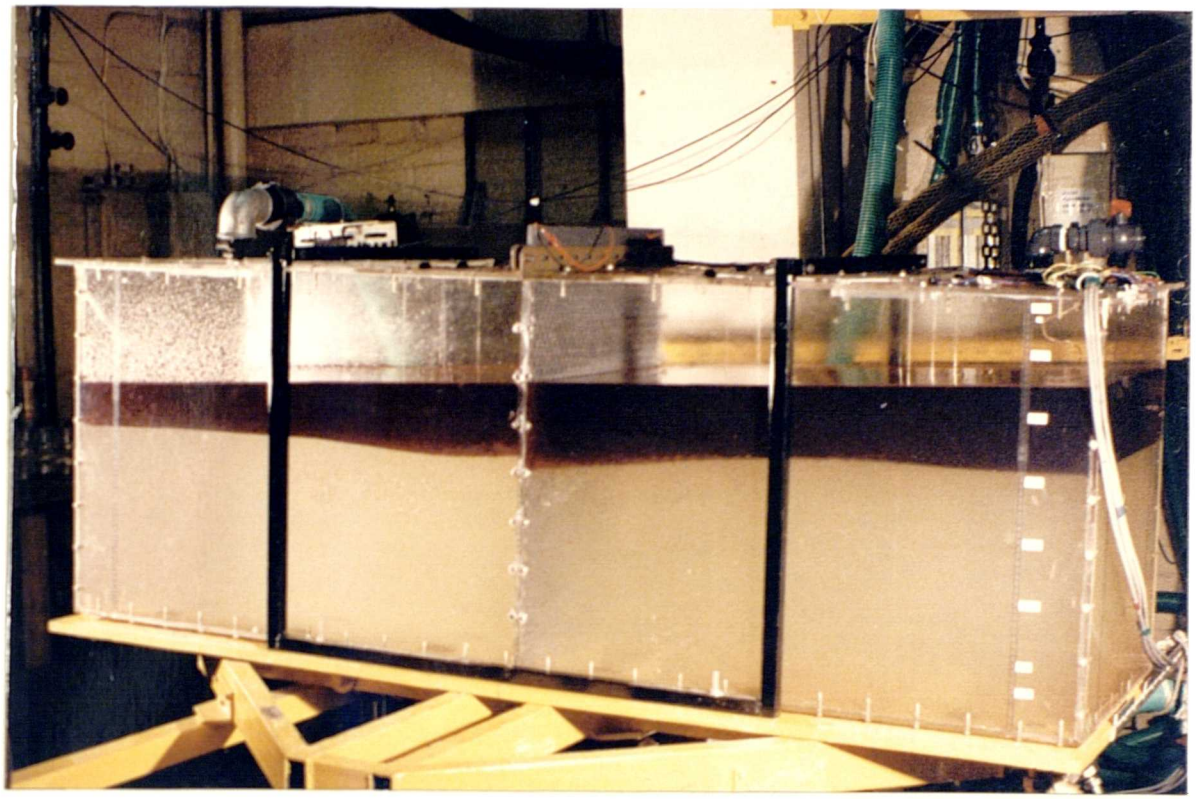

Photograph 10.13: Interface profiles under pitch forcing motion at 3 seconds, ±4° amplitude with the 53% perforated baffle touching the oil/water interface. Oil depth 460mm, water depth 355mm.

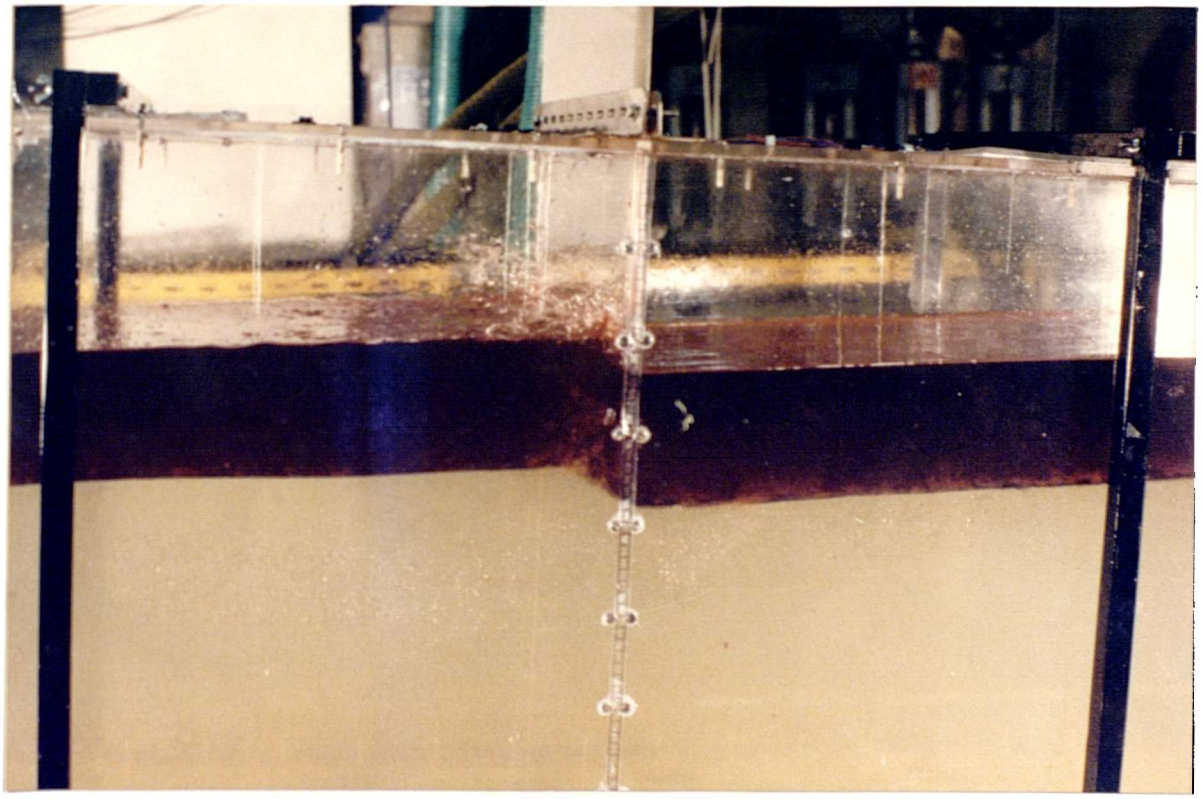

Photograph 10.14: Interface profiles under pitch forcing motion at 3 seconds, ±4° amplitude with the solid plate baffle. Oil depth 460mm, water depth 355mm.

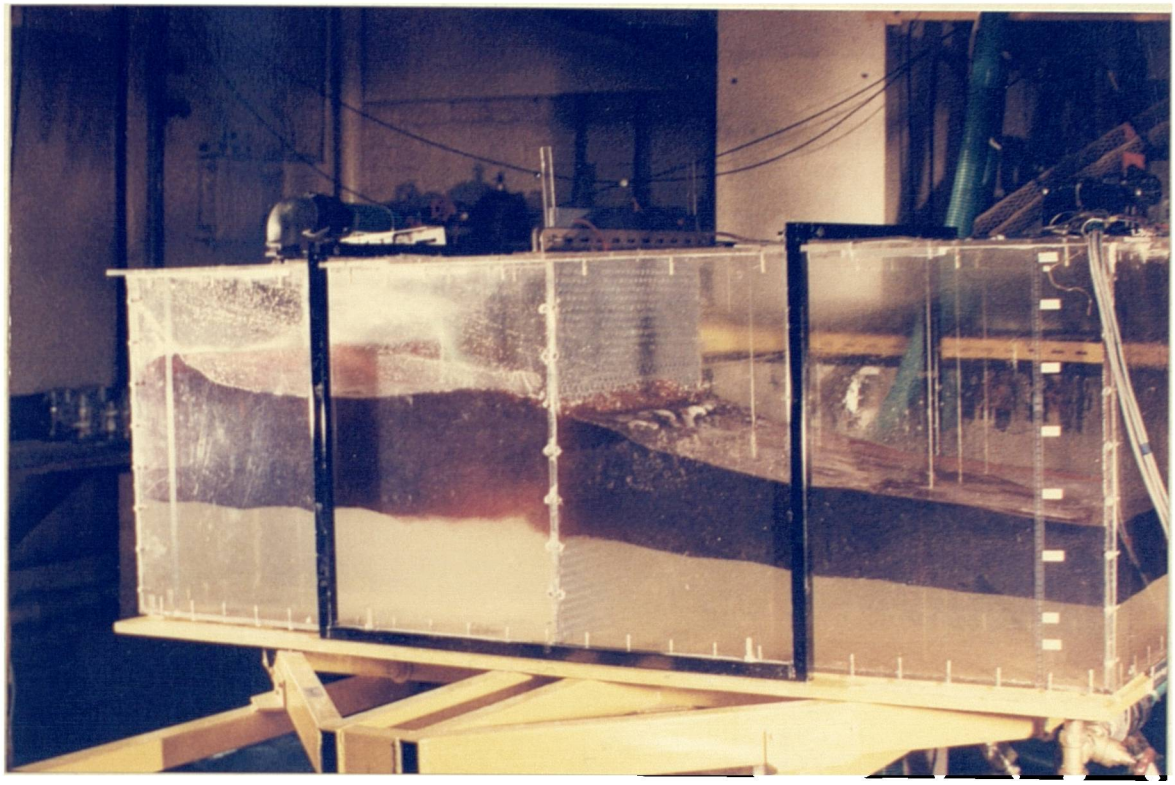

Photograph 10.15: Interface profiles under pitch forcing motion at 3 seconds, ±4° amplitude with the 53% perforated baffle. Oil depth 356mm, water depth 180mm.

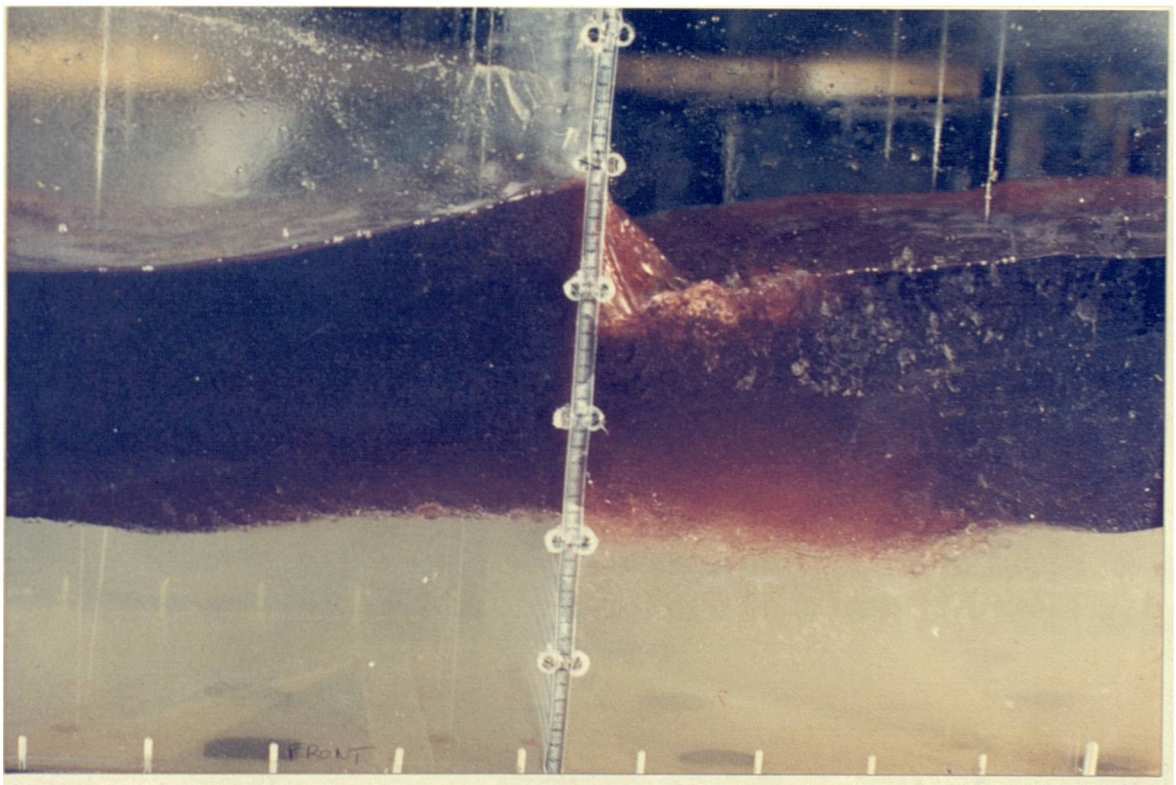

Photograph 10.16: Oil/Water interface profiles under pitch forcing motion at 3 seconds, ±4° amplitude with the 53% perforated baffle. Oil depth 356mm, water depth 180mm.

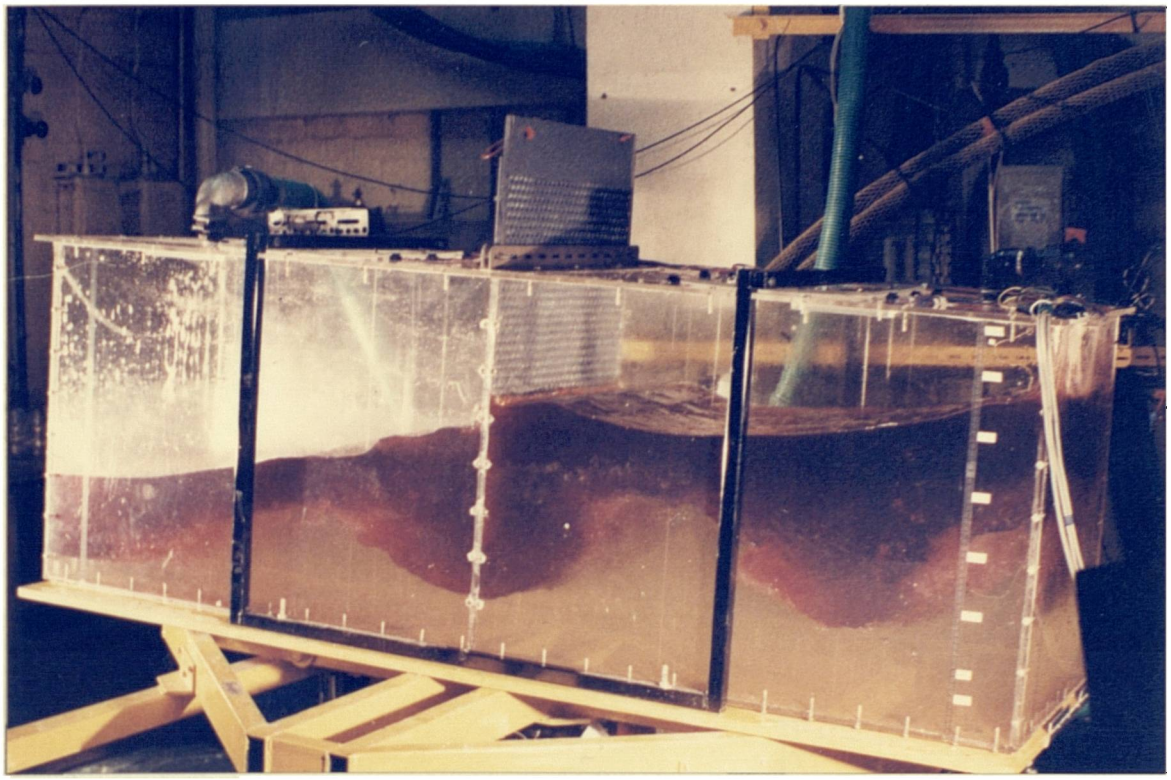

Photograph 10.17: Interface profiles under pitch forcing motion at 3 seconds, ±4° amplitude with the 53% perforated baffle touching the oil/water interface. Oil depth 360mm, water depth 180mm.

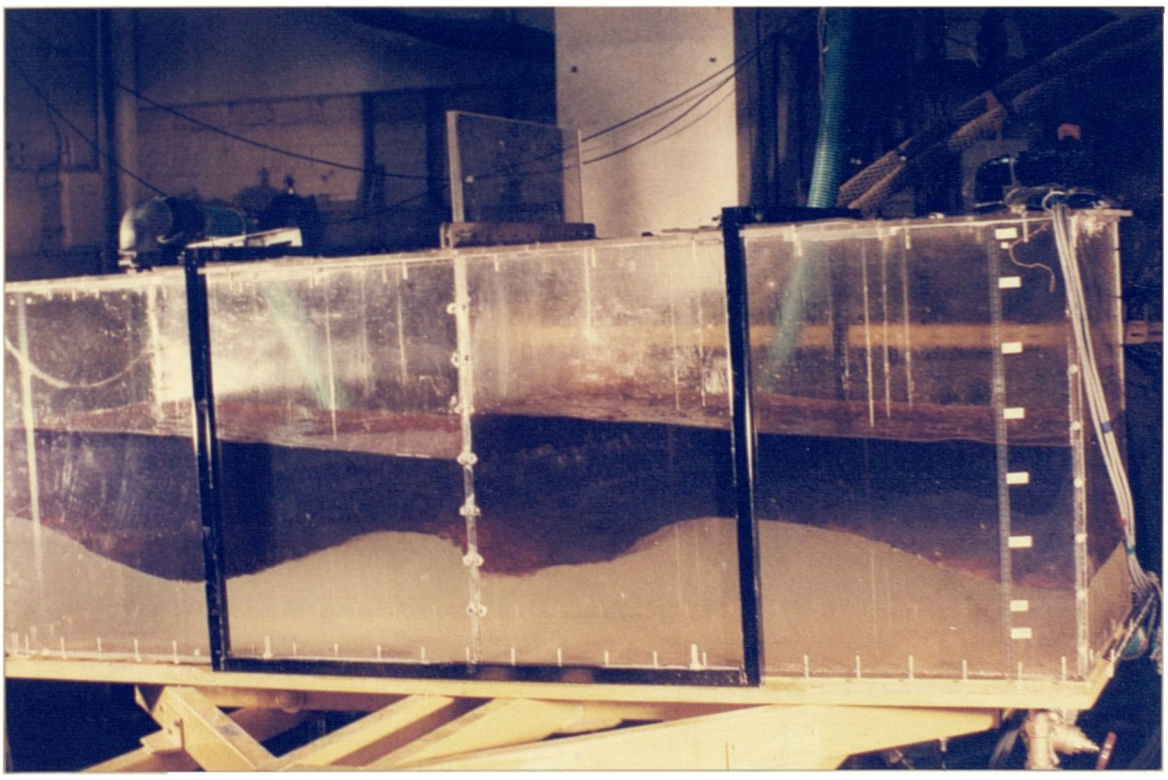

Photograph 10.18: Interface profiles under pitch forcing motion at 3 seconds, ±4° amplitude with the solid plate baffle. Oil depth 360mm, water depth 180mm.

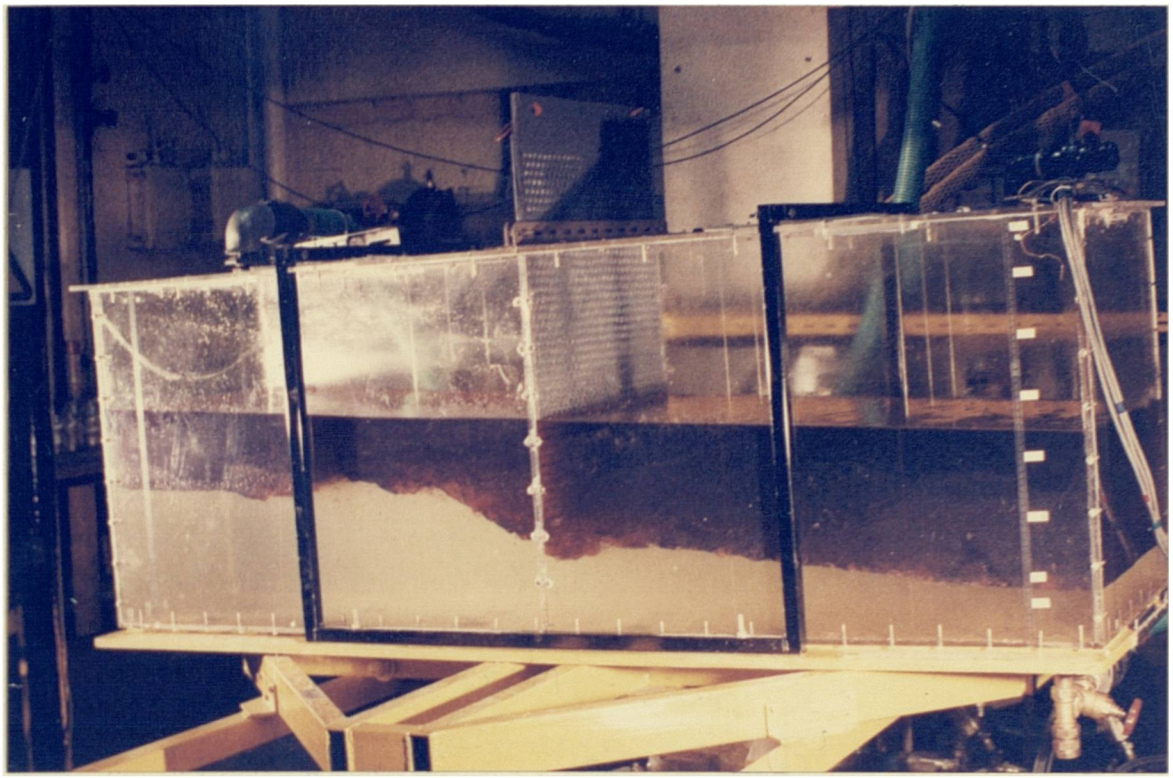

Photograph 10.19: Interface profiles under pitch forcing motion at 12 seconds, ±4° amplitude with the 53% perforated baffle touching the oil/water interface. Oil depth 360mm, water depth 180mm.

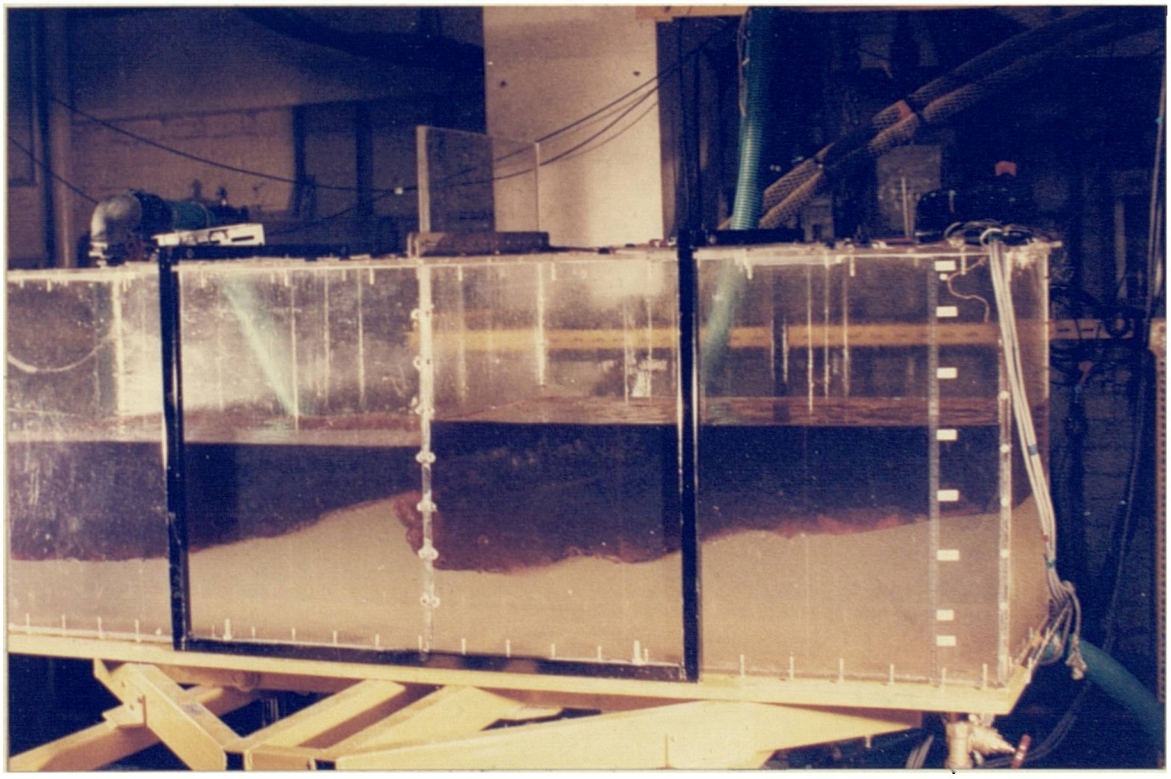

Photograph 10.20: Interface profiles under pitch forcing motion at 12 seconds, ±4° amplitude with the solid plate baffle. Oil depth 360mm, water depth 180mm.

Fill Depth		Predicted Natural Periods Modes			
		Air/Oil		Oil/Water	
Water (mm)	Oil (mm)	Mode 1 (sec)	Mode 2 (sec)	Mode 1 (sec)	Mode 2 (sec)
180	535	1.8	0.9	8.9	3.5
360	535	1.8	0.9	9.0	3.5
190	400	2.0	0.9	9.6	3.6

Table 10.1: Predicted first and second natural period modes for air/oil and oil/water interfaces at different oil/water fill depths in the large rectangular vessel.

CHAPTER 11.

ON THE AMOUNT OF OIL TRANSFERRED TO WATER DURING FORCING EXPERIMENTS.

11.1 INTRODUCTION.

In previous oil/water forcing experiments (1,12,42) the amount of fluid (e.g. oil and water) transferred from one phase to the other, has not been reported. Linear and non-linear theories do not model interface breakup. To attempt to study the effect of forcing motion on fluid transfer, two experiments were devised. Firstly, to use the ACORN ATOM data logging system to measure the transfer of a tracer (Benzoic Acid) from gas oil to water during forcing, with and without baffles. A second set of experiments were later conducted to measure the concentration of oil-in-water by analysis of water samples extracted during forcing.

This chapter provides details on techniques and results from both the benzoic acid and oil-in-water experiments. All forcing experiments were conducted using the large rectangular vessel with gas oil. Pitch forcing motion was applied at various periods including resonance, with an amplitude of $\pm 4°$.

11.2 BENZOIC ACID TRANSFER FROM GAS OIL TO WATER.

11.2.1 Introduction.

Determining the amount of oil transferred to water as a result of forcing, requires water samples to be taken from a test vessel during forcing. However, the natural period of a system, has been shown to depend on liquid fill depth (equation 4.18). A reduction in oil/water fill depth during forcing, would therefore cause fluid responses to alter. Even the addition of fresh water may alter the characteristics of the system. Further problems with direct sampling, concerns the way in which samples

can be taken, avoiding interfacial disturbances (e.g. dipped sample containers).

A method was devised to gauge the effect of forcing on oil-to-water transfer, by measuring the transfer of an organic acid from oil to water. Using the data logging system, water conductivity at specific points inside the large rectangular vessel, was recorded during forcing experiments. The concentration of the organic acid could then be determined from calibration data.

11.2.2 Background to Principle.

Organic acid tracer techniques have been applied to liquid/liquid mass transfer experiments (86,87), due to the ease of detection by titration with alkali or by conductivity (88,89). Taylor (90) discussed a set of experiments simulating the uptake of various organic acids by nerve cells. The acid was first dissolved in water, shaken with samples of oil and resulting water titrated with alkali.

To gauge the transfer of oil to water, if the acid were dissolved in the oil, then increases in water conductivity would indicate transfer of acid to the water. Enhanced transfer of acid from oil to water over normal diffusion during forcing, might then simulate the transfer of oil to water during forcing.

11.2.3 Preliminary Experiments.

Prior to forcing experiments, several bench scale experiments were performed both to verify the principle and to calibrate a set of custom designed conductivity probes.

Firstly, 40 ml of gas oil with acid concentration 4g/l was taken from an initial 100ml and vigorously shaken by hand with 20 ml of distilled water for 1 minute i.e. oil/water ratio of 2:1. By shaking in

this manner, it was assumed that some equilibrium condition would be reached between acid in oil to acid in water. The water was separated and titrated with 0.05NaOH to determine the concentration of acid. By mass balance, the acid remaining in the oil was calculated. To the remaining 60ml of gas oil was added 40ml of fresh oil and the process repeated.

Graph 11.1 shows a plot of acid concentration in water and oil layers after shaking for 1 minute. The results indicate that from an initial stock solution of 4 grams benzoic acid per litre of Gas Oil, if full equilibrium was achieved during a forcing experiment (with oil/water ratio 2:1), then the resulting concentration of acid in water would be approximately 1.5g/l and that in oil would be approximately 3.6g/l.

To prevent contamination of oil in the departments storage facility (see chapter 10), benzoic acid was dissolved in gas oil using two 45 gallon oil drums. Although a number of forcing tests were performed, it was *not found necessary to add additional acid to oil.* This will be discussed later in this chapter.

11.2.4 Conductivity Probe Design.

A total of twelve probes were attached to three vertical rods (four probes per rod) placed so that at least two probes per rod resided in the water when the vessel was at zero angle. Each probe consisted of two washers fixed to the rods via insulating bolts with insulation between washer and rod (figure 11.1). The probes were calibrated in water of known acid concentration using the data logging system. These calibration values were later used to determine acid concentrations during forcing experiments. The use of washers posed several difficulties in cleaning, as the build up of rust was thought to alter probe calibration values. During some experiments, bubbles of oil-in-water interfered with all but the

bottom row of probes. Therefore, averaged results from probes 1,3 and 5 are presented in graphs 11.2 to 11.5.

11.2.5 Effect of Forcing in an Unbaffled Vessel.

Experiments were carried out on the unbaffled vessel at water depth 180mm, oil depth 535mm for pitch forcing motion at ±4° amplitude at three periods, 3, 9 and 10 seconds. Equation 4.19 predicted a resonant forcing period for this oil/water fill depth combination to be 8.9 seconds. Graph 11.2 shows the change in average acid concentration measured continuously with respect to time for each forcing period. Note that the ratio of oil to water is approximately 2:1, the same as used in bench shake tests.

The following points can be made :

1) At short forcing periods away from oil/water resonance (Ω=3 secs), no change in acid concentration is seen. This indicates that for the duration of forcing applied (approximately 8 minutes), no transfer took place between oil and water.

2) At a forcing period of 10 seconds, a slight increase in acid concentration is seen towards the end of applied forcing motion. Significant transfer is seen at forcing period closer to resonance (Ω=9 secs). Visual observations indicated that interfacial mixing occurred more at 9 seconds than 10 seconds forcing period i.e. more oil-in-water bubbles were seen for Ω=9 seconds than Ω=10 seconds.

To clarify the result for 9 seconds forcing period, this forcing period was applied for 20 minutes, the results of which are shown in graph 11.3. The positive value of acid concentration at time 0 arises due to continual use of oil from previous forcing experiments. The graph indicates a steady increase in acid concentration as the experiment progressed.

11.2.6 Effect of Forcing in a Baffled Vessel.

Experiments were carried out at the same fill depth and forcing conditions as in the previous section, using the 53% free area perforated baffle fully immersed in fluid (see chapters 8 and 10). Graph 11.4 shows the change in average acid concentration for the duration of forcing as determined from probes 1,5 and 8. The results indicate that acid concentration remains unaffected for the duration of applied forcing motion.

11.2.7 Transfer of Benzoic Acid Under Static Conditions.

To determine natural diffusion of acid from oil to water, a static experiment was carried out. Here water and gas oil at fill depths 180mm and 535mm respectively, were left in the vessel for a number of days. The vessel was placed in a horizontal position and the data logging system was adjusted to take probe readings at periodic intervals.

Graph 11.5 show the results of average acid concentration (probes 1,5 and 8) over a recording time of 80 hours. This graph indicates that acid concentration rises steadily until a constant concentration of 0.35 Kg/m^3 is reached after some 60 hours. The unusual result close to time 0 was probably due to error in the data logging system, since the results after this point show a smooth curve i.e. the data logger recovered.

11.2.8 Discussion.

These results suggest that significant acid transfer occurs only during resonant forcing conditions in an unbaffled vessel. Assuming therefore that acid transfer is related to oil transfer, it is further suggested that the 53% perforated baffle offers some beneficial effect in reducing oil transfer. Visual comparisons between unbaffled and baffled experiments (chapter 10) suggest similar resonant oil/water interface

profiles but differences in oil-in-water bubble formation. In the unbaffled vessel, oil-in-water bubbles were produced which became distributed along the vessel length throughout the water layer (photograph 10.1). For the baffled vessel, the quantity of oil-in-water bubbles appeared less. Therefore, associating bubble formation with increasing oil/water interfacial area, the lack of benzoic acid transfer observed with baffles is not surprising.

However, caution must be advised when interpreting the acid transfer results for the 53% baffle. Photographic evidence (photograph 10.8) clearly shows oil/water interfacial breakup round the baffle. This would lead to localized increases in acid concentration. It may be then be argued that conductivity probes round the baffle might register increasing concentration. Certainly, over a long period of time, it may be expected that continual interface breaking round the baffle will give increased acid concentrations.

The results from the static transfer test indicate that equilibrium concentration of acid in water is $0.35 Kg/m^3$. This value is then significantly lower than recorded in bench scale shake tests ($1.5 Kg/m^3$). However, the static transfer value is of similar magnitude to the concentration noted for the 9 second forcing period, in the unbaffled vessel ($0.4 Kg/m^3$). As the conductivity method records acid present only in the water not the oil phase, it is suggested that slight differences in probe calibration may be responsible for differences between static and forcing experimental values. The discrepancy between bench scale shake test and forcing/static experiments may be attributed to the determination of acid concentration. In the bench scale shake tests, settled water samples were titrated with alkali. If after settling, oil drops remained suspended in the water phase (e.g. by adhesion on the container walls or due to a short settling time), then oil drops with a relatively high

concentration of acid would also be titrated with alkali. It is then questionable if the titration analysis would detect the acid contained in the water phase together with acid in the oil phase.

The lack of acid transfer for all forcing experiments except those under resonant forcing conditions, explains why no further additions of acid were made to the original stock of gas oil.

Regardless of exact questions of mass transfer rates between oil and water under static or forcing conditions, these experiments show that :

1) The 53% perforated baffle does not increase acid transfer for same duration of forcing, at the same forcing periods as the unbaffled vessel i.e. baffles reduce material transfer across the oil/water interface.

2) It is only at resonant forcing periods in the unbaffled vessel, that increased acid transfer occurs.

11.3 ON THE AMOUNT OF OIL DISSOLVED IN WATER AS A RESULTS OF FORCING.

11.3.1 Introduction.

The benzoic acid experiments indicated significant transfer of material occurred only at resonance in the unbaffled vessel. To clarify this result, actual oil-in-water content had to be measured during forcing, irrespective of the possible consequences of on-line sampling.

Sample volume was carefully controlled so as not to influence resonant response by changing water levels.

11.3.2 Experimental Technique.

A total of seven sample ports were drilled into the vessel, six along its length and one in the "left" wall. Fluid from all ports was taken off through lengths of stainless steel tubes, terminating in a brass

ball valve. Ports 1 to 6 had tubes (2mm ID) reaching to the vessels centre line, while port 7 (tube 4mm ID) protruded approximately 100mm from the wall. Figure 11.2 presents details of sample port positions.

Appendix VII presents details of the method adopted to analyze the water samples. In essence, oil was extracted from water by the solvent 112-Trichlorotrifluoroethane. The solvent was then separated and analyzed by a Horiba OCAM-220 Oil Content Analyzer with range 0 to 20ppm dissolved oil-in-water. During the experiments, it was necessary to adopt two measuring techniques as some samples were found to be greater than 20ppm. The methods were :

1) The *standard sample analysis method*, centered on shaking equal volumes of solvent with water and analyze the solvent sample, by methods described in Appendix VI.

2) If results from the *standard* procedure gave dissolved oil content >20ppm, the extraction procedure was modified. After shaking 20ml of solvent with 20ml of sample, 10ml of extracted solvent was diluted to 100ml with fresh solvent. This *diluted* sample was then analysed, preventing off-scale readings.

11.3.3 Experimental Results.

Four experiments were carried out, using two water fill depths (360mm and 180mm) with one oil depth (535mm). Pitch forcing motion was again applied at ±4° amplitude at resonant periods predicted by equation 4.19. Different sample ports were accessed for each experiment.

Table 11.1 provides details of forcing period, fill depth, sample ports and duration of applied forcing motion. Reference is also given to graphs of oil content as a function of time.

Graph 11.6a shows averaged oil content from ports 1-3 for the high water fill depth (360mm). The results shown that oil content rises from

0.6ppm, to a maximum of 3.2ppm towards the end of forcing. During the decay, oil content steadily drops. Graph 11.6b for the same fill depth shows results from two sample ports, port 5 closer to the oil/water interface than ports 1-3, and the "end port". Referring to port 5, the graph indicates that soon after the start of motion, oil content reaches 5 ppm and peaks at 5.5ppm before motion was stopped. For the "end port", the graph shows an initial oil content of 3ppm which peaks at 4.5ppm prior to motion stop. After forcing motion had ceased, oil content from both sample ports begins to fall.

Graph 11.7 shows the results from port 2 for water depth of 180mm. For this particular experiment, oil content was greater than 20ppm therefore the analysis method had to be adjusted. The results show substantial scatter with initial oil content rising from 0ppm to peak at approximately 200ppm but falling to 0ppm once forcing motion had ceased. Visual observations indicated the present of free oil (i.e. floating oil layer) on the water surface, of samples which gave 200ppm results.

11.3.4 Discussion.

These results suggest that :

1) During resonant forcing conditions, oil content of the water increases. Graphs 11.6b and 11.7 show that changes in oil-in-water content vary. Visual observations of samples indicated the presence of free oil on the water surface.

2) Once forcing motion has ceased, oil content reduces. This is particulary evident from the low water (180mm) fill depth experiment.

3) Graphs 11.6a and 11.6b suggest that background oil-in-water may be of the order 0.6ppm to 3ppm.

Visual observations indicated that while an oil/water resonant interface profile (i.e. a solitary travelling wave) occurred in both fill depth cases, more oil-in-water bubbles appeared to be produced in the low water fill depth (180mm) experiment. This perhaps explains the significant difference in oil-in-water content between graphs 11.6a-b and 11.7. It is suggested that these experiments recorded free droplets of oil suspended in the water as a result of interface breakup, rather than dissolved oil. Evidence for this comes from :

1) The indication of free oil in some water samples and the decrease in oil-in-water content once forcing motion had ceased to background level.

2) Published oil-in-water solubility data (91) suggests the *maximum* solubility of gas oil to be 0.003ppm, and that of decane to be 0.2ppm. This data supports the experimental results recording the presence of free oil drops as opposed to dissolved oil.

Establishing that forcing increases free oil content rather than dissolved oil content, does pose some question as to the analogous behaviour between benzoic acid and oil transfer. The measurement of conductivity indicates only the benzoic acid dissolved in water, and not in oil. The benzoic acid results therefore indicate increases in oil/water interfacial area and fluid turbulence i.e. resonance increases fluid turbulence hence leads to the breaking of the oil/water interface. Therefore, the benzoic acid experiments are not a true representation of oil transfer, rather an indication of interfacial breakup.

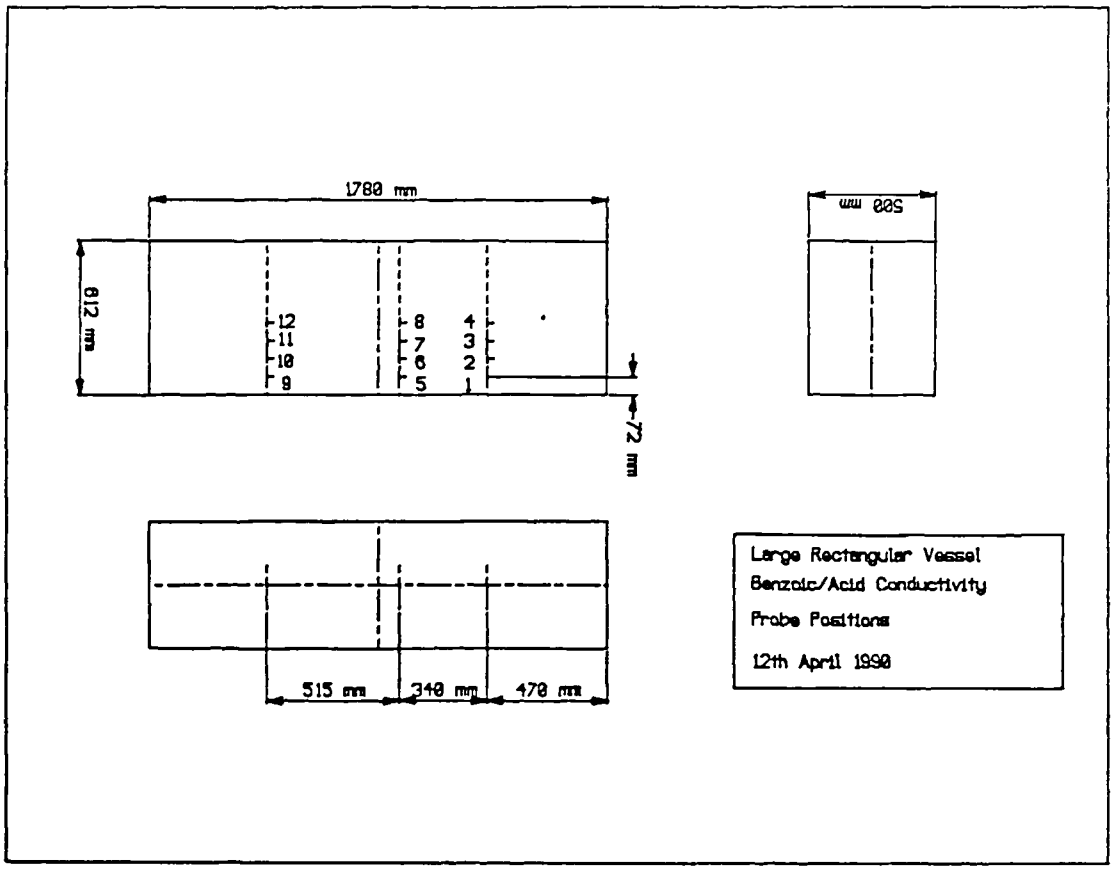

Figure 11.1a: Location of benzoic acid conductivity probes in the large rectangular vessel.

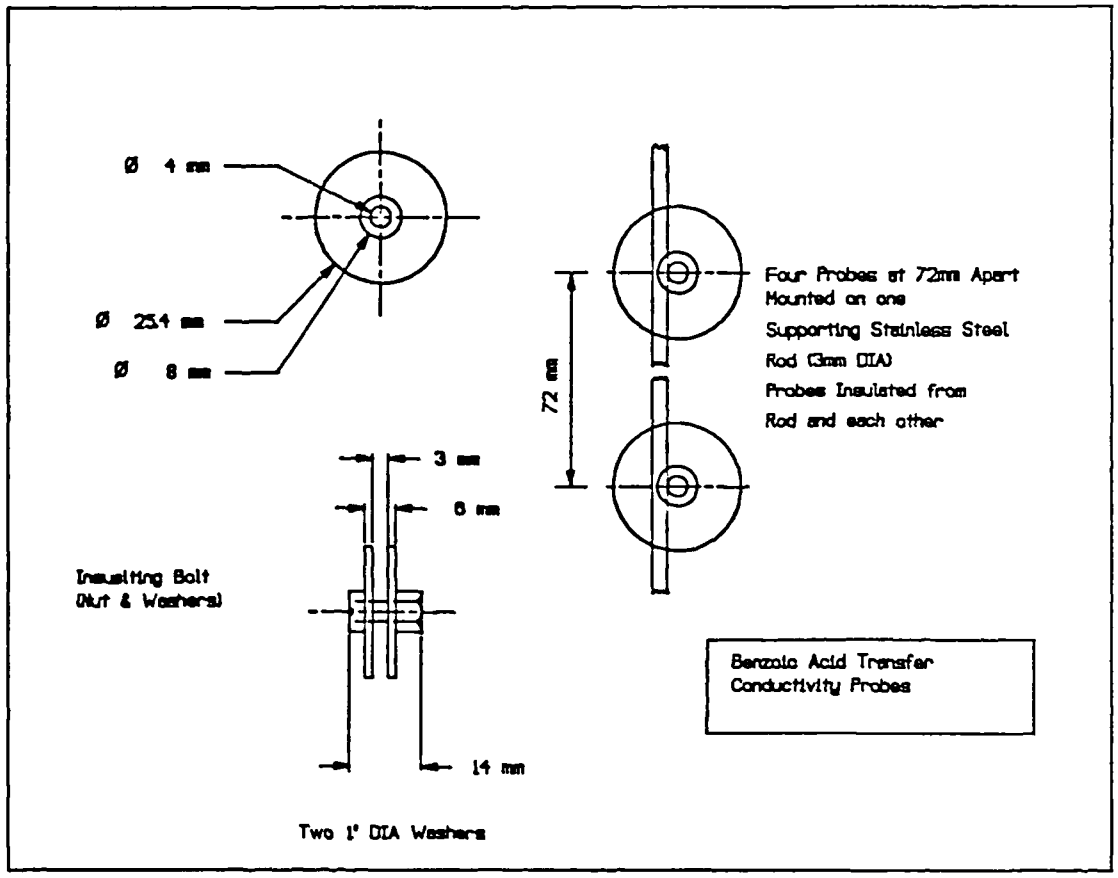

Figure 11.1b: Construction details of benzoic acid conductivity probes.

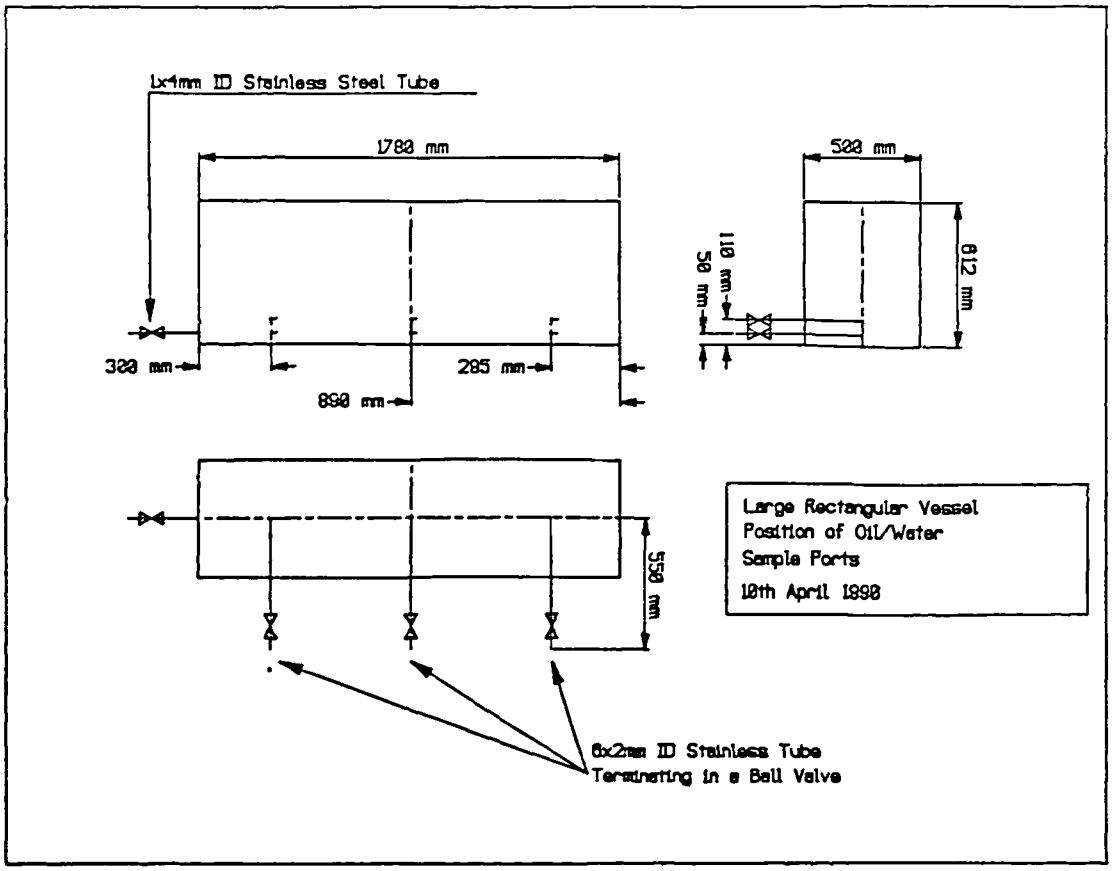

Figure 11.2: Water sample port positions in the large rectangular vessel.

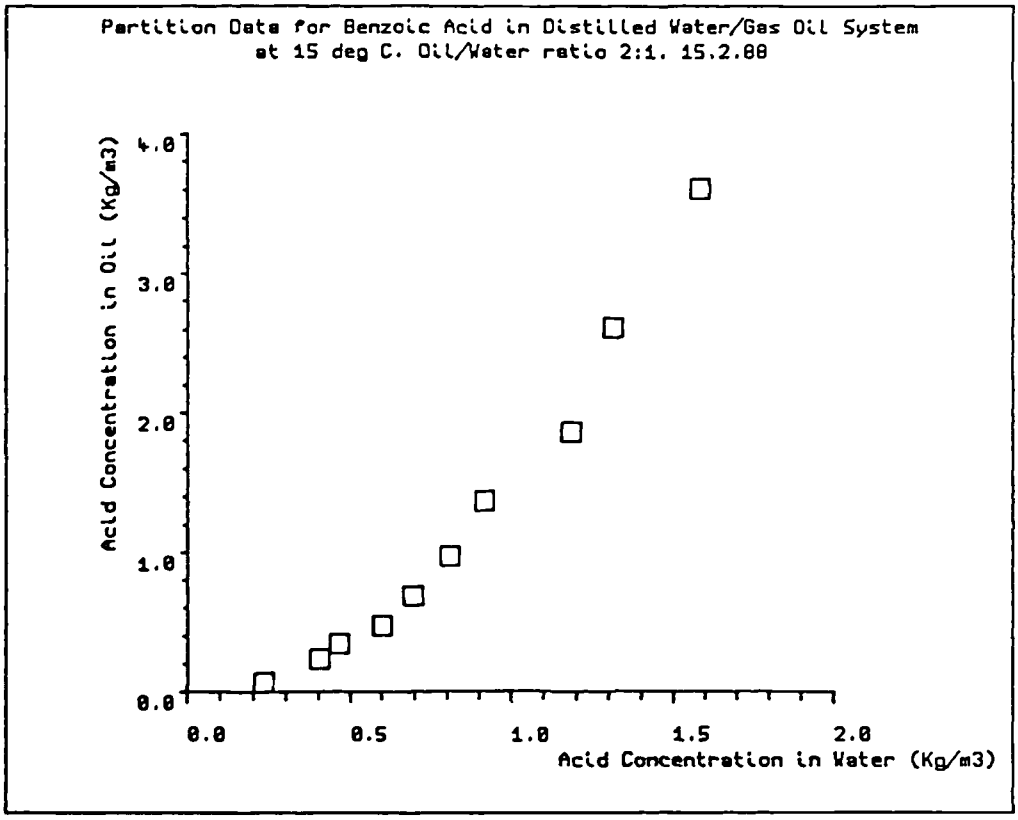

Graph 11.1: Benzoic acid concentration in oil and water as a result of bench scale shake tests.

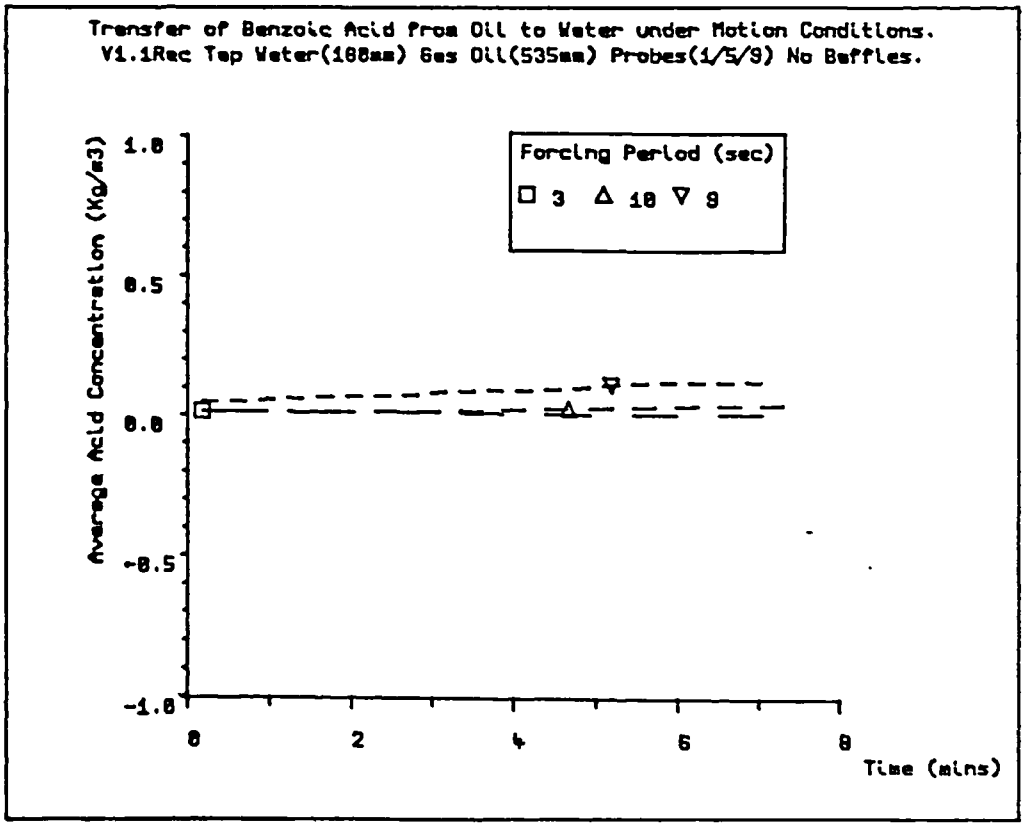

Graph 11.2: Change in benzoic acid concentration as a function of time for various pitch forcing periods at ±4°, in the unbaffled vessel. Oil depth 535mm, water depth 180mm.

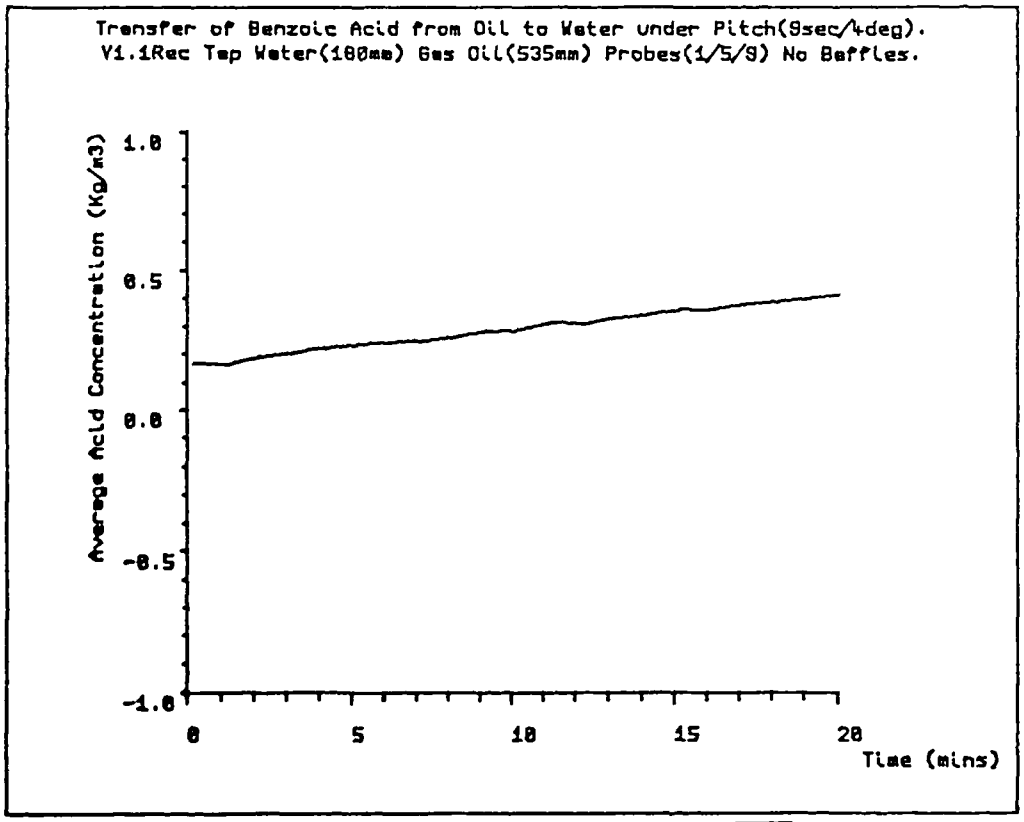

Graph 11.3: Change in benzoic acid concentration as a function of time (to 20 minutes) for pitch forcing period of 9 seconds, ±4°, in the unbaffled vessel. Oil depth 535mm, water depth 180mm.

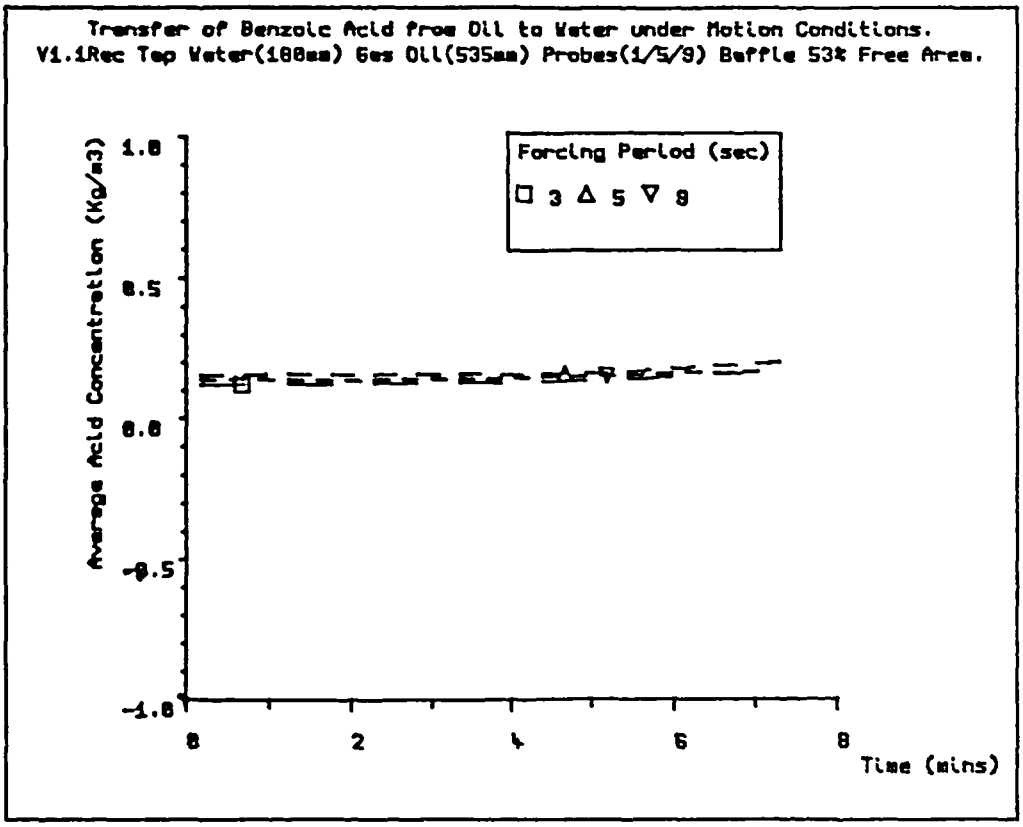

Graph 11.4: Change in benzoic acid concentration as a function of time for various pitch forcing periods at ±4°, with the 53% perforated baffle. Oil depth 535mm, water depth 180mm.

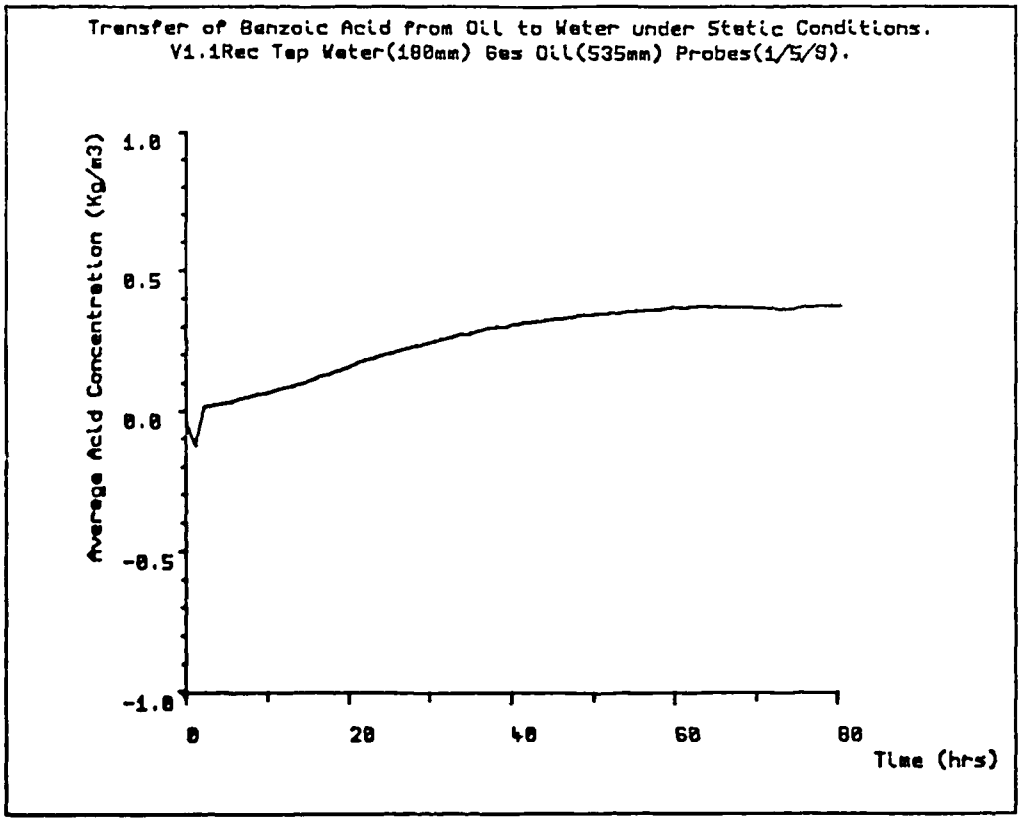

Graph 11.5: Change in benzoic acid concentration as a function of time under static conditions. Oil depth 535mm, water depth 180mm.

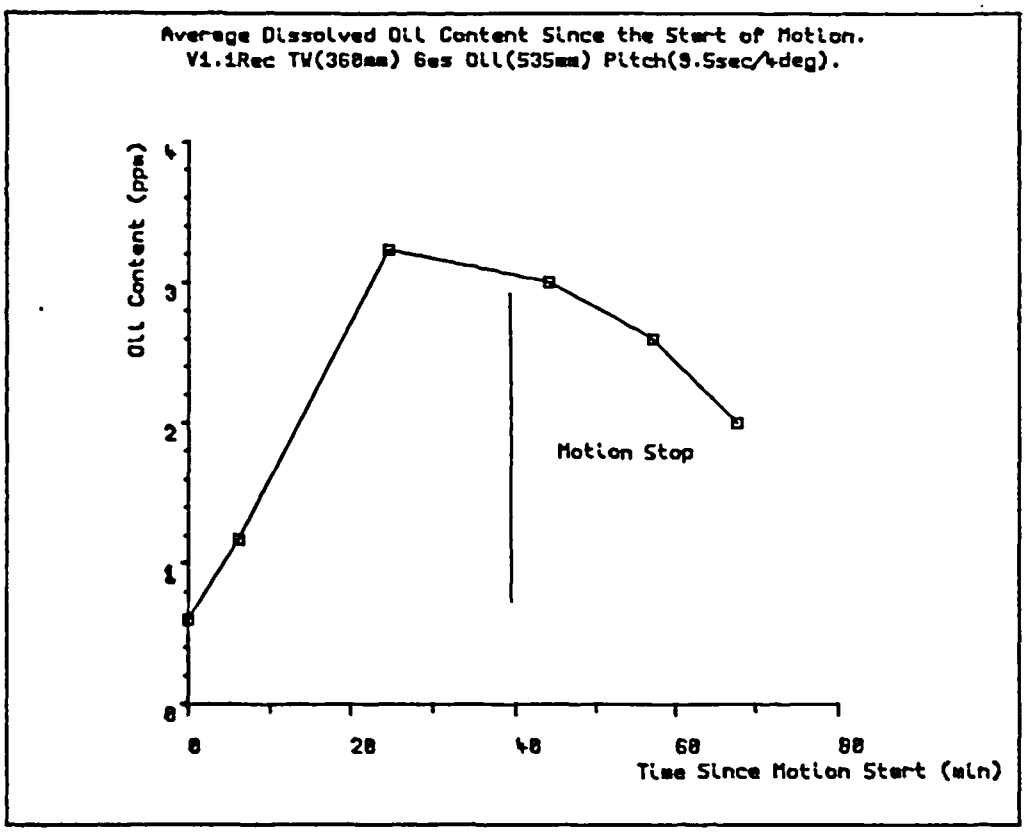

Graph 11.6a: Average oil content from sample ports 1,2,3 under pitch forcing at 9.5 seconds, ±4°. Oil depth 535mm, water depth 360mm.

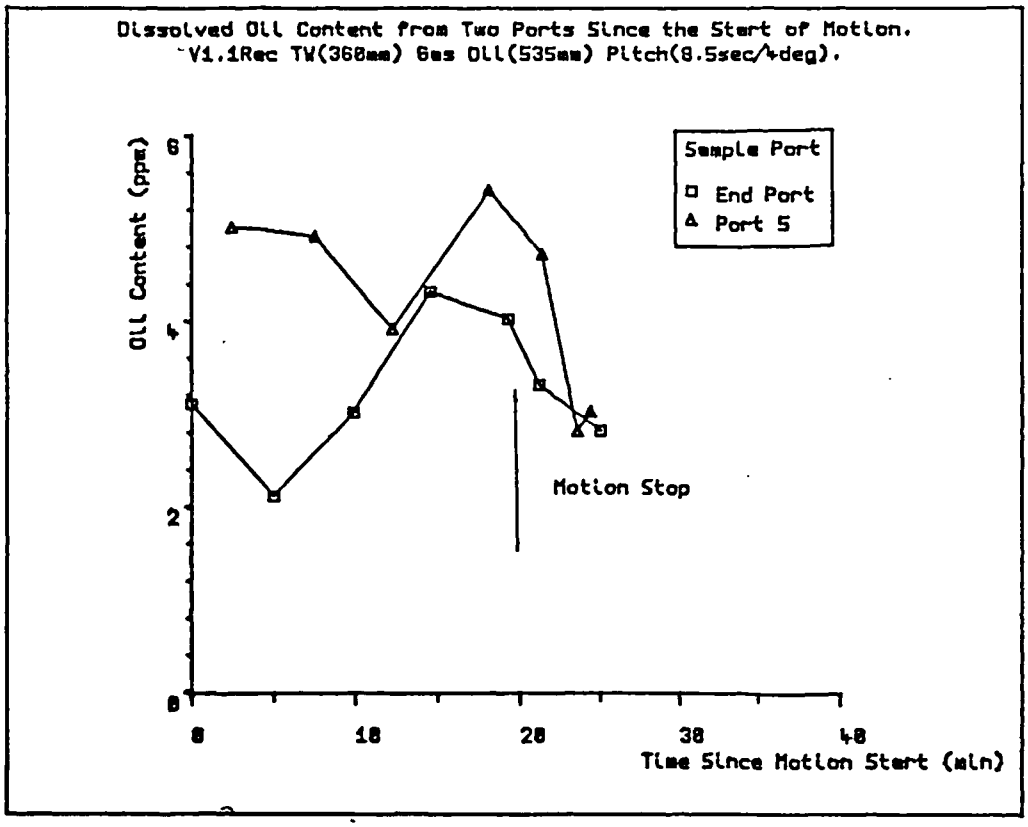

Graph 11.6b: Oil-in-water content from ports 5 and 7 under pitch forcing at 9.5 seconds, ±4°. Oil depth 535mm, water depth 360mm.

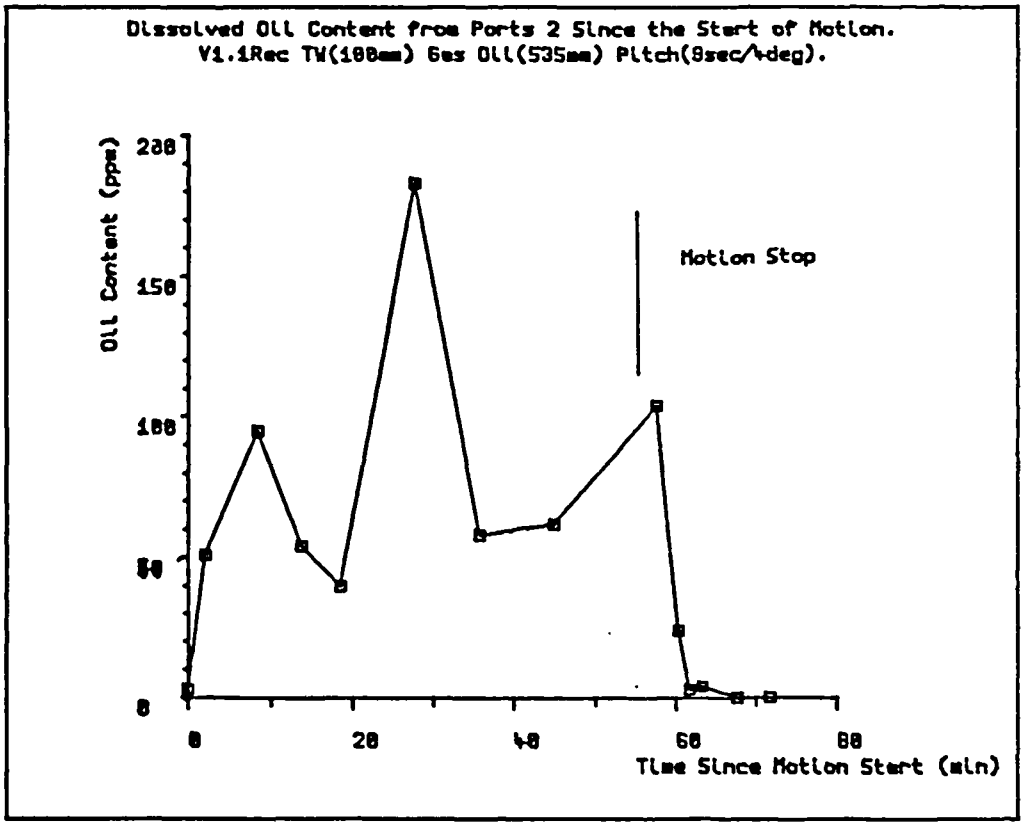

Graph 11.7: Oil-in-water content from port 2 under pitch forcing at 9 seconds, ±4°. Oil Depth 535mm, water depth 180mm.

Water Depth (mm)	Pitch Period (sec)	Sample Ports	Duration of Forcing (mins)	Graph
360	9.5	1,2,3	40.8	11.6a
360	9.5	7	20.5	11.6b
360	9.5	5	20.5	11.6b
180	9.0	2	56.8	11.7

Table 11.1: Water fill depths, pitch forcing motion periods and sample ports used in oil-in-water experiments.

Fraction	Carbon Number	Extrapolated Solubility in Fresh water (ppm).
Kerosene	C_{10} to C_{17}	$2x10^{-1}$ to $1x10^{-4}$
Gas Oil	C_{16} to C_{25}	$3x10^{-4}$ to 10^{-8}
Lube Oil	C_{23} to C_{37}	10^{-7} to 10^{-14}
Bitumen	$>C_{37}$	$<10^{-14}$

Table 11.2: Solubilities of crude oil fractions in fresh water (91).

CHAPTER 12.

RESULTS FROM AIR/OIL/WATER NUMERICAL SIMULATION EXPERIMENTS.

12.1 INTRODUCTION.

The development of the numerical model outlined in chapter 4, required direct comparison with physical experimental data. Program modifications configured the model to produce data files compatible with those of air/water experiments allowing both sets to be analyzed by the same data processing software.

Simulation experiments were carried out on two vessels of same dimensions as the large and small rectangular containers. Fluid properties (i.e. density) were again the same as those used in physical experiments. Forcing conditions applied in the majority of simulation experiments, concentrated on pitch forcing motion at $\pm 4^{\circ}$ amplitude and covered periods of 1 to 12 seconds. Physical position of each vessel in relation to the motion simulators pivot point location was also considered (see chapter 5).

Simulation experiments were extended to include the effects of viscosity and pivot point location on air/water sloshing in the small rectangular container.

This chapter presents comparisons between physical and simulation experiments on the large and small rectangular vessels. Results are also presented for a simulation experiment of an offshore separator containing oil and water.

12.2 METHOD IN COLLECTING SIMULATION RESULTS.

The simulation program, developed on the Acorn Cambridge Workstation (ACW) was transferred to the Universities VAX Cluster and re-

compiled. Unfortunately, the screen shots of velocity vectors and interface profiles were not available for analysis from the VAX, as :

1) The programs graphic drivers were compatible only with the ACW and although conversion to GINO graphics was not carried out.

2) The saved screen information (i.e. velocity and free surface plots at small time intervals) produced very large data files for which transfer from VAX to ACW or even storage on the VAX, was uneconomic.

3) The effort needed to produce hardcopy plots by either video recorder of pen plotter was considerable and not considered practical for all simulation experiments.

Only peak velocity and simulated probe information was stored on the VAX for later collection by the ACW. Special precautions had to be introduced on the VAX, to prevent exceeding storage space allocation and CPU time. The procedure to simulate one fill depth/amplitude condition and 1 to 12 second forcing periods in 1 second time steps, was :

1) A single batch job was submitted (started) with data for one forcing period. Upon completion, this job would then submit the next in sequence. Sufficient program time was allocated to cover at least five forcing cycles, before recording decay data for a further program minute. This allowed frequency and transient effects to be analyzed.

2) Result files (probe and peak data) would be placed in VAX archive and deleted from on-line storage.

3) On completion of all runs, archived data was retrieved and transferred (via Kermit utility) to the ACW. Files were then organized and the probe information processed as for physical air/water experiments (chapter 6).

The CPU time available per VAX batch job was set at the maximum of 5 hours. In the majority of cases, jobs were found to last for 1-2 hours CPU time, although actual time in the system varied. To produce velocity profiles, runs were carried out on the ACW. Depending on forcing conditions, these runs took on average 4-5 days to complete.

12.3 COMPARISON WITH OIL/WATER EXPERIMENTS IN THE SMALL RECTANGULAR VESSEL.

12.3.1 Introduction.

As the numerical model deals with a two fluid system (e.g. oil/water), physical experimental data was needed to test this model. The oil/water results from the small rectangular vessel allow direct comparisons between simulation and physical experiment. In the numerical experiments, two water fill depths (87mm and 174mm) were tried with oils of density 851 Kg/m^3 and 890 Kg/m^3 (i.e. FK851 and FK890). These compare to physical experiments reported in chapter 9. The actual density of oils FK851 and FK890 used in the physical experiments were later measured as 858 Kg/m^3 and 885 Kg/m^3 respectively. Some difference in interface response would therefore be expected, since natural period varies with density. Table 12.1 presents predicted oil/water interface natural periods for all fill depths used in simulation experiments.

In each simulation experiment, a variable mesh of 20x10 cells was found suitable for this vessel to achieve numerical stability.

12.3.2 The Effect of Forcing Period on Oil/Water Interface Amplitude by Simulation.

Graphs 12.1 and 12.2 show the effect of forcing period on oil/water interface amplitude for low (87mm) and high (174mm) water fill depths, as obtained from simulation. Oil occupied the space above the water.

These results show :

1) Simulation probes produce symmetrical responses i.e. probe 2 corresponds to probe 14. Exact symmetry does not occur at some forcing periods (e.g. Ω=7 secs in graph 12.1)

2) Maximum interface amplitude occurs at forcing periods higher than predicted natural periods.

3) The value for maximum interface amplitude seems to depend on the difference between oil and water depth e.g. 75mm for 87mm fill depth and 85mm for 174mm fill depth.

12.3.3 Comparison Between Simulation and Physical Experiment.

Graphs 12.3 and 12.4 compare results from probe 2 at low (87mm) and high (174mm) water fill depths for oil FK851. Graphs 12.5 and 12.6 compare results from the same water fill depths using oil FK890. A forcing amplitude of $\pm 4°$ and periods 1 to 12 seconds were applied in all simulation cases.

These results indicate :

1) The shape of the interface amplitude response for both simulation and physical experiments are similar.

2) The point of maximum interface amplitude occurs at similar forcing periods in both simulation and physical experiment.

3) Simulation appears to produce lower interface amplitudes at forcing periods close to resonance and higher ones away from resonance.

12.3.4 Discussion.

For simulation experiments, the effect of forcing period on interface amplitude produces symmetrical probe responses. Deviations from this at some forcing periods are probably due to mesh resolution and

interface detection method. Increasing mesh resolution might have resulted in a symmetrical probe response at all forcing periods. Interface detection methods for both simulation and physical experiment may have to be improved to achive better comparison between the two experiments.

In physical experiments (chapter 9), it was observed that maximum interface amplitude occurs at higher forcing periods than predicted resonance. The simulation is seen to produce compatible results i.e. the forcing period corresponding to maximum interface amplitude appears to be the same in simulation and physical experiment.

As regards the effect of density, the simulation is again supported by physical experimental observations. Increasing fluid density increases natural period, hence the forcing period producing maximum interface amplitude.

Comments regarding the general performance of the simulation will be discussed later in this chapter.

12.4 COMPARISON WITH OIL/WATER EXPERIMENTS IN THE LARGE RECTANGULAR VESSEL.

12.4.1 Introduction.

Physical experiments using oil and water were carried out in the large rectangular vessel in the presence of a gas cap, (chapter 10). As simulation was based on a two fluid (oil/water) system, direct comparison between simulation and physical results are not possible. The simulation does however, offer the possibility of comparing the effects of a gas cap in the large vessel.

Simulation experiments were carried out at water fill depths 180mm and 360mm, with oil of density 860 Kg/m^3. Predicted natural periods together with fill depths used in corresponding physical experiments are given in table 12.2.

A mesh of 20x10 cells as used in the small vessel was found to be unstable for the large vessel, and was therefore changed to 32x16 cells.

12.4.2 The Effect of Forcing Period on Oil/Water Interface Amplitude.

Graphs 12.7 and 12.8 compare simulation and physical experimental results for low (180mm) and high (360mm) water fill depth with oil of density 860 Kg/m^3. These results indicate :

1) For low water depth (180mm) both simulation and physical results are similar. Peak interface amplitude occurs around 9 seconds forcing period, higher than predicted resonance. At shorter forcing periods ($4<\Omega<8$), simulation is seen to produce higher interface amplitude readings.

2) For the high water depth (360mm), there appears no similarity with physical and experimental results, other than maximum interface amplitude occurs at similar forcing periods.

12.4.3 Discussion.

As the small vessel oil/water simulations conform with physical experiments, the difference in large vessel simulation and physical experiments at high water fill depth (360mm) must be due to the effect of a gas cap. Physical experiments show (chapter 10) that the presence of a gas cap not only reduces interface amplitude but also alters natural periods.

In regards to the low water fill depth, although maximum interface amplitude is similar for simulation and physical experiment, the breadth of the response in not. Simple linear theory (chapter 4, graph 4.4) indicates that for any oil/water ratio, a gas cap narrows the natural period response i.e. the range of forcing periods that produce resonant type waves is wider for no gas cap than with a gas cap. At forcing periods

away from resonance it might then be expected, that interface amplitude will be higher for situations without a gas cap than with. This was observed in the physical experiments with the small rectangular vessel (comparing graphs 9.6a and 9.1).

The simulation results from this vessel appear to agree with experimental data, but show the inadequacy of the two fluid model when applied to a three fluid system.

12.5 COMPARISON WITH AIR/WATER EXPERIMENTS IN THE LARGE RECTANGULAR VESSEL.

12.5.1 Introduction.

Resonant behaviour in an oil/water system has been shown (chapter 10) to consist of a single travelling wave. In contrast, resonant air/water behaviour is characterised by the more turbulent hydraulic jump (chapter 8). Simulation experiments were carried out with air and water in the large rectangular container. Water fill depths of 175mm and 360mm were used with pitch forcing motion at $\pm 4°$ amplitude and a range of forcing periods. Table 12.3 presents predicted air/water natural periods for both water fill depths.

As in oil/water large vessel experiments, a mesh of 32x16 cells was used. However, as will be pointed out, some forcing conditions gave rise to unstable solutions. No satisfactory mesh configuration has yet been found for these conditions.

12.5.2 Effect of Forcing Period on Interface Amplitude.

Graphs 12.9 and 12.10 compare simulation with physical experiment for two water fill depths 175mm and 360mm. As a result of numerical instability close to resonance, each graph shows simulation results in two parts.

These results indicate :

1) Simulation interface amplitude is lower than physical, at all forcing periods. As forcing period increases, (Ω>8 secs) the difference between simulation and physical experiment reduces.

2) Simulation is seen not to cope with resonance at $\pm 4°$ forcing amplitude i.e. an unstable solution scheme.

Appendix VII shows wave profiles and corresponding FFT frequency spectra for these simulation experiments, their physical equivalents were presented in Appendix IV. Comparing profile plots from the same forcing periods (i.e. Ω=5.0, 5.8, 7.0 seconds), the results show :

1) During applied forcing motion, both simulation and physical profiles are very similar both in shape and form i.e. the same irregular profile exists between the two at similar places in time. The same comment can be made regarding the frequency spectrum, although the physical experiment appears to contain natural period components of higher magnitude.

2) The simulation tends to produce *smoother* profile traces than those from physical experiments.

3) During initial startup, both physical and simulation show irregular profiles of similar shape and duration.

4) The decay profiles from simulation are of much lower amplitude than their physical counterparts. The frequency spectra indicates more high frequency components in the physical spectrum compared to the simulation.

5) Away from resonance (e.g. Ω=9.1 secs) both simulation and physical experiments seem to agree. Closer to resonance (Ω=5.8 secs) a more rapid decay is seen for the simulation rather than physical experiment.

12.5.3 Discussion.

The simulation instability, can be related to the differences between oil/water and air/water interface resonant profiles. From the results presented in chapters 8 and 10, the air/water hydraulic jump is more turbulent than the oil/water travelling wave. This suggests the numerical model is unable to cope with large interface disturbances which occur at resonance in a gas/liquid system. However, it must be pointed out that numerical stability is partly controlled by mesh size and fluid velocity. Two problems arose during attempts to reduce mesh spacing for all unstable numerical experiments :

1) Calculation time steps became of the order 10^{-4} seconds, and resulted in the simulation exceeding computer CPU time allocation. Although modifications were made to the program to restart such experiments, difficulties remain in joining wave profile results together.

2) Through mesh changes, stability was achieved for some low (180mm) water depth experiments. Unstable solutions resulted from all mesh configuration changes, made to the high (360mm) water fill depth experiments.

Although the agreement of air/water interface amplitude response between physical and simulation (graphs 12.9 and 12.10) appears less than that for oil/water (graph 12.7), the profile results presented in appendix IV and VIII show remarkable similarity. The relatively poor agreement for interface amplitude results could be due to :

1) Mesh resolution resulting in poor definition of the air/water interface.

2) Simulation interface detection method using incorrect application of volume of fluid function.

3) During physical experiments, *splashing* waves may have caused *spray* which produced artificially high probe readings. This would also account for irregular peaks which were observed in some experiments, particularly near resonance. Such splashing would be difficult to simulate using the numerical model, and therefore result in lower interface amplitudes than physical experiments.

The relatively good agreement between profile and frequency spectra, especially away from resonance, would support the suggestion of splashing waves interfering with physical probe measurements.

Further discussion on performance of the simulations will be made later.

12.6 FREQUENCY ANALYSIS OF SIMULATION DATA.

12.6.1 Introduction.

Previous physical air/water experiments indicated the presence of natural frequency modes in the wave spectrum as predicted by derived simple linear theory (chapter 4). Similar frequency data from oil/water experiments were not available due to oil/water interface measuring relying on video recordings of one forcing cycle (frequency data had to be taken from 256 points over many forcing cycles). Processing simulation data by the FFT technique, allowed frequency analysis of not only air/water but oil/water simulation experiments.

Simulation data from one oil/water experiment with the small vessel, one air/water and oil/water experiment with the large vessel, were analyzed by FFT techniques as described in chapter 6.

12.6.2 Oil/Water Experiments in the Small Rectangular Vessel.

Table 12.4 presents frequency component data for the duration of forcing (upper line) and for decay (lower line) for a simulation experiment with water to a depth of 87mm, oil density 851 Kg/m^3. Pitch forcing motion was applied at ±4° amplitude.

Referring to the frequency data for decay, it would appear that measured first and second oil/water interface natural periods were 6.99 and 3.59 seconds, respectively. These are higher than predicted ones shown in table 12.1. Oil/water interface amplitude comparison between simulation and physical experiments were presented in graph 12.3. It would seem that maximum oil/water interface amplitude from simulation occurs at forcing periods equal to the measured natural period.

As regards the frequency spectrum during applied forcing, for forcing periods lower that resonance (Ω<4 secs), the second major frequency component is seen to correspond to the natural frequency. Far from resonance (Ω=0.9 secs), the oil/water interface is seen to oscillate at its natural period and not that of the forcing motion. At longer forcing periods (Ω>7.9 seconds), the major frequency component during forcing is higher than the forcing period. This discrepancy becomes more acute at even longer forcing periods (Ω=11.9 secs) where the second major frequency component becomes equal to that of measured natural period.

12.6.3 Oil/Water Experiments in the Large Rectangular Vessel.

Table 12.5 presents frequency component data for the duration of forcing (upper line) and for decay (lower line) for a simulation experiment with water to a depth of 175mm, and oil of density 860 Kg/m^3 (gas oil). Pitch forcing motion was applied, at ±4° amplitude.

The data shows similar trends to that for oil/water experiments in the small rectangular container, i.e. :

1) Measured first and second mode natural periods are higher than predicted (9.59 and 4.53 seconds respectively).

2) The point of maximum interface amplitude occurs at forcing periods corresponding to the measured first mode natural period (Ω=9 to 10 seconds in graph 12.7).

3) At long forcing periods (Ω>9.1 secs), the major frequency component during forcing, is greater than the actual forcing period.

As regards the content of the frequency spectrum, again similar comparisons between small and large vessel can be made. However, table 12.5 shows at forcing periods shorter than resonance (Ω<5.8 secs) the second major frequency component corresponds to the measured natural period. With the small vessel, this behaviour is not seen until a forcing period of 4.2 seconds (table 12.4). This is then entirely due to small vessel natural period occurring at 6.99 seconds as opposed to the large vessel at 9.59 seconds.

12.6.4 Air/Water Experiments in the Large Rectangular Vessel.

Table 12.6 presents frequency component data for the duration of forcing (upper line) and for decay (lower line) for a simulation experiment with water to a depth of 175mm, and air. Pitch forcing motion was applied, at $\pm 4°$ amplitude.

It would appear that measured first and second air/water interface natural periods were 2.8 and 1.42 seconds, respectively. These are higher than predicted ones given in table 12.3. Interface amplitude comparison between simulation and physical experiments was presented in graph 12.3.

Table 12.6 indicates :

1) At forcing periods higher than resonance (Ω>5.8 secs) the second major frequency component corresponds to the measured first mode natural period. This is the similar to the oil/water results at forcing periods lower than resonance.

2) At longer forcing periods (Ω>9.1 secs), the major frequency component during forcing, is greater than the actual forcing period. This observation is similar to those for simulation oil/water experiments in both vessels.

12.6.5 Discussion of Frequency Results.

The results from both large and small vessel with oil/water and air/water show similar trends :

1) At forcing periods away from resonance, the second major frequency component during forcing corresponds to measured first mode natural period.

2) Measured natural periods are higher than those predicted by equation 4.19.

3) Maximum interface amplitude seems to occur at a forcing period corresponding to the measured natural period, and not that predicted from equation 4.19.

The above comments also apply in comparing simulation with physical FFT data (table 12.6 and table 8.3). In addition, table 12.6 shows at long forcing periods, the major frequency component during forcing was higher than the forcing period. This behaviour was also seen from physical air/water experiments (table 8.3). In the physical experiments, it might have been suggested that generation of forcing period by computer program was incorrect. In the simulation forcing motion was generated from exact equations. Therefore, the common factor between simulation and physical

data, concerns the 8 bit resolution of data (i.e. numbers between 0 and 255 for amplitude ±10°) and the data processor. These results then suggest that either the data processor is at fault or the frequency effects are due to resolution of amplitude at long periods.

In relation to the differences between measured and predicted natural periods, previous workers (62) have derived expressions for natural period involving surface tension. In the simulation experiments, although surface tension was not introduced, the results still show that differences exist between predicted and measured natural periods. The predicting equation (equation 4.19) was derived using the velocity potential technique (chapter 4) which is then different from the simulations use of primary variables (e.g. velocity and pressure). This would suggest that some assumptions applied to the velocity potential technique become invalid.

12.7 ADDITIONAL SIMULATION EXPERIMENTS.

12.7.1 Introduction.

Numerical simulations offer the possibility of conducting experiments which would be difficult in practice (3). Caution however, would have to be given to results as comparisons between simulation and physical experiments show some inconsistencies.

Two sets of simulation experiments were carried out to see firstly, the effect of liquid viscosity on interface profile and secondly to compare velocity profiles in a baffled and unbaffled vessel.

12.7.2 The Effect of Viscosity on Interface Amplitude.

Previous workers (2) have indicated the importance of scaling viscous forces in model experiments, especially when dealing with LNG tankers. In the majority of cases, viscosity is thought to have little

effect on interface profiles (60) although forces exerted on vessel walls are reduced (8). Data from air/water and numerical models, suggested that viscous forces determine the strength of natural frequency components in the forced wave spectrum. In this respect, viscosity would play an important role.

Simulation experiments were carried out using the small rectangular vessel filled with air and water to a depth of 87mm. Pitch forcing motion was applied at 3 seconds period, ±4° amplitude. Between each experiment, kinematic viscosity was multiplied by factors from 1 to 1000. Graphs 12.11 to 12.13 present the wave profile and corresponding frequency spectra for three kinematic viscosity values, x1, x100 and x1000 respectively. It must be noted that SOLA-VOF requires only one viscosity value which is applied for both fluids, throughout the mesh.

The results indicate :

1) The amplitude of the major frequency component as defined by equation 6.1 (chapter 6) reduces with increasing viscosity. The actual values are 13.5mm for x1 factor, 12.9mm for x100 and 10.8mm for x1000.

2) The wave profiles during forcing *start up* for x1 factor (between 3 to 6 seconds as in graph 12.11) appear to be more uniform than for x100 (graph 12.12). A similar difference is noted for x1000 (graph 12.13) over 3 to 12 seconds.

3) No significant difference occurs in the composition of the frequency spectra for all viscosity values.

These results show that viscosity has an effect on wave profiles during initial *start up* but has little effect on reducing wave amplitude.

12.7.3 Velocity Profiles in Oil/Water Baffled and Unbaffled Vessels.

In addition to predicting interface profiles, the numerical model can give graphical representation of the velocity profile in both fluids at any instant. Oil/water simulation experiments were carried out in the large rectangular vessel, with and without a 50% free area perforated baffle. Oil density was 860 Kg/m^3, water fill depth 180mm, pitch forcing motion period of 9.17 seconds, ±2.9° amplitude. In each simulation experiment, a mesh of 40x20 cells was used. Graphs 12.14a-h show initial settings, initial fluid configuration and velocity profiles at 18 and 19 seconds during applied forcing motion in the unbaffled vessel.

The results show :

1) At 18 seconds (graph 12.14e) a velocity circulation profile is seen on the oil/water interface at the right of the vessel.

2) At 18.5 seconds (graph 12.14f) a travelling wave develops as the vessel changes position from -0.685° to 0.314°. The velocity circulation profile is seen to increase in amplitude.

3) At 19 and 19.5 seconds (graphs 12.14g-h) a full travelling wave profile is observed. The velocity vectors indicate a possible circulation flow path over the wave.

The volume of fluid change at 19 seconds is 0.023% while at 19.5 seconds, it is 0.019%. This implies the water fill depth changed from 179.95mm to 179.97mm during each time step (e.g. 180mm - 0.023%).

Graphs 12.15a-h show the velocity profiles for the baffled vessel at the same times as the unbaffled vessel. Graph 12.15c shows the initial configuration of a still fluid, and the baffle placed at the vessel's centre. Construction of baffles for simulation experiments, relies on the designation of mesh cells to be either fluid or boundary cells. The baffle used in this experiment was formed by alternate cells at the vessel's

centre to be designated as boundary cells. Size of the baffle perforations is then governed by the cell spacing in both x and y directions at the vessel centre. This explains the use of a variable 40x20 spaced mesh shown in graphs 12.14b/12.15b. The mesh is seen to converge at the vessel's centre. Therefore, the baffle can be said to have 50% free area at equal hole spacing.

With reference to graphs 12.15e-h :

1) At 18 seconds (graph 12.15e) a velocity circulation profile is seen on the oil/water interface at the right of the vessel. In addition, a significant flow is seen through the baffle holes in both oil and water layers.

2) At 18.5 seconds (graph 12.15f) a form of travelling wave develops as the vessel changes position from -0.688° to 0.307°. The velocity circulation profile is seen to increase in amplitude as the wave moves towards the baffle. Flow through the baffle is seen to reduce.

3) At 19 and 19.5 seconds (graphs 12.15g-h) again a form of travelling wave profile is observed, passing through the baffle. A velocity circulation profile is still present.

Thus, similar oil/water interface and velocity profiles occur in both unbaffled and baffled vessels, except :

1) Oil/water interface amplitude at any position inside the vessel is lower in the baffled vessel than in the unbaffled vessel.

2) The circulation velocity round the travelling wave appears to be reduced in the presence of the baffle.

The volume of fluid, graphs 12.15g-h indicates the mesh had lost a total of 0.049% of original fluid (water). This is then higher than the

unbaffled vessel, an indication of problem complexity and interface disturbance by the baffle.

12.7.4 Discussion of Velocity Profile Experiments.

The simulation oil/water interface profiles and those observed during physical experiments (chapter 10) appear to be remarkably similar. In addition, the actual velocity profiles produced by simulation, aid the interpretation of physical experiments. During physical oil/water experiments, regions of interface breaking occur over the top of the travelling wave (chapter 10 for low water depth of 180mm). This corresponds to the opposing velocity profiles in the oil and water layers, as seen in graphs 12.14g-h. It is then suggested that where a circulating velocity profiles across an interface occur in simulation experiments, interface breaking is likely to occur. Comparing unbaffled with baffled vessel, graphs 12.15g-h show that the baffle reduces circulation velocity amplitude. Thus, interface breaking would be less for a baffled vessel. This compares favorably with physical experiments where interface breakup seemed to be less with a baffle than without (chapter 10).

Questions about a velocity profile extending from one fluid to the other, across the interface have been raised. However, the flow profiles observed in simulation experiments compares favorably with those observed by Handa & Tayima (42) and are reproduced in figure 12.1.

It should be noted that no satisfactory method has been found to store fluid velocity data for the duration of a simulation experiment. Hence, no comment can be made regarding exact values of velocity components observed during these two experiments.

12.8 GENERAL COMMENTS ON PROGRAM OPERATION.

12.8.1 Introduction.

The major concern of any simulation program is the stability of the numerical scheme and the equations solved. The simulation experiments presented in this chapter, have shown numerical instability to be a function of forcing conditions and fluid system.

12.8.2 Solution Stability in Air/Water Simulation Experiments.

The air/water simulation experiments in the large rectangular vessel show that close to resonance, numerical instability causes the solution to break down. However, oil/water experiments in both vessels indicate the numerical system is capable of dealing with interfacial breaking. This suggests that the program cannot cope with large turbulent mixing processes which occur during air/water resonance i.e. the hydraulic jump.

Preliminary examination of the problem has resulted in the main area of difficulty, centering on the interfacial boundary conditions between air and water. The air being a fluid with near negligible density causes the pressure iteration loop to fail, presumable at the interface where velocity and pressure differentials would be quite high. The original SOLA-VOF algorithm operates on a basis of a single fluid with a free surface. Special free surface boundary conditions were then used to remove the upper fluid. If a single fluid designation (NMAT=1 in the program input parameters) was applied, it was found that stable solutions could be produced from the previous unstable forcing conditions. This suggests that a modification is required to aid the pressure iteration loop around the air/water interface when specifying a two fluid system (NMAT=2).

12.8.3 The Single Viscosity Value.

The original SOLA-VOF code as supplied (17), was set up for a single fluid with a free surface. Therefore only one viscosity value was required. Most of the modifications carried out for this project centred on the introduction of a rotational co-ordinate system to produce forcing motion effects. Unfortunately, attention was not paid to the change in viscosity throughout the mesh.

In simulation experiments presented in the earlier sections, the effect of changing viscosity was found to be negligible in the small vessel. This might be a result of viscosity applying to the whole mesh rather than one fluid.

12.9 EXAMPLE OF MODELING AN OFFSHORE SEPARATOR.

12.9.1 Introduction.

Departmental activities in the offshore processing area revealed the importance of reducing fluid motion effects in oil/water separation equipment. Figure 12.2 shows an example of a gas/oil/water separator in which oil, separated by gravity, is collected over a weir plate. During departmental experiments, forcing motion effects caused spilling of water over the weir plate, reducing the quality of separated oil.

A simulation experiment was set up in an attempt to model the above behaviour in a rectangular vessel (1.89m by 0.5m) filled with water to a depth of 250mm and oil of density 860 Kg/m^3. Pitch forcing motion at 10 seconds period and ±4° amplitude was applied. Appendix VII presents full time stepped velocity and oil/water interface profile at 0.5 second time intervals during forcing, till 29.5 seconds. Oil/water resonance for this configuration was predicted by equation 4.18 as 10.2 seconds.

12.9.2 Velocity and Oil/Water Interface Profile in the Separator.

The computer was allowed to continue the simulation beyond 29.5 seconds, but plotting more profiles would have proved time consuming.

Several features of these profiles are :

1) At time 3.5 seconds, the interface is seen close to the vessel roof on the vessel's left side. On the right, the interface is seen well below the tip of the weir.

2) At 6 seconds, a velocity circulation profile has developed, although there appears no indication of a travelling wave. The oil/water interface is now close to the tip of the weir.

3) At 7 seconds, flow of water over the weir has started. Large velocity vectors are seen on the oil side of the weir, as water flows into this section.

4) At 10.5 seconds, water is seen flowing towards the left side of the vessel, away from the weir.

5) At 13.5 seconds, the water begins to flow back towards the weir. A velocity circulation profile is seen to develop at the vessel centre. Note that the oil/water interface nearly touches the vessel base close to the weir's left side.

6) At 16 seconds, water again begins to flow over the weir.

7) At 18 to 19 seconds, a velocity circulation profile develops as water flows away from the weir. On the weir's right hand side, strong circulation profile is seen.

8) At 29 seconds, the weir's right side is seen full of water.

It is unfortunate that space does not permit further profile frames to be included with this report, although by 30 seconds the spilling over the weir plate would now be periodic.

12.9.3 Discussion.

By comparison with a gas/oil/water separator (figure 12.2) and previous physical experiments (chapter 10), the separator simulation experiment shows several important effects.

The first effect, regards the water spilling over the weir to be collected in the oil take off side. In offshore separators, this would result in water taken off along with oil product hence a reduction in oil quality. Sloshing therefore, has important consequences for the design and specification of downstream processing equipment.

The second effect, regards the velocity circulation profile around the oil/water interface. Results presented earlier in this chapter have suggested that a velocity circulation profile on the oil/water interface, is related to breakup of that interface. Physical experiments (chapters 9 and 10) indicated that this oil/water interface breakup produces bubbles of oil-in-water and water-in-oil. Such behaviour would also have a detrimental effect of separation performance. In offshore separators, it may be possible for some of these bubbles to be taken off in the water stream which again affects downstream processing requirements. At certain times, the oil/water interface is seen close to the vessel base which may result in the presence of oil in the water take off stream.

The simulation deals with a two fluid (oil/water) system and therefore the results are not directly applicable to a real gas/oil/water separator. However, results from physical experiments (chapters 9 and 10) show that oil/water interface behaviour in a two fluid (oil/water) system is similar to that in a three fluid (gas/oil/water) system i.e. the upper gas/oil interface behaves in a similar way to the vessel top. Therefore, results from the simulation experiment may be valid for a gas/oil/separator.

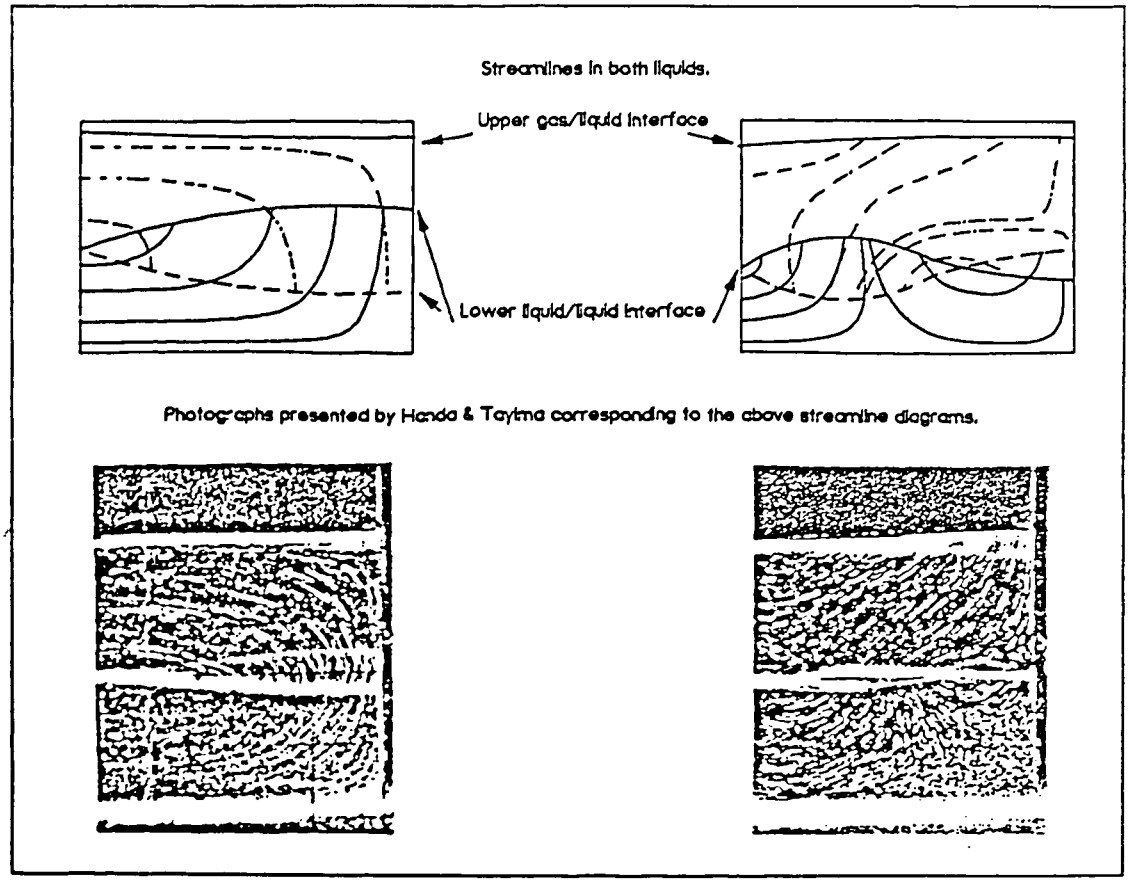

Figure 12.1: Flow profiles in air/oil/water filled vessel as observed by Handa & Tayima (42).

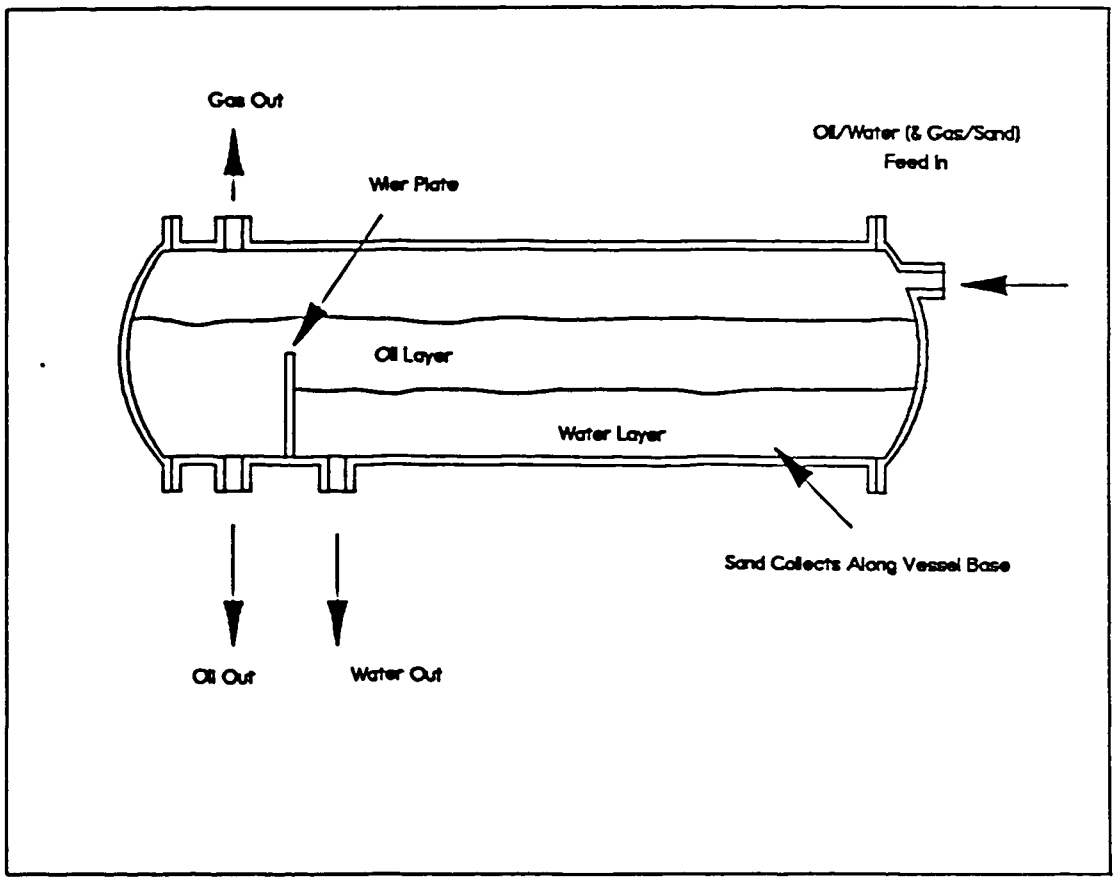

Figure 12.2: Sketch of a gas/oil/water separator.

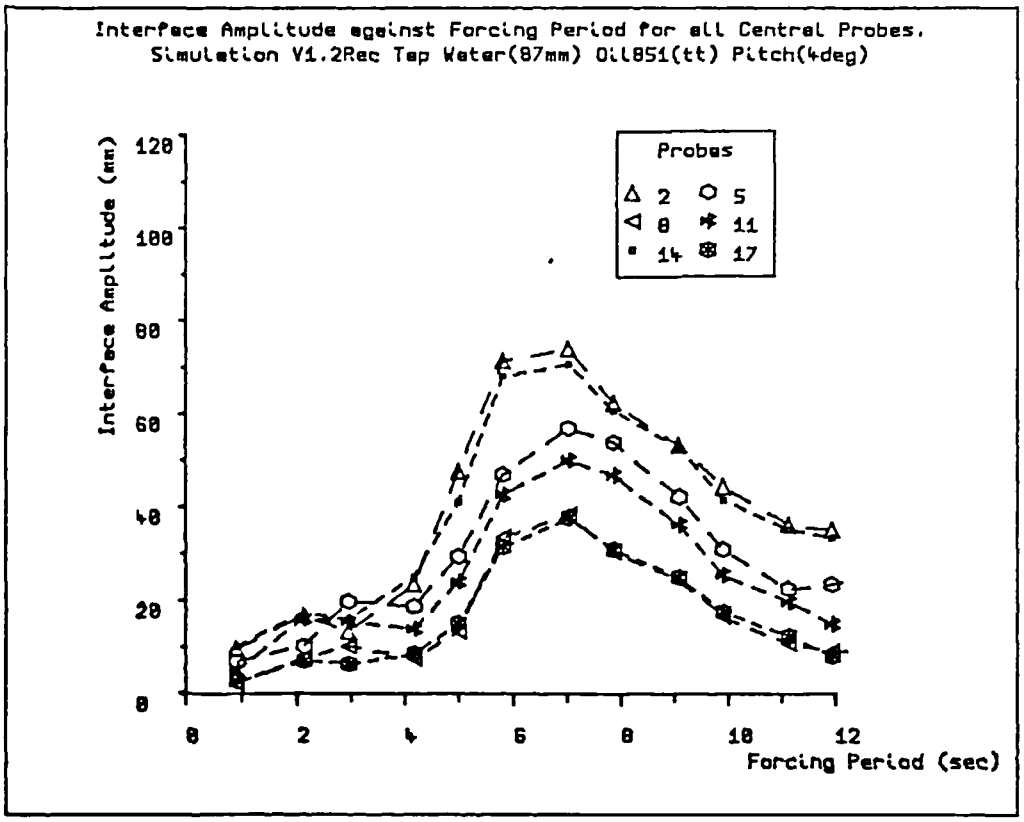

Graph 12.1: Effect of forcing period on oil/water interface amplitude from simulation experiment in the small rectangular vessel under pitch forcing motion at ±4° amplitude. Oil: FK851, water fill depth of 87mm.

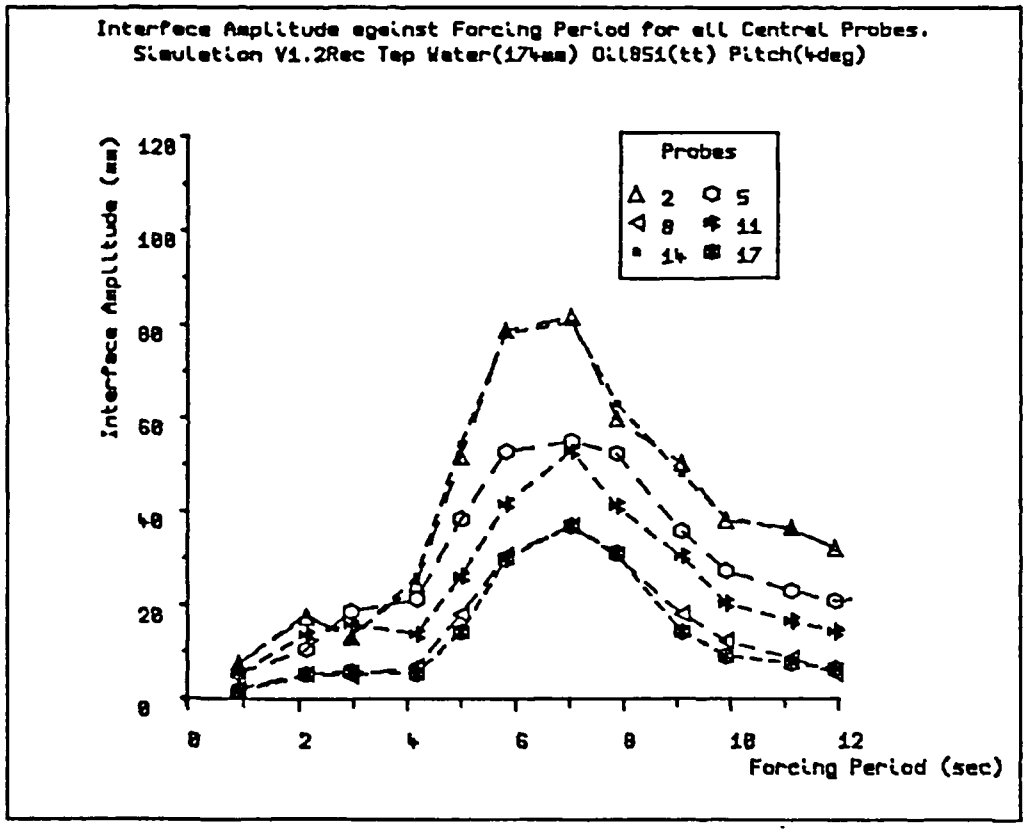

Graph 12.2: Effect of forcing period on oil/water interface amplitude from simulation experiment in the small rectangular vessel under pitch forcing motion at ±4° amplitude. Oil: FK851, water fill depth of 174mm.

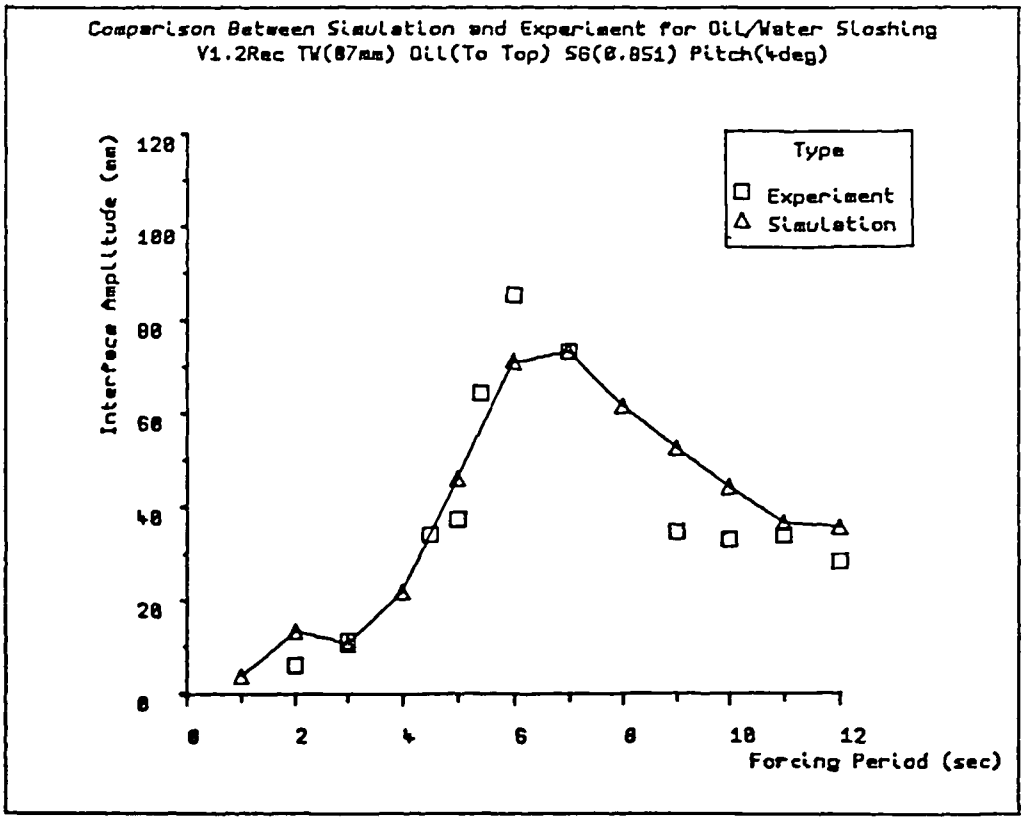

Graph 12.3: Comparison of simulation to physical experiment on oil/water interface amplitude in the small rectangular container under pitch forcing motion at ±4° amplitude. Oil: FK851, water depth 87mm.

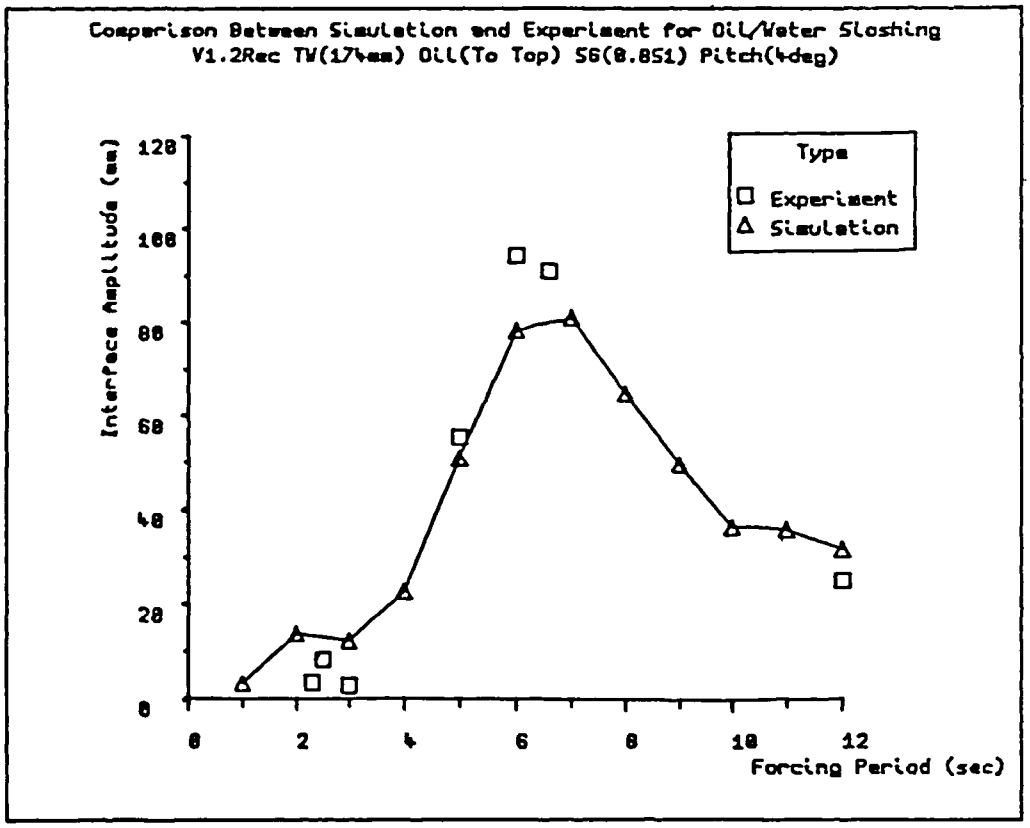

Graph 12.4: Comparison of simulation to physical experiment on oil/water interface amplitude in the small rectangular vessel under pitch forcing motion at ±4° amplitude. Oil: FK851, water depth 174mm.

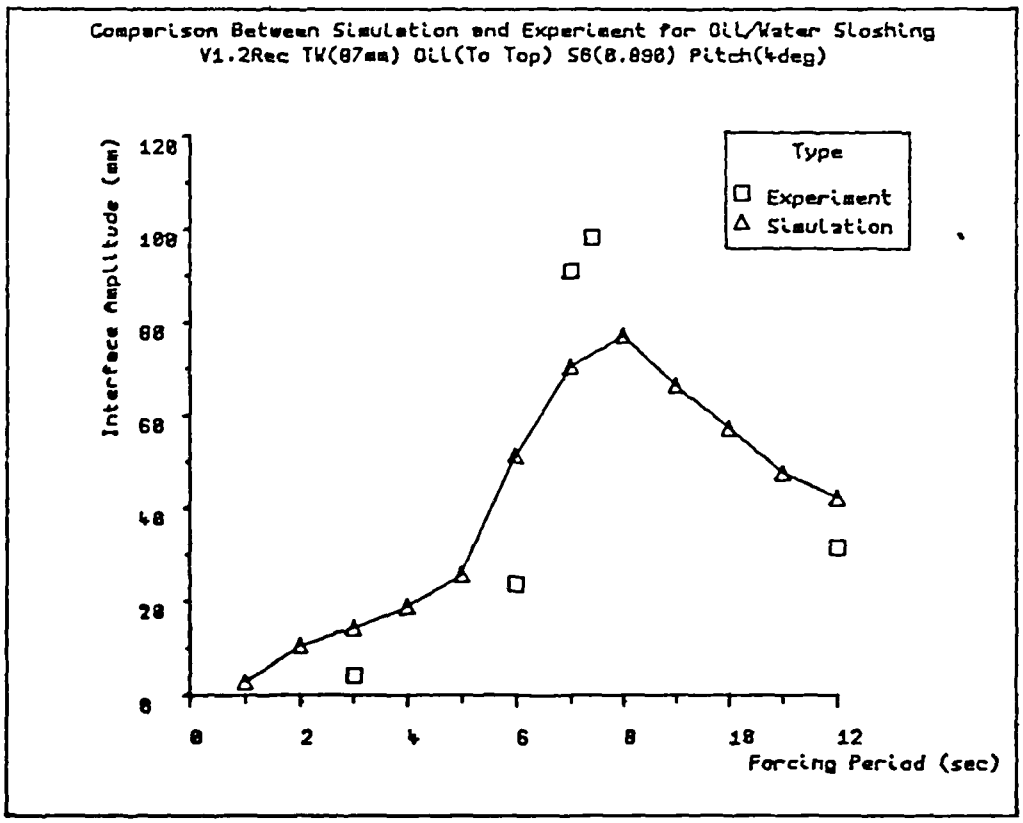

Graph 12.5: Comparison of simulation to physical experiment on oil/water interface amplitude in the small rectangular vessel under pitch forcing motion at ±4° amplitude. Oil: FK890, water depth 87mm.

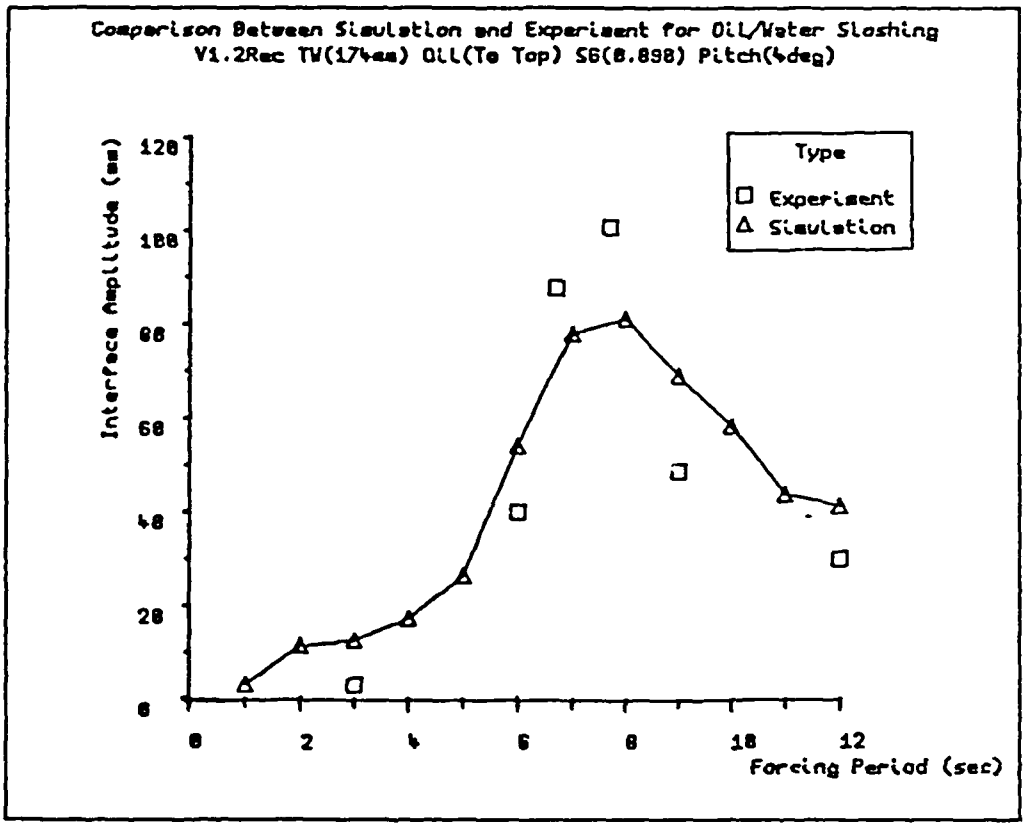

Graph 12.6: Comparison of simulation to physical experiment on oil/water interface amplitude in the small rectangular vessel under pitch forcing motion at ±4° amplitude. Oil: FK890, water depth 174mm.

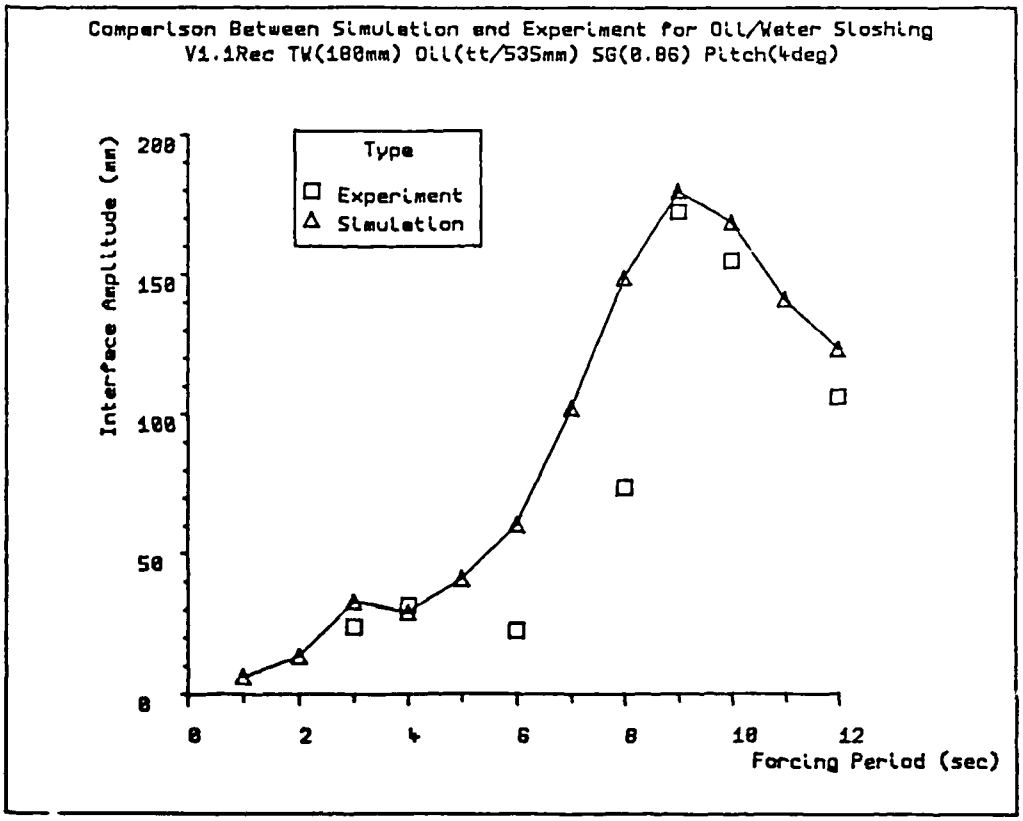

Graph 12.7: Comparison of simulation to physical experiment on oil/water interface amplitude in the large rectangular container under pitch forcing motion at ±4° amplitude. Gas Oil, water depth 180mm.

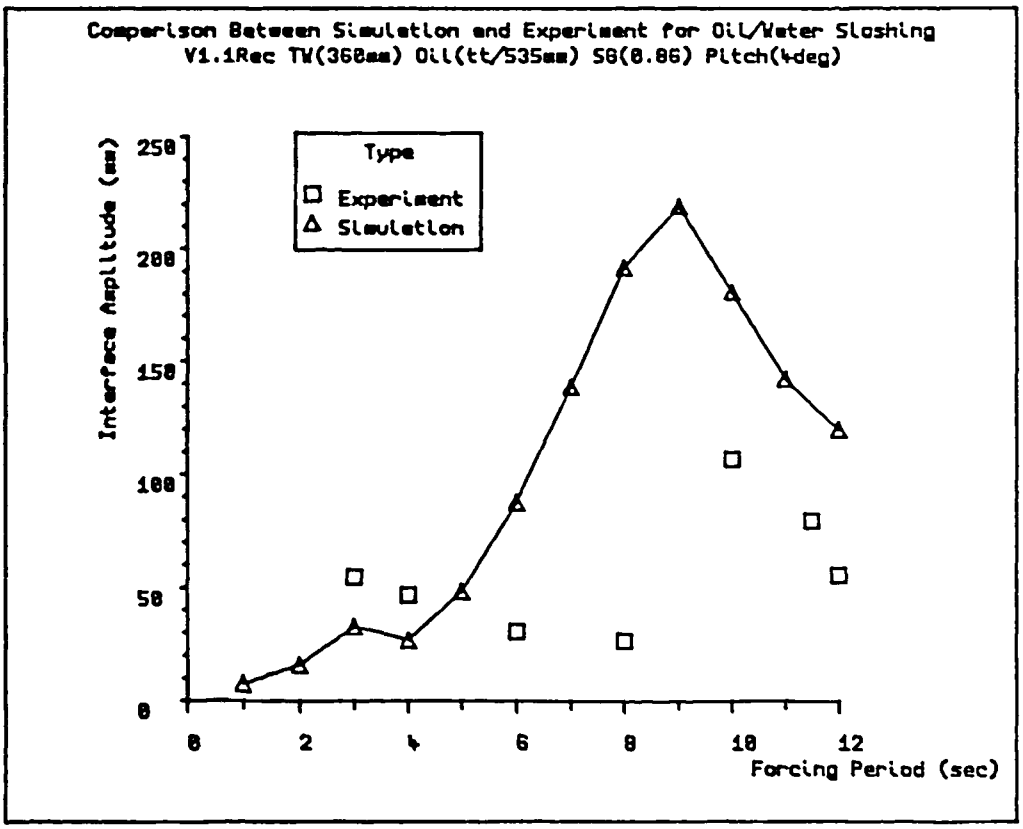

Graph 12.8: Comparison of simulation to physical experiment on oil/water interface amplitude in the large rectangular container under pitch forcing motion at ±4° amplitude. Gas Oil, water depth 360mm.

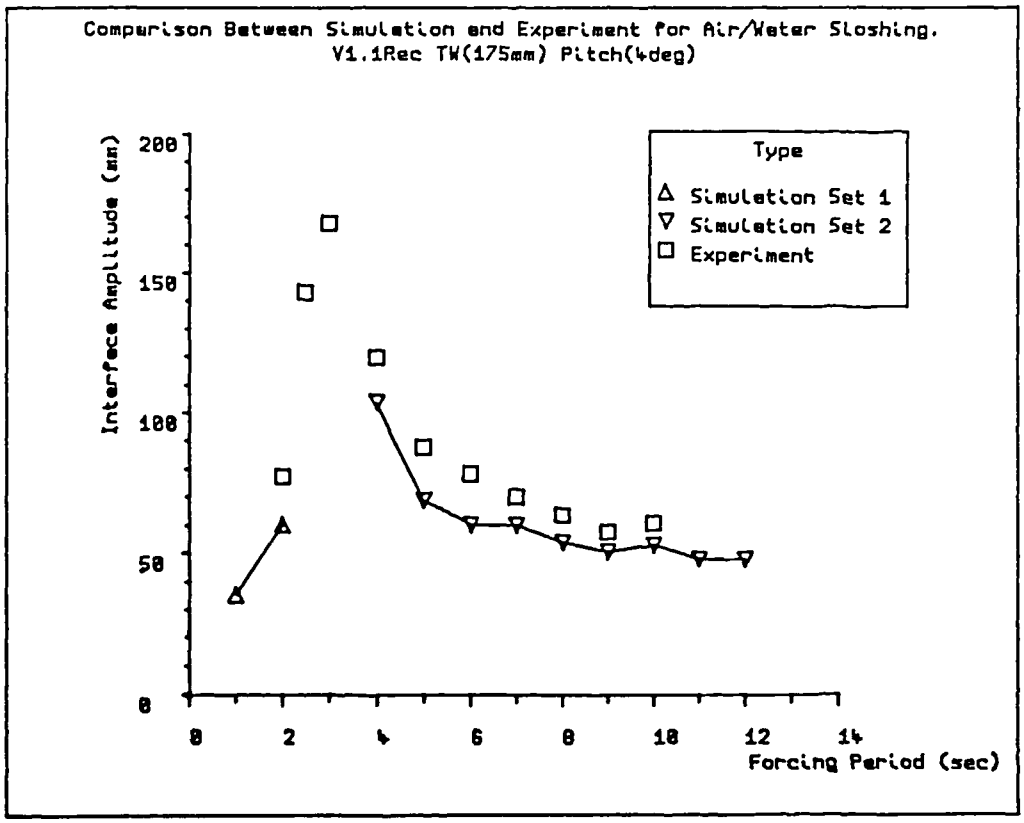

Graph 12.9: Comparison of simulation to physical experiment on air/water interface amplitude in the large rectangular container under pitch forcing motion at ±4° amplitude. Water depth 175mm.

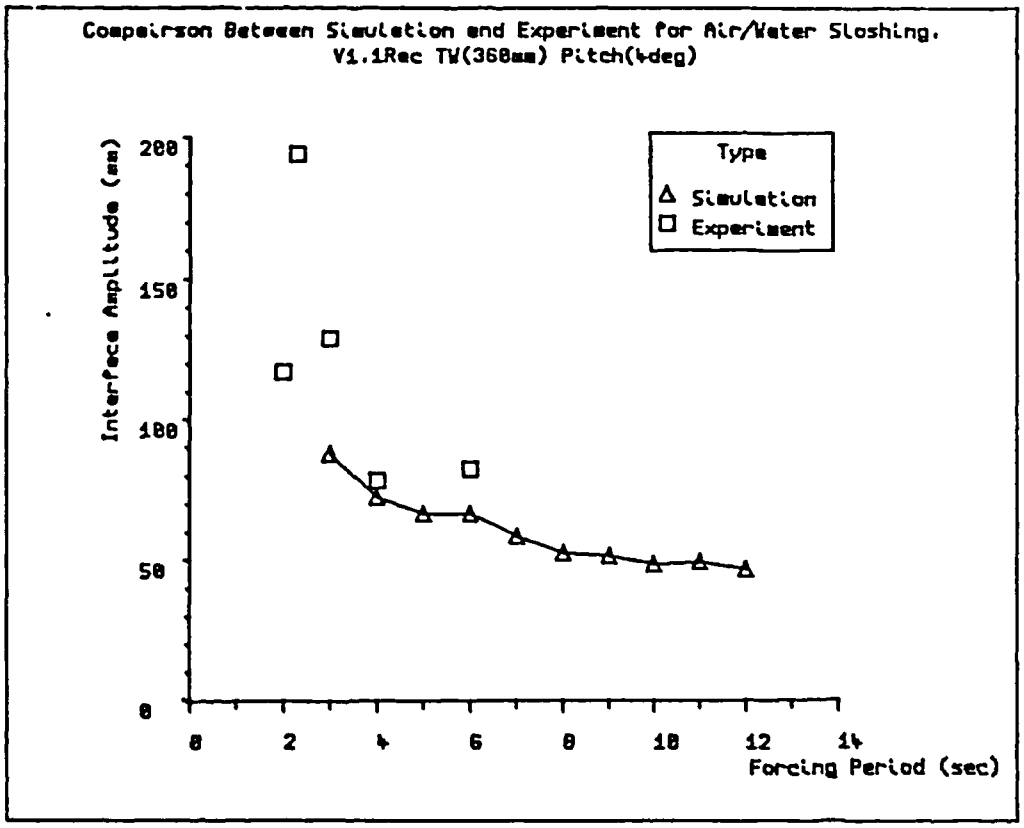

Graph 12.10: Comparison of simulation to physical experiment on air/water interface amplitude in the large rectangular container under pitch forcing motion at ±4° amplitude. Water depth 360mm .

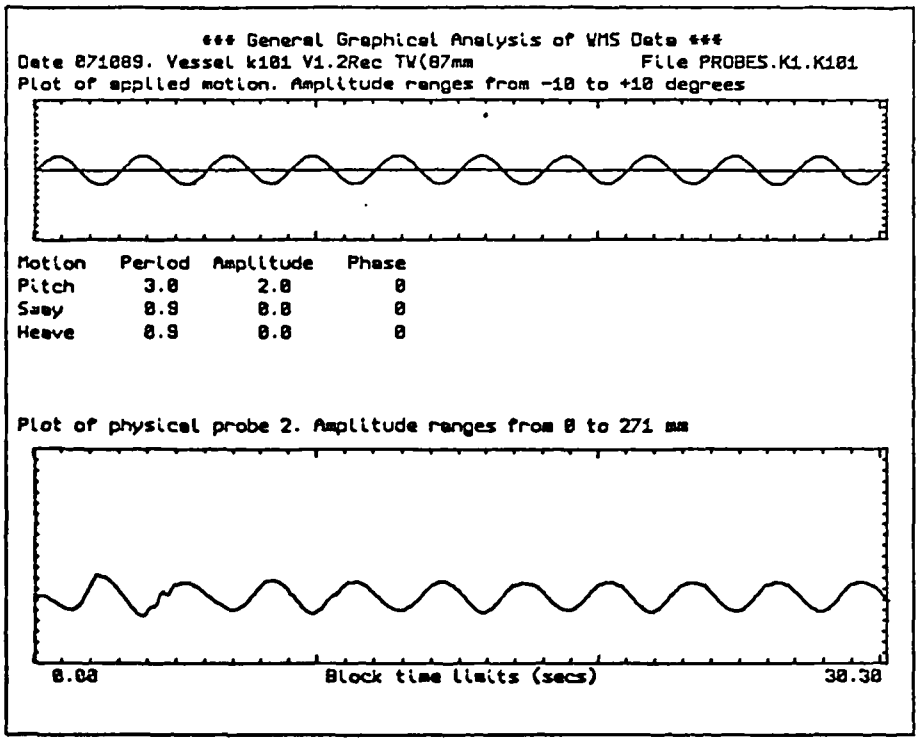

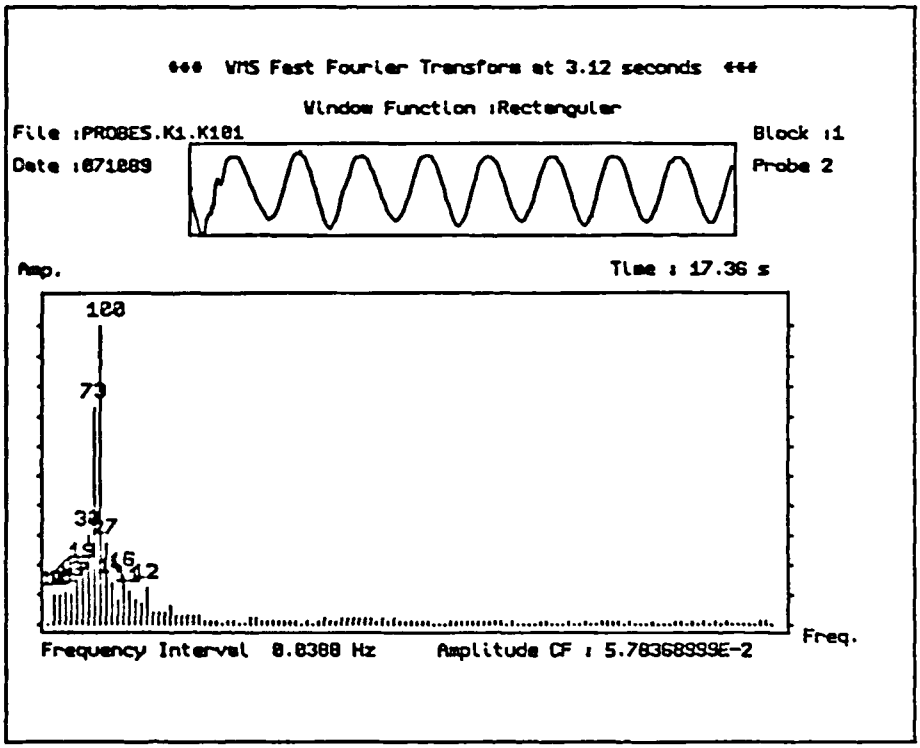

Graph 12.11: Wave profile and FFT frequency spectrum for probe 2 in the air/water simulation of the small rectangular vessel with viscosity factor x1. Water depth 87mm, pitch forcing motion at 3 secs, $\pm 4°$.

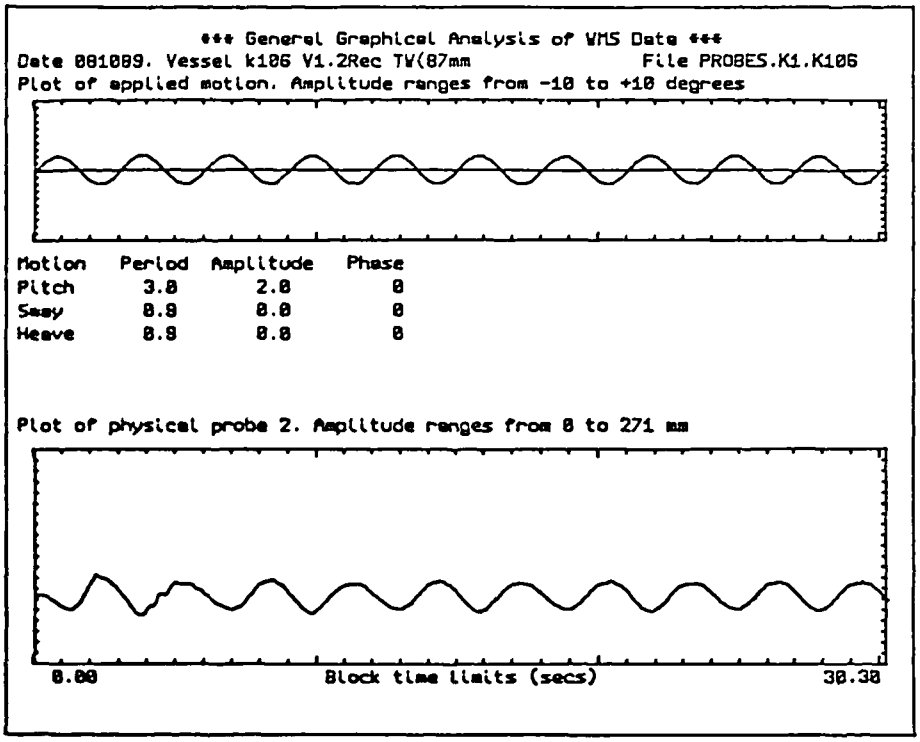

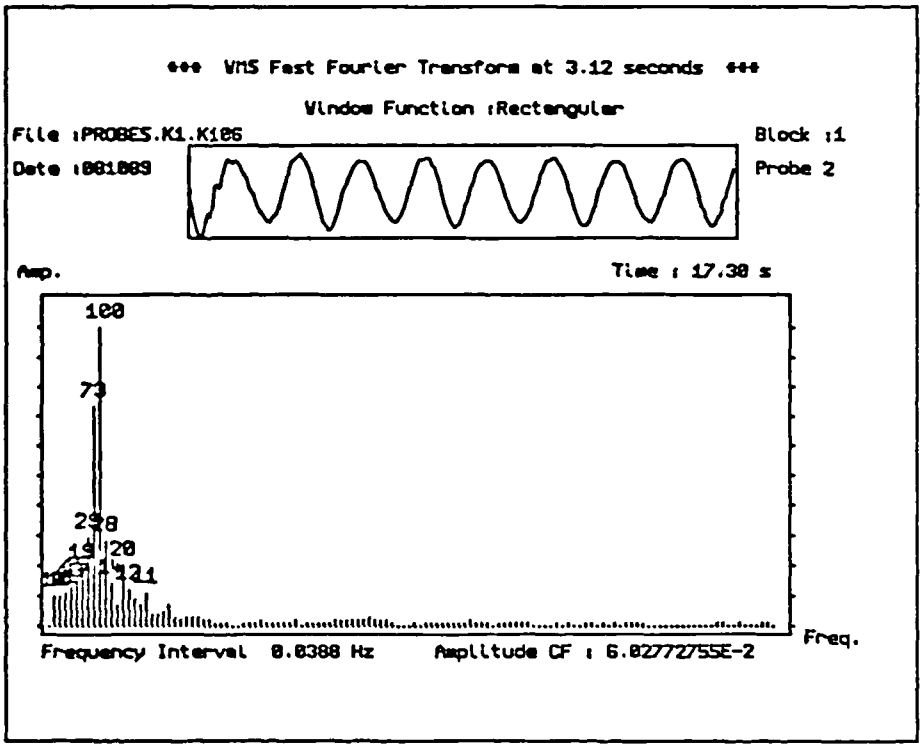

Graph 12.12: Wave profile and FFT frequency spectrum for probe 2 in the air/water simulation of the small rectangular vessel with viscosity factor x100. Water depth 87mm, pitch forcing motion at 3 secs, ±4°.

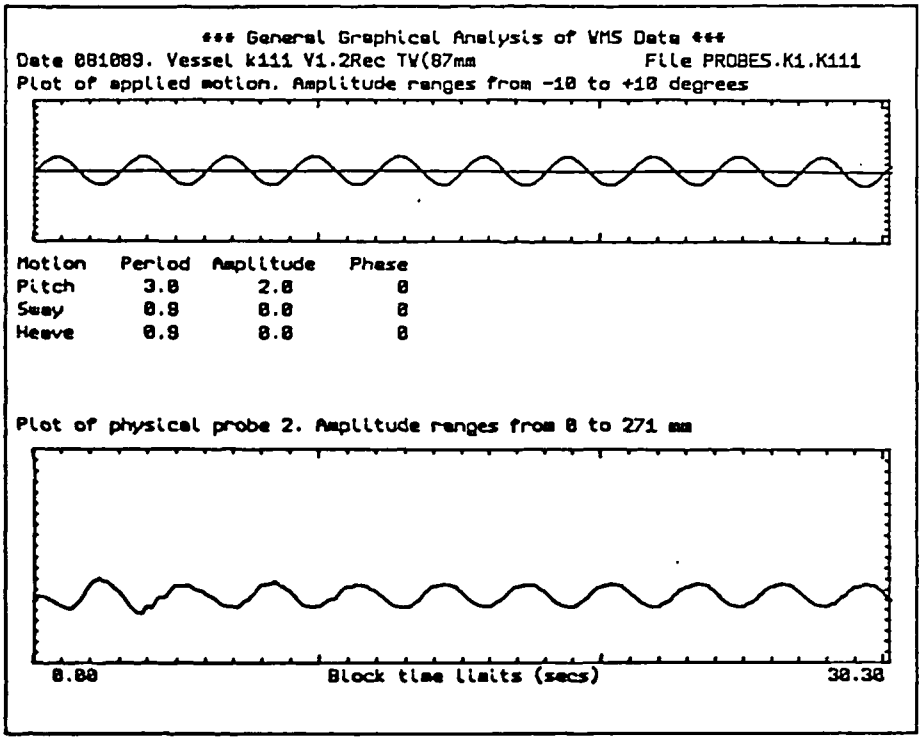

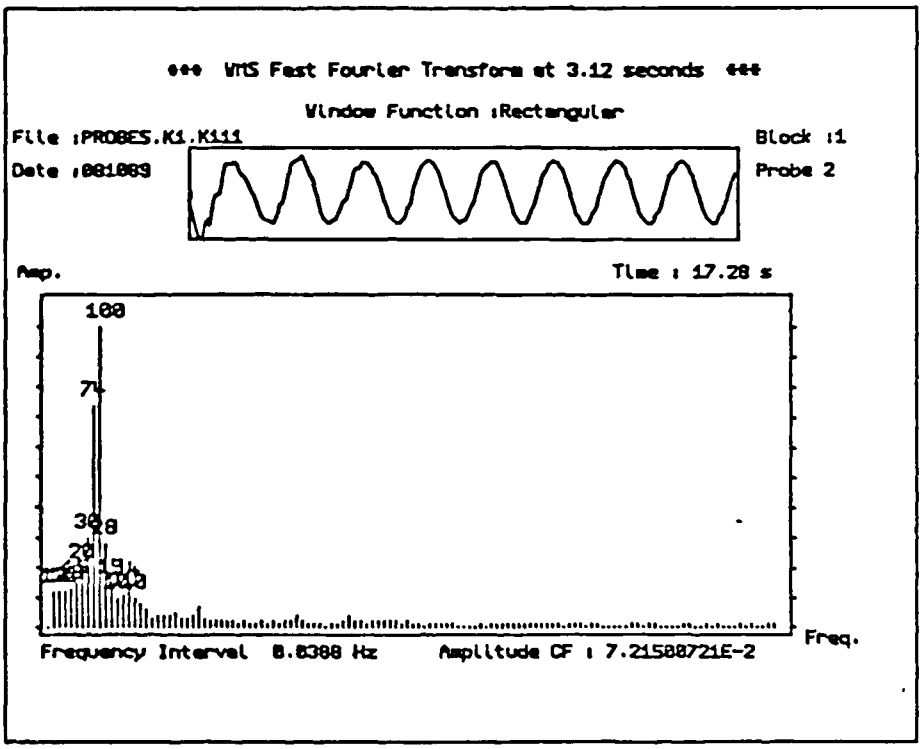

Graph 12.13: Wave profile and FFT frequency spectrum for probe 2 in the air/water simulation of the small rectangular vessel with viscosity factor x1000. Water depth 87mm, pitch forcing motion at 3 secs, ±4°.

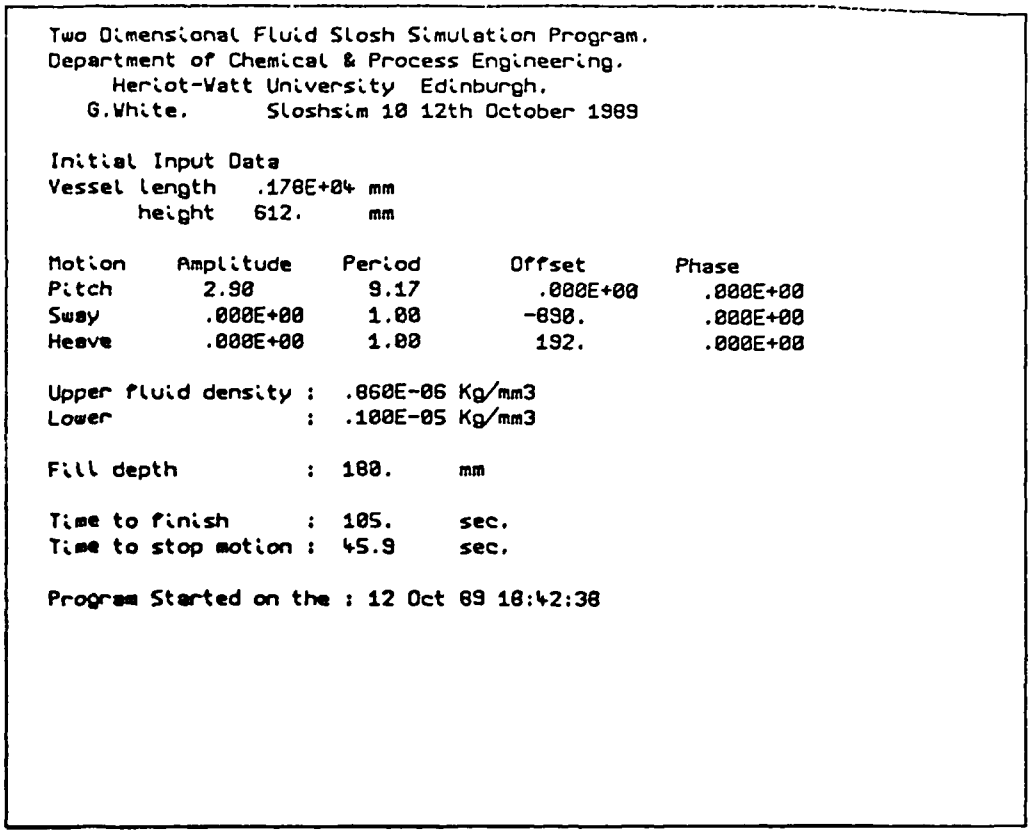

Graph 12.14a: Simulation of oil/water unbaffled vessel for pitch forcing motion at 9.17secs, ±2.9°. Water fill depth 180mm. Initial information screen.

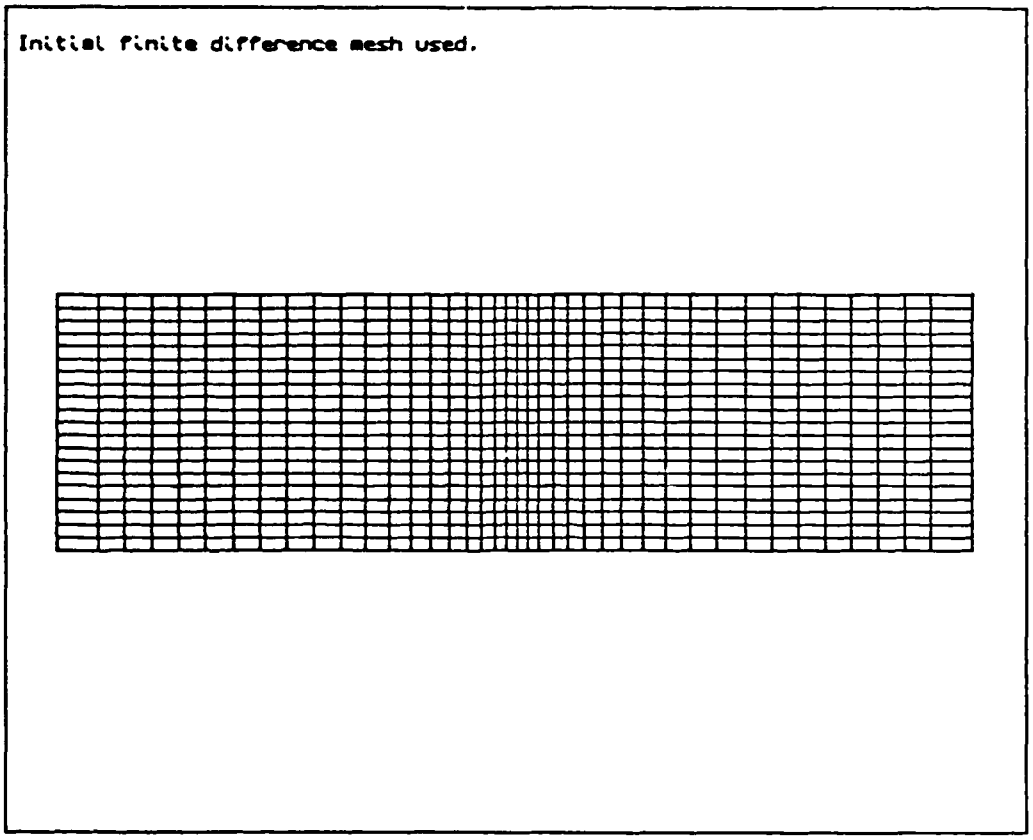

Graph 12.14b: Simulation of oil/water unbaffled vessel for pitch forcing motion at 9.17 secs, ±2.9°.Water fill depth 180mm. Initial mesh configuration.

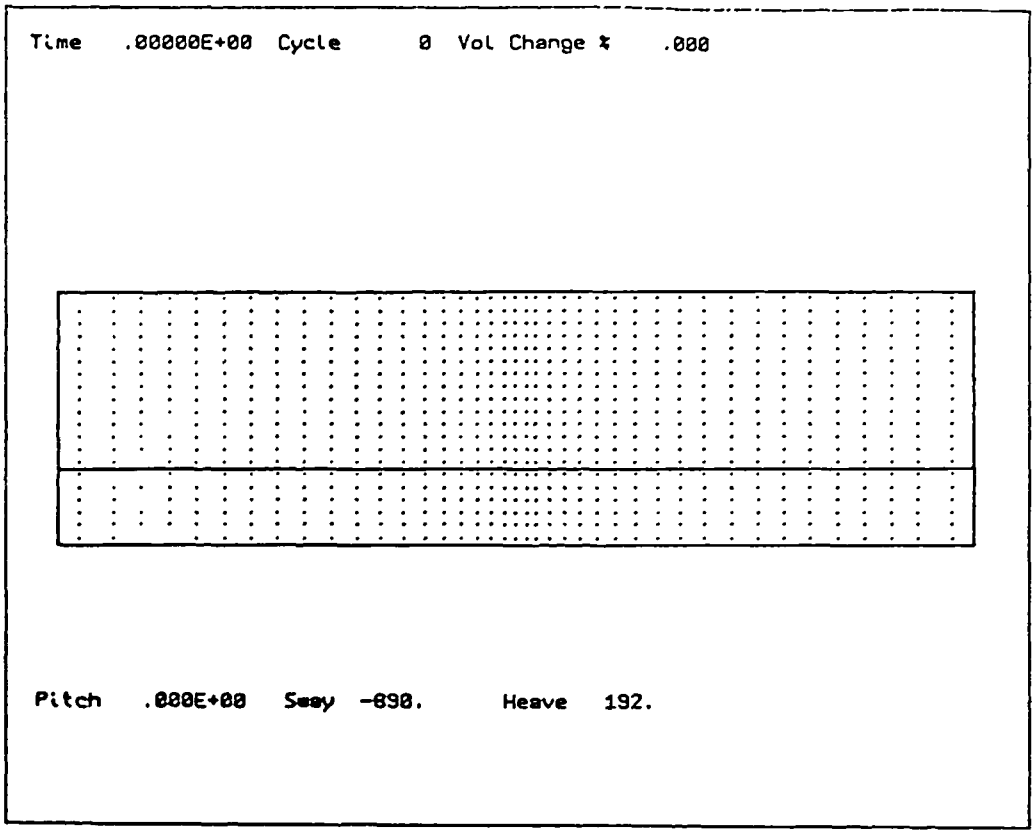

Graph 12.14c: Simulation of oil/water unbaffled vessel for pitch forcing motion at 9.17 secs, ±2.9°.Water fill depth 180mm. At time 0 seconds.

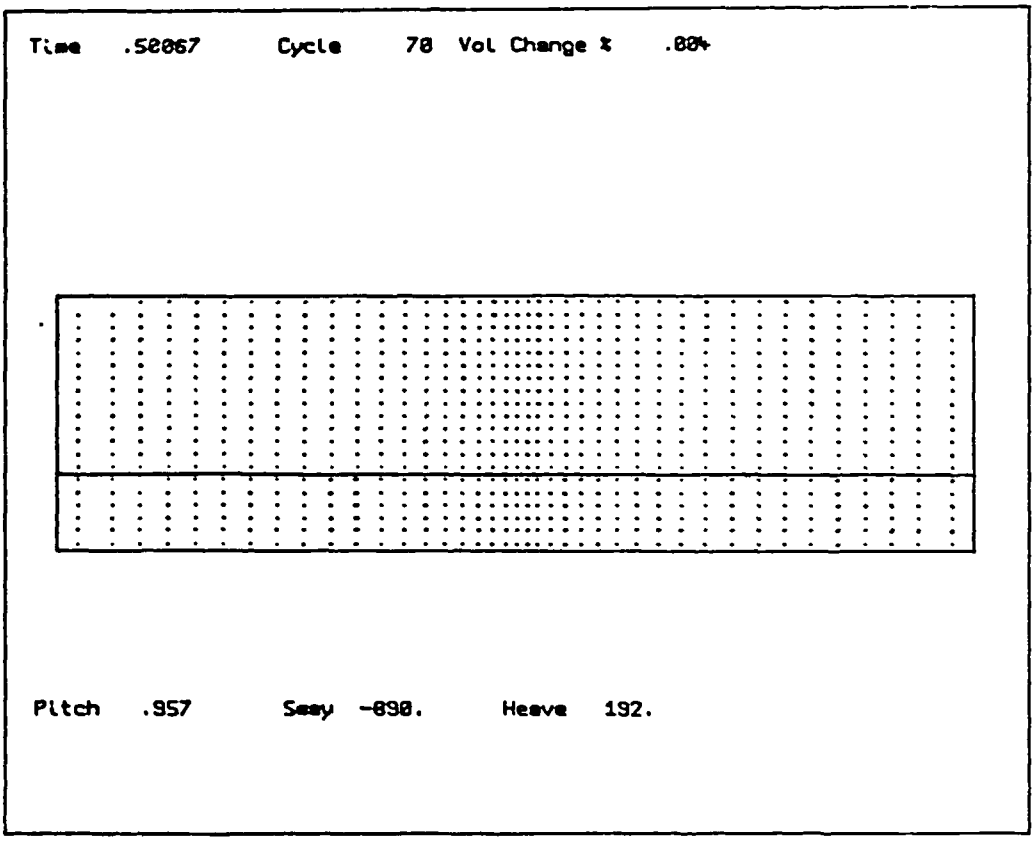

Graph 12.14d: Simulation of oil/water unbaffled vessel for pitch forcing motion at 9.17 secs, ±2.9°.Water fill depth 180mm. At time 0.5 seconds.

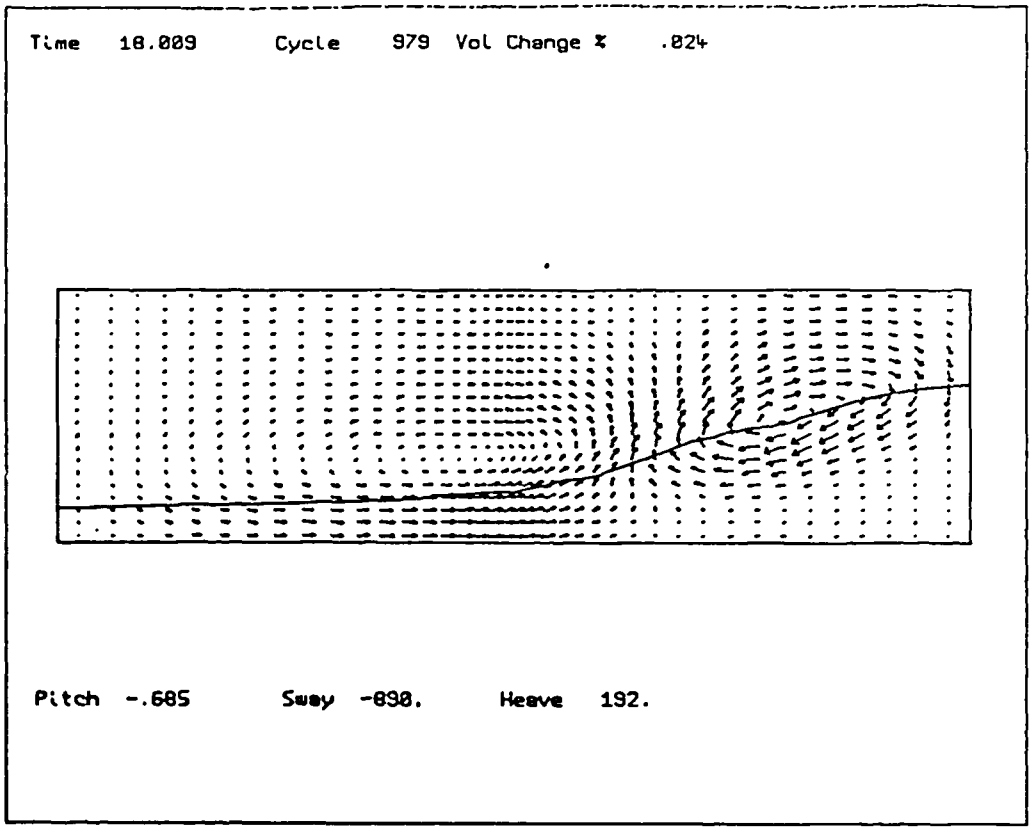

Graph 12.14e: Simulation of oil/water unbaffled vessel for pitch forcing motion at 9.17 secs, ±2.9°.Water fill depth 180mm. At time 18 seconds.

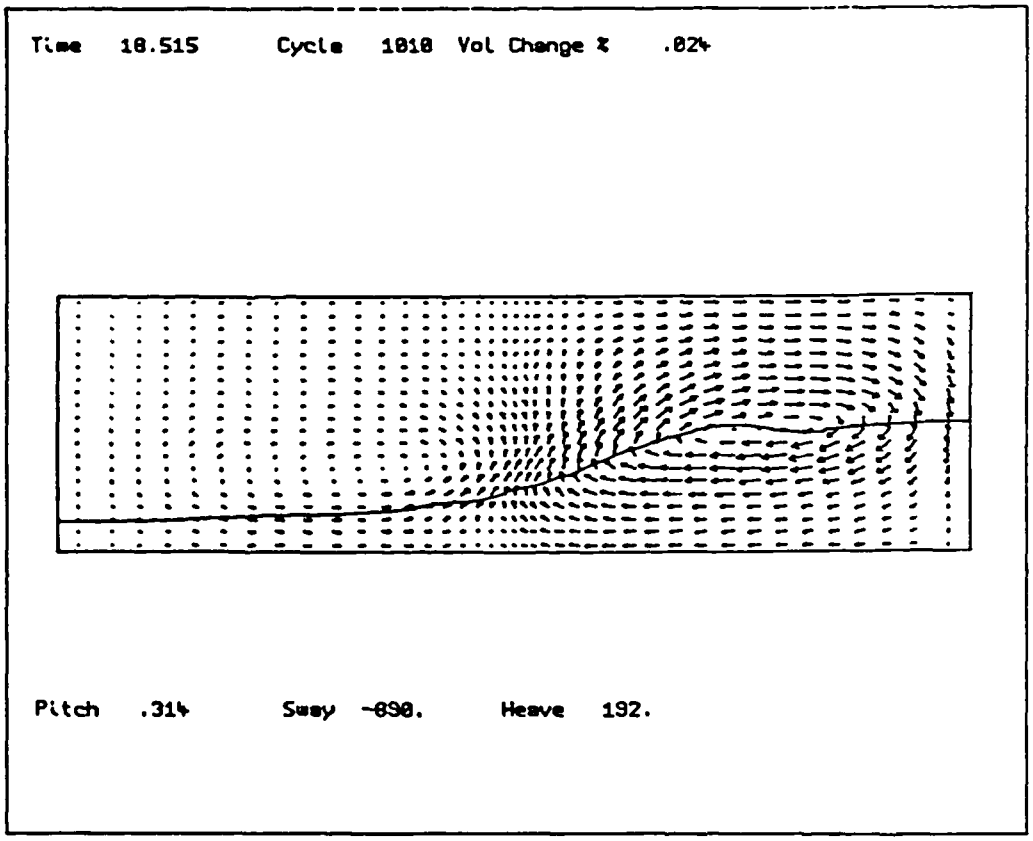

Graph 12.14f: Simulation of oil/water unbaffled vessel for pitch forcing motion at 9.17 secs, ±2.9°.Water fill depth 180mm. At time 18.5 seconds.

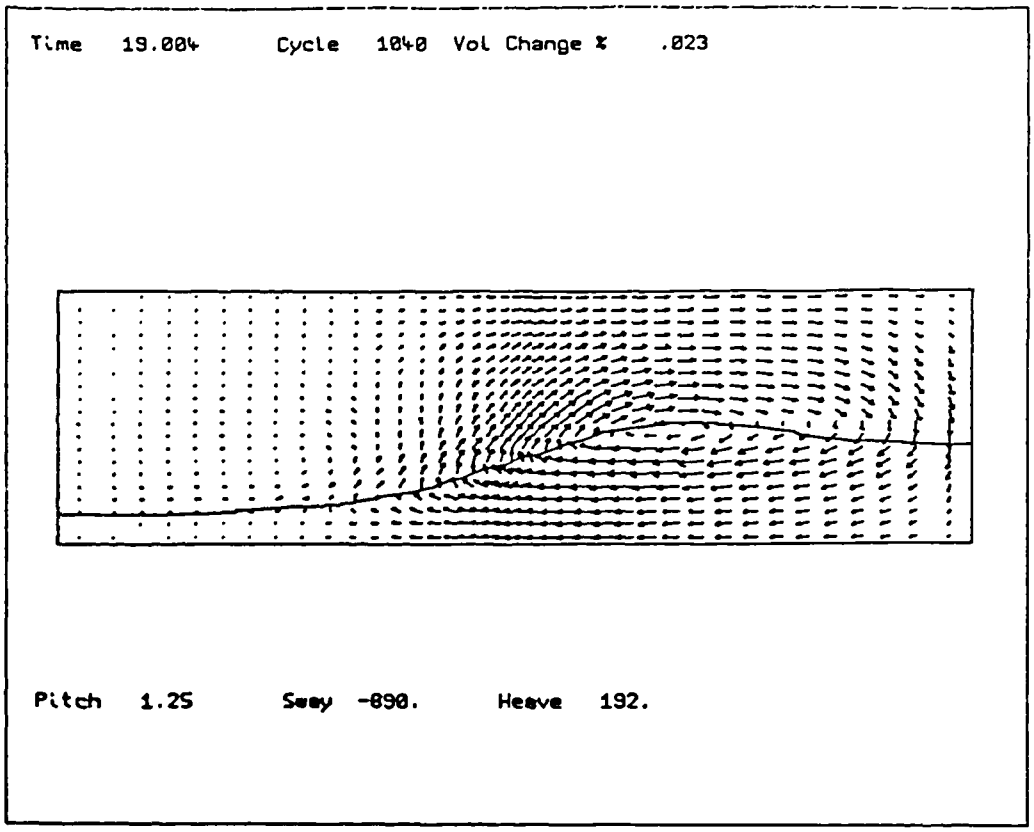

Graph 12.14g: Simulation of oil/water unbaffled vessel for pitch forcing motion at 9.17 secs, ±2.9°.Water fill depth 180mm. At time 19 seconds.

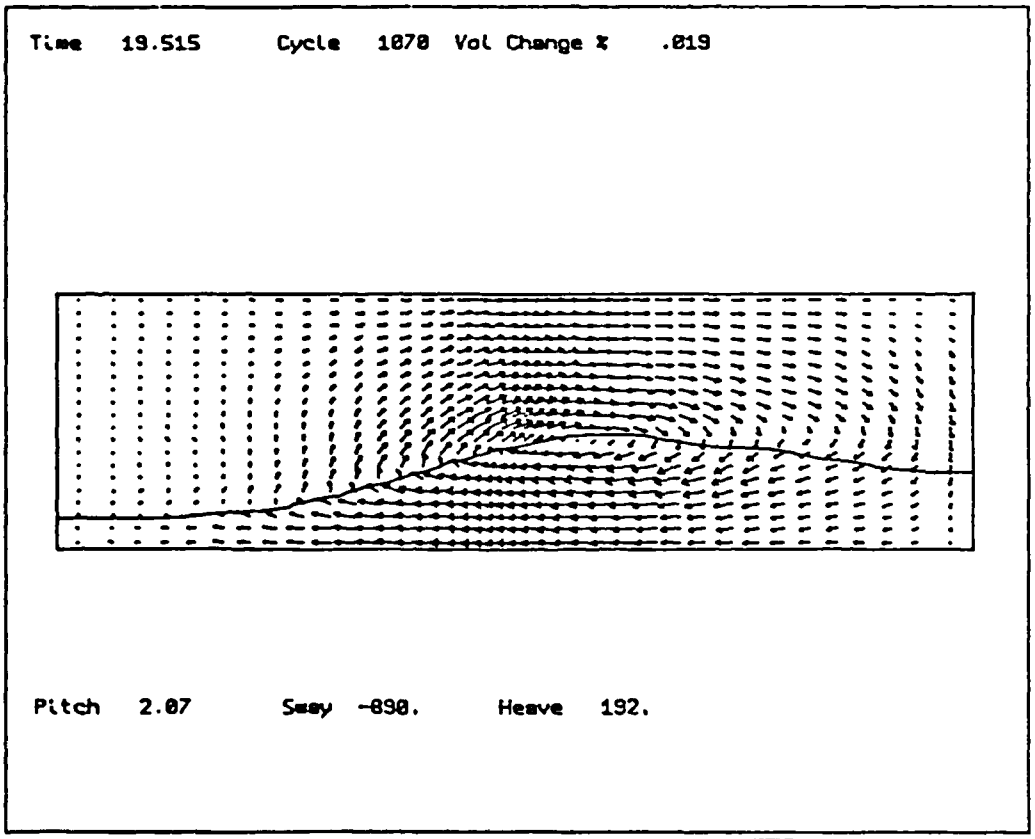

Graph 12.14h: Simulation of oil/water unbaffled vessel for pitch forcing motion at 9.17 secs, ±2.9°.Water fill depth 180mm. At time 19.5 seconds.

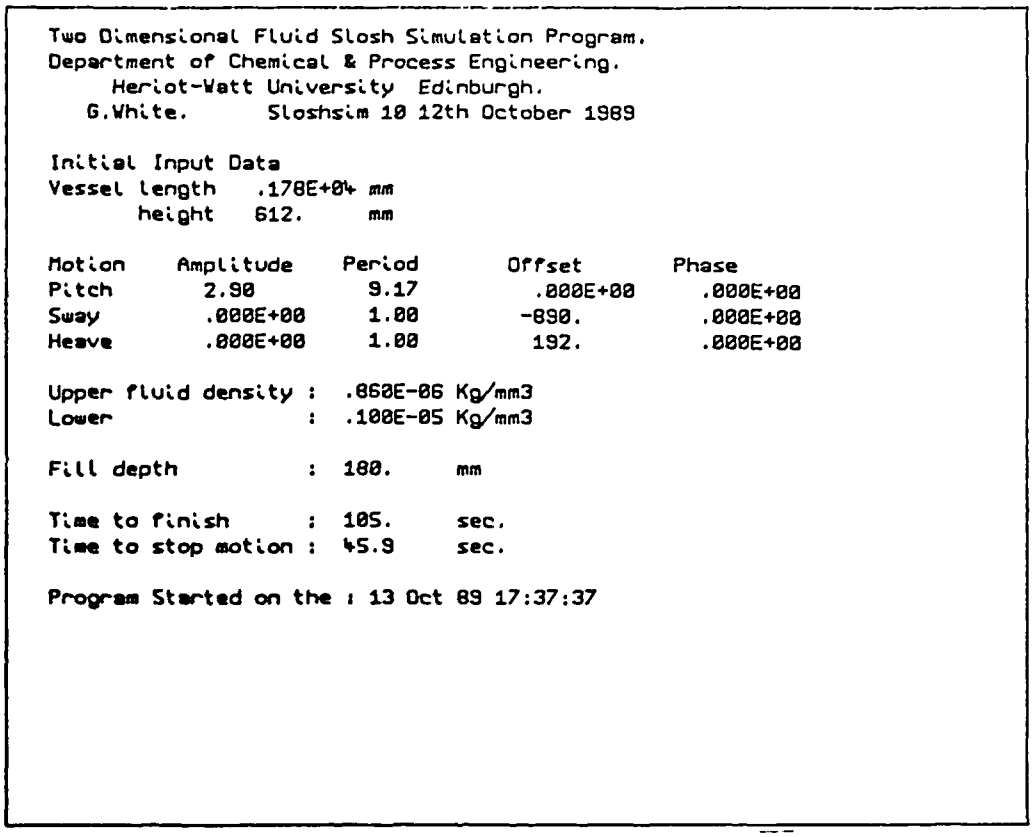

Graph 12.15a: Simulation of oil/water baffled vessel for pitch forcing motion at 9.17 secs, ±2.9°.Water fill depth 180mm. Initial information screen.

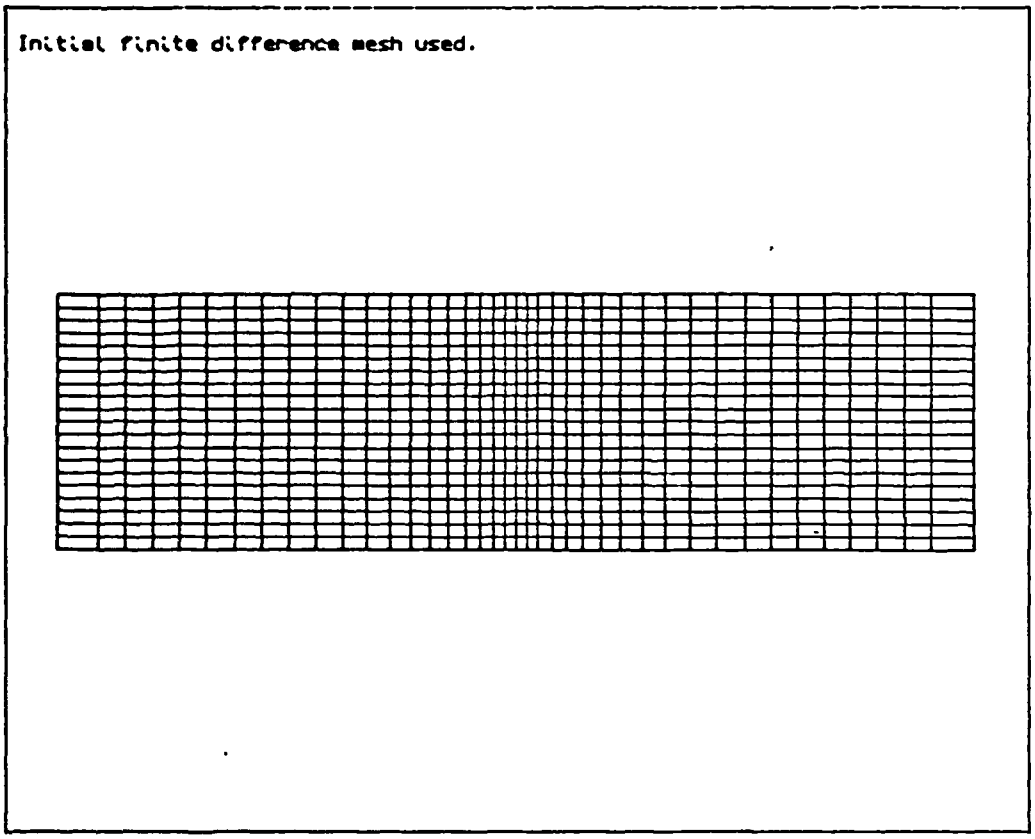

Graph 12.15b: Simulation of oil/water baffled vessel for pitch forcing motion at 9.17 secs, ±2.9°.Water fill depth 180mm. Initial mesh configuration.

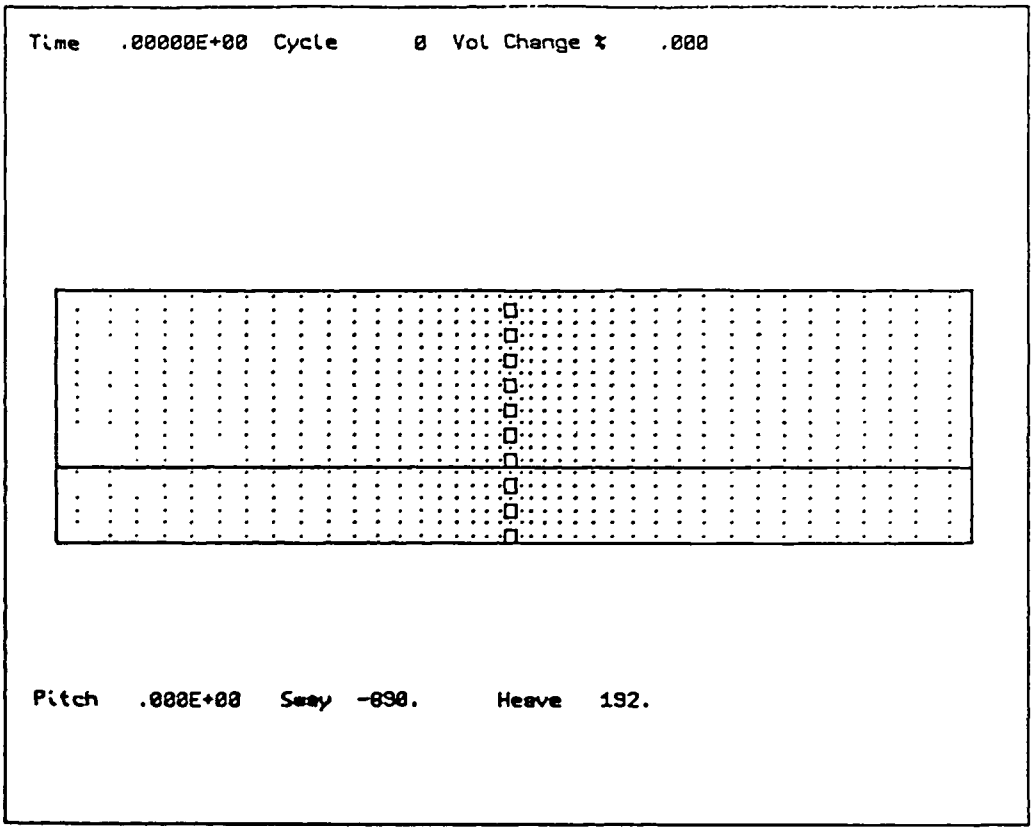

Graph 12.15c: Simulation of oil/water baffled vessel for pitch forcing motion at 9.17 secs, ±2.9°.Water fill depth 180mm. At time 0 seconds.

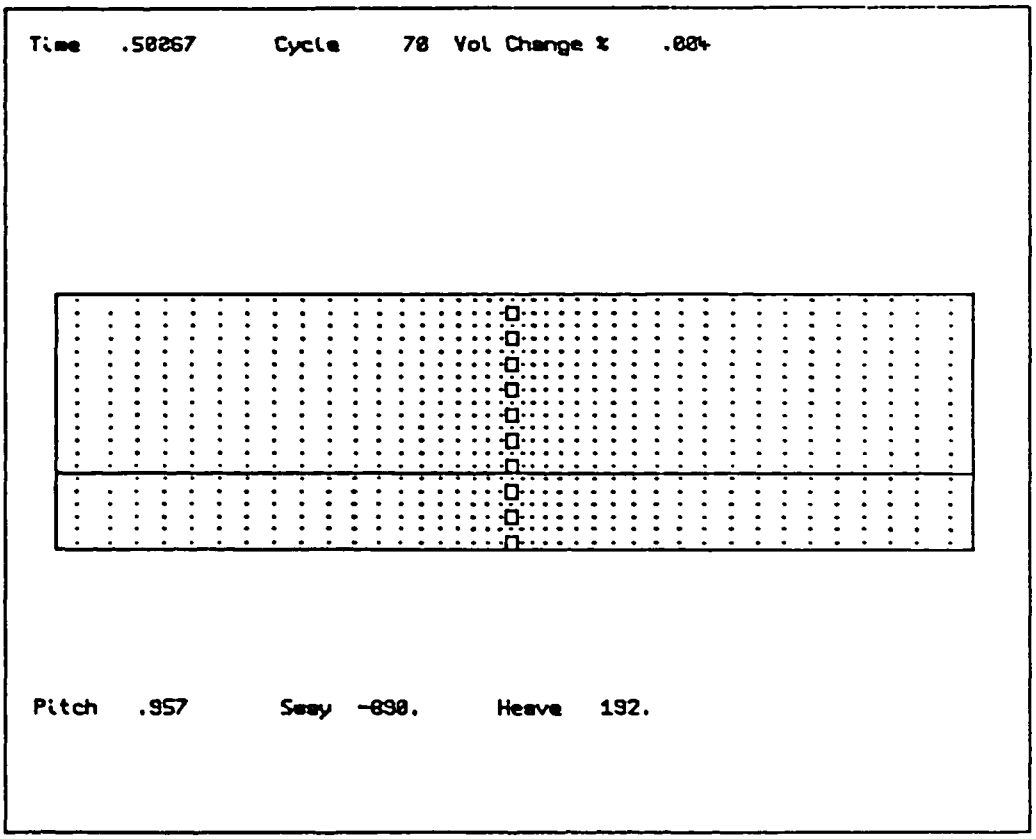

Graph 12.15d: Simulation of oil/water baffled vessel for pitch forcing motion at 9.17 secs, ±2.9°.Water fill depth 180mm. At time 0.5 seconds.

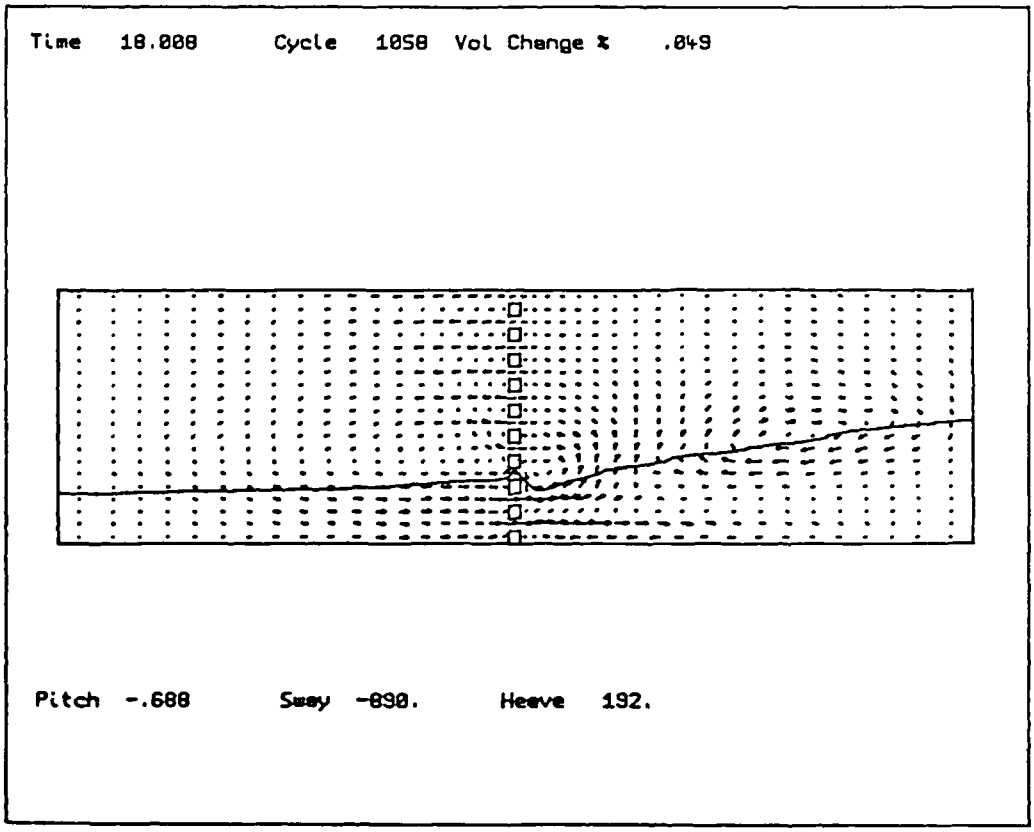

Graph 12.15e: Simulation of oil/water baffled vessel for pitch forcing motion at 9.17 secs, ±2.9°.Water fill depth 180mm. At time 18 seconds.

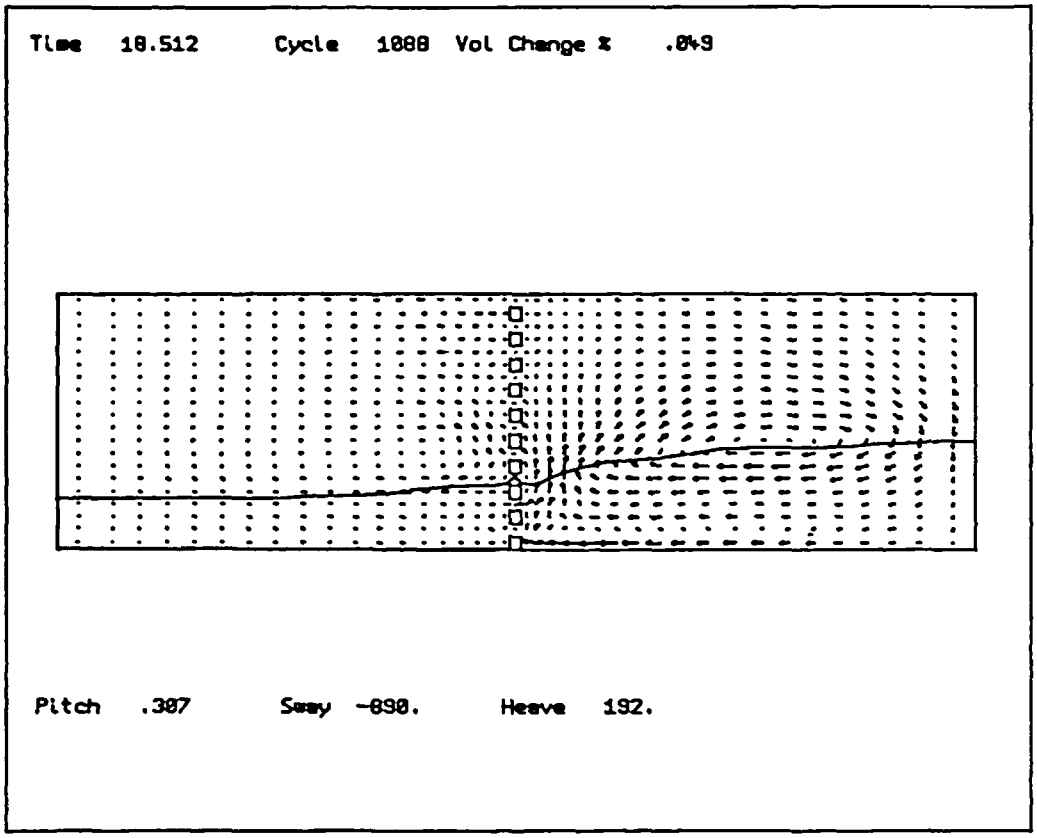

Graph 12.15f: Simulation of oil/water baffled vessel for pitch forcing motion at 9.17 secs, ±2.9°.Water fill depth 180mm. At time 18.5 seconds.

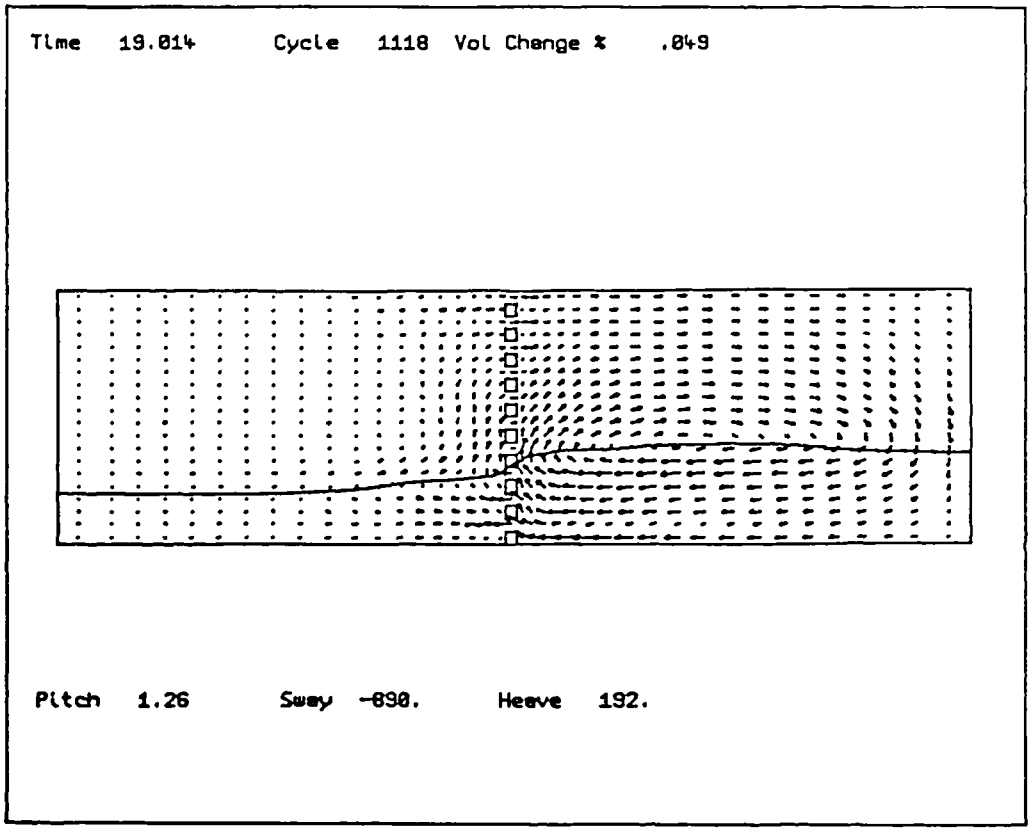

Graph 12.15g: Simulation of oil/water baffled vessel for pitch forcing motion at 9.17 secs, ±2.9°.Water fill depth 180mm. At time 19 seconds.

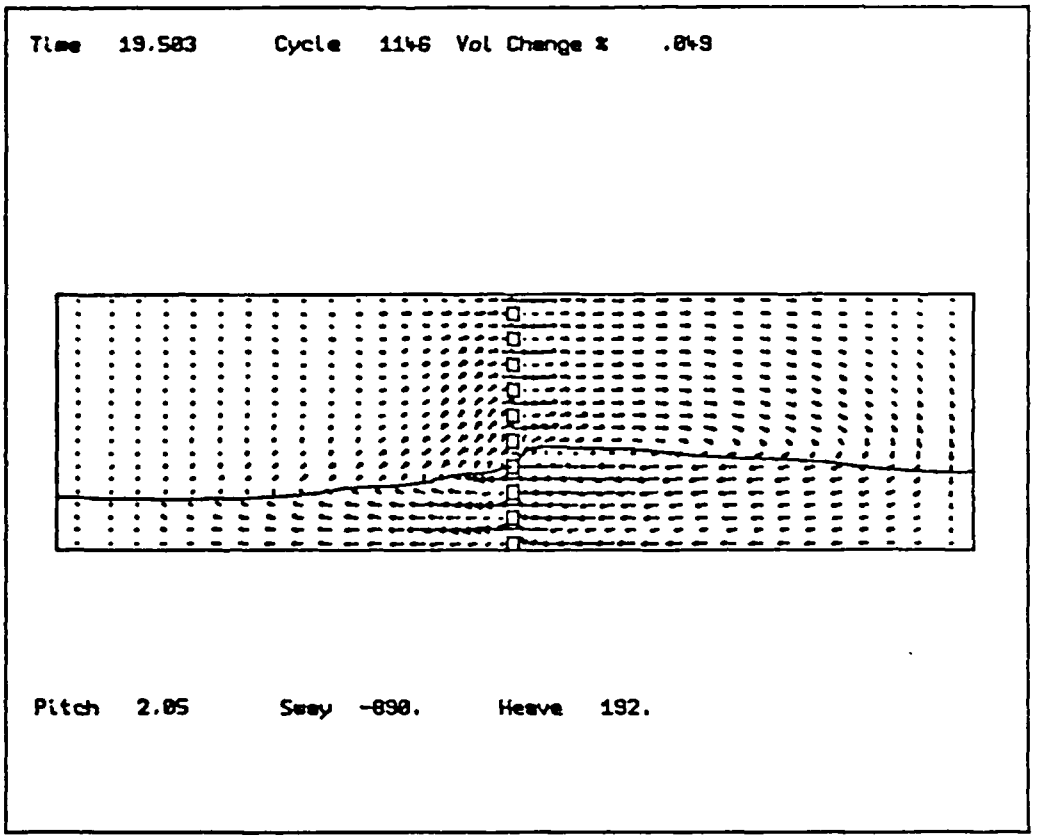

Graph 12.15h: Simulation of oil/water baffled vessel for pitch forcing motion at 9.17 secs, ±2.9°.Water fill depth 180mm. At time 19.5 seconds.

Water Fill Depth (mm)	Oil Density (Kg/m^3)	Predicted Natural Period Modes		Graph
		Mode 1 (sec)	Mode 2 (sec)	
87	851	5.96	2.36	12.1/3
174	851	5.69	2.31	12.2/4
87	890	6.99	2.78	12.5
174	890	6.71	2.72	12.6

Table 12.1: Predicted natural periods for simulation comparison experiments in the small rectangular vessel at different water fill depths.

Notes: 1) Predicted natural periods apply to those from equation 4.19 for the oil/water interface for a two fluid system.

2) Comparison results from physical experiments were presented in chapter 9.

3) Predicted natural periods for physical experiments was presented in chapter 9, table 9.1.

Water Fill Depth (mm)	Predicted Natural Period Modes		Graph
	Mode 1 (sec)	Mode 2 (sec)	
180	8.85	3.48	12.7
360	7.90	3.32	12.8

Table 12.2: Predicted natural periods for oil/water simulation comparison experiments in the large rectangular vessel at different water fill depths.

Notes: 1) Predicted natural periods apply to those from equation 4.19 for the oil/water interface, for a two fluid system.

2) "Gas Oil" density was 860 Kg/m^3

3) Comparison results from physical experiments were presented in chapter 10, graph 10.1 for which the oil fill depth was 535mm.

Water Fill Depth (mm)	Predicted Natural Period Modes	
	Mode 1 (sec)	Mode 2 (sec)
180	2.72	1.01
360	2.01	0.89

Table 12.3: Predicted natural periods for air/water simulation comparison experiments in the large rectangular vessel at different water fill depths.

Pitch Forcing Period (sec)	FFT Frequency Component Data					
	Mode 1		Mode 2		Mode 3	
	Period (sec)	Amp (mm)	Period (sec)	Amp (mm)	Period (sec)	Amp (mm)
0.9	6.99	3				
	6.99	4				
2.1	2.03	8	6.99	3		
	6.99	3	2.03	1		
3.0	3.15	6	6.99	3		
	6.99	6				
4.2	4.16	14	6.99	5		
	6.99	9	3.59	2		
5.0	5.50	31	2.53	3	2.97	2
	6.99	12	3.59	2		
5.8	6.15	44	3.15	14	3.85	4
	6.99	15	3.35	3	3.59	2
7.0	8.08	50	3.59	14	2.41	5
	6.99	17	3.59	6	2.03	1
7.9	9.59	38	4.16	10	2.66	2
	6.99	10	3.59	4		
9.1	9.59	42	4.53	5	1.82	2
	6.99	10	3.59	4		
9.9	11.78	36	4.97	3		
	6.99	8	3.59	2		
11.1	11.78	29	4.16	2	5.50	1
	6.99	9	3.59	2		
11.9	15.27	26	6.99	5	4.53	2
	6.99	7	3.59	1		

Table 12.4: FFT analysis of simulation wave profile data during pitch forcing at $\pm 4°$ amplitude and various periods. Probe 2 in the small rectangular container with oil FK851 and water to depth 87mm. First line corresponds to duration of applied motion, the second to decay.

Pitch Forcing Period (sec)	FFT Frequency Component Data Mode 1 Period (sec)	Mode 1 Amp (mm)	Mode 2 Period (sec)	Mode 2 Amp (mm)	Mode 3 Period (sec)	Mode 3 Amp (mm)
0.9	9.59	4				
	9.59	6				
2.1	9.59	7	2.03	4		
	9.59	11	4.97	1		
3.0	3.15	16	9.59	7	4.97	2
	9.59	11	2.97	2	4.97	1
4.2	4.16	9	9.59	8	2.03	2
	9.59	13	3.85	4	4.97	2
5.0	5.50	19	9.59	16	3.59	2
	9.59	21	4.97	4	3.85	2
5.8	6.15	24	9.59	23	4.97	6
	9.59	27	4.97	4	3.85	2
7.0	8.08	62	4.16	7	3.59	6
	9.59	35	4.53	5	5.05	3
7.9	9.59	108	4.16	23	37.48	3
	9.59	45	4.53	7	4.97	4
9.1	9.59	120	4.97	36	6.15	6
	9.59	48	4.53	11	5.50	7
9.9	11.78	123	5.50	41	3.59	12
	9.59	32	5.50	11	4.53	4
11.1	11.78	102	5.50	20	3.85	10
	9.59	31	4.97	6	5.50	4
11.9	15.27	86	6.15	17	4.97	5
	9.59	31	4.97	6	5.50	4

Table 12.5: FFT analysis of simulation wave profile data during pitch forcing at ±4° amplitude and various periods. Probe 2 in the large rectangular container with "gas oil" and water to depth 180mm. First line corresponds to duration of applied motion, the second to decay.

Pitch Forcing Period (sec)	FFT Frequency Component Data Mode 1 Period (sec)	Mode 1 Amp (mm)	Mode 2 Period (sec)	Mode 2 Amp (mm)	Mode 3 Period (sec)	Mode 3 Amp (mm)
0.9	1.00	14	0.50	9	0.51	3
	2.80	5	1.04	3	1.46	2
2.1	2.03	51	1.02	6	2.41	5
	2.80	12	1.46	6	2.11	4
4.2	4.16	86	2.03	13	0.58	6
	2.80	6	1.46	6	3.85	6
5.0	5.50	53	3.15	6	2.53	5
	2.80	10	4.97	3	1.46	3
5.8	6.15	41	2.97	7	1.54	2
	2.80	11	6.99	3	1.42	2
7.0	8.08	41	2.80	6	3.35	3
	2.80	12	8.08	4	1.42	2
7.9	9.59	35	2.80	7		
	2.80	14	1.42	1		
9.1	9.59	42	2.80	4	3.35	1
	2.80	14	1.38	2		
9.9	11.78	44	2.80	5	3.59	2
	2.80	12				
11.1	11.78	39	2.80	3	3.59	1
	2.97	5	3.85	1		
11.9	15.27	39	2.80	4	3.59	2
	2.97	2				

Table 12.6: FFT analysis of simulation wave profile data during pitch forcing at ±4° amplitude and various periods. Probe 2 in the large rectangular container with air and water to depth 87mm. First line corresponds to duration of applied motion, the second to decay.

CHAPTER 13.

GENERAL DISCUSSION AND APPLICATION OF EXPERIMENTAL RESULTS TO THE EFFECTS OF SEA MOTION ON OFFSHORE PROCESS EQUIPMENT.

13.1 INTRODUCTION.

The main objective of this research project was to study the effects of sea motion on the interface between gas/oil and oil/water layers, representing those in non-segregated oil/water storage tanks and gas/oil/water separators on floating production systems. Following definitions in chapter 3, these two items of offshore equipment involve the effects of forcing motion (i.e. *sloshing*) on single, twin and three fluid systems.

During this project, fundamental data on sloshing was gained from air/water experiments conducted in two rectangular vessels. Interface amplitudes and wave frequency spectra were measured using a computer based data logging system. Later, experiments with air/oil/water were carried out, recording interface profiles on video tape, and measuring the amount of oil transferred to water as a result of forcing motion. A numerical model was developed in an attempt to predict fluid behaviour.

This chapter presents a general discussion of the effects of forcing on single, twin and three fluid systems. The effects of baffles and comparisons with the numerical model will be made where appropriate.

13.2 EFFECTS OF FORCING MOTION IN A SINGLE FLUID (AIR/WATER) SYSTEM.

13.2.1 Introduction.

From experiments in this project, the effects of forcing motion on a single fluid (air/water) system, comply with findings published by previous workers. Unlike previous studies, this project investigated the effect of combined forcing motions (e.g. pitch and roll) and the influence

of baffles on interface amplitude. The frequency analysis (by Fast Fourier Transform) of wave profile data from single and combined forcing motion data, was found to be a very useful analysis technique.

The numerical model was found suitable for predicting single fluid behaviour. Numerical stability became a problem close to air/water resonance forcing periods.

13.2.2 General Interface Behaviour in an Unbaffled Vessel.

The air/water experiments discussed in chapters 7 and 8 for the unbaffled vessel, resulted in a classic interface response to forcing i.e. air/water interface amplitude approaches a maximum value as forcing period approaches the natural period predicted from linear theory (equation 4.19). This is the condition of *resonance.*

Linear theory does not predict one natural period but an infinite number of modes, although in practice only the first mode is of any major significance (84). Linear theory also predicts infinite fluid response (e.g. interface amplitude, velocities) when forcing period equals any natural period mode (i.e. n=1,2,3.. in equation 4.15). However in practice, interface amplitude reaches a maximum value, usually accompanied by breaking waves. All previous investigations of single fluid sloshing (e.g. 2,7,9,38) have concluded that interface amplitude peaks at these *harmonic* modes. In addition, Dodge et al (7) quoted the existence of *super-harmonic* modes i.e. a resonant type response at forcing periods *higher than predicted natural period.* During this project, evidence for super-harmonic modes occurred only for surge forcing motion in the large rectangular vessel (section 8.3).

The shape of the air/water interface during forcing was found to depend on liquid fill depth and forcing conditions. From both published work and experimental results, wave profiles may be summarized as :

1) Resonant forcing at low fill depths ($h/l<0.2$) produces hydraulic jumps while standing/travelling waves develop at high fill depths ($h/l>0.2$). During the experiments with the large vessel, as fill depth to length ratios were all less than 0.2 (i.e. 175/1780 & 360/1780) only hydraulic jumps occurred at resonance. In the small rectangular vessel, predicted resonant forcing periods for high fill depths were too short to be studied on the motion simulator (e.g. Ω=1.55 secs for 139mm fill depth).

2) Close to resonance, the air/water interface adopts a standing/travelling wave profile. Further from resonance, a smooth flat profile develops similar to a *spirit level response* i.e. the water surface remains horizontal for any vessel angle.

Although previous investigations have usually applied a single forcing motion, offshore platforms may be subject up to six degrees of freedom (figure 2.5). Two or three of these motions may dominate depending on platform design. Lou et al (40) derived a two dimensional non-linear sloshing theory in which combined forcing motions (e.g. surge/heave/pitch, sway/heave/roll) had a negligible effect on fluid response at resonance. Chapter 8 presented experiments on the effect of combined pitch/surge and pitch/roll on interface amplitude. These results can be summarised as :

1) For combined pitch & surge, interface amplitude may be increased if surge acts in the same direction (phase) as pitch i.e. resultant accelerations are additive.

2) The addition of roll to pitch forcing motion has the effect of reducing interface amplitude.

The degree of increase or decrease in interface amplitude was found to depend on forcing amplitude and proximity of pitch forcing period to the vessels natural period.

In addition to interface amplitude data, wave profiles were also analyzed by Fast Fourier Transform (FFT) to determine the wave *frequency spectra*. Table 8.3 and 8.4 presented the first three *major frequency components* for the duration of forcing and decay profiles resulting from single pitch and surge forcing motions. These results showed two important effects. Firstly, a slight difference occurs between measured (by FFT analysis) and predicted natural periods e.g. 10% in the case of 175mm fill depth (table 8.3). This difference could be due to data processing errors, differences in water fill depth or even failure of the prediction. Previous workers (44,63) have suggested that interfacial tension should be included into the prediction for natural period. However, following discussions presented in chapter 12 it is suggested that interfacial tension has a negligible effect on natural period. The discrepancies between predicted and measured natural periods are therefore thought to be due to slight errors in the FFT technique.

The second result from FFT analysis, concerns the composition of the wave profile frequency spectra. During forcing, the wave profile was found to contain frequency components due to both forcing motion and natural period modes. The equation of the free surface profile derived here from linear theory (chapter 4) supports this basic form. To derive equations for linear and in some cases non-linear theory, previous workers (5,7,10,38,47-49) assume a *time factor* to be of similar form to the forcing motion. As a consequence, such equations cannot predict natural period components in wave frequency spectra.

Linear theory, both derived here (in chapter 4) and by previous workers, appears deficient in two aspects. Firstly, linear theories break

down close to resonance, regardless of forcing amplitude. This is possibly due to the application of the kinematic free surface boundary condition, where particles of fluid on the free surface stay at the free surface (74). Clearly at resonance, particles of water will not remain on the air/water interface. It is interesting to note that non-linear theories which apply the kinematic boundary condition, break down close to resonance. Other theories such as that due to Verhagen & Wijngaarden (54) do not apply this condition and can predict resonant behaviour.

The second aspect of linear theory is the inability to predict non-steady state effects such as *start-up effects*. Experiments in chapter 8, suggested start-up effects were governed by the amplitude of natural period components, which were in turn related to viscosity. The equations for free surface profile derived from simple linear theory (chapter 4 equations 4.14, 4.17), neglected fluid viscosity and therefore cannot predict such start-up effects.

13.2.3 General Interface Behaviour in a Baffled Vessel.

Baffles have been used previously to reduce the effects of sloshing in spacecraft (6) and offshore separators (1). Chapter 8 discussed experiments with three types of baffles, perforated baffles of 22% and 53% free area, a solid plate baffle and two *interfacial* baffles.

Although Rush et al (23) suggested that baffles shift natural periods, results presented in graphs 8.9 and 8.10 suggested that baffles simply *reduce* interfacial amplitude around resonance. The reduction of interface amplitude depends on baffle type and location. With regards resonant forcing periods with baffles, the experimental results indicate that resonance based on the unbaffled vessel, results in worst case sloshing i.e. the baffle does not shift the natural period response. Measurement of natural periods for all baffles showed that the period of

decaying wave motion was equivalent to the second natural period mode, predicted for the unbaffled vessel i.e. the natural period predicted from equation 4.15 with n=2. It might be expected that baffles at the vessel centre would half the vessel and subsequent modes would be based on half lengths. Table 8.9 indicates that predicted full length 1^{st} and 2^{nd} modes were 2.77 and 1.02 seconds and those based on half vessel length were 1.44 and 0.63 seconds (vessel of length 1.78m, fill depth 175mm). Measured natural periods for the unbaffled vessel were 2.97 and 1.5 seconds, the 1^{st} mode for the baffled vessels were 1.5 seconds. There are two suggestions to support the statement of 2^{nd} full length modes :

1) Assuming that the unbaffled vessel recorded 1^{st} and 2^{nd} natural modes, then the baffled vessel must be recording full length 2^{nd} modes. However, through some non-linear action it may be that unbaffed results record both 1^{st} period modes based on full and half vessel length.

2) The FFT analysis produces first natural period modes which are higher than those predicted by equation 4.15. Therefore, it may be expected that second natural period modes will also be higher. Hence, it is suggested that a result of 1.5 seconds corresponds to 1.02 seconds.

3) Perforated baffles fully immersed in water might result in half length period modes since the vessel will be essentially halved. However, the same natural period data was measured for the solid plate touching the water surface and the interface baffles. It is suggested that baffles touching the water surface do not half the vessel.

Further investigation is required to measure natural periods for baffles at other locations before the further discussions can be made.

The condensed FFT profile results (chapter 8) show that baffles quickly reduce interface amplitude once forcing motion has ceased. Compared with any other baffle, the solid plate baffle placed halfway into the water showed increased damping. What may be surprising is that interface baffles appeared to increase damping to the same degree as the other more extensive and complex baffles. It is therefore suggested that any obstacle which removes wave motion on the air/water, provides an effective wave damper.

13.2.4 Comparison Between Physical and Simulation Experiments in an Unbaffled Vessel.

The methods used to derived non-linear expressions for fluid behaviour were shown to be complex (chapter 3) and unable to deal with internal obstacles. Various numerical methods have been used (3,13,14,30) to predict fluid response to forcing in a variety of two and three dimensional vessels. As described in chapter 4, modifications to the numerical model developed by Nichols et al (17) (SOLA-VOF) introduced sloshing through a rotating reference frame. Subsequent *simulation experiments* on both small and large rectangular vessels produced similar trends to physical air/water results.

From air/water simulation experiments, interface amplitude approaches a maximum finite value as forcing period approaches the first natural period mode. Unfortunately for conditions close to resonance with low water fill depths, numerical instability caused the simulation to fail. For these fill depths, physical experiments have shown that hydraulic jumps form with *strength/amplitude* increasing as the forcing period approaches the natural period. Away from resonance, the air/water interface is free from breaking waves. As simulation failure coincides with the development of a the hydraulic jump, it appears that the program

has difficulty in dealing with air/water mixing. Possible solutions to this breakdown were discussed in chapter 12.

As regards the FFT analysis of simulated air/water wave profiles (table 12.6), both forcing and natural period components appear in the frequency spectra during forcing. It was encouraging to see that this prediction agrees with the physical observations noted in chapter 12.

Although the simulation reproduces some physical results, there appear to be several deficiencies in the code. The basic sloshing equations derived in chapter 4 in which density is variable, suggest additional terms in the *Navier-Stokes* equation. Such a system of equations has been used by Daly (92) to study *Rayleigh-Taylor* Instability i.e. a heavier fluid on top of a lighter one. In the numerical model, the Navier-Stokes equations are applied with a constant density throughout the finite difference mesh. It is only through the volume of fluid function that SOLA-VOF changes fluid density across the interface. Although it may be argued that SOLA-VOF cannot correctly deal with mixing of two fluids, it is suggested that density terms only affect fluid interfaces i.e. the boundary between one homogeneous fluid and another. This may be the reason why special boundary conditions within SOLA-VOF can predict air/water resonance.

A second deficiency with SOLA-VOF regards the single viscosity input value. As in the case of density, the Navier-Stokes equations as applied in the program do not consider a variable fluid viscosity i.e. one viscosity value covers both fluids. All simulation experiments were conducted with the viscosity value corresponding to water. Further investigation into the action of viscosity on the air/water interface is required.

13.3 EFFECTS OF FORCING MOTION IN A TWIN FLUID (OIL/WATER) SYSTEM.

13.3.1 Introduction.

For an oil/water filled vessel, linear theories (equations 4.19 and 3.17) predict longer natural periods (graph 4.3) than the equivalent air/water system (i.e. same water depth). The same theories also predict infinite oil/water interface amplitude at resonance. Several experiments were conducted in the small rectangular vessel to study the effects of forcing on oil/water interface amplitude. Attention was paid to the shape of the interface, the effects of oil density and oil/water fill depths.

A frequency analysis of oil/water profiles was only obtained from simulation experiments as physical experiments were recorded on video tape for one forcing cycle. However, the numerical simulation of oil/water sloshing did allow frequency spectra to be determined.

13.3.2 General Interface Behaviour.

The results of oil/water experiments presented in chapter 9, show the general trends suggested by linear theory i.e. increasing oil/water natural periods for increasing oil density. Theoretically, as oil density approaches that of water, the oil/water interface becomes unstable. In physical terms, this might suggest that the smallest movement of the container would lead to oil/water mixing (93).

Although the basic effects of forcing period on interface amplitude occur in both oil/water and air/water systems, there are some important differences. Unlike air/water, maximum oil/water interface amplitude occurs at longer forcing periods than predicted natural periods. However like air/water systems, measured natural periods agree with predicted ones (equation 4.19). Linear theory however, predicts that maximum interface response occurs when forcing and natural periods are equal (i.e. resonance). One possible reason for this discrepancy may be related to the

formation of bubbles on the oil/water interface. As shown in chapter 4, natural period heavily depends on density ratio between two fluids. Therefore, changes in density along the oil/water interface via bubble formation would change the *local density* along the oil/water interface. Then, with the onset of resonance, *interfacial density* rather than bulk density would determine resulting fluid behavior. Indeed, the quantity of bubbles produced and hence degree of density change, may be related to forcing amplitude e.g. higher amplitude may produce more bubbles.

A further difference between oil/water and air/water experiments concerns the shape of the interface :

1) For oil/water resonance at a low fill depth (h/l=0.1), a *solitary travelling wave* was observed (photographs 9.3a-b). On the tip of this wave, vortices formed producing *bubbles of oil-in-water and water-in-oil.* These bubbles were found to disperse quickly once forcing motion had ceased. The formation of bubbles of oil-in-water and water-in-oil has not been reported in the literature, although similar characteristics exist with oil/water interfacial breakup in oil slicks (94).

2) At resonance for high fill depth (h/l>0.2), an *inverted solitary travelling wave* developed. Bubbles were seen to form from vortex action below the wave tip.

As air/water resonance is characterised by a hydraulic jump, then oil/water resonance is characterised by a solitary travelling wave. It should also be noted that a hydraulic jump can be considered as a *special* travelling wave (8). Comparing, in general, the behaviour of air/water with oil/water systems, it is suggested that air/water is a special case of a two fluid system

13.3.3 Comparison Between Physical and Simulation Experiments.

Comparisons between oil/water physical and simulation experiments presented in chapter 12 are perhaps better than those for air/water experiments.

As with oil/water physical experiments, the numerical model shows maximum interface amplitude occurs at forcing periods higher than predicted natural periods. With both maximum interface amplitude and corresponding forcing periods, predicted and measured values compare well. Unlike air/water simulation, oil/water resonant behavior is numerically stable.

From earlier discussions on single fluid systems, instability may be related to density changes along the air/water interface. With oil/water systems, density differences are small hence the simulation produces a stable solution at resonance. This provides further support that SOLA-VOF code should use modified boundary conditions along a gas/liquid interface.

However, there appears to be a major difference between simulation and physical oil/water experiments, as regards natural period. Physical experiments show good agreement between measured (by observation) and predicted natural periods (equation 4.11). However, the simulation natural periods determined by FFT frequency analysis, do not agree with predicted natural periods. It is suggested that errors exist in the FFT analysis technique which fail to resolve long period components i.e. those above 6 seconds. This inability was seen in the failure of the FFT to match long forcing period motions with wave spectra (tables 12.5 and 12.6). Additional support for inaccuracies in the data processing system arise from differences between predicted and measured air/water natural periods (section 13.3).

As regards the oil/water interface profile at resonance, the simulation produced a solitary travelling wave similar in shape to that seen in physical experiments. Graphs 12.14a-h presented an example of simulation oil/water interface profiles, resulting from resonant pitch forcing motion at ±2.9° amplitude. Important points from these velocity profile graphs may be summarised as :

1) The simulation showed no sign of vortex action along the oil/water interface. At the expense of computer time, it is suggested that an increased mesh resolution would produce signs of vortex action. It is also suggested that increased mesh resolution may indicate transport of material from one phase to the other.

2) A *circulation velocity profile* exists round the region where vortex action would be expected. It is suggested that opposing velocity components, one in oil and the other in water layers, lead to vortex action.

3) Velocity profile plots show that on either side of the travelling wave the velocity vectors are in opposing directions. This profile agrees with the behaviour of a breaking wave (95).

13.4 EFFECTS OF FORCING MOTION IN A THREE FLUID (AIR/OIL/WATER) SYSTEM.

13.4.1 Introduction.

In offshore separators and storage systems, it would be expected that above the oil layer some sort of inert blanketing or gas cap would be present. To study the effects of a gas cap, experiments were conducted at different oil and water fill depths in both vessels. Experiments discussed in chapter 10, were also conducted on the large vessel to study the effect of baffles.

Additional experiments were conducted on the large vessel, to determine the transfer of material from the oil layer to the water, as a

result of forcing. Two methods were used, firstly benzoic acid transfer and secondly, the measurement of oil content of water.

13.4.2 General Interface Behaviour in an Unbaffled Vessel.

Close to oil/water resonant forcing periods, a three fluid (air/oil/water) system was found be behave in two distinct parts, one part due to air/oil and the other to oil/water. The results presented in chapters 9 and 10 showed that general oil/water interface behaviour is similar to that in a two fluid system in two respects :

1) Oil/water interface amplitude peaks at forcing periods slightly higher than natural periods predicted from equation 4.19. This appears to be a common feature of oil/water experiments, not of air/water experiments.

2) The second common feature between two and three fluid oil/water systems concerns the shape of resonant waves. A three fluid system was seen to produce a normal solitary travelling wave at high oil/low water fill depth and an inverted wave at low oil/high water fill depths.

Dealing with the effect of forcing on the upper air/oil interface, linear theory predicts natural periods of similar values to those for air/water. Air/oil response was in fact found similar to that for air/water i.e. maximum interface amplitude occurs at resonance, with large amplitude standing waves at high liquid fill depths. However, photographs presented in chapters 9 and 10, suggested that in some cases upper air/oil resonant waves may influence lower oil/water behaviour. It is suggested that velocity profiles beneath the air/oil interface may be responsible for the observed effects. Linear theory (45) predicts that velocity profiles beneath a gas/liquid interface decrease in magnitude with

increasing depth from the interface. In a three fluid system, velocity profiles generated in the upper liquid layer, will influence those in the lower layer provided the oil depth is small.

13.4.3 General Interface Behaviour in an Baffled Vessel.

Chapter 10 presented results from experiments dealing with the effects of baffles on both air/oil and oil/water interfaces in the large vessel. Similar to air/water experiments, baffles were seen to reduce interface amplitude around resonance rather than shifting natural period. As oil/water resonance occurs at longer forcing periods than air/water, any shift in natural period due to baffles would have been noted during the experiments.

Comparisons between baffle performance, indicated that the solid plate baffle touching the oil/water interface was more effective in reducing both air/oil and oil/water interface amplitude than any other baffle tested.

In the unbaffled vessel, production of oil-in-water bubbles occurred as a result of vortices formed on the crest of the resonant travelling wave. For all baffles, including the 53% perforated baffle, bubble formation was reduced. Although the basic resonant oil/water interface profile still appeared (photographs 10.7 to 10.10), bubble formation tended to remain localized round the baffle itself. At shorter forcing periods, baffles have two effects depending on location :

1) For the 53% perforated baffle fully immersed, short forcing periods appeared to produce droplets of oil-in-water rather than bubbles. This kind of disturbance was caused by the baffle itself.

2) For baffles touching the oil/water interface, large amplitude standing waves developed. Such behaviour was observed by Thorpe (41) in resonant internal waves in stratified fluids.

13.4.4 Transfer of Oil to Water In Baffled and Unbaffled Vessels.

Oil/water resonance consists of travelling waves which produce bubbles of oil-in-water and water-in-oil. Although these bubbles were seen to disperse once forcing motion had ceased, some oil might remain in the water either as dissolved oil or suspended droplets. To gauge the potential of forcing to increase oil content of water, the transfer of benzoic acid from oil to water was measured by conductivity. Later, actual amount of oil-in-water was measured using a direct sampling technique. Chapter 11 presented techniques and results from these experiments. No corresponding analytical technique was available to assess changes in water content of the oil.

Material transfer across the oil/water interface will depend on several factors including interfacial area and fluid turbulence. Therefore, since oil/water resonance results in bubble formation, an increase in contact area and turbulence, material transfer may be expected to be higher than non-resonant forcing conditions. The benzoic acid experiments supported the concept that bubble formation increased material transfer. These experiments also demonstrated that baffles may reduce material transfer as bubble formation is reduced. However, prolonged forcing in a baffled vessel may eventually cause some material transfer.

Chapter 11 indicated that forcing increases oil content of water whilst motion is applied. Also once forcing stops, the oil content of the water decreases to an initial value. Together with published data on oil solubilities, this suggested that instead of dissolved oil, the oil-in-water experiments indicate predominantly, the presence of suspended oil drops i.e. *free oil.*

13.5 RELATION OF EXPERIMENTAL RESULTS TO THE EFFECT OF MOTION ON OFFSHORE PROCESS EQUIPMENT.

13.5.1 Introduction.

To compare experimental results with the effects of forcing motion on offshore process equipment, consideration must be given to process vessel design and to platform design.

13.5.2 Range of Applied Forcing Motions.

In scaling model data for application to LNG tankers, previous workers (2,72,73,96) have applied Froude scaling laws (chapter 3).

With surge motion, scaling can be done by ratio of forcing amplitude to vessel length. To scale pitch forcing amplitude, a literature review suggests full scale amplitudes should be applied to models :

1) Abramson et al (2) quoted periodic roll forcing motion of ±5° (3.5° RMS) and ±10° (7.0° RMS) amplitude in LNG model tests and ±2.9° RMS for full scale *random* motion. Forcing periods corresponded to resonance on a model on 1m size scaled down by 1:30 from full size.

2) Hoerner et al (27) applied full scale random pitch and roll forcing motions at maximum angles 3.66° and 6° respectively, on model absorption columns.

3) Froude scaling laws suggest overall acceleration of model and full scale should be the same. Hence, scaling motion amplitude by length ratio, maximum accelerations may allow scaling of forcing periods. In addition to periods scaled by Froude scaling laws, the condition of resonance must be covered. It is only at resonance that *worst case sloshing* occurs.

The decision to use ±4° pitch amplitude motion for all physical experiments applied throughout this project, was an attempt to cover an average forcing amplitude, based upon published data.

13.5.3 Relation of Experiments to Non-Segregated Storage Tanks.

One of the objectives of this research project was to study the effect of forcing on oil/water behavior for application to a non-segregated storage tank on a semi-submersible floating production system. In the absence of specific design details, only estimates of vessel shape and internals can made. The storage system may consist of rectangular elements with supporting internal *struts*, as in LNG cargo tanks (96). Also, oil/water fill depths would vary throughout production and the possibility of resonant oil/water forcing would be high. Following the study of a Tension Leg Platform storage system, Hisamatsu (25) suggested that the storage tank would remain full of liquid. Therefore, the storage system may be compared to experimental results from the large rectangular vessel with a high oil fill depth.

The effect of sea motion on non-segregated oil/water storage systems will then include :

1) Natural periods for an oil/water system increase as vessel length increases which may increase the possibility of vessel movement causing resonance. Consider ships cargo hold (length 34m, height 37m) (91) half filled with water and oil (ρ=860 Kg/m^3). The natural period of the oil/water interface as predicted by equation 4.18 would be 15.8 seconds. This figure is within the range of possible marine motion periods (see figure 2.6). However, the effects of actual sea conditions on the structure would have to be determined.

2) Oil/water resonant forcing produces bubbles of oil-in-water and water-in-oil close to the oil/water interface. Although these bubbles quickly disperse once forcing has ceased, continual sea motion will result in permanent suspension of oil-in-water. Therefore, water displaced from the storage area by produced oil will require separation treatment (e.g. hydrocyclone separation) prior to disposal at sea. Similarly, oil extracted for transportation to shuttle tanker may require additional processing to remove bubbles of water.

3) The experiments in this project used refined oils which separate easily from water, It may be expected therefore, that crude oils will behave differently due to their more complex composition. Then, depending on oil properties, continual oil/water interface mixing may create stable emulsions. These emulsions will require further treatment prior to oil and water storage/disposal.

4) Baffles and internals may reduce oil/water turbulence and interface amplitude, thus perhaps relaxing further processing requirements. However, baffles may increase oil/water mixing under some forcing conditions.

5) The use of baffles may assist in platform stability. One of the principle aims of baffles in single fluid (air/water) sloshing experiments is the reduction of internal forces which cause instability and may result in vessel damage. Bauer's (62) proposal of a motion damper, suggested significant internal forces maybe produced in an oil/water filled vessel. Further investigation will be required to assess possible beneficial effects of baffles on platform stability.

13.5.4 Relation of Experiments to Primary Separators.

Primary separators designed to continually separate gas, oil and water from a flowing stream present a variety of problems not associated with storage tanks :

1) The classical method to design such separators is based on the time required to coalesce oil droplets above a minimum size. It is important to maintain the designed gas/oil and oil/water fill depths and near plug flow characteristics throughout the separator.

2) Well head fluids entering the separator may consist of emulsions and particulates (e.g. sand). This effectively means that the separator is a *three phase separator* i.e. gas, liquid and solid). Further, the gas and liquid constitutes a four fluid system i.e. gas, oil, emulsion and water.

3) Collection of separated oil and water involves the spilling of oil over a weir plate and pumping the water from one side and oil from the other side. The separator then acts with continuous flow.

In addition to the physical experiments, the numerical simulation example presented in chapter 12, indicated that forcing could cause several problems in separator design.

The first problem concerns the formation of bubbles of oil-in-water and water-in-oil at resonance. These bubbles could be carried over the weir into the oil take off, or taken off in the water outlet stream. Although physical experiments indicated that baffles may reduce bubble production at oil/water resonance, baffles may promote droplet formation at short forcing periods. This describes primary and secondary turbulence (1).

Further more, the water itself can spill over the weir plate causing problems in contamination of oil, and downstream processing

equipment. Thus, it may be necessary to either reduce the water level close to the weir plate or to re-design the oil take off systems to allow a *clean* oil flow.

At the upper gas/oil interface, forcing may develop unstable (breaking) waves. These breaking waves would allow mixing of gas and oil. Although gas/oil resonance is an obvious source of unstable waves, given a sufficiently high gas velocity particles of oil may be stripped from non-resonant waves and be carried out of the separator in the gas stream. In addition, wave motion on the gas/oil interface may restrict the gas flow at some points in the separator and alter the gas velocity. This will affect demisting equipment.

CHAPTER 14.

CONCLUSIONS AND RECOMMENDATIONS FOR FURTHER WORK.

14.1 INTRODUCTION.

The response of fluid contained within a vessel to some external force, has been shown to be complex in theory and in practice. Previous investigations of motion effects on partially filled liquid containers have concentrated on single fluid (air/water) systems. Studies with three fluid (gas/oil/water) systems are few. The experiments conducted during this project have provided basic information of fluid behaviour in single, two and three fluid systems.

This chapter presents some conclusions regarding experimental and predicted effects of forcing on gas/oil/water systems. Recommendations are given to extend the numerical model and additional experiments on oil/water mixing.

14.2 CONCLUSIONS.

During this study of sea motion effects on offshore process equipment, information was collected from physical experiments with air, oil and water from two rectangular vessels at various fill depths. Motion conditions varied from single pitch and surge to combined pitch/roll and pitch/surge at various forcing periods. A pitch forcing amplitude of ±4° and surge amplitude of ±120mm was used exclusively for single forcing motion combinations in the large rectangular vessel. In the study of the effect of combined forcing motions on fluid response, various forcing amplitude and phases were applied.

The theory behind fluid sloshing was found to be complex. A new linear theory was developed which gave predictions for natural periods in single, twin and three fluid systems. This theory failed to predict the

exact free surface response as it broke down (i.e. interface amplitude reached infinite values) close to resonance. To model near resonant forcing conditions, a numerical model was developed from the SOLA-VOF algorithm. This model proved useful to study velocity profiles in addition to free surface profiles.

Over the range of conditions tested, the following conclusions can be drawn from theoretical discussions and from results of physical and numerical experiments :

1) Simple linear theory derived from velocity potential theory can suitably predict natural period modes of single, two and three fluid systems i.e. air/water, oil/water and air/oil/water respectively. The complexity of the equations increases with each additional fluid.

2) Current non-linear theories are complex and unable to deal with the effects of vessel internals on fluid behaviour.

3) Linear theory predicts that the maximum interface amplitude occurs when the forcing period equals the first natural period mode i.e. the condition of resonance. Experiments have indicated that maximum interface amplitude occurs at a forcing period somewhat higher than the first mode natural period. This may be due to interfacial mixing adjusting the effective density along the oil/water or air/water interface.

4) To predict interface profiles, analytical theories (both linear and non-linear) should derive expressions which have a frequency response containing terms due to both natural and forcing periods.

This behaviour was seen in the derivation of the new linear equation based upon Laplace transforms. Both physical and simulation experimental data supported the general from of the linear theory.

5) The numerical model developed from SOLA-VOF has proved capable of predicting both the interface amplitude and the frequency response for the air/water filled small rectangular vessel. There is good agreement between model and physical results using both oil/water filled vessels.

6) The velocity profiles from numerical model compared favourably to visual observations from physical experiments. It was not possible to compare the magnitude of velocity between physical and numerical model.

7) In an unbaffled vessel, single fluid (air/water) resonance is characterized by hydraulic jumps at low fill depths. However, further from resonance, the interface assumes a spirit level profile.

8) Pitch forcing motion produced a more turbulent air/water profile at resonance than surge motion. Presumably, this was due to differences in motion acceleration (i.e. forcing amplitude) between pitch (at $\pm 4°$) and surge (at $\pm$120mm).

9) With the addition of roll motion onto pitch, interface amplitude reduces. However, interface amplitude may increase or decrease with the addition of surge motion to pitch, depending on the phase angle

between the two. Combined pitch and surge with resulting acceleration adding, will result in a more turbulent fluid response that pure pitch or pure surge.

10) In an unbaffled vessel, twin fluid (oil/water) resonance produces only one wave form. At low water depths, a solitary (upright) travelling wave appears. At high water depths, the wave appears inverted. Mixing occurs as a result of these resonant wave forms producing droplets and bubbles of oil-in-water and water-in-oil. These bubbles are caused by shearing along the wave's crest. The numerical model predicted a circulating velocity profile around the crest of the oil/water resonant travelling wave. It is suggested that this circulation profile leads to interfacial breakup in oil/water systems.

11) Close to oil/water resonant conditions in an unbaffled vessel, a three fluid (gas/oil/water) system divides into two distinct sections. In such cases, the upper air/oil interface behaves as if the vessel were a single fluid system. This applies to the fill depths used in this study.

12) Both air/water and oil/water results have suggested that solid plate baffles immersed in liquid will reduce interface amplitude. The results from the interface baffles in air/water systems suggested that immersion depth governs baffle performance.

13) When compared to an empty vessel, reducing the free area of a perforated baffle reduces interface amplitude. Over the range of experimental conditions used in this project, a solid plate baffle

immersed in liquid performed better in reducing interface amplitudes than either the 22% or 53% free area baffle fully immersed in water.

14) The condensed FFT profiles showed that all baffles produced similar amounts of damping which were greater than that in an unbaffled vessel.

15) There remains some controversy regarding the effect of baffles on natural period. The experiments suggest that baffles remove the first natural period component from the decay waves frequency spectrum, leaving only the second.

16) Significant transfer of material from oil to water occurs only when resonant forcing is applied in an unbaffled vessel. This applies to the refined oils (gas oil and kerosene). With an oil of more complex composition (e.g. crude oil), transfer characteristics may be different.

17) All perforated and solid plate baffle configurations were found to reduce the production of oil-in-water and water-in-oil bubbles which are formed at resonance. However, at short forcing periods away from oil/water resonance, perforated baffles showed clear evidence of increasing droplet formation.

14.3 RECOMMENDATIONS FOR FUTURE WORK.

14.3.1 Introduction.

This research project, represents a preliminary study of the effects of motion on offshore processing equipment. Additional work is

required with the numerical model to improve solution method and the storage of velocity profile data. Further physical experiments are also required to study the formation of oil/water emulsions and the transfer of material across the oil/water interface.

14.3.2 Modifications to the Numerical Model.

The numerical model used in this project deals with sloshing in closed rectangular vessels. To allow simulation of an offshore gas/oil/water separator, the following modifications are suggested :

1) **Addition of a Flow Through Mesh.** The current program version deals with a confined mass of fluid and thus lacks the capability to fully simulate offshore separators. Examination of the program suggests that boundary cells may be modified to allow material transfer in and out of the finite difference calculation mesh.

2) **Extension To Three Fluids.** Physical experiments suggest that a three fluid system can be sub-divided into two twin fluid systems. However, to deal with gas separation, the program must be modified to three fluids. It is expected that such a modification would result in significant code changes.

3) **Improved Result Presentation.** Although the modifications to SOLA-VOF (chapter 4) were required to compare physical with simulation experiments, velocity profile data was useful to interpret wave profiles. At present such output has to be discarded for memory storage and transfer of files from the VAX system. It is suggested that the storage of velocity, fluid configuration and

pressure data could be compacted and additional programs written to extract the data.

14.3.3 Additional Simulation Experiments.

In light of the recommended modifications (above), further simulation experiments are suggested in addition to those involving motion effects on separators :

1) **Formation of a Databank.** With improved presentation of velocity and pressure data, it may be possible to construct a databank, relating velocity and pressure profiles to different forcing conditions. Such information could then be used by the model to predict velocity profiles at different forcing conditions.

2) **Perform scale up simulations.** Simulation experiments should be carried out on vessels of different scales and various forcing conditions. The results may provide information on correct procedures to scale both forcing and wave motion data. However, it must be recognised that increasing vessel size would require a smaller mesh size and hence the time taken to solve the entire mesh would increase. It may be that computer time will limit the size of vessel and/or forcing conditions to model.

14.3.4 Further Physical Experiments.

The experiments conducted during this project are by no means a complete investigation of forcing effects on fluid behaviour. Although the effects of forcing amplitude could be studied for a range of forcing periods, such a program would be demanding on time and resources.

For applications to offshore separators, more fundamental data is required :

1) **Mechanism of Oil Transfer.** Oil/water transfer experiments indicated a lack of knowledge regarding the transfer mechanism in the formation of suspended bubbles and droplets of oil. Studies into the factors affecting oil transfer are suggested e.g. velocity profile and oil physical properties. Such experiments would also allow study of how emulsions form as a result of interfacial turbulence.

2) **Velocity Profiles.** To study the performance of separators, the velocity profiles of both fluids during applied forcing and static conditions are required. This would provide additional comparison data for simulation experiments and indicate the conditions at which oil/water turbulence is generated. Such information could be programed into the numerical model to determine probabilities of interfacial shear.

3) **Baffles Design.** Baffles placed at the vessels centre have been shown to reduce oil/water resonant behaviour. Experiments will be required to see the effect of baffle location both along vessel length and at different immersion depths.

4) **Separator Design.** Simulation experiments suggest possible difficulties in current separator design i.e. spilling of water over the weir plate, oil bubbles in water take off stream. Further physical and simulation experiments with different separator designs may suggest suitable solutions.

APPENDIX I

LINEAR SOLUTION OF THE SLOSHING EQUATIONS.

1.1 INTRODUCTION.

This appendix presents full workings of three solutions to the sloshing equation for a closed rectangular container undergoing a sinusoidal transverse forcing motion. The wave motion is assumed irrotational and viscosity is neglected.

1.2 *SINGLE FLUID TRANSVERSE SLOSHING.*

1.2.1 Problem Description.

Single fluid sloshing refers to a situation where a vessel is partially filled with say water, the space above begin air. Here the pressure on the air/liquid interface may be taken as zero.

Consider a closed vessel which is free to move in the x-axis (Figure A1.1), then the forcing terms in equation 4.11 (chapter 4) become :

$$D = 1 = x_o \mathrm{Sin}(\Omega t+\varepsilon) = X \text{ say, } \theta = 0 \text{ and } \Omega_z = 0$$

Then :

$$\frac{da_x}{dt} = x_o \Omega \mathrm{Cos}(\Omega t+\varepsilon) = \frac{dX}{dt} = X'$$

$$\frac{d^2a_x}{dt^2} = -x_o \Omega^2 \mathrm{Sin}(\Omega t+\varepsilon) = X''$$

Neglecting viscosity, the basic sloshing equation reduces to :

$$\rho\frac{Du}{Dt} = -\frac{\partial P}{\partial x} - \rho X'' \text{ and } \rho\frac{Dv}{Dt} = -\rho g - \frac{\partial P}{\partial y} \qquad \ldots \text{ A1.2.1}$$

The linear solution of A1.2.1 now relies on the assumption that the resulting wave motion is irrotational hence a velocity potential can be applied.

Define : $u = -\frac{\partial\phi}{\partial x}$, $v = -\frac{\partial\phi}{\partial y}$

Representing the forcing and body force terms by a force potential, such that :

$$\frac{\partial\Omega}{\partial x} = -X'' \text{ and } \frac{\partial\Omega}{\partial y} = -g, \text{ then } \Omega = -X''x - gy$$

Following the usual method, the velocity potential from the sloshing equation gives :

$$-\frac{\partial\phi}{\partial t} + \frac{(u^2+v^2)}{2} + \frac{P}{\rho} - \Omega = f(t) \qquad \ldots \text{ A1.2.2}$$

The above, is the usual form of the Navier-Stokes equation as applied to wave mechanics. At this stage another simplification is made. It is assumed that the fluid velocity is sufficiently small enough to enable the velocity product terms to be neglected. Following a previous example (44) where the pressure is set to zero, A1.2.2 can be written as :

$$-\frac{\partial\phi}{\partial t} + g\eta = -xX'' \qquad \text{at } y = h+\eta \qquad \forall\ x,t$$

In the solution method the above is used as a boundary condition to the usual Laplace Wave equation.

1.2.2 Solution.

The problem reduces to :

$$\text{Solve} \quad \frac{\partial^2\phi}{\partial x^2} + \frac{\partial^2\phi}{\partial y^2} = 0 \qquad \forall\ x,y,t \qquad \ldots \text{ A1.2.3}$$

Subject to the boundary conditions :

$$-\frac{\partial\phi}{\partial y} = 0 \qquad \text{at } y = 0 \qquad \forall\ x,t$$

$$-\frac{\partial\phi}{\partial\phi} = 0 \qquad \text{at } x = 0,1 \qquad \forall\ y,t$$

$$-\frac{\partial\phi}{\partial t} + g\eta = -xX'' \qquad \text{at } y = h + \eta \qquad \forall\ x,t$$

$$\frac{\partial\eta}{\partial t} = -\frac{\partial\phi}{\partial y} \qquad \text{at } y = h + \eta \qquad \forall\ x,t$$

... A1.2.4

By separation of variables ,

$$\phi(x,y,t) = T(t)(A\text{Sin}(kx)+B\text{Cos}(ky))(C\text{Cosh}(kx)+D\text{Sinh}(ky))$$

Applying boundary conditions :

$\frac{\partial\phi}{\partial y} = 0$ at $y = 0$, then $C = 0$

$\frac{\partial\phi}{\partial x} = 0$ at $x = 0$ & 1, then $A = 0$, $\text{Sin}(kl)=0$

Then :

$$\phi(x,y,t) = \frac{T_0(t)}{2} + \sum_{n=1}^{\infty} T_n(t)\text{Cos}\left(\frac{n\pi x}{l}\right)\text{Cosh}\left(\frac{n\pi y}{l}\right)$$

The other two remaining boundary conditions are then used to solve for the unknown function of time.

Applying the dynamic conditions (equation A1.2.4c) gives :

$$-\frac{\partial^2\phi}{\partial t^2} + g\frac{\partial\eta}{\partial t} = -xX^{(3)} \qquad \text{at } y = h + \eta$$

Then the kinematic condition gives :

$$\frac{\partial^2\phi}{\partial t^2} + g\frac{\partial\phi}{\partial y} = xX^{(3)} \qquad \text{at } y = h + \eta$$

Applying Laplace transforms on the time function gives :

$$s^2\bar{\phi}(s) - s\phi(0) - \frac{\partial\phi(0)}{\partial t} + g\frac{\partial\bar{\phi}(s)}{\partial y} = xX^{(3)}(s) \qquad \text{... A1.2.5}$$

Note that :

$$X = x_o \mathrm{Sin}(\Omega t+\varepsilon) + S_o$$

$$X' = x_o \Omega \mathrm{Cos}(\Omega t+\varepsilon), \quad X'' = -x_o \Omega^2 \mathrm{Sin}(\Omega t+\varepsilon)$$

$$X^{(3)} = -x_o \Omega^3 \mathrm{Cos}(\Omega t+\varepsilon)$$

$$L\{X^{(3)}\} = - \frac{x_o \Omega^3 (s\mathrm{Cos}(\varepsilon) - \Omega \mathrm{Sin}(\varepsilon))}{(s^2+\Omega^2)}$$

Denote $\varepsilon_c = \mathrm{Cos}(\varepsilon)$ and $\varepsilon_s = \mathrm{Sin}(\varepsilon)$

The other unknown values of ϕ are found from the boundary conditions :

1) $\phi(0) = 0$ assuming no initial motion

2) $\dfrac{\partial \phi(0)}{\partial t} = xX^{(2)}(t=0)$ by virtue of A1.2.4d

Then :

$$s^2 \bar{\phi}(s) + x \Omega^2 x\varepsilon + g \frac{\partial \bar{\phi}(s)}{\partial y} = - \frac{x_o \Omega^3 (s\varepsilon_c - x\varepsilon_s) x}{(s^2+\Omega^2)}$$

Replacing for ϕ gives :

$$s^2 \frac{\bar{T}_0(s)}{2} + \sum_{n=1}^{\infty} \bar{T}_n(s) \mathrm{Cos}\left(\frac{n\pi x}{l}\right) \left[\mathrm{Cosh}\left(\frac{n\pi h}{l}\right) s + \frac{gn\pi}{l} \mathrm{Sinh}\left(\frac{n\pi h}{l}\right) \right]$$

$$= - \left[\frac{x_o \Omega^3 (s\varepsilon_c - \Omega\varepsilon_s)}{(s^2+\Omega^2)} + x_o \Omega^2 \varepsilon \right] x$$

Replacing the variable x on the RHS by its Fourier Cosine Series approximation :

$$x = \frac{a_0}{2} + \sum_{n=1}^{\infty} a_n \mathrm{Cos}\left(\frac{n\pi x}{l}\right)$$

where :

$$a_0 = \frac{2}{l}\int_0^l x\,dx = l \qquad \text{and}$$

$$a_n = \frac{2}{l}\int x\cos\left(\frac{n\pi x}{l}\right)dx = \frac{2}{l}\left[\frac{l^2}{n^2\pi^2}\right]((-1)^n-1)$$

this gives $a_{2n-1} = -\dfrac{4l}{(2n-1)^2\pi^2}$

Hence :

$$s^2\frac{\bar{T}_0(s)}{2} + \sum_{n=1}^{\infty}\bar{T}_n(s)\cos(kx)\left[\cosh(kh) + gk\sinh(kh)\right]$$

$$= -\left[\frac{1}{2} - \sum_{n=1}^{\infty}\frac{4l}{(2n-1)^2\pi^2}\cos(kx)\right]\left[\frac{x_0\Omega^2 s(\Omega\varepsilon_c+s\varepsilon_s)}{(s^2+\Omega^2)}\right]$$

where $k = (2n-1)\pi/l$

Then, define a function ω such that :

$$\omega^2 = \omega_{2n-1}^2 = g\,\frac{(2n-1)\pi}{l}\,\tanh\,\frac{(2n-1)\pi h}{l} \qquad \ldots \text{A1.2.6}$$

Collecting like terms :

1) $$s^2\frac{\bar{T}_0(s)}{2} = -\frac{lx_0\Omega^2 s(\Omega\varepsilon_c+s\varepsilon_s)}{2(s^2+\Omega^2)}$$

Taking inverse transforms :

$$T_0(t) = -x_0\Omega l(\varepsilon_s\sin(\Omega t) - \varepsilon_c\cos(\Omega t) + \varepsilon_c)$$

Defining an appropriate constant C_a :

2) $$\bar{T}_n(s)(s^2+\omega^2) = C_a\left[\frac{s(\Omega\varepsilon_c+s\varepsilon_s)}{(s^2+\Omega^2)}\right]$$

Taking inverse transforms :

$$T_n(t) = C_a\left[\frac{\varepsilon_s(\omega\sin(\omega t) - \Omega\sin(\Omega t)) + \Omega\varepsilon_c(\cos(\Omega t - \cos(\omega t))}{(\omega^2-\Omega^2)}\right]$$

Hence, the full expression for the velocity profile is :

$$\phi(x,y,t) = -x_o\Omega l(\varepsilon_s Sin(\Omega t)-\varepsilon_c Cos(\Omega t)+\varepsilon_c)/2$$

$$+\sum_{n=1}^{\infty}\left[\frac{4lx_o\Omega^2[\varepsilon_s(\omega Sin(\omega t)-\Omega Sin(\Omega t))+}{(2n-1)^2\pi^2 Cosh((2n-1)\pi h/l)(\omega^2-\Omega^2)}\right.$$

$$\left.\varepsilon_c(Cos(\Omega t)-Cos(\omega t))]Cos[\frac{(2n-1)\pi x}{l}]Cosh[\frac{(2n-1)\pi y}{l}]\right]$$

... A1.2.7

The equation for the free surface profile can be obtained from the dynamic boundary condition :

$$g\eta = -x\ddot{X}+\frac{\partial\phi}{\partial t} \qquad \text{at } y = h + \eta$$

$$g\eta = -\left[\frac{1}{2}-\sum_{n=1}^{\infty}\frac{4l}{(2n-1)^2\pi^2}Cos(\frac{(2n-1)\pi x}{l})\right]x_o\Omega^2 Sin(\Omega t+\varepsilon)$$

$$-x_o\Omega l(\varepsilon_s\Omega Cos(\Omega t)+\varepsilon_c\Omega Sin(\Omega t))/2$$

$$+\sum_{n=1}^{\infty}\frac{4lx_o\Omega^2[\varepsilon_s(\omega^2 Cos(\omega t)-\Omega^2 Cos(\Omega t))}{(2n-1)^2\pi^2(\omega^2-\Omega^2)}$$

$$-\Omega\varepsilon_c(\Omega Sin(\Omega t)-\omega Sin(\omega t))]Cos[\frac{(2n-1)\pi x}{l}]$$

Then :

$$\eta = \sum_{n=1}^{\infty}\frac{4lx_o\Omega^2\omega[\omega\varepsilon_s Cos(\omega t)+\Omega\varepsilon_c Sin(\omega t)-\omega Sin(\Omega t+\varepsilon)]}{(2n-1)^2\pi^2(\omega^2-\Omega^2)g}Cos[\frac{(2n-1)\pi x}{l}]$$

... A1.2.8

Note: $\varepsilon_s=0$ and $\varepsilon^c=0$ for no phase angle.

1.3 TWIN FLUID TRANSVERSE SLOSHING.

1.3.1 Problem Description.

Twin fluid theory applies to the case of oil/water sloshing. Unlike single fluid theory, physical properties of the upper fluid cannot be

neglected. This introduces additional complications at the oil/water interface.

Consider a vessel in filled with two fluids of density ρ_1 and ρ_2 such that $\rho_1 > \rho_2$ (figure A1.2). Allow the vessel to under go a simple transverse oscillation.

In this case the equation A1.2.2 has to be applied to both fluids. To eliminate the pressure term it is assumed that at every point on the interface the pressure in both fluids is equal :

$$-\frac{\partial\phi_i}{\partial t} + \frac{P}{\rho_i} - \Omega = 0 \quad \text{for fluid i at } y = h_1 \quad (i=1,2)$$

Then define $r = \rho_2/\rho_1$:

$$-\frac{\partial\phi_1}{\partial t} + r\frac{\partial\phi_2}{\partial t} = \Omega(1-r) \text{ at } y = h_1$$

This is then the dynamic free surface boundary condition. The problem reduces to :

$$\text{Solve } \frac{\partial^2\phi_i}{\partial x^2} + \frac{\partial^2\phi_i}{\partial y^2} = 0 \qquad \forall\ x,y,t \quad \ldots \text{ A1.3.1}$$

Subject to the boundary conditions :

$$-\frac{\partial\phi_1}{\partial y} = 0 \qquad \text{at } y = 0 \qquad \forall\ x,t$$

$$-\frac{\partial\phi_2}{\partial y} = 0 \qquad \text{at } y = H \qquad \forall\ x,t$$

$$-\frac{\partial\phi_i}{\partial x} = 0 \qquad \text{at } x = 0,1 \qquad \forall\ y,t \quad \ldots \text{ A1.3.2}$$

$$-\frac{\partial\phi_1}{\partial t} + r\frac{\partial\phi_2}{\partial t} = \Omega(1-r) \text{ at } y = h+\eta \quad \forall\ x,t$$

$$\frac{\partial\eta_i}{\partial t} = -\frac{\partial\phi_i}{\partial y} \qquad \text{at } y = h+\eta \quad \forall\ x,t$$

1.3.2 Solution.

Now, separation of variables gives two velocity potential equations as :

$$\phi_1(x,y,t) = \frac{T_0^1(t)}{2} + \sum_{n=1}^{\infty} T_n^1(t)\,\mathrm{Cos}\left(\frac{n\pi x}{l}\right)\mathrm{Cosh}\left(\frac{n\pi y}{l}\right) \qquad \ldots \text{A1.3.3a}$$

and

$$\phi_2(x,y,t) = \frac{T_0^2(t)}{2} + \sum_{n=1}^{\infty} T_n^2(t)\,\mathrm{Cos}\left(\frac{n\pi x}{l}\right)\mathrm{Cosh}\left(\frac{n\pi (y-H)}{l}\right) \qquad \ldots \text{A1.3.3b}$$

Using the dynamic boundary condition as before :

$$-\frac{\partial^2\phi_1}{\partial t^2} + r\frac{\partial^2\phi_2}{\partial t^2} - g(1-r)\frac{\partial\phi_1}{\partial y} = -xX^{(3)} \text{ at } y = h + \eta \qquad \ldots \text{A1.3.4}$$

where the forcing terms are defined as :

$$X = x_o\mathrm{Sin}(\Omega t) + S_o$$

$$X' = x_o\Omega\mathrm{Cos}(\Omega t), \qquad X'' = -x_o\Omega^2\mathrm{Sin}(\Omega t)$$

$$X^{(3)} = -x_o\Omega^3\mathrm{Cos}(\Omega t)$$

At y = h, assume that :

$$\frac{\partial\phi_1}{\partial y} = \frac{\partial\phi_2}{\partial y} \text{ and } T_0^1(t) = T_0^2(t)$$

Then :

$$T_n^1(t)\,\mathrm{Sinh}(n\pi h/l) = T_n^2(t)\,\mathrm{Sinh}(n\pi(h-H)/l)$$

Define a constant C_a such that :

$$T_n^1(t) = -C_a T_n^2(t)$$

Using the dynamic equation at t=0 to give :

$$-\frac{\partial\phi_1}{\partial t} + r\frac{\partial\phi_2}{\partial t} = 0 \text{ at } t=0$$

Then taking Laplace transforms of A1.3.4 :

$$s^2(\bar{\phi}_1(s)-r\bar{\phi}_2(s))+g(1-r)\frac{\partial\bar{\phi}_1(s)}{\partial y} = -\frac{x_o\Omega^3 s(1-r)}{(s^2+\Omega^2)}$$

As previous (section 1.2), replace for $\phi(x,y,t)$ and collecting like terms :

1)
$$s^2T^1_\emptyset(s)(1-r) = -\frac{1x_o\Omega^3 s(1-r)}{(s^2+\Omega^2)}$$

i.e. $$T^1_\emptyset(t) = T^2_\emptyset(t) = -x_o\Omega 1[1-\text{Cos}(\Omega t)]$$

2) $$s^2T^1_n(s)[\text{Cosh}(kh)+r\text{Cosh}(k(H-h)] + g(1-r)k\text{Sinh}(kh)$$

$$= \frac{41x_o\Omega^3(1-r)}{(2n-1)^2\pi^2(s^2+\Omega^2)}$$

Define two constants :

$$C_b = \frac{\text{Cosh}(kh)\text{Sinh}(k(H-h))+r\text{Cosh}(k(H-h)\text{Sinh}(kh)}{\text{Sinh}(k(H-h))}$$

$$C_c = \frac{41x_o\Omega^3(1-r)}{(2n-1)^2\pi^2 C_b}$$

Then define :

$$\omega^2 = \omega^2_{2n-1} = \frac{g(1-r)k}{[\text{Coth}(kh)+r\text{Coth}(k(H-h))]} \qquad \ldots \text{A1.3.5}$$

Hence :

$$T^1_n(s)(s^2+\omega^2) = \frac{C_c s}{(s^2+\Omega^2)}$$

Taking inverse transforms, gives :

$$T^1_n(t) = \frac{C_c(\text{Cos}(\Omega t)-\text{Cos}(\omega t))}{(\omega^2-\Omega^2)}$$

The full expressions for the two velocity potentials are then :

$$\phi_1(x,y,t) = - x_o \Omega l [1-\cos(\Omega t)]/2$$

$$+ \sum_{n=1}^{\infty} \frac{4 l x_o \Omega^3 (1-r)}{(2n-1)^2 \pi^2 (\omega^2-\Omega^2)} \left[\frac{\sinh(kh)(\cos(\Omega t)-\cos(\omega t))\cos(kx)\cosh(ky)}{(\cosh(kh)\sinh(k(H-h))+r\cosh(k(H-h)\sinh(kh)} \right]$$

... A1.3.6a

$$\phi_2(x,y,t) = - x_o \Omega l [1-\cos(\Omega t)]/2$$

$$- \sum_{n=1}^{\infty} \frac{4 l x_o \Omega^3 (1-r)}{(2n-1)^2 \pi^2 (\omega^2-\Omega^2)} \left[\frac{\sinh(kh)(\cos(\Omega t)-\cos(\omega t))\cos(kx)\cosh(k(y-H)}{(\cosh(kh)\sinh(k(H-h))+r\cosh(k(H-h)\sinh(kh)} \right]$$

... A1.3.6b

Applying the dynamic boundary condition the equation for the interface (free) surface profile can be found :

$$- \frac{\partial \phi_1}{\partial t} + r\frac{\partial \phi_2}{\partial t} = (1-r)(-g\eta - xX'') \text{ at } y = h + \eta$$

Replacing the appropriate values and defining a constant f as :

$$f = \frac{\sinh(k(H-h))\cosh(kh) - r\sinh(kh)\cosh(k(H-h))}{\sinh(k(H-h))\cosh(kh) + r\sinh(kh)\cosh(k(H-h))}$$

Then :

$$(1-r)g\eta = \left[\frac{1}{2} - \sum_{n=1}^{\infty} \frac{4 l \cos(kx)}{(2n-1)^2 \pi^2} \right] x_o \Omega^2 \sin(\Omega t)(1-r)$$

$$- x_o l \Omega^2 \sin(\Omega t)(1-r)/2$$

$$- \sum_{n=1}^{\infty} \frac{4 l x_o f \Omega^2 (1-r)[\Omega \sin(\Omega t) - \omega \sin(\omega t)]\cos(kx)}{(2n-1)^2 \pi^2 (\omega^2-\Omega^2)}$$

Thus :

$$\eta = -\sum_{n=1}^{\infty} \frac{4lx_o\Omega^2[(\omega \mp \Omega)(1-f))Sin(\Omega t)-\omega\Omega fSin(\omega t)]Cos(kx)}{g(2n-1)^2\pi^2(\omega^2-\Omega^2)} \quad \ldots A1.3.7$$

If r=0, then the above reverts to the equation derived for a single fluid.

1.4 THREE FLUID TRANSVERSE SLOSHING.

1.4.1 Problem Description.

Equation A1.3.5 gives the natural frequency of a two fluid system as a function of fill depth 'h' and density ratio 'r'. Applying a similar method, a three fluid expression can be obtained.

With reference to figure A1.3, three fluids of densities ρ_1, ρ_2 and ρ_3 are filled to a depth h_1, h_2 and H.

The basic sloshing equation can be applied to all fluids as before :

Fluid 1 :

$$\nabla^2\phi_1 = 0 \qquad 0<y<h_1 \qquad \forall\ x,t$$

$$-\frac{\partial\phi_1}{\partial y} = 0 \qquad \text{at } y = 0 \qquad \forall\ x,t$$

$$-\frac{\partial\phi_1}{\partial x} = 0 \qquad \text{at } x = 0,l \qquad \forall\ y,t$$

$$-\frac{\partial\phi_1}{\partial t} + \frac{P_{12}}{\rho_1} - \Omega = 0 \qquad \text{at } y = h_1 \qquad \forall\ x,t$$

Then :

$$\phi_1(x,y,t) = T_1(t)Cos(kx)Cosh(y)$$

$$k = n\pi/l$$

Fluid 3 : $\nabla^2\phi_3 = 0$ $\quad h_2 < y < H$ $\quad \forall\ x,t$

$$-\frac{\partial\phi_3}{\partial y} = 0 \qquad \text{at } y = H \qquad \forall\ x,t$$

$$-\frac{\partial\phi_3}{\partial x} = 0 \qquad \text{at } x = 0,1 \qquad \forall\ y,t$$

$$-\frac{\partial\phi_3}{\partial t} + \frac{P_{23}}{\rho_3} - \Omega = 0 \qquad \text{at } y = h_2 \qquad \forall\ x,t$$

Then :

$$\phi_3(x,y,t) = T_3(t)\,\mathrm{Cos}(kx)\,\mathrm{Cosh}(y-H)$$

Fluid 3 : $\nabla^2\phi_2 = 0$ $\quad h_1 < y < h_2$ $\quad \forall\ x,t$

$$-\frac{\partial\phi_2}{\partial x} = 0 \qquad \text{at } x = 0,1 \qquad \forall\ y,t$$

$$-\frac{\partial\phi_2}{\partial t} + \frac{P_{12}}{\rho_2} - \Omega = 0 \qquad \text{at } y = h_1 \qquad \forall\ x,t$$

$$-\frac{\partial\phi_2}{\partial t} + \frac{P_{23}}{\rho_2} - \Omega = 0 \qquad \text{at } y = h_2 \qquad \forall\ x,t$$

1.4.2 Solution.

Since there is no vertical velocity boundary condition for fluid 2, the velocity potential cannot be separated as before :

$$\phi_2(x,y,t) = \mathrm{Cos}(kx)\,[A(t)\,\mathrm{Sinh}(ky) + B(t)\,\mathrm{Cosh}(ky)]$$

The unknown function of time A & B, have to be written in terms of the velocity potentials of fluids 1 & 2 using the interfacial condition that the vertical velocity in each fluid is equal at the interface :

Between 1 & 2 $\qquad \dfrac{\partial\phi_1}{\partial y} = \dfrac{\partial\phi_2}{\partial y} \qquad \text{at } y = h_1$

Then: $T_1(t)\text{Sinh}(kh_1) = A(t)\text{Sinh}(kh_1)+B(t)\text{Cosh}(kh_1)$

... A1.3.1a

And between 2 & 3 :

$$T_3(t)\text{Sinh}(h_2-H) = A(t)\text{Sinh}(kh_2)+B(t)\text{Cosh}(kh_2)$$

... A1.3.1b

Solving for A(t) & B(t) gives :

$$A(t) = \frac{T_1(t)\text{Sinh}(kh_1)\text{Cosh}(kh_2)-T_3(t)\text{Sinh}(k(h_2-H))\text{Cosh}(kh_1)}{\text{Sinh}(k(h_1-h_2))}$$

$$= a_1T_1(t) + a_3T_3(t) \quad \text{... A1.3.2a}$$

$$B(t) = \frac{\text{Sinh}(kh_1)[T_1(t)\text{Sinh}(kh_2)-T_3(t)\text{Sinh}(k(h_2-H))]}{\text{Sinh}(k(h_2-h_1))}$$

$$= b_1T_1(t) + b_3T_3(t) \quad \text{... A1.3.2b}$$

By applying the dynamic boundary conditions at each interface a pair of simultanious equations will result, from which, the unknown time functions can be solved.

Taking Laplace transforms as before :

At $y = h_1$

$$s^2(\bar{\phi}_1(s)-r_{21}\bar{\phi}_2(s))+g(1-r_{21})\frac{\partial\bar{\phi}_1(s)}{\partial y} = -\frac{x_o\Omega^3 s(1-r_{21})}{(s^2+\Omega^2)}$$

At $y = h_2$

$$s^2(\bar{\phi}_3(s)-r_{23}\bar{\phi}_2(s))+g(1-r_{23})\frac{\partial\bar{\phi}_3(s)}{\partial y} = -\frac{x_o\Omega^3 s(1-r_{23})}{(s^2+\Omega^2)}$$

where : $r_{21} = \rho_2/\rho_1$, and $r_{23} = \rho_2/\rho_3$

1) Evaluating the time functions, first assume that the $T_{\emptyset 1}(t) = T_{\emptyset 2}(t)$, then :

$$s^2 T^1_{\emptyset 1}(s)(1-r_{21}) = -\frac{1x_o\Omega^3 s(1-r_{21})}{(s^2+\Omega^2)}$$

By similar assumption :

$$s^2 T^1_{\emptyset 3}(s)(1-r_{23}) = -\frac{1x_o\Omega^3 s(1-r_{23})}{(s^2+\Omega^2)}$$

Hence : $T_{\emptyset 1}(t) = T_{\emptyset 2}(t) = T_{\emptyset 3}(t) = -x_o\Omega l[1-\text{Cos}(\Omega t)]$

2) For the other time function terms, denote :

Sinh(kx) = Sx and Cosh(kx) = Cx

k = (2n-1)π/l, then :

$$s^2[T_1 Ch_1 - r_{21}((a_1 Sh_1 + b_1 Ch_1)T_1 + (a_3 Sh_1 + b_3 Ch_1)T_3)]$$

$$+ g(1-r_{21})kSh_1 T_1 = \frac{4lx_o\Omega^3(1-r_{21})s}{(2n-1)^2\pi^2(s^2+\Omega^2)} \qquad \text{... A1.3.3a}$$

And

$$s^2[T_3 C(h_2-H) - r_{23}((a_1 Sh_2 + b_1 Ch_2)T_1 + (a_3 Sh_2 + b_3 Ch_2)T_3)]$$

$$+ g(1-r_{23})kS(h_2-H)T_3 = \frac{4lx_o\Omega^3(1-r_{23})s}{(2n-1)^2\pi^2(s^2+\Omega^2)} \qquad \text{... A1.3.3a}$$

Re-arranging gives :

$$T_1(s^2+\omega_1^2) - \frac{r_{21}(a_3 Sh_1 + b_3 Ch_1)T_3}{(Ch_1 - r_{21}(a_1 Sh_1 + b_1 Ch_1))}$$

$$= \frac{4lx_o\Omega^3(1-r_{21})s}{(2n-1)^2\pi^2(s^2+\Omega^2)(Ch_1 - r_{21}(a_1 Sh_1 + b_1 Ch_1))}$$

$$T_3(s^2+\omega_3^2) - \frac{r_{23}(a_1Sh_2+b_1Ch_2)T_1}{(C(h_2-H)-r_{23}(a_3Sh_2+b_3Ch_2))}$$

$$= \frac{4lx_o\Omega^3(1-r_{23})s}{(2n-1)^2\pi^2(s^2+\Omega^2)(Ch_1-r_{23}(a_3Sh_2+b_3Ch_2))}$$

Where :

$$\omega_1^2 = \frac{g(1-r_{21})kSh_1}{(Ch_1-r_{21}(a_1Sh_1+b_1Ch_1))} \qquad \text{... A1.3.4a}$$

$$\omega_3^2 = \frac{g(1-r_{23})kS(h_2-H)}{(C(h_2-H) -r_{23}(a_3Sh_2+b_3Ch_2))} \qquad \text{... A1.3.4b}$$

Denote :

$$c_1 = \frac{r_{21}(a_3Sh_1+b_3Ch_1}{(Ch_1-r_{21}(a_1Sh_1+b_1Ch_1))} \qquad \text{... A1.3.5a}$$

$$d_1 = \frac{4lx_o\Omega^3(1-r_{21})}{(2n-1)^2\pi^2(Ch_1-r_{21}(a_1Sh_1+b_1Ch_1))} \qquad \text{... A1.3.5b}$$

and similarly for c_3 and d_3.

Then :

$$T_1(s^2+\omega_1^2) - c_1T_3 = \frac{d_1s}{(s^2+\Omega^2)} \qquad \text{... A1.3.6a}$$

$$T_3(s^2+\omega_3^2) - c_3T_1 = \frac{d_3s}{(s^2+\Omega^2)} \qquad \text{... A1.3.6b}$$

Solving for the two time functions, gives :

$$T_1 = \frac{d_1s^3+(d_3c_1+d_1\omega_3^3)s}{(s^4+(\omega_1^2+\omega_3^2)s^2+\omega_1^2\omega_3^2-c_3c_1)(s^2+\Omega^2)} \qquad \text{... A1.3.7a}$$

$$T_3 = \frac{d_3s^3+(d_1c_3+d_3\omega_1^3)s}{(s^4+(\omega_1^2+\omega_3^2)s^2+\omega_1^2\omega_3^2-c_3c_1)(s^2+\Omega^2)} \qquad \text{... A1.3.7b}$$

Both these equations are of the form :

$$T(s) = \frac{As^3 + Bs}{(s^2+\omega_1'^2)(s^2+\omega_3'^2)(s^2+\Omega^2)}$$

Taking inverse transforms, the expression for the time factors is of the form :

$$T_i(t) =$$

$$\left[(A_i\omega_1'^2 - B_i)(\omega_3'^2-\Omega^2)\cos(\omega_1' t) - (A_i\omega_3'^2 - B_i)(\omega_1'^2-\Omega^2)\cos(\omega_3' t) \right.$$

$$\left. + (A_i\Omega^2 - B_i)(\omega_1'^2-\omega_3'^2)\cos(\Omega t) \right]$$

$$\left[(\omega_1'^2-\omega_3'^2)(\omega_3'^2-\Omega^2)(\Omega^2-\omega_1'^2) \right]^{-1} \qquad \ldots \text{ A1.3.8}$$

The two natural frequency terms, one for each fluid interface, are evaluated from the roots of the denominator in equation A1.3.7.

Following the previous twin fluid example, the equations describing the interface profiles can be obtained.

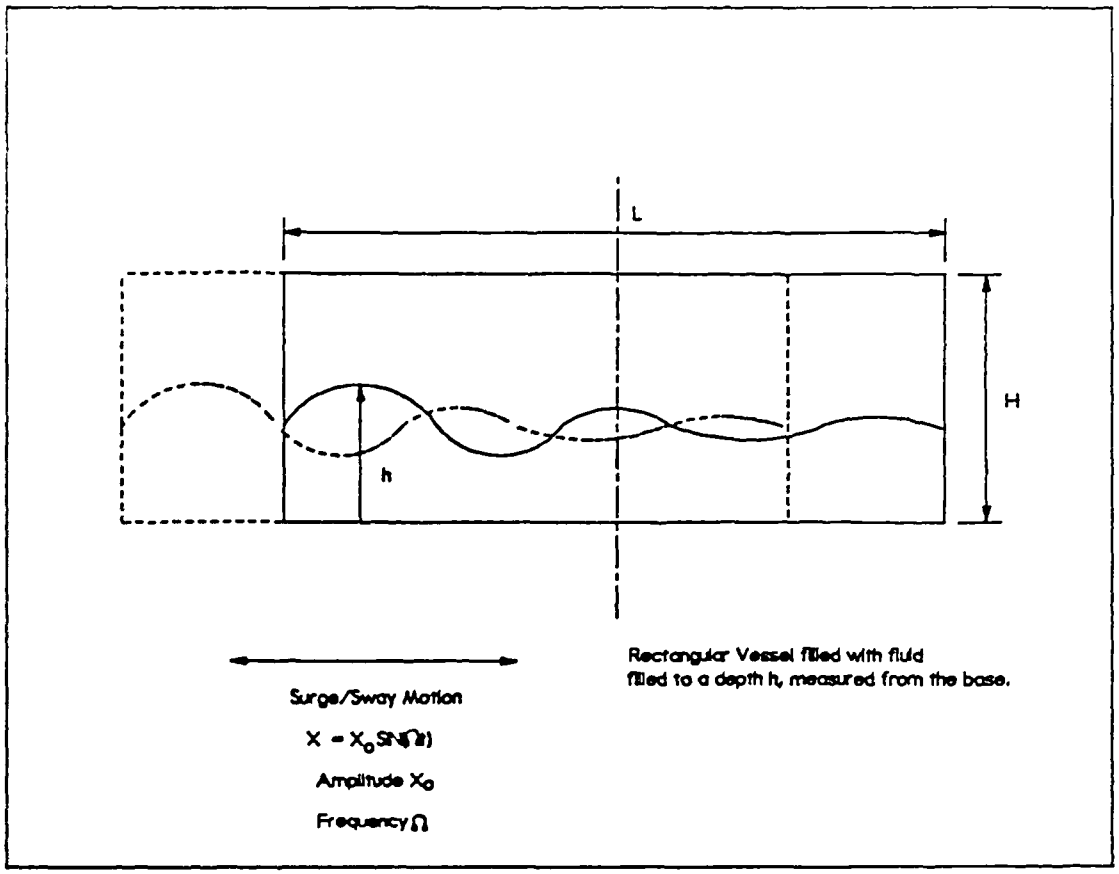

Figure A1.1: Nomenclature applied to a single fluid (gas/liquid) system.

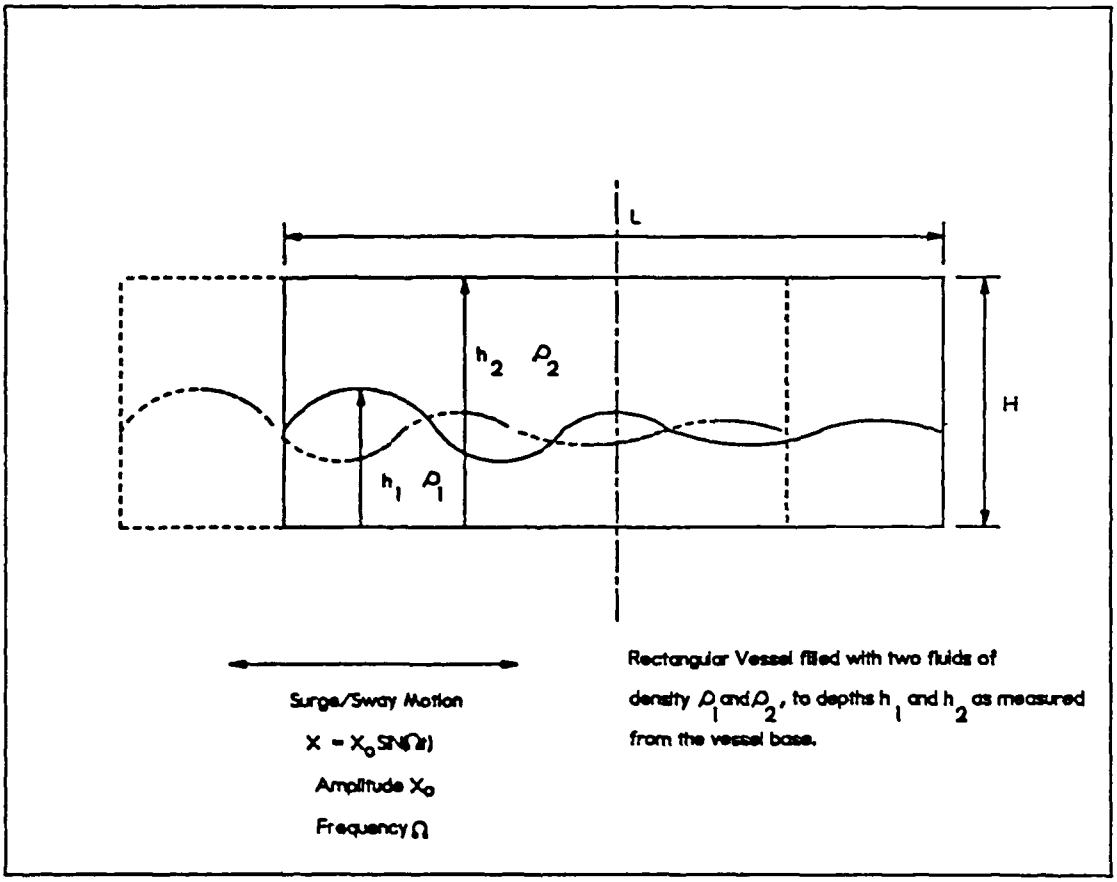

Figure A1.2: Nomenclature applied to a twin fluid (liquid/liquid) system.

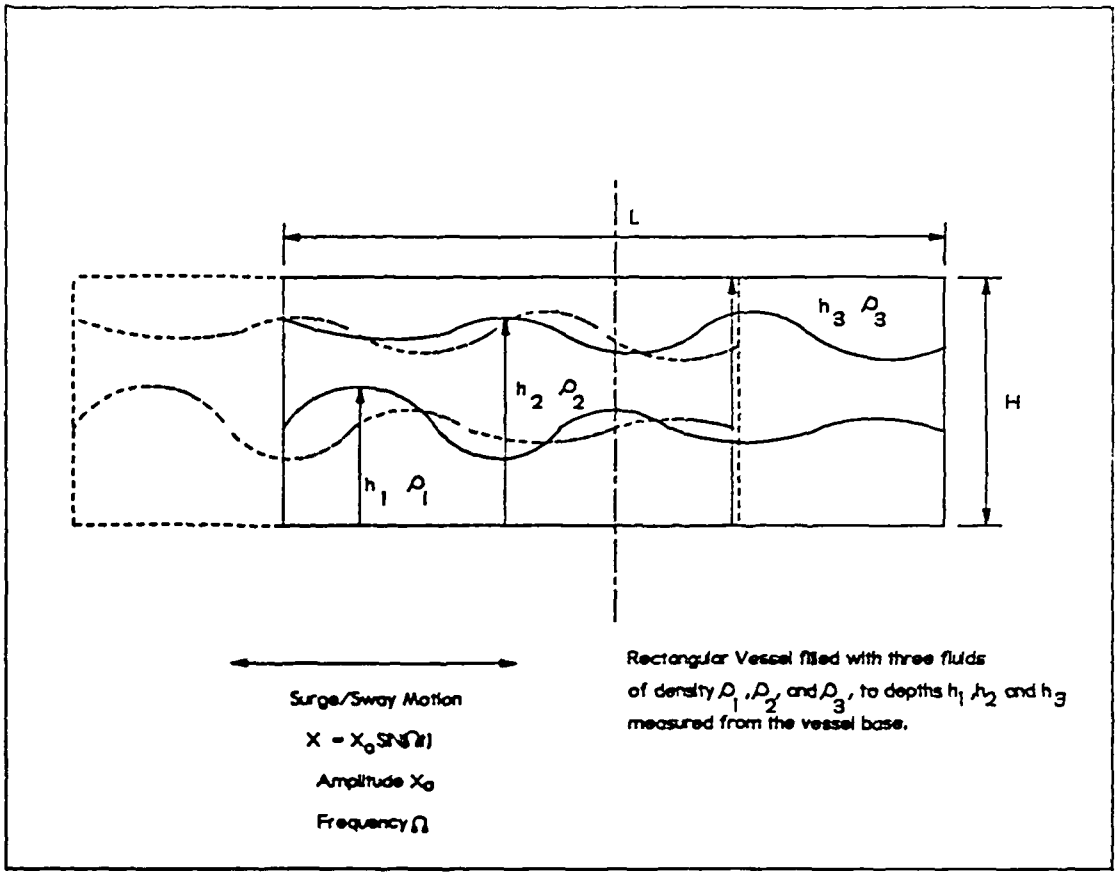

Figure A1.3: Nomenclature applied to a three fluid (gas/liquid/liquid) system.

APPENDIX II

DESCRIPTION OF THE DATA LOGGER *HEADER DATA BLOCK.*

1.1 INTRODUCTION.

Chapter 5 introduced the concept of a *header data block* to convey information from the data logger, to the motion controller and the data processor. Two header block structures were used, one for wave probe calibration, the other to convey forcing conditions. During data logging, wave and simulator position information was stored after a header, in a unique format. This appendix provides details on formats of header blocks and raw data files.

1.2 HEADER FORMATS.

1.2.1 General Header Format.

The general header format common to both calibration and forcing conditions was :

1) Sync: A 5 character syncronisation string "*ATOM" to detect a valid simulator data file.
2) Date Code: A date 6 character code string for general information with format "ddmmyy".
3) Vessel Code: A general 20 character vessel code string to identify vessel and internals e.g "V1.1REC BAFF1".
4) Probe Code: A general 10 character probe identification code string, to relate the exact probe connections to the user e.g. "PB SET 1".
5) Run Code: A single character to identify the type of run i.e. "M" for motion, "C" for calibration. For simulation experimental data files this was replaced by a "S".

6) Run number: A single byte number giving the run number of the current forcing/calibration sequence i.e. from Ø to 255.

7) Fill Depth: A single byte number to represent the fill depth (usually air/water or oil/water). The user would be expected to record the actual depth corresponding to the fill depth number.

8) Number of Probes: A single byte number giving the total number of wave probes connected (1 to 16).

This makes up the general header format.

Apart from checking syncronisation, the motion controller also checked the run code e.g. calibration sequence must have run code "C". If a run code error was detected, the motion controller produced an audible warning to the user that communication had failed and all operations were halted.

1.2.2 Calibration File Header Block.

With run code of "C", the calibration file header continued as :

9) Positions: A two byte number representing the position to move the simulator to for the next calibration reading (pitch, roll, surge/sway). The actual value was 10x the value entered by the user (in degrees).

1.2.3 Forcing Motion File Header Format.

Following the general header block, the forcing motion header (run code "M") continued as :

10) Periods: A single byte representing the forcing periods of each motion (pitch, roll, surge/sway). The number was converted from *real* periods by a calibration factor.

11) Centre: A two byte number representing the offset of each forcing motion (pitch, roll surge/sway) i.e. the default centre. The actual value was 10x the value entered by the user (in degrees).

12) Amplitudes: A two byte number representing the amplitude of each forcing motion (pitch, roll, surge/sway). As with phase angle, these numbers were 10x the requested forcing amplitudes (in degrees).

13) Phase Angle: A two byte number representing the phase angle between each forcing motion. This number gave the position within each *look-up* table, for the program to start the forcing motion.

14) Number of Run Cycles: A two byte number giving the total number of forcing cycles to perform before halting the motion. This number was calculated on the required *length of run* and the forcing motion with the greatest period e.g. for 5 minutes run at 11 second period, number of run cycles was 5*60/11 = 27.3, rounded to 28.

15) Number of Decay Cycles: A two byte number representing the length of wave decay logging.

1.3 DATA BLOCK FORMATS.

1.3.1 Introduction.

Two data block formats were used, one for wave probes and simulator position and the second, to identify the end of the data block. Although the header block contained run length information, it was thought prudent to insert a special block to allow the data processor to detect the end of the data. Data blocks were common to calibration and forcing experiments.

1.3.2 Wave and Simulator Data Block Format.

Following the header block information, the data files continued as :

1) Syncronisation: A single byte to signify the start of a block i.e. "*". This was used by the data processor to detect errors within the data file.

2) Position Data: Three *single* bytes representing the simulator position (pitch,roll, surge/sway). These numbers were as measured by the A/D convertor.

3) Wave Probe Data: Single bytes representing wave probe information as obtained from the A/D convertor. The number of bytes was given by the *number of probes* as specified by the header block.

This loop repeated itself for the duration of data logging. Note that no direct information on when these measurements were taken is contained within the block. It must be recognised that fixed loops were used to sample both simulator position and wave probe information. These fixed loops would be of specific duration, dependant only on the number of probes accessed. Using the computers internal timing system (i.e. the 6522 VIA's), calibration factors were determined relating the length of each collection loop to the number of wave probes. These values were used by the data processor to determine time information.

1.3.3 "End Data" Block Format.

The end block followed the data as three loops, of similar structure to the wave/position data block, but with all data bytes set to equal the same number. The data processor detected this end block using a counter to see if all data was the same.

APPENDIX III

EXAMPLES OF VIDEO DIGITIZING SEQUENCE FOR OIL/WATER INTERFACE MEASUREMENT.

1.1 INTRODUCTION.

The figures presented in this appendix, serve to illustrate the method used to determine the oil/water interface location from digitizing HSV-400 video frames. Each frame has the following format :

1) Frame identification (top right).

2) Time and sequence number for the particular frame (top left).

3) Interface profile inside the vessel (centre). The vertical lines from the vessel base to the oil/water interface, represent the *wave probes* measuring the interface position.

4) Actual wave probe measurements (bottom lines).

On starting the analysis, an initial frame was taken, to provide information on the vessel. The last frame (frame 26 in this case) provides information on the maximum interface amplitude recorded from each probe. It was this data that was used to construct graphs of the effects of forcing period on interface amplitude, presented in chapters 9 and 10.

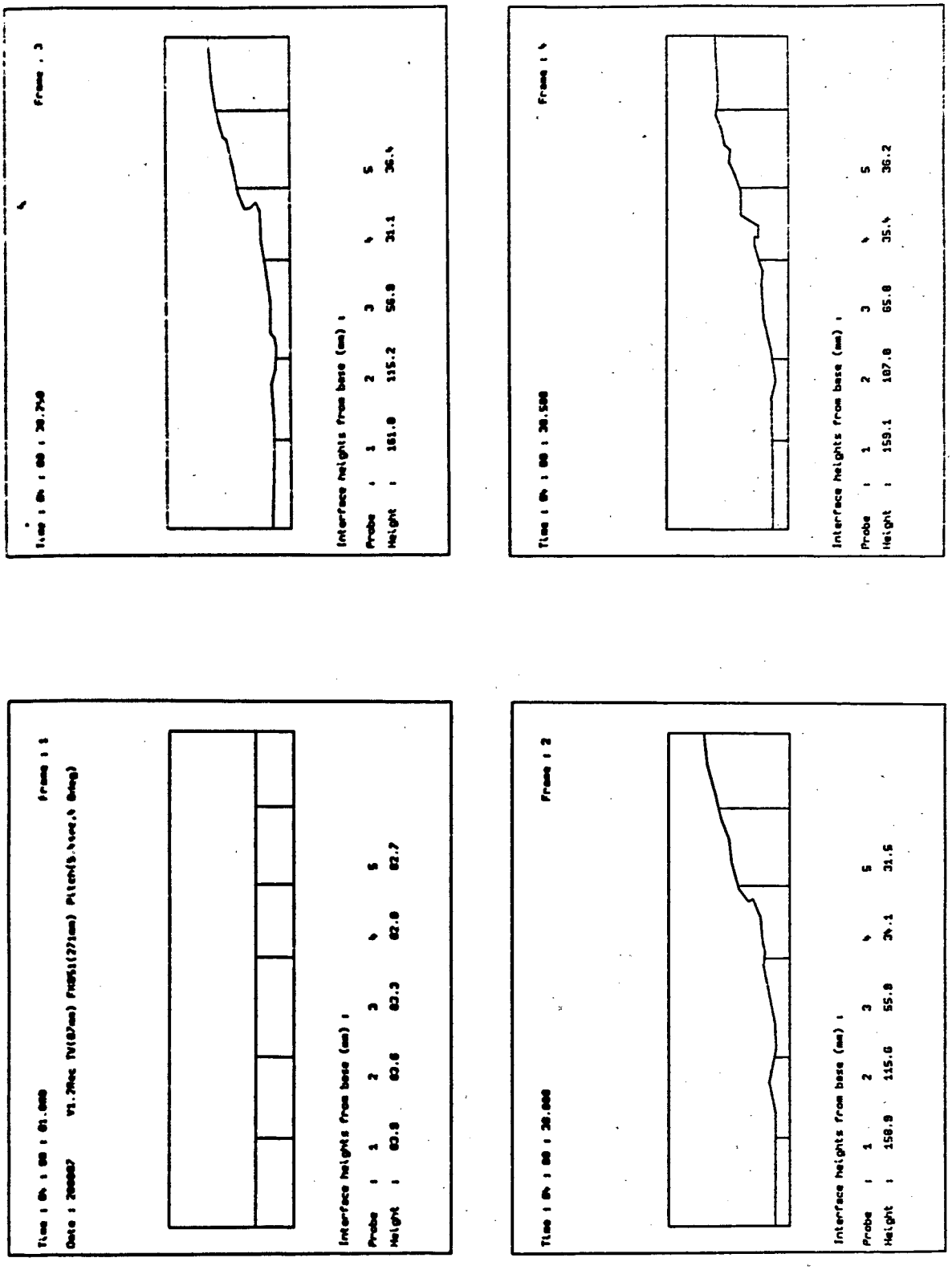

Frames 1 to 4

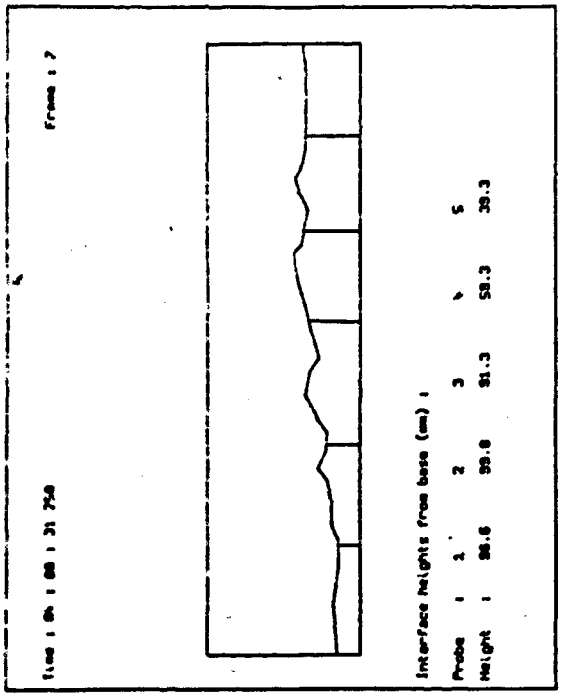
Frame : 7
Interface heights from base (mm) :
Probe : 1 2 3 4 5
Height : 98.6 99.8 91.3 58.3 39.3

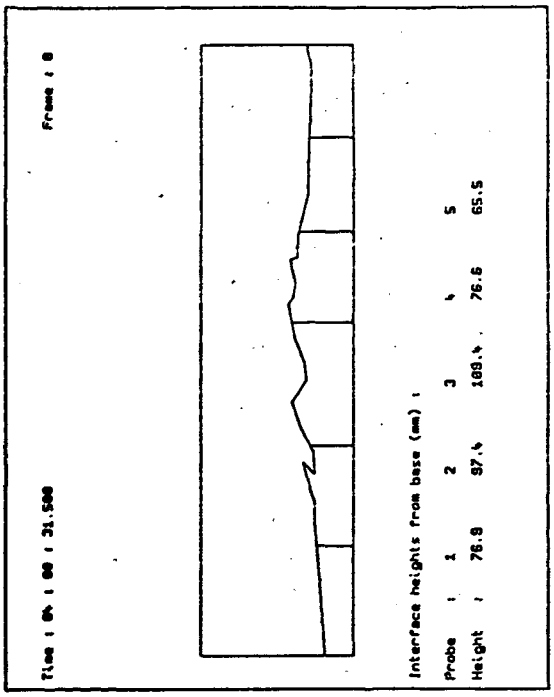
Frame : 8
Interface heights from base (mm) :
Probe : 1 2 3 4 5
Height : 76.8 97.4 100.4 76.6 65.5

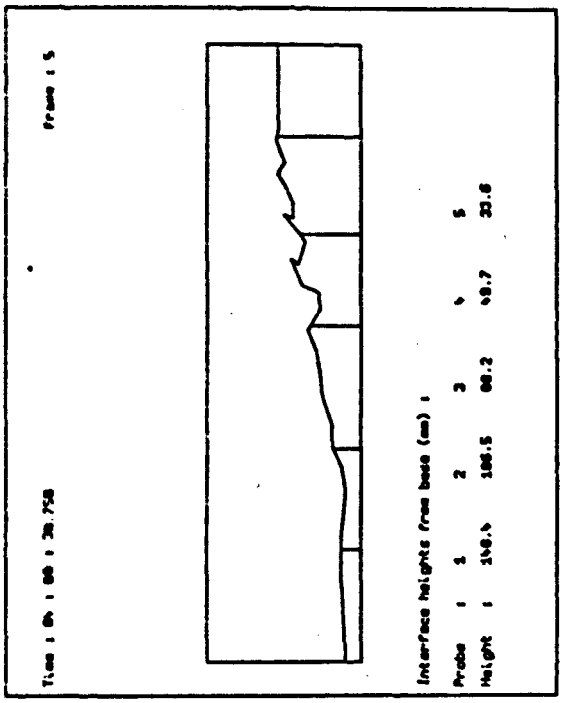
Frame : 5
Interface heights from base (mm) :
Probe : 1 2 3 4 5
Height : 140.4 100.5 80.2 49.7 23.8

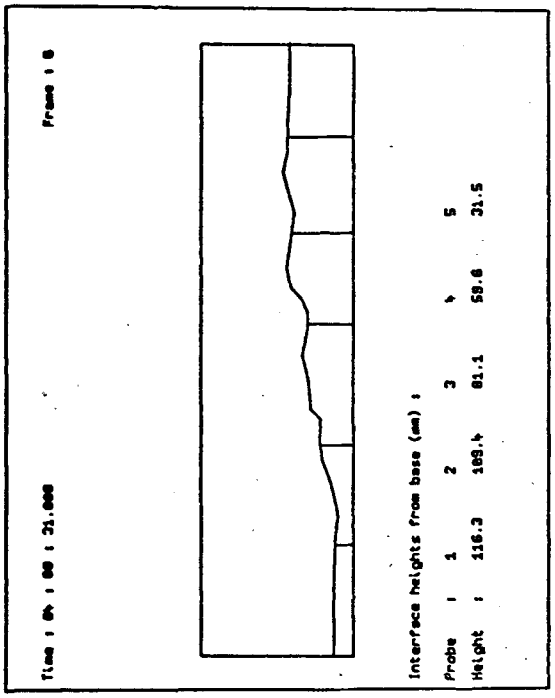
Frame : 6
Interface heights from base (mm) :
Probe : 1 2 3 4 5
Height : 116.3 100.4 81.1 58.6 31.5

Frames 5 to 8

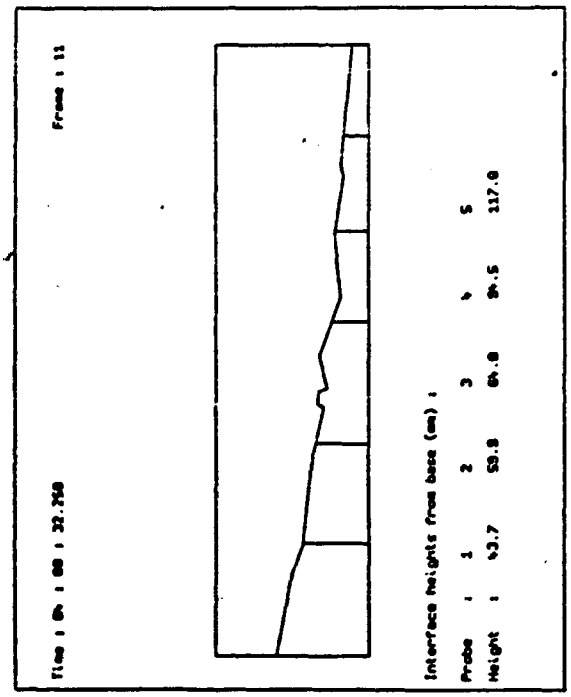

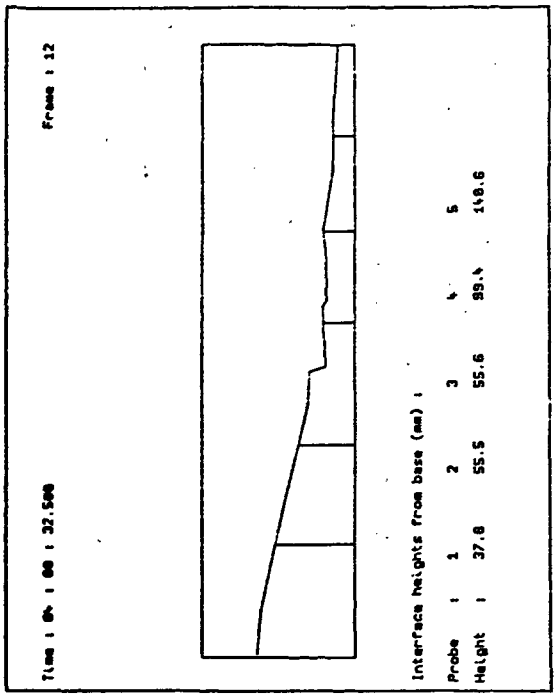

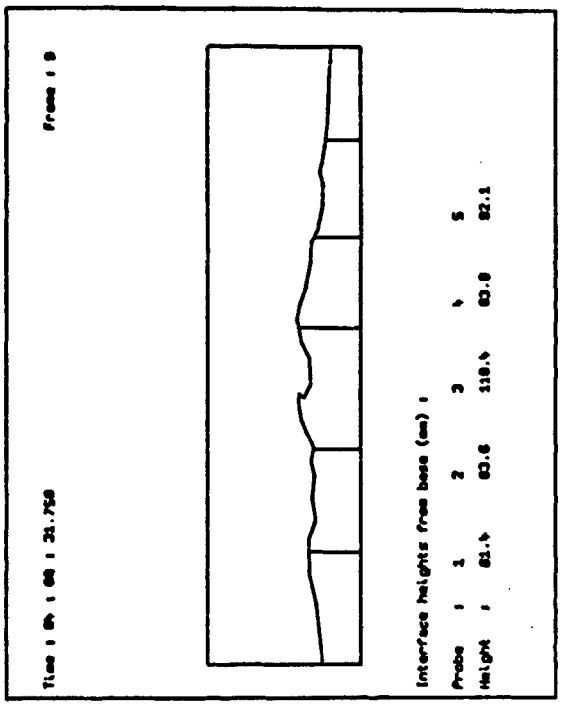

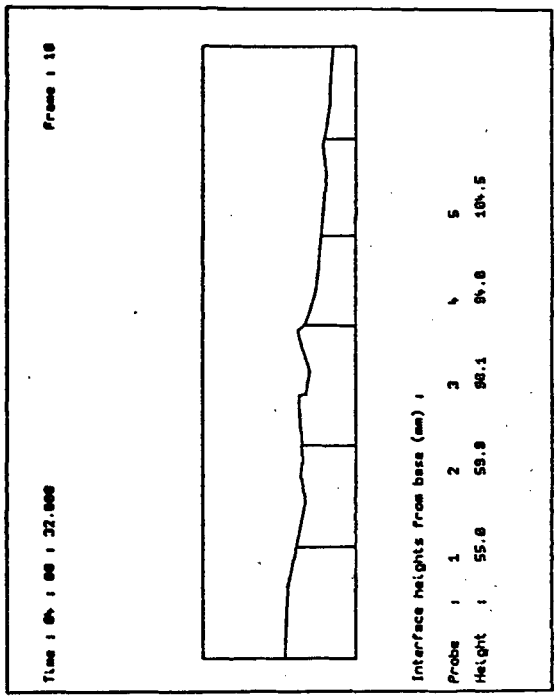

Frames 9 to 12

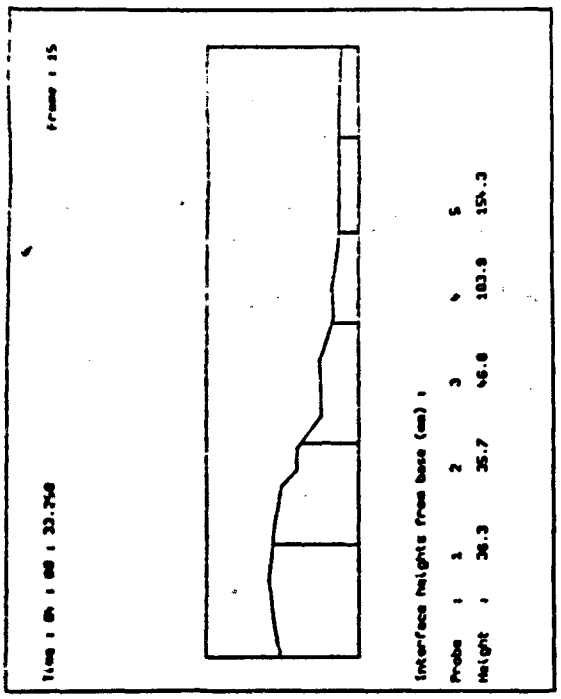

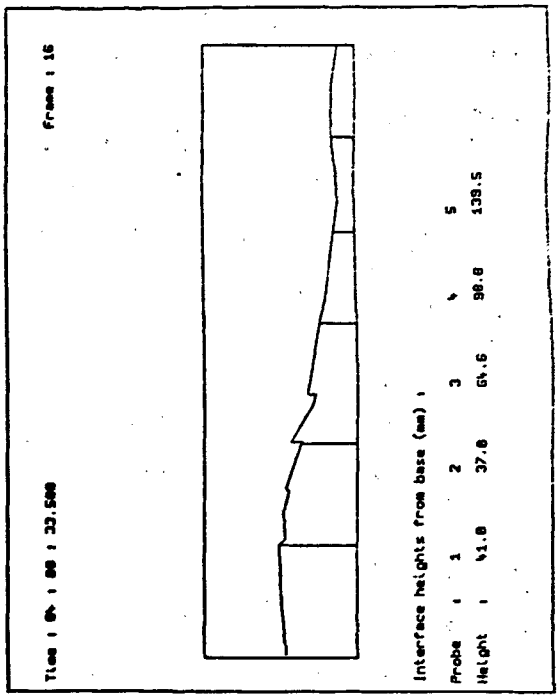

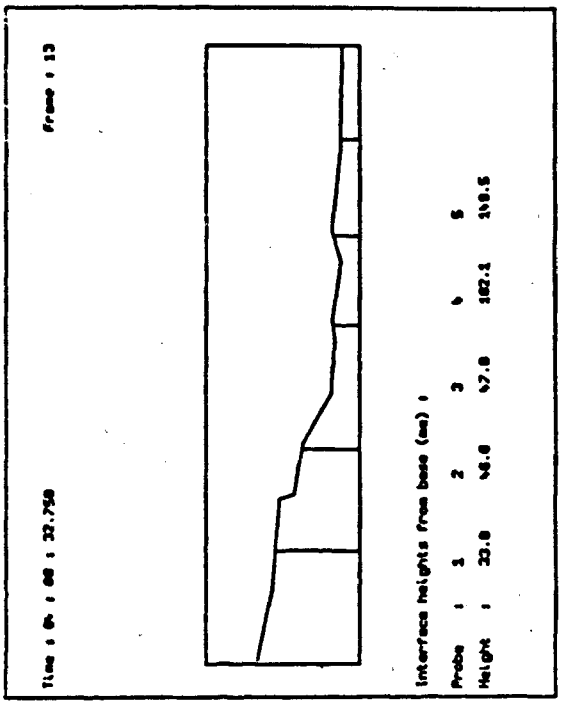

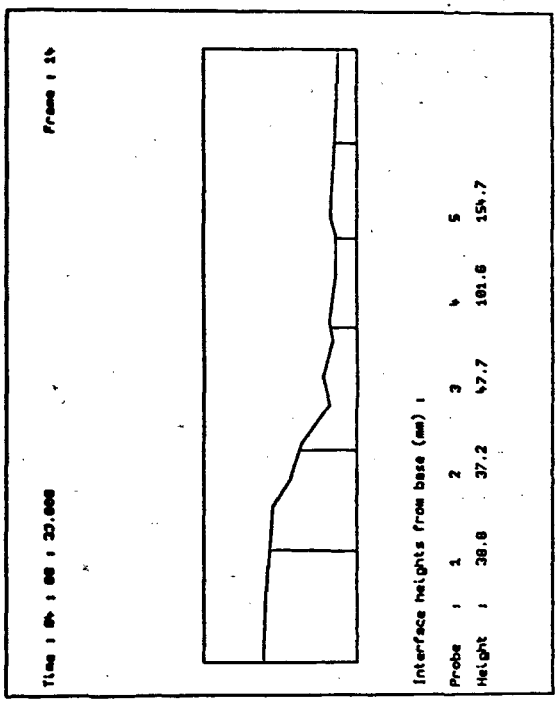

Frames 13 to 15

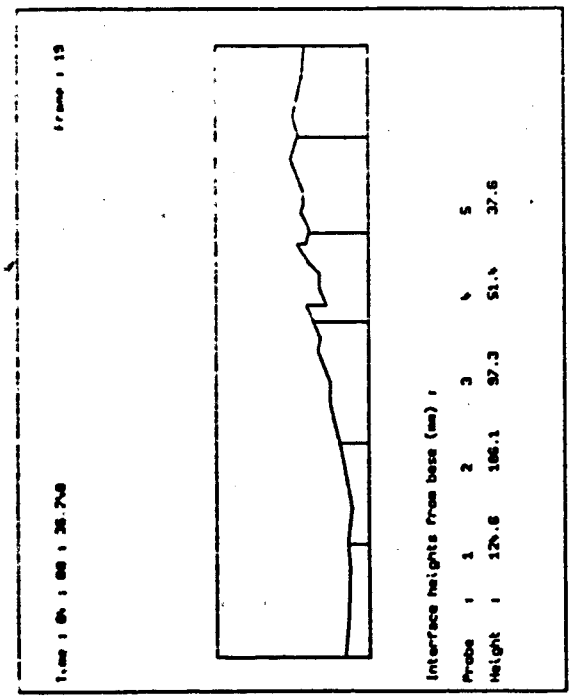

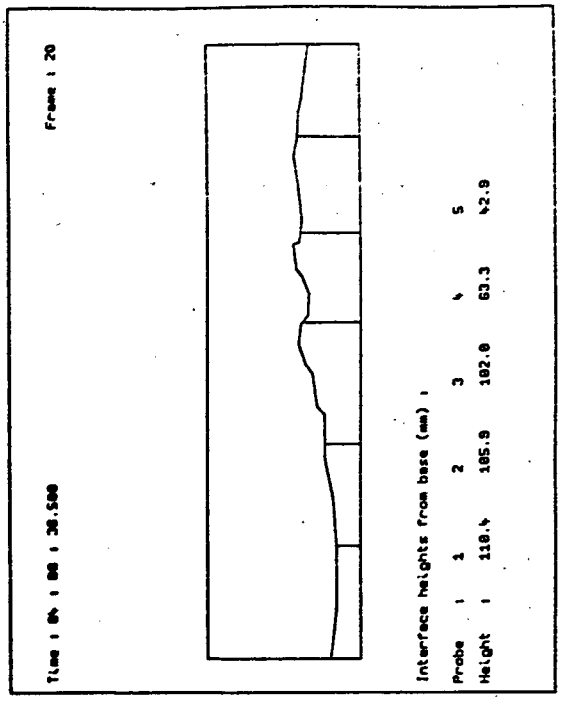

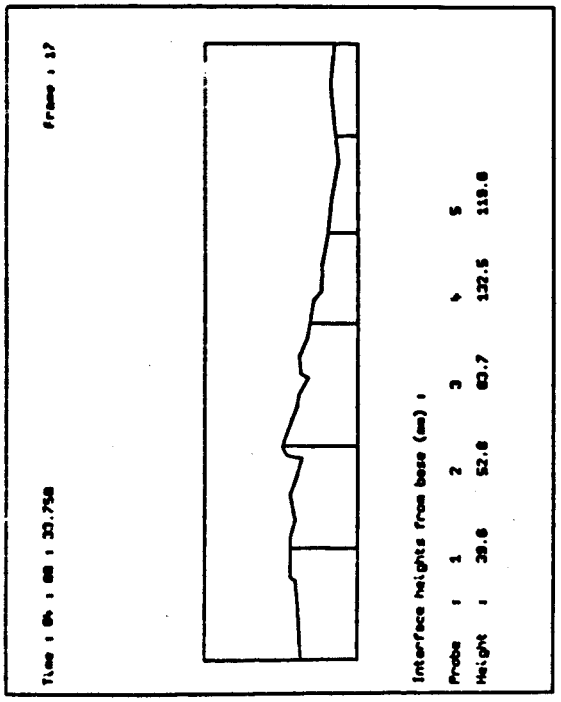

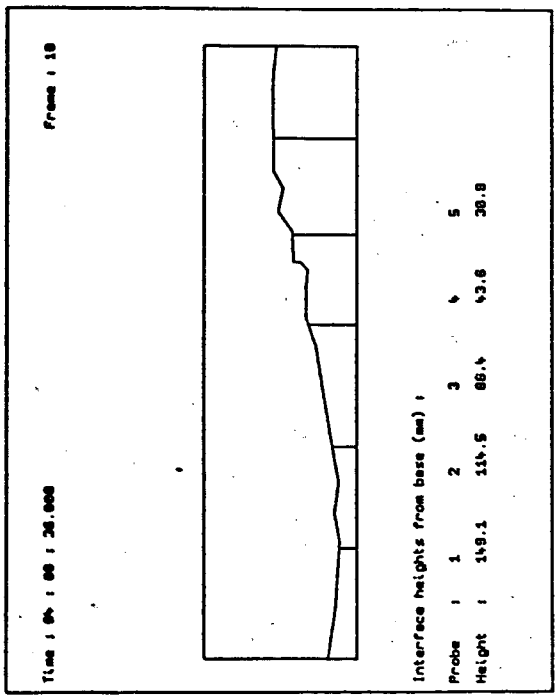

Frames 17 to 20

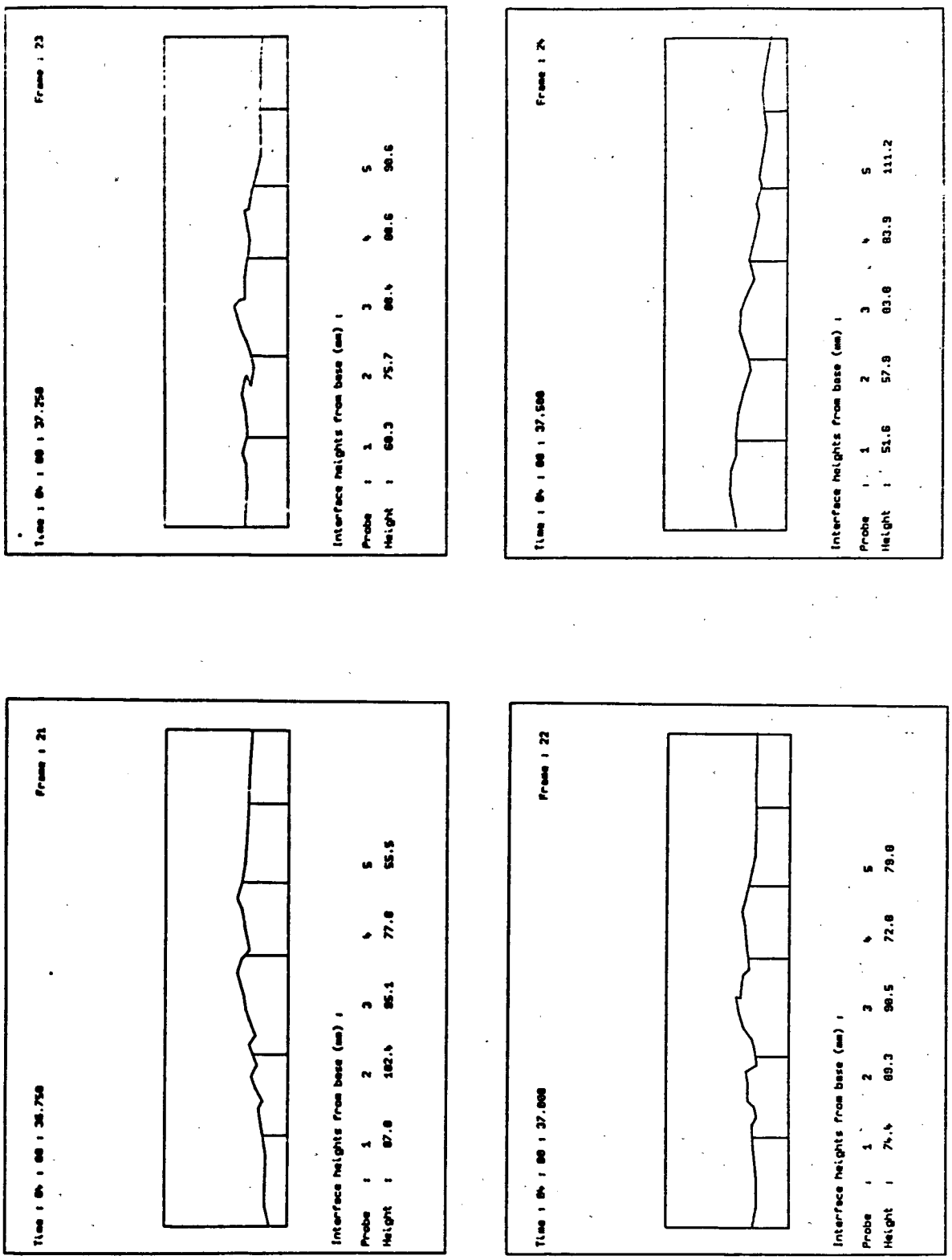

Frames 21 to 24

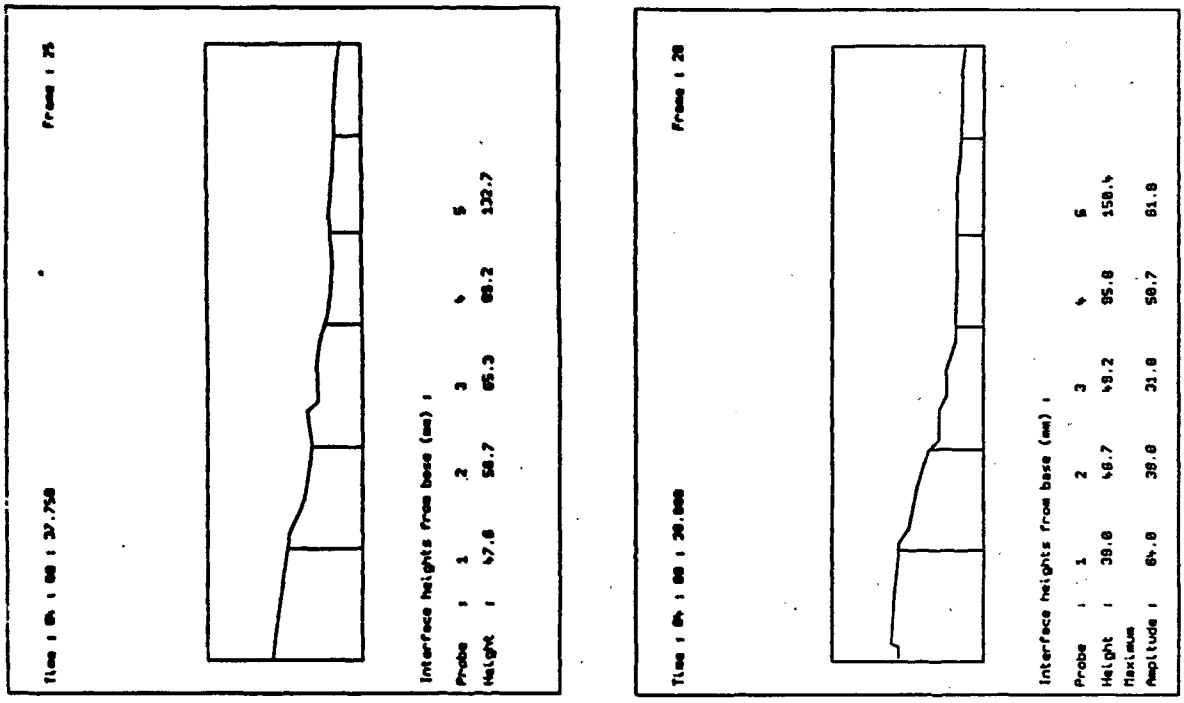

Frames 25 to 26

APPENDIX IV

PROBE 2 WAVE PROFILES AND FFT FREQUENCY SPECTRA FOR AIR/WATER EXPERIMENTS IN THE LARGE RECTANGULAR VESSEL UNDER SINGLE FORCING MOTIONS.

1.1 INTRODUCTION.

This appendix presents wave profile data and corresponding FFT frequency spectra for probe 2 in the large rectangular vessel resulting from pitch and surge forcing motion at ±4° amplitude. Format of these plots was given in chapter 6.

Each graph (A4.1 to A4.17) shows two sets of profile and spectra data. The first plot starts at time 0 and applies to the first minute of forcing. The second plot refers to some time later when forcing motion has ceased i.e. the decay profile.

Chapter 8 discussed the effects observed in the graphs presented here.

Graph A4.1: Pitch forcing motion at forcing period 1.7 seconds, ±4° amplitude.

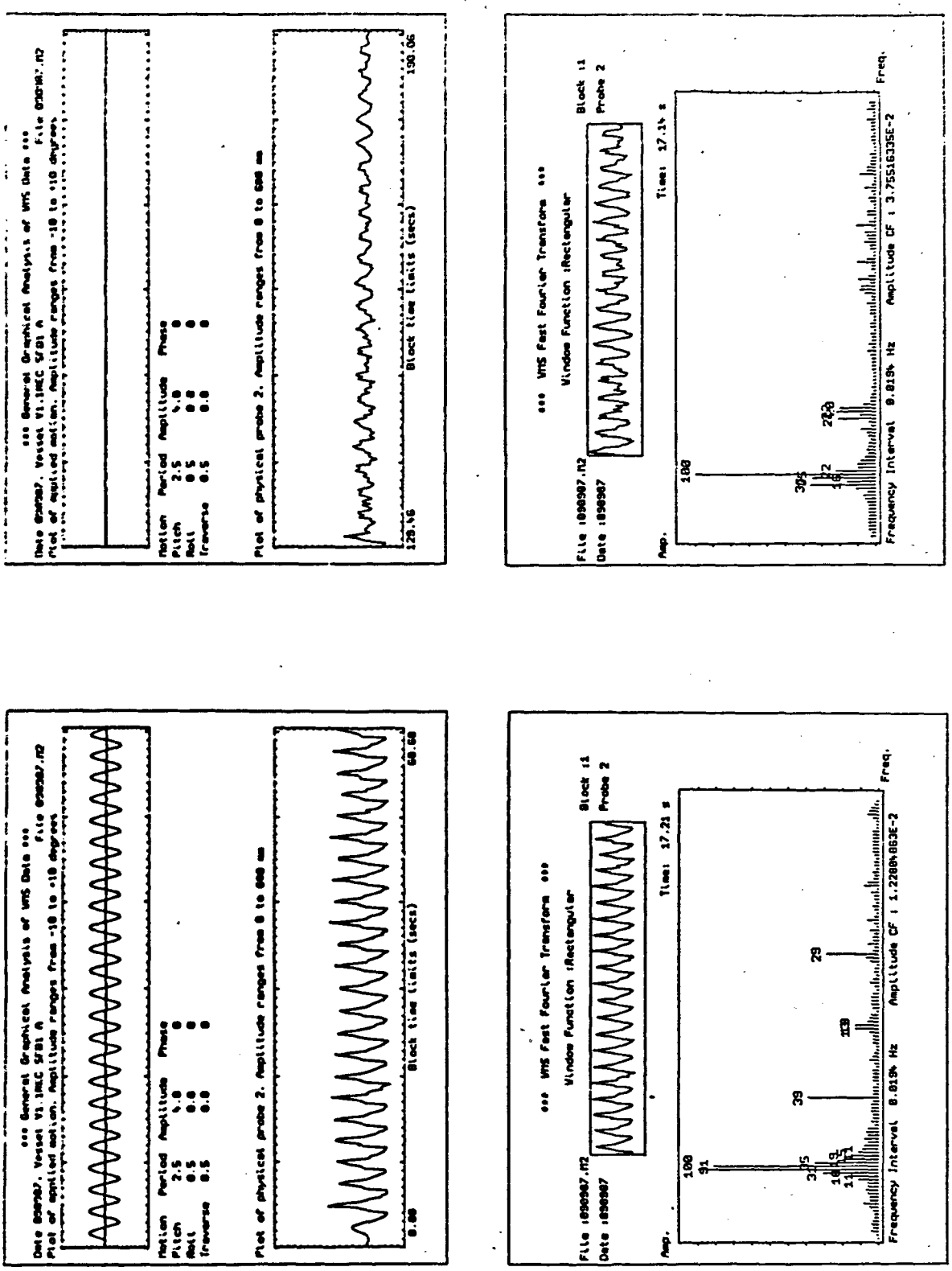

Graph A4.2: Pitch forcing motion at forcing period 2.5 seconds, ±4° amplitude.

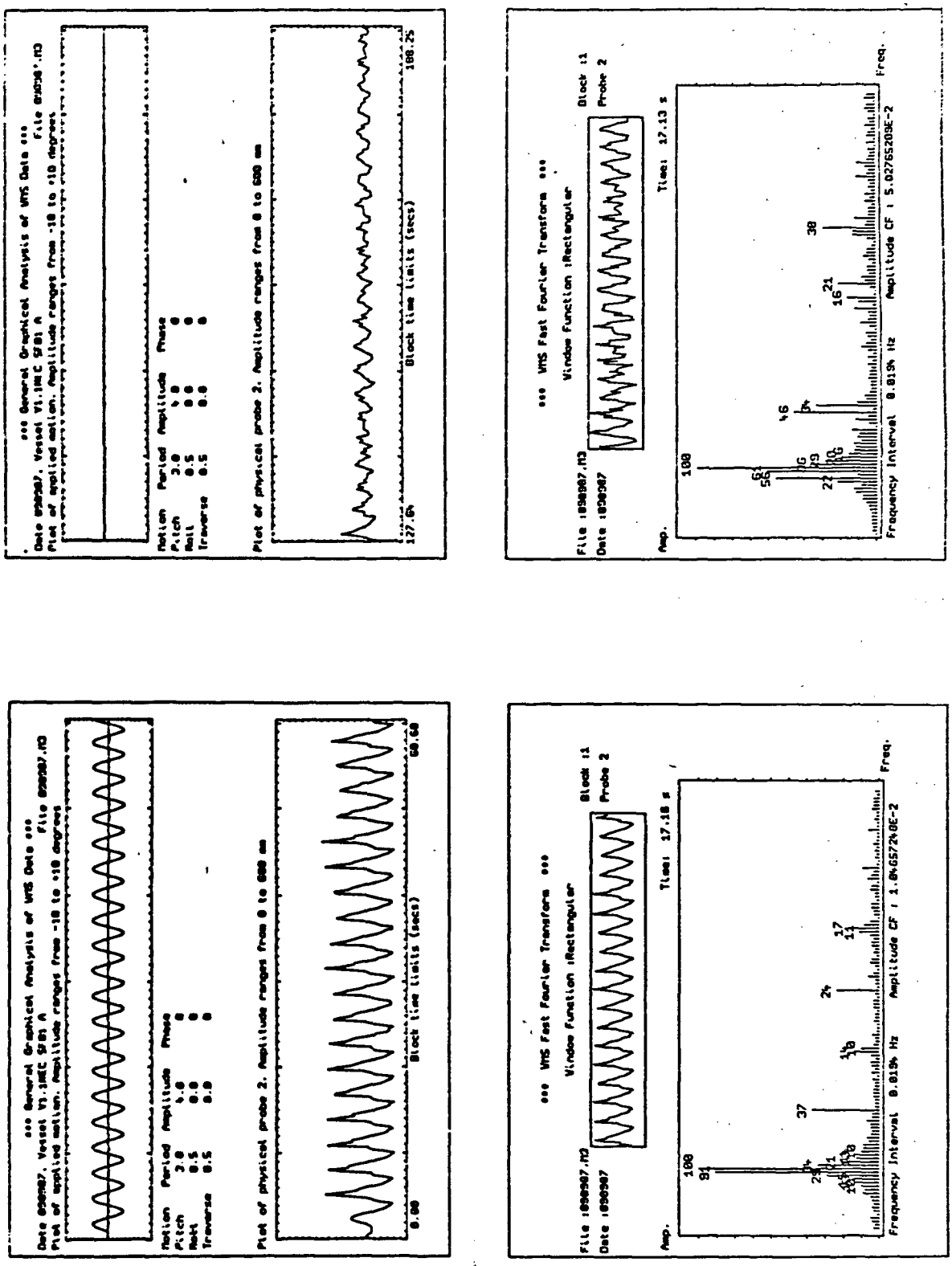

Graph A4.3: Pitch forcing motion at forcing period 3.0 seconds, ±4° amplitude.

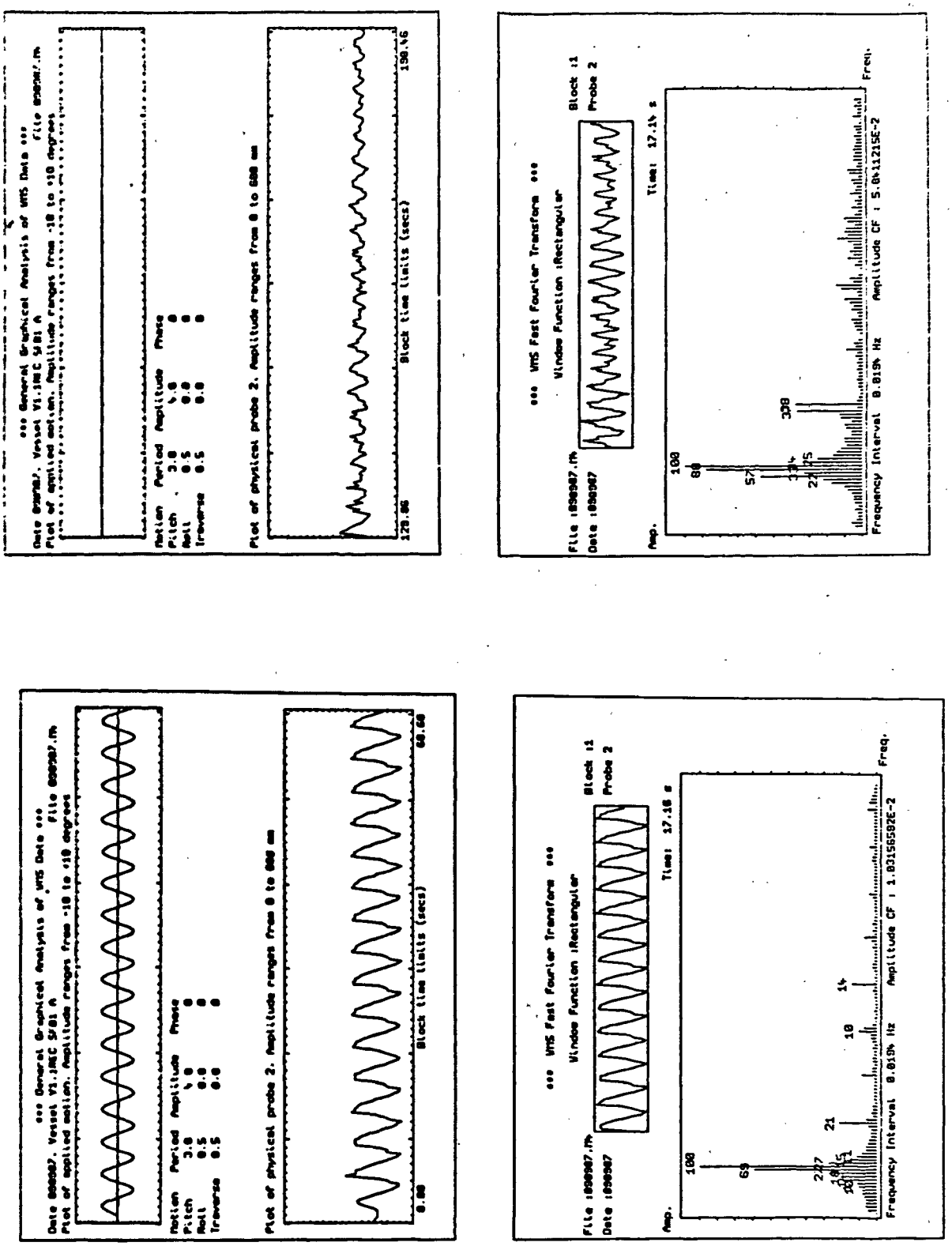

Graph A4.4: Pitch forcing motion at forcing period 3.8 seconds, ±4° amplitude.

Graph A4.5: Pitch forcing motion at forcing period 5.0 seconds, ±4° amplitude.

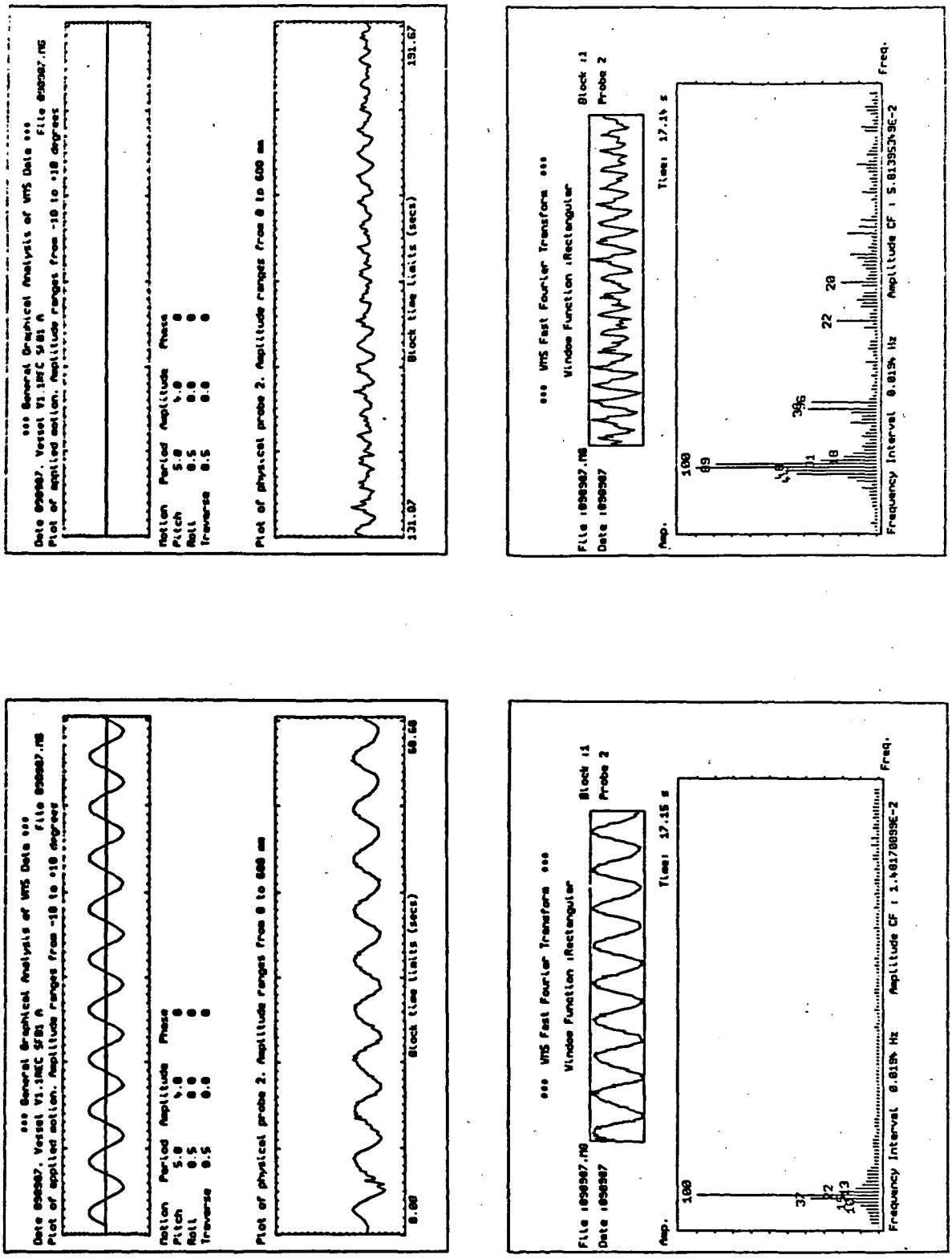

Graph A4.6: Pitch forcing motion at forcing period 5.8 seconds, ±4° amplitude.

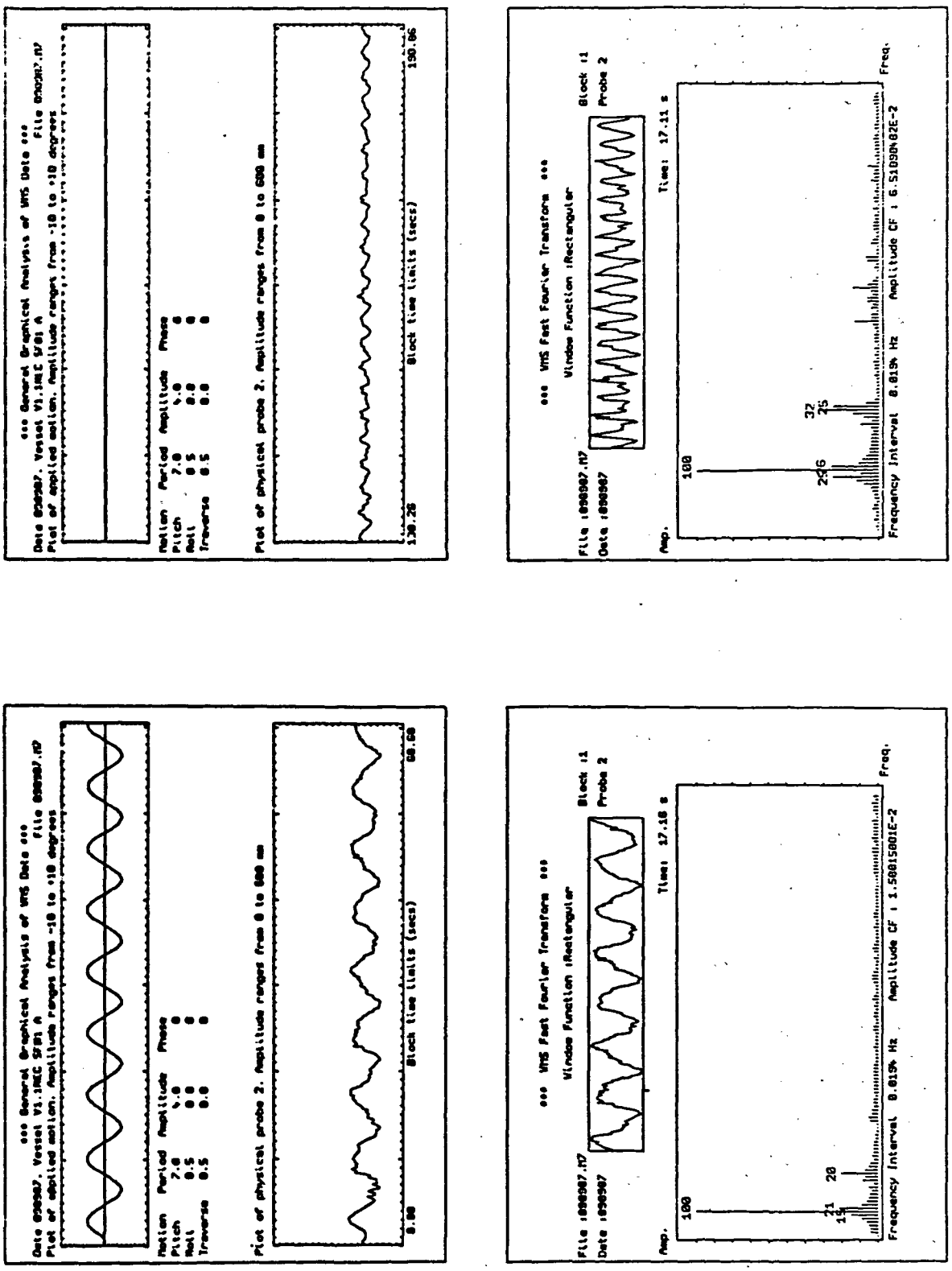

Graph A4.7: Pitch forcing motion at forcing period 7.0 seconds, ±4° amplitude.

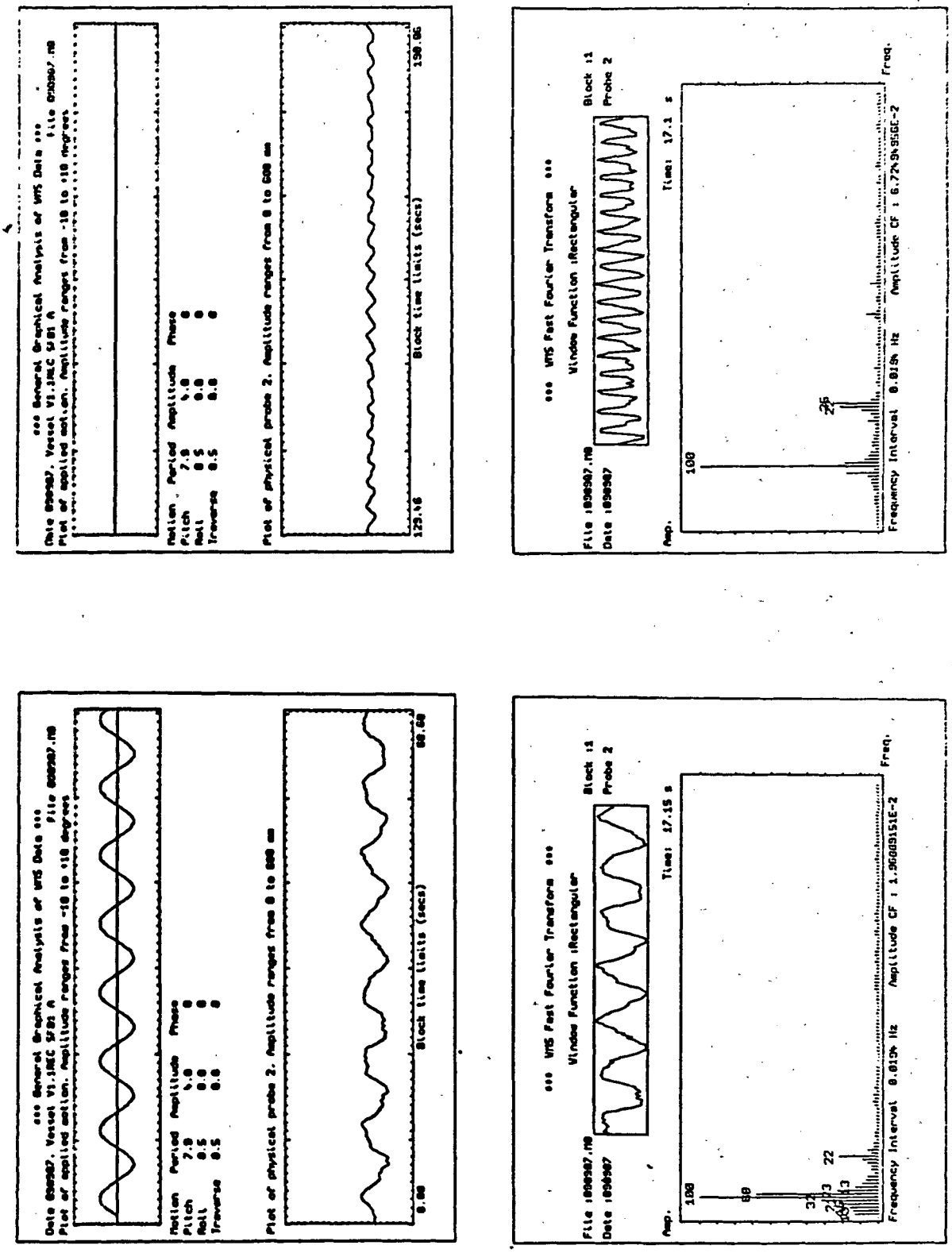

Graph A4.8: Pitch forcing motion at forcing period 7.9 seconds, ±4° amplitude.

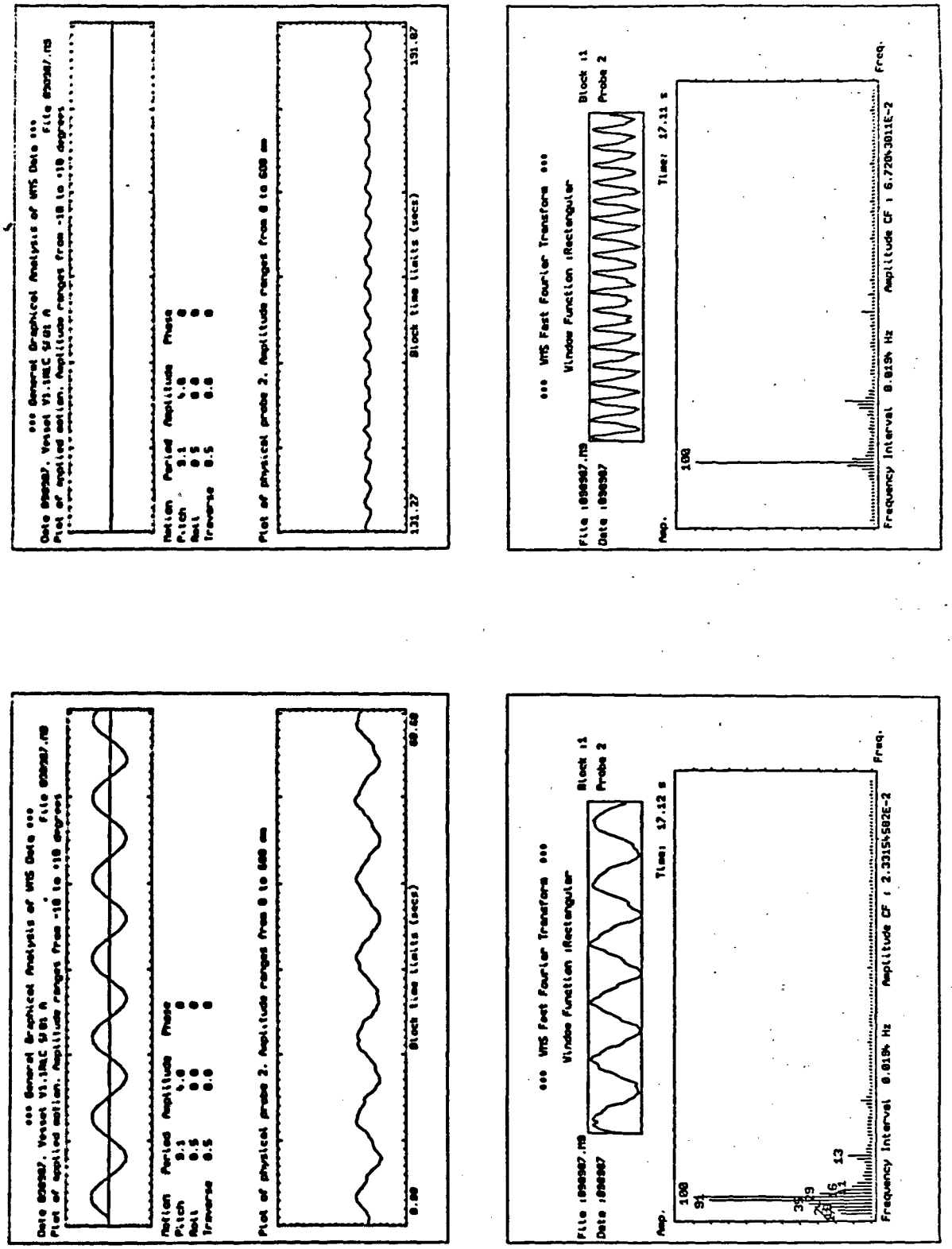

Graph A4.9: Pitch forcing motion at forcing period 9.1 seconds, ±4° amplitude.

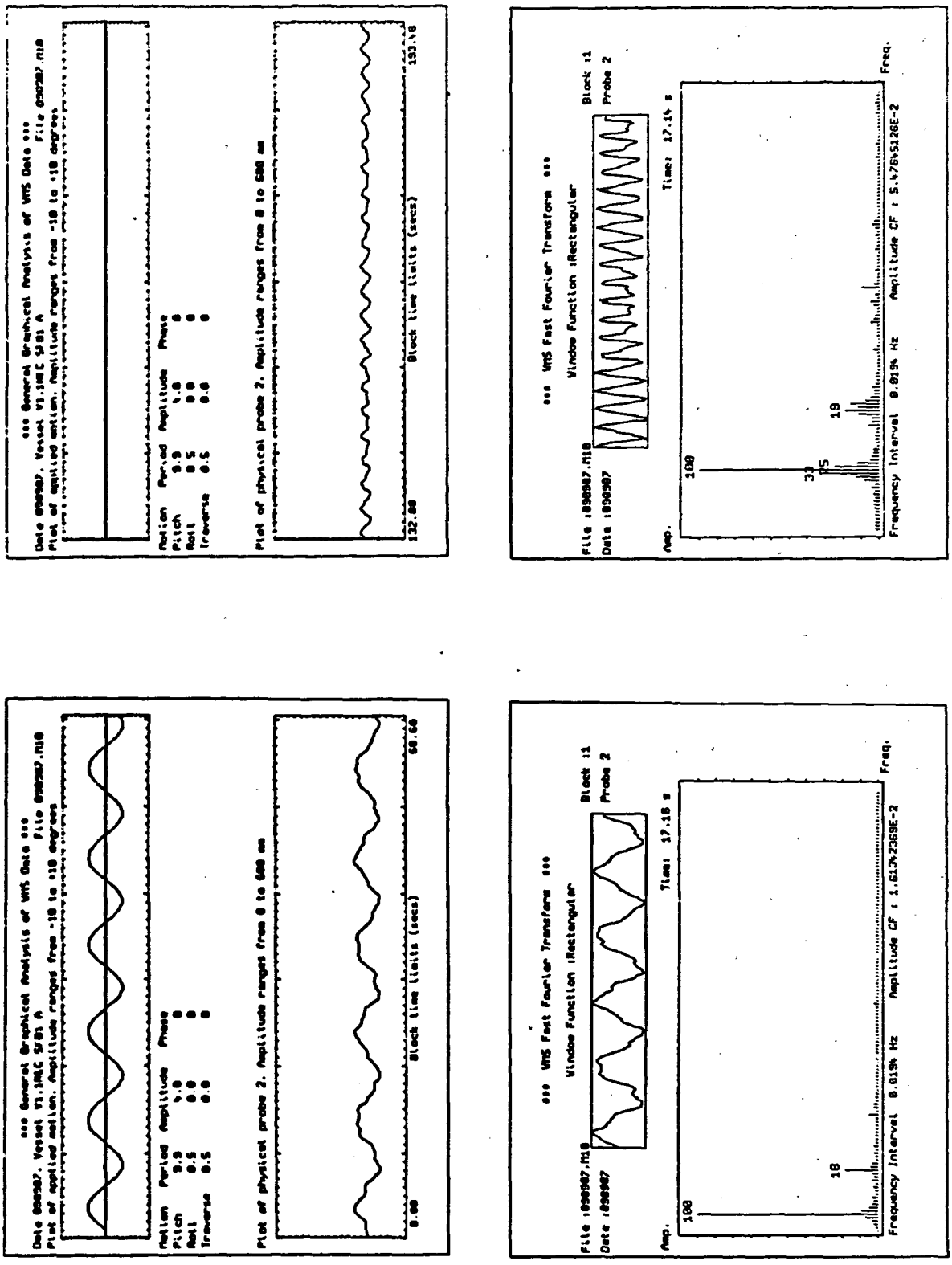

Graph A4.10: Pitch forcing motion at forcing period 9.9 seconds, ±4° amplitude.

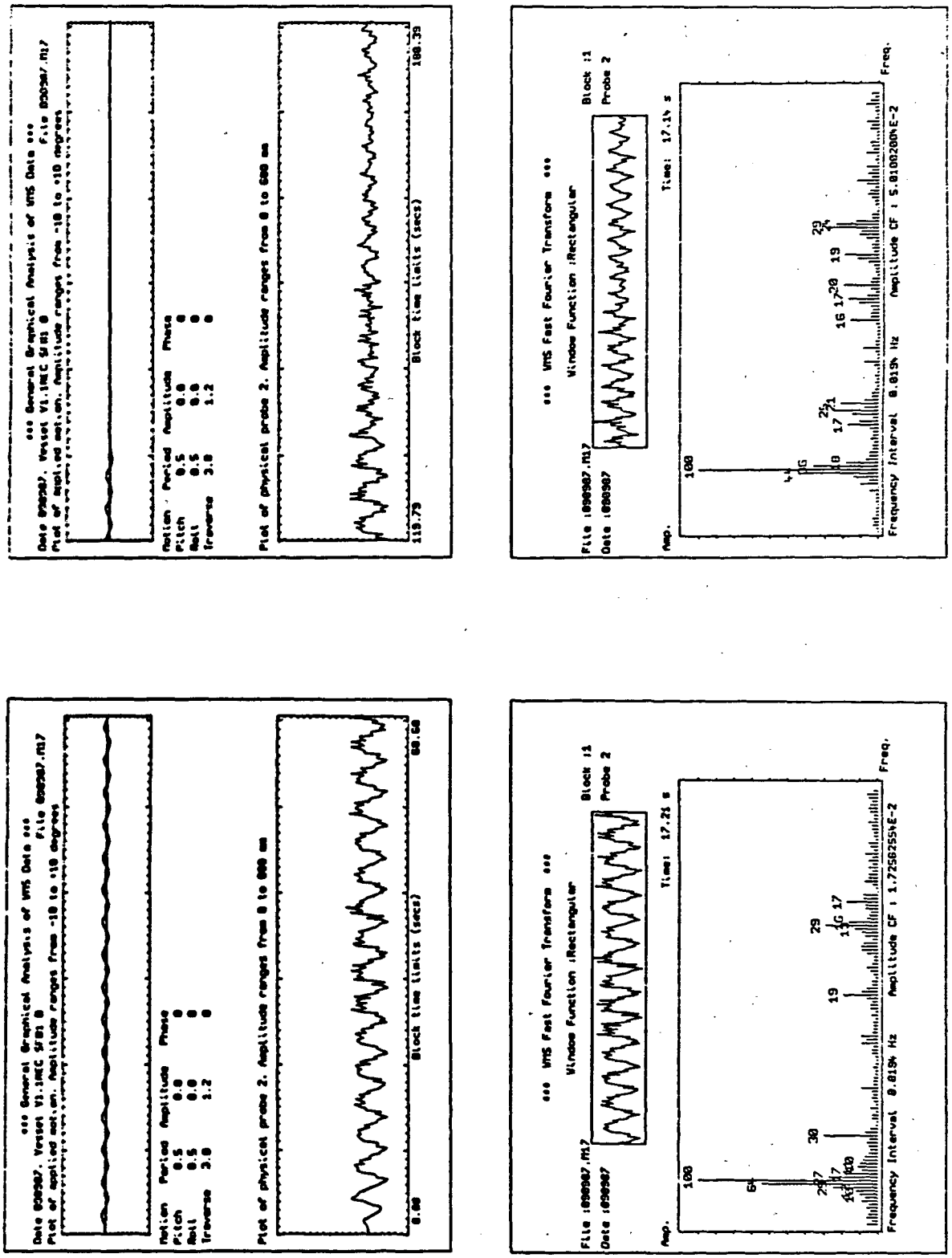

Graph A4.11: Surge forcing motion at forcing period 3.8 seconds, ±120mm amplitude.

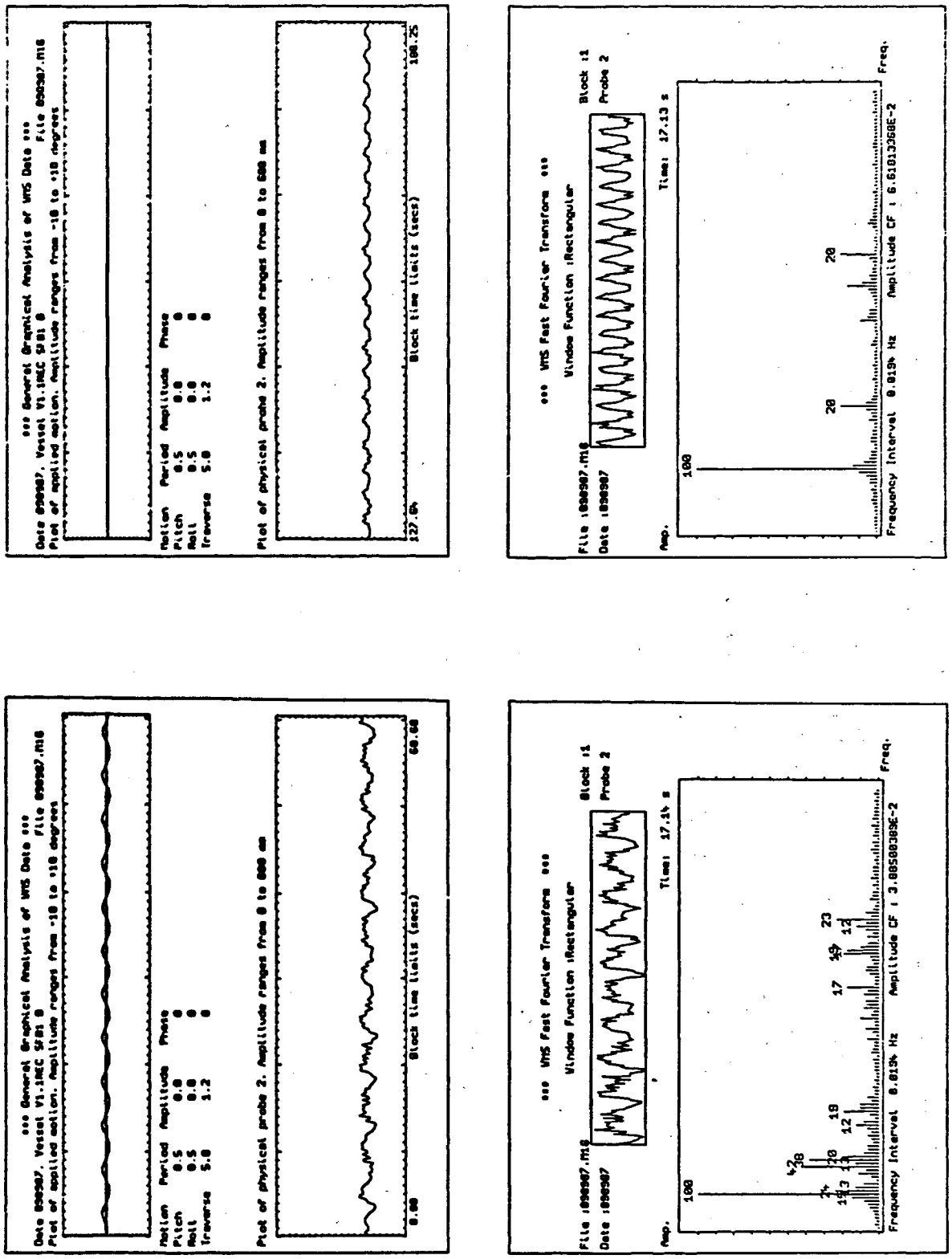

Graph A4.12: Surge forcing motion at forcing period 5.0 seconds, ±120mm amplitude.

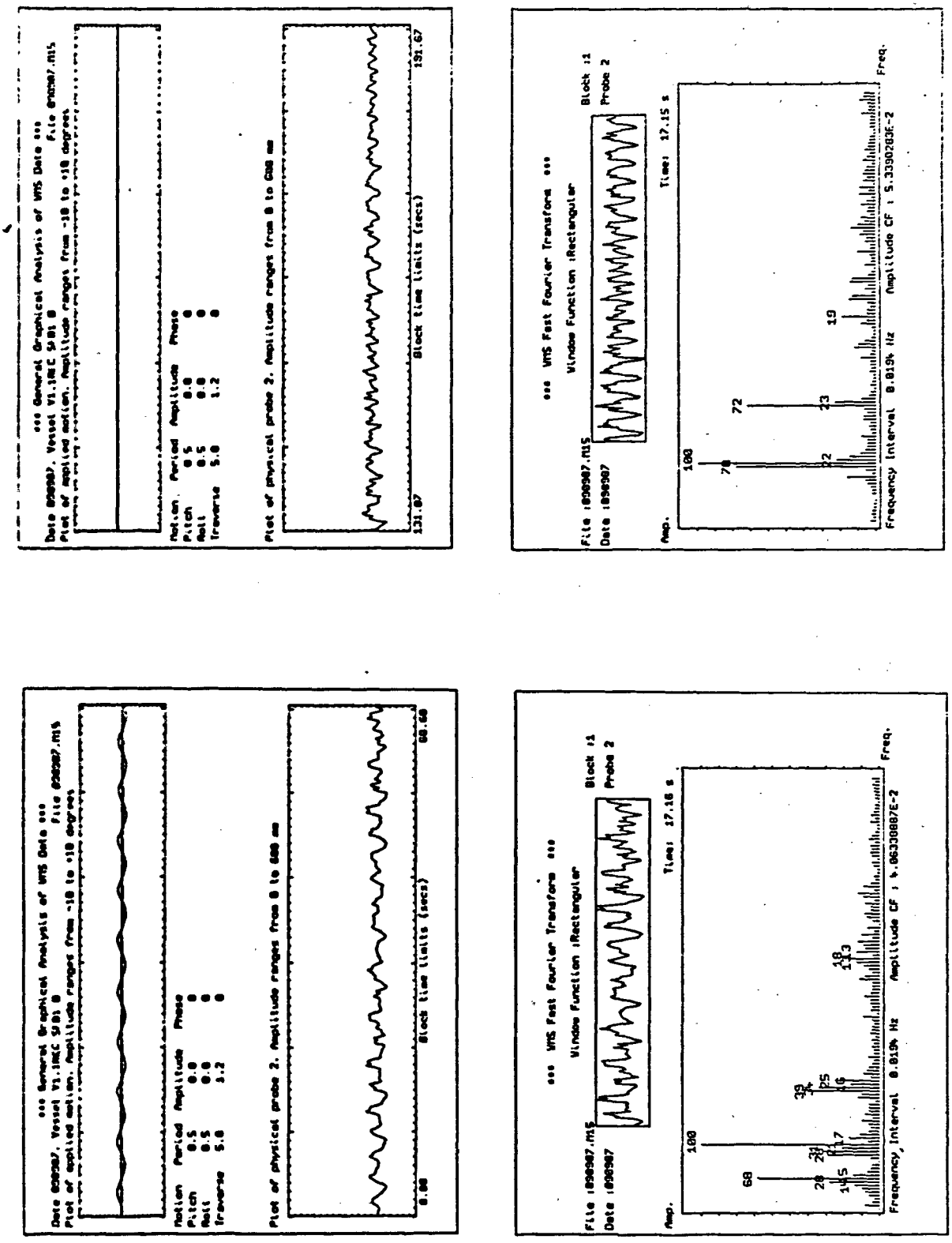

Graph A4.13: Surge forcing motion at forcing period 5.8 seconds, ±120mm amplitude.

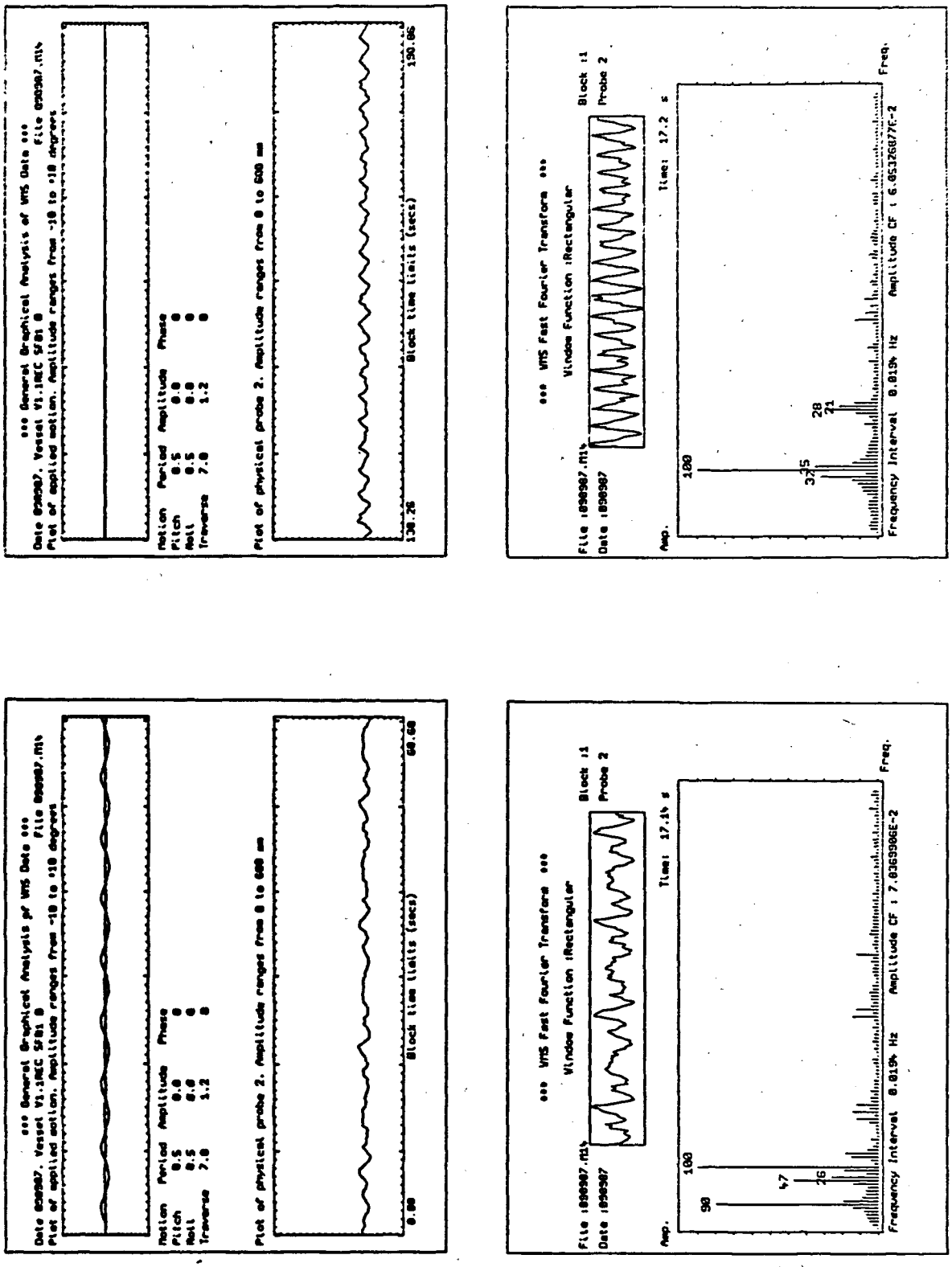

Graph A4.14: Surge forcing motion at forcing period 7.0 seconds, ±120mm amplitude.

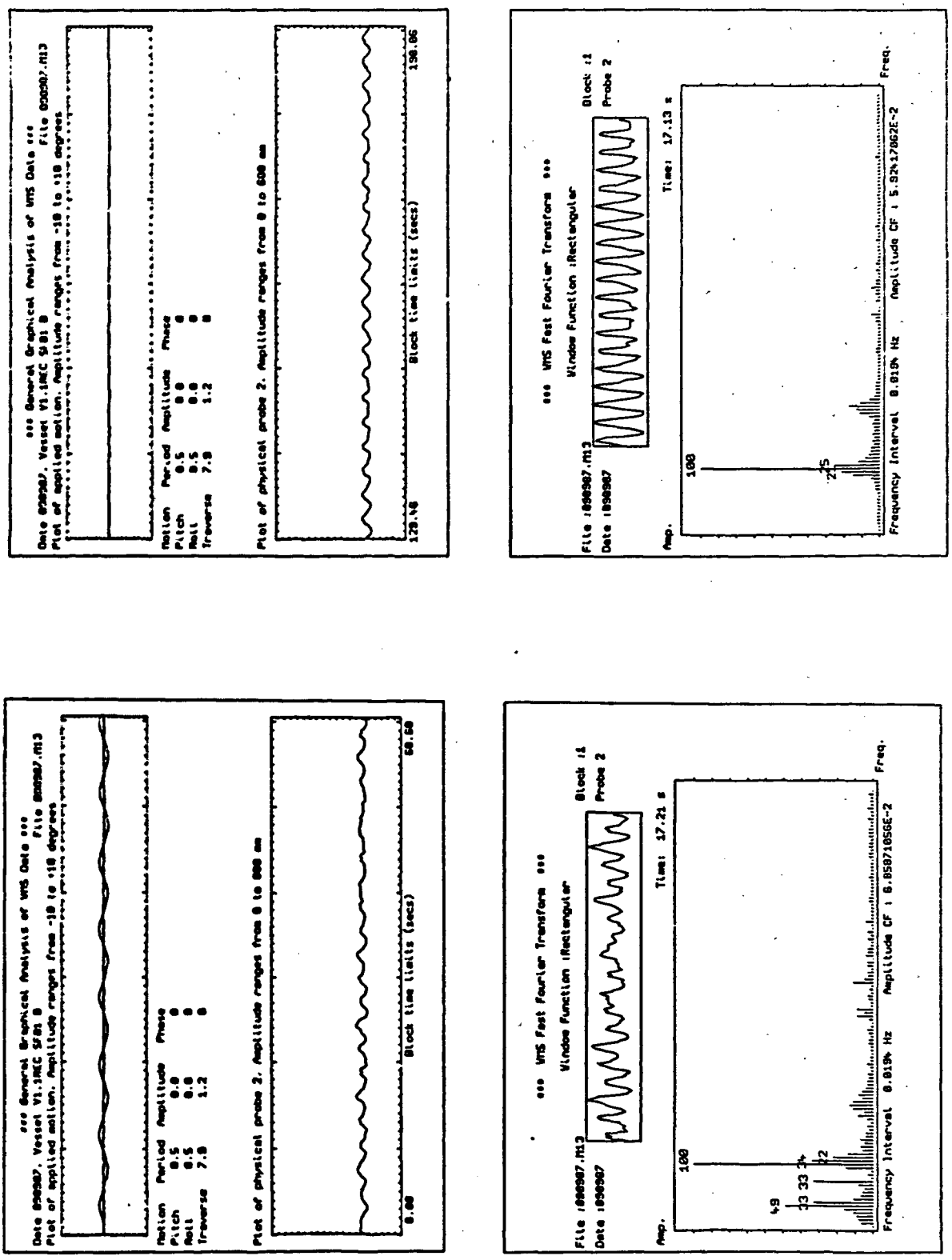

Graph A4.15: Surge forcing motion at forcing period 7.9 seconds, ±120mm amplitude.

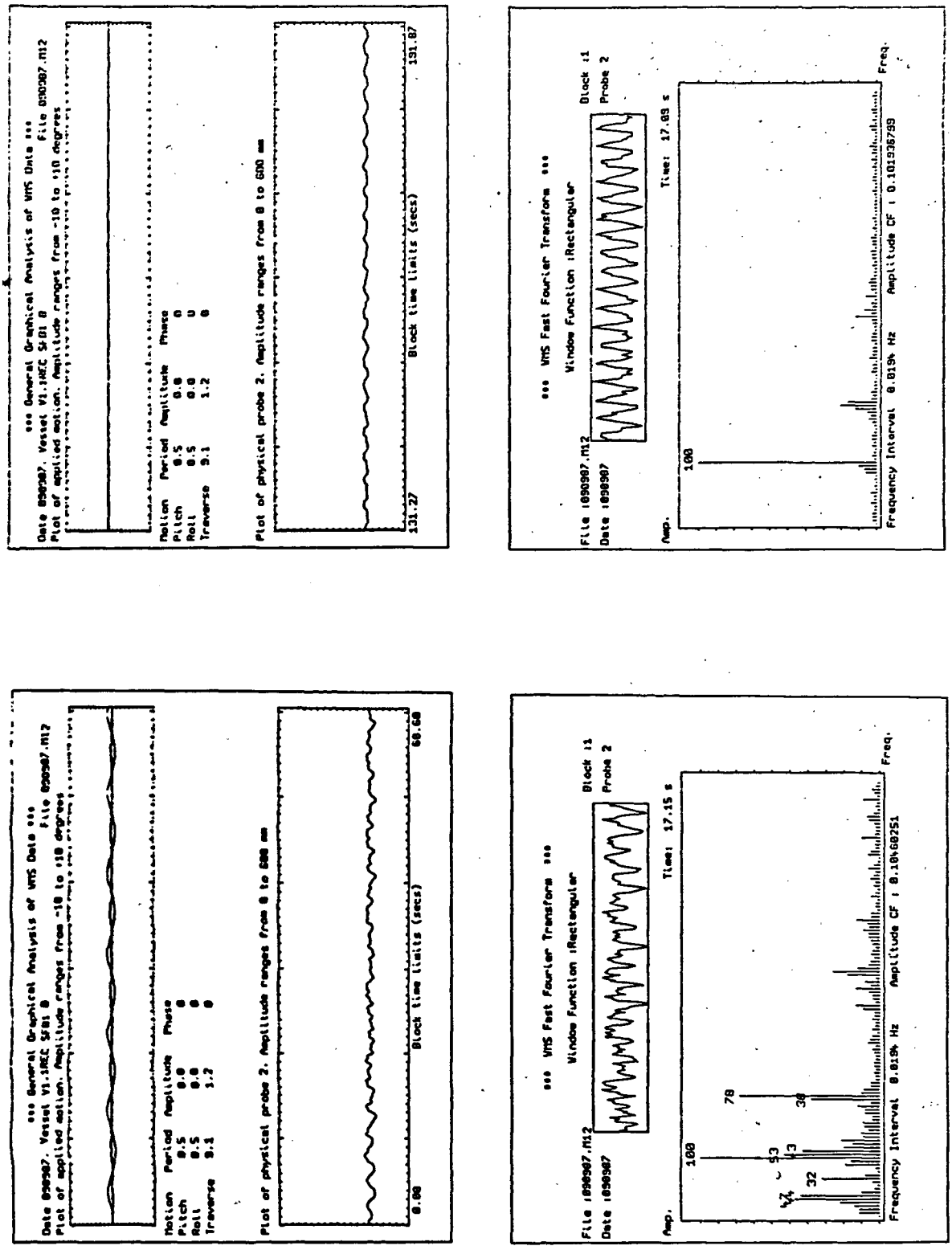

Graph A4.16: Surge forcing motion at forcing period 9.1 seconds, ±120mm amplitude.

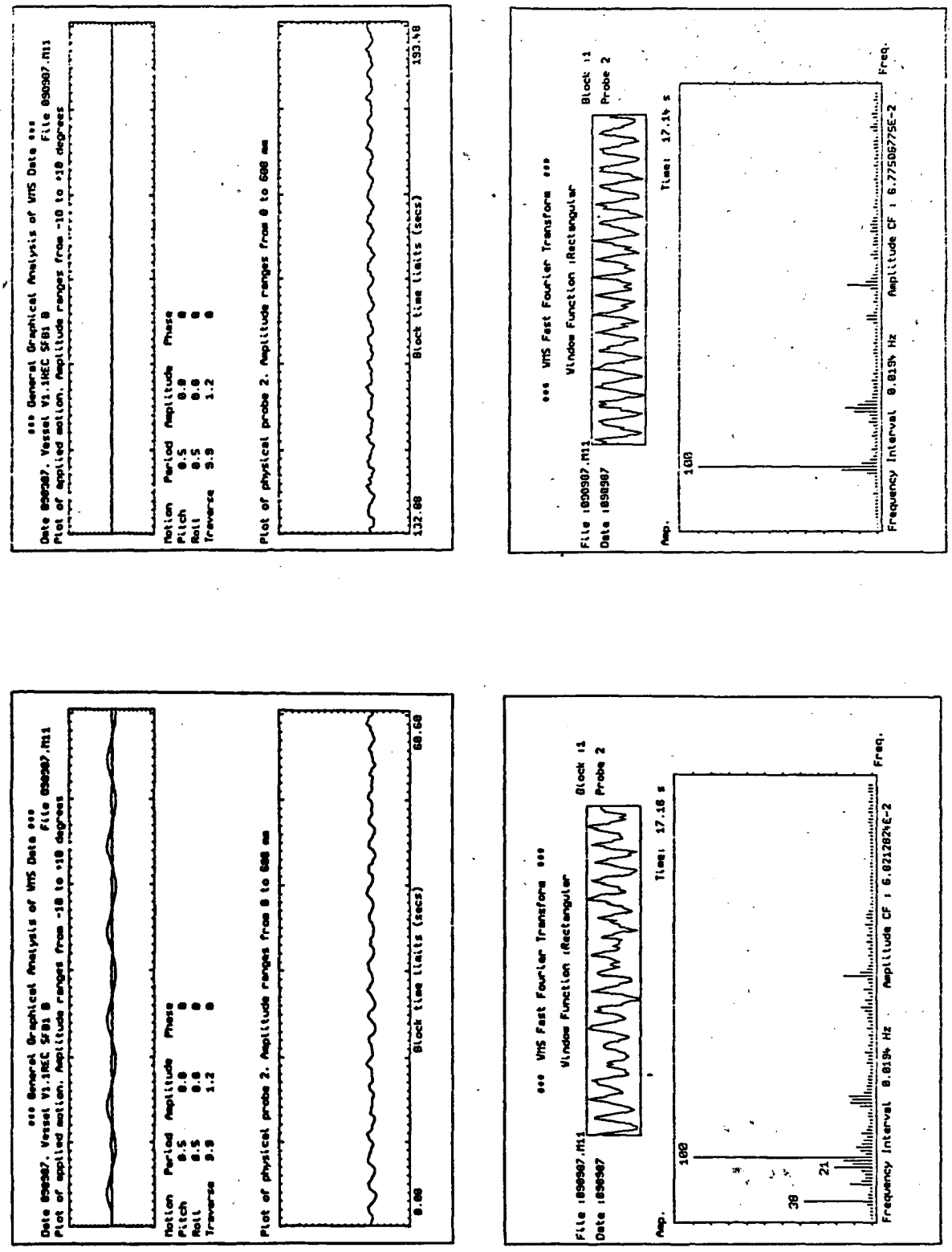

Graph A4.17: Surge forcing motion at forcing period 9.9 seconds, ±120mm amplitude.

APPENDIX V

PROBE 2 WAVE PROFILES AND FFT FREQUENCY SPECTRA FOR AIR/WATER EXPERIMENTS IN THE LARGE RECTANGULAR VESSEL UNDER SIMULTANEOUS FORCING MOTIONS.

1.1 INTRODUCTION.

This appendix presents wave profile data and corresponding FFT frequency spectra for probe 2 in the large rectangular vessel resulting from simultaneous pitch & roll, and pitch & surge forcing motions. Format of each plot, was given in chapter 6.

Each graph (A5.1 to A5.11) shows two sets of profile and spectra data. The first plot starts at time Ø and applies to the first minute of forcing. The second plot refers to some time later when forcing motion has ceased i.e. the decay profile.

Where two graphs are presented (i.e. graphs A5.5a-b and A5.10a-b) the first two plots refer to forcing and decay, the third plot refers to some time during forcing motion. These serve to illustrate the effect of natural period components within the wave spectrum (chapter 8).

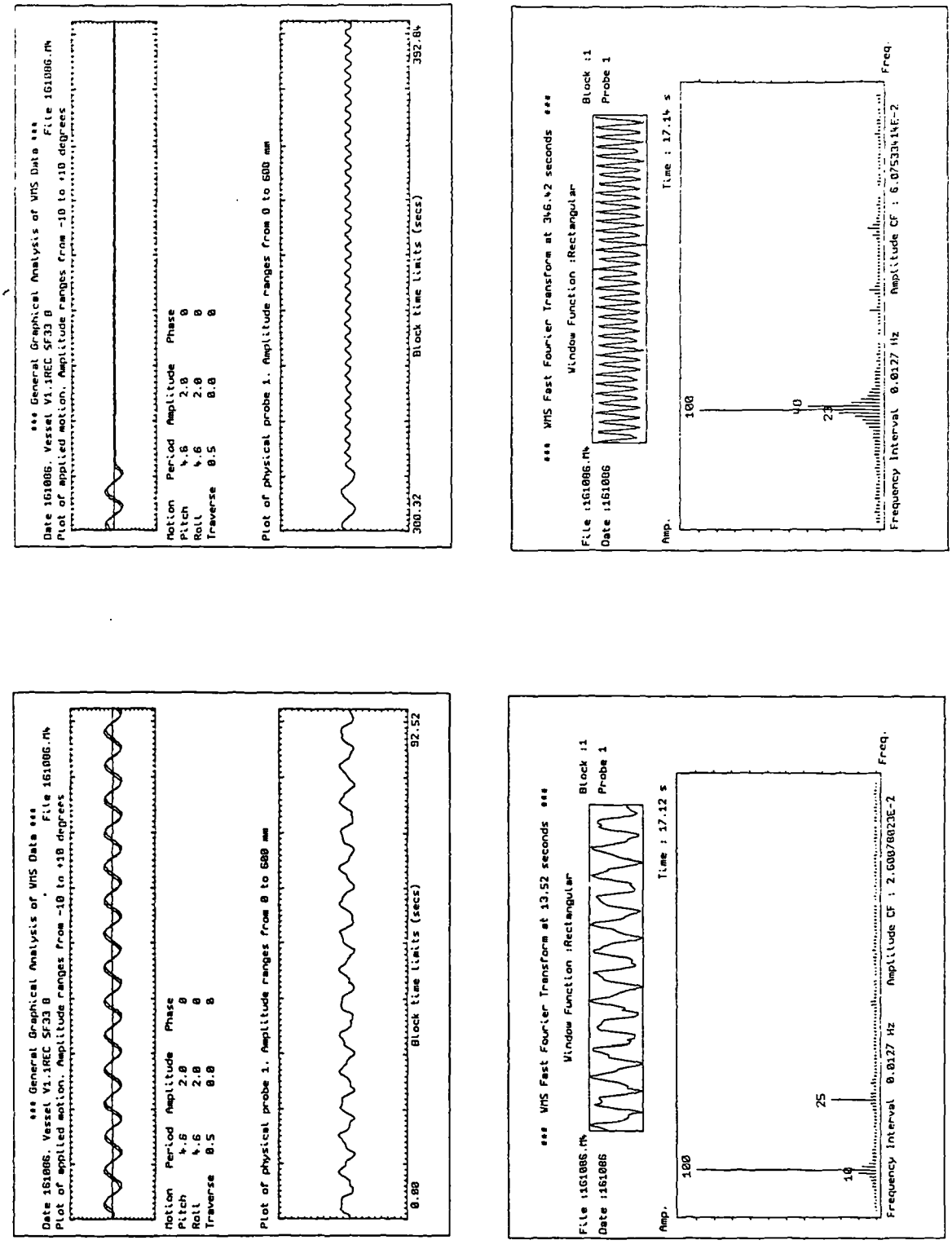

Graph A5.1: Combined pitch & roll forcing motion at forcing periods 4.6, 4.6 seconds, ±2°, ±2° amplitude respectively. Phase angle Ø°.

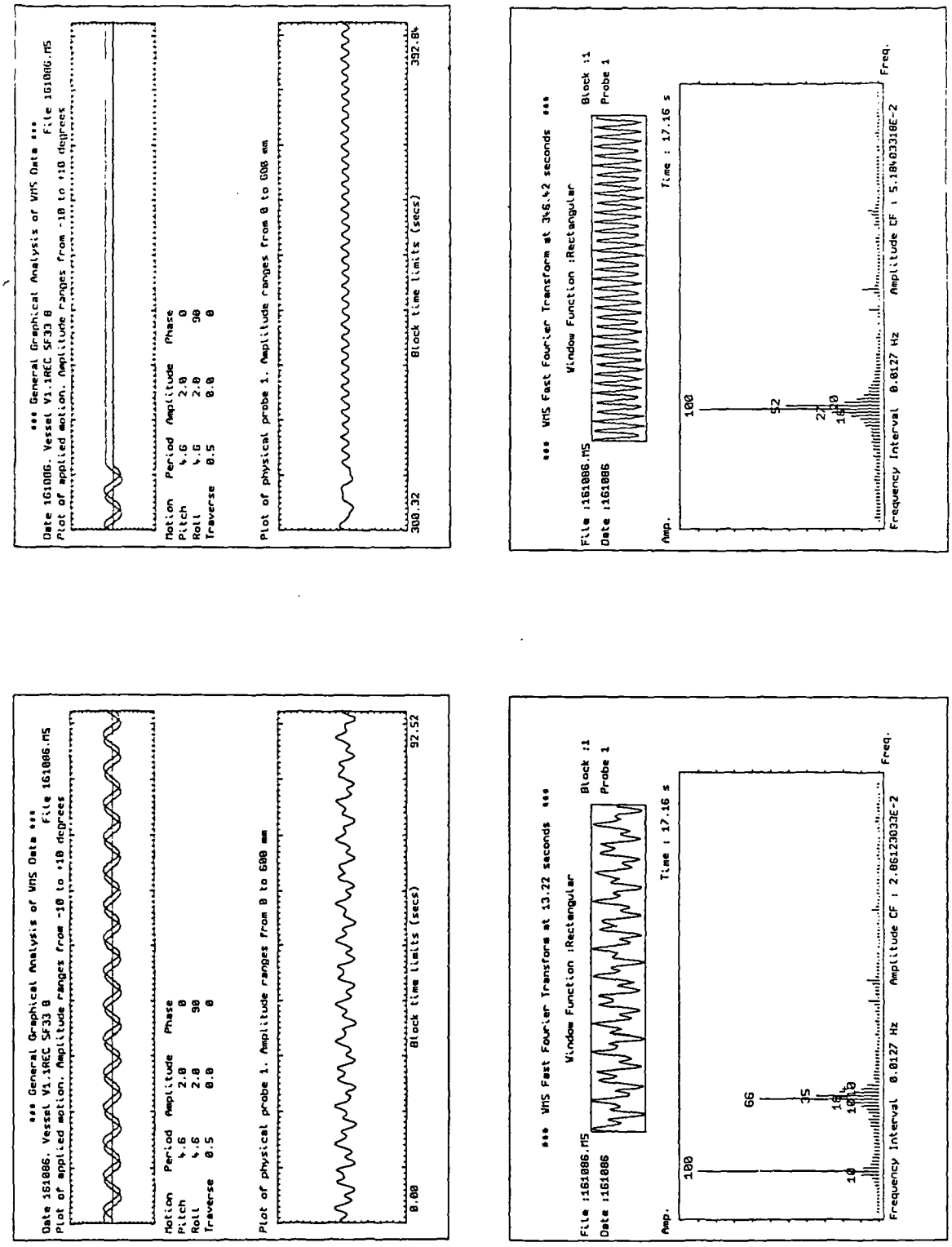

Graph A5.2: Combined pitch & roll forcing motion at forcing periods 4.6, 4.6 seconds, ±2°, ±2° amplitude, respectively. Phase angle 90°.

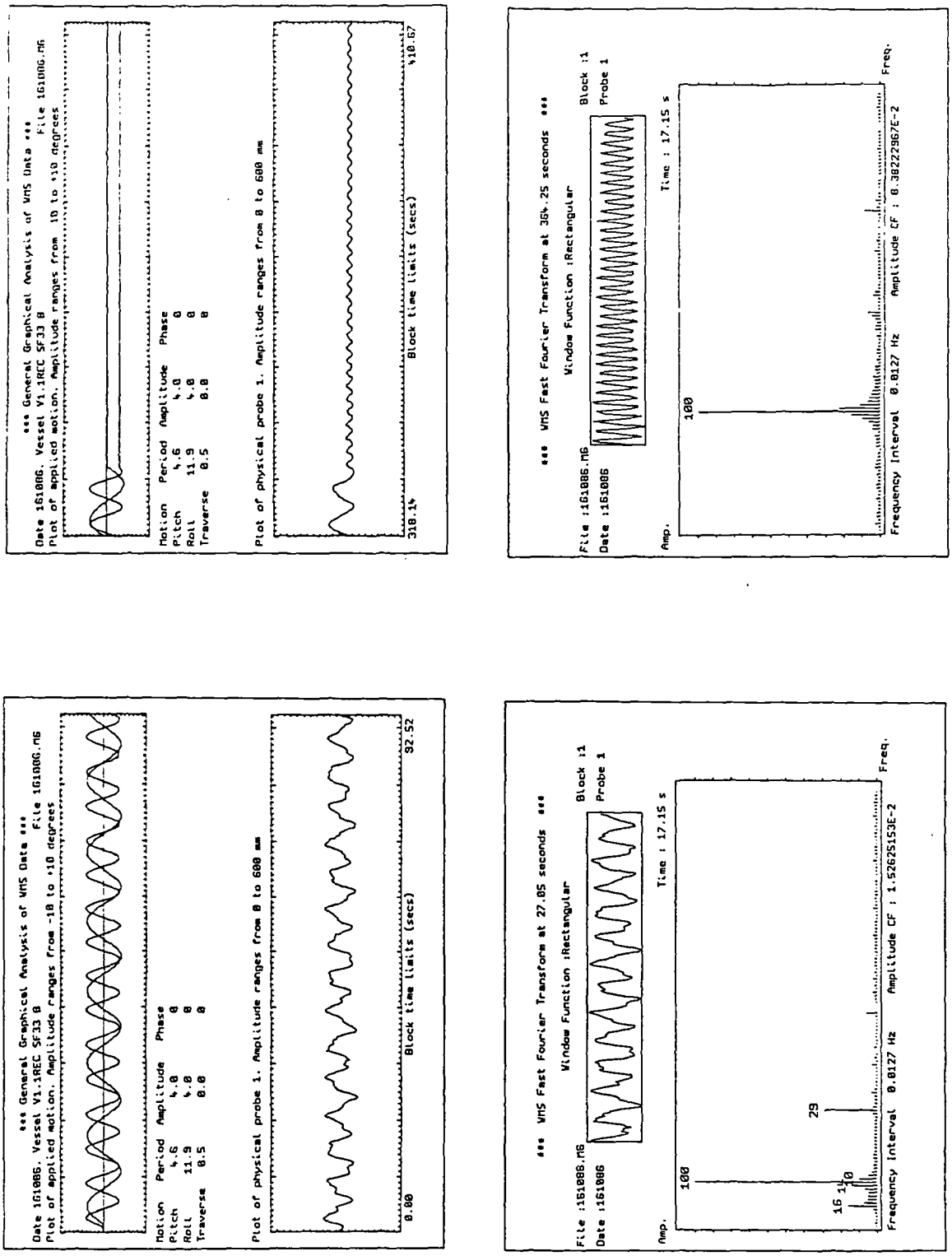

Graph A5.3: Combined pitch & roll forcing motion at forcing periods 4.6, 11.9 seconds, ±4°, ±4° amplitude, respectively. Phase angle 0°.

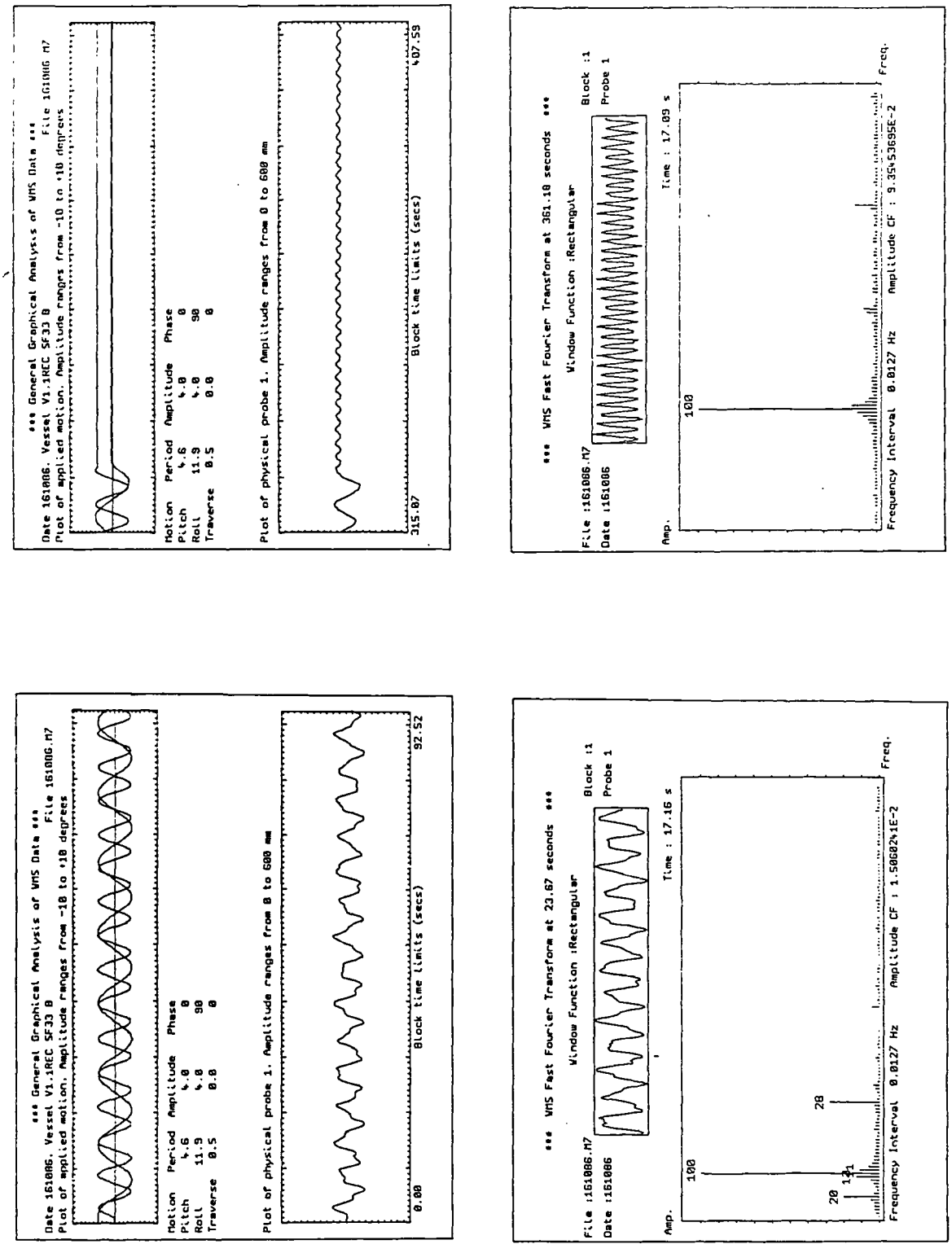

Graph A5.4: Combined pitch & roll forcing motion at forcing periods 4.6, 11.9 seconds, ±4°, ±4° amplitude, respectively. Phase angle 90°.

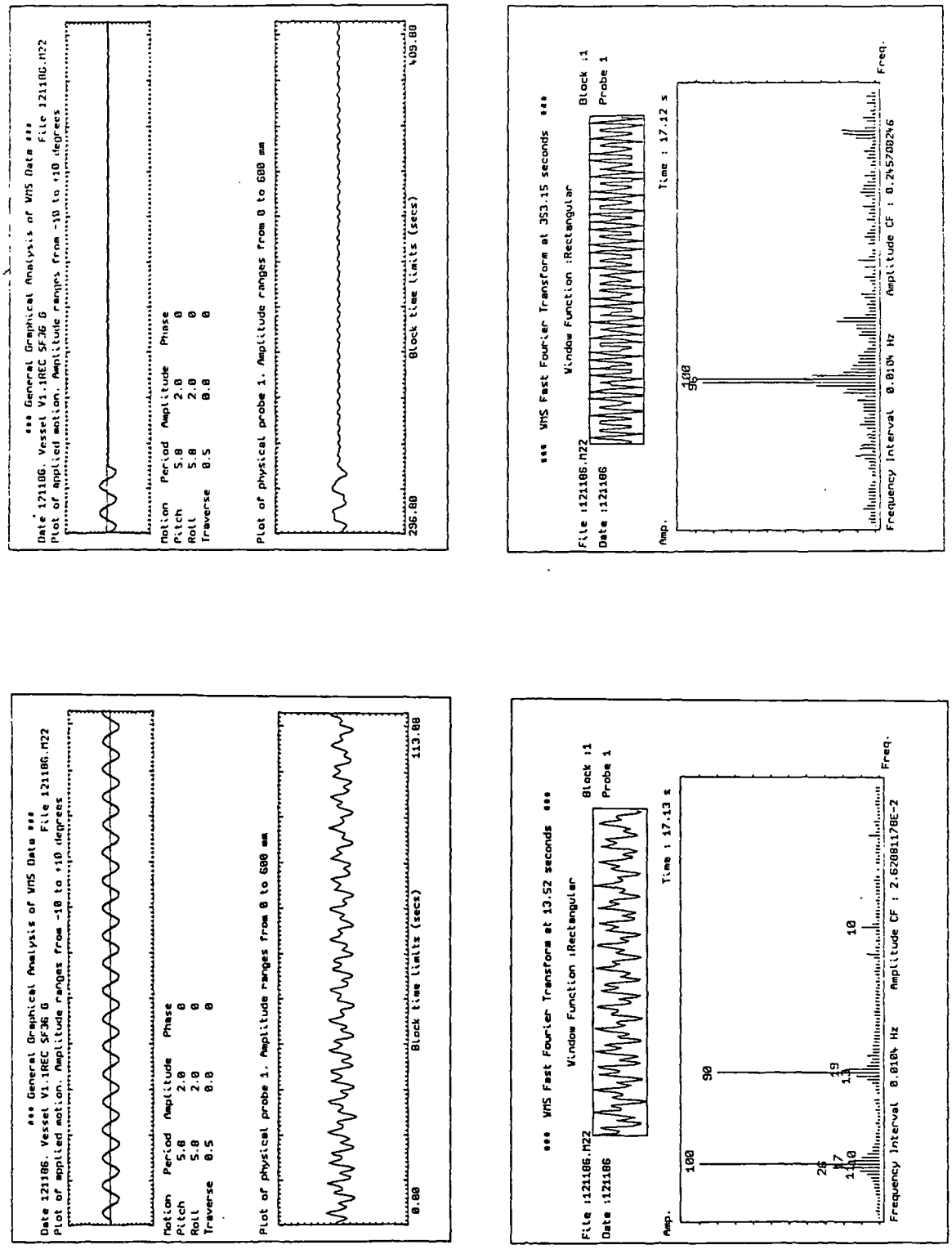

Graph A5.5a: Combined pitch & roll forcing motion at forcing periods 5.8, 5.8 seconds, ±2°, ±2° amplitude, respectively. Phase angle 0°.

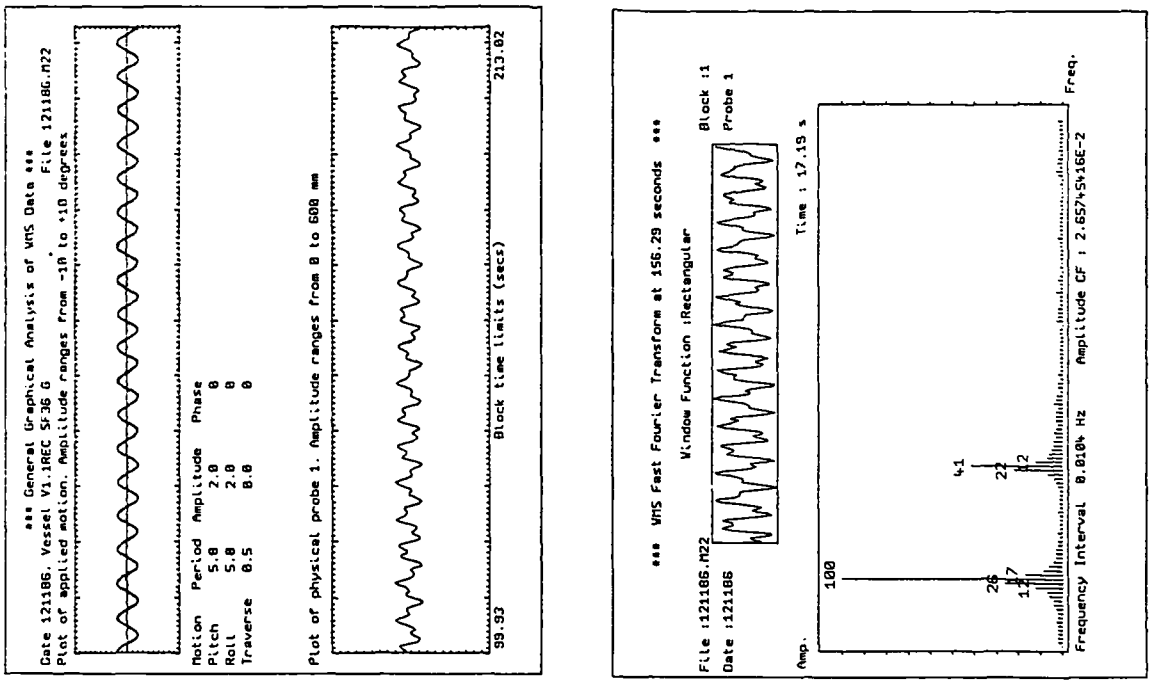

Graph A5.5b: Combined pitch & roll forcing motion at forcing periods 5.8, 5.8 seconds, ±2°, ±2° amplitude, respectively. Phase angle 0° (cont).

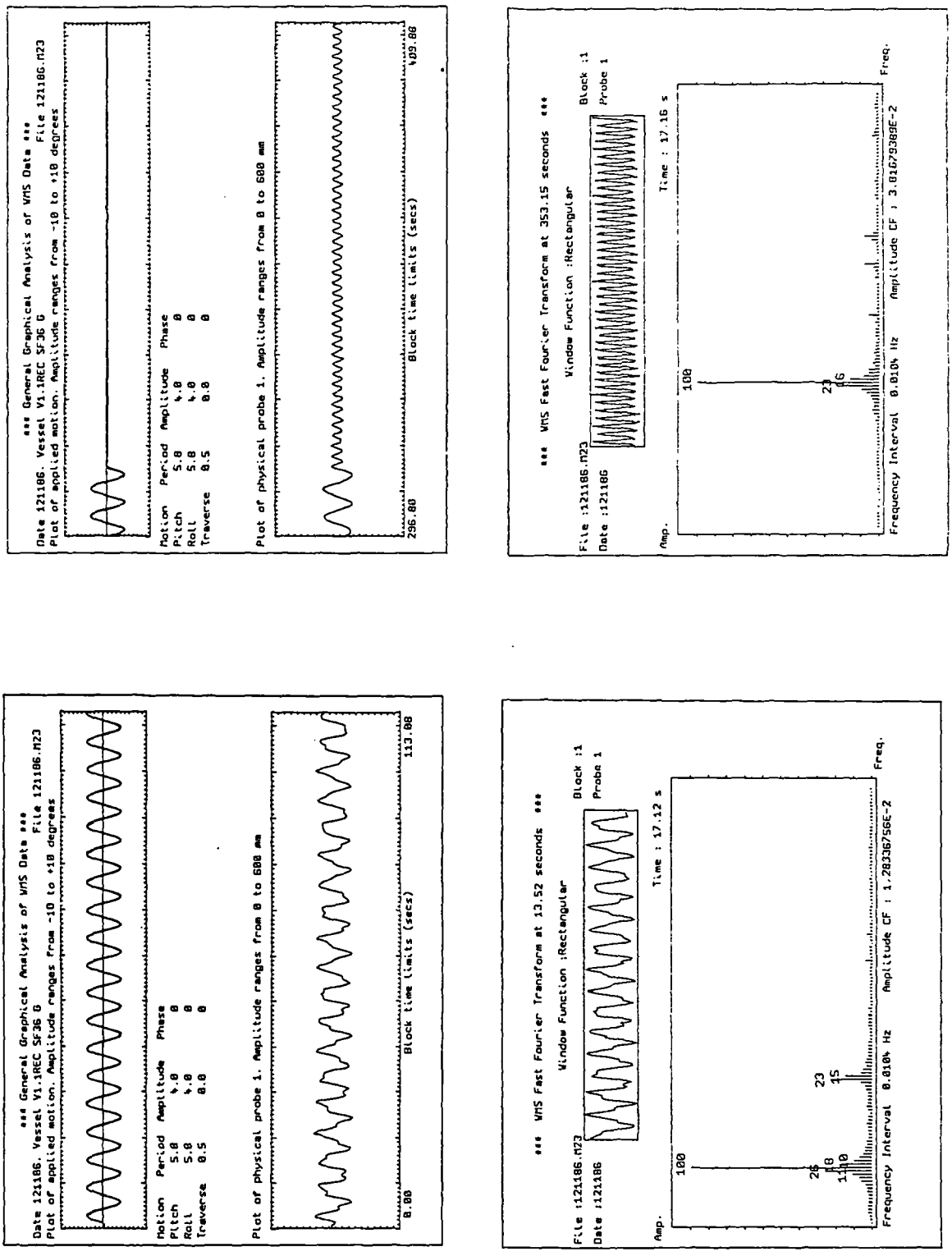

Graph A5.6: Combined pitch & roll forcing motion at forcing periods 5.8, 5.8 seconds, ±4°, ±4° amplitude, respectively. Phase angle 0°.

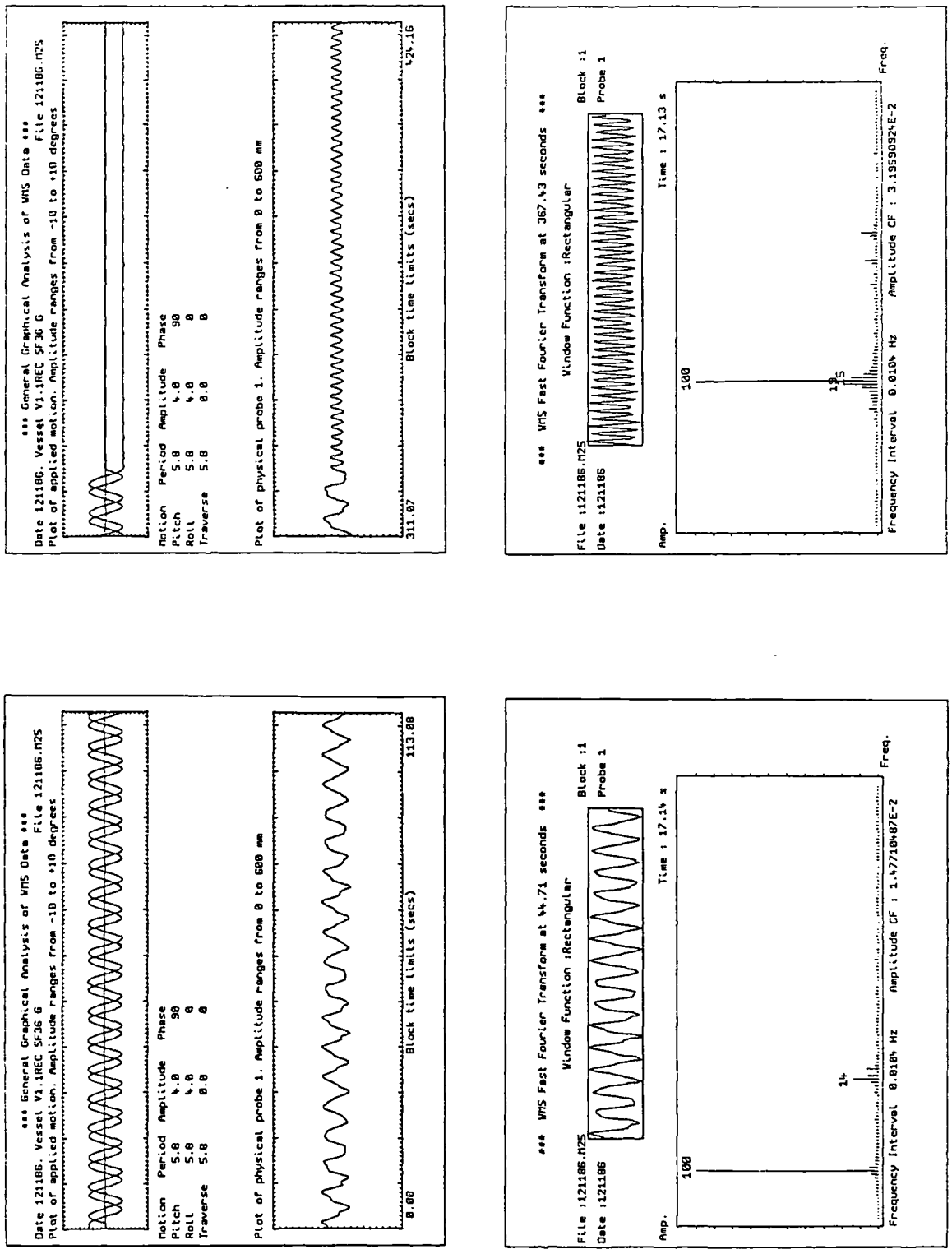

Graph A5.7: Combined pitch & roll forcing motion at forcing periods 5.8, 5.8 seconds, ±4°, ±4° amplitude, respectively. Phase angle 90°.

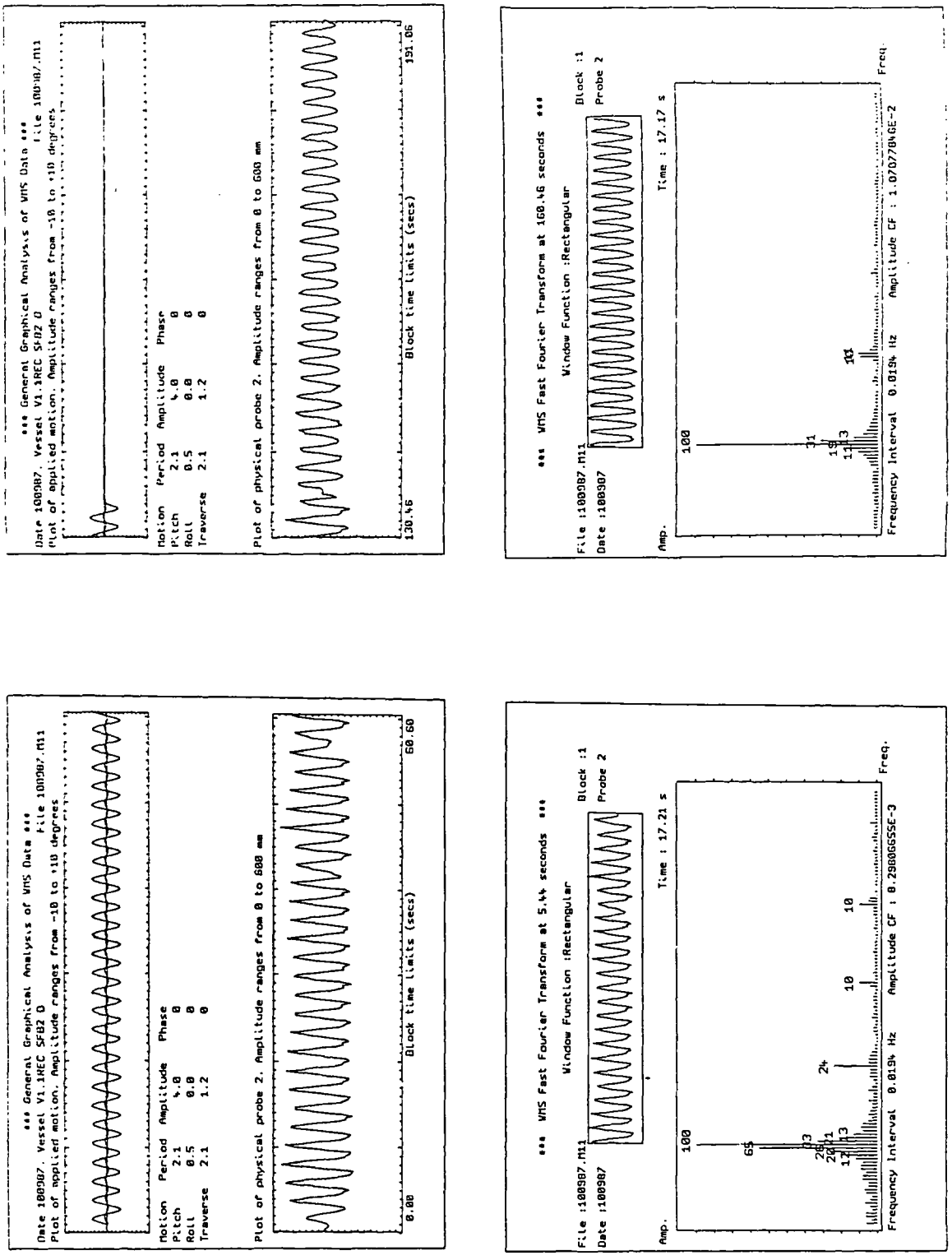

Graph A5.8: Combined pitch & surge forcing motion at forcing periods 2.1, 2.1 seconds, ±4°, ±120mm amplitude, respectively. Phase angle 0°.

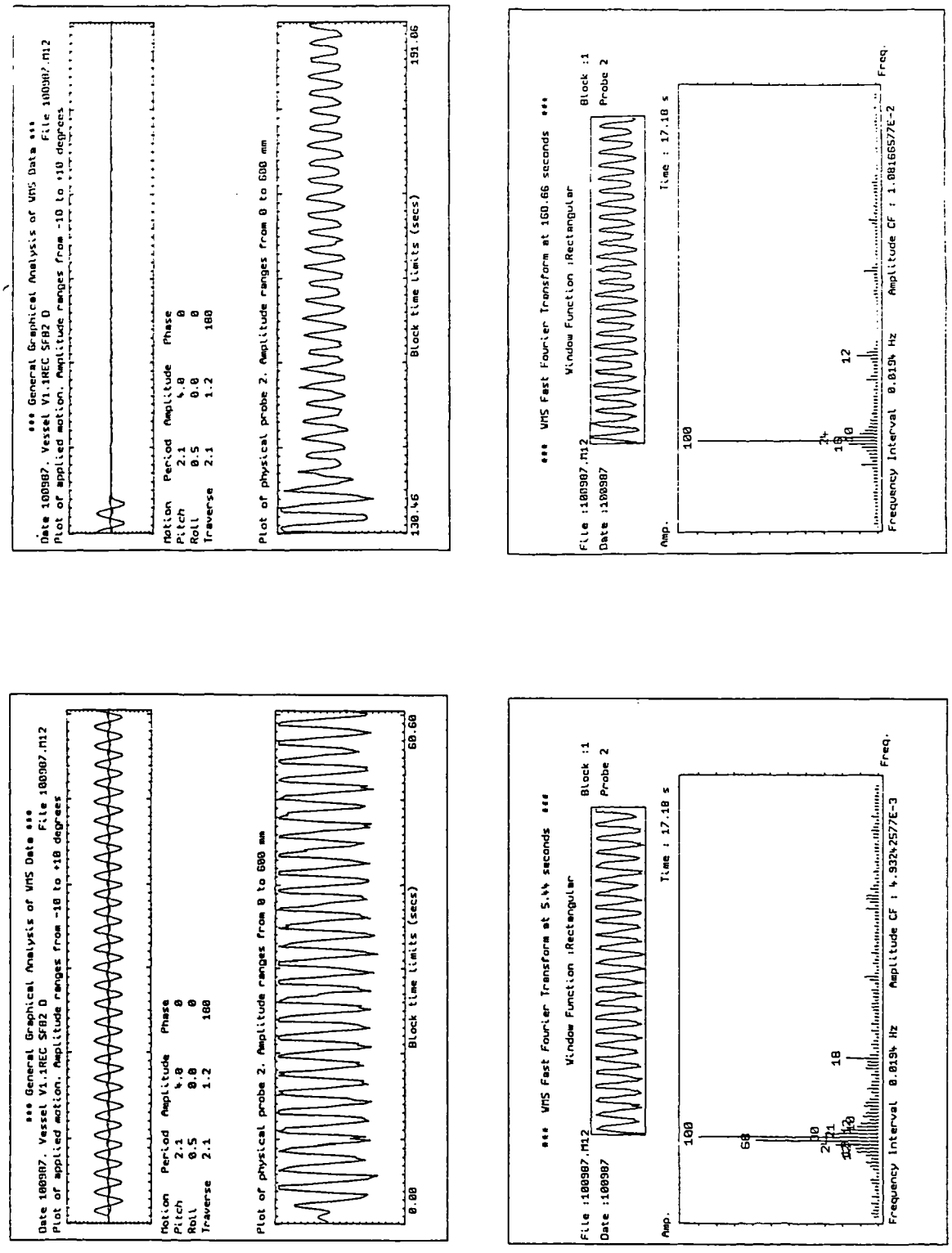

Graph A5.9: Combined pitch & surge forcing motion at forcing periods 2.1, 2.1 seconds, ±4°, ±120mm amplitude, respectively. Phase angle 180°.

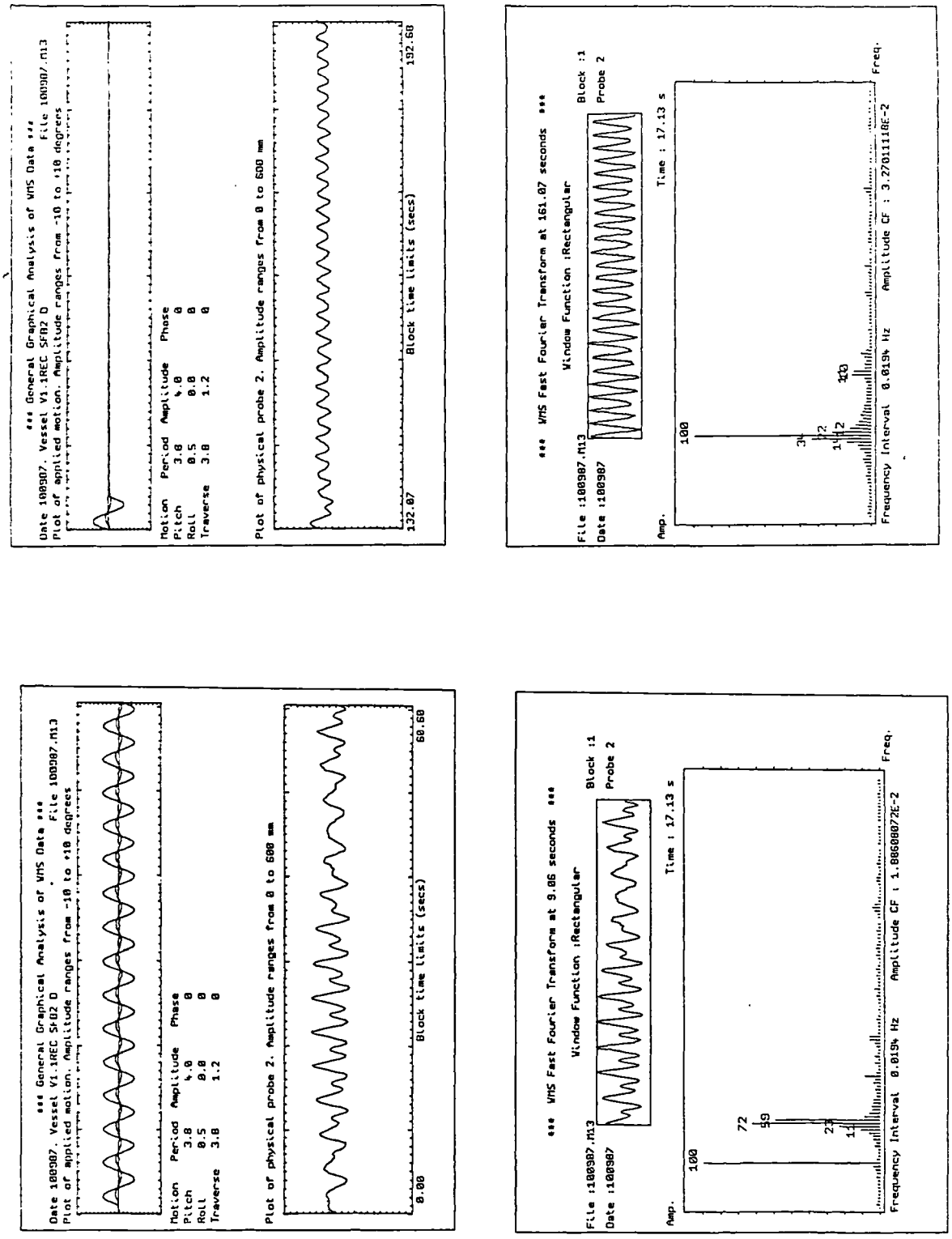

Graph A5.10a: Combined pitch & surge forcing motion at forcing periods 3.8, 3.8 seconds, ±4°, ±120mm amplitude, respectively. Phase angle 0°.

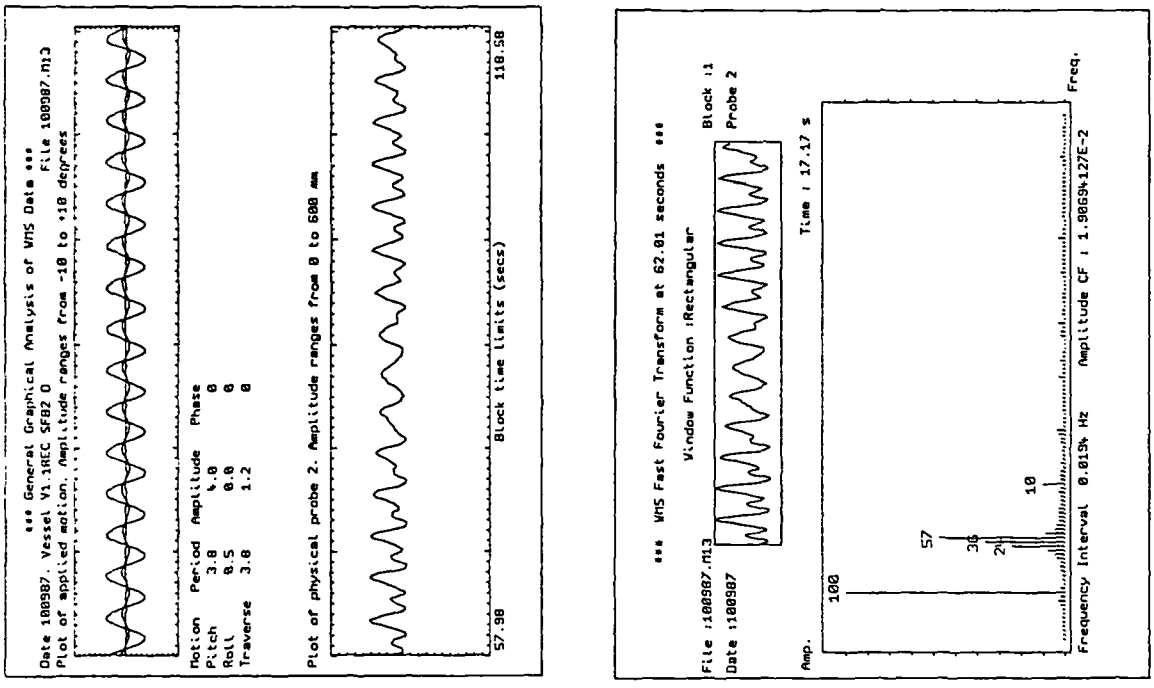

Graph A5.10b: Combined pitch & surge forcing motion at forcing periods 3.8, 3.8 seconds, ±4°, ±120mm amplitude, respectively. Phase angle 0° (cont).

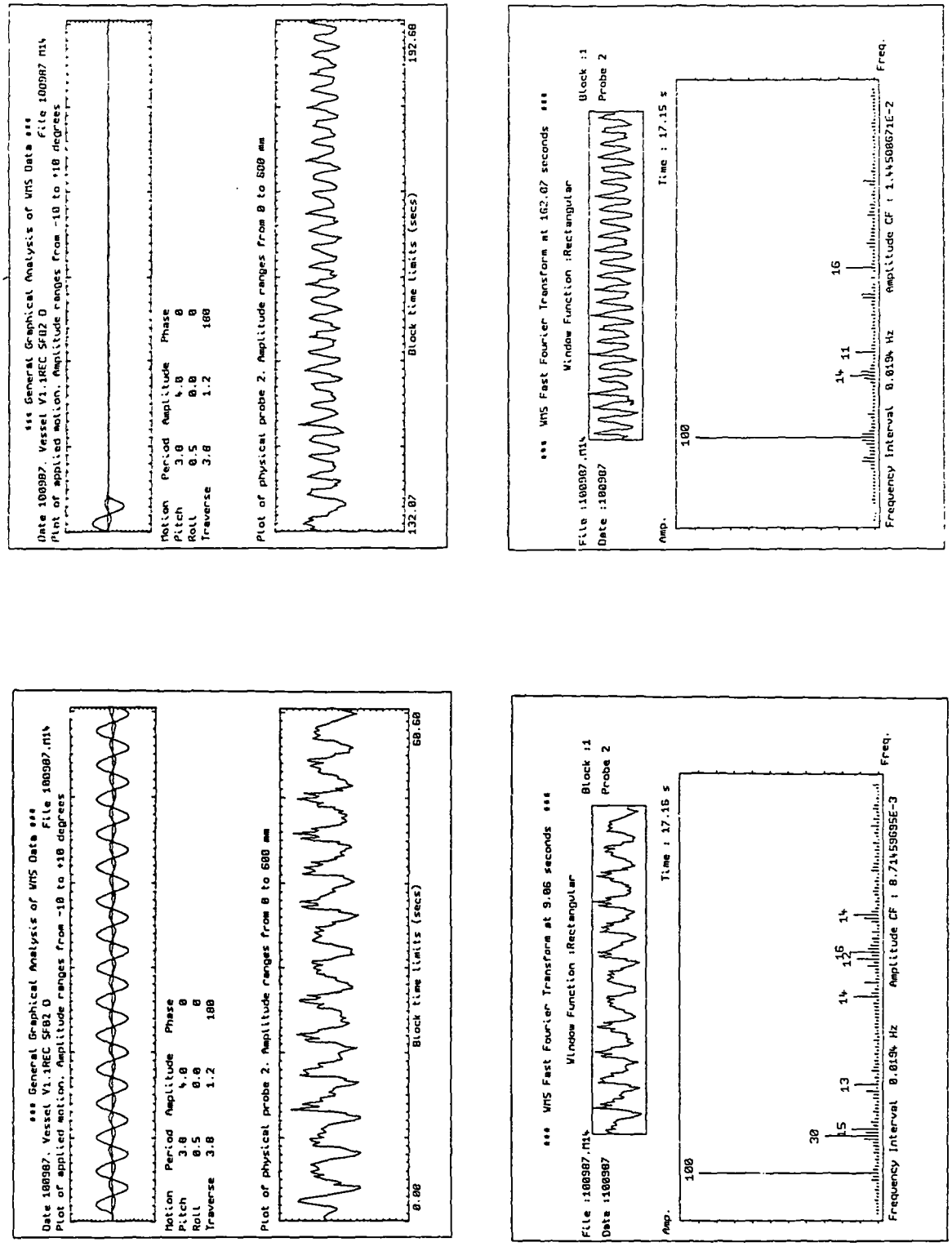

Graph A5.11: Combined pitch & surge forcing motion at forcing periods 3.8, 3.8 seconds, ±4°, ±120mm amplitude, respectively. Phase angle 180°.

APPENDIX VI

EXPERIMENTAL PROCEDURE AND SAMPLE ANALYSIS FOR OIL-IN-WATER EXPERIMENTS IN THE LARGE RECTANGULAR VESSEL.

1.1 INTRODUCTION.

This appendix presents the experimental procedure followed to determine the concentration of oil in water from samples, obtained during experiments with the large rectangular vessel.

The results and further details were presented in chapter 11.

1.2 EXPERIMENTAL PREPARATION.

The procedure adopted for oil-in-water measurement required all sample containers to be made of glass with sealed lids to prevent hydrocarbon contamination by external sources. The following procedure was adopted prior to experimentation :

1) Glass sample bottles were washed and then left overnight in Decon 90 (10-20%), to be rinsed with distilled water before sealing with aluminum foil. Steeping in Decon 90 ensured that IR active components would be removed from the glass surface. The foil prevented possible contamination from the sample bottle tops.

2) During testing, a quantity of water was allowed to flow through the sample ports before collecting in a sample jar. The jar was then sealed, again with aluminum foil.

3) Samples were stored until analysis the following day.

1.3 SAMPLE ANALYSIS.

In analysing samples, the equipment used (Horiba OCAM-220 Oil Content Analyser) relied on extraction of oil from a water sample by shaking with the solvent 112-Trichlorotrifluoroethane (Freon 113). For

this purpose the unit was supplied with a built in extractor system unit which, during calibration, was found to cause problems due to contamination of the extraction chamber by successive samples. An external extraction process was adopted both for calibration of the unit and sample analysis :

1) Water sample of 100ml was placed in a 250ml separating funnel.

2) Five drops of HCl was then added (diluted as recommended 1:1 with distilled water).

3) 100ml of Freon 113 solvent was added.

4) The mixture was then shaken by hand for 2 minutes and allowed to settle.

5) The heavier solvent layer was drawn from the base of the funnel. All the oil originally in the water would now be in the solvent.

6) 15ml of extracted solvent was placed into the OCA and the oil concentration recorded. This was repeated until three consecutive reading were taken.

As in the actual sampling procedure, all utensils were made from glass previously immersed in a Decon 90 bath for 2 to 12 hours.

APPENDIX VII

PROBE 2 WAVE PROFILES AND FFT FREQUENCY SPECTRA FOR AIR/WATER NUMERICAL SIMULATION EXPERIMENTS IN THE LARGE RECTANGULAR VESSEL.

1.1 INTRODUCTION.

This appendix presents wave profile data and corresponding FFT frequency spectra for probe 2 resulting from numerical simulation experiments with the large rectangular vessel. Pitch forcing motion was applied at various periods at $\pm 4^{\circ}$ amplitude. The format of each plot was given in chapter 6.

Each graph (A7.1 to A7.10) shows two sets of profile and spectra data. The first plot starts at time 0 and applies to the first minute of forcing. The second plot refers to some time later when forcing motion had ceased i.e. the decay profile.

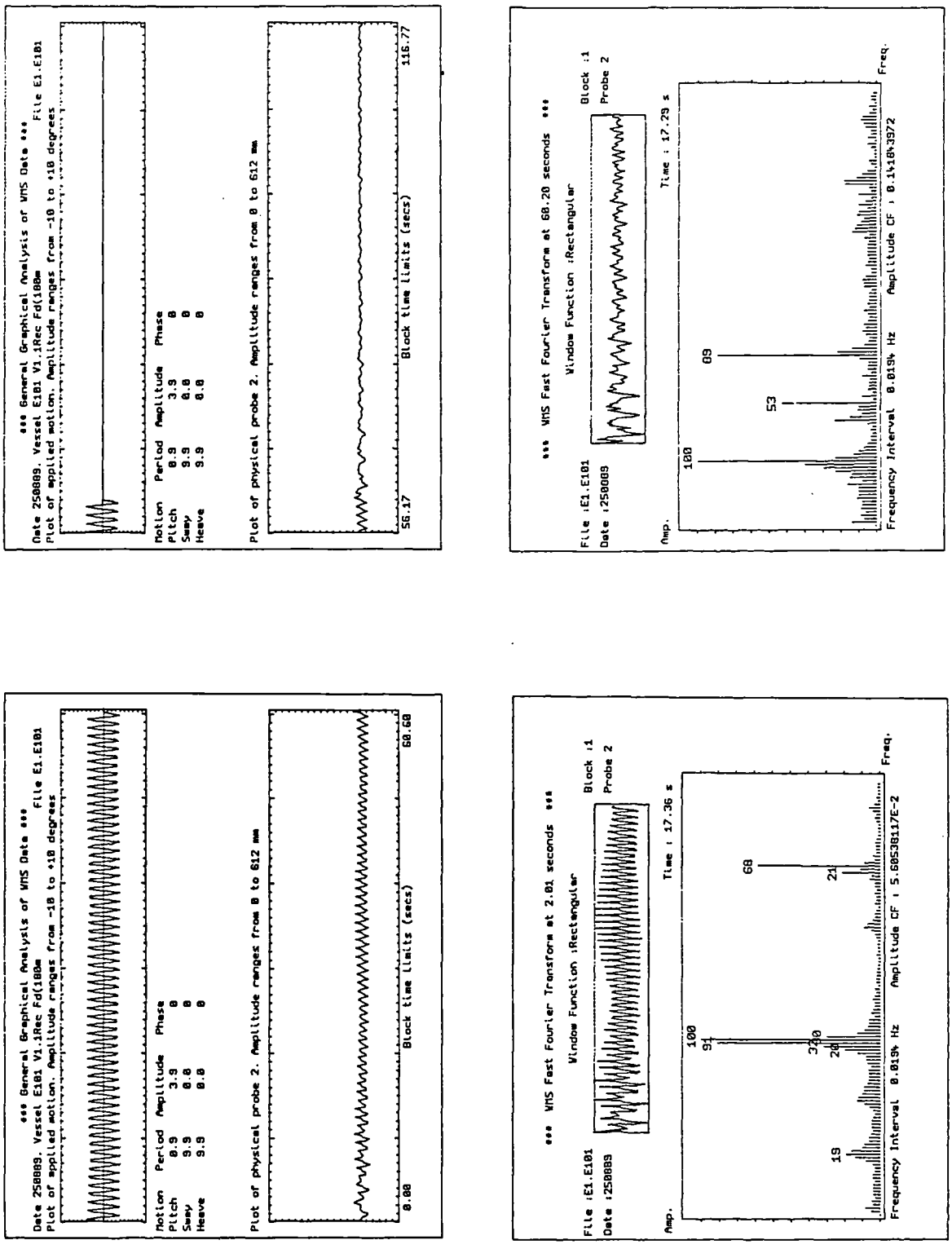

Graph A7.1: Pitch forcing motion at forcing period 0.9 seconds, ±4° amplitude.

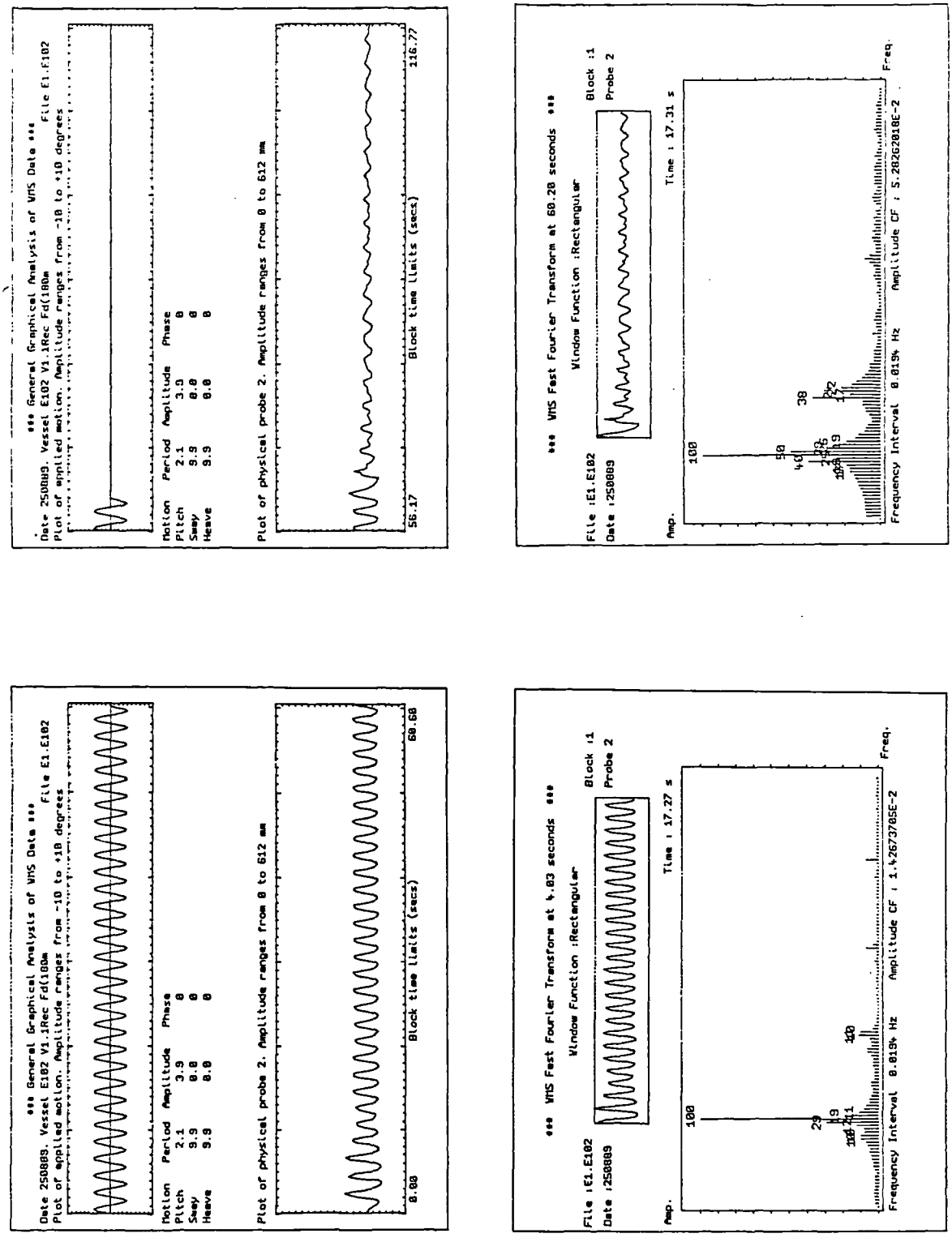

Graph A7.2: Pitch forcing motion at forcing period 2.1 seconds, ±4° amplitude.

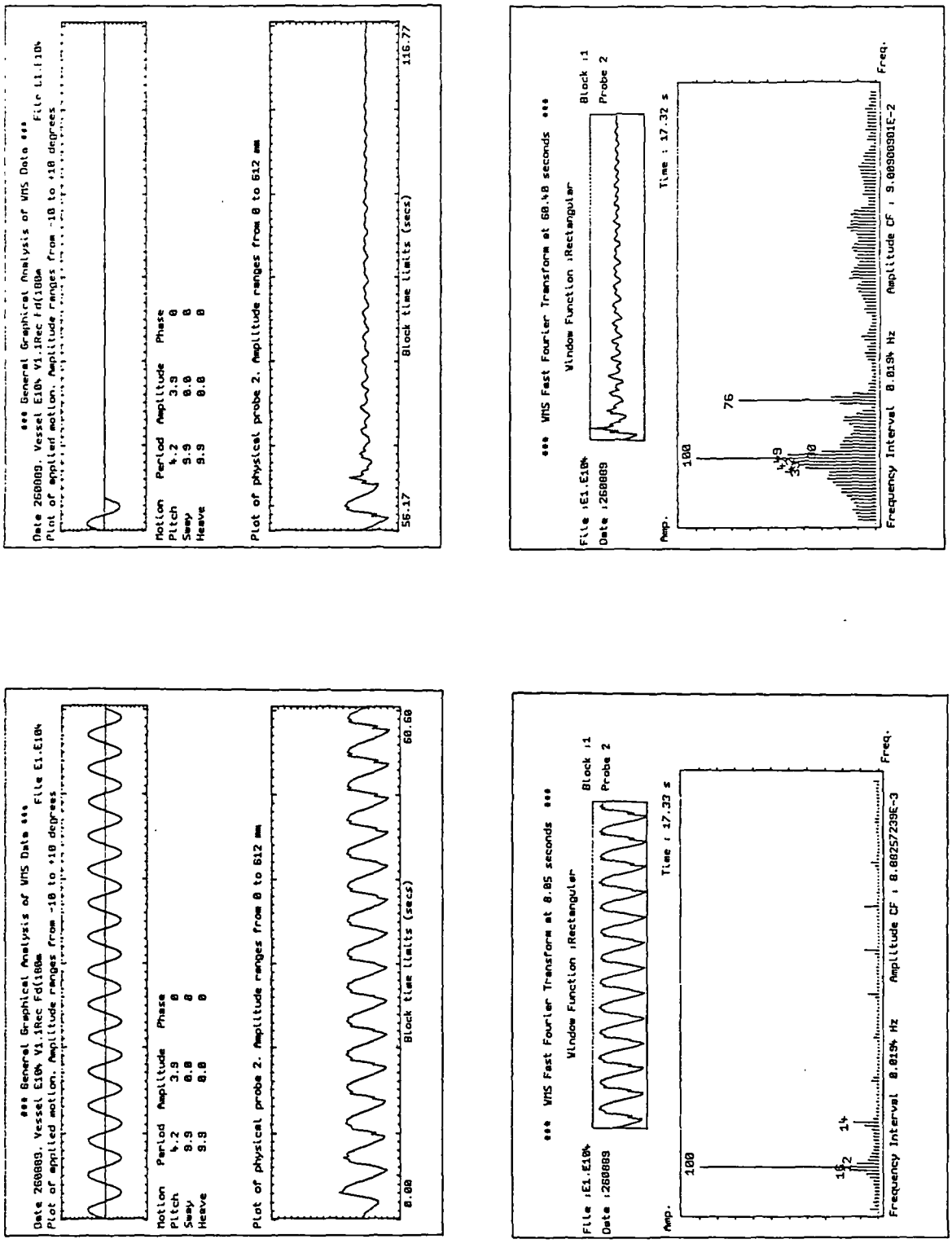

Graph A7.3: Pitch forcing motion at forcing period 4.2 seconds, ±4° amplitude.

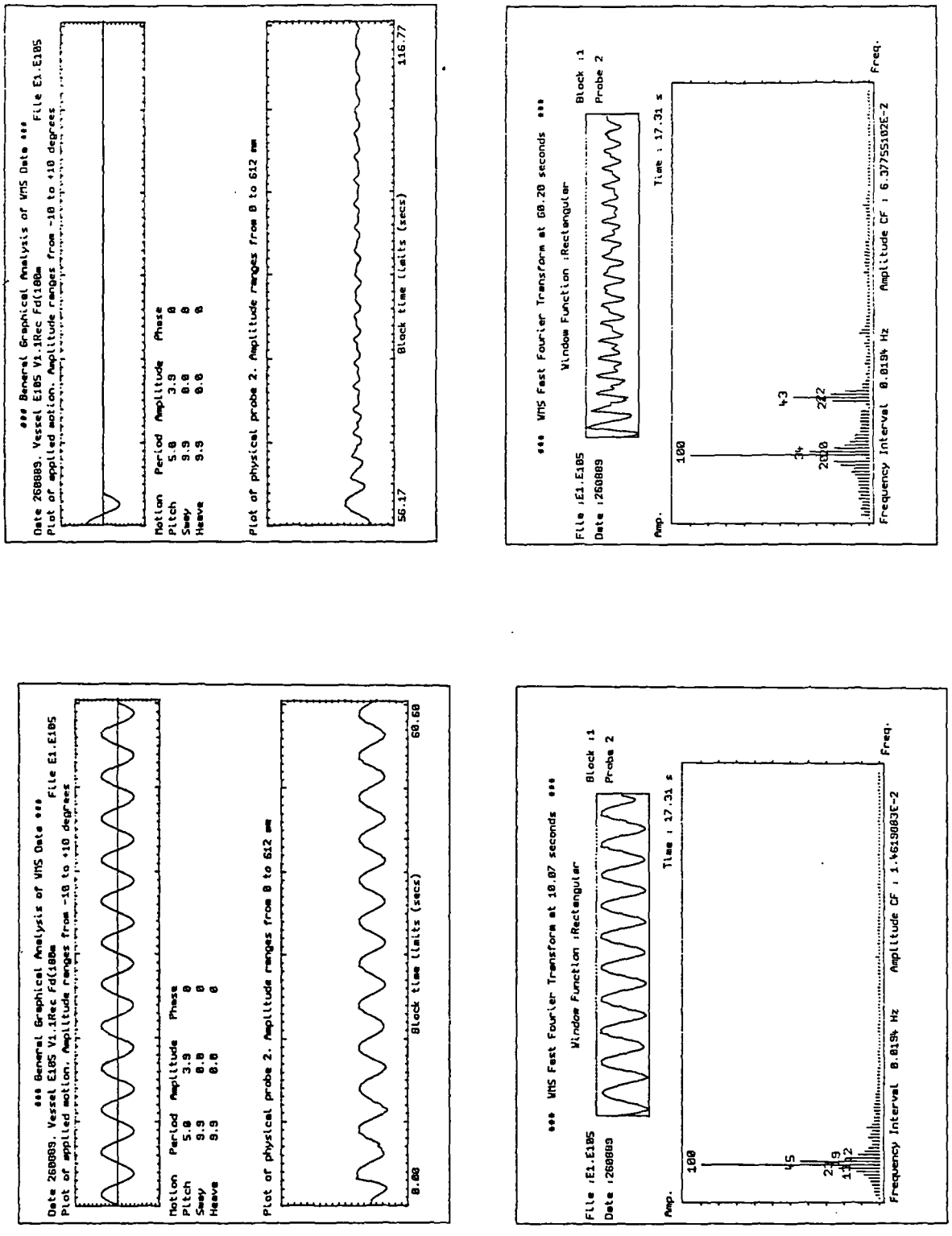

Graph A7.4: Pitch forcing motion at forcing period 5.0 seconds, ±4° amplitude.

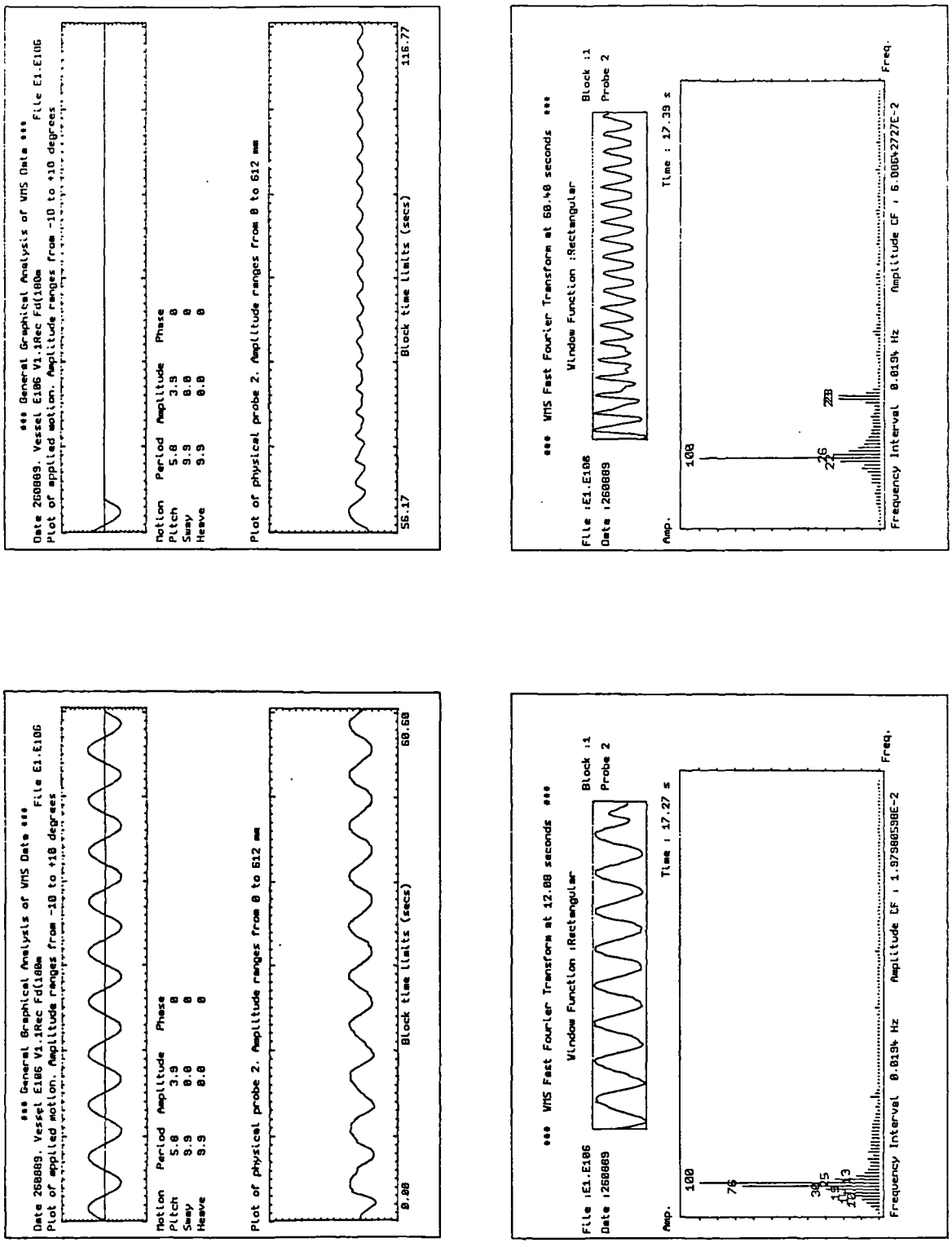

Graph A7.5: Pitch forcing motion at forcing period 5.8 seconds, ±4° amplitude.

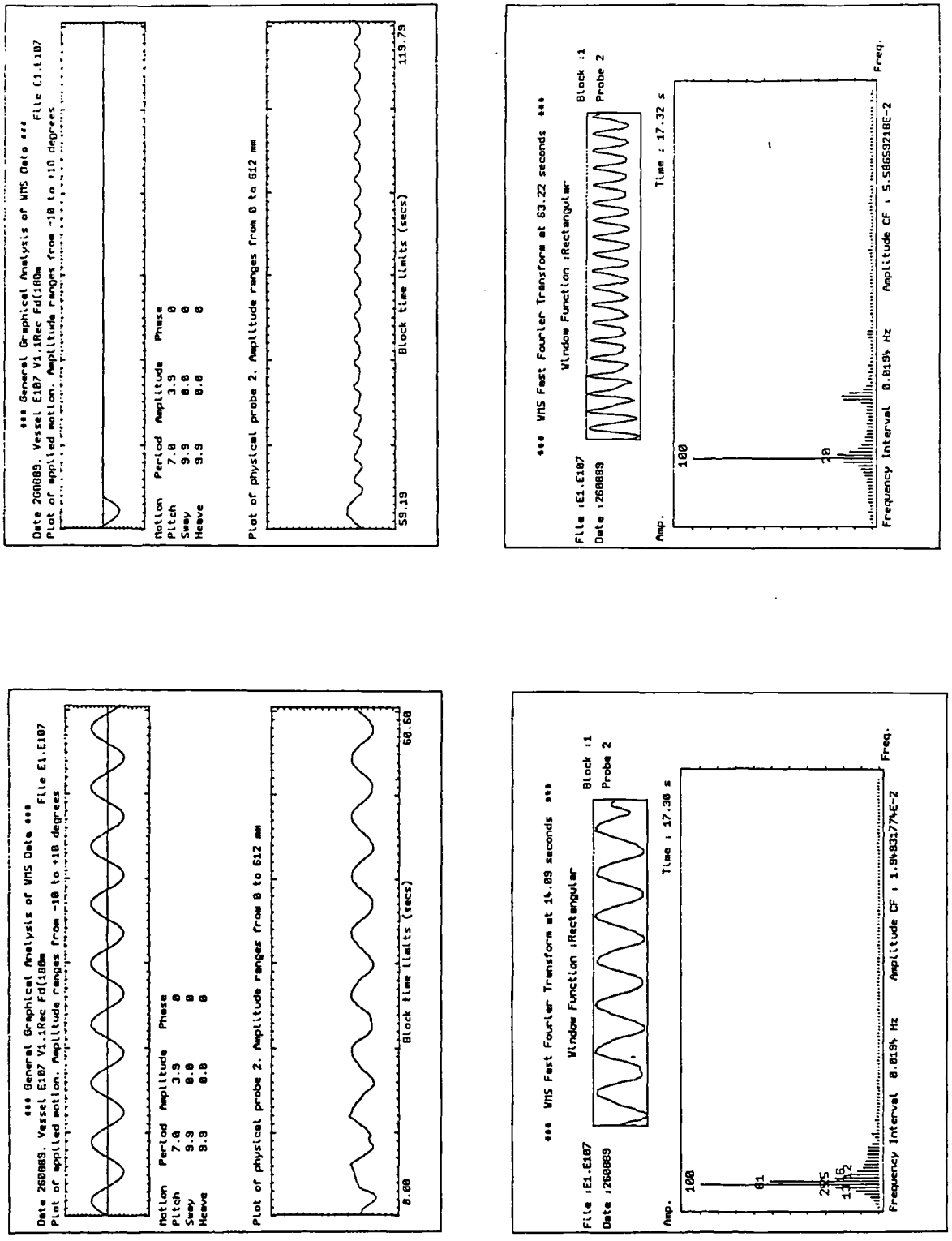

Graph A7.6: Pitch forcing motion at forcing period 7.0 seconds, ±4° amplitude.

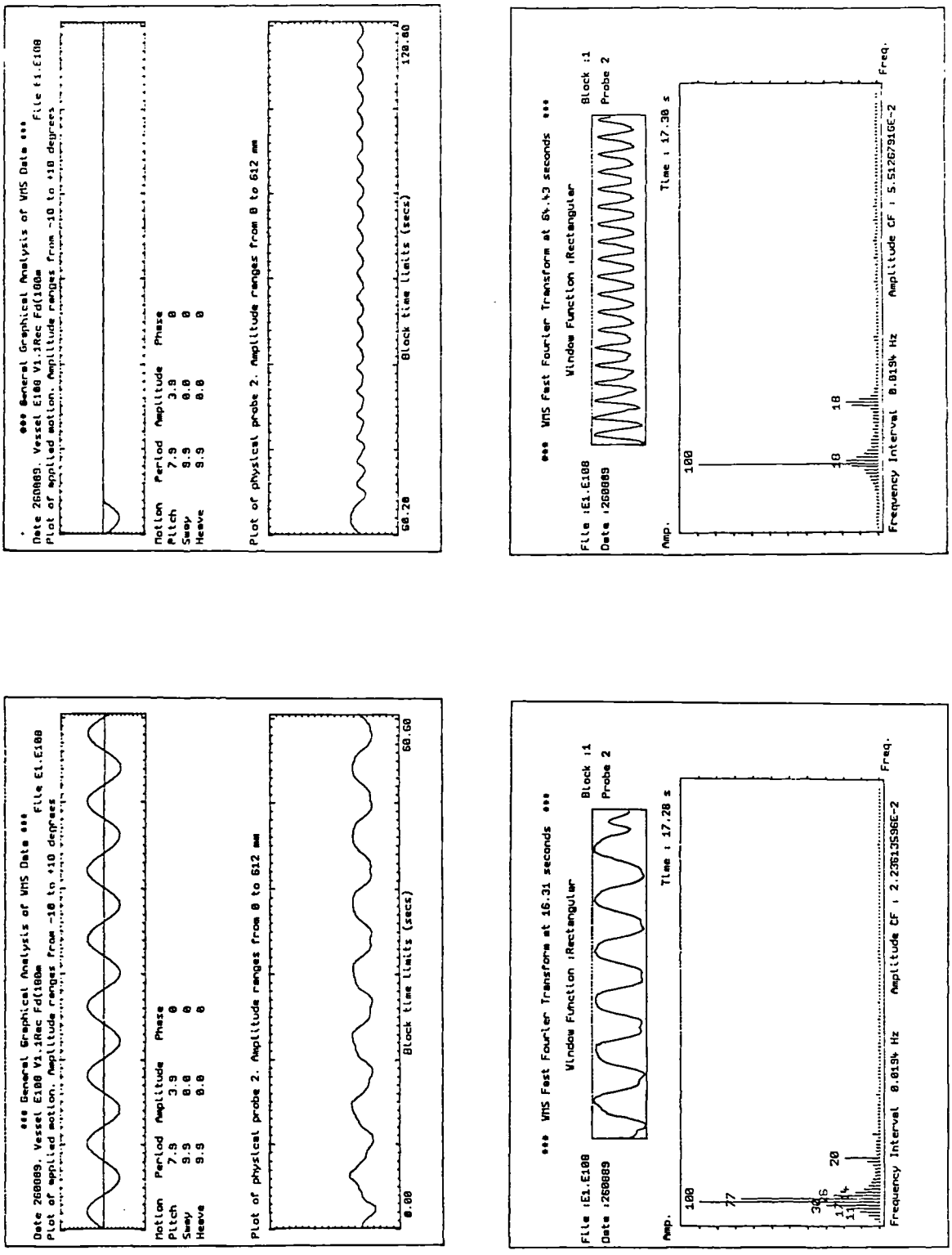

Graph A7.7: Pitch forcing motion at forcing period 7.8 seconds, ±4° amplitude.

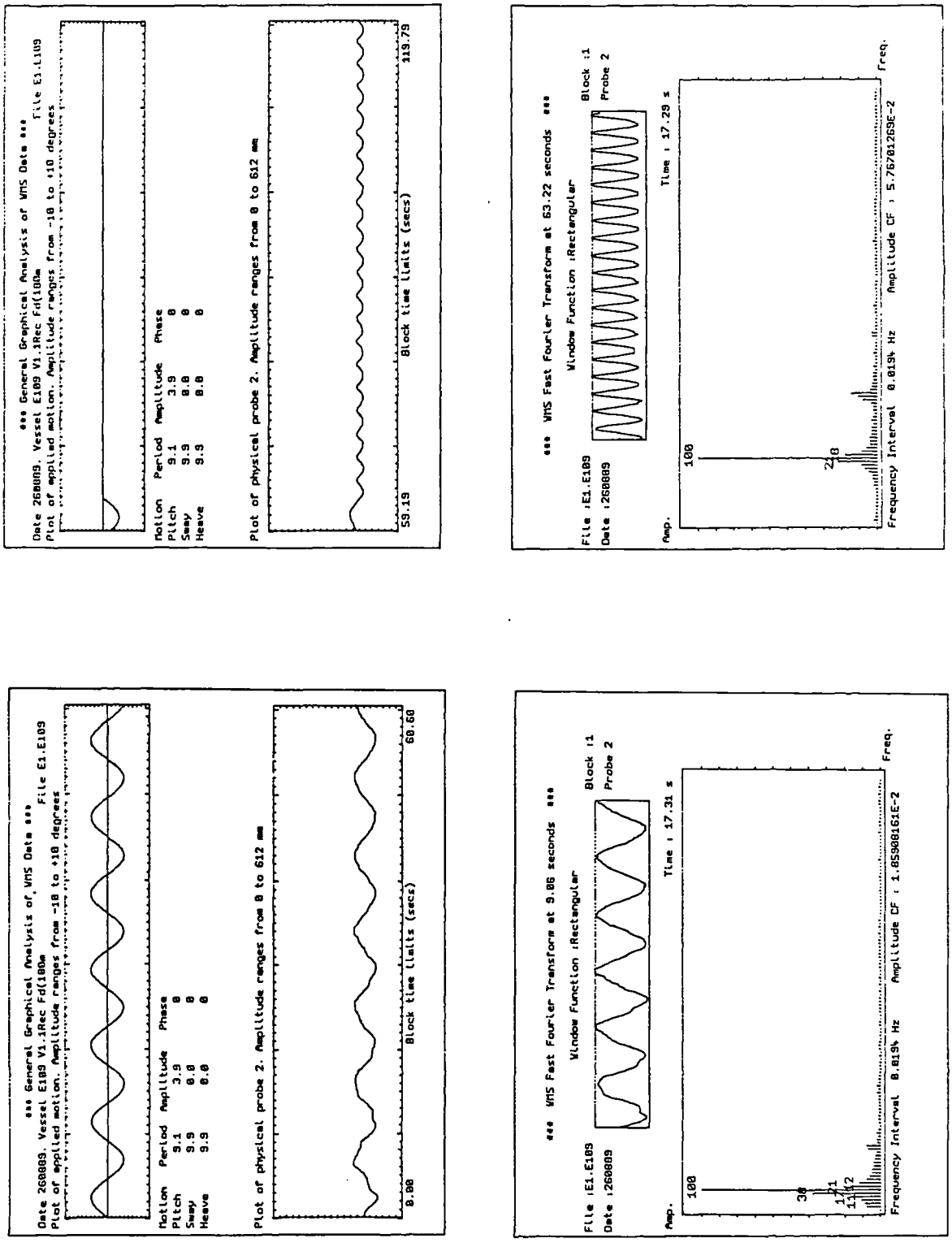

Graph A7.8: Pitch forcing motion at forcing period 9.1 seconds, ±4° amplitude.

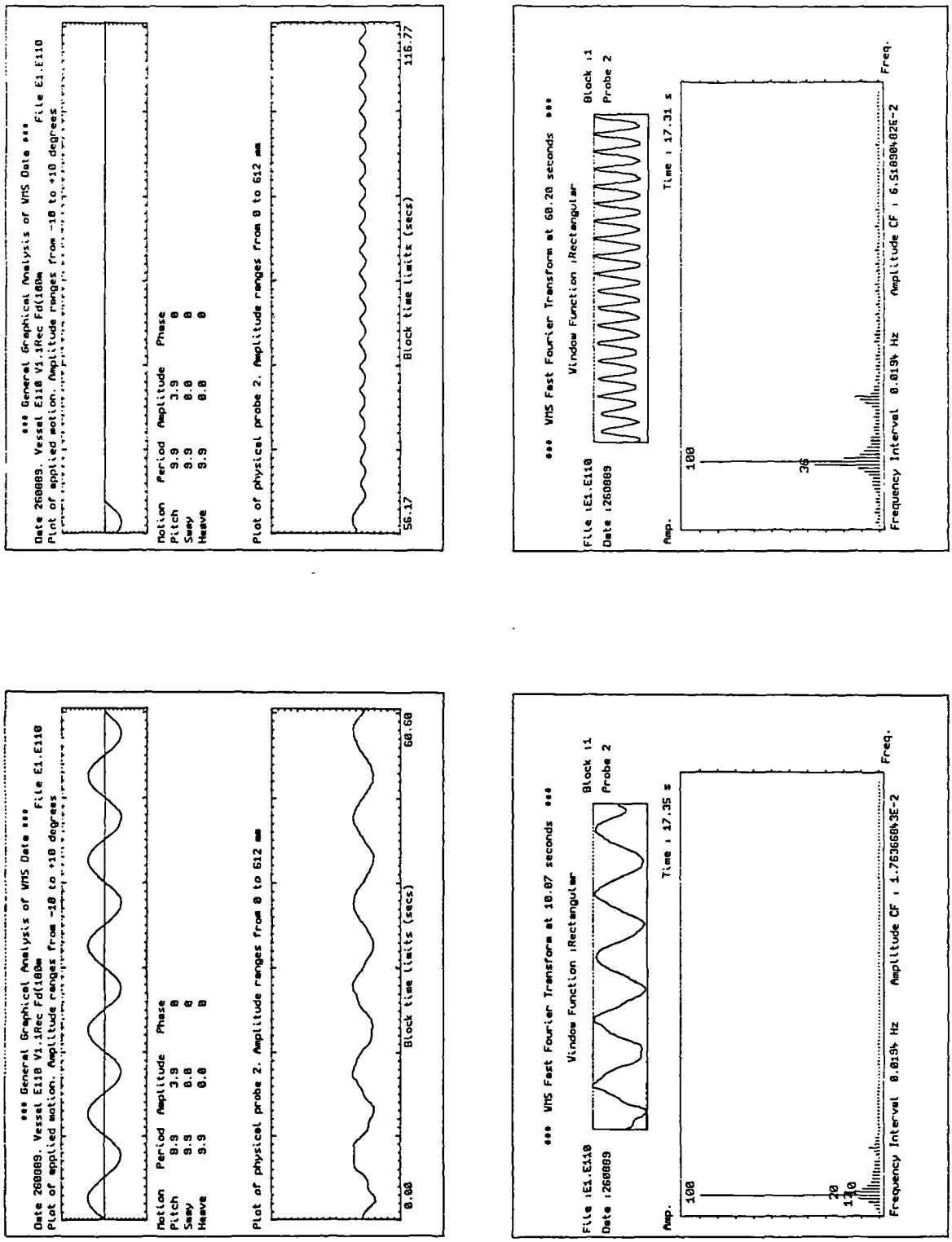

Graph A7.9: Pitch forcing motion at forcing period 9.9 seconds, ±4° amplitude.

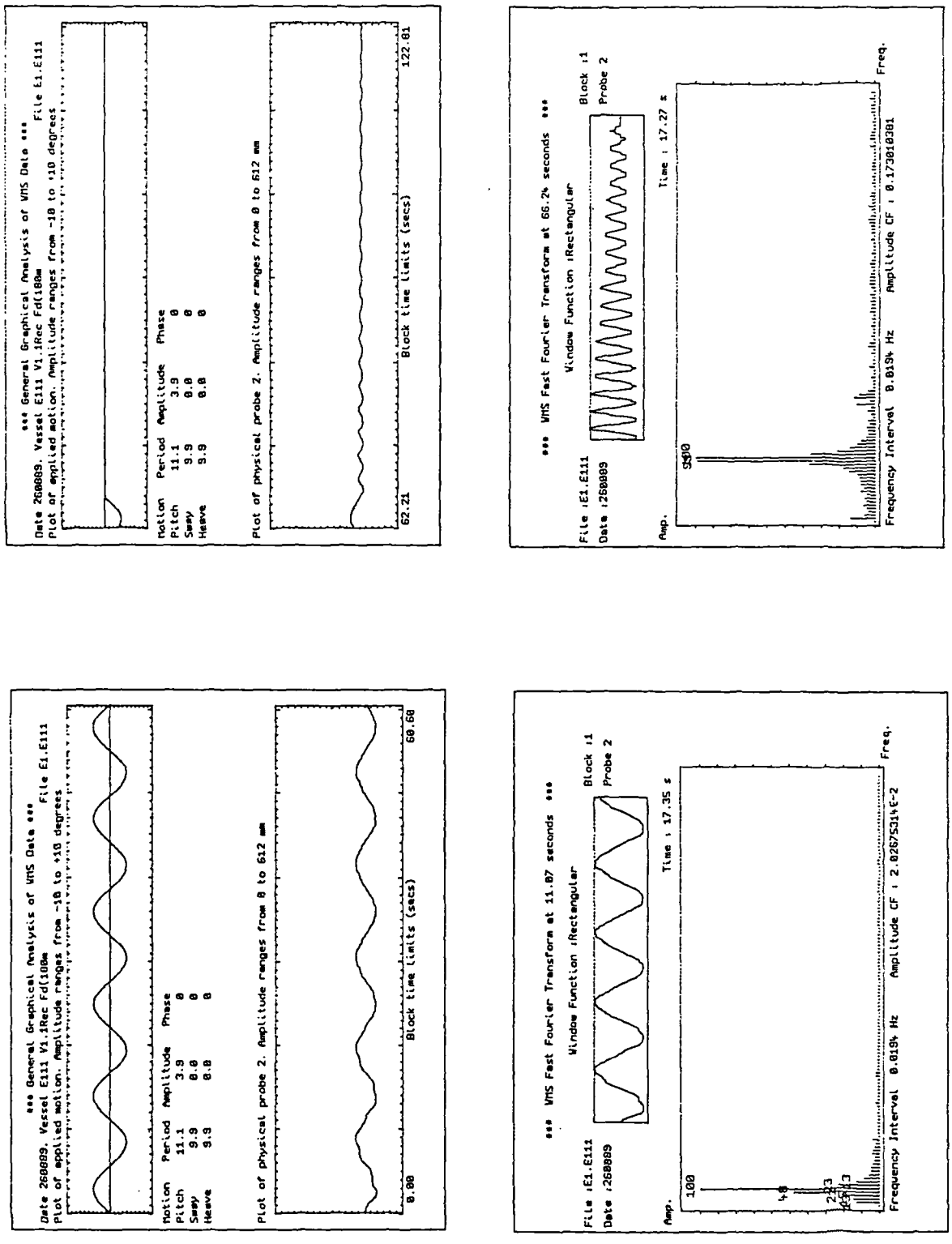

Graph A7.10: Pitch forcing motion at forcing period 11.1 seconds, ±4° amplitude.

APPENDIX VIII

VELOCITY AND OIL/WATER INTERFACE PROFILES IN A RECTANGULAR MODEL OF AN OFFSHORE SEPARATOR PREDICTED BY NUMERICAL SIMULATION.

1.1 INTRODUCTION.

This appendix presents velocity and oil/water interface profiles in a rectangular vessel filled with oil and water. Discussions on the important points from this numerical experiment were presented in chapter 12. For applications to an offshore separator, a *weir* plate was included into the mesh, with oil occupying all mesh cells to the right of the weir.

The profiles clearly show that water can be carried over the weir to be drawn off in the oil product stream.

```
Two Dimensional Fluid Slosh Simulation Program.
Department of Chemical & Process Engineering.
     Heriot-Watt University  Edinburgh.
   G.White..      Sloshsim 10 12th October 1989

Initial Input Data
Vessel length    .189E+04 mm
       height    500.     mm

Motion     Amplitude     Period        Offset        Phase
Pitch        4.00          10.0          .000E+00      .000E+00
Sway         .000E+00      1.00         -943.          .000E+00
Heave        .000E+00      1.00          .000E+00      .000E+00

Upper fluid density :  .860E-06 Kg/mm3
Lower               :  .100E-05 Kg/mm3

Fill depth          :  250.     mm

Time to finish      :  180.     sec.
Time to stop motion :  60.0     sec.

Program Started on the : 22 Dec 89 09:19:50
```

Initial finite difference mesh used.

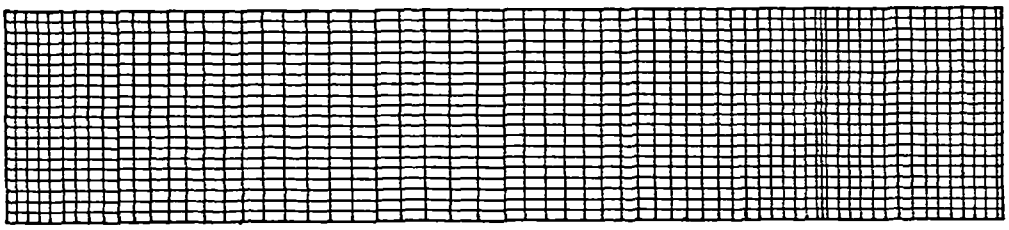

Time .00000E+00 Cycle 0 Vol Change % .000

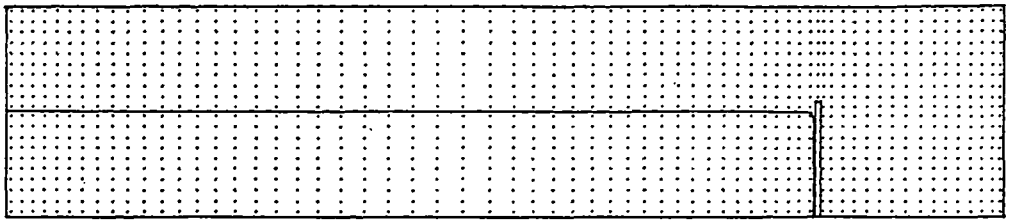

Pitch .000E+00 Sway -943. Heave .000E+00

Time .50093 Cycle 82 Vol Change % .002

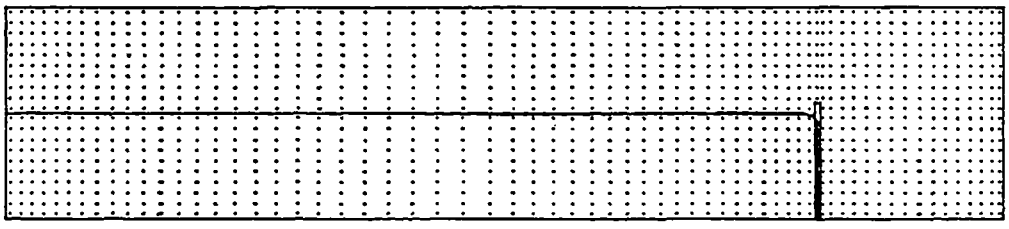

Pitch 1.22 Sway -943. Heave .000E+00

Time 1.0014 Cycle 160 Vol Change % .005

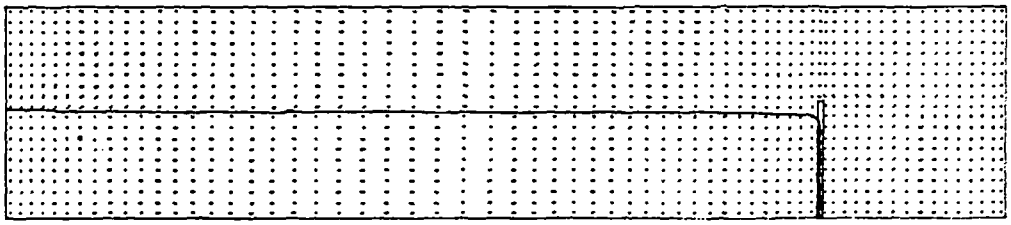

Pitch 2.34 Sway -943. Heave .000E+00

Time 1.5023 Cycle 231 Vol Change % .008

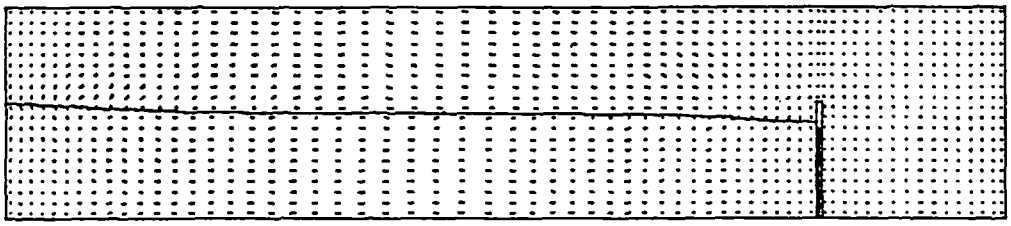

Pitch 3.23 Sway -943. Heave .000E+00

Time 2.0026 Cycle 286 Vol Change % .010

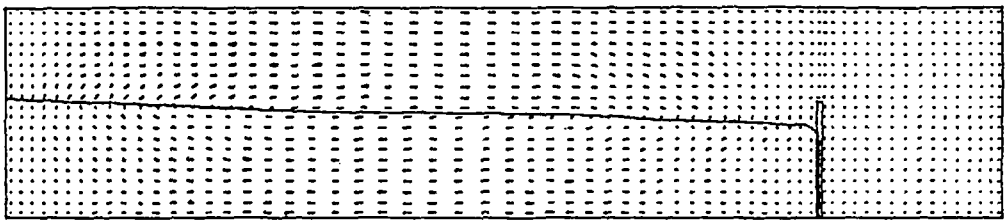

Pitch 3.80 Sway -943. Heave .000E+00

Time 2.5009 Cycle 329 Vol Change % .012

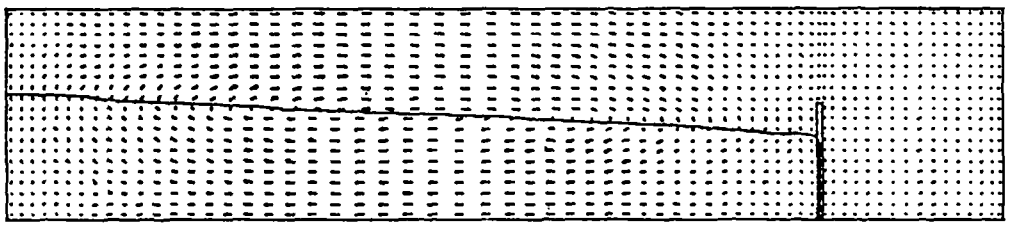

Pitch 4.00 Sway -943. Heave .000E+00

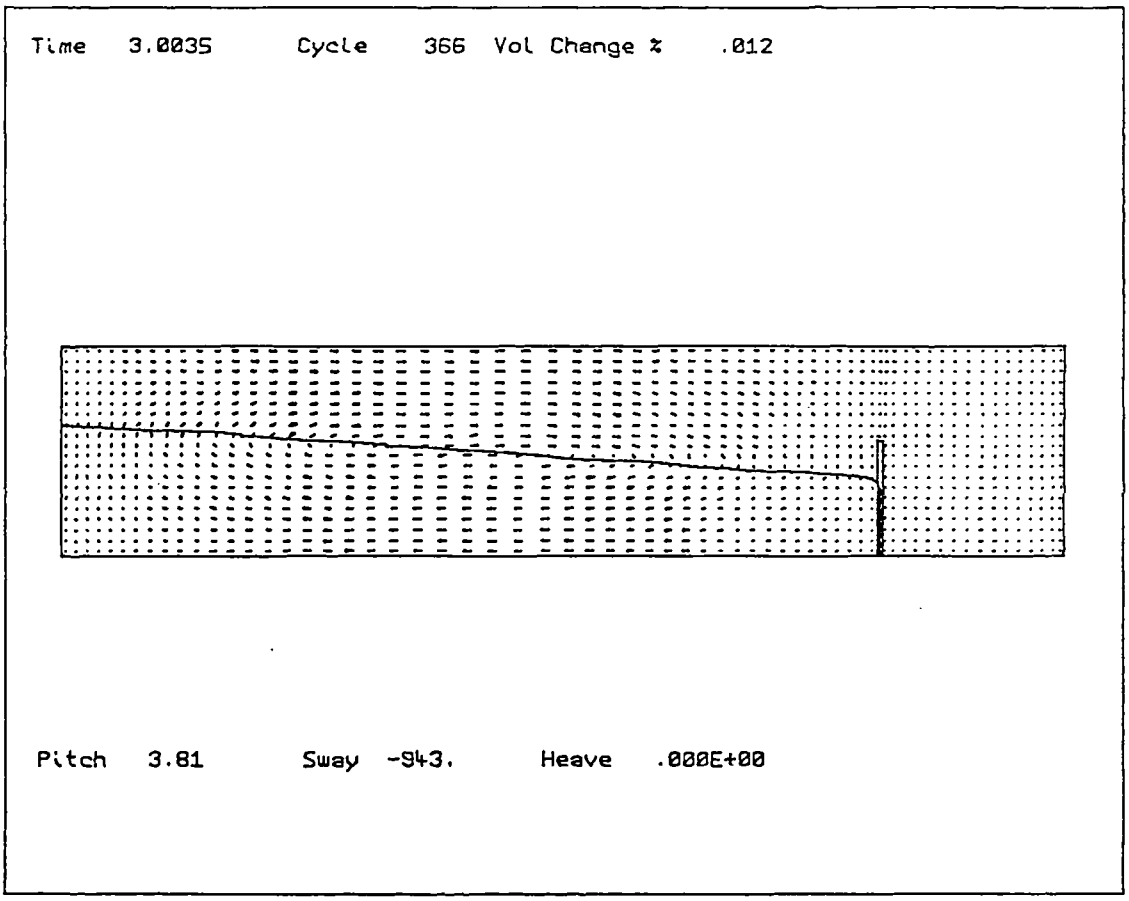
Time 3.0035 Cycle 366 Vol Change % .012
Pitch 3.81 Sway -943. Heave .000E+00

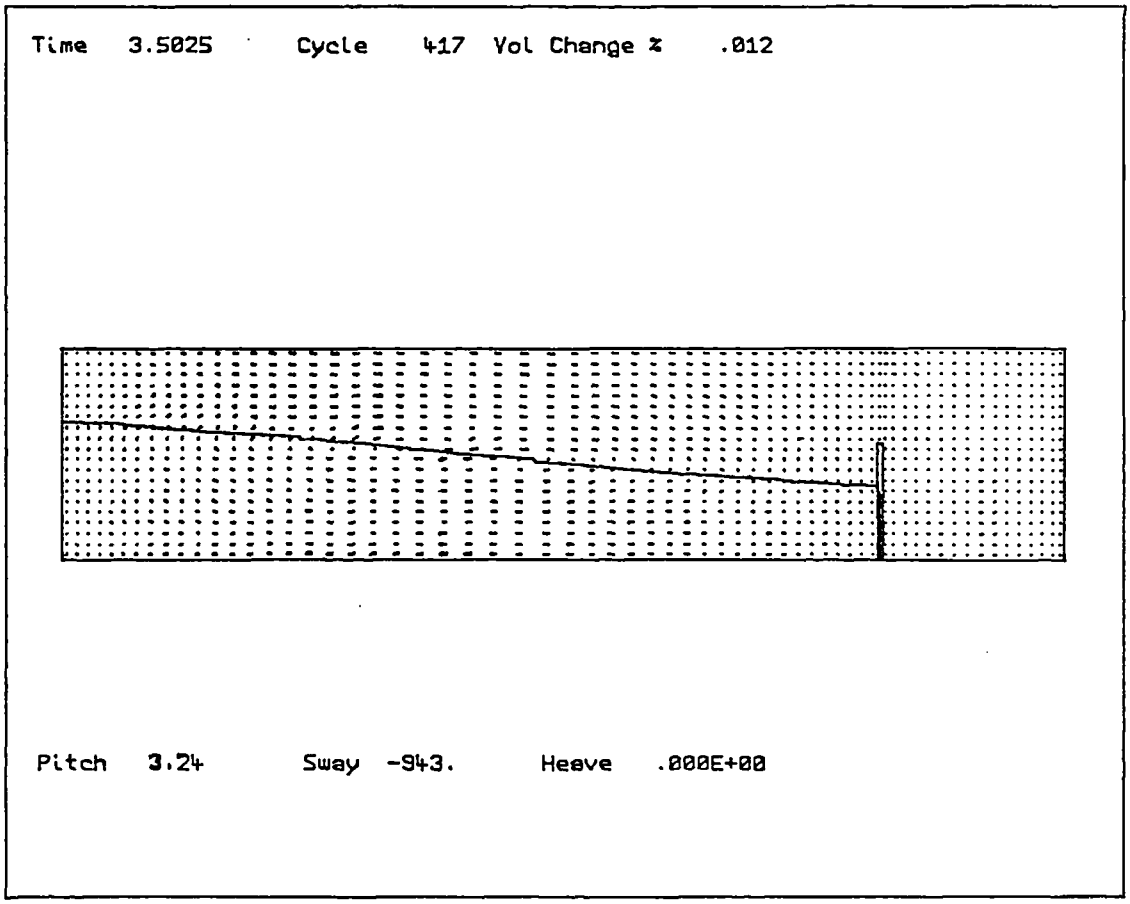
Time 3.5025 Cycle 417 Vol Change % .012
Pitch 3.24 Sway -943. Heave .000E+00

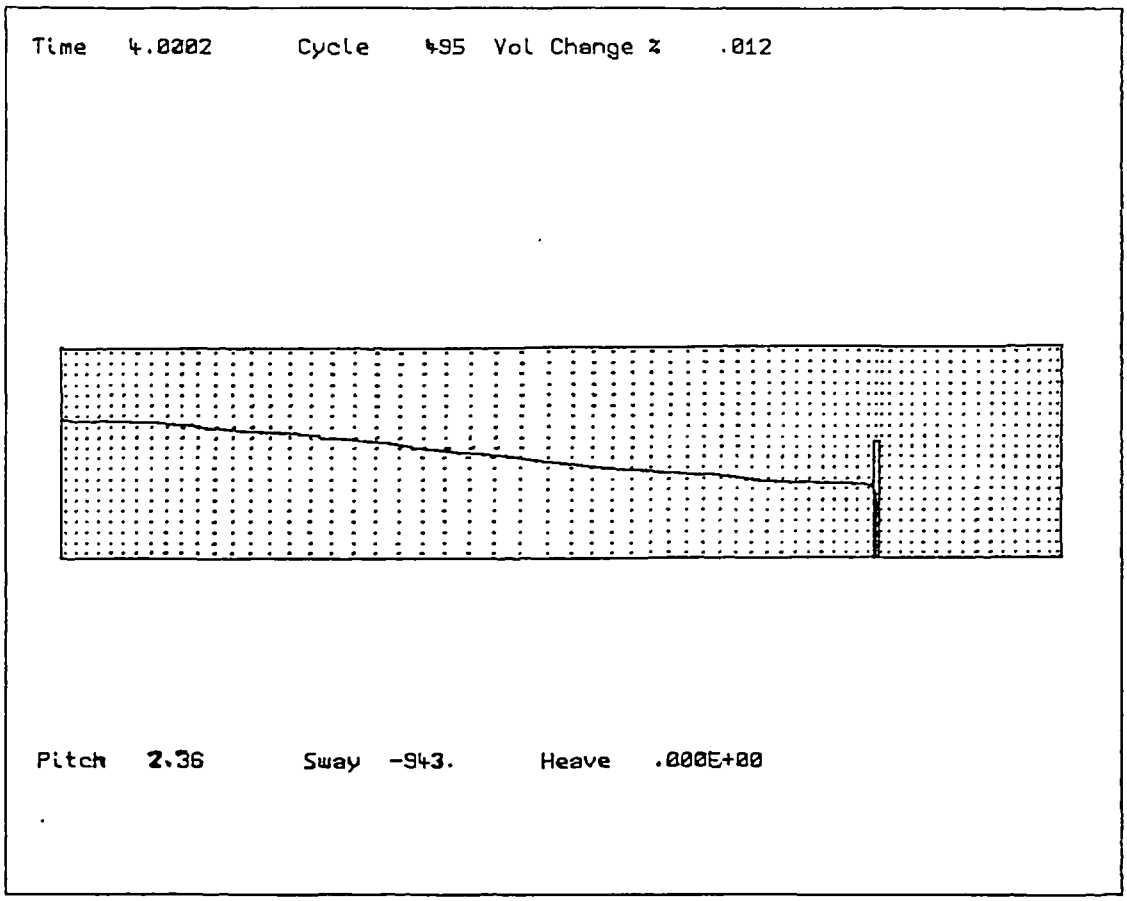
Time 4.0202 Cycle 495 Vol Change % .012
Pitch 2.36 Sway -943. Heave .000E+00

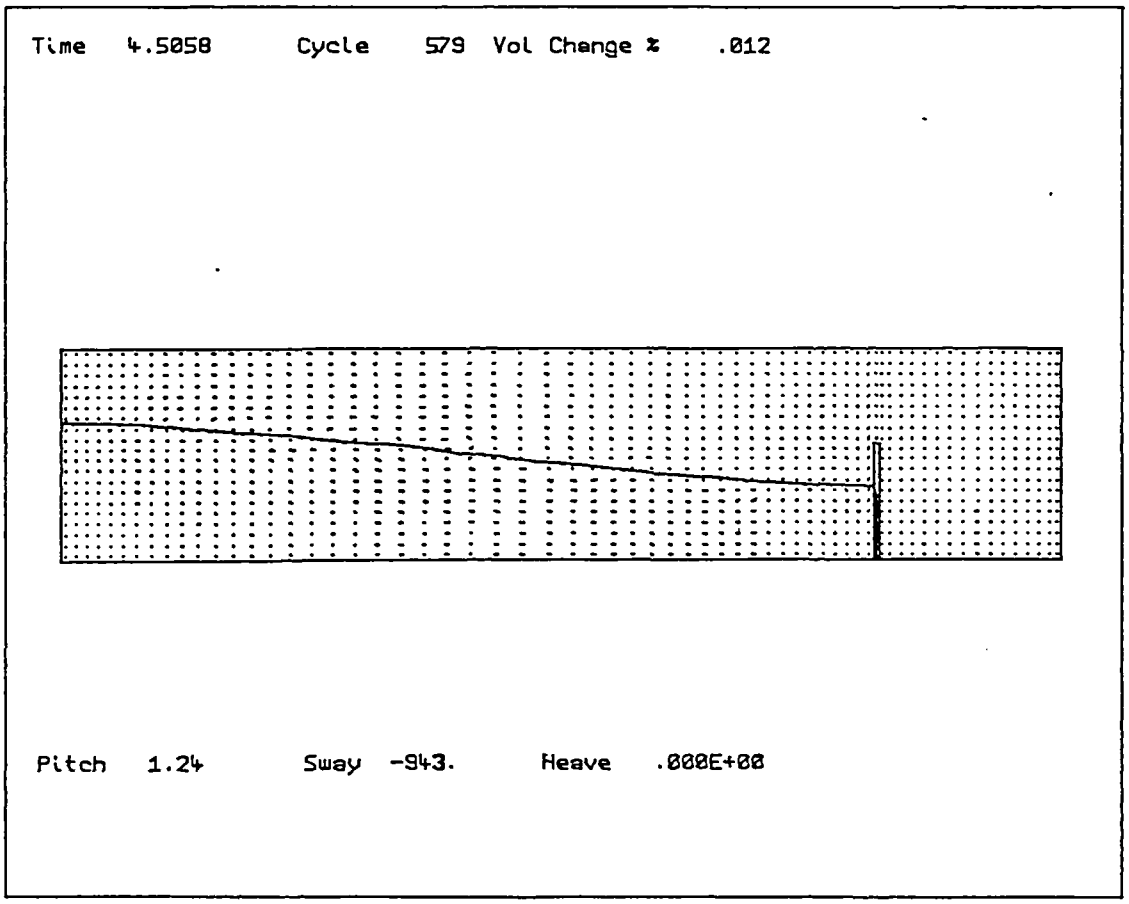
Time 4.5058 Cycle 579 Vol Change % .012
Pitch 1.24 Sway -943. Heave .000E+00

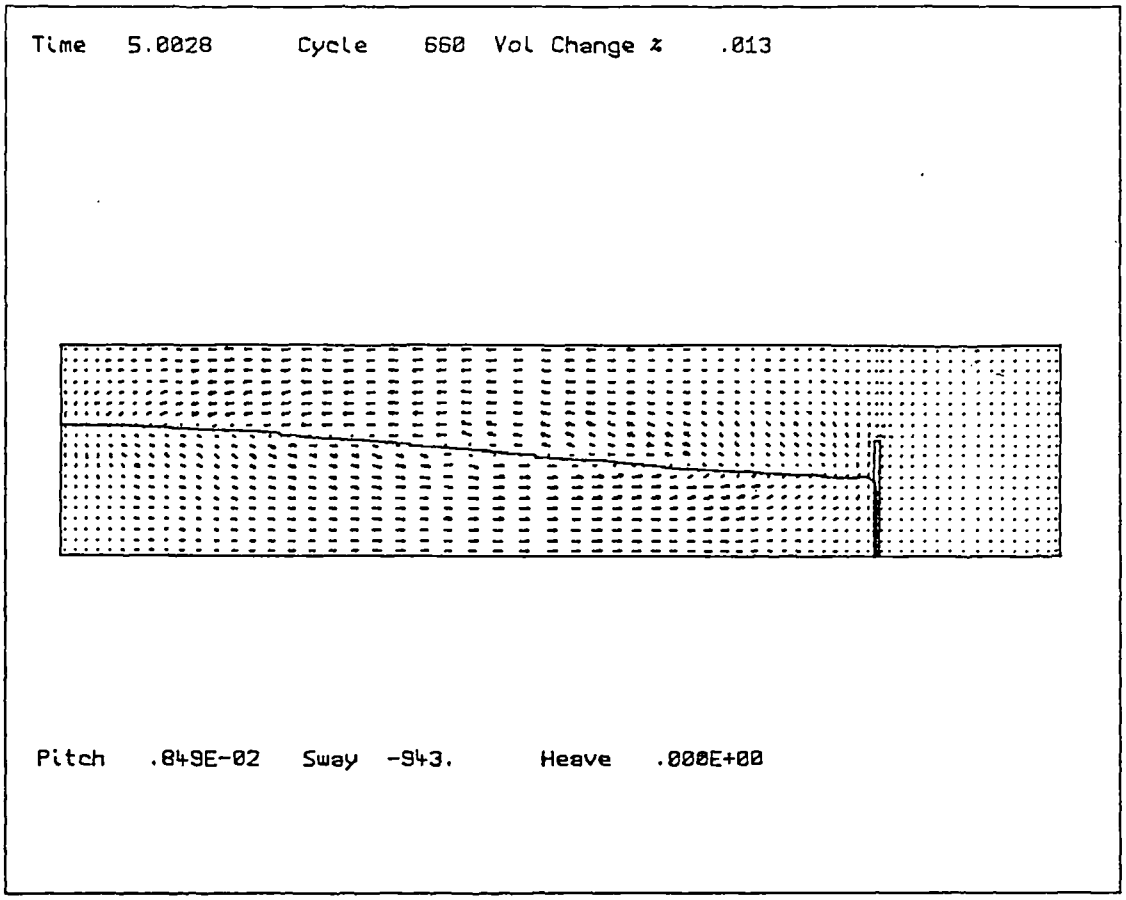
Time 5.0028 Cycle 660 Vol Change % .013
Pitch .849E-02 Sway -943. Heave .000E+00

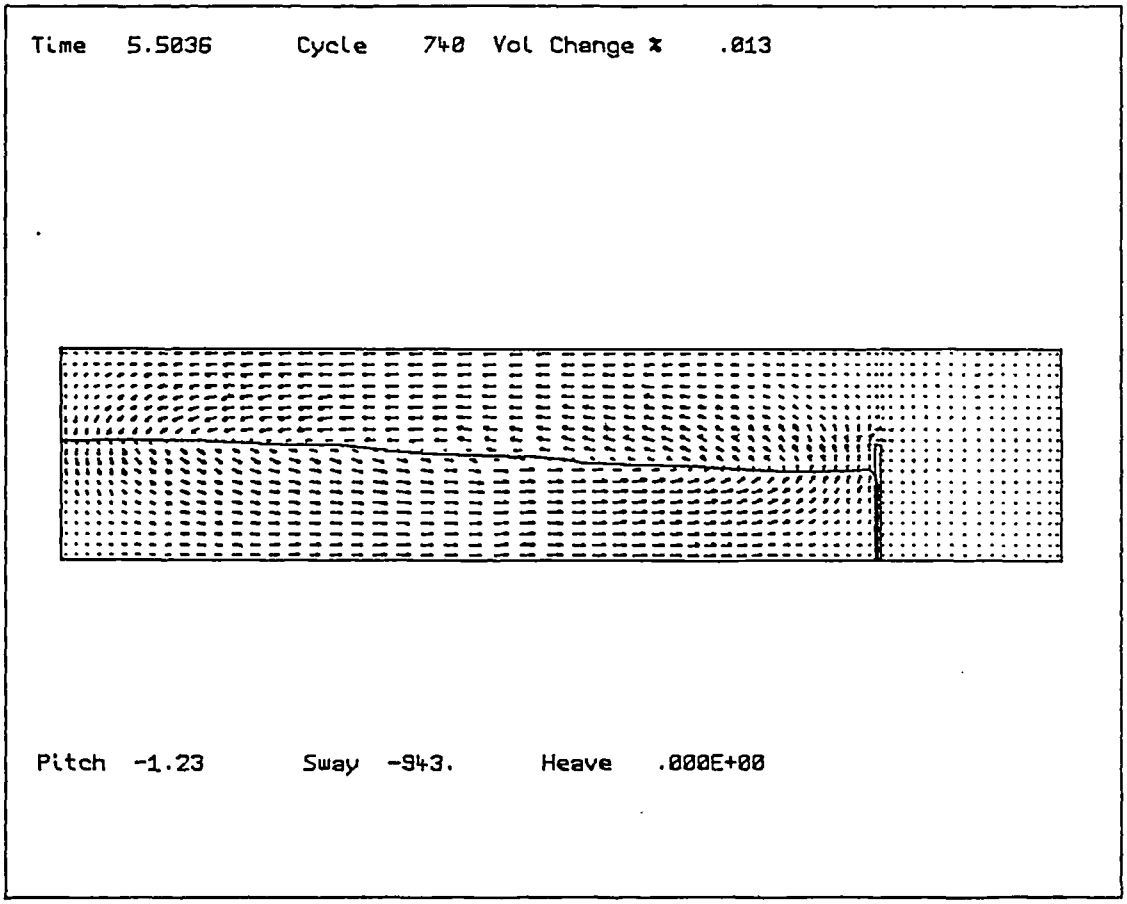
Time 5.5036 Cycle 740 Vol Change % .013
Pitch -1.23 Sway -943. Heave .000E+00

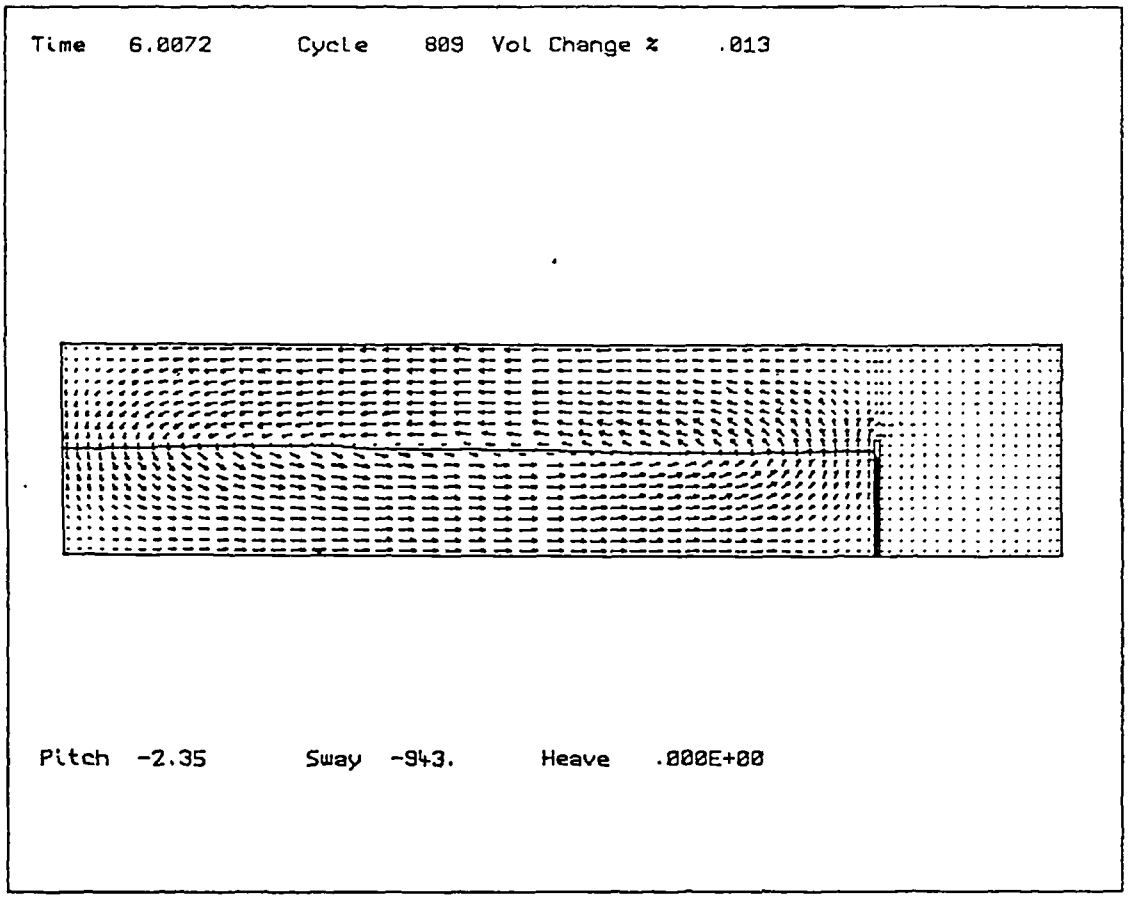
Time 6.0072 Cycle 809 Vol Change % .013
Pitch -2.35 Sway -943. Heave .000E+00

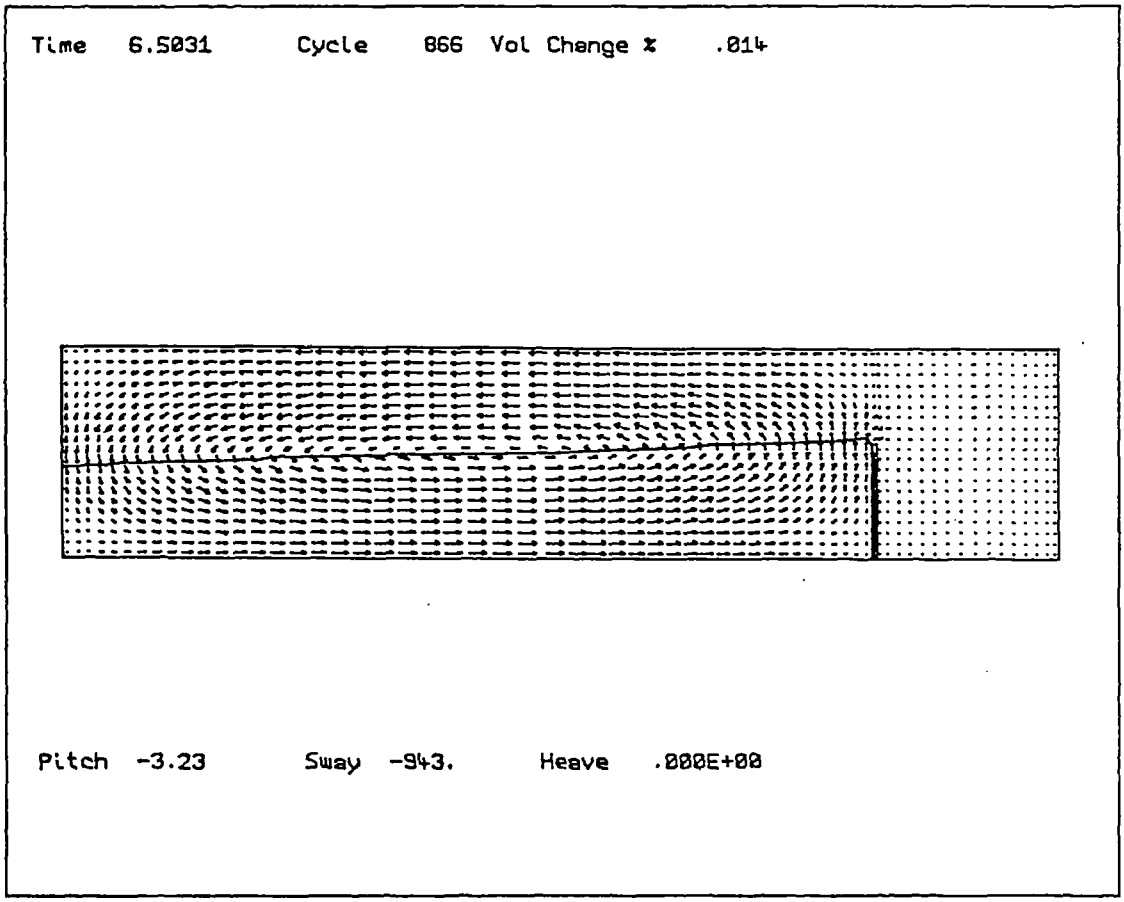
Time 6.5031 Cycle 866 Vol Change % .014
Pitch -3.23 Sway -943. Heave .000E+00

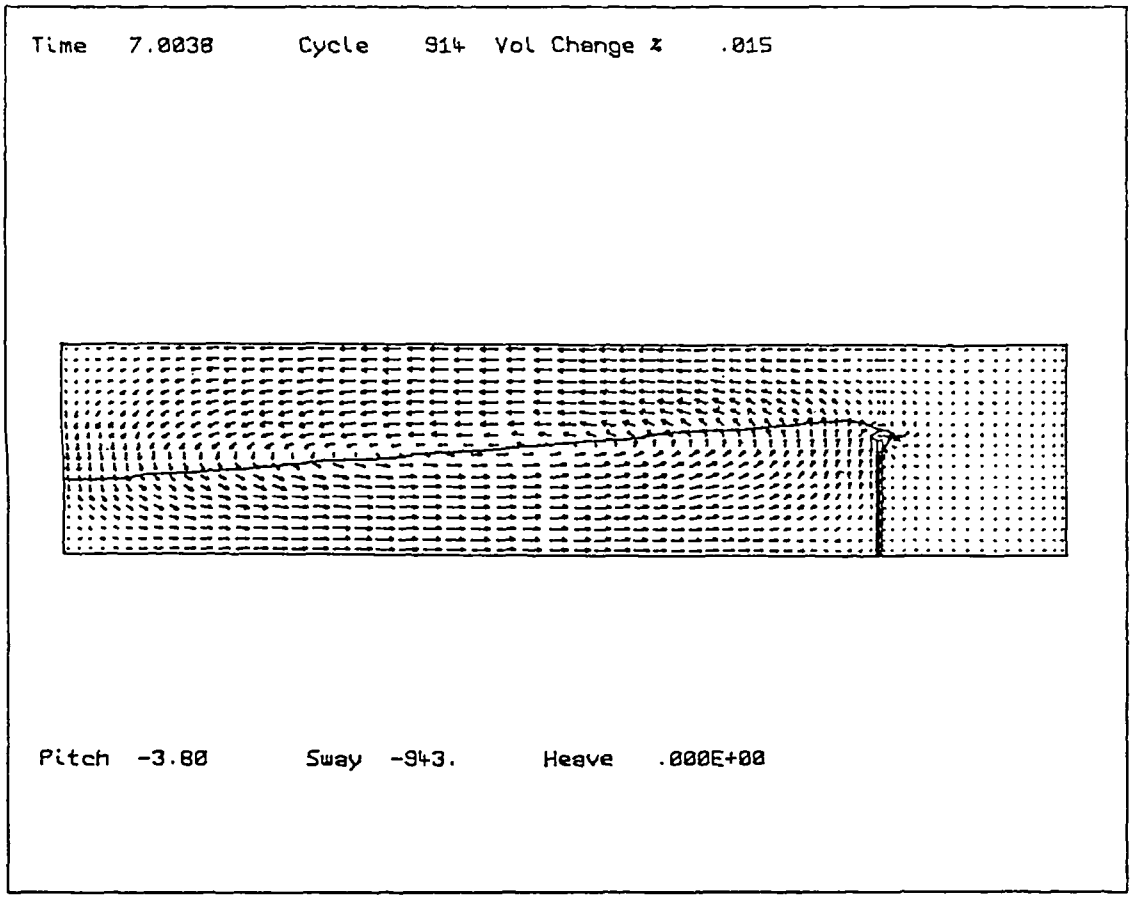
Time 7.0038 Cycle 914 Vol Change % .015
Pitch -3.80 Sway -943. Heave .000E+00

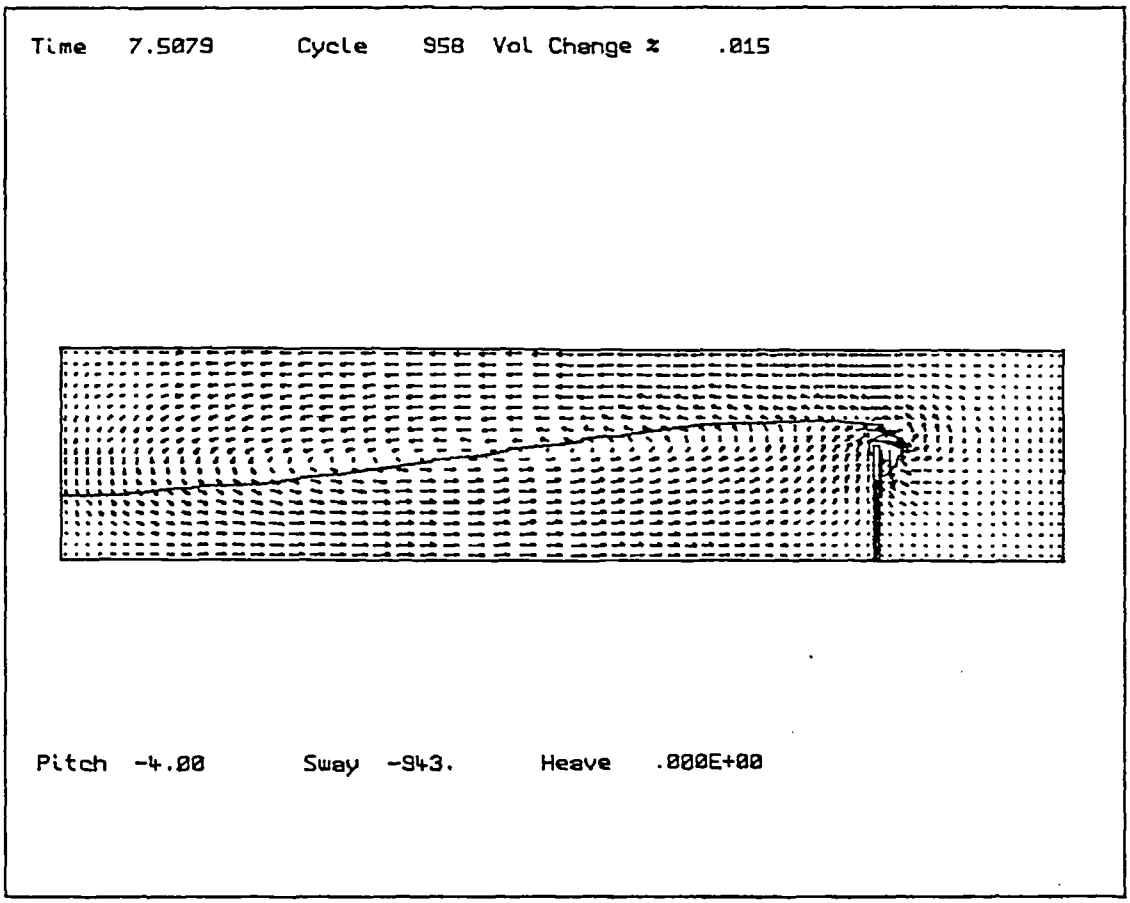
Time 7.5079 Cycle 958 Vol Change % .015
Pitch -4.00 Sway -943. Heave .000E+00

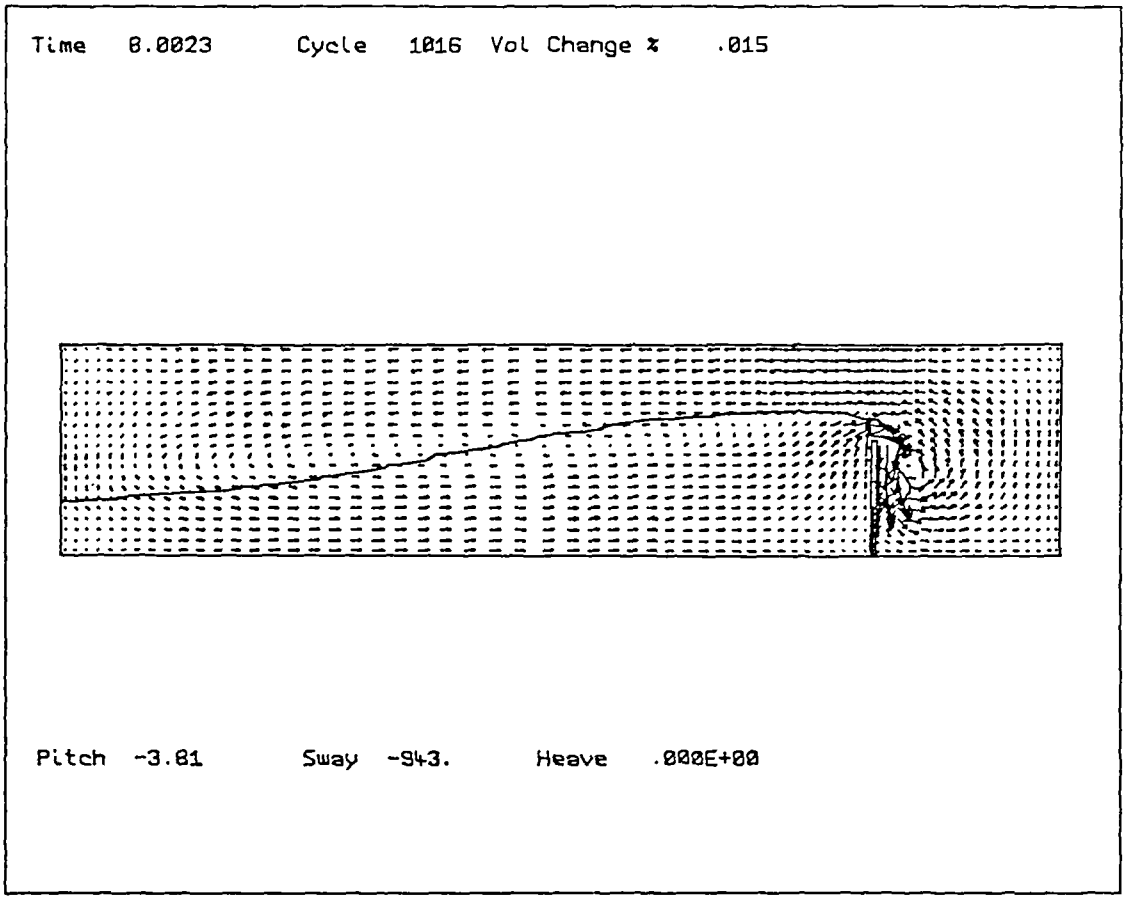
Time 8.0023 Cycle 1016 Vol Change % .015
Pitch -3.81 Sway -943. Heave .000E+00

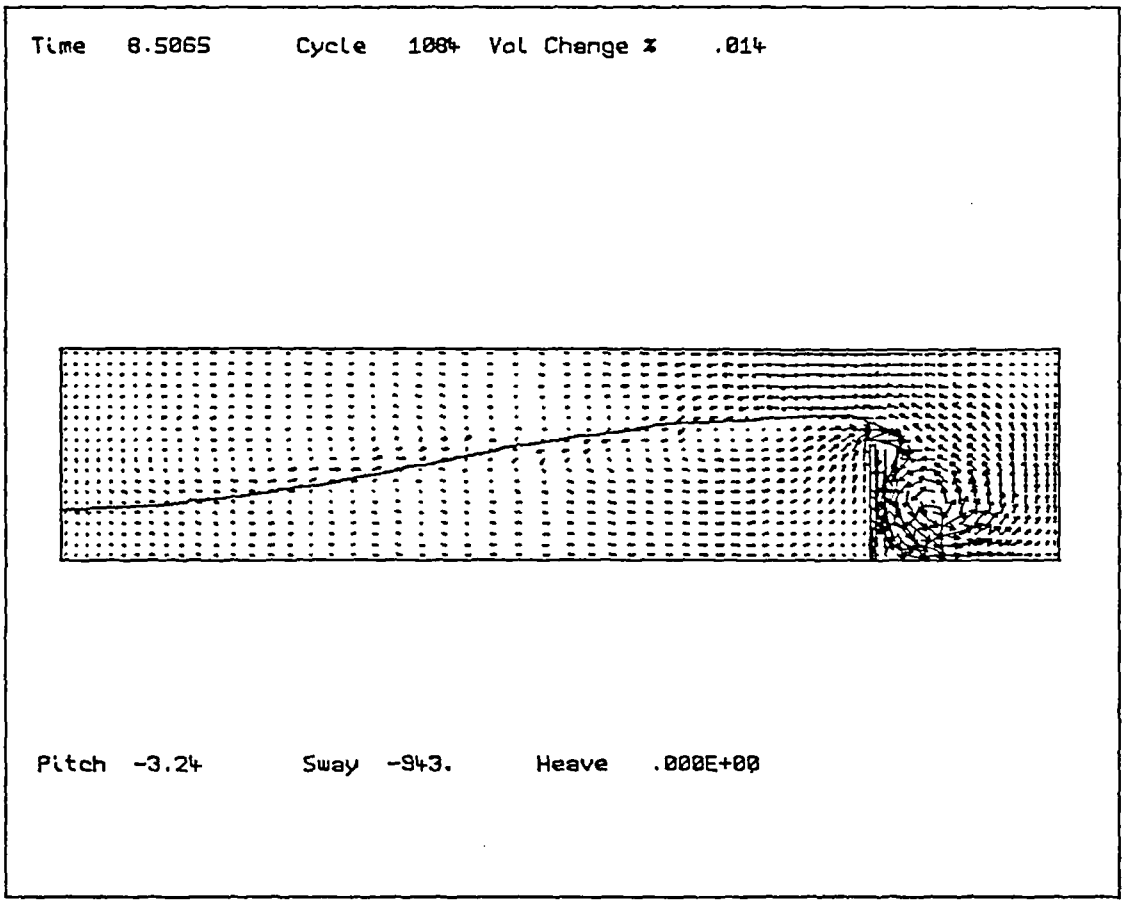
Time 8.5065 Cycle 1084 Vol Change % .014
Pitch -3.24 Sway -943. Heave .000E+00

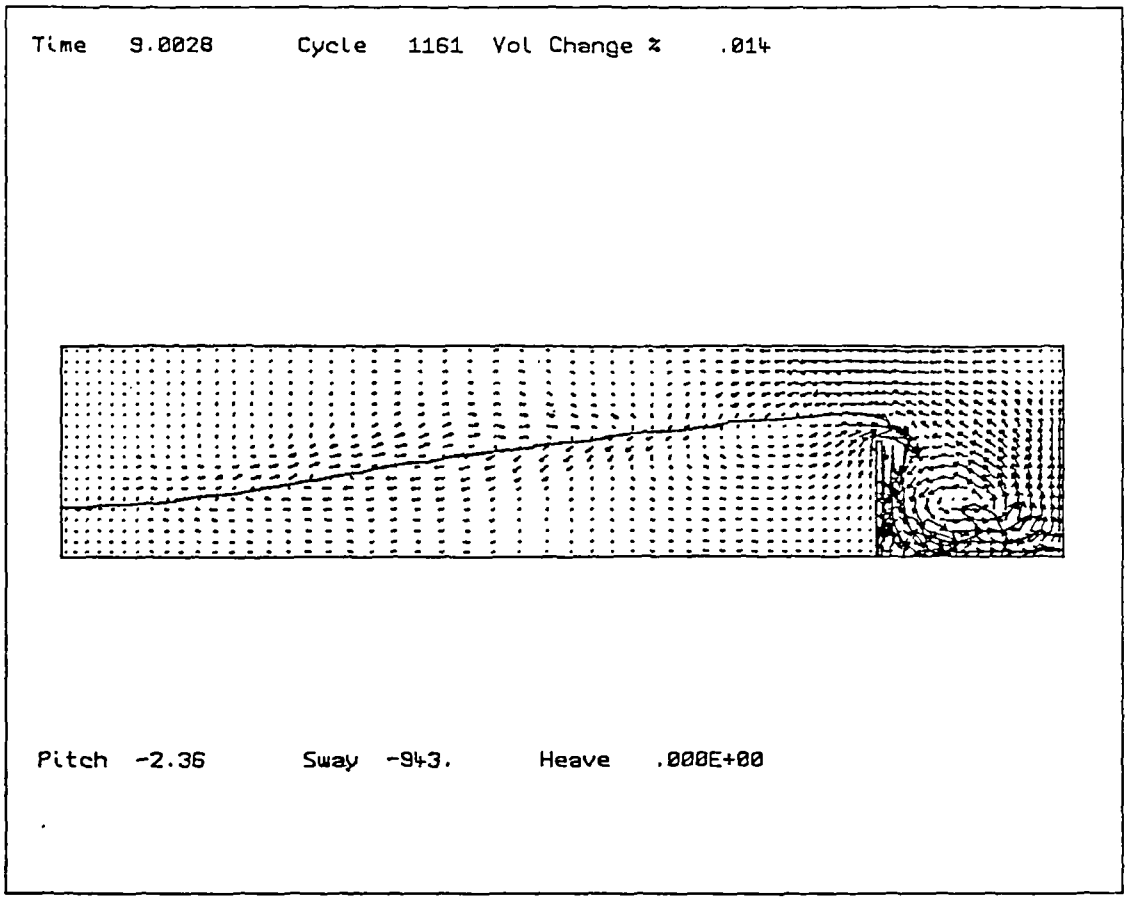
Time 9.0028 Cycle 1161 Vol Change % .014
Pitch -2.36 Sway -943. Heave .000E+00

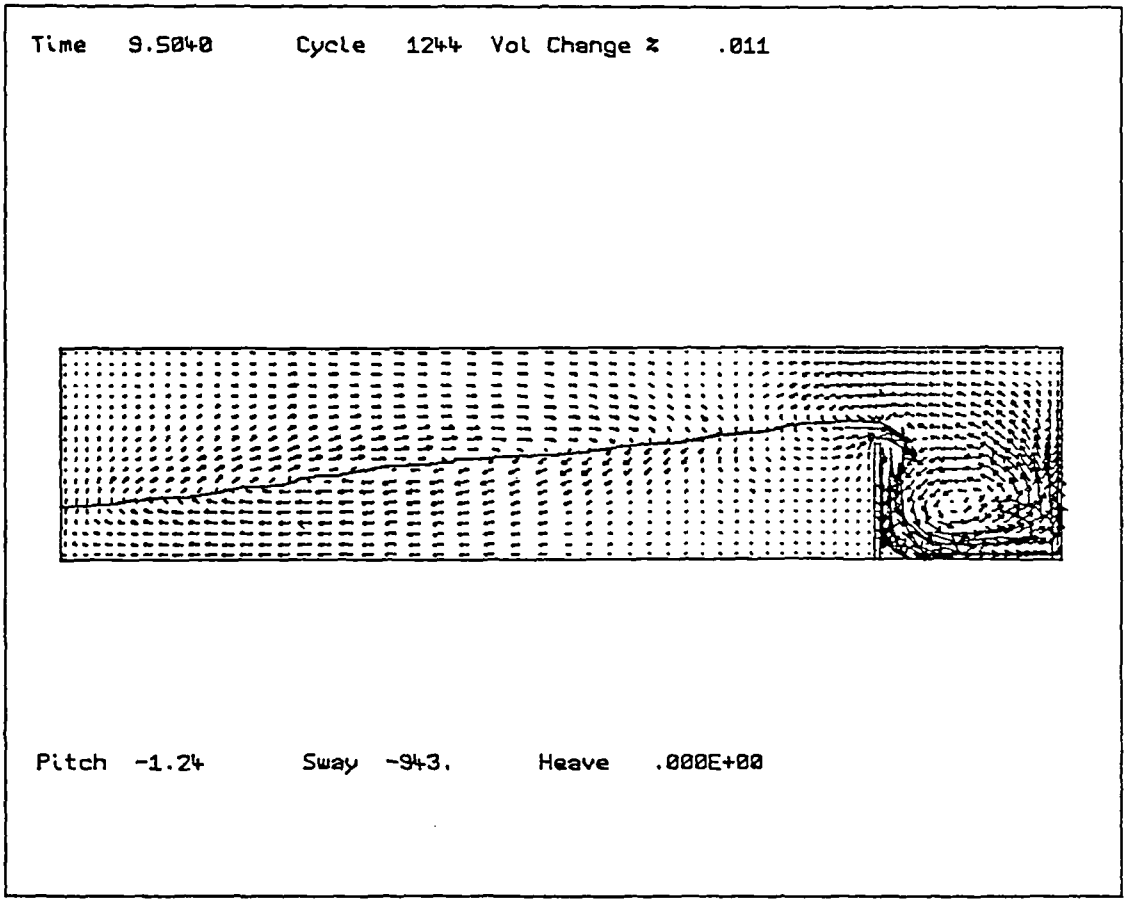
Time 9.5040 Cycle 1244 Vol Change % .011
Pitch -1.24 Sway -943. Heave .000E+00

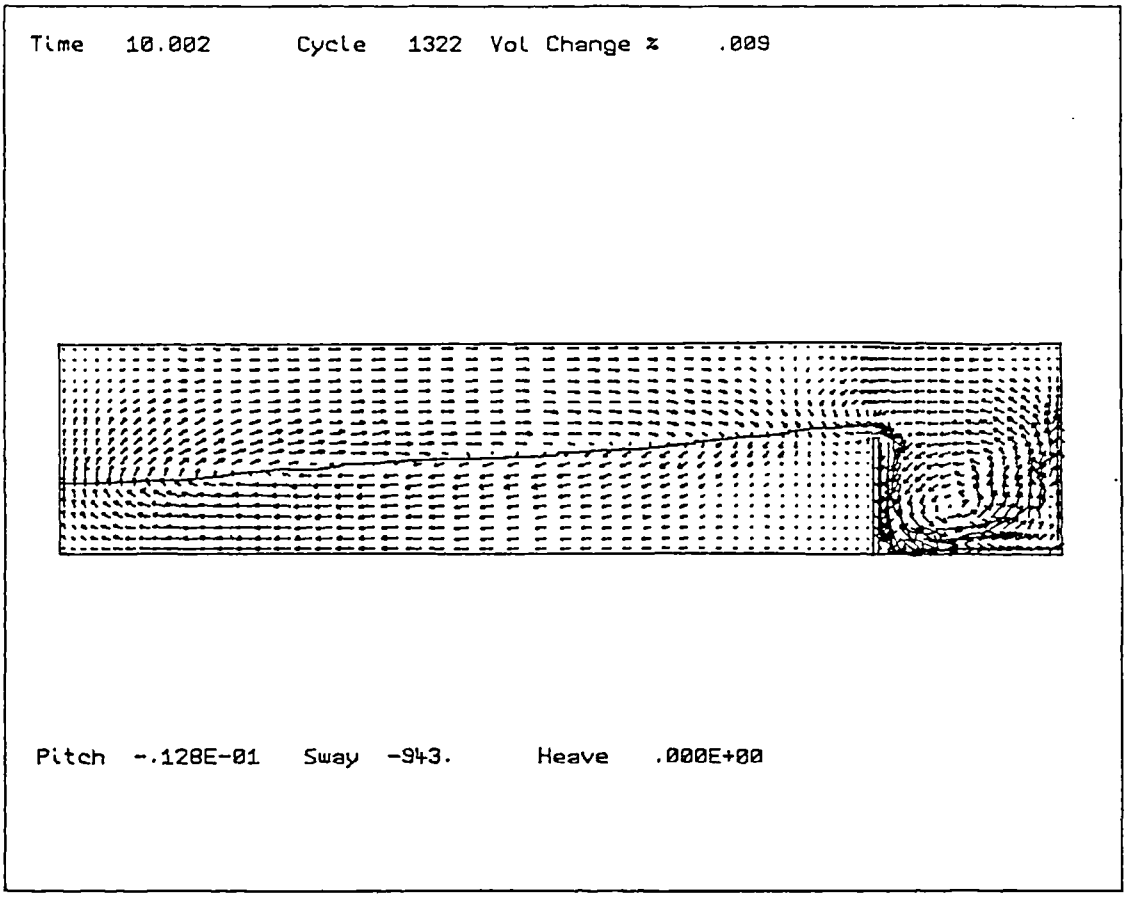
Time 10.002 Cycle 1322 Vol Change % .009
Pitch -.128E-01 Sway -943. Heave .000E+00

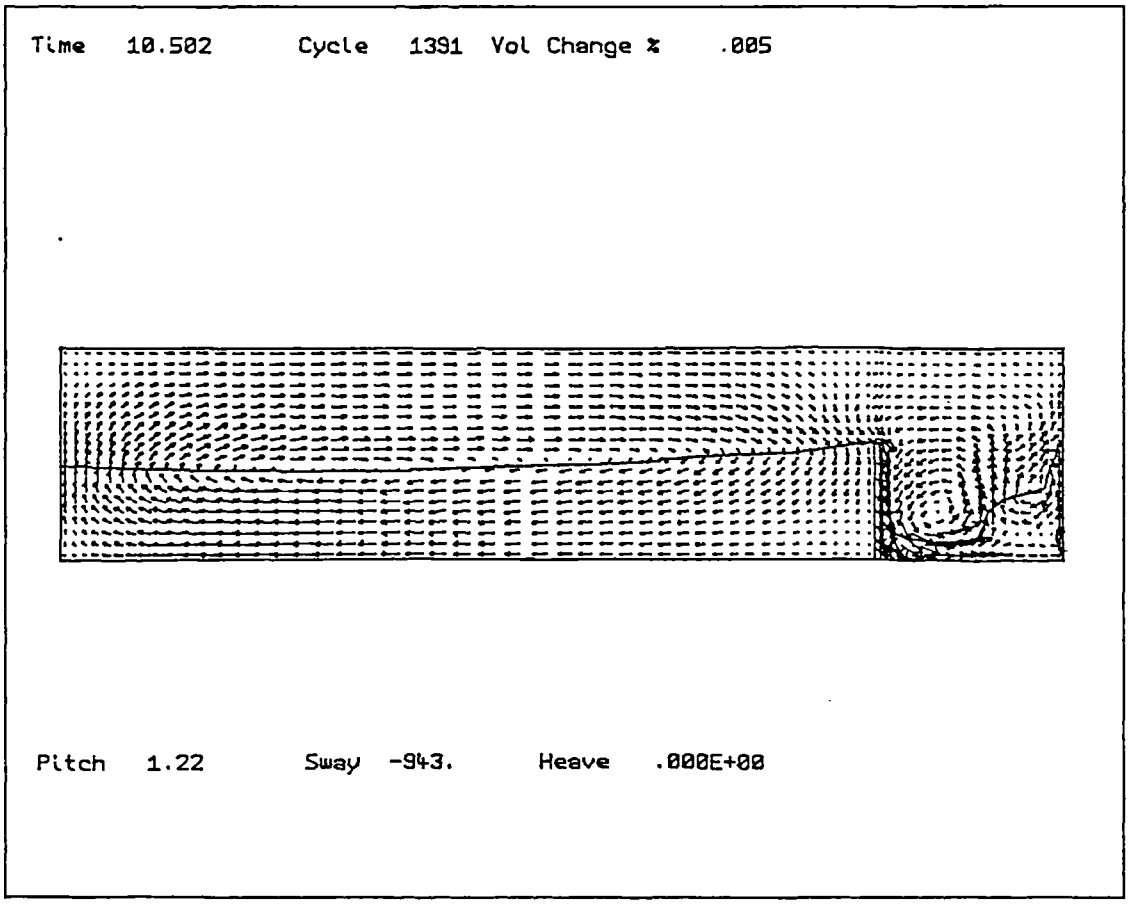
Time 10.502 Cycle 1391 Vol Change % .005
Pitch 1.22 Sway -943. Heave .000E+00

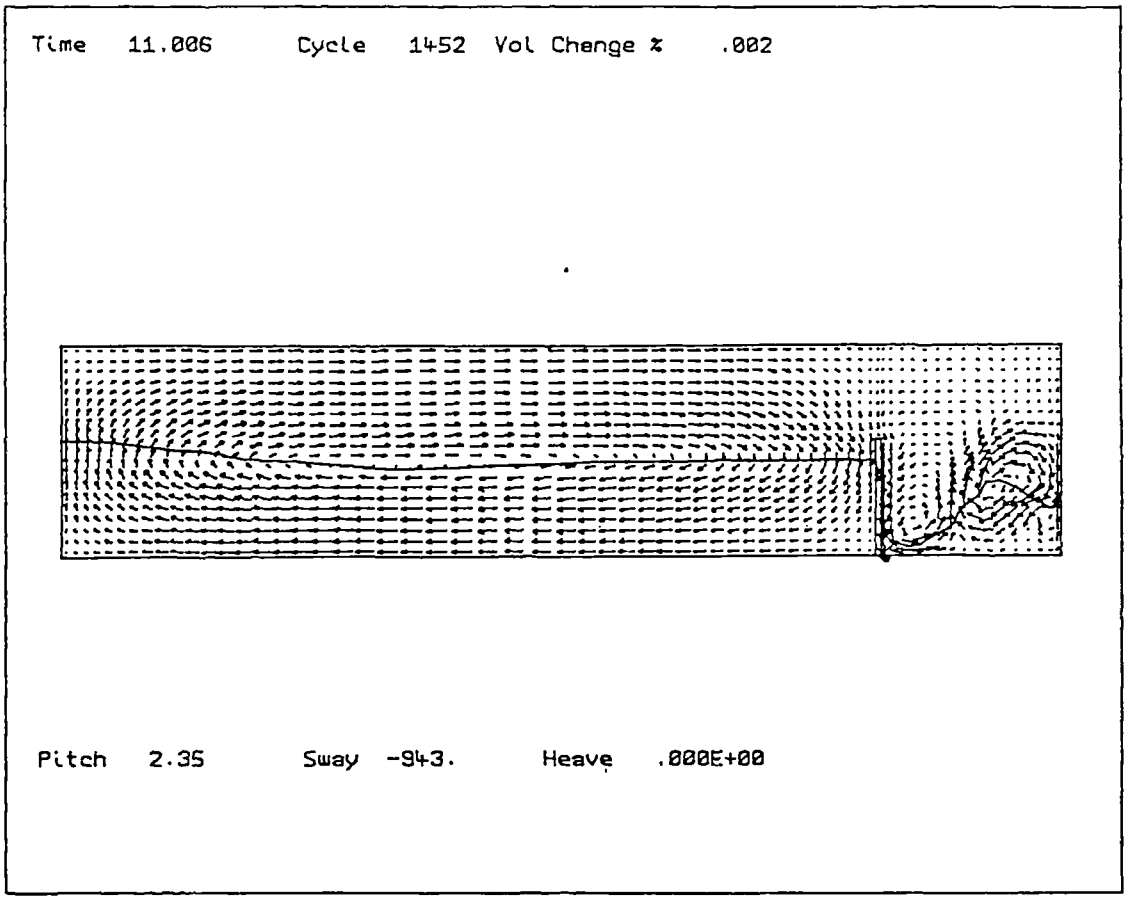
Time 11.006 Cycle 1452 Vol Change % .002
Pitch 2.35 Sway -943. Heave .000E+00

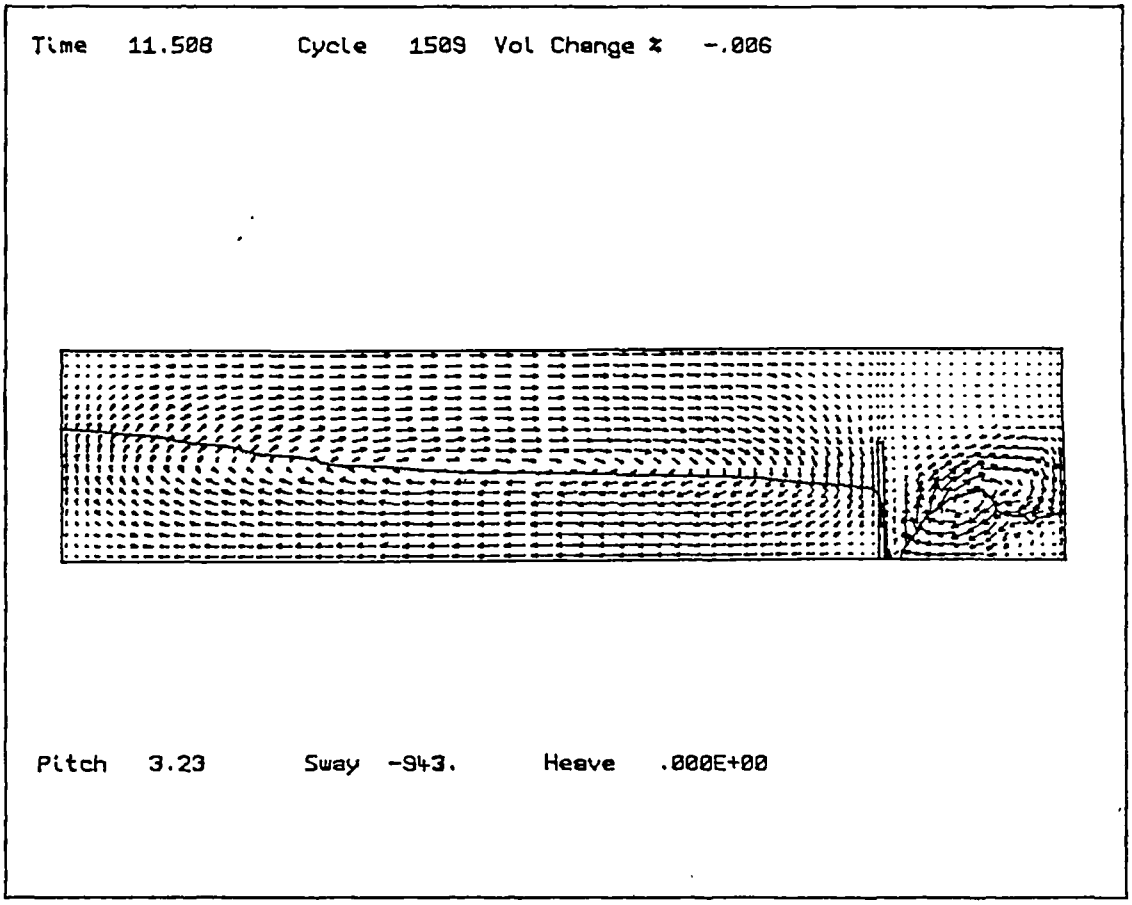
Time 11.508 Cycle 1509 Vol Change % -.006
Pitch 3.23 Sway -943. Heave .000E+00

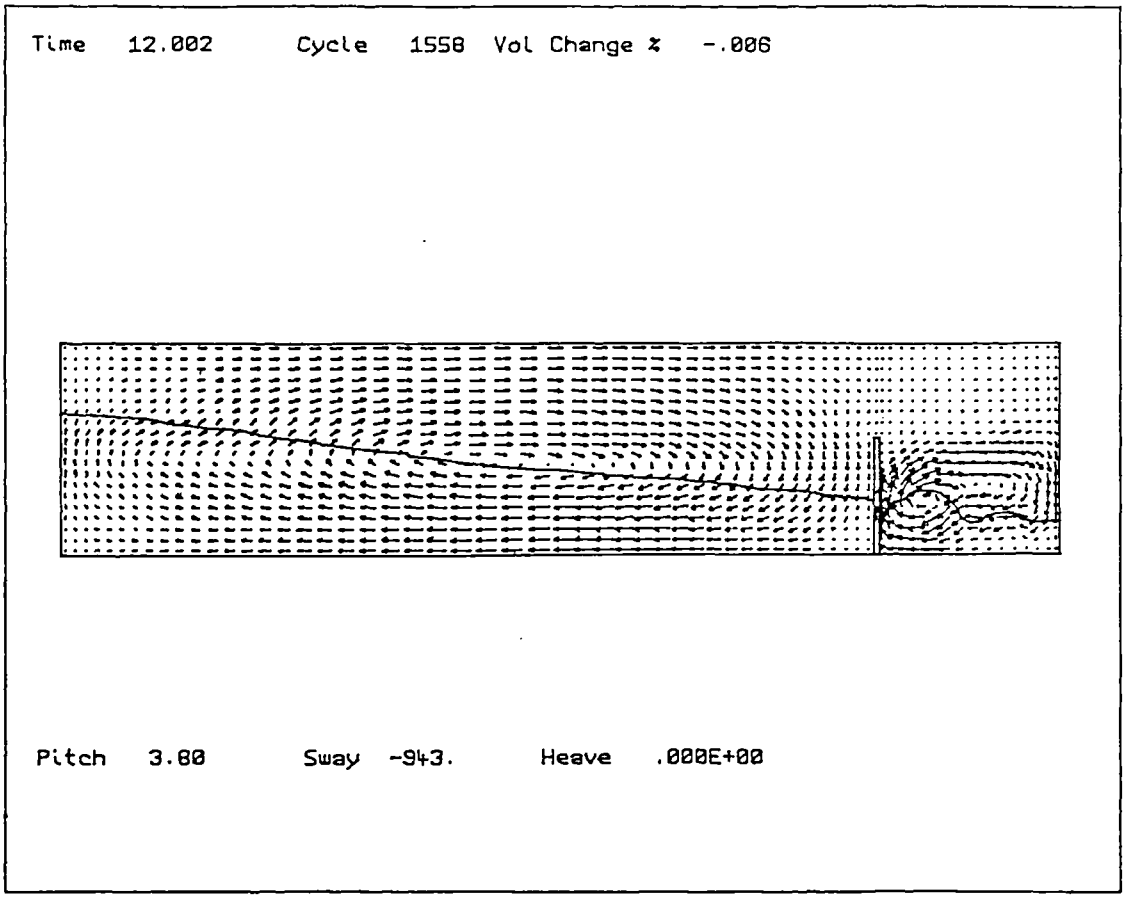
Time 12.002 Cycle 1558 Vol Change % -.006
Pitch 3.80 Sway -943. Heave .000E+00

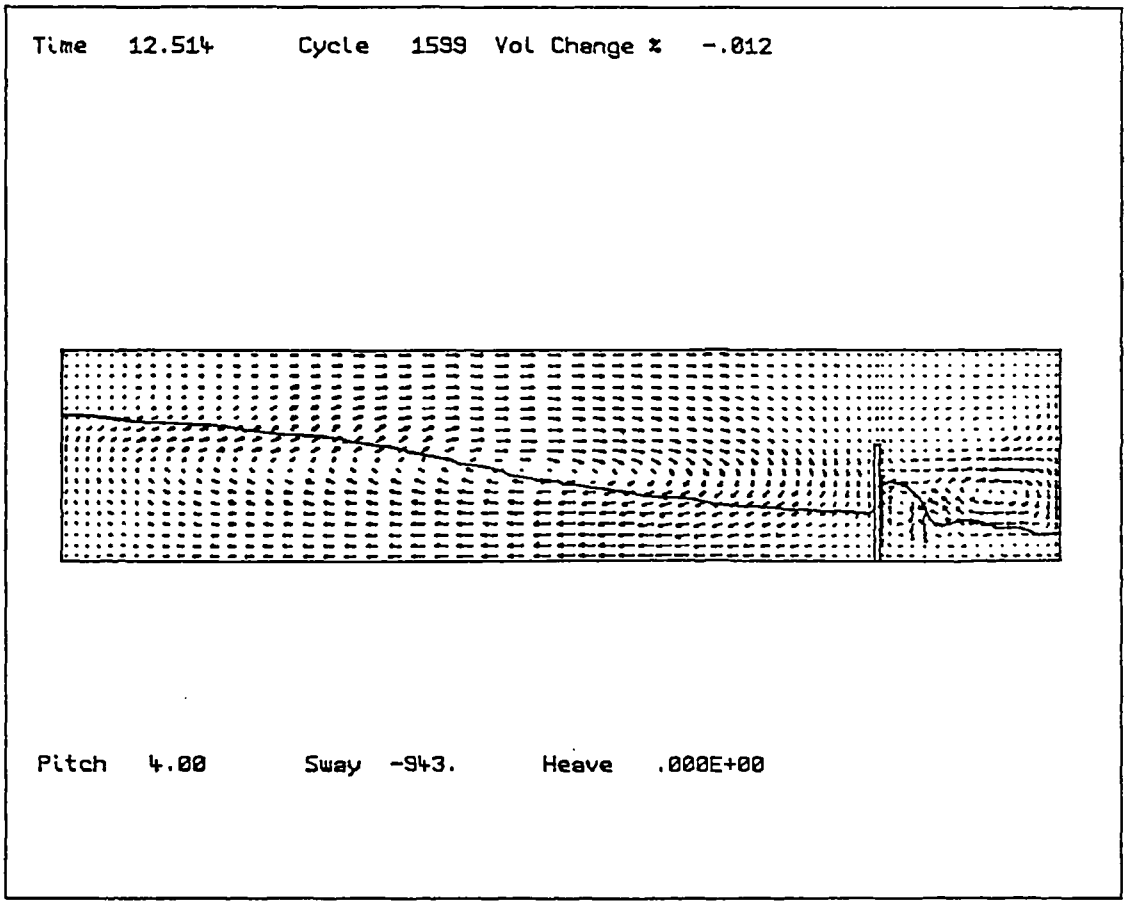
Time 12.514 Cycle 1599 Vol Change % -.012
Pitch 4.00 Sway -943. Heave .000E+00

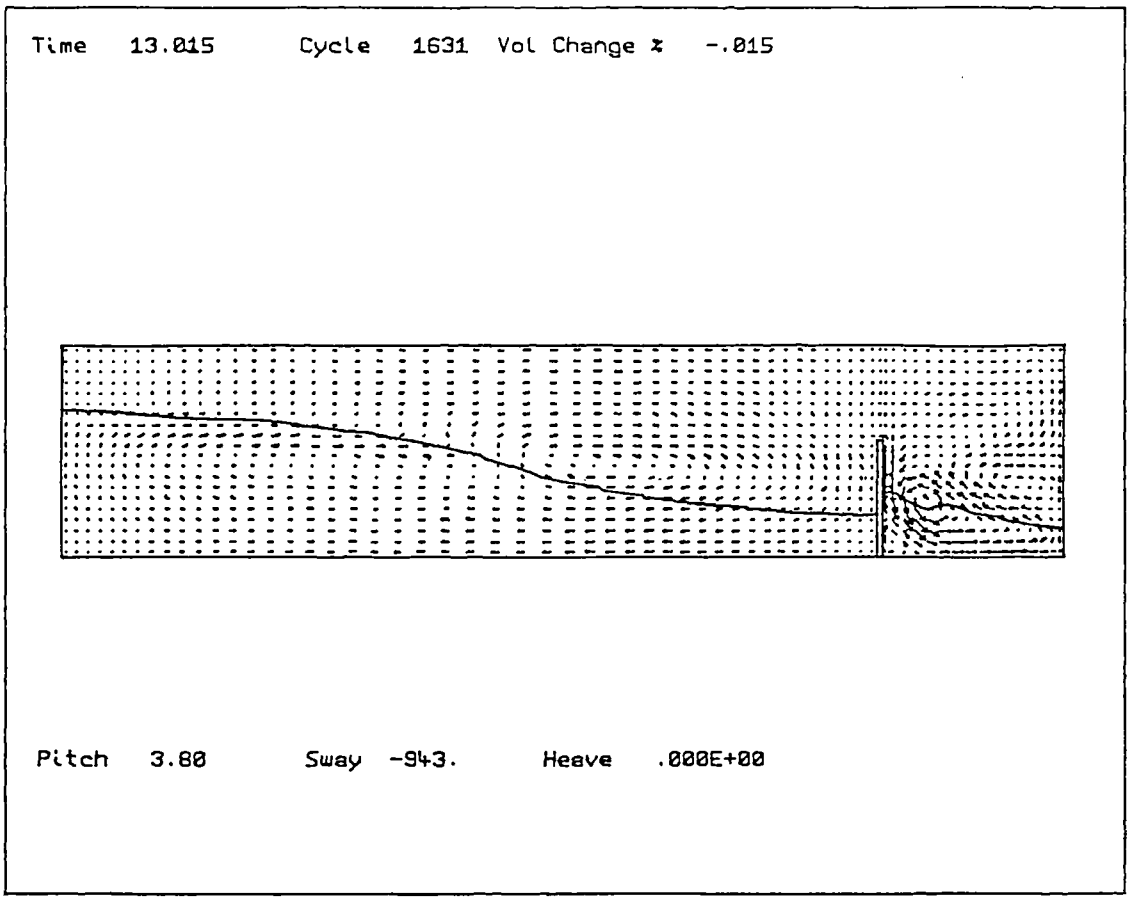
Time 13.015 Cycle 1631 Vol Change % -.015
Pitch 3.80 Sway -943. Heave .000E+00

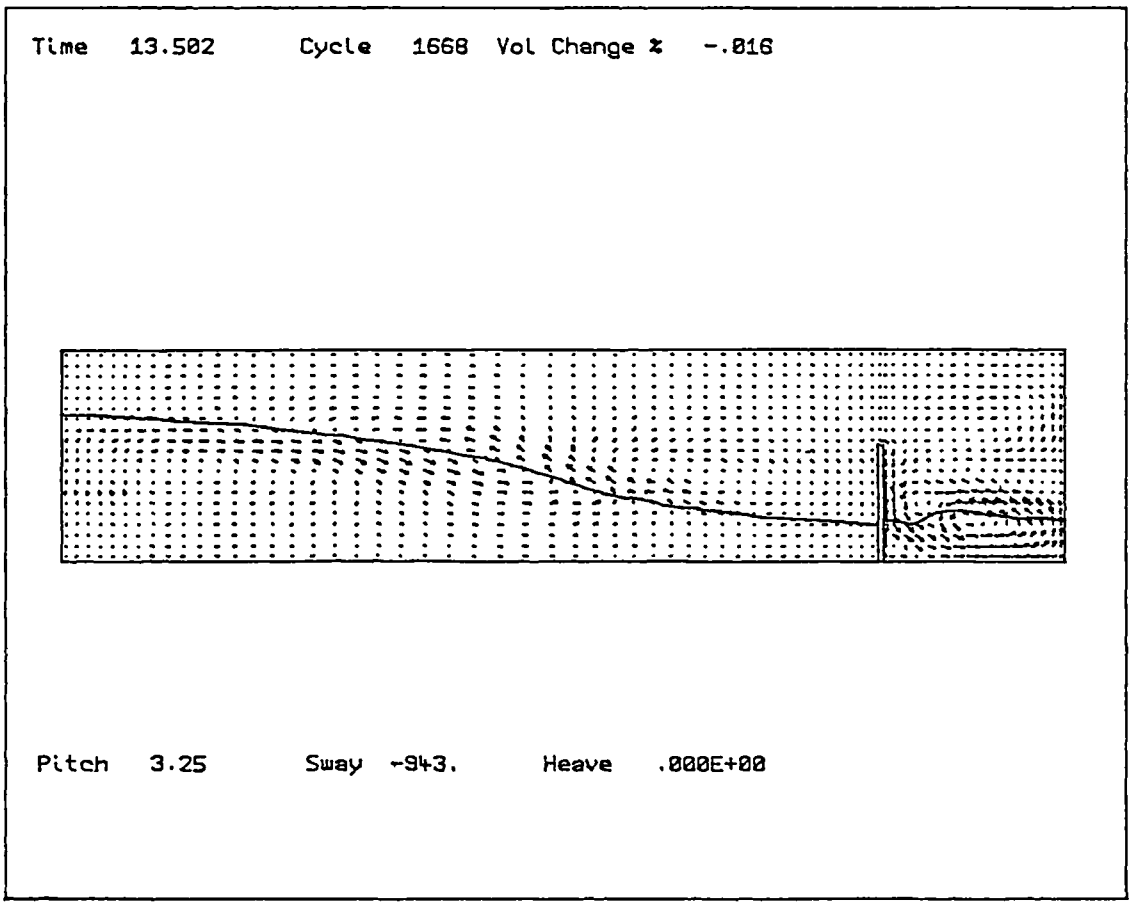
Time 13.502 Cycle 1668 Vol Change % -.016
Pitch 3.25 Sway -943. Heave .000E+00

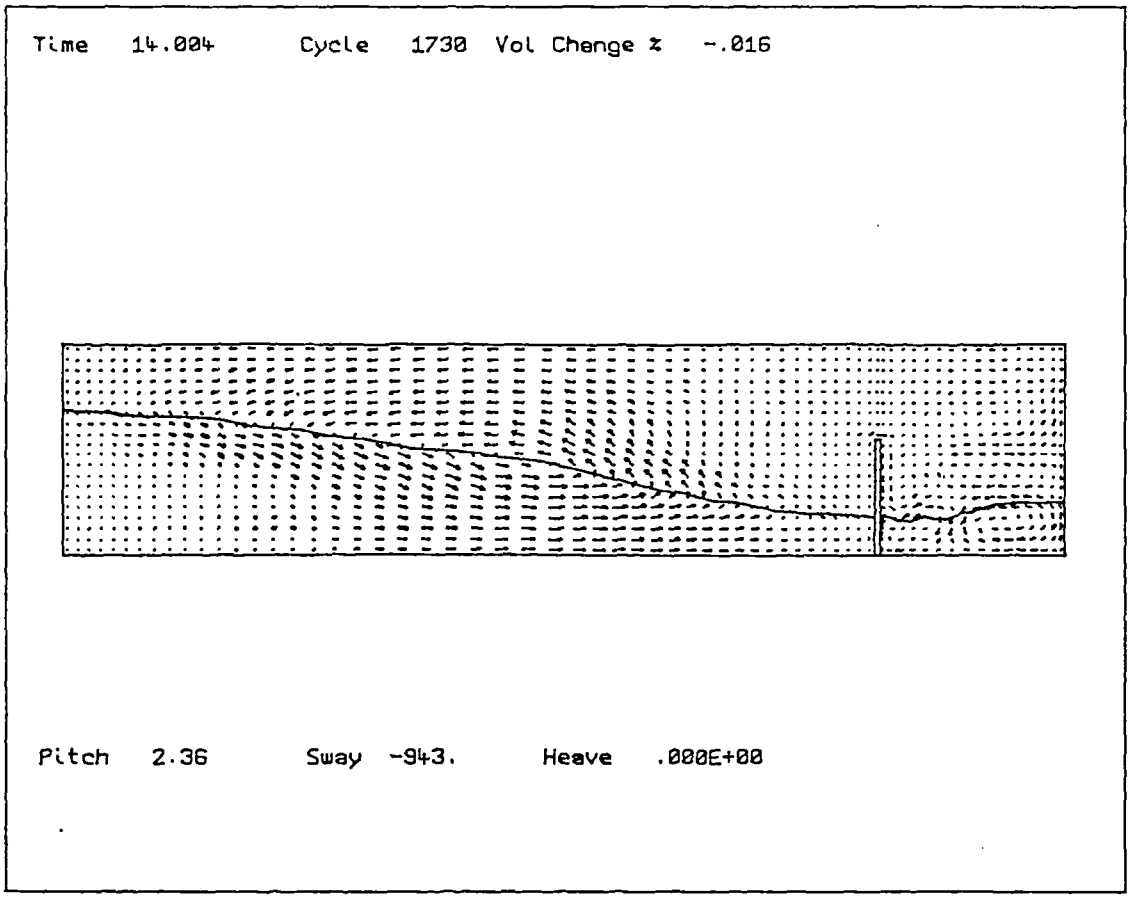
Time 14.004 Cycle 1730 Vol Change % -.016
Pitch 2.36 Sway -943. Heave .000E+00

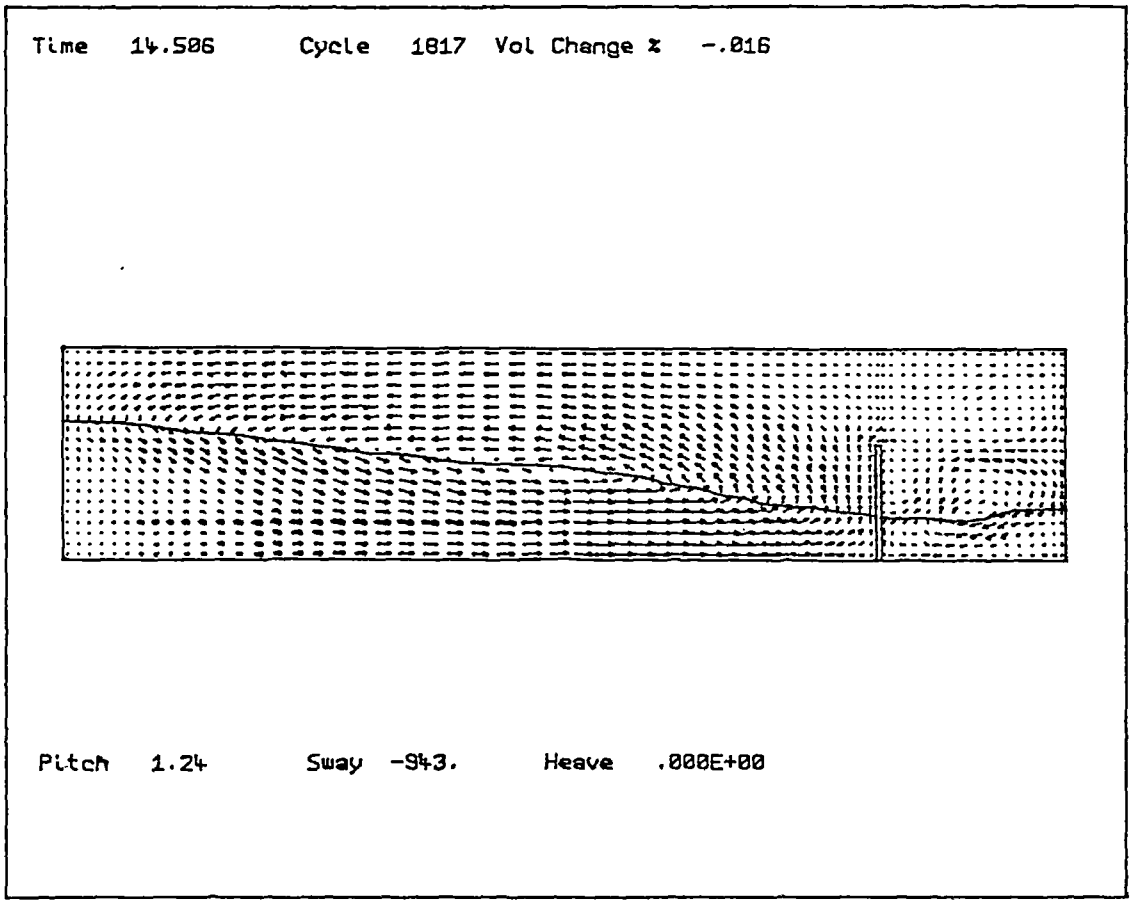
Time 14.506 Cycle 1817 Vol Change % -.016
Pitch 1.24 Sway -943. Heave .000E+00

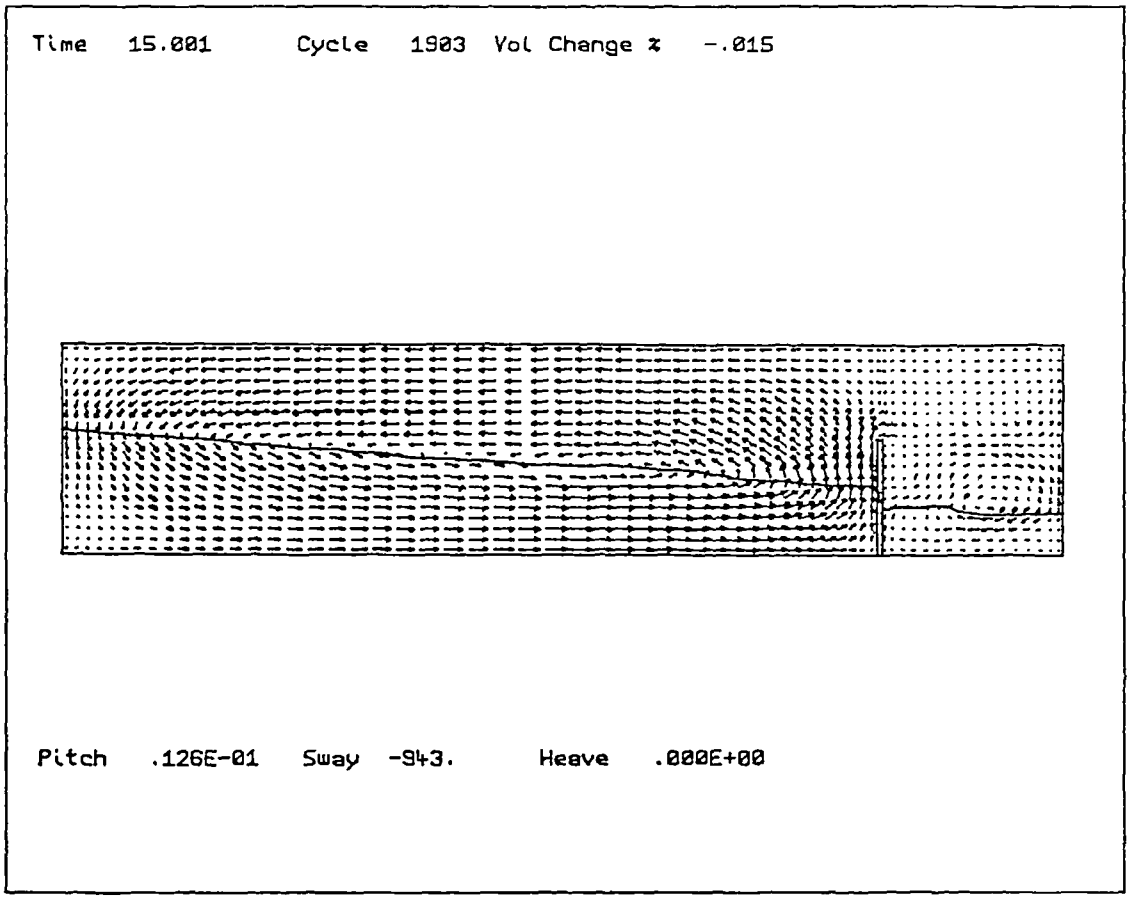
Time 15.001 Cycle 1903 Vol Change % -.015
Pitch .126E-01 Sway -943. Heave .000E+00

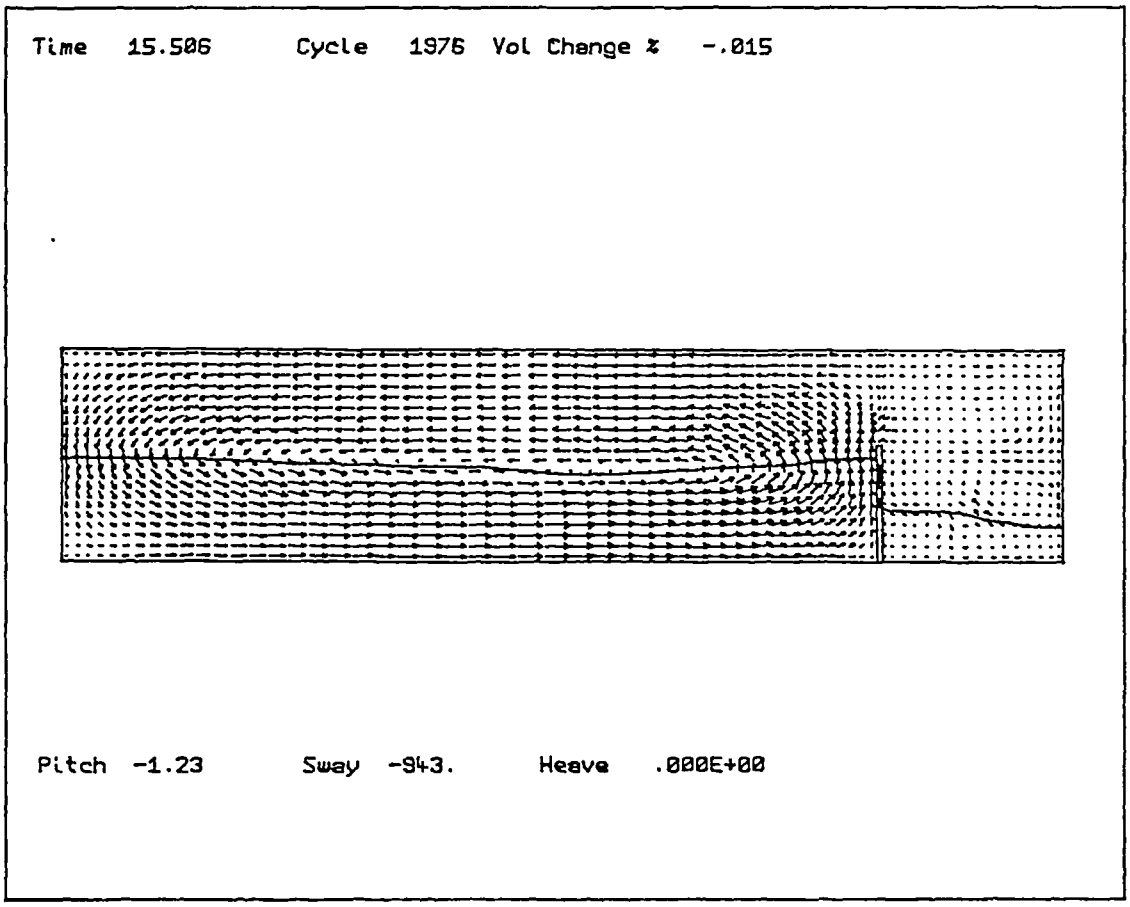
Time 15.506 Cycle 1976 Vol Change % -.015
Pitch -1.23 Sway -943. Heave .000E+00

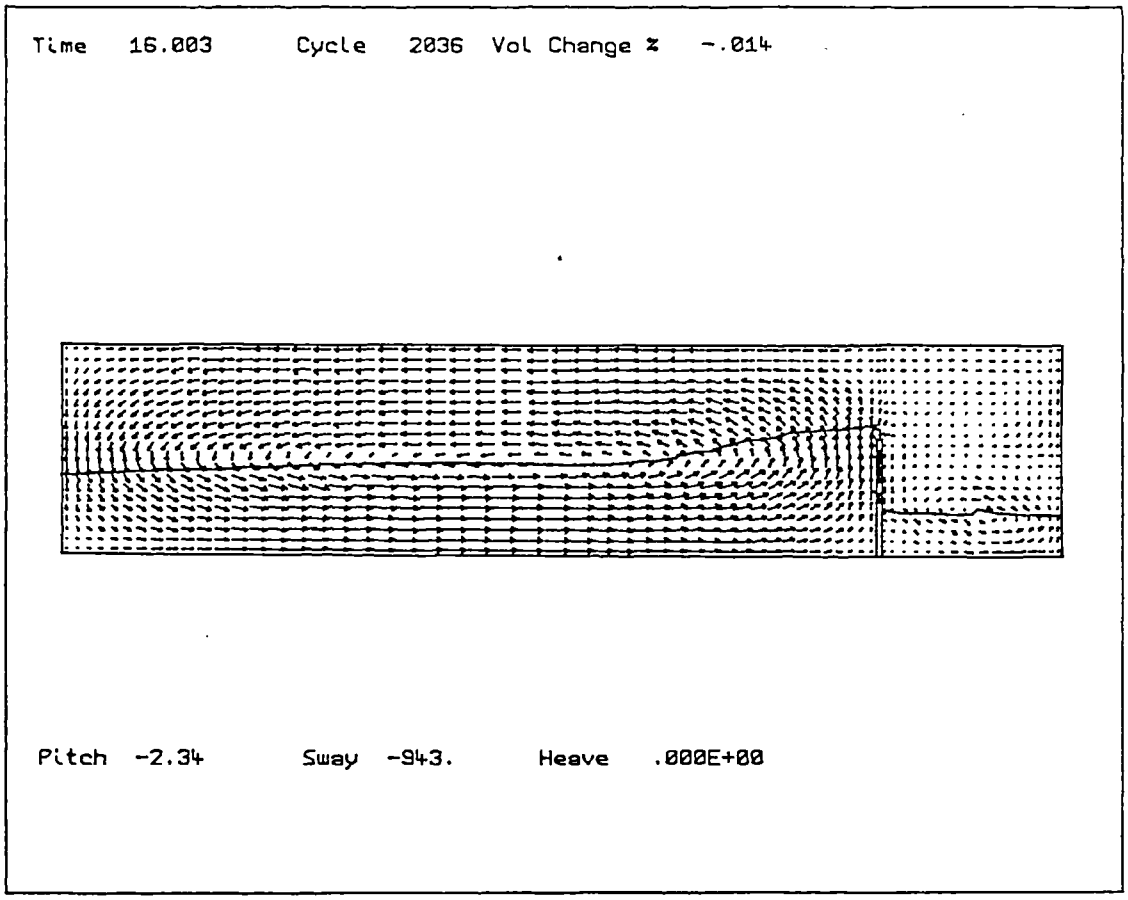
Time 16.003 Cycle 2036 Vol Change % -.014
Pitch -2.34 Sway -943. Heave .000E+00

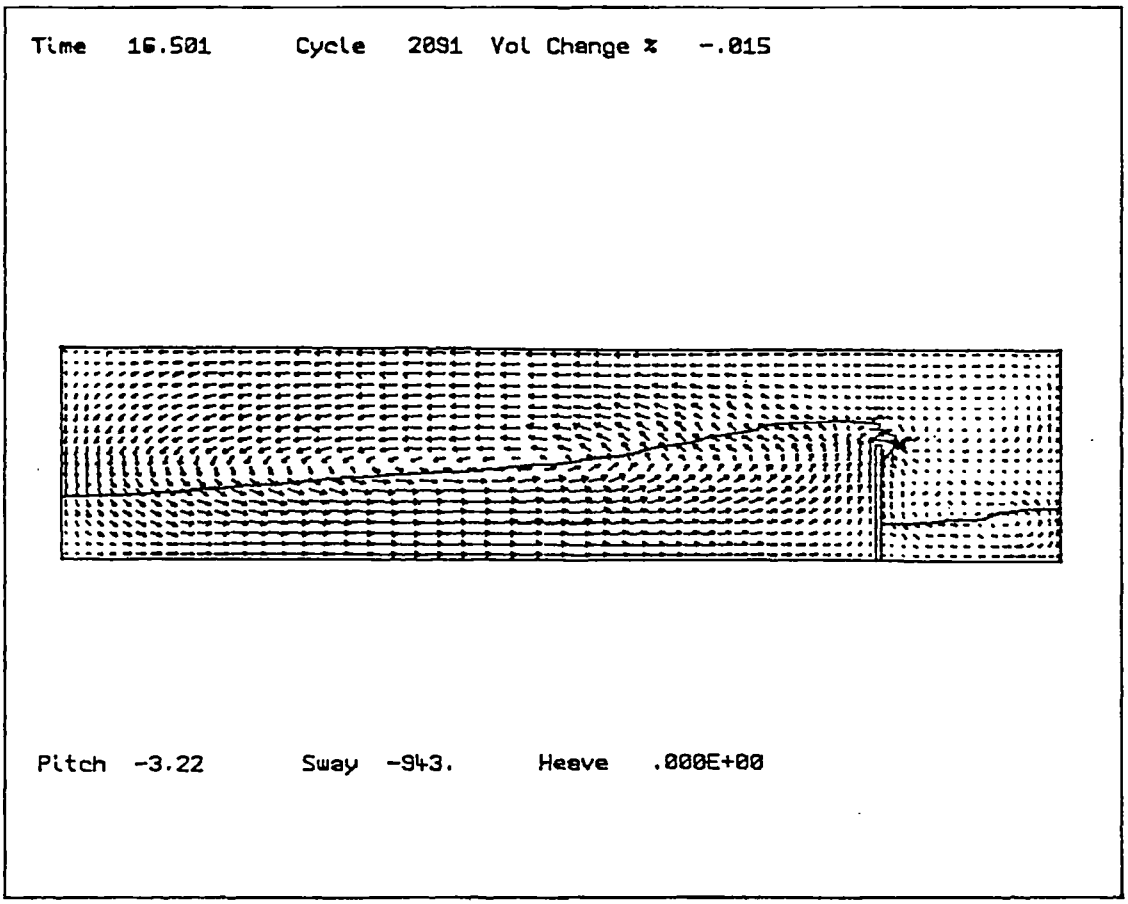
Time 16.501 Cycle 2091 Vol Change % -.015
Pitch -3.22 Sway -943. Heave .000E+00

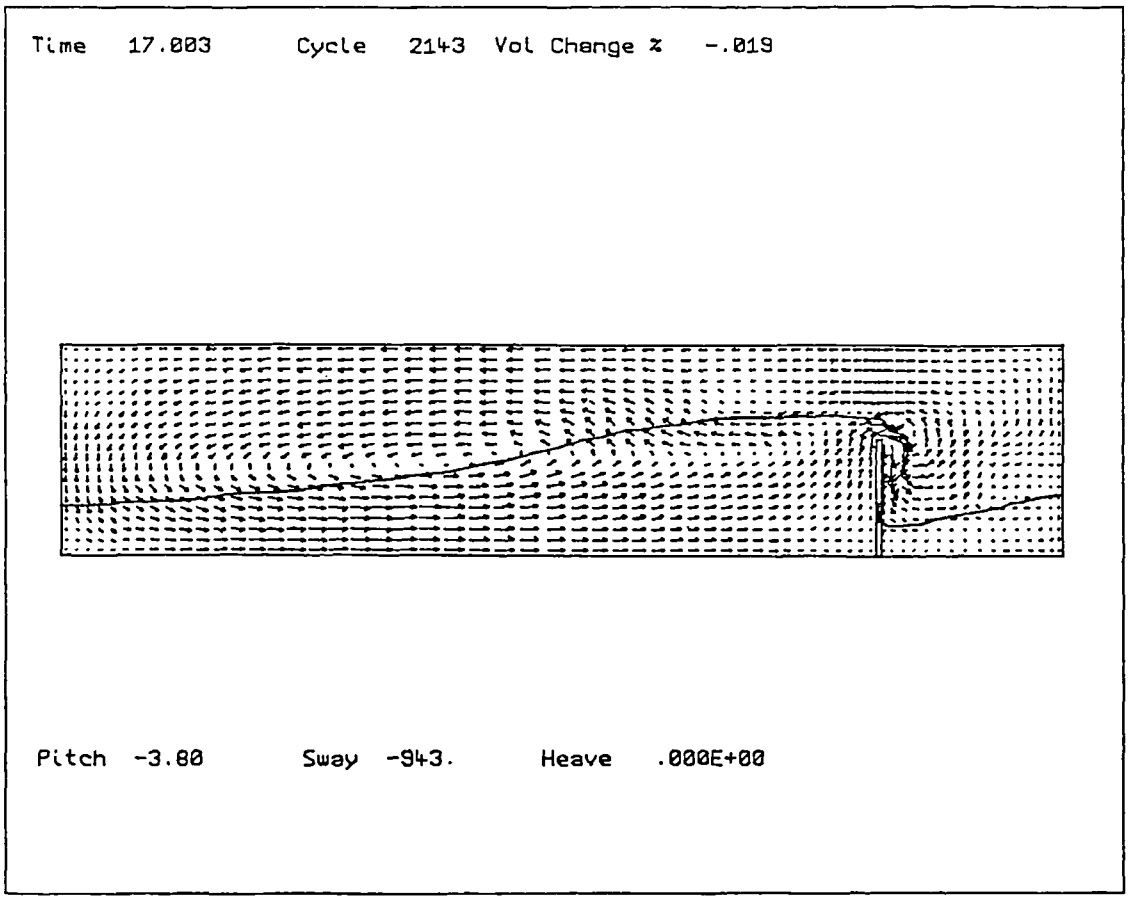
Time 17.003 Cycle 2143 Vol Change % -.019
Pitch -3.80 Sway -943. Heave .000E+00

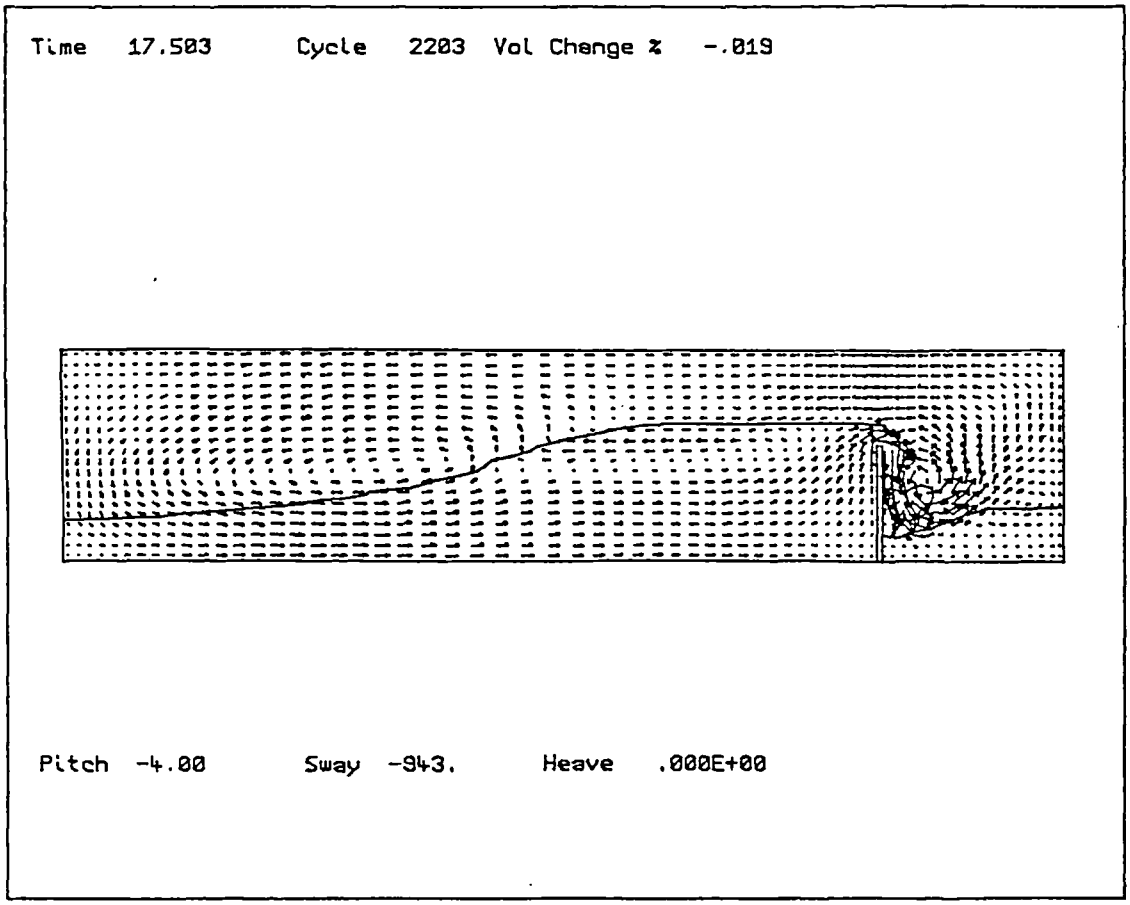
Time 17.503 Cycle 2203 Vol Change % -.019
Pitch -4.00 Sway -943. Heave .000E+00

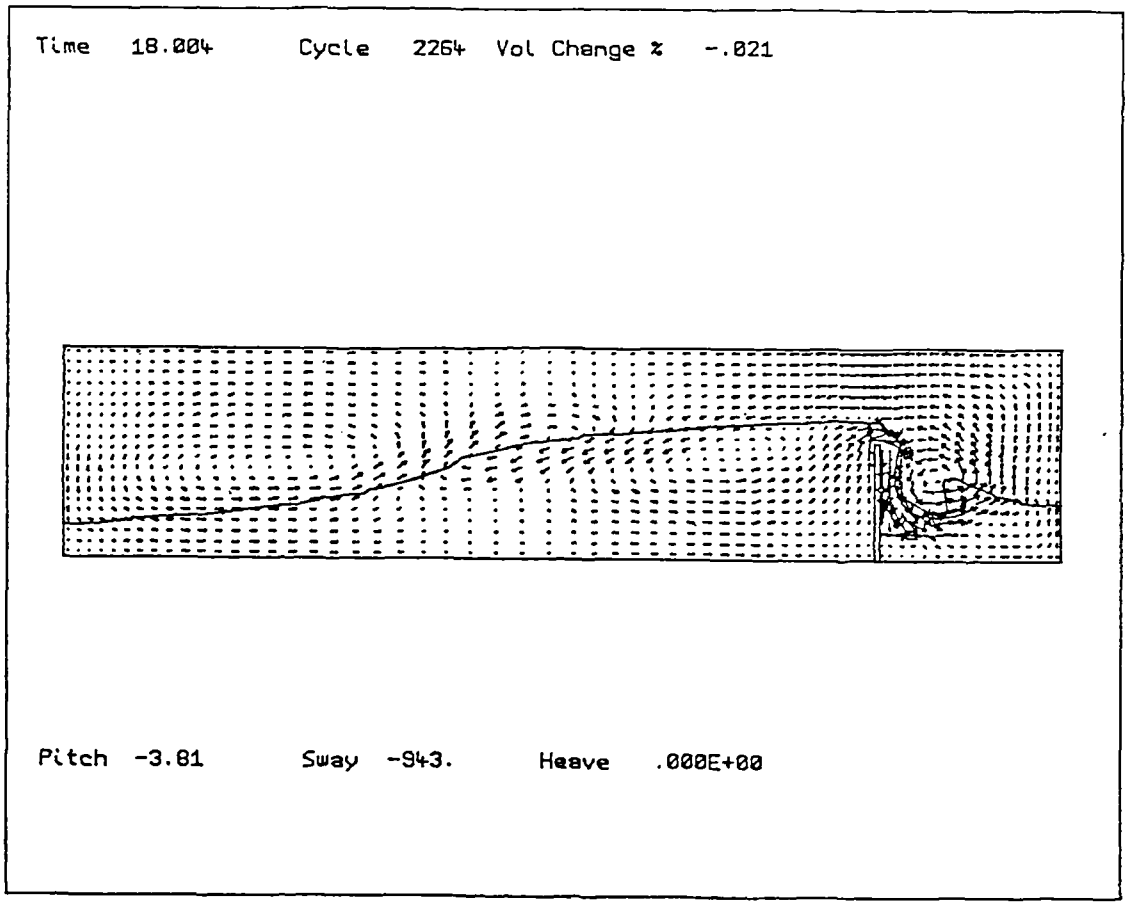
Time 18.004 Cycle 2264 Vol Change % -.021
Pitch -3.81 Sway -943. Heave .000E+00

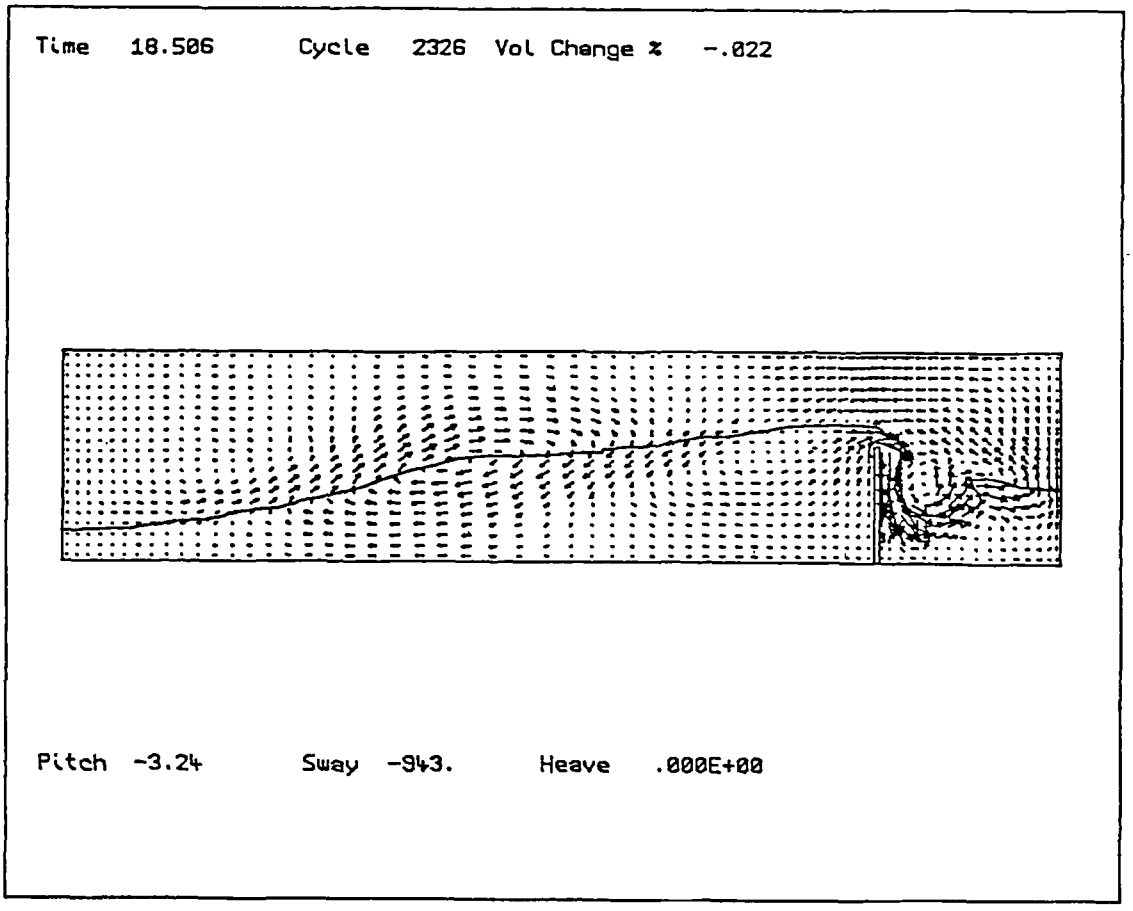
Time 18.506 Cycle 2326 Vol Change % -.022
Pitch -3.24 Sway -943. Heave .000E+00

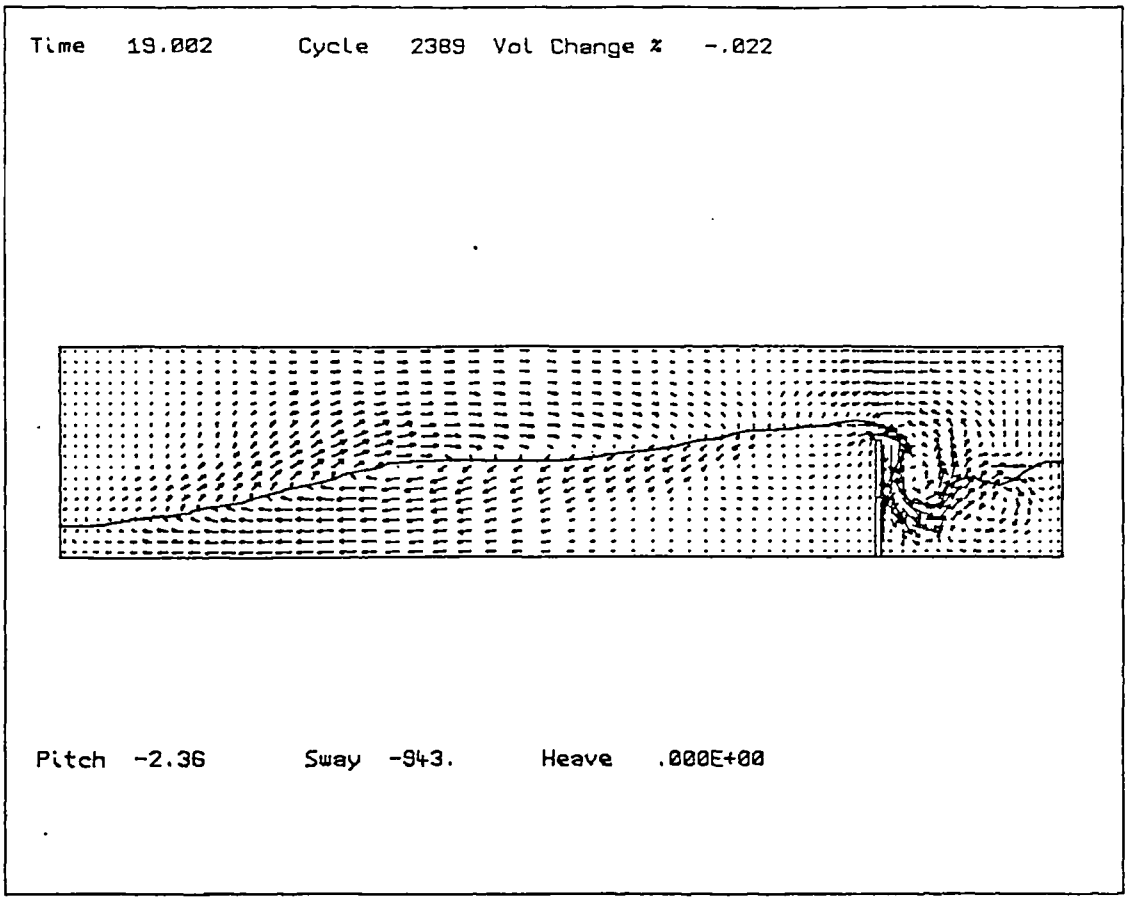
Time 19.002 Cycle 2389 Vol Change % -.022
Pitch -2.36 Sway -943. Heave .000E+00

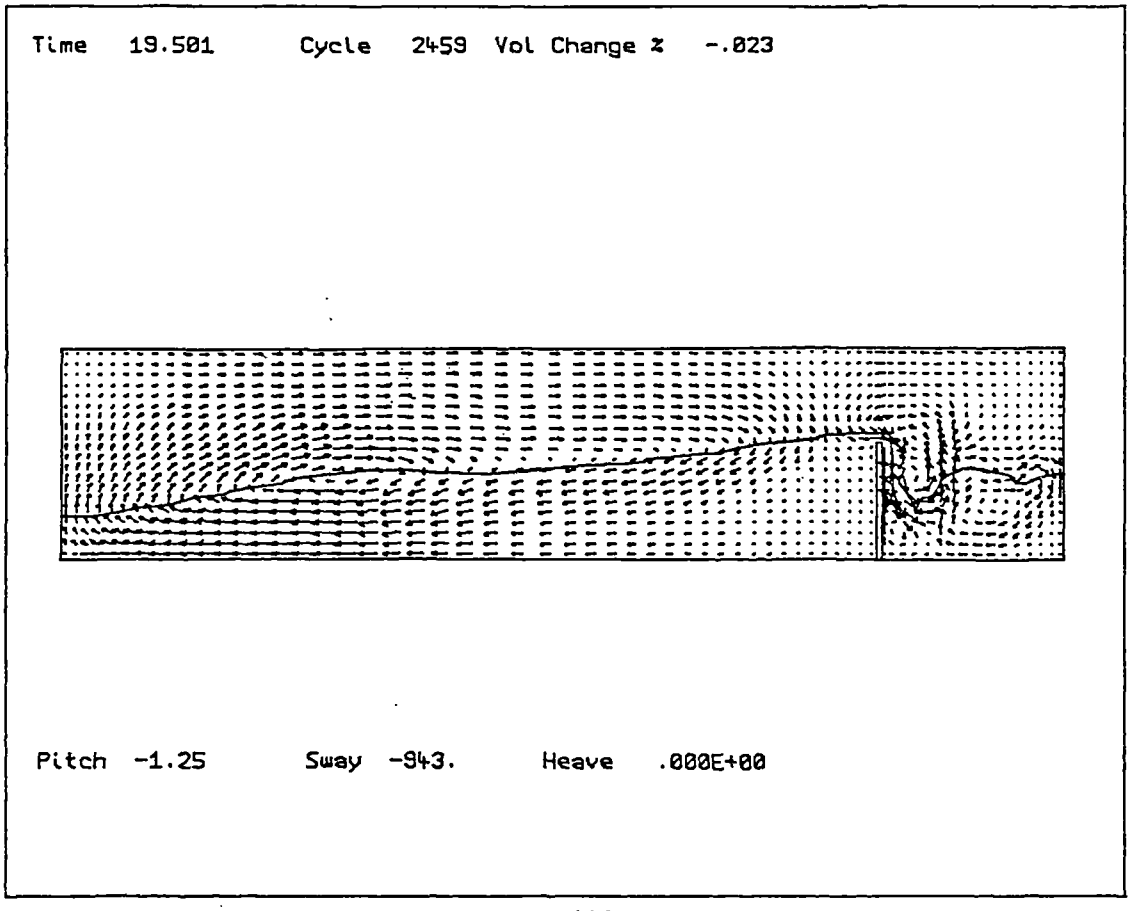
Time 19.501 Cycle 2459 Vol Change % -.023
Pitch -1.25 Sway -943. Heave .000E+00

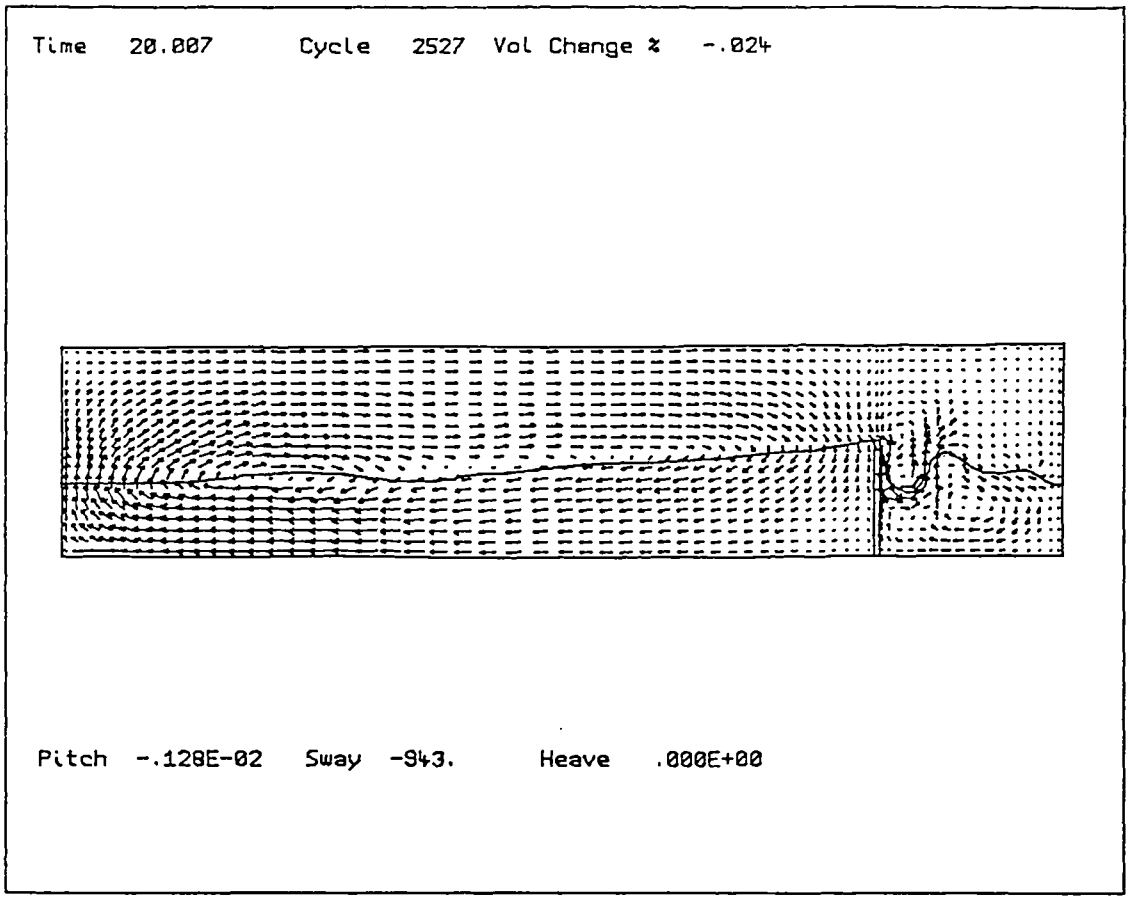
Time 20.007 Cycle 2527 Vol Change % -.024
Pitch -.128E-02 Sway -943. Heave .000E+00

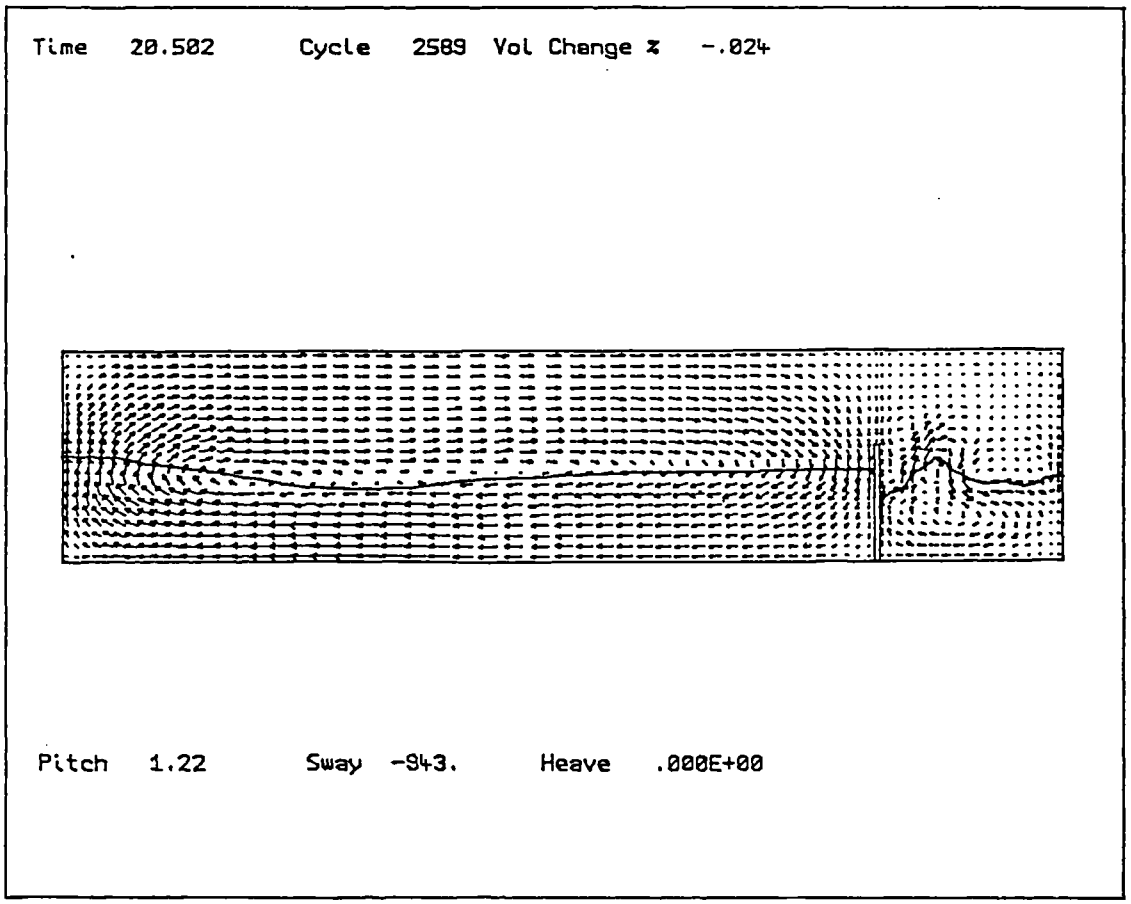
Time 20.502 Cycle 2589 Vol Change % -.024
Pitch 1.22 Sway -943. Heave .000E+00

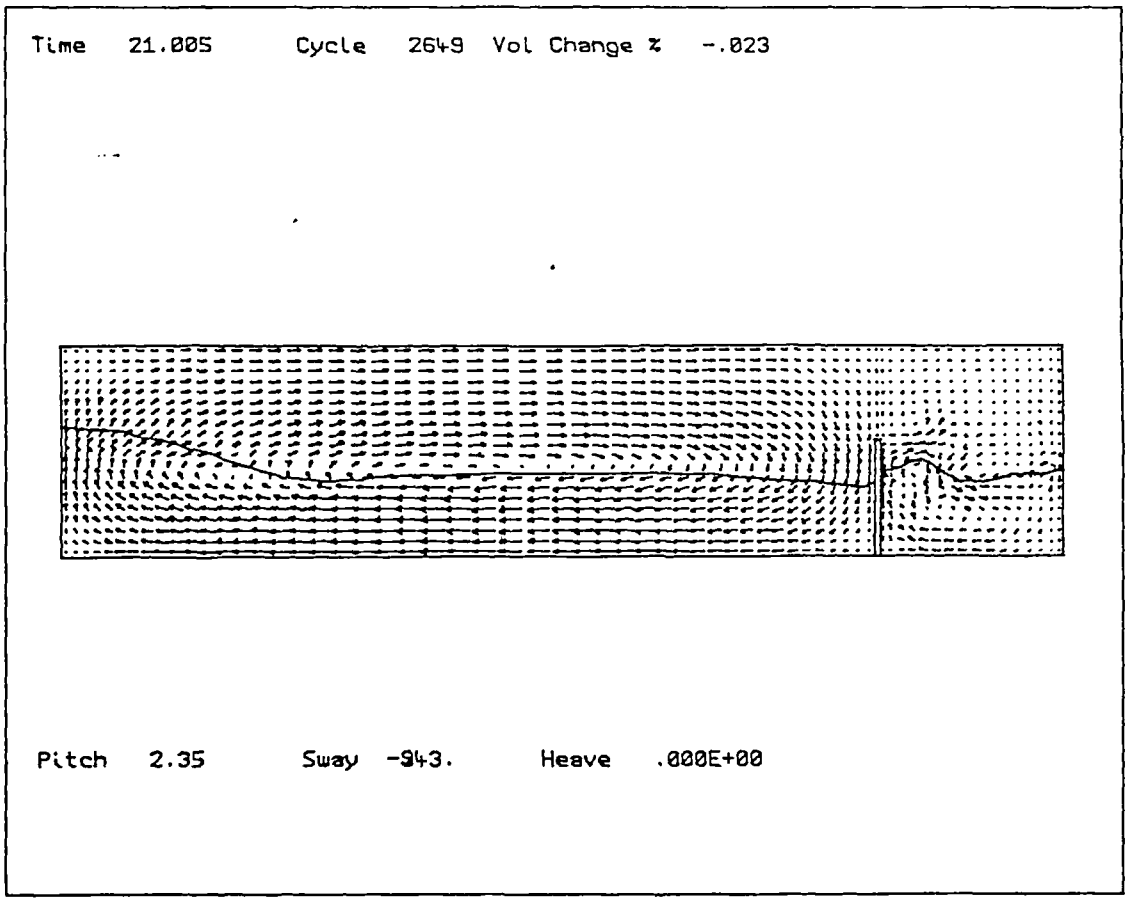
Time 21.005 Cycle 2649 Vol Change % -.023
Pitch 2.35 Sway -943. Heave .000E+00

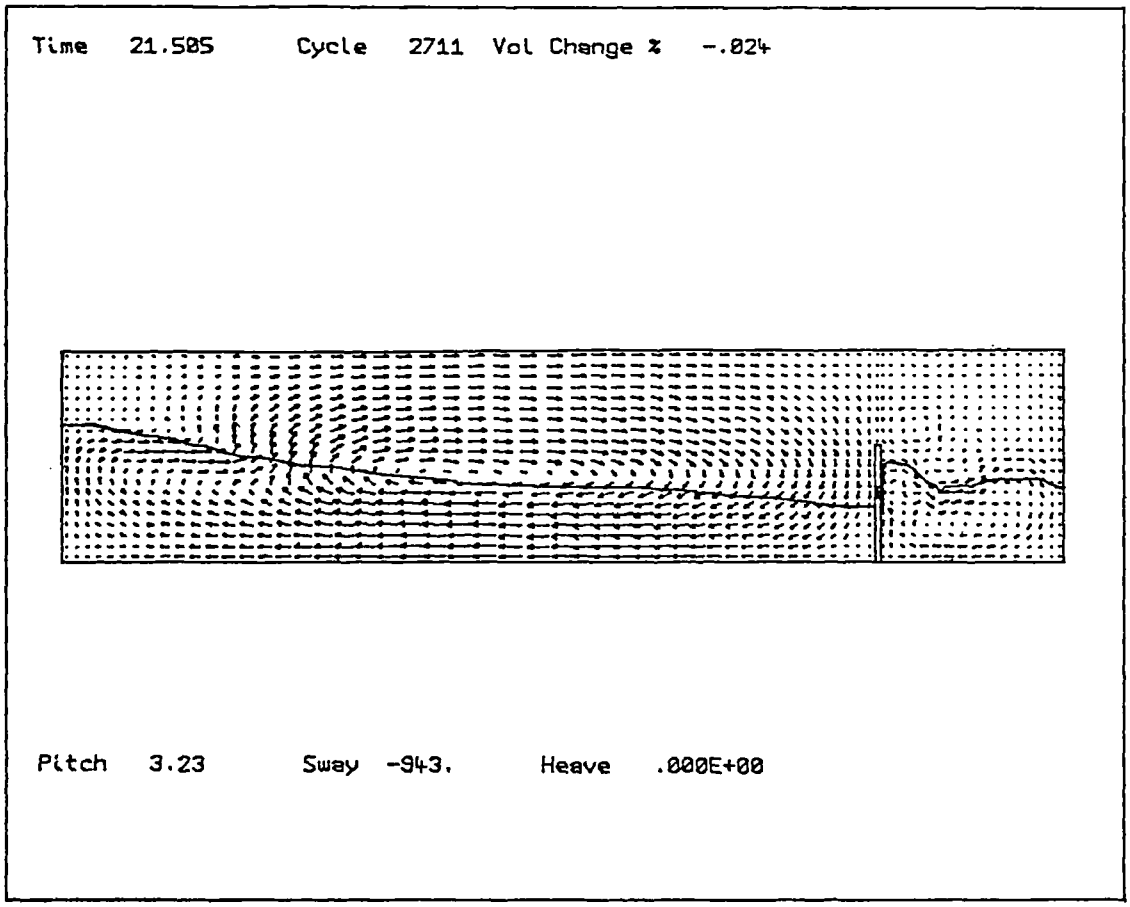
Time 21.505 Cycle 2711 Vol Change % -.024
Pitch 3.23 Sway -943. Heave .000E+00

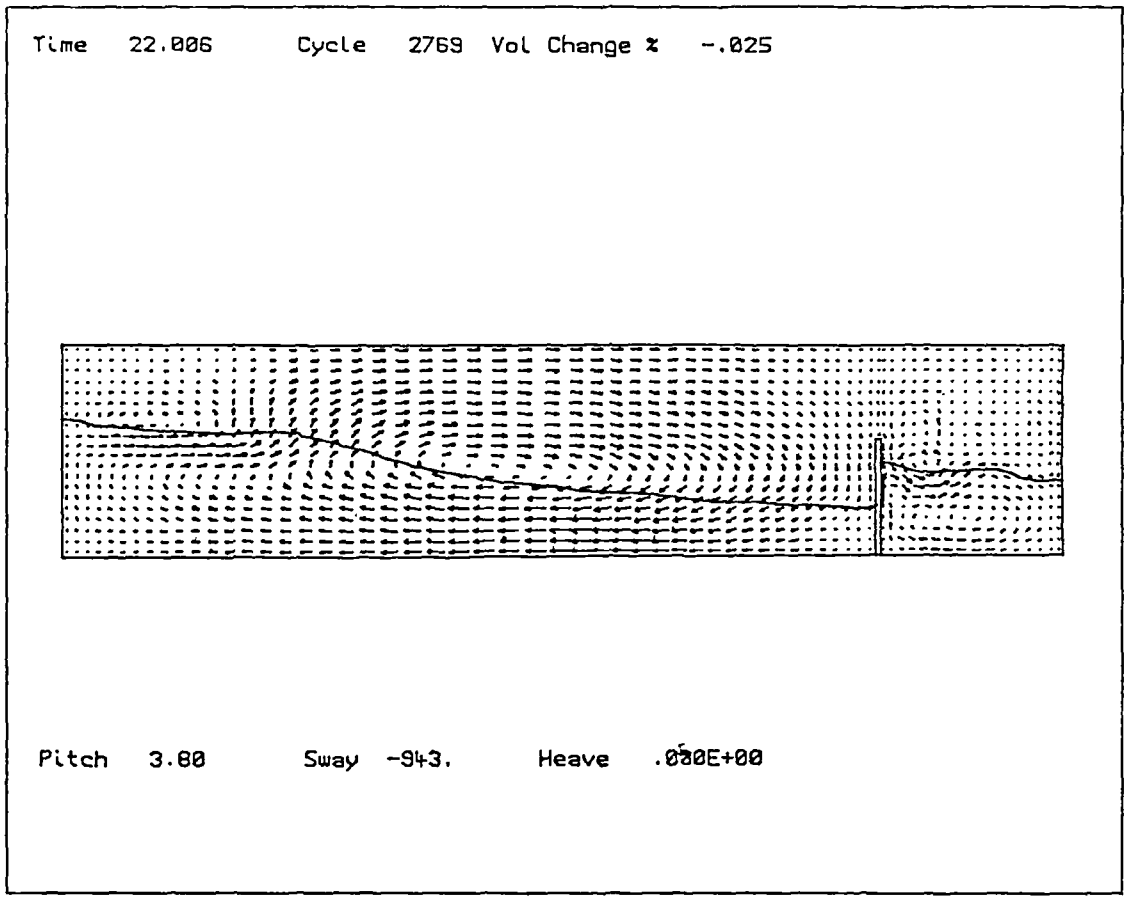
Time 22.006 Cycle 2769 Vol Change % -.025
Pitch 3.80 Sway -943. Heave .000E+00

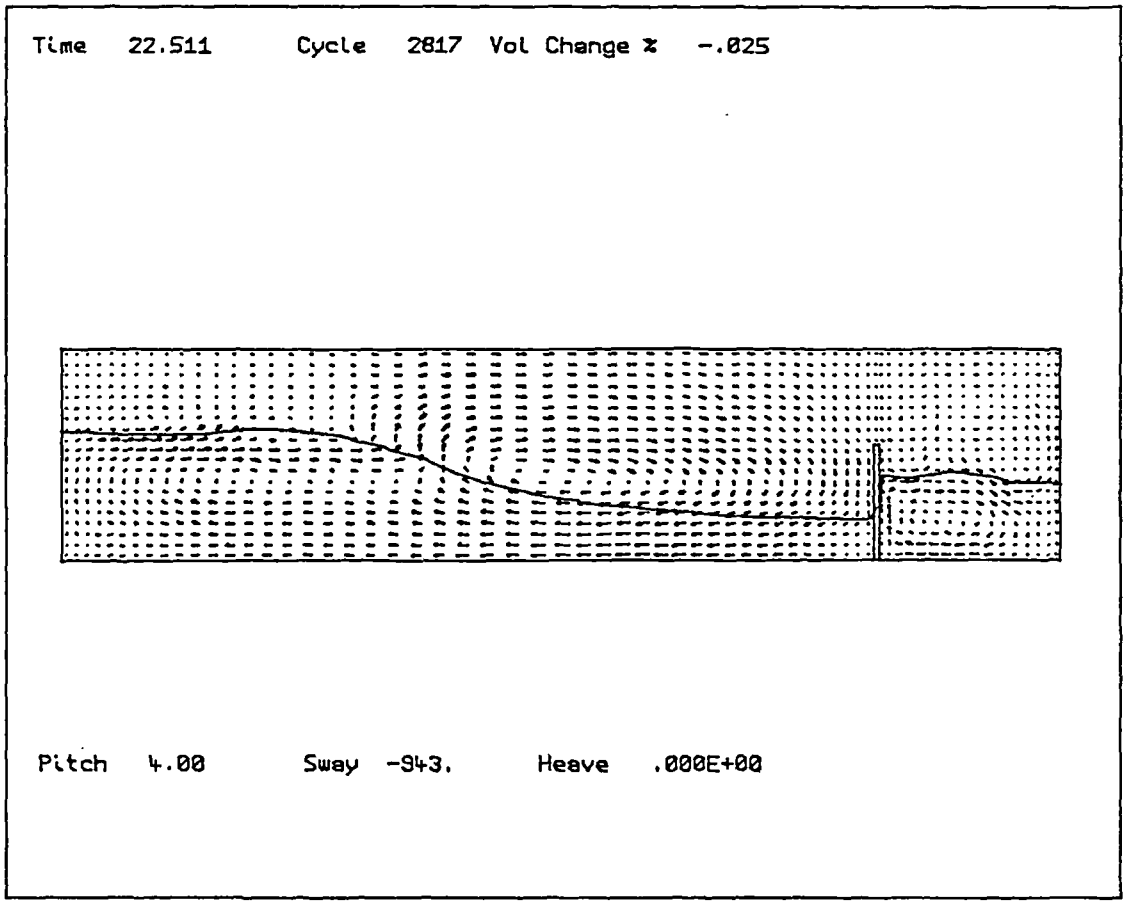
Time 22.511 Cycle 2817 Vol Change % -.025
Pitch 4.00 Sway -943. Heave .000E+00

Time 23.002 Cycle 2853 Vol Change % -.025

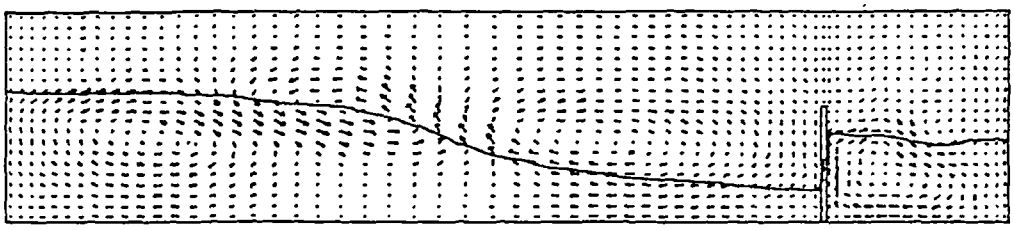

Pitch 3.81 Sway -943. Heave .000E+00

Time 23.504 Cycle 2904 Vol Change % -.025

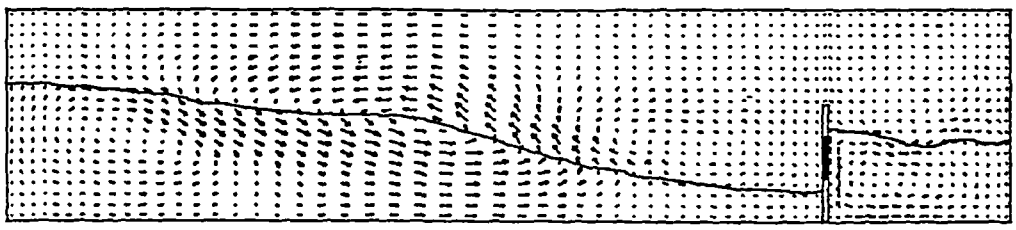

Pitch 3.24 Sway -943. Heave .000E+00

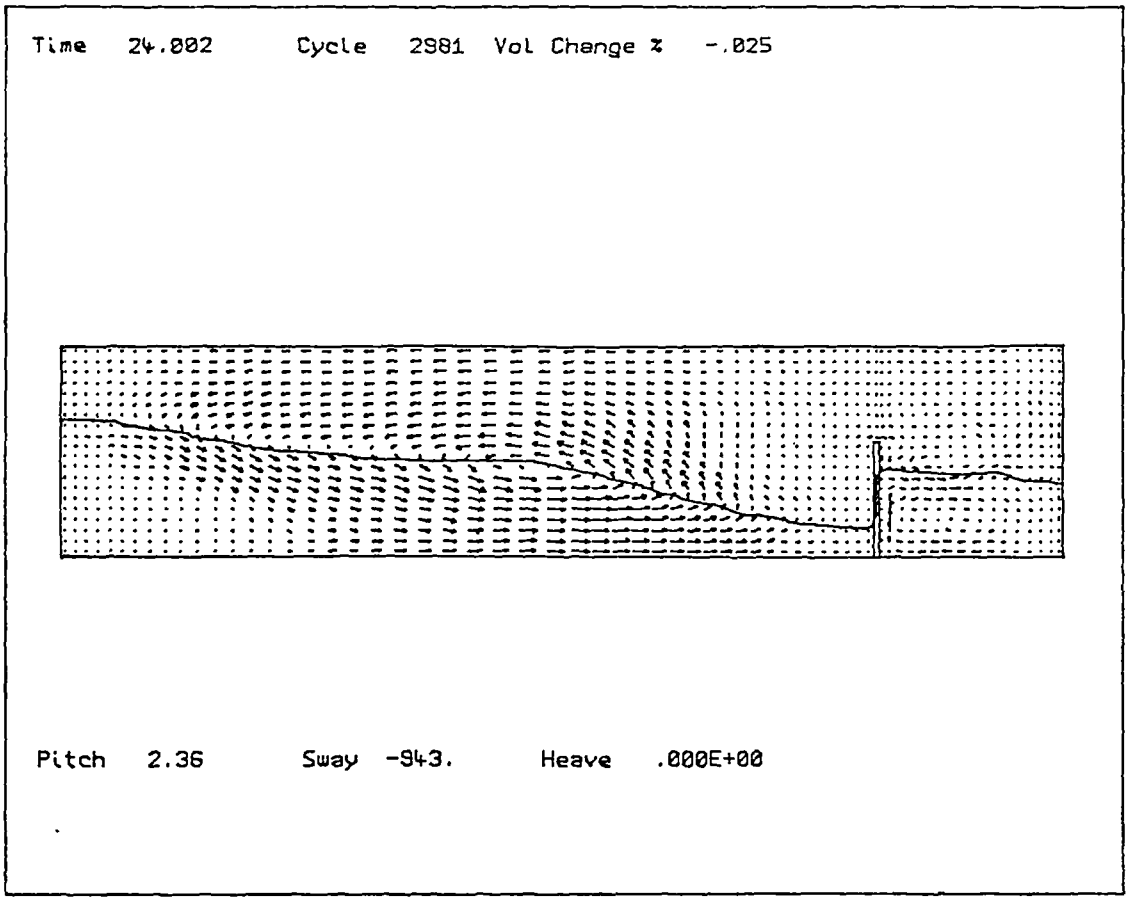
Time 24.002 Cycle 2981 Vol Change % -.025
Pitch 2.36 Sway -943. Heave .000E+00

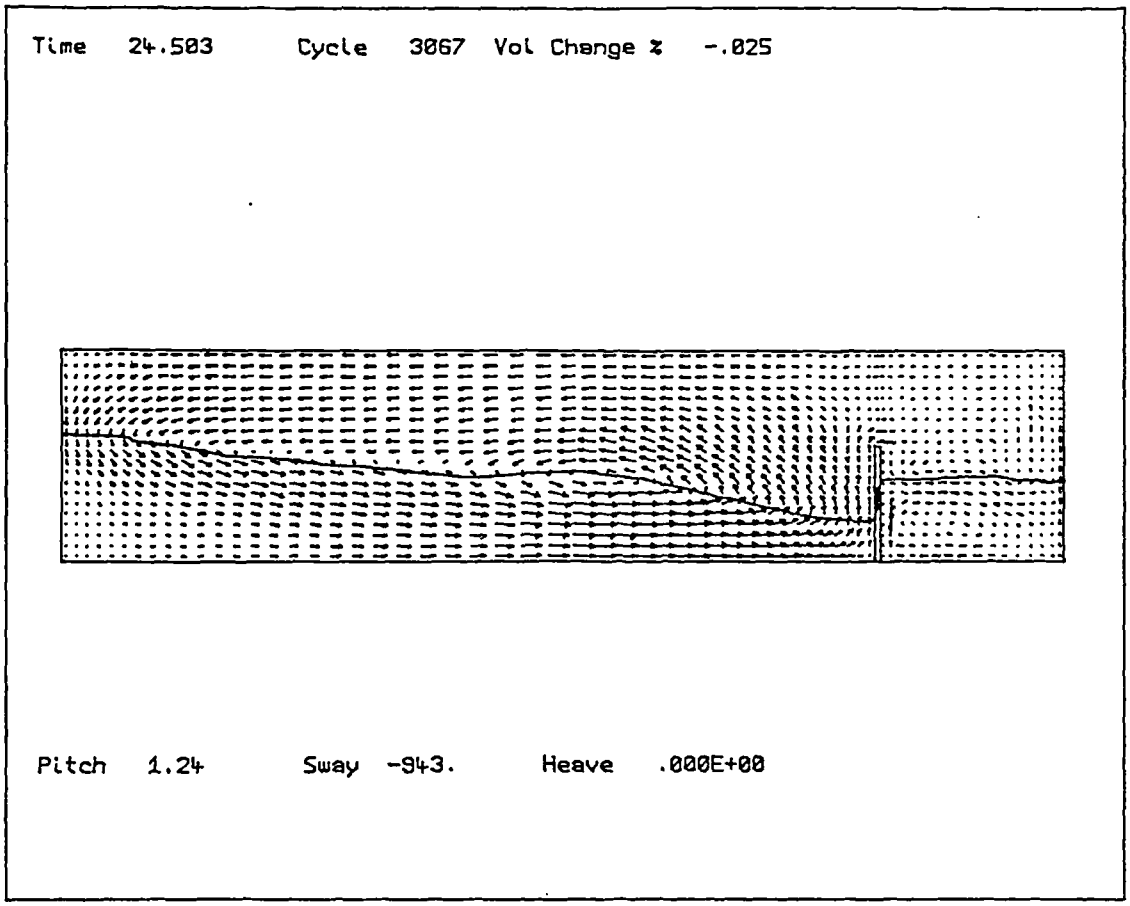
Time 24.503 Cycle 3067 Vol Change % -.025
Pitch 1.24 Sway -943. Heave .000E+00

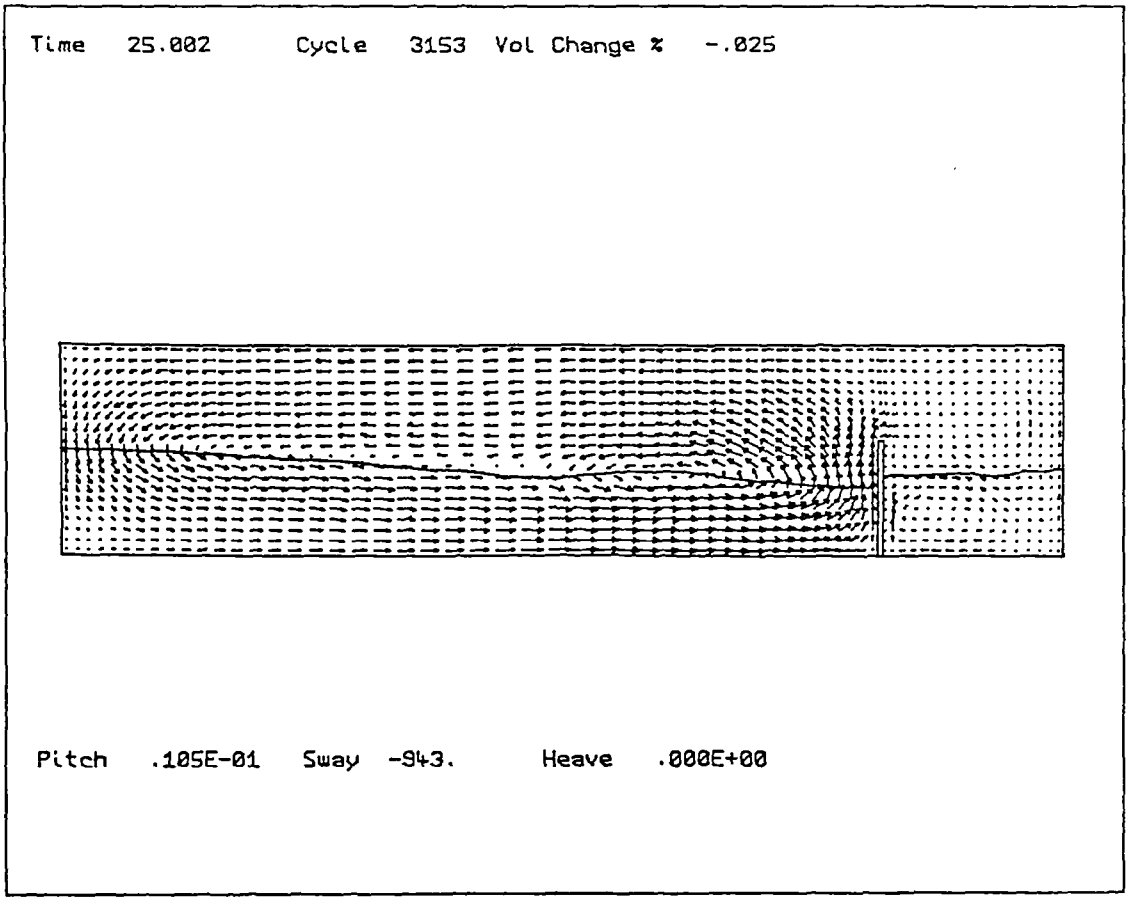
Time 25.002 Cycle 3153 Vol Change % -.025
Pitch .105E-01 Sway -943. Heave .000E+00

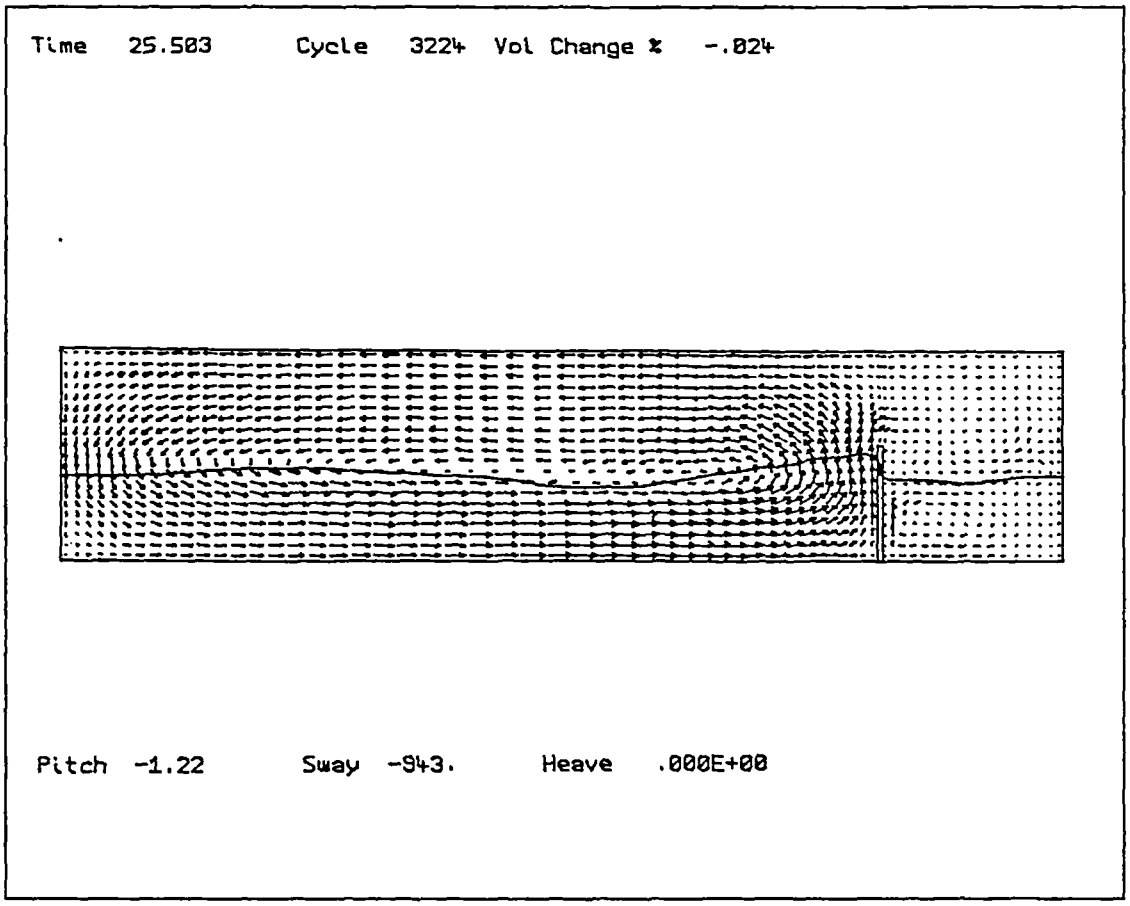
Time 25.503 Cycle 3224 Vol Change % -.024
Pitch -1.22 Sway -943. Heave .000E+00

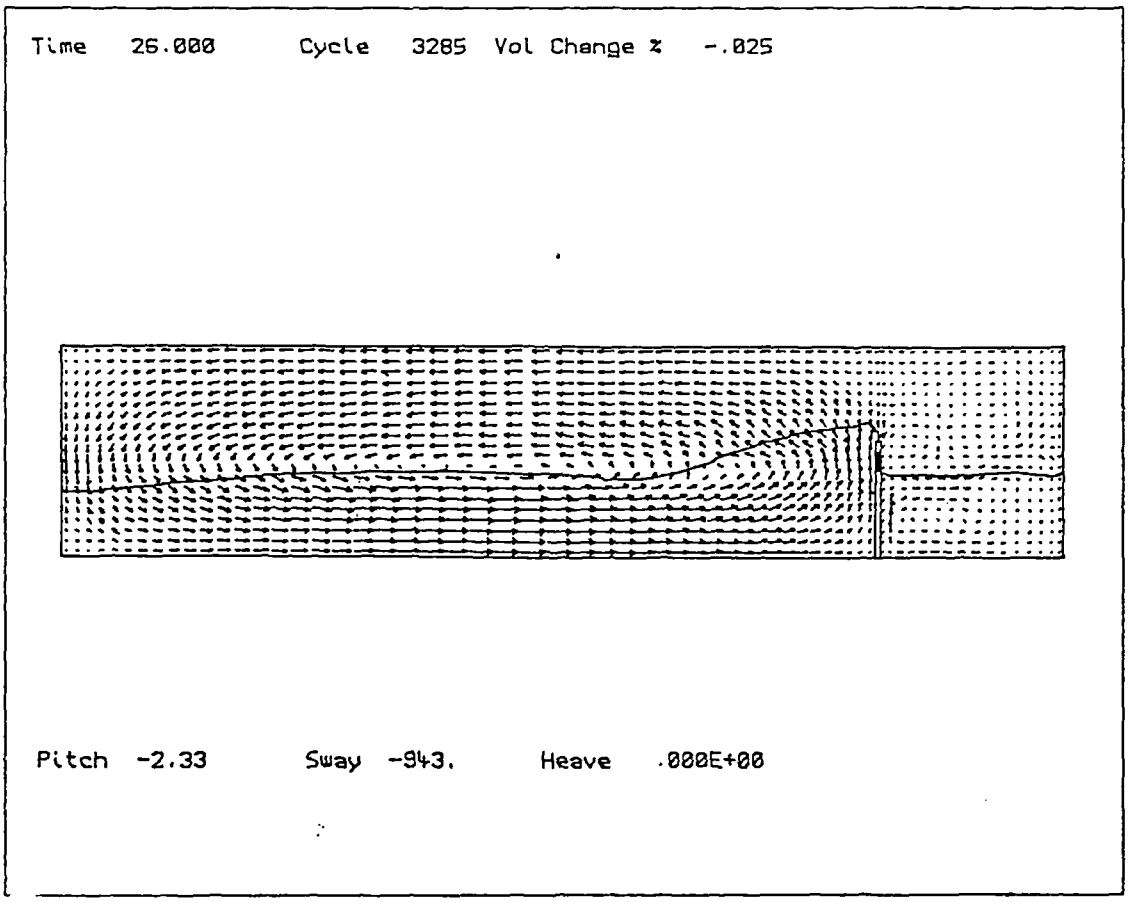
Time 26.000 Cycle 3285 Vol Change % -.025
Pitch -2.33 Sway -943. Heave .000E+00

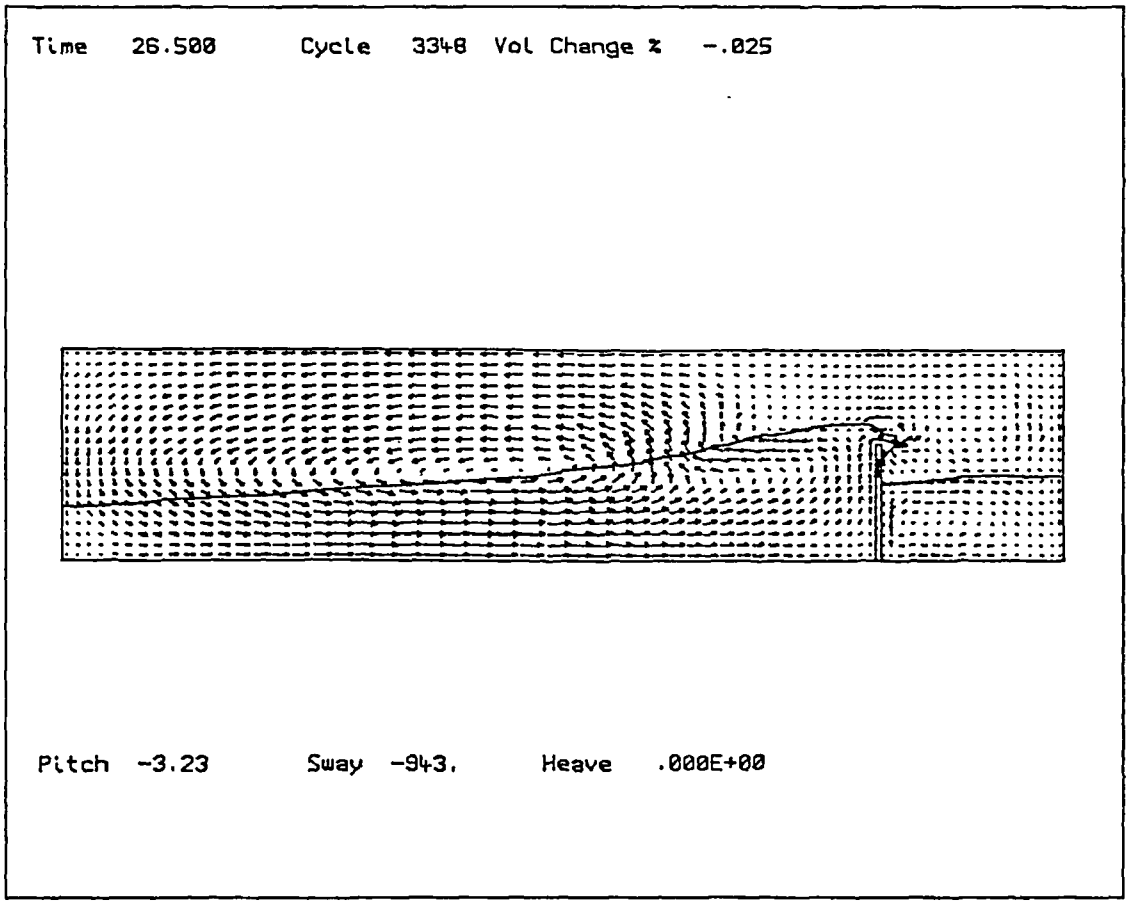
Time 26.500 Cycle 3348 Vol Change % -.025
Pitch -3.23 Sway -943. Heave .000E+00

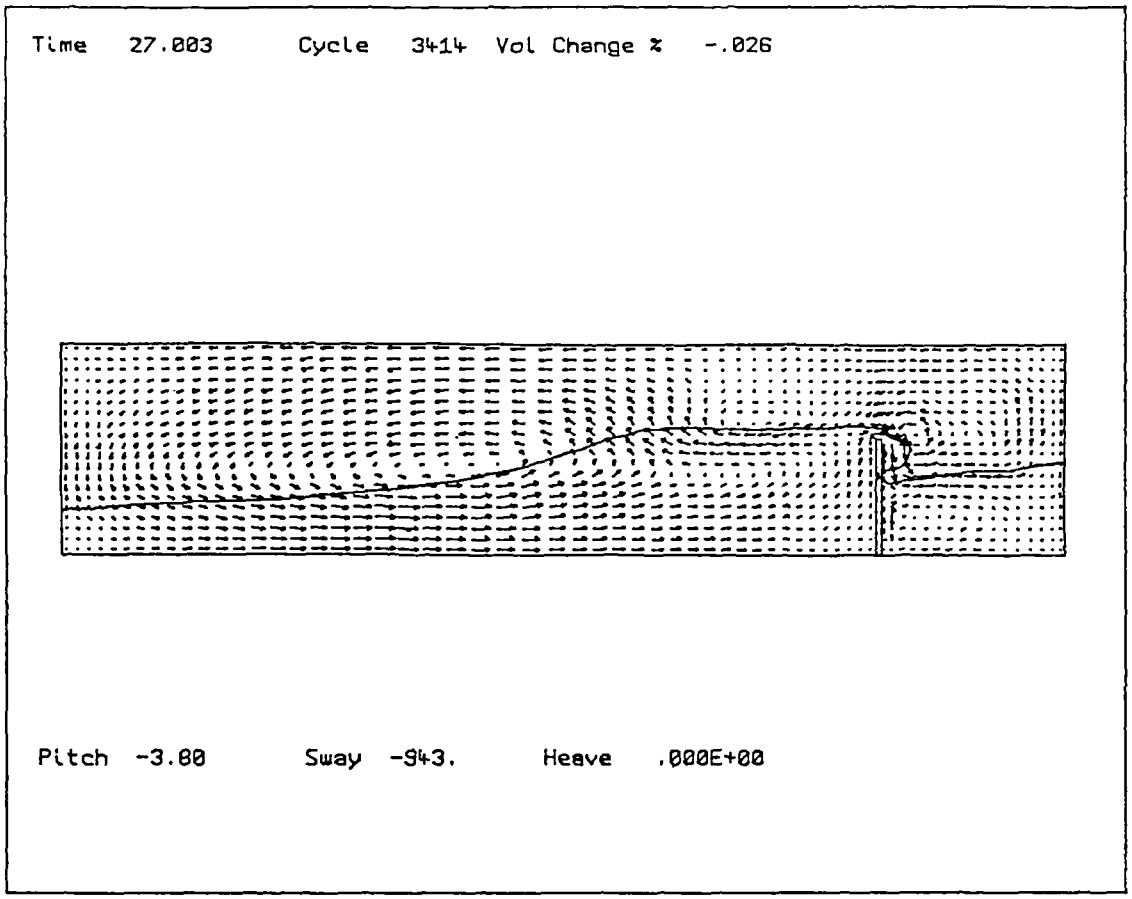
Time 27.003 Cycle 3414 Vol Change % -.026
Pitch -3.00 Sway -943. Heave .000E+00

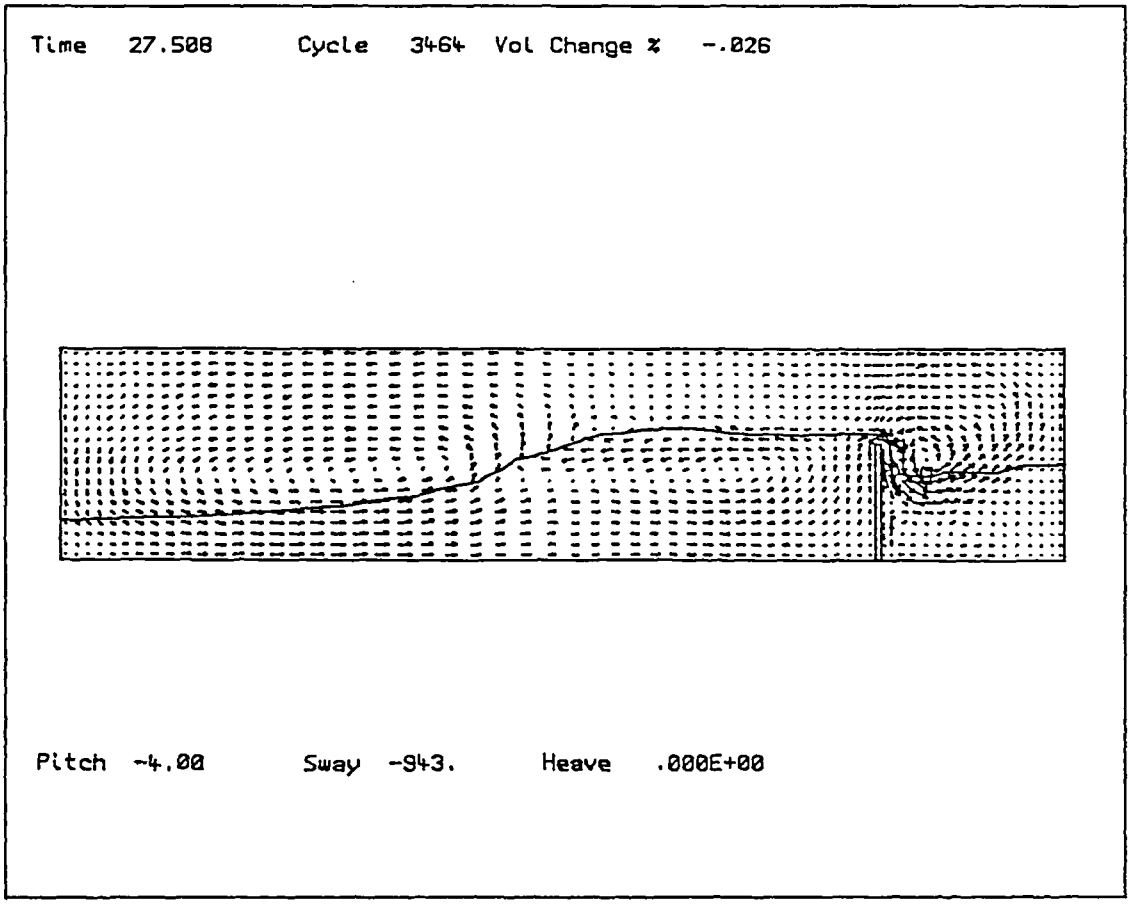
Time 27.508 Cycle 3464 Vol Change % -.026
Pitch -4.00 Sway -943. Heave .000E+00

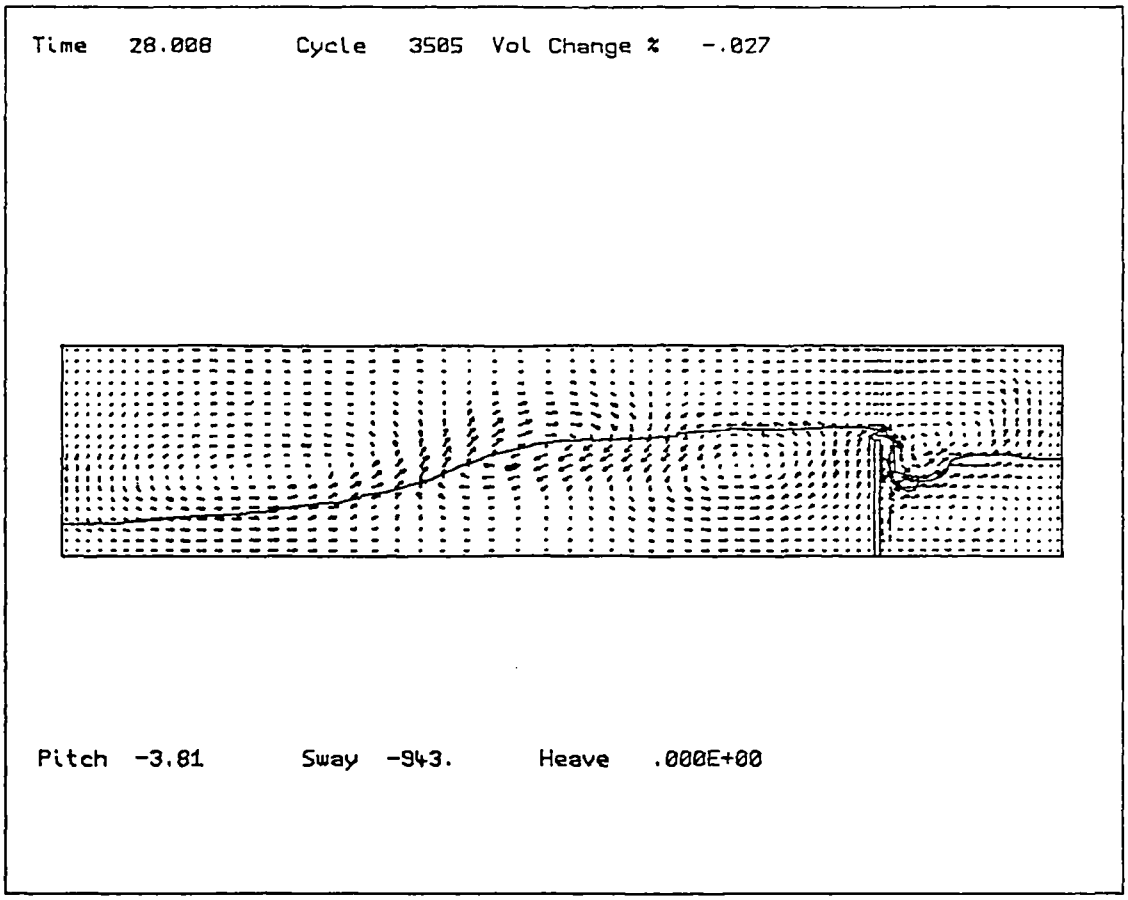
Time 28.008 Cycle 3505 Vol Change % -.027
Pitch -3.81 Sway -943. Heave .000E+00

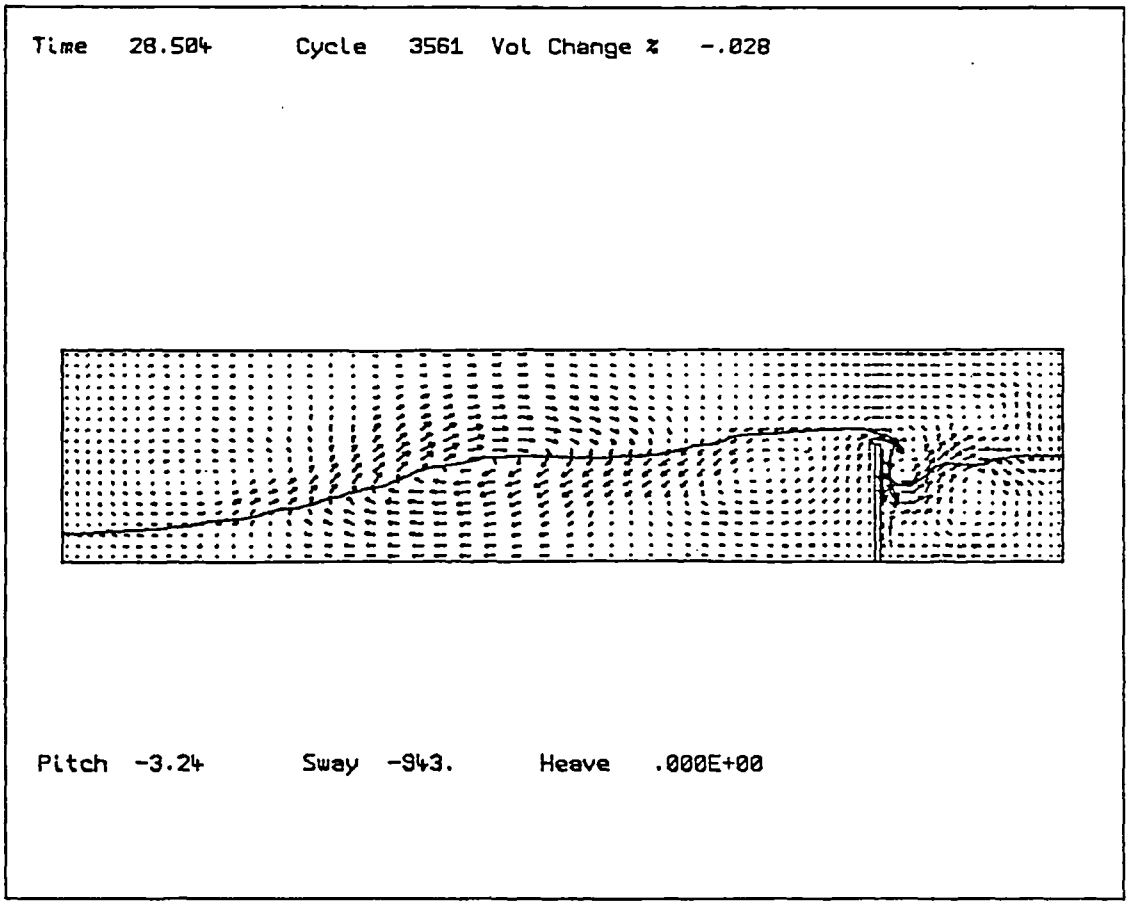
Time 28.504 Cycle 3561 Vol Change % -.028
Pitch -3.24 Sway -943. Heave .000E+00

LIST OF REFERENCES.

1) Rice C.L.
"Effects of Motion on Design of Process Facilities for Floating Production Systems."
17th Annual Offshore Technology Conference, Texas
6-9th May 1985 Vol. 4 No. 5034 (119-127)

2) Abramson H.N. Bass R.L. Faltinsen O. Olsen H.A.
"Liquid Slosh in LNG Carriers."
10th Symposium of Naval Hydrodynamics.
24-28th June 1974 (371-388)

3) Mikelis N.E. Miller J.K. Taylor K.V.
"Sloshing in Partially Filled Liquid Tanks and its Effects on Ship Motions: Numerical Simulations and Experimental Verification."
Naval Archit.
October 1984 (267-281)

4) Roberts J.R. Basurto E.R. Chen P-Y.
"SLOSH Design Handbook I."
Report NASA-CR-406.
May 1966

5) Lamb H.
"Hydrodynamics 6th Edition."
Cambridge University Press
1932

6) Abramson H.N.
"Dynamic Behaviour of Liquid in Moving Container."
Applied Mechanics Reviews
July 1963 Vol. 16 No 7 (501-506)

7) Dodge F.T. Kana D.D. Abramson H.N.
"Liquid Surface Oscillations in Longitudinally Excited Rigid Cylindrical Containers."
AIAA Journal
April 1965 Vol. 3 No. 4 (685-695)

8) Olsen H.A. Hysing,T.
"A Study of Dynamic Loads Caused by Liquid Sloshing in LNG Tanks. Volume I. Text and Figures."
Norske Veritas, Oslo, Norway.
December 1974 Report 74-276-C

9) Eulitz W.R. Glaser R.F.
"Comparative Experimental and Theoretical Considerations on the Mechanisims of Fluid Oscillations on Cylindrical Containers."
George C. Marshall Space Flight Center.
29th May 1961 NASA MTP-M-S&M-P-61-11

10) Graham E.W. Rodriguez A.M.
"The Characteristics of Fuel Motion which Affect Airplane Dynamics."
Journal of Applied Mechanics (Trans ASME).
September 1952 Vol. 19 Part 3 (381-388)

11) Haroun M.A. Chang R.
"Internal Seismic Forces on Submerged Oil Tanks."
Journal of Waterway, Port, Coastal and Ocean Engineering.
November 1985 Vol. 111 No. 6 (1000-1008)

12) Karve S. Fenner C.J.
"Prediction of Process Equipment Performance on Floating Production Systems."
Int. Symp. Dev. Float. Prod. Systems, Royal Inst. Naval Arch. London.
21st-22nd March 1985 Paper 13

13) Feng G.C.
"Dynamic Loads due to Moving Liquid."
14th Structures, Structural Dynamics and Materials Conference, Virginia.
20th-22nd March 1973 AIAA Paper. No. 73-409

14) Bridges T.J.
"A Numerical Simulation of Large Amplitude Sloshing."
3rd Int. Symp. Numerical Ship Hydrodynamics, Paris."
June 1981 (269-284)

15) Arai M.
"Experimental and Numerical Studies of Sloshing Pressure in Liquid Cargo Tanks."
Journal of Soc. Naval Arch. of Japan.
1984 No. 155 (114-121)

16) Harlow F.H. Welch J.E.
"Numerical Calculation of Time Dependant Viscous Incompressible Flow of Fluid with Free Surface."
The Physics of Fluids
December 1965 Vol.8 No.12 (2182-2189)

17) Nichols B.D. Hirt C.W. Hotchkiss R.S.
"SOLA-VOF: A Solution Algorithm for Transient Fluid Flow with Multiple Free Boundaries."
Los Alamos Scientific Laboratory Report.
August 1980 LA-8355

18) Westray T.
"Experience Counts with Floaters."
The Oilman
July 1963 (65-66)

19) Carter J.H.T. Foolen J.
"Evolutionary Developments Advancing the Floating Production, Storage and Offloading Concept."
14th Annual Offshore Technology Conference, Texas.
3rd-6th May 1982 No. 4273 (503-513)

20) Whitfield M.
"Oil/Water Separation: Environmental Requirements."
I.Chem.E. Symposium "Offshore Separation Processes."
15th May 1986 Paper 3

21) Carlisle D. Jenkins R.A. Swift P.M.
"Tanker to Floating Storage Unit: Experience and Future Development."
Int. Symp. Dev. Float. Prod. Systems, Royal Inst. Naval Arch., London.
21st-22nd March 1985 Paper 10

22) Curtis L.B.
"How Conoco Developed the Tension Leg Platform."
Ocean Industry
August 1984 (35-48)

23) Rush H. Craig P. Davidsen N.
"The BP SWOPS Vessel."
Inst. Pet. Eng. Meeting, Report by Marine Management (Holdings) Ltd
8th April 1986

24) Anon
"NOROIL Special: Offshore Europe."
Noroil Publishing House Ltd.
August 1985 Vol. 13 Issue 8 (Page 97)

25) Hisamatsu Y.
"Conceptual Study of a Deepwater Oil Production and Storage System."
Ph.D. Dissertation, University of California, Berkeley.
1981

26) Cormack D. Nichols J.A.
"The Natural and Chemical Dispersion of Oil in the Sea."
RAPP-P-v Reun. Cons. Int. Explor. Mer.
1977 Vol. 171 (97-100)

27) Hoerner B.K. Wiessner F.G. Berger E.A.
"Influence of Irregular Motion of a Floating Structure on Absorption and Distillation Processes."
14th Annual Offshore Technology Conference, Texas
3rd-6th May 1982 No.4276 (527-531)

28) Nobel P. McDowall J. Munson M.
"Floating Offshore Production Systems for Ice Infested Waters."
Int. Symp. Dev. Float. Prod. Systems, Royal Inst. Naval Arch.
London
21st-22nd March 1985

29) Natvig B.J. Pendered J.W.
"Motion response of Floating Structures to Regular Waves."

30) Remery G.F.M.
"Developing Tanker Based Floating Production Systems."
Int. Symp. Dev. Float. Prod. Systems, Royal Inst. Naval Arch. London
21st-22nd March 1984 Paper 7

31) Williams L.M. Pierce D.M. Berkel P. Van
"FPSO II - A Second Generation Floating Production System for Offshore Philippines."
14th Annual Offshore Technology Conference, Texas
3rd-6th May 1982 (515-520)

32) Baitis A.E. Bales S.L. Meyers W.G.
"Design Acceleration and Ship Motions for LNG Cargo Tanks."
10th Symposium Naval Hydrodynamics
24-28th June 1974 (351-370)

33) Anon
"Santa Fe's Deepwater Floating Production Systems."
Ocean Industry.
June 1984 (48-50)

34) Geodfrey J.W. Barakis S.E. Devine W.B. Fedak M.E.
"Offshore Storage and Treating of Crude Oil Aboard a Modified Oil Tanker."
14th Annual Offshore Technology Conference, Texas
3rd-6th May 1982 No.4271 (495-499)

35) Anon
"BP SWOPS Publication."
1988

36) Waldie B.
"Chemical Engineering at Sea."
The Chemical Engineer
June 1986 No. 426 (17-19)

37) Booth D.
"Trend to Floaters Puts New Emphasis on Subsea Route."
The Oilman
December 1985 (28-32)

38) Abramson H.N. Chu W.H. Kana D.D.
"Some Studies of Nonlinear Lateral Sloshing in Rigid Containers."
Journal of Applied Mechanics, Trans ASME.
December 1966 (777-784)

39) Chen P-Y.
"Nonlinear Characteristics of Liquid Sloshing in Rigid Tanks."
3rd Int. Conf. on Pressure Vessel Technology, Tokyo.
April 1977 No. 1 (375-387)

40) Lou Y.K. Su T.C. Flipse J.E.
"A Nonlinear Analysis of Liquid Sloshing in Rigid Containers."
Ocean Engineering Program, Texas A & M University College Station.
August 1980 DOT-RSPA-DMA 50-8211

41) Thorpe S.A.
"On Standing Internal Gravity Waves of Finite Amplitude."
Journal of Fluid Mechanics.
1968 Vol. 32 Part 3 (489-528)

42) Handa K. Tayima K.
"Sloshing of Two Superimposed Liquid Layers in Rectangular Tank."
Trans. Jap. Soc. Mech. Engineers Series B.
1979 Vol. 45 No. 398 (1450-1457)

43) Thorpe S.A
"Turbulence in Stably Stratified Fluids: A Review of Laboratory Experiments."
Boundary-Layer Meteorology
1973 Vol. 5 (95-119)

44) Trefil J.S.
"Introduction to the Physics of Fluids and Solids."
Pergamon Press Inc.
1975

45) Sarpkaya T. Isaacson M.
"Mechanics of Wave Forces on Offshore Structures."
Van Nostrand Reinhold Company.
1981

46) Faltinsen O.M.
"A Nonlinear Theory of Sloshing in Rectangular Tanks."
Journal of Ship Research.
December 1974 Vol. 18 No. 4 (224-241)

47) Bauer H.F.
"Nonlinear Propellant Sloshing in a Rectangular Container of Infinite Length."
Proceedings of the S.E.C.T.A.M.
1966 Vol. 3 (725-760)

48) Binnie A.M.
"Waves in an Open Oscillating Tank."
Engineering.
1941 Vol. 151 (224-226)

49) Graham E.W. Rodriguez A.M.
"The Characteristics of Fuel Motion which Affect Airplane Dynamics."
Douglas Aircraft Company Report, Santa Monica Division.
27th November 1951 SM-14212

50) Skalak R. Yarymovych M.
"Forced Large Amplitude Surface Waves."
Proc. 4th US National Congress on Applied Mechanics, Berkeley.
June 1962 (1411-1418)

51) Chu W.H.
"Subharmonic Oscillations in an Arbitray Tank Resulting from Axial Excitation."
Journal of Applied Mechanics, (Trans ASME).
March 1968 (148-154)

52) Chwang A.T. Wang K.H.
"Nonlinear Impulsive Force on an Accelerating Container."
Journal of Fluids Endineering.
June 1984 Vol. 106 (233-240)

53) Sakata M. Kimura K. Utsumi M.
"Non-stationary Response of Non-linear Liquid Motion in a Cylindrical Tank Subjected to Random Base Exitation."
Journal of Sound and Vibration.
8th June 1984 Vol. 94 No. 3 (351-363)

54) Verhagen J.H.G. Wijngaarden L. Van
"Non-linear Oscillations of Fluid in a Container."
Journal of Fluid Mechanics.
1965 Vol. 22 Part 4 (737-751)

55) Chester W.
"Resonant Oscillations of Water Waves I. Theory."
Proc. Royal Soc. London Series A
1968 Vol. 306 (5-22)

56) Faltinsen O.M.
"A Numerical Nonlinear Method of Sloshing in Tanks with 2-Dimensional Flow."
Journal of Ship Research
September 1978 Vol. 22 No. 3 (193-202)

57) Vandiver J.K. Mitome S.
"Effect of Liquid Storage Tanks on the Dynamic Response of Offshore Platforms."
Applied Ocean Research.
1979 Vol. 1 No. 2 (67-74)

58) Ames W.F.
"Numerical Methods for Partial Differential Equations, 2nd Edition."
Academic Press Inc.
1977

59) Hirt C.W. Shannon J.P.
"Free Surface Stress Conditions for Incompressible Flow Calculations."
Journal of Computational Physics.
1968 Vol. 2 (403-411)

60) Liu W.K. Ma D.C.
"Coupling Effect Between Liquid Sloshing and Flexible Fluid Filled Systems."
Nuclear Engineering and Design.
1982 Vol. 72 (345-357)

61) Navickas J. Peck J.C. Bass R.L. Bowles E.B. Yoshimura N. Endo S.
"Sloshing of Fluids at High Fill Levels in Closed Tanks."
ASME Winter Meeting, Washington
1981 (191-198)

62) Bauer H.F.
"Oscillations of Immiscible Liquids in a Rectangular Container: A New Damper for Excited Structures."
Journal of Sound and Vibration.
1984 Vol. 93 No. 1 (117-133)

63) Manna R.K.
"Forced Oscillations in a Two-Layer Fluid of Finite Depth."
Journal of Applied Mechanics, (Trans. ASME)
September 1983 Vol. 50 (506-510)

64) Anderson G.L. Weiss H.J.
"Baffling of Fluid Sloshing in Cylindrical Tanks."
General Dynamics/Convair.
1st April 1966 NASA-CR-61434 N6815457

65) O'Neil J.P.
"Semiannual Report on Experimental Investigation of Sloshing."
TRW Space Technology Labs, Los Angeles. Report STL/TR-59-0000-00713
June 1959 AD 607 341

66) Keulegan G.H.
"Energy Dissipation in Standing Wavesin Rectangular Basins."
Journal of Fluid Mechanics.
1959 (33-50)

67) Case K.M. Parkinson W.C.
"Damping of Surface Waves in an Incompressible Liquid."
Journal of Fluid Mechanics.
March 1957 Part 2 (172-184)

68) Abranson H.N.
"The Dynamic Behavior of Liquids in Moving Containers with Applications to Space Vehicle Technology."
Southwest Research Institute Report NASA-SP106
1966 N67-15884

69) Howell E. Ehler F.G.
"Experimental Investigation of the Influence of Mechanical Baffles on the Fundamental Sloshing Mode of Water in a Cylindrical Tank."
Guided-Missile Research Division, The Ramo-Wooldridge Corporation.
6th July 1956 Report No. GM-TR-69

70) Fox D.W. Kuttler J.R.
"Upper and Lower Bounds for Sloshing Frequencies by Intermediate Problems."
Journal of Applied Mathematics and Physics
1981 Vol. 32 (667-682)

71) Fox D.W. Sigillito V.G.
"Sloshing Eigenvalues of Two-Dimensional Regions with Holes."
Journal of Applied Mathematics and Physics
1982 Vol. 32 (658-666)

72) Abramson H.N. Nevil G.E. Jr
"Some Modern Developments in the Application of Scale Models in Dynamic Testing."
ASME Meeting, "Use of Models and Scaling in Shock and Vibration."
19th November 1963 (1-15)

73) Bass R.L. Bowles E.B Jr. Trudell R.W. Navickas J. Peck J.C. Yoshimura N. Endo S. Pots B.F.M
"Modeling Criteria for Scaled LNG Sloshing Experiments."
Journal of Fluids Engineering, (Trans. ASME)
June 1985 Vol. 107 (272-280)

74) Yih C-S.
"Fluid Mechanics."
McGraw Hill Book Company Inc.
1969

75) Raudkivi A.J. Callander R.A.
"Advanced Fluid Mechanics. An Introduction."
Edward Arnold.
1975

76) Hirt C.W. Cook J.L. Butler T.D.
"A Lagrangian Method for Calculating the Dynamics of an Incompressible Fluid with Free Surface."
Journal of Computational Physics
1970 Vol. 5 (103-124)

77) Noh W.F.
"CEL: A Time-Dependant Two-Space-Dimensional Coupled Eulerian-Lagrange Code."
Methods in Computational Physics
1964 Vol. 3 (117-179)

78) Anon.
"Liquid Sloshing Course Notes."
Wessex Institue of Technology, Southampton.
17-18th April 1985

79) Wyk R. Van
"Variable Mesh Multistep Methods for Ordinary Differential Equations."
Journal of Computational Physics.
1970 Vol. 5 (244-264)

80) Rennie G.
"Final Year Experimental Report"
Heriot-Watt University, Dept. Chemical & Process Engineering.
1984

81) Smith C.L.
"Liquid Measurement Technology."
Chemical Engineer.
3rd April 1978 Vol. 85 No. 8 (155-164)

82) Liu H.T. Katsaros K.B. Weissman M.A.
"Dynamic Response of Thin-Wire Wave Gauges."
Journal of Geophysical Research.
20th July 1982 Vol. 87 No. C8 (5686-5698)

83) Larsen T. Dyrik G.
"Fast Fourier Transforms using a Microcomputer."
Electronics & Wireless World.
September 1985 (80-82)

84) Omer W.
"Fast Fourier Transforms."
Electronics & Wireless World.
June 1986 (23-25)

85) Harker J.H. Backhurst J.R.
"Fuel and Energy."
Academic Press
1981

86) Said I. Anderson B.
"Concentration Dependant Diffusivity of Benzoic Acid in Water and its Influence on the Liquid-Solid Mass Transfer."
Canadian Journal of Chemical Engineering
December 1986 Vol. 64 (954-959)

87) Murdoch R. Pratt H.R.C.
"Liquid-Liquid Extraction: Part III. The Extraction of Uranyl Nitrate in a Wetted Wall Column.""
Trans. Inst. Chem. Eng.
1953 Vol. 31 (307-326)

88) Rushton J.H.
"Measurements of Mass Transfer Coefficients in Liquid-Liquid Mixing."
A.I.Chem.E.J
May 1964 Vol. 10 (298-302)

89) Yoshitome H. et al
"Mass Transfer of Bubble Bed Dissolution of Benzoic Acid in Water."
Chem. Eng. Japan
March 1964 Vol. 28 (228-232)

90) Taylor N.W.
"The Nature of the Nerve Receptor for the Acid Taste as Indicated by the Absorption of Organic Acids by Fats and Proteins."
Protoplasma.
1930 Vol. 10 (98-105)

91) Anon.
"The Fate of Oil Spilt at Sea."
M.O.D. Working Party Report, Defence Research Information Centre
1973

92) Daly B.J.
"Numerical Study of Two Fluid Rayleigh-Taylor Instability."
The Physics of Fluids
Febuary 1967 Vol. 10 No. 2 (297-307)

93) Davis R.E. Acrivos A.
"The Stability of Oscillatory Internal Waves."
Journal of Fluid Mechanics
1967 Vol. 30 No. 4 (723-736)

94) Milgram J.H. Houten R.J. Van
"Mechanics of a Restrained Layer of Floating Oil above a Water Current."
Journal of Hydronautics
July 1978 Vol. 12 No. 3 (93-108)

95) Basco D.R.
"A Qualitative Description of Wave Breaking."
Journal of Waterway, Port, Coastal and Ocean Engineering
March 1985 Vol. 111 No. 2 (171-188)

96) Huther M. Olsen H. Thomsson O.
"Liquid Sloshing in Tanks with Internal Structures."
The Swedish Ship Research Foundation, Summary Report
1977 SSF Project 5609

97) Cox P.A. Bowles E.B. Bass R.L.
"Evaluation of Liquid Dynamic Loads in Slack LNG Cargo Tanks."
Southwest Research Institute Report.
May 1980 SWRI-SR-1251 SSC-297